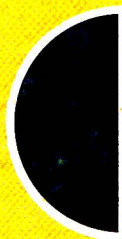
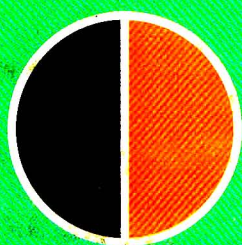


APRIL 1, 1992

Analytical CHEMISTRY



**LIGHT IN AN
ELECTROCHEMICAL TUNNEL**
429 A

The only thing better
than our new
Accumet® pH Meter
is our free offer.



Fisher's new microprocessor-controlled Accumet 50 is the **most advanced pH meter on the market**, bar none. The *only* benchtop meter that measures conductivity, as well as ion concentration and pH. With simple intuitive controls and a big, easy-to-read help screen that's really an electronic operator's manual at your fingertips. Plus dual electrode inputs, an internal 50-point datalog, print-when-stable function, and more. Much more. But don't take our word for it. **Try it free for 30 days.**

The Accumet Model 50 pH Meter comes standard with a Fisher glass-body combination electrode. At the end of the 30-day trial, **you keep the electrode**—whether you keep the meter or not. Absolutely no risk to you. Also very little risk to us. Because once you've tried the Accumet 50, we think you'll keep it.



To schedule your free trial, call 800-766-7000. To receive information about the other innovative new pH meters in the Accumet line, check the reader-service card number below.



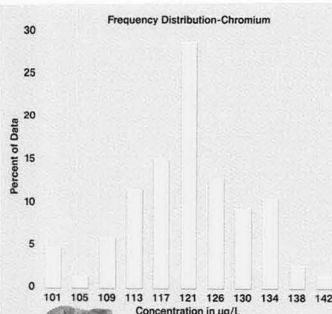
Fisher Scientific

CIRCLE 40 ON READER SERVICE CARD

THE PERFECT STANDARD. Emerged By Consensus.

We can all agree that the value of any standard is directly related to its level of documentation. The more you know about the standards you use, the greater your confidence. Only APG brings you the first true consensus laboratory standards for environmental analysis.

APG *Setpoint Laboratory Standards*™ are verified in a unique nationwide round-robin program which includes over five hundred laboratories. The data you get is the data you need for your analysis: True Values, Means, Standard Deviations, Number of Laboratories, and Confidence Intervals.



It's all there with no estimates based on prior studies, no unexplained Certified Values, no extra charges.

For developing QC charts, solving problems, or evaluating commercial laboratories, *Setpoint Laboratory Standards* are your best choice for external quality control. Only APG can give real world interlaboratory Means and Deviations based upon the strength—and numbers—of our unmatched database.

Hundreds of labs throughout the U.S. and Canada currently rely on *Setpoint Laboratory Standards* for their environmental quality control. You can too. Call today.

Certified Reference Material

Setpoint Laboratory Standards are verified in a nationwide interlaboratory program. The data supplied with this standard was developed based upon analysis of the standard in this program. Laboratories reporting data analyzed this sample as an unknown.

Standard: Trace Metals Lot No. 7749
Parameter: Chromium Units: ug/L

Interlaboratory Data

True Value:	119.65
Mean of Reporting Laboratories:	119.462
Actual Standard Deviation:	8.678
Standard Error of the Mean:	0.919
Number of Laboratories	
Reporting:	89
Average % Recovery:	99.842
95% Confidence Limit:	102.45-136.47
99% Confidence Limit:	97.07-141.85

1-800-272-4442

The Measure of Quality.

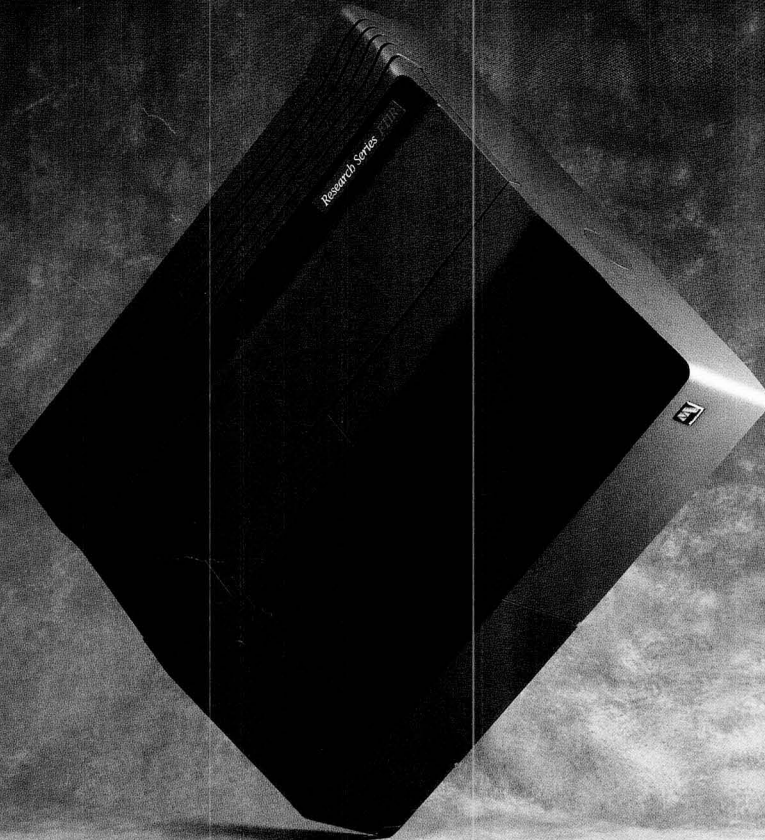
APG

**Analytical Products
Group, Inc.**

2730 Washington Blvd., Belpre, OH 45714
FAX 1-614-423-5588

CIRCLE 5 ON READER SERVICE CARD

Turning spectroscopy on its ear.
Once again.



Mattson introduces the Research Series™ FTIR spectrometer.

Once again, we're introducing a first. The first spectrometer with signal-to-noise ratios exceeding 50,000:1. That's the highest signal-to-noise you can get.

Our Research Series is the only high-end spectrometer that works on a standard computer platform. (We were the first to introduce that concept, too.) So every time one of the computer biggies makes a big breakthrough, you're right there with them. Upgrading. Evolving. You can upgrade your software just as easily. What's more, you can choose from 8 different plug-and-play options to add on as your research needs change.

You just can't get a better spectrometer. Call us at Mattson Instruments today. 1-608-831-5515. We're taking you into tomorrow. And beyond.



Mattson
Revolutionary. Evolutionary.

Mattson Instruments, Orion Research, Cahn Instruments and Unicam are operating divisions of Analytical Technology, Inc.
Research Series is a trademark of Mattson Instruments.
© 1992, Mattson Instruments, Inc.

APRIL 1, 1992

VOLUME 64

NUMBER 7

AN The ANCHAM
Audit: 64(7) 411A-462A/705-832 (1992)
Bureau ISSN 0003-2700

Registered in U.S. Patent and Trademark Office;
©Copyright 1992 by the American Chemical Society

EDITOR: ROYCE W. MURRAY

ASSOCIATE EDITORS: Catherine C. Fenselau,
Georges Guiochon, James W. Jorgenson,
Robert A. Osteryoung, Edward S. Yeung

Editorial Headquarters

1155 Sixteenth St., N.W.

Washington, DC 20036

Phone: 202-872-4570

Telefax: 202-872-4574

Bitnet: rmh96@cas

Internet: rmh96@acs.org

Managing Editor: Mary Warner

Senior Editor: Louise Vorets

Associate Editor: Grace K. Lee

Assistant Editors: Julie Poudrier Skinner, Felicia
Wach

Contributing Editor: Marcia Vogel

Director, Operational Support: C. Michael
Phillippe

Head, Production Department: Leroy L.
Corcoran

Art Director: Alan Kahan

Composition Systems Administrator: Vincent L.
Parker

Designers: Peggy Corrigan, Robert Sargent

Production Editor: Elizabeth Wood

Circulation: David Schulbaum

LabGuide

Managing Editor of Directories and Databases:
Kathleen Strum

Associate Editor: Joanne Mullican

Journals Dept., Columbus, Ohio

Associate Head: Marianne Brogan

Editorial Office Manager: Mary E. Scanlan

Journals Editing Managers: Kathleen E. Duffy,
Joseph E. Yurvati

Assistant Editors: Stephanie R. Harrell,
Diane E. Needham

Advisory Board: Michelle V. Buchanan, M.
Bonner Denton, William S. Hancock, Joel M.
Harris, Timothy D. Harris, Franz Hillenkamp,
Dennis C. Johnson, Richard A. Keller, Philip D.
LaFleur, Alan G. Marshall, John F. Rabolt, Ger-
aldine Richmond, Ralph Riggan, Debra R. Rol-
ison, Shigeru Terabe, Michael Thompson
Ex Officio: Charles L. Wilkins

Instrumentation Advisory Panel: Daniel W.
Armstrong, Anna Brajer-Toth, Thomas L.
Chester, Raymond E. Clement, Norman J. Dov-
ichi, Jack D. Henion, John W. Olesik, Dallas L.
Rabenstein, Brenda R. Shaw

Publications Division

Director: Robert H. Marks

Head, Special Publications: Anthony Durniak

Journals: Charles R. Bertsch

Published by the
AMERICAN CHEMICAL SOCIETY

1155 Sixteenth Street, N.W.

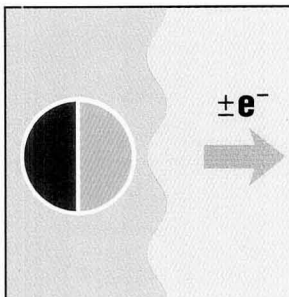
Washington, DC 20036

(202) 872-4600

TDD (202) 872-8733

FAX (202) 872-4615

Analytical[®] CHEMISTRY



REPORT

429 A

On the cover. Light in an electrochemical tunnel? Spectroscopic methods increasingly are being used to solve analytical problems in electrochemistry. Krishnan Rajeshwar of the University of Texas at Arlington and co-workers focus on the central role of optical spectroscopies in the study of electrode reactions and boundary layers



FOCUS

453 A

Have LC lab, will travel. At the conclusion of Operation Desert Storm, it was necessary to test the stability of unused propellant. Gail Y. Stine of the Naval Surface Warfare Center describes the problems that had to be overcome in establishing a mobile LC lab in the Saudia Arabian desert

UPCOMING RESEARCH

421 A

EDITORIAL

425 A

August in New Hampshire. The JOURNAL shares with the Analytical Chemistry Gordon Conference a commitment to a general approach to analytical chemistry and an aim of presenting the best current science across the discipline

NEWS

427 A

New Head of Special Publications. • 1993 Waters Symposium proposals. • **Washing an aquifer**

MEETINGS

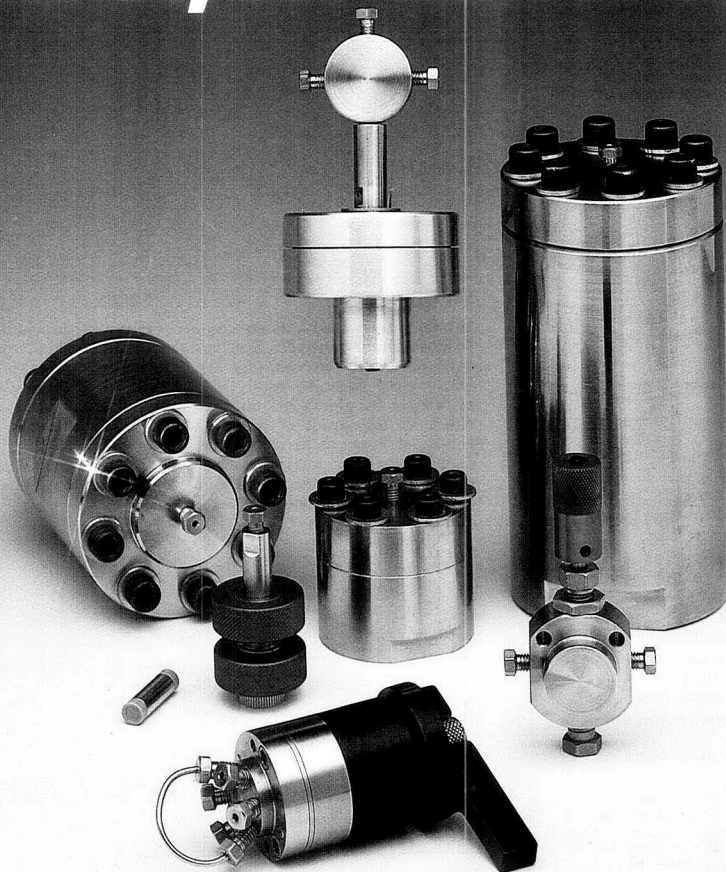
443 A

Fourteen of this year's **Gordon Research Conferences** are of particular interest to analytical chemists

NEW PRODUCTS AND MANUFACTURERS' LITERATURE

456 A

NEW PRODUCTS FOR HPLC, SFE AND SFC.



Introducing VICI's new line of high performance flat rotary valves, SFE on/off valves, and vessels for supercritical fluid extraction. The new Cheminert® HPLC and SFE/SFC valves are available in manual and automated versions and are rated at 7,000 psi. The manual version features front panel loading via standard syringes.

Valco's new fixed and removable seat on/off valves feature standard cobalt alloy stems and have the lowest internal volume of any two port valve. These valves have low-force manual or automatic actuation and are available in Hastelloy C-22® and titanium. All models are suitable for prime and purge or SFE applications.

Our supercritical fluid extraction vessels range in size from the finger-tight 250µl model to the 50ml version and are operable to 200°C at 10,000 psi. Large models may be opened and closed with ease, so large wrenches and bench vises are not required.

VICI® offers you the most advanced accessories and components for HPLC, SFE and SFC.

VICI

Valco Instruments Co. Inc.
P.O. Box 55603, Houston, TX 77255
Telephone (713) 688-9345
Telefax (713) 688-8106
Sales Calls 1-800-FOR VICI

VICI AG

Valco Europe
Untertannberg 7 CH-6214 Schenkon, Switzerland
Telex 868342 VICI CH
Telefax (045) 21 30 20
Telephone (045) 21 68 68

ANALYTICAL CHEMISTRY (ISSN 0003-2700) is published semimonthly by the American Chemical Society at 1155 Sixteenth St., N.W., Washington, DC 20036. Editorial offices are located at the same ACS address (202-872-4570; fax 202-872-4574; Bitnet rmh96@cas; TDD 202-872-8733). Second-class postage paid at Washington, DC, and additional mailing offices. Postmaster: Send address changes to ANALYTICAL CHEMISTRY, Member & Subscriber Services, P.O. Box 3337, Columbus, OH 43210. Canadian GST Reg. No. R127571347.

Copyright Permission: An individual may make a single reprographic copy of an article in this publication for personal use. Reprographic copying beyond that permitted by Section 107 or 108 of the U.S. Copyright Law is allowed, provided that the appropriate per-copy fee is paid through the Copyright Clearance Center, Inc., 27 Congress St., Salem, MA 01970. For reprint permission, write Copyright Administrator, Publications Division, ACS, 1155 Sixteenth St., N.W., Washington, DC 20036.

Registered names and trademarks, etc., used in this publication, even without specific indication thereof, are not to be considered unprotected by law.

Subscription and Business Information

1992 subscription rates include air delivery outside the U.S., Canada, and Mexico. Canadian subscriptions are subject to 7% GST.

	Members	Nonmembers (personal)	Nonmembers (institutional)
U.S.	\$ 33	\$ 76	\$ 373
Canada and Mexico	69	112	409
Europe	117	233	457
Other countries	150	266	490

Nonmember rates in Japan: Rates above do not apply to nonmember subscribers in Japan, who must enter subscription orders with Maruzen Company Ltd., 3-10, Nihonbashi 2-chome, Chuo-ku, Tokyo 103, Japan. Tel: (03) 272-7211.

For multi-year and other rates, call toll free 800-227-5558 in the U.S. and Canada; in the Washington, DC, metropolitan area and outside the U.S., call 202-872-4363; fax 202-872-4615.

Single issues, current year, \$16.00 except review issue, \$40.00, and LabGuide, \$50.00; **back issues and volumes and microform editions** available by single volume or back issue collection. For information or to order, call the number listed for subscription orders by phone; or write the Microform & Back Issues Office at the Washington address.

Subscription orders by phone may be charged to VISA, MasterCard, or American Express. Call toll free 800-333-9511 in the continental U.S.; in the Washington, DC, metropolitan area and outside the continental U.S., call 202-872-8065. Mail orders for new and renewal subscriptions should be sent with payment to American Chemical Society, Department L-0011, Columbus, OH 43268-0011.

Changes of address must include both old and new addresses with ZIP code and a recent mailing label. Send all address changes to the ACS Columbus address. Please allow 6 weeks for change to become effective. **Claims for missing numbers** will not be allowed if loss was due to failure of notice of change of address to be received in the time specified; if claim is dated (a) North America—more than 90 days beyond issue date, (b) all other foreign—more than 180 days beyond issue date. Hard copy claims are handled at the ACS Columbus address.

ACS membership information: Lorraine Bowlin (202-872-4567)

Articles

- Rapid Functional Group Characterization of Gas Chromatography/Fourier Transform Infrared Spectra by a Principal Components Analysis Based Expert System** **705**
*Erik J. Hasenoeher, Jonathan H. Perkins, and Peter R. Griffiths**

- Determination of Amino Acids by Capillary Zone Electrophoresis Based on Semiconductor Laser Fluorescence Detection** **711**
Toshiyuki Higashijima, Tetsuhiro Fuchigami, Totaro Imasaka, and Nobuhiko Ishibashi*

- Drug Release Profiles of Ophthalmic Formulations. 1. Instrumentation** **715**
*Larry E. Stevens, Paul J. Missel, and John C. Lang**

- Determination of Selenium by Inductively Coupled Plasma Mass Spectrometry Utilizing a New Hydride Generation Sample Introduction System** **724**
Wayne T. Buckley, James J. Budac, David V. Godfrey, and Karen M. Koenig*

- Simultaneous Determination of Mixtures by Kinetic Analysis of General-Order Reactions** **729**
Israel Schechter

- Preconcentration of Trace Rare-Earth Elements in Seawater by Complexation with Bis(2-ethylhexyl) Hydrogen Phosphate and 2-Ethylhexyl Dihydrogen Phosphate Adsorbed on a C₁₈ Cartridge and Determination by Inductively Coupled Plasma Mass Spectrometry** **737**
Mohammad B. Shabani, Tasuku Akagi, and Akimasa Masuda*

- Is Plasma Desorption Mass Spectrometry Useful for Small-Molecule Analysis? Fragmentations of the Natural α -Amino Acids** **743**
Stephane Bouchonnet, Jean-Pierre Denhez, Yannik Hoppilliard, and Christine Mauriac*

- Neutral-Ion Correlation Measurements: A Novel Tandem Mass Spectrometry Data Acquisition Mode for Tandem Magnetic Sector/Reflectron Time-of-Flight Instruments** **754**
*F. H. Strobel, L. M. Preston, K. S. Washburn, and D. H. Russell**

- Mass Discrimination in Laser Desorption/Fourier Transform Ion Cyclotron Resonance Mass Spectrometry Cation-Attachment Spectra of Polymers** **763**
*Jeremiah D. Hogan and David A. Laude, Jr.**

- Pulsed Sample Introduction Interface for Combining Flow Injection Analysis with Multiphoton Ionization Time-of-Flight Mass Spectrometry** **769**
*Alan P. L. Wang and Liang Li**

- Quadrupole Mass Spectrometry in Combination with Lithium Ion Attachment for Sampling at Atmospheric Pressure: Possible Coupling to Supercritical Fluid Chromatography** **775**
Toshihiro Fujii

- Capillary Zone Electrophoretic Detection of Biological Thiols and Their S-Nitrosated Derivatives** **779**
*Jonathan S. Stamler and Joseph Loscalzo**

*Corresponding author

continued on p. 419 A

DIGITAL'S POWERFUL SOLUTIONS HELP SPEED YOUR NEXT DISCOVERY TO MARKET.

Whatever it is that's slowing you down, the world won't wait for you to announce your next discovery. Which is why you should call Digital soon.

Our robust workstations, vectors, and networks empower scientists and researchers to choose the resources needed to speed the latest discoveries to market.

Visualization - The powerful DECstation 5000 provides windows so you can manipulate and view molecules, and determine their optimum structure, stability and possible reaction mechanisms.

Information - Digital's open computing environment puts molecular and reaction databases, such as

CPSS®, ISIS™, MACCS-II and REACCS, quickly at your fingertips.

Computation - Our VAX 6000 and VAX 9000 vector systems perform analyses up to 400 times faster than general processing systems, enabling you to quickly calculate structures using vectorized applications such as CHARMM™, DISCOVER, GAUSSIAN 90™, MOPAC and others.

Collaboration - Digital's networking and open systems environment mean test results can be transmitted to remote sites immediately instead of the weeks required by mail.

Digital's workstations, vectors, and networks. A major find for bringing your discoveries to market **digital**™ sooner.

BECAUSE THE MARKET WON'T WAIT FOREVER.

NAS FROM DIGITAL. THE OPEN ADVANTAGE.

©DIGITAL EQUIPMENT CORPORATION 1991. THE DIGITAL LOGO, DIGITAL AND VAX ARE TRADEMARKS OF DIGITAL EQUIPMENT CORPORATION. CHARMM IS A TRADEMARK OF POLYGEN CORP. GAUSSIAN 90 IS A TRADEMARK OF GAUSSIAN, INC. CPSS IS A REGISTERED TRADEMARK, AND ISIS IS A TRADEMARK OF MOLECULAR DESIGN LTD.

Editorial Information

Instructions for authors of AC RESEARCH are published in the January 1 issue, p. 107. Guidelines for the INSTRUMENTATION, REPORT, ANALYTICAL APPROACH, and A/C INTERFACE features are available from the Washington editorial office. Please consult these instructions and guidelines prior to submitting a manuscript for consideration for publication.

Manuscripts for publication (4 copies of text and illustrative material) should be submitted to ANALYTICAL CHEMISTRY at the ACS Washington address. Please include a signed copyright status form; a copy of this document appears on p. 111 of the January 1 issue. Correspondence regarding manuscripts under review should be directed to the Washington editorial staff; correspondence regarding accepted papers and proofs should be directed to the Journals Dept. in Columbus at the address below.

For individual reprints of AC RESEARCH or A-page articles, please contact the authors directly. Bulk reprints of individual articles are available from ACS. For information, write or call the Distribution office at the ACS Washington address (202-872-4539; fax 202-872-4615).

ACS Division of Analytical Chemistry
Chair, Charles Wilkins (714-787-3518)
Secretary, Sarah Rutan (804-367-1298)

ACS Information

Library Services	202-872-4515
Education Division	202-872-4388
Meetings Dept.	202-872-4397
Member Services	202-872-4414
Employment Services	202-872-6120
Public Outreach	202-872-4091

Supplementary material is noted in the table of contents with a ■. It is available as photocopy (\$10.00 for up to 3 pages and \$1.50 per page for additional pages, plus \$2.00 for foreign postage) or as 24X microfiche (\$10.00, plus \$1.00 for foreign postage). Canadian residents should add 7% GST. See supplementary material notice at end of journal article for number of pages. Orders must state whether for photocopy or for microfiche and give complete title of article, names of authors, journal, issue date, and page numbers. Prepayment is required and prices are subject to change. Order from Microforms & Back Issues Office at the ACS Washington address.

The paper used in this publication meets the minimum requirements of American National Standard for Information Sciences—Permanence of Paper for Printed Library Materials, ANSI Z39.48-1984.

Journals Department

American Chemical Society
2540 Olentangy River Road
P.O. Box 3330
Columbus, OH 43210
614-447-3600, Ext. 3171
TELEX 6842086; FAX 614-447-3745

Member & Subscriber Services

American Chemical Society
P.O. Box 3337
Columbus, OH 43210
614-447-3776
800-333-9511

Advertising Office: Centcom, Ltd., 1599 Post Road East, P.O. Box 231, Westport, CT 06881

The American Chemical Society and its editors assume no responsibility for the statements and opinions advanced by contributors. Views expressed in the editorials are those of the editors and do not necessarily represent the official position of the American Chemical Society.

Microscopic Order as a Function of Surface Coverage in Alkyl-Modified Silicas: Spin Probe Studies **785**
*Paul B. Wright, Edward Lamb, John G. Dorsey, and Robert G. Kooser**

Separation and Molecular Weight Distribution of Anionic and Cationic Water-Soluble Polymers by Flow Field-Flow Fractionation **790**
*Maria Anna Benincasa and J. Calvin Giddings**

Migration Behavior of Inorganic Anions in Micellar Electrokinetic Capillary Chromatography Using a Cationic Surfactant **798**
Takashi Kaneta, Shunitz Tanaka, Mitsuhiro Taga, and Hitoshi Yoshida*

Combined Supercritical Fluid Extraction/Solid Phase Extraction with Octadecylsilane Cartridges as a Sample Preparation Technique for the Ultratrace Analysis of a Drug Metabolite in Plasma **802**
*Hanjia Liu, Linda M. Cooper, Douglas E. Raynie, J. David Pinkston, and Kenneth R. Wehmeyer**

Intravenous Microdialysis Sampling in Awake, Freely-Moving Rats **806**
*Martin Telting-Diaz, Dennis O. Scott, and Craig E. Lunte**

Parts-per-Trillion Determination of Trihalomethanes in Water by Purge-and-Trap Gas Chromatography with Electron Capture Detection **810**
Louis Lépine and Jean-François Archambault*

Selective Sorption and Column Concentration of Alkali-Metal Cations by Carboxylic Acid Resins with Dibenzo-14-crown-4 Subunits and Their Acyclic Polyether Analogues **815**
*Takashi Hayashita, Joung Hae Lee, Matthew G. Hankins, Jong Chan Lee, Jong Seung Kim, John M. Knobloch, and Richard A. Bartsch**

Correspondence

Continuous Rods of Macroporous Polymer as High-Performance Liquid Chromatography Separation Media **820**
*Frantisek Svec and Jean M. J. Fréchet**

Mass Spectrometric Identification of Methylphosphonic Acid: The Hydrolysis Product of Isopropyl Methylphosphonofluoridate and Pinacolyl Methylphosphonofluoridate **823**
Durgesh N. Tripathi, Karuna S. Pandey, Arabinda Bhattacharya, and Ramamoorthy Vaidyanathaswamy*

Technical Notes

Recovery of Submilligram Quantities of Carbon Dioxide from Gas Streams by Molecular Sieve for Subsequent Determination of Isotopic (¹³C and ¹⁴C) Natural Abundances **824**
James E. Bauer, Peter M. Williams, and Ellen R. M. Druffel*

Inverse Sampling Valve Interface for On-Line Process Monitoring with a Mass Spectrometer **827**
Jennifer S. Brodbelt, Reid S. Willis, and A. Kasem Chowdhury*

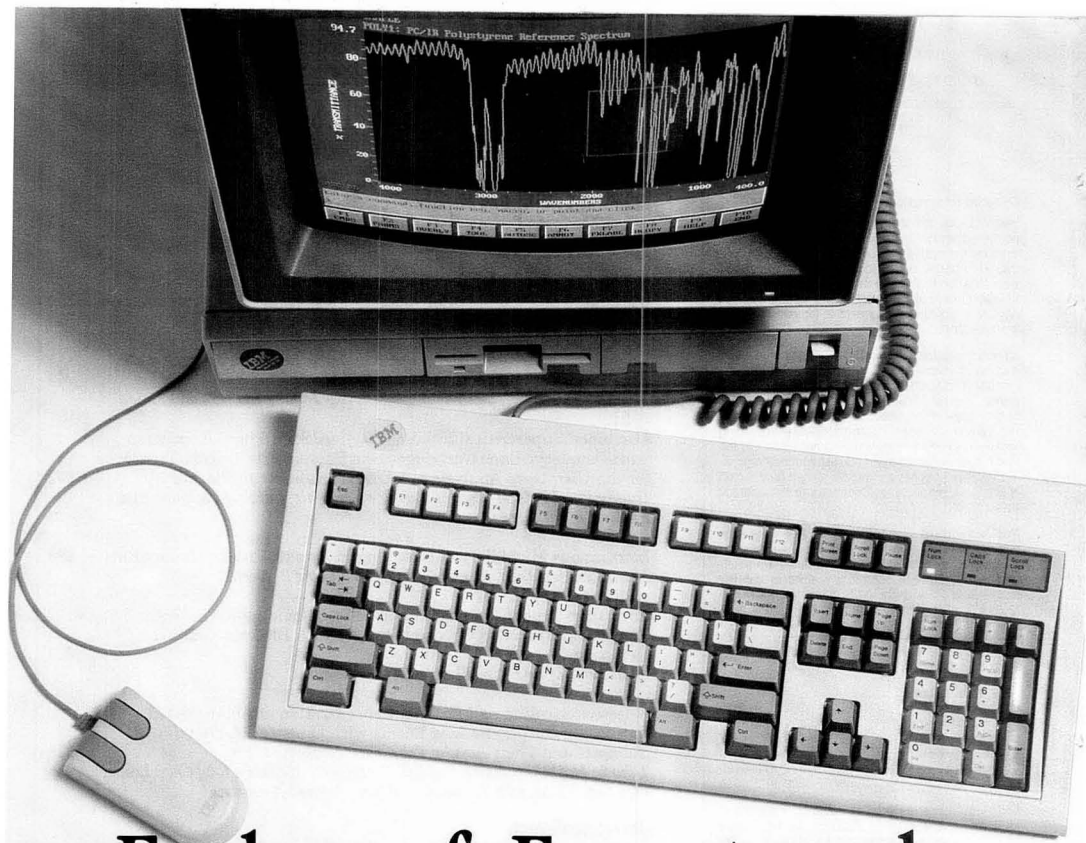
Extraction Technique for the Determination of Oxygen-18 in Water Using Prevacuated Glass Vials **829**
Richard A. Socki, Haraldur R. Karlsson, and Everett K. Gibson, Jr.*

Correction

Enzymatic Flow Injection Analysis in Nonaqueous Media **831**
Lorenzo Braco, José A. Darós, and Miguel de la Guardia

Author Index

832



Fool proof. Expert ready.

You gave our engineers a challenge. You asked for a PC FT-IR system so simple, so easy to use, that you could generate an IR spectrum, manipulate it, save it and plot it—*on your first try!*

Then you wanted to be able to grow with your system—add hyphenated techniques, speed up your analysis processing, and learn advanced programming as you became more experienced with the software system.

Our engineers asked, "You want it nice-and-easy AND you want it powerful and flexible?"

You said, "*Exactly.*"

Experience Nicolet's improved PC FT-IR systems.

Nicolet
INSTRUMENTS OF DISCOVERY



Analytical Division / 5225 Verona Road / Madison, WI 53711 / TEL: 608-271-3333 / FAX: 608-273-5046

CIRCLE 94 ON READER SERVICE CARD

UPCOMING RESEARCH

Comparison of Methods To Assess Surface Acidic Groups on Activated Carbons

Carbon surface properties after oxidation are studied by inverse GC and Boehm titration. A correlation of carbon acidity is found between chromatographic and Boehm titration results.

Teresa J. Badosz, Jacek Jagiello, and James A. Schwarz*, Department of Chemical Engineering and Materials Science, Syracuse University, Syracuse, NY 13244-1190

Development of an Elutropic Series for the Chromatography of Lewis Bases on Zirconium Oxide

Retention data show that the thermodynamics and kinetics of solute Lewis base interaction with the Lewis acid sites present on the zirconia surface are greatly affected by the structure of competing eluent Lewis bases. Eluent Lewis bases with complex structures produce different selectivities than simple Lewis bases, suggesting secondary interactions between these species on the support surface.

John A. Blackwell*, Group Analytical Laboratory, Specialty Adhesives and Chemicals Division, 3M Company, 236-2B-11, 3M Center, St. Paul, MN 55144-1000 and **Peter W. Carr**, Department of Chemistry and Institute for Advanced Studies in Bioprocess Technology, University of Minnesota, 207 Pleasant Street SE, Minneapolis, MN 55455

The Role of Lewis Acid-Base Processes in Ligand-Exchange Chromatography of Benzoic Acid Derivatives on Zirconium Oxide

Retention on zirconium oxide is closely related to a solute's Lewis basicity over a wide range of pH in aqueous media. Secondary interactions caused by chelation or steric hindrance cause significant deviations from this trend.

John A. Blackwell*, Group Analytical Laboratory, Specialty Adhesives and Chemicals Division, 3M Company, 236-2B-11, 3M Center, St. Paul, MN 55144-1000 and **Peter W. Carr**, Department of Chemistry and Institute for Advanced Studies in Bioprocess Technology, University of Minnesota, 207 Pleasant Street SE, Minneapolis, MN 55455

Mechanistic Studies of Electrostatic Potentials on Antigen-Antibody Complexes for Bioanalyses

The mechanistic studies of induced changes in the electrostatic potentials around the antigen-antibody complex attributable to antigen binding are presented for directly sensing the antigen-antibody reaction.

Ping Yu Huang and Cheng S. Lee*, Department of Chemical and Biochemical Engineering, University of Maryland Baltimore County Campus, Baltimore, MD 21228

These articles are scheduled to appear in AC RESEARCH in the near future.

*Corresponding author

Instrumental, Theoretical, and Experimental Aspects of Determining Thermodynamic and Kinetic Parameters from Steady State and Non-Steady-State Cyclic Voltammetry at Microelectrodes in High-Resistance Solvents: Application to the *fac/mer*-[Cr(CO)₃](η^3 -Ph₂PCH₂CH₂P(Ph)CH₂CH₂-PPh₂)]^{+/0} Square Reaction Scheme in Dichloromethane

Kinetic and thermodynamic aspects of complex electrode processes in high-resistance solvents can be determined by newly developed instrumental, theoretical, and experimental approaches to steady-state and transient voltammetry at microelectrodes.

Alan M. Bond*, **Stephen W. Feldberg**, **Howard B. Greenhill**, and **Peter J. Mahon**, Department of Chemical and Analytical Sciences, Deakin University, Geelong, Victoria 3217, Australia and **Ray Colton and Tania Whyte**, Inorganic Chemistry Section, School of Chemistry, University of Melbourne, Parkville, Victoria 3052, Australia

Analysis of Polystyrene/PVME Blends by Coincidence Counting Time-of-Flight Mass Spectrometry

A new method for determining surface heterogeneity down to the submicrometer level is described. Phase-separated and miscible PS/PVME blends are analyzed.

B. Dwain Cox*, **Melvin A. Park**, **R. Gene Kaercher**, and **Emile A. Schweikert**, Center for Chemical Characterization and Analysis, Chemistry Department, Texas A&M University, College Station, TX 77840

Enhancement of the Thermal and Storage Stability of Urease by Covalent Attachment to Phospholipid-Bound Silica

Stabilization of the activity of urease under dry storage conditions, or upon thermal treatment simulating sterilization conditions, can be achieved by the covalent attachment of the enzyme to phospholipids immobilized on silanized silica surfaces.

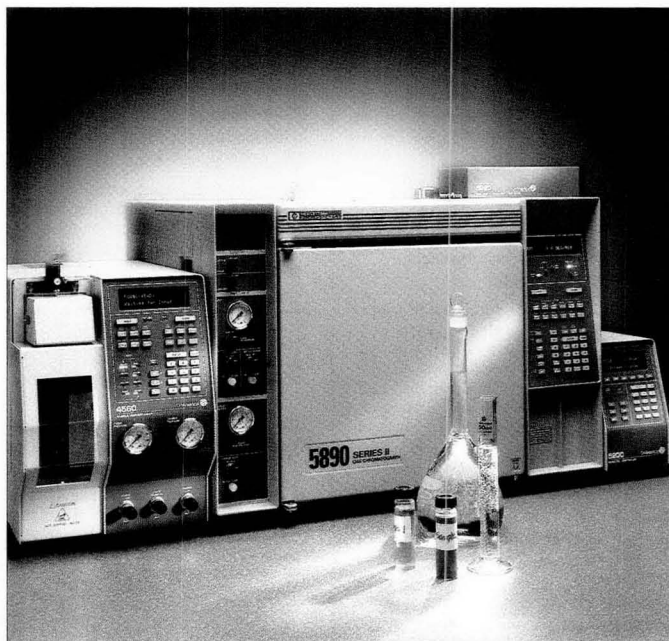
Krishna M. R. Kallury, **William E. Lee***, and **Michael Thompson**, Department of Chemistry, University of Toronto, 80 St. George St., Toronto, Ontario M5S 1A1 Canada and Defence Research Establishment Suffield, P. O. Box 4000, Medicine Hat, Alberta T1A 8K6 Canada

Effect of Direct Control of Electroosmosis on Peptide and Protein Separations in Capillary Electrophoresis

Studies for enhancing the separation resolution and efficiency of peptide and protein mixtures in capillary zone electrophoresis with the direct control of electroosmosis are discussed. The direction and flow rate of electroosmosis are directly manipulated by using an additional electric field applied from outside the capillary.

Chin-Tiao Wu, **Teresa Lopes**, **Bhisma Patel**, and **Cheng S. Lee***, Department of Chemical and Biochemical Engineering, University of Maryland Baltimore County Campus, Baltimore, MD 21228

Unique sample heating option uses advanced technology to measure actual sample temperature, providing greater accuracy and reliability.



New features include Internal Carrier Gas Control option and protective sparge filter. Filter protects internal components from foaming samples and reduces sample rerun.



The Model 4560 keypad is easy to learn and is designed to minimize operator error. 14+ method storage improves lab efficiency with pre-programmed methods, minimizing both keystrokes and errors.

OI Analytical's System VOC features the new generation Model 4560 Purge and Trap Sample Concentrator and Model 5240 PID/ELCD for greater productivity in your lab. New purge-and-trap technology includes built-in Cyclone™ water management that removes 99.8% of water interference, improving peak shape. Rapid trap heating/cooling cuts cycle time and increases sample throughput. PATTI® II software allows for "Super-Sequencing" with GCs and data systems. System VOC is fast, accurate, and easy to use—making maximum use of your lab resources.



Solutions for
Environmental Analysis

P.O. Box 2980 College Station, Texas 77841-2980 409 690-1711 FAX 409 690-0440

- Systems for VOCs, BTX/BTEX, Pesticides
- 5220 ELCD, 4430 PID, 5240 PID/ELCD, 4450 PID/FID, 5250 PID/FID

- 4560 Purge & Trap, PATTI® II Software, Cryo-Focusing Module™, Autosamplers
- 700 TOC Analyzer, Autosamplers

Azide-Induced Reversible Voltammetric Reduction of Gallium(III) from Room-Temperature, Low Ionic Strength Acid Media

Low concentrations of dissolved free azide (≤ 0.58 M) are found to enable the reversible reduction of Ga(III) to the amalgam within a band of pH ranging from ~ 3 to 5 at room temperature and low ionic strength. Peak currents increase linearly with increasing Ga concentrations of 0–0.985 M. Effects of changing the pH and azide are also discussed.

E. D. Moorhead* and **T. S. Robison**, Department of Chemical Engineering, University of Kentucky, Lexington, KY 40506-0046

Determination of pH with Surface-Enhanced Raman Fiber Optic Probes

Experiments that demonstrate the possibility of remotely determining pH with SERRS/SERS fiber optic probes are described. The data are explained in terms of Gouy–Chapman–Stern theory.

Ken I. Mullen, DaoXin Wang, L. Gayle Crane, and Keith T. Carron*, Department of Chemistry, University of Wyoming, Laramie, WY 82071-3838

Universal Sandwich Membrane Cell and Detector for Optical Flow Injection Analysis

An integrated cell for spectrophotometric and chemiluminescent measurements that allows membrane separation and gas diffusion is described.

José Luis Pérez Pavón, Encarnación Rodríguez Gonzalo, Gary D. Christian, and Jaromir Ruzicka*, Department of Chemistry, University of Washington, BG-10, Seattle, WA 98195

Secondary Isotope Effect: The Resolution of Deuterated Glucoses by Anion-Exchange Chromatography

D-Glucose-1-*d* and D-glucose-2-*d* are separated in < 30 min by using the secondary isotope effect. Dissociation constants are predicted for two deuterated glucoses.

Jeffrey S. Rohrer* and **Joseph D. Olechno**, Dionex Corporation, 470 D Lakeside Dr., Sunnyvale, CA 94086

Separation of Poly(styrenesulfonates) by Capillary Electrophoresis with Polymeric Additives

The effect of hydroxyethyl cellulose additives on the resolution enhancement of poly(styrenesulfonate) standards is demonstrated for capillary electrophoresis using wall-coated capillary columns over a wide range of solute molecular weights.

Janet Beebe Poli* and **Mark R. Schure***, Analytical Research and Computer Applications Research, Rohm and Haas Company, 727 Norristown Road, Spring House, PA 19477

Collisionally Induced Dissociation in the Study of A-Ring Hydroxylated Vitamin D Type Compounds

The position of hydroxylation on the A-ring of vitamin D type compounds is determined by collision-induced dissociation of the methyl styryl ion formed in the EI mass spectrum of the compound.

David C. Young and Paul Vouros*, Department of Chemistry and Barnett Institute, Northeastern University, Boston, MA 02115, **Michael F. Holick**, Vitamin D Laboratory, Boston University Medical School, Boston, MA 02118, and **Tetsuo Higuchi**, JEOL U.S.A., Inc., 11 Dearborn Road, Peabody, MA 01960

Multiple Enantioselective Retention Mechanisms on Derivatized Cyclodextrin Gas Chromatographic Chiral Stationary Phases

An evaluation of homologous series retention, enthalpy–entropy compensation, mass overloading, and other data indicates that at least two different chiral recognition mechanisms may be operative with dipentyltrifluoroacetyl-derivatized β - and γ -cyclodextrin GC stationary phases.

Alain Berthod, Weiyong Li, and Daniel W. Armstrong*, University of Missouri—Rolla, Department of Chemistry, Rolla, MO 65401

Monitoring Cholesterol Auto-Oxidation Processes Using Multideuterated Cholesterol

Deuterated cholesterol is used to correct for artifactually produced cholesterol oxidation products in samples rich in cholesterol.

Bruce A. Wasilchuk, P. W. Le Quesne, and Paul Vouros*, Department of Chemistry and Barnett Institute of Chemical Analysis, Northeastern University, Boston, MA 02115

Sample Stacking of Extremely Large Injection Volume in High-Performance Capillary Electrophoresis

The technique is based on the principle that the local electrophoretic velocity of the ions inside the diluted sample buffer is much faster than the bulk electroosmotic velocity of the solution. Improved resolution is achieved for large sample volumes.

Ring-Ling Chien* and **Dean S. Burgi**, Gintz Research Center, Varian Associates, Inc., 3075 Hansen Way, Palo Alto, CA 94304

Ultraviolet Resonance Spectroscopy of 4-Aminopyridine Adsorbed on Zeolite Y

UV resonance Raman spectroscopy with excitation at 266 nm makes it possible to examine selectively the vibrations of protonated 4-aminopyridine formed by reaction with weak acidic groups on zeolite Y.

Michael R. Jakupca and Prabir K. Dutta*, Department of Chemistry, The Ohio State University, 120 West 18th Ave., Columbus, OH 43210

ANALYTICAL CHEMISTRY, VOL. 64, NO. 7, APRIL 1, 1992 • 423 A

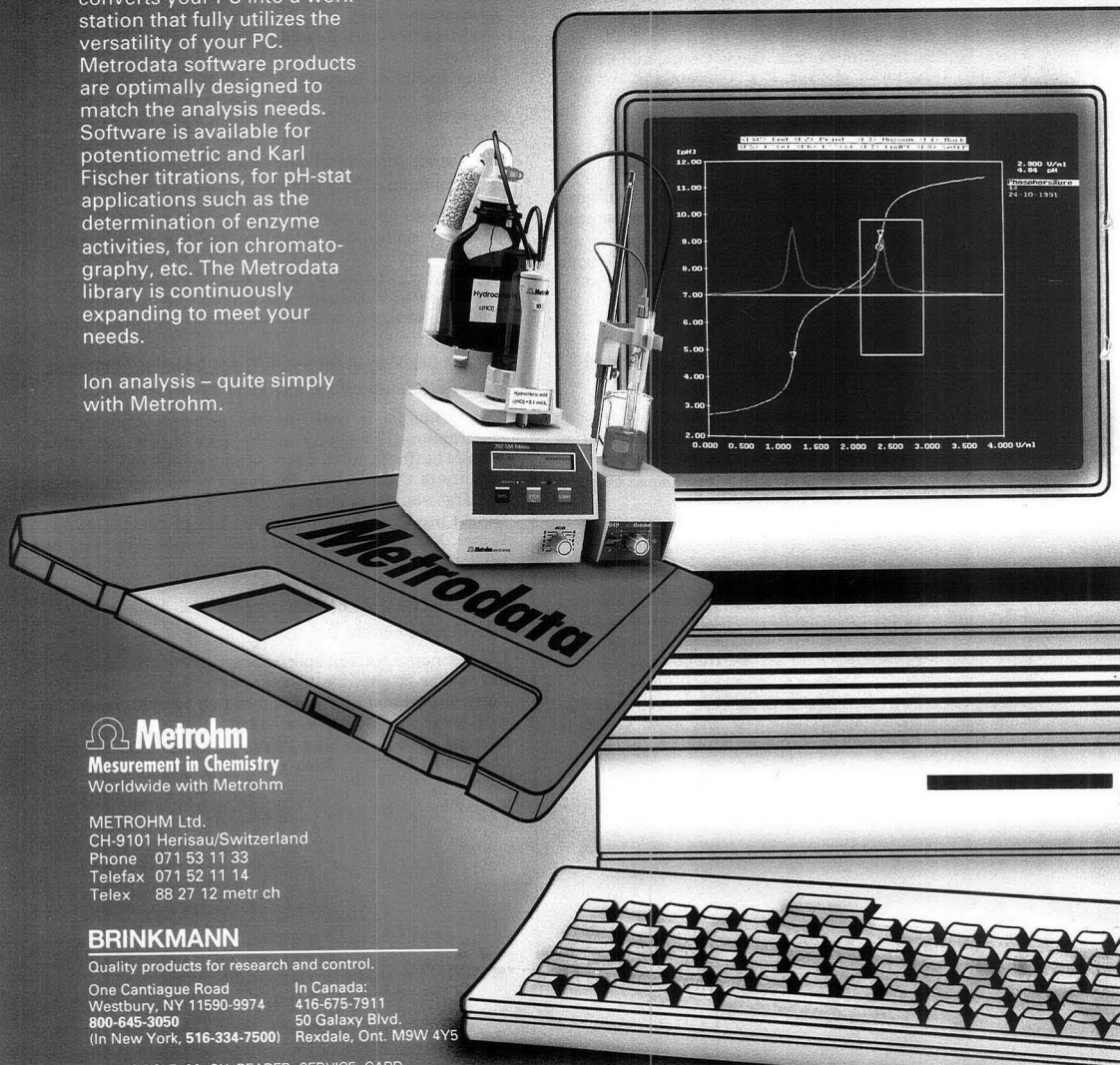
Metrodata software.

The intelligent link between PC and Metrohm

Data storage on state-of-the-art media is important in your laboratory now. Just think of quality assurance programs, both short and long term, GLP or ISO 9000.

The software-products of the Metrodata line allow the efficient management of your data. Metrodata software converts your PC into a work station that fully utilizes the versatility of your PC. Metrodata software products are optimally designed to match the analysis needs. Software is available for potentiometric and Karl Fischer titrations, for pH-stat applications such as the determination of enzyme activities, for ion chromatography, etc. The Metrodata library is continuously expanding to meet your needs.

Ion analysis – quite simply with Metrohm.



Metrohm
Measurement in Chemistry
Worldwide with Metrohm

METROHM Ltd.
CH-9101 Herisau/Switzerland
Phone 071 53 11 33
Telefax 071 52 11 14
Telex 88 27 12 metr ch

BRINKMANN

Quality products for research and control.

One Cantiague Road
Westbury, NY 11590-9974
800-645-3050
(In New York, 516-334-7500)

In Canada:
416-675-7911
50 Galaxy Blvd.
Rexdale, Ont. M9W 4Y5

August in New Hampshire

August 3–7, 1992, at New Hampton School in rural New Hampton, NH, is the time and place for the next Gordon Research Conference on Analytical Chemistry. I would like to invite you to consider participating in this conference, which is to be chaired by Isiah Warner. Program information is found elsewhere in this issue.

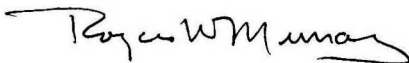
For those of you unfamiliar with the Gordon Conference format for meetings, they are held at sites remote from other distractions and offer the attributes of scenic beauty and a pleasant climate. Morning and evening lecture sessions are graced by a generous opportunity for discussion and questioning. More importantly, the rules forbid subsequent citation of lectures and discussion so that you are apt to hear the latest results and their preliminary interpretations, and thereby encounter more often the cutting edges of chemistry as they emerge. Afternoons are free for walking in the woods or for arguing chemistry with other conferees. Throughout my career I have attended at least one Gordon Conference a year, and I give their format a strong endorsement for the serious scholar. I also have many fond memories of the pleasant environment at New Hampton and the many wonderful analytical chemistry scholars outside my own specialty that I met and came to know there.

The Analytical Chemistry Gordon Conference is especially important to the analytical community because it gathers together leading scholars across a broad face of analytical sciences. The ever-increasing complexity of our subdiscipline (a characteristic shared by all vigorous chemical subdisciplines) has led to our increasingly narrow specialization. Conference planners and chemists in general have reflected this tendency toward specialization in their organization

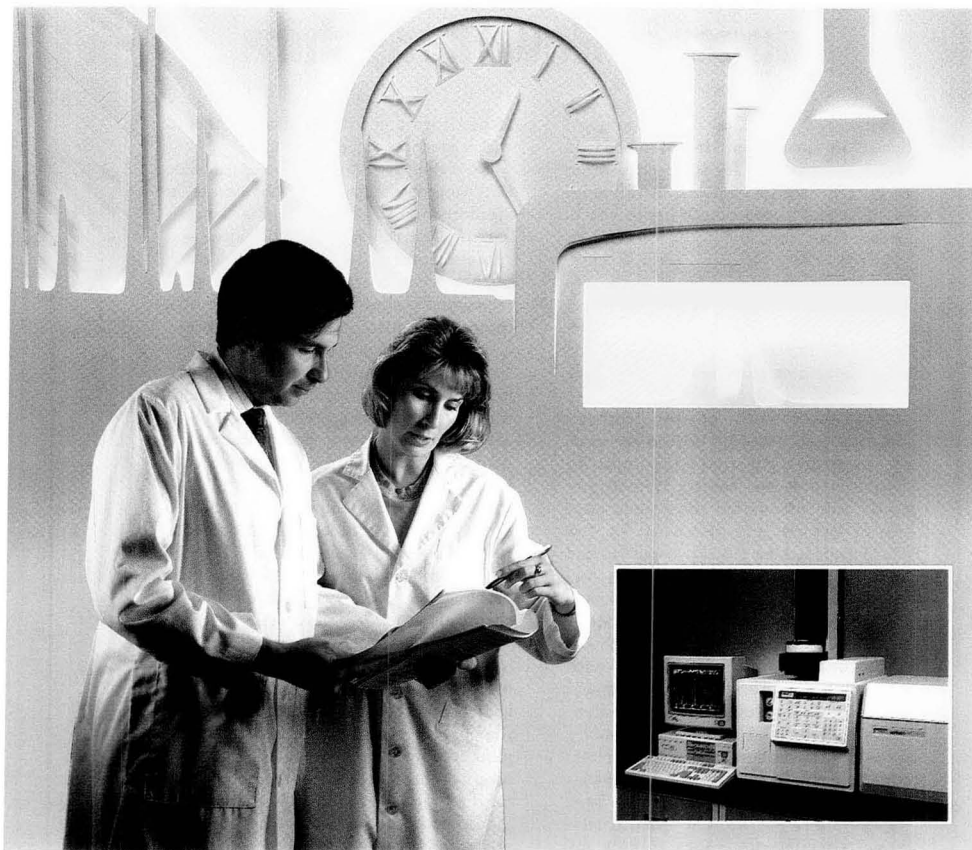
of meetings and in their decisions as to which journals are published.

We chemists at times act like grackles that congregate together and cackle in similar ways. Electrochemists congregate in electrochemistry conferences and rub electrons with their fellow electron pushers; chromatographers and spectroscopists similarly congregate and compare columns and photons. Birds-of-a-feather behavior is of course intellectually useful in advancing knowledge in individual subjects, but it leads to isolation in our thinking about science and about our community. Analytical chemists must think of their discipline in a broader framework. Educators must consider a balanced approach to the education of their students; industrialists must have the intellectual breadth to launch multitechnique approaches to the problems of analysis of diverse bodies of chemicals in diverse matrices.

The JOURNAL shares with the Analytical Chemistry Gordon Conference a commitment to a general approach to analytical chemistry and an aim of presenting the best current science across the discipline. Analytical chemists need to stay aware of the developments in the analytical discipline that are outside their individual specialties. Such awareness is maintained only by a willingness to be exposed to and—in the natural scheme of scientific discussion, to inquire into and challenge for understanding—specialties outside our own niches. It is in this spirit of discouraging overspecialization that I urge everyone to examine the Analytical Chemistry Gordon Conference program for this summer. Isiah Warner has assembled an excellent representation of the breadth of analytical chemistry.



Ask Tough Questions.



Saturn II GC/MS gives the right answers.

Don't compromise on results. You shouldn't have to rely merely on selected ion monitoring in order to see the whole "picture".

Demand the best. The Saturn® II GC/MS, with new generation ion trap technology, provides library-searchable, full scan, classical spectra of compounds at ultra trace levels, even parts per trillion. That's why Saturn easily meets, and exceeds, the high demands mandated for air monitoring and drinking water analysis.

Saturn provides this superb sensitivity, even for labile or toxic compounds in dirty samples like soil and sludge. Therefore, smaller sample sizes can be used for solid phase and solvent extractions, making sample preparation less costly and less time consuming.

Let us show you how Saturn II provides the best overall GC/MS performance. Call 1-800-944-1826. In Canada, call 1-800-387-2216.

GC • GC/MS • HPLC • AAS • ICP-AES • UV-Vis-NIR • NMR • Sample Preparation

varian 

CIRCLE 142 ON READER SERVICE CARD

New Head of Special Publications



Anthony Durniak has been named Head of the ACS Special Publications Department. Durniak comes to the ACS with considerable publishing experience, primarily from McGraw-Hill, Inc., where he held a variety of editorial and management positions. He holds a B.E.E. degree in electronic engineering from the City College of New York and an

M.S. degree in journalism from Columbia University. In his role as Head, Special Publications, Durniak is responsible for managing the staff functions of ANALYTICAL CHEMISTRY, *Environmental Science & Technology*, CHEMTECH, *Today's Chemist at Work*, and the ACS Buyers' Guides.

1993 Waters Symposium Proposals

Proposals are solicited for the 1993 James L. Waters Annual Symposium, which will recognize the collaborative work of groups involved in the invention, development, and implementation of analytical instrumentation of established exceptional importance. Previous symposia have covered GC, atomic absorption spectrometry, and IR spectrometry. Proposals should include recommendations for the analytical instrumentation to be recognized as well as names of inventors, entrepreneurs producing and marketing commercial instruments, and additional researchers at the forefront of the technology. Proposals should also recommend speakers who can authoritatively address the invention, production, and use of the instrumentation. Proposals should be submitted by April 30 to Singh Manocha, PPG Industries, Glass R&D, P.O. Box 11472, Pittsburgh, PA 15238-0472.

Washing an Aquifer

All manner of laundry detergents promise to get your clothes their whitest and brightest, but can a detergent actually save your drinking water supply?

John Fountain, associate professor of geology at the State University of New York at Buffalo, has developed a process that uses surfactants, the active ingredient in laundry detergents, to literally wash toxic chemicals out of contaminated groundwater aquifers. The technique, called surfactant flooding, involves repeatedly pumping the contaminated water to the surface, adding the surfactants, and pumping the water back into the ground, allowing the treatment solution to pass through the contaminated area several times.

In a recent field test near Ontario, Canada, the method was successfully used to eliminate the separate, insoluble phase of dense nonaqueous-phase liquids (DNAPLs) that form in aquifers where significant volumes of organic liquids have been spilled. Fountain and

his colleagues walled off part of an aquifer that had already sustained chemical contamination. Injection and extraction wells were installed on opposite sides of the cell, and the aquifer was flooded with surfactants. After six months of treatment, the DNAPLs were removed. Fountain believes that the aquifer can now be treated with conventional procedures and restored to drinking water quality.

An actual toxic waste site in Texas is undergoing surfactant flooding; results are expected this summer.

For Your Information

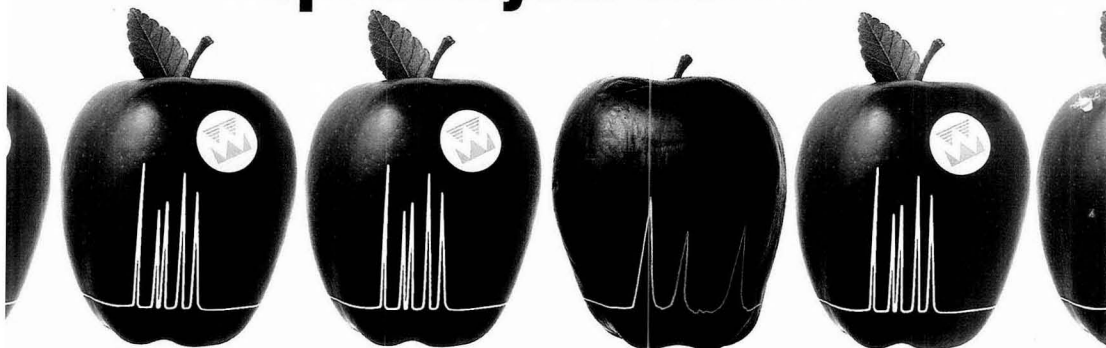
Daniel W. Armstrong, Curators' Professor of Chemistry at the University of Missouri-Rolla, is the winner of the 1991 Isco Award in chemical separations. Armstrong is being honored for his research in developing chiral separation methods.

A new **brochure on quality** is available from the National Institute of Standards and Technology. *Questions and Answers on Quality: The ISO 9000 Standard Series, Quality System Registration, and Related Issues* (NISTIR 4721) provides answers to commonly asked questions about quality and quality systems. Included are brief descriptions of the ISO 9000 standards and the conformity assessment scheme of the European Community; a comparison of the ISO 9000 standards with the Malcolm Baldrige National Quality Award; contacts for industry assistance in getting information on current domestic and foreign standards, regulations, and certification activities; and a list of standards-related and certification directories. To obtain a copy, send a self-addressed mailing label to Standard Code and Information Program, A629 Administration Bldg., NIST, Gaithersburg, MD 20899 (301-975-4031).

The American Institute of Chemical Engineers has just published the ninth edition of its **Directory of Chemical Engineering Consultants**. The volume lists consultants alphabetically according to whether they are full time or part time consultants and what their specialties are. Cost is \$15 for members and \$25 for nonmembers. Contact the Publications Sales Dept., 345 E. 47th St., New York, NY 10017 (212-705-7657).

The U.S. Environmental Protection Agency (EPA) has released **Access EPA**, a new 500-page directory that lists the agency's resources, services, and products. The directory's seven sections contain contacts and descriptions of clearinghouses and hotlines, public information tools, rule-making procedures, databases, library services, and records management programs. The directory is color-coded and has a comprehensive index. A form for comments is included for those who wish to make new entries or update information. To order the directory (stock no. 055-000-00378-5), send \$18 to Mail Order, Superintendent of Documents, P.O. Box 371954, Pittsburgh, PA 15250-7954. To order by phone, call 202-783-3238.

Why let one bad apple spoil all your work?



Get reproducible results with Whatman.

**Call 1-800-242-7530
for a free sample and more information.**

Reproducibility problems are more than just frustrating: They cast doubt on the validity of your analysis. Why not get the reproducible results you need from Whatman?

Whatman has the most complete line of sample prep products in the industry—over 500 in all—and every one is unconditionally guaranteed to work within your exacting tolerances. In fact, reproducible results are the #1 reason so many professionals have made the switch to Whatman.

Our technical staff is ready to help you improve your method's reproducibility—whether your problems are procedural or involve the shortcomings of another manufacturer's product.

So the next time you're less than satisfied with the results you're getting, call Whatman. We'll spoil you, not your work.

CIRCLE 148 ON READER SERVICE CARD



Whatman®

Whatman Laboratory Division

Whatman Inc., 9 Bridewell Place, Clifton, New Jersey 07014

Telephone: 201-773-5800 Telex: 133426 Fax: 201-472-6949

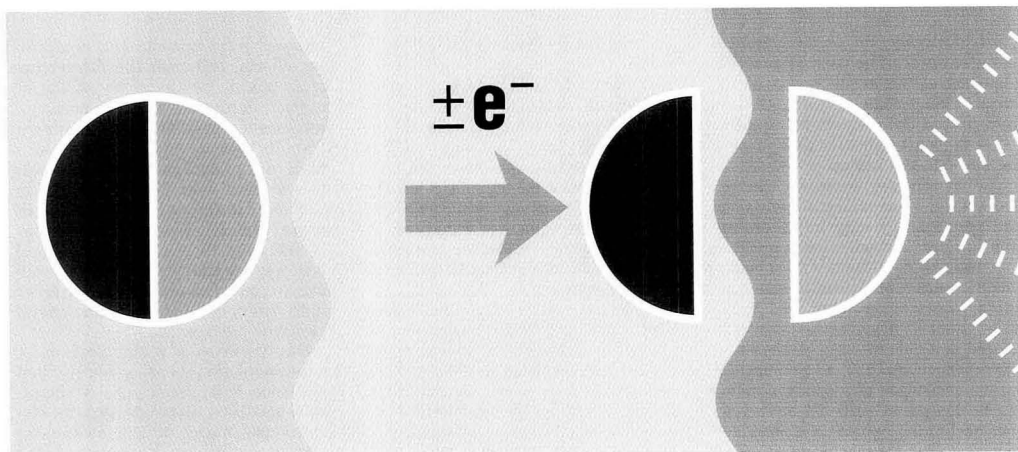
Whatman (word and device) and Whatman (word only) are trademarks of Whatman Paper Ltd. 746-11-203

The reproducible results you need. Guaranteed.



Whatman
SPE ODS-1





LIGHT IN AN ELECTROCHEMICAL TUNNEL?

Solving Analytical Problems in Electrochemistry via Spectroscopy

Krishnan Rajeshwar

Department of Chemistry
Box 19065
The University of Texas at Arlington
Arlington, TX 76019-0065

Reynaldo O. Lezna and

Norma R. de Tacconi

INIFTA, Universidad Nacional de La Plata
Suc. 4, C. C. 16
La Plata (1900), Argentina

Electrochemical phenomena have an impact on a wide spectrum of technologies ranging from the traditional corrosion, electrolytic, chemical, and metal alloy industries to exciting new areas involving chemical and biological sensors, semiconductors, and superconductor materials. Historically, electrochemists' reliance on the measurement of current, potential, or charge has resulted in an evolution of the discipline that would appear to be somewhat less molecularly oriented than other areas of chemistry. However, this trend is rapidly changing. Indeed, we are at an exciting juncture wherein electrochemical science and technology is poised for breakthroughs in structural details associated with the electrode-solution interphase, microscopic de-

lineation of the participating interphase, and the dynamics of electrode processes.

Recent advances have been facilitated by the advent of new characterization tools amenable to assimilation within an electrochemical context (e.g., ultrahigh vacuum techniques) and by improved sensitivity in traditional spectroscopic techniques (e.g., IR and Raman spectroscopies). Paralleling these have been rapid strides in the "indirect" electrochemical approaches (based on the measurement of current, potential,

matter across the electrode-solution boundary, or interphase (Figure 1). Aside from the flow of an electronic current, this process may result in the deposition of an insoluble layer atop the underlying electrode (e.g., as in electroplating procedures) or in the transfer of ionic and/or neutral species (e.g., solvent) across the boundary. In addition, processes within the boundary layer itself (e.g., adsorption) are important from both fundamental and practical perspectives. Several analytical questions related to composition and structure are of interest in the system depicted in Figure 1, and the use of spectroscopy enhances interpretative capability (1).

The analytical strategies may be classified within a global perturbation-response framework as in Figure 2 (1). An optical perturbation combined with an electrochemical measurement (e.g., photocurrent) thus furnishes a rich array of information on the solid (insoluble) layer. This photoelectrochemical strategy has proven useful for the analyses of inorganic semiconductor, conducting polymer, and anodic oxide and other passive film-based electrochemical systems, as illustrated by the following examples.

REPORT

or charge) that make it possible to examine electrode processes on shorter time scales and with finer spatial resolution than ever before. In this REPORT, we will focus on the role of optical spectroscopies in the study of electrode reaction participants and of boundary layers exhibiting high chemical specificities.

Mating electrochemistry with spectroscopy

An electrochemical process generally involves the transfer of charge and/or

Alternatively, an electrochemical perturbation can be used to generate a species, either in solution or at the support electrode surface, that is then probed optically. Some spectroscopic tools available for this purpose are listed in the box on p. 431 A.

The synergism between electrochemistry, photoelectrochemistry, and spectroscopy may be taken one step further. Indeed, a laser pulse in spectroscopy corresponds to a coulometric injection of charge in semiconductor electrochemistry (2). Similarly, chopped illumination is closely related to a current step method or a galvanostatic method, and sinusoidal optical excitation of a semiconductor can be compared with the ac impedance technique, which is a standard tool for the electrochemist. The choice of optical probe and other design considerations related to the electrochemistry-spectroscopy approach depend critically on which of the three components in the overall system (the solid layer, the interphase, or the bulk solution) is being probed.

An analytical prerequisite for the electrochemistry-spectroscopy approach obviously is that one or more system components of interest (the solid layer, the electrogenerated species in solution, or the adsorbed species within the interphase) be intrinsically photoresponsive. Alternatively, an optically silent species (e.g., H^+) could be derivatized in situ with a dye probe and then tagged, as described below.

Analysis of the solid layer

There are some inherent experimental difficulties in the use of spectroscopic tools for probing the solid (electrode) phase. For example, the use of a transmission-mode UV-vis absorption probe may be precluded by a thick, optically dense sample. Recourse to alternative modes of detection (such as reflectance or opto-

thermal methods) obviates this difficulty.

Particularly informative are measurements obtained *in situ* by reflecting a polarized light beam off the electrode surface. This approach has been successfully applied in the UV-vis and IR spectral regions (3, 4). The very small signals containing the relevant information are enhanced by modulating the electrode potential and thereby the intensity reflected by the electrode.

At a later stage, the time-dependent optical profiles can either be obtained by digital signal averaging or, if the time variation is not required, demodulated by a lock-in amplifier. In the IR region, the modulation can also be carried out by a Michelson interferometer; the spectra are calculated through fast Fourier transform (FFT) of the corresponding interferograms. The information in the form of a differential, (dR/R) , or integral, $\Delta R/R$, is displayed as a function of either photon energy or electrode potential. Such information has been useful in identifying the participating species in the electrochemical system and in determining the orientation and type of interaction between the adsorbed molecules and the electrode surface.

Time-resolved measurements with millisecond resolution are also feasible by using diode array detection in the UV-vis region and step-scan FFT in the IR region. Ellipsometry, which yields data on composition and thicknesses of surface films, is also a popular technique. Reflectance techniques in the UV-vis and IR spectral regions are continually being developed, fueled by advances in both instrumentation and methodologies.

Luminescence probing of the solid layer has high sensitivity but is often fraught with difficulties from

quenching phenomena and inner-filter effects, although the former are often useful for the study of charge carrier dynamics. Furthermore, luminescence probing (and, similarly, Raman spectroscopy) results in a high (noisy) background attributable to scattered light from the electrode surface. However, claims have been made that FT-Raman spectroscopy in the near-IR ($\sim 1 \mu\text{m}$ wavelength) is less prone than luminescence probing to interference from scattered light from, for example, the metal electrode surface (5).

Incorporation of a chromophore or a luminophore into an optically silent electrode framework (i.e., a chemically modified electrode system) circumvents many of the aforementioned problems because of the diluteness of the optically responsive entity. On the other hand, photoelectrochemical approaches for probing the solid layer do not suffer from many of the problems inherent in optical detection schemes, because a photocurrent or photovoltage signal rather than an optical signal is measured.

Probing the interphase

The electrode-solution boundary that nominally spans 10–1000 Å is the "scene of action" of all electrochemical phenomena. This Helmholtz region can assume relatively simple geometry for planar (smooth) electrode surfaces as well as more complicated contours and diffuse boundaries for porous (spongelike) electrodes. The structural aspects of this boundary region traditionally have fallen within the realm of physical electrochemistry, although many structural and compositional issues are amenable to attack by new electroanalytical methodologies (6).

It is fair to say that in choosing a

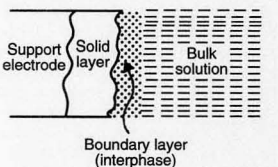


Figure 1. Components of an electrochemical system.

Only the working electrode is considered.

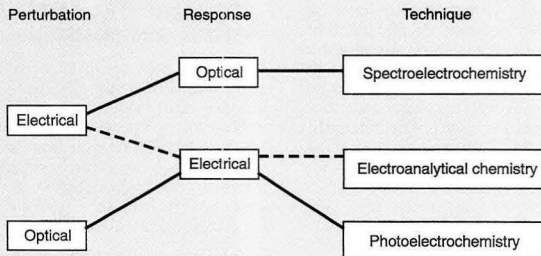


Figure 2. Analytical strategies for combining spectroscopy with an electrochemical experiment.

spectroscopic technique, the attributes related to spatial resolution and sensitivity are of foremost importance. Perhaps it is not surprising that vibrational spectroscopies (IR and Raman) and surface analysis methods (photoelectron spectroscopies) have been popular techniques for the study of metal-solution interphasial phenomena.

Several factors have contributed to the rather spectacular advances in this area. First, the advent of potential-modulated IR reflection techniques (e.g., EMIRS) and FT-IR instrumentation has opened the door to fine detail characterization of adsorbed species (3, 4). Second, the discovery of the surface-enhanced Raman spectroscopy (SERS) effect (7) and resonance enhancement modes (8) has salvaged an otherwise hopeless situation with the intrinsically weak Raman scattering phenomenon. Finally, techniques and instrumentation to effectively and faithfully transfer an electrochemical interphase into a UHV chamber for subsequent examination by surface analysis techniques (X-ray photoelectron spectroscopy, or XPS, Auger electron spectroscopy, and electron diffraction) (9) have been significant factors. It is a safe bet that these approaches, along with X-ray spectroscopic methods, will continue to play pivotal roles in further advances in this area.

Analysis of the bulk solution

From an experimental perspective, the solution component of the overall system is perhaps the easiest to probe optically. Indeed, most "bread-and-butter" spectroscopic analyses of interest to chemists are confined to

the solution phase. When the electrochemical perturbation is used to alter the solution composition, exhaustive electrolysis is facilitated by the use of a thin-layer electrochemical cell (10). A transparent support electrode material (e.g., Au minigrid, indium tin oxide glass) is also necessary for transmission spectroscopic techniques.

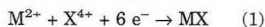
Another spectroelectrochemical approach, developed by Rajeshwar and co-workers (11, 12), uses electrochemistry to trigger the release of a species of interest from the solid layer into the adjacent solution. These species can be either chosen for spectroscopic properties that make them amenable to tagging or derivatized in situ with a dye or a luminophore (11-13) to generate optically responsive probes. By moving the analysis zone from the solid layer to the bulk solution, we obviate many of the analytical difficulties with the solid layer. Use of a thin-layer cell in this case enhances the analytical sensitivity of the method by shrinking the solution volume.

Spectroelectrochemical methodology has involved most of the common spectroscopic tools available to the chemist, including some rather tricky combinations involving NMR (14) and MS (15).

Applications of photoelectrochemistry and spectroelectrochemistry

The combination of electrochemistry and optical spectroscopy can provide particularly valuable insights. We will highlight compositional issues in the *in situ* analysis of electrochemical systems.

Inorganic semiconductor thin films. Electrosynthesis offers a facile means for depositing micrometer-thick layers of chalcogenide thin films atop suitable "substrate" electrodes (e.g., Ti, glassy carbon) for a variety of optoelectronic applications (16). These thin films are electrogenerated via a cathodic process



where X represents a chalcogen such as Se or Te. Thus CdTe thin films may be prepared in this manner via the co-reduction of Cd^{2+} and $H_2TeO_3^2$ in an aqueous electrolyte.

How can we characterize these thin films *in situ* while gaining useful insights into the electrosynthesis process itself (e.g., potential regimes for semiconductor formation and dissolution)? Voltammetric scanning is a useful approach, but when done in the dark it often has little or no in-

formation content. On the other hand, superimposition of chopped illumination on the excitation potential ramp yields a modulation of the current flow when a photoresponsive layer is present (Figure 3).

This modulation could arise from either a bulk photoconductive effect (a change in the electrode resistance on illumination) or a surface photoelectrochemical (or photovoltaic) effect resulting from minority carriers generated by light (holes for n-type semiconductors and electrons for p-type materials). In the latter, the direction of the modulation yields valuable information about the type of semiconductor thin film electrogenerated.

As shown in Figure 3, CdSe thin films as formed are n-type, whereas CdTe films are p-type. These observations can be rationalized on a chemical basis (17). Interestingly enough, it is possible to electrochemically generate, *in situ*, mixed n- and p-type materials within the same layer. We demonstrated this capability in the $Cd_{1-x}Zn_xSe$ system electrosynthesized from an aqueous medium containing Cd^{2+} , Zn^{2+} , and Se^{4-} (18). Such band-gap engineered materials (the end members, CdSe and ZnSe, have optical band gaps of

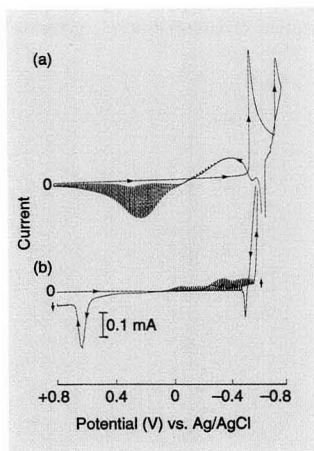


Figure 3. Cyclic photovoltammetry of inorganic semiconductor thin films on a glassy carbon electrode in 0.5 M H_2SO_4 .

(a) CdSe (4×10^{-3} M H_2SeO_3 and 1×10^{-2} M $CdSO_4$). (b) CdTe (1×10^{-3} M H_2TeO_3 and 2×10^{-2} M $CdSO_4$). Scan rate is 0.02 V/s with chopped white light (100 mW/cm²). The photocurrent modulations are predominantly anodic for CdSe and cathodic for CdTe. (Adapted with permission from Reference 17.)

Spectroscopic tools useful in electrochemical situations

UV-vis spectroscopy
Transmission, reflection, and diffraction techniques
Photoacoustic, photothermal, and probe beams
Deflection modes
Ellipsometry
IR spectroscopy
Raman spectroscopy
Luminescence spectroscopy
NMR spectrometry
MS
Photoelectron spectroscopies (such as XPS)
X-ray absorption, fluorescence, and diffraction techniques

1.7 and 2.6 eV, respectively) are relevant to a variety of optoelectronic applications such as solar cells and electroluminescent displays.

In the type of experiments exemplified by Figure 3, one must ensure that the observed photoeffects are truly electronic in origin and not derived from spurious secondary effects such as enhanced mass transport from heating of the electrode and the solution. In fact, much of the published photocurrent data on conducting polymer thin films appears to suffer from such artifacts.

Coupling of light with an electrochemical procedure is also useful for the compositional analysis of advanced semiconductor materials such as (Al,Ga)As/GaAs heterostructures grown by molecular beam epitaxy (MBE). For example, we recently demonstrated (19) how the layer-by-layer geometry prevalent in MBE-grown structures is ideally suited to photoelectrochemical depth profiling. Each layer is first characterized in terms of its photoaction spectrum (which, in turn, yields compositional information) and then precisely removed by photoelectrochemical etching, exposing a fresh epilayer.

Anodic oxide and chalcogenide systems. Many anodic electrochemical processes result in the deposition of insoluble layers on the native metal surface. In fact, the passivation of metals toward corrosion

results from the formation of oxide films that are semiconductors or insulators (20). Photoelectrochemical and other analytical techniques such as XPS or Raman and IR spectroscopies are important tools in mechanistic corrosion studies because they can provide a combination of electronic, structural, and chemical information on a corroding surface.

Some general aspects in the optical-electrochemical analyses of anodic films are worthy of mention. First, the layers are often very thin (a few Angstroms) so that only a fraction of the excitation light is usually absorbed. Reflected signals from the underlying metal layer must also be taken into account. Second, because the compositional makeup of the passive films generally is very sensitive to the environment, a passive film on Fe often changes its identity when removed from its formation environment (21). In fact, many of the controversies surrounding the Fe system could well result from ex situ characterization techniques (22). Raman spectroscopy especially continues to provide a wealth of in situ information on passive films on Fe, Ni, Cu, Ag, and Zn surfaces. The organic inhibitor agents often used in corrosion systems (e.g., benzimidazole, benzotriazole) also offer intriguing avenues for in situ optical "tags" in the electrochemical cell.

The passivation of a metal in aqueous chalcogenide media has many parallels with the oxide system. The anodic behavior in these media is also dependent on the chemistry of the electrode material itself. For example, noble metals form a sulfur multilayer at potentials negative of the oxide formation regime (23). On the other hand, more reactive metals such as Cu, Ag, and Cd develop multilayer sulfide films (Cu_2S , Ag_2S , and CdS) with semiconductor properties (24, 25).

The sulfur multilayer formation at a Au electrode is preceded by the development of a Au_2S monolayer in two stages (A_1 and A_2), as seen in the UV-vis reflectance spectrum (Figure 4). This monolayer catalyzes the H_2 evolution reaction, which renders the electrochemical detection of monolayer formation susceptible to interference from the proton reduction currents. The two stages have been proposed to correspond to adsorption of SH^- and Au_2S monolayer formation, the latter commencing after a critical amount of SH^- accumulates on the surface (23). Similar effects with other sulfur-containing compounds and the optical detection of polysulfide intermediates during growth of the sulfur multilayer are noteworthy (23, 26).

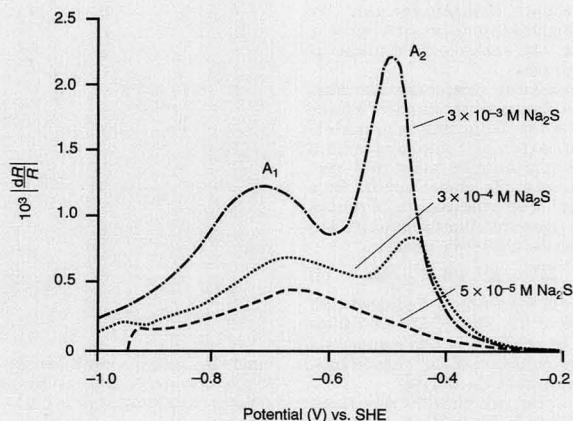


Figure 4. Differential reflectivity of a sulfide-modified Au electrode as a function of potential in pH 7 borate buffer with variable Na_2S concentrations.

Source energy is 2.5 eV, angle of incidence of the polarized light is 60° , and potential modulation frequency is 11 Hz. (Adapted with permission from Reference 23.)

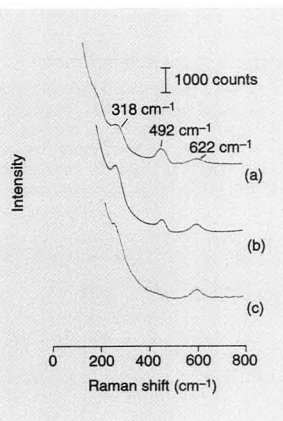


Figure 5. In situ Raman detection of hydrated cadmium oxide intermediate during the anodic electrosynthesis of CdS thin films.

Raman spectra shown for a Cd anode held at +0.35 V (vs. SCE) in 1 M NaOH/0.1 M Na_2S for (a) 2 min, (b) 20 min, and (c) 180 min. The 318 cm^{-1} and 622 cm^{-1} features arise from CdS, and the 492 cm^{-1} band is attributable to the oxide intermediate. An Ar ion laser with a 488-nm line was used. (Adapted with permission from Reference 25.)



re•li•a•bil•i•ty \ ri·lī·ə·bil·ət·ē \ *n*

1: the quality or state of being reliable;
2: the extent to which an experiment, test, or
measuring procedure yields the same results
on repeated trials; 3: **METTLER**

You can count on most balances to weigh with the specified accuracy throughout their full range...but one million times in a row within specs? Now, that's reliability. And that's a METTLER PM Balance quality control standard. METTLER balances are available only from Fisher Scientific or VWR Scientific. All products are backed by METTLER Service Plus®. For information, call 1-800-METTLER.

The last word in reliability is

METTLER

CIRCLE 87 ON READER SERVICE CARD

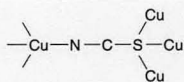
Mettler Instrument Corporation, P.O. Box 71, Hightstown, NJ 08520, 1-800-METTLER, (NJ 609-448-3000) FAX 609-490-0917

Oxide formation and chalcogenization of the electrode surface may be intertwined in the same system, depending on experimental conditions (e.g., pH, chalcogen concentration). Figure 5 illustrates Raman spectroelectrochemistry data on the Cd-S system (25). The temporal profile of the 492 cm^{-1} feature and its sensitivity to the sulfide concentration, along with suitable calibration standards, identify CdO/CdOH as a key intermediate in the formation of CdS, which in turn yields the Raman signals at 318 cm^{-1} and 622 cm^{-1} .

A final related example concerns very recent Raman spectroelectrochemistry experiments in our laboratories on the Cu/SCN system (27). Voltammetry reveals a region of double-layer charging at potentials below -0.45 V (vs. Ag/AgCl) and an "active" regime at higher potentials. The SCN probe has a $\nu(\text{CN})$ band in the 2050–2200 cm^{-1} region as well

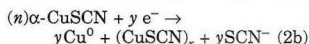
as the normal $\nu(\text{CS})$ and $\delta(\text{NCS})$ vibrational modes in the 420–480 cm^{-1} and 710–800 cm^{-1} regions, respectively.

Figure 6 shows the evolution of the Raman bands in the 2000–2250 cm^{-1} region in the Cu/SCN system. Aside from the 2067 cm^{-1} band attributable to the free SCN^- ion, there are two bands for film formation at the Cu surface: a 2172 cm^{-1} band for SCN groups in a bridged configuration



and a 2120 cm^{-1} feature that is prominent at open circuit (-0.41 V) or slightly more negative potentials (Figure 6, inset). The 2172 cm^{-1} band conclusively identifies the thin film

formed at the Cu surface as $\alpha\text{-CuSCN}$. On the other hand, the 2120 cm^{-1} feature peaks during the electroreduction of the $\alpha\text{-CuSCN}$ film and decreases to almost zero in the double-layer potential region. This trend makes it possible for us to assign this band to the formation of aggregates $(\text{CuSCN})_x$



where $x + y = n$. Thus electroreduction and bond-breaking in $\alpha\text{-CuSCN}$ facilitate aggregation via reaction 2b. Support for this model accrues from a previously reported 2111 cm^{-1} IR feature for CuSCN aggregate formation on alumina (28).

Dye-modified electrodes. Photoresponsive dye molecules that are also electrochemically active serve as useful probes of the electrode-solution interphase. Electrochromic devices, photogalvanic cells, and spectral sensitization of wide band-gap semiconductors provide practical incentives for studying metal-dye solution interphases.

A methylene blue layer may be attached to a gold surface using a sulfur transition layer (29). Voltammetry of this system, in the absence of the dye in bulk solution, displays a region of double-layer charging and a redox couple

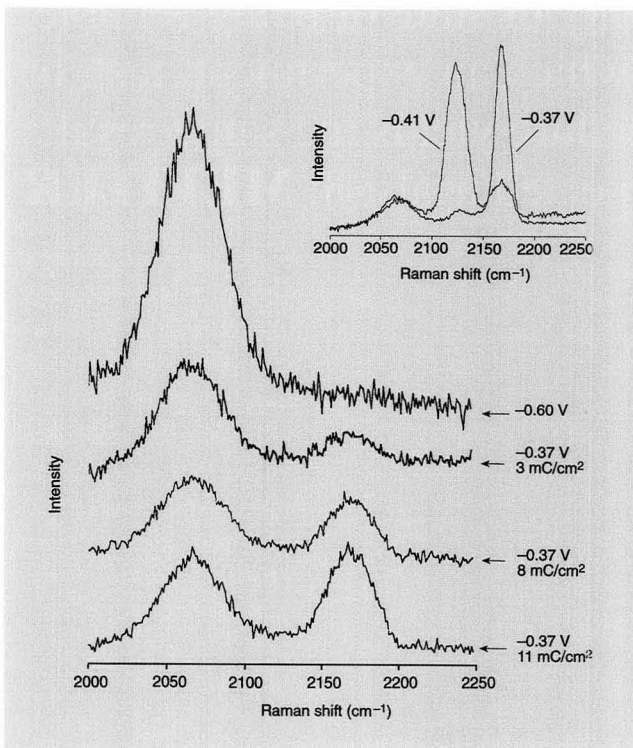
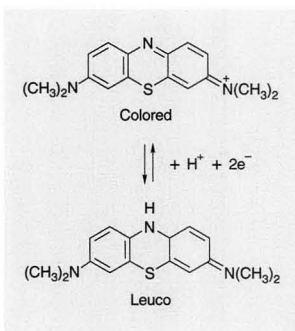


Figure 6. In situ Raman spectra of the anodic Cu/SCN system.

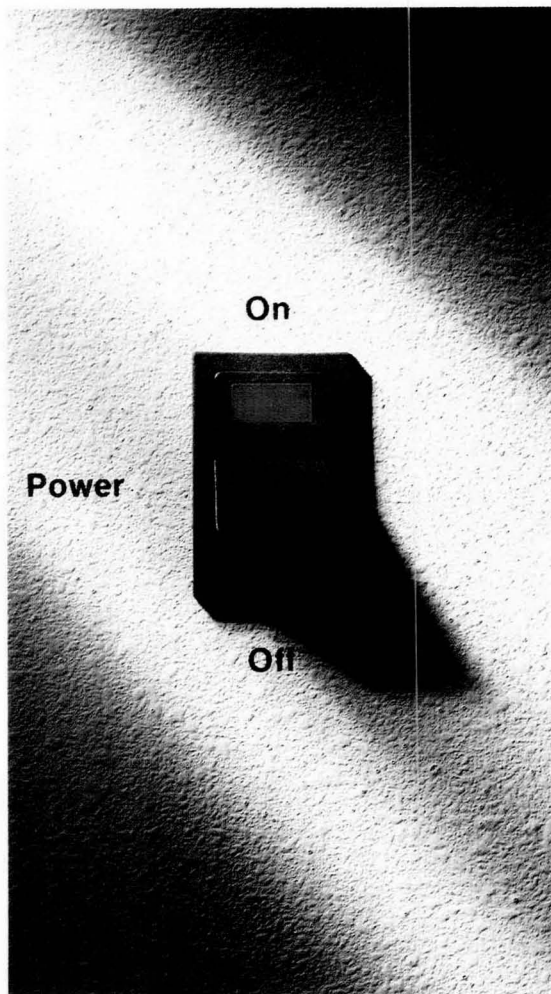
Spectra are shown at -0.60 V (vs. Ag/AgCl reference) in the double-layer region and at -0.37 V where $\alpha\text{-CuSCN}$ is gradually formed. The inset contains a comparison of the Raman spectra for a film formed at -0.37 V and one obtained at open circuit (-0.41 V).



Integration of the voltammetric charge in the redox waves allows the adsorbed dye to be determined. However, further information at the molecular level is not accessible without recourse to in situ spectroscopic measurements.

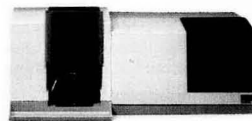
Figure 7 shows the normalized change of reflectance ($-\Delta R/R$) in response to a modulation of potential in the region of double-layer charging.

Our Affordable New AA Requires Knowledge Of A Fundamental Scientific Principle.



AA

Anyone who knows the difference between "on" and "off," between "automated" and "manual," between "affordable" and "expensive," will appreciate Perkin-Elmer's new Model 3300 AA Spectrometer—the state of the art in low-cost, fully automated AA.



The Model 3300: cost effective, automated AA.

Simple to learn and easy to use, the Model

3300 is powered by the best software available—the same software that runs all Perkin-Elmer AA systems.

And it's compatible with all of Perkin-Elmer's AA accessories. Like our unique Stabilized Temperature Platform Furnace for simpler analyses with fewer interferences. And our flow injection system for time-saving automated sample pretreatment.

Compare the Model 3300 to any other fully automated AA. Compare quality. Compare features. Compare price. The difference is easy to see.

For more information, contact your local Perkin-Elmer office. For product literature in the U.S., call **1-800-762-4000**.

PERKIN ELMER

The Perkin-Elmer Corporation, Norwalk, CT 06859-0012 U.S.A.

Circle 110 for Information Only. Circle 111 for Sales Call.

ing. Two bands, observed at 1.79 eV and 2.05 eV, have been assigned to adsorbed methylene blue monomers and dimers, respectively (Figure 7a). These bands, which represent the differential optical response attributable to the component bands at the two modulation potential limits, stem from the electrochromic effect produced by the high double-layer electric field (10^7 V/cm) on the methylene blue transition moment (i.e., a change of its extinction coefficient).

Analysis of the polarization dependence of these bands indicates that the dye is oriented on the surface with its molecular axis at an intermediate angle ($\sim 25^\circ$ – 40°) with respect to the surface. This conclusion is in agreement with other studies of sulfur-modified Pt electrodes using second harmonic generation (30).

For dye coverages of less than a monolayer, potential modulation in the region of double-layer charging gives rise, interestingly enough, to monomer and dimer bipolar bands. These and other data show that the monomer–dimer interconversion is

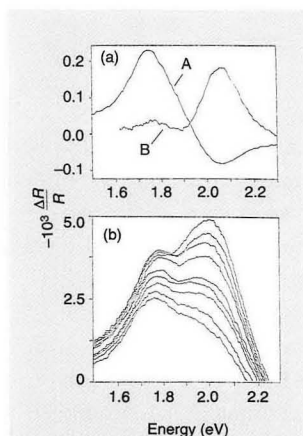


Figure 7. Normalized change of reflectance in response to modulation of potential.

(a) Differential reflectance spectra of a Au/S/methylene blue film at -0.10 V (vs. SCE) in the region of double-layer charging in pH 7.9 phosphate buffer. Potential modulation amplitude is 0.1 V $p-p$, modulation frequency is 40 Hz, and angle of incidence of polarized light is 60° . Curve A: 0.3 monolayer dye coverage; curve B: 1 monolayer dye coverage. (b) Time-resolved spectra in the redox region (integral measurements) obtained by subtracting the reflectance at -0.5 V (leuco species) from that at -0.2 V (colored species). (Adapted with permission from Reference 29.)

a dynamic process; the dimer becomes the predominant species as the bias potential of the modulation is made more negative (29).

On the other hand, when the potential modulation encompasses the redox region, the measurements show that the monomeric dye molecules grow at the expense of the dimeric species (Figure 7b) (29). This behavior can be explained by noting that the N and S heteroatoms change their hybridization from sp^2 to sp^3 when electroreduction takes place. The ensuing conformational change precludes the π -interaction between

the monomers and leads to destabilization of the dimer.

Electrosorption of CO. Strongly adsorbed intermediates such as CO have deleterious consequences in the operation of methanol-based fuel cells and similar energy conversion systems because they block the electrode surface. Fortunately, these electrode "poisons" also have useful spectroscopic signatures in the IR region that facilitate their spectroelectrochemical monitoring (3).

Figures 8 and 9 show representative EMIRS data on Pt (31, 32) and spectra acquired by polarization modulation of the IR radiation between s and p states on Rh electrode surfaces (33). The latter are absolute spectra because of the null contribution from the s polarization (the surface selection rule).

Three main contributions from the CO species can be observed in these spectra: a 2050 – 2100 cm^{-1} band assignable to linear CO (CO_L), a bridged CO species (CO_B) at 1870 – 1960 cm^{-1} , and a complex band at 1620 – 1700 cm^{-1} , which is thought to be a composite of contributions from adsorbed water and a carbonyl-containing functional group. The latter, along with the CO_B band, disappears at high CO coverage, leading to a surface covered predominantly with CO_L species. On the other hand, on a Rh electrode, the surface cover-

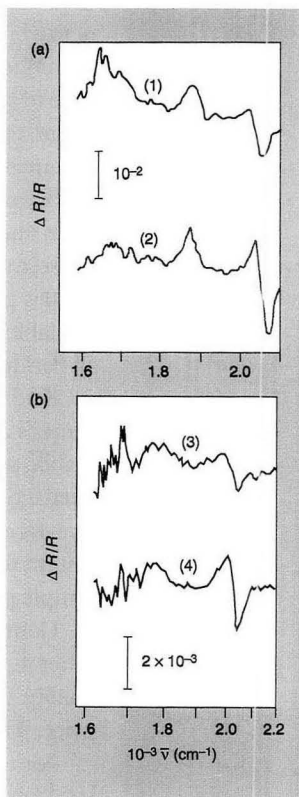


Figure 8. EMIR spectra of the adsorbed species obtained from CH_3OH chemisorption (a) on a Pt(100) single crystal and (b) for a preferentially oriented Pt electrode.

Potentials (vs. RHE) are (1) 0.2 V, (2) 0.35 V, (3) 0.2 V, and (4) 0.3 V. Potential modulation amplitude is 0.4 V $p-p$; modulation frequency is 13.5 Hz. (Adapted with permission from Reference 32.)

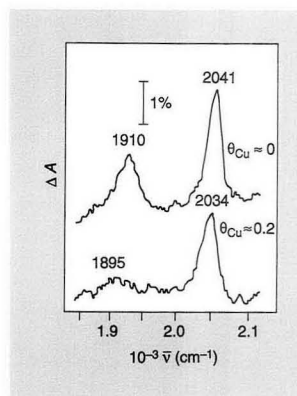
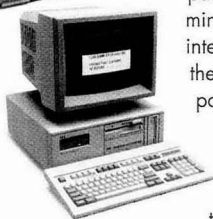


Figure 9. IR spectra of adsorbed CO on a Rh electrode showing the influence of Cu atoms at 0.37 V (vs. RHE).

The spectra were obtained under two sets of conditions: in 0.5 M H_2SO_4 CO-saturated solution ($\theta_{\text{Cu}} = 0$) and after depositing Cu at 0.37 V from 0.5 M $\text{H}_2\text{SO}_4 + 5 \times 10^{-5}$ M CuSO_4 ($\theta_{\text{Cu}} = 0.2$) and then adsorbing CO at the same potential. (Adapted with permission from Reference 33.)

The Millennium™ 2010 Chromatography Manager. It's not just a new product. It's a milestone.



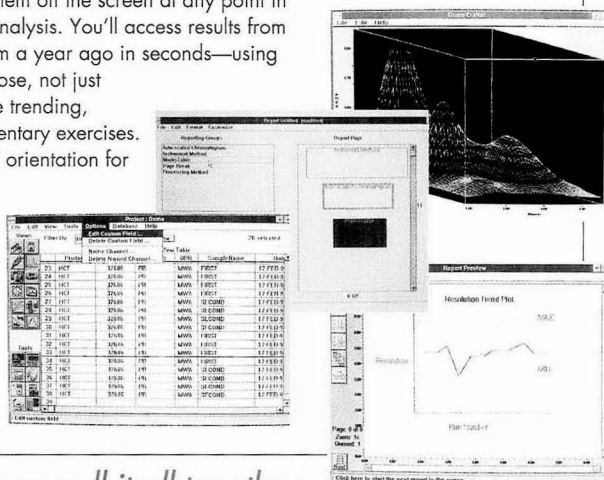
Adancing far beyond current workstation technology, the Millennium™ 2010 Chromatography Manager makes history out of every other way of collecting and reporting data. It adapts to the way you do chromatography, giving you an unprecedented degree of control and flexibility.

When you first sit down at the keyboard—where all your method information is developed—you'll graphically select the instrument components and control parameters for your analysis and acquire your first chromatogram in minutes. The software will then use that chromatogram to develop peak integration parameters, set up your component table, and assist you with the entry of calibration information. You can even enter your own custom parameters to add information to your samples.

When you're ready for results, you can pick them off the screen at any point in the analysis. You'll access results from today or from a year ago in seconds—using any criteria you choose, not just sample or file name. Sample trending,

tracking, and summarizing all become elementary exercises. And you'll decide content, size, layout, and orientation for printing publication-quality reports using our exclusive Report Publisher.

Chalk up a few milestones of your own with the Millennium™ 2010 Chromatography Manager. Increased productivity. Improved quality of results. Easier compliance with GLP standards. To see how it adapts to your lab, call **1-800-252-4752**.



What separates Waters is how we pull it all together.



MILLIPORE

Waters Chromatography

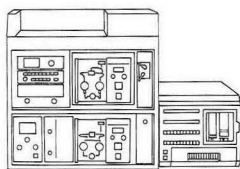
©1992 Millipore Corporation

CIRCLE 146 ON READER SERVICE CARD



Kontes' **ULTRAWARE**
Solvent
System

*Helping people
do things with HPLC.*



+ Your
Chromatograph
and
Autosampler



+ Kimble's
NEW Large
Opening
Vials

**ULTRAWARE Integrated Analytical
HPLC Mobile Phase Handling Systems**

• Unique four valve cap for single system
stepwise filtration, sparging, storage and
delivery. Ask for our FREE brochure.

**NEW LOVIAL Large Opening Vials
Designed to Fit Newer Autosamplers**

• 40% larger opening means fewer bent
needles and more flexibility when using
inserts. Ask for our FREE brochure.

**KIMBLE
KONTES**

Your most complete source
for laboratory glassware products.

Also available through major scientific distributors.

Call 1-800-223-7150.

CIRCLE 72 ON READER SERVICE CARD

NIST

UNITED STATES
DEPARTMENT OF COMMERCE
NATIONAL INSTITUTE OF STANDARDS
AND TECHNOLOGY

**QUALITY
MEASUREMENTS =
STANDARD REFERENCE
MATERIALS**



The National Institute of Standards and
Technology has developed a series of
SRM's to serve as calibrants, test
mixtures, and standardization materials
for Quality Control of analytical
instrumentation and methodology.

MEASUREMENTS and STANDARDS are
important to everyone who needs quality.
NIST has over 1,000 Standard Reference
Materials that can help you calibrate
instruments and check on measurement
accuracy. For more information phone or
write for a free catalog.

Telephone (301) 975-0SRM (6776)
FAX (301) 948-3730

**STANDARD REFERENCE MATERIAL
PROGRAM**

Building 202, Room 204
National Institute of Standards
and Technology
Gaithersburg, MD. 20899

CIRCLE 98 ON READER SERVICE CARD

438 A • ANALYTICAL CHEMISTRY, VOL. 64, NO. 7, APRIL 1, 1992

REPORT

age of CO_B is comparable to that of
 CO_L and increases at negative poten-
tials (33). Recent in situ scanning
tunneling microscopy measurements
on CO adsorbed at Rh(111) (34) ap-
pear to be in agreement with the
composition of the adsorbed CO layer
predetermined by IR spectroscopy
(33).

When the Rh electrode is partially
covered with Cu atoms ($\theta_{\text{Cu}} \sim 0.2$) the
 CO_B species disappear almost en-
tirely, whereas the CO_L adsorption
remains unaffected. One possible ex-
planation for this phenomenon is
that the presence of the Cu atoms
leads to a decrease in the number of
free neighboring Rh sites necessary
for the CO species to adopt a bridge
configuration. Access to this type of
molecular-specific information would
have been difficult to obtain by em-
ploying only conventional electro-
chemical measurements.

**Conducting polymer thin
films.** Thin films of electronically
conductive polymers such as polypyr-
role, polythiophene, and polyaniline
are being considered for diverse ap-
plications ranging from controlled
drug release and chemical sensors to
electrochromic displays and smart
windows (35). Most of these applica-
tions depend critically on the ability
of the polymer to switch from an in-
sulating (reduced) form to an elec-
tronically conductive (oxidized) form.
The dynamics of this process, how-
ever, depend critically on the ionic
fluxes that accompany the polymer
redox process, and both anion and

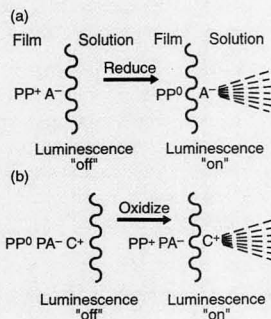
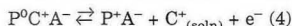
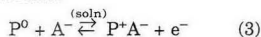


Figure 10. Scheme for in situ
luminescence monitoring of ion
transport during redox
electrochemistry of a
polypyrrole-modified electrode.

Strategies for monitoring (a) anion (A^-) and
(b) cation (C^+) fluxes. (Adapted from Reference
36.)

cation fluxes are known to play important roles.



P, A, and C represent the polymer, "dopant" anion, and "pseudo-dopant" cation, respectively. The compositional changes undergone by the polymer during redox and the dynamics of the processes may be probed in situ by a luminescence strategy, as shown in Figure 10 (36).

The important point with this strategy is that A^- and C^+ have been chosen to have both a dopant (ionic) functionality and a photophysical core, the latter serving as the probe. Species such as ClO_4^- , which are commonly used as dopant anions, however, have no useful spectroscopic

properties in the UV-vis. (ClO_4^- does have vibrational features that are amenable to tagging, as exemplified by the study in Reference 37.) Furthermore, the cation C^+ in Equation 4 could also be a proton with facile transport characteristics. In these two cases, in situ derivatization provides a viable measurement strategy. A pyrylium reagent can be used for ClO_4^- to generate a green fluorescent complex (13), and Bromocresol purple can be used as the spectroscopic tag for protons (11, 12).

The conducting polymer thin films themselves also undergo spectroscopic transitions in the UV-vis and near-IR regions. Furthermore, the radical cations formed during oxidation are amenable to in situ examination by electron spin resonance (ESR) techniques.

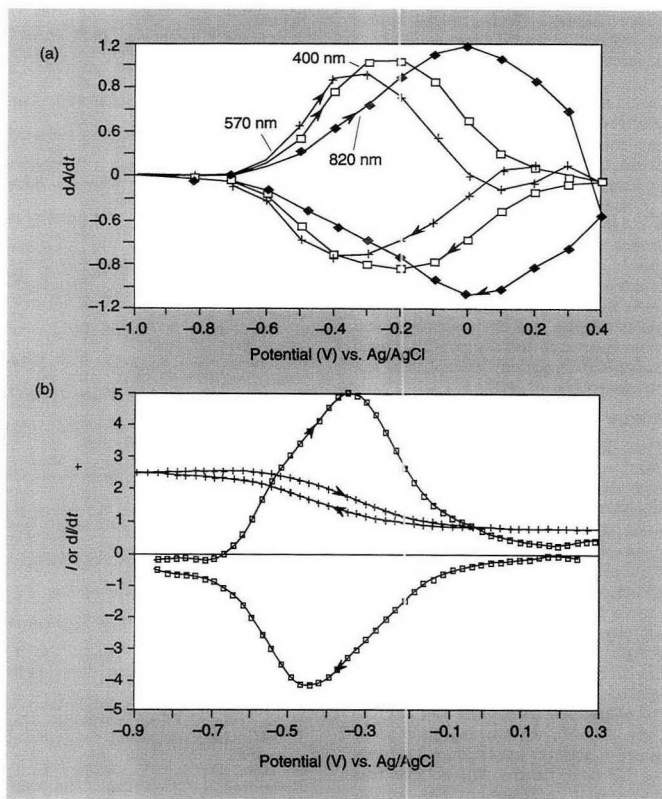


Figure 11. Modulation of spectroscopic signals as polymer is driven through the redox transition.

(a) UV-vis absorption. dA/dt vs. potential is plotted for a polypyrrole thin film in N_2 -saturated 0.1 M KCl. The potential scan rate was 5 mV/s. (b) Raman scattering. Integral and differential plots of the 1576 cm^{-1} Raman band intensity vs. potential for a polypyrrole thin film in N_2 -saturated 0.1 M KCl are shown. The potential scan rate was 5 mV/s. (Adapted with permission from Reference 38.)

Discover new solutions

Don't pollute your lab

SFE sample prep avoids toxic organic solvents

- Supercritical fluid extraction uses low-cost, non-toxic CO_2 instead of hazardous and expensive solvents.
- Process samples in a fraction of the time required for Soxhlet methods.



Call today.

We'll send you SFE application bulletins along with our new catalog of SFE instruments.

Isco, Inc.
P.O. Box 5347
Lincoln NE 68505 U.S.A.
Tel (800)228-4250
Fax (402)464-4543



Isco Europe AG,
Brüschstr. 17
CH8708 Männedorf, Switzerland
Fax (41-1)920 62 08

CIRCLE 64 ON READER SERVICE CARD



DEVELOPING A CHEMICAL HYGIENE PLAN

Jay A. Young
Warren K. Kingsley
George H. Wahl, Jr.

PUBLISHED BY
THE AMERICAN CHEMICAL SOCIETY

Developing a Chemical Hygiene Plan

This essential "how-to" book tells you what you need to know to comply with the federal regulation known as the "OSHA Laboratory Standard" which requires chemical hygiene plans. Developed by the ACS Committee on Chemical Safety, the guide presents hygiene plans that can be modified according to the particulars of individual laboratories. Among the topics covered in this valuable book you'll find

- application of the OSHA Laboratory Standard
- history of the OSHA Laboratory Standard
- standard operating procedures
- control measures and equipment
- records and recordkeeping

In addition, several appendices are provided, including employee information and training techniques, exposure assessment procedures, the elements of an emergency procedure plan, the OSHA Laboratory Standard, a list of contacts for states that have OSHA-approved state plans, and a list of acronyms.

This reference is critical to all lab supervisors who must have in place by January 31, 1991, a chemical hygiene plan that outlines specific work practices and procedures ensuring employee protection from health hazards associated with hazardous chemicals.

by Jay A. Young, Warren K. Kingsley, and George H. Wahl

Developed by the Committee on Chemical Safety of the American Chemical Society

72 pages (1990) Paperbound
ISBN 0-8412-1876-5 LC 90-46721
\$18.95

ORDER FROM

American Chemical Society
Distribution Office, Dept. 87
1155 Sixteenth St., N.W.
Washington, DC 20036

or CALL TOLL FREE

800-227-5558

(in Washington, D.C. 872-4363) and use your credit card!

REPORT

Figure 11 illustrates the modulation in the UV-vis absorption and Raman scattering cross sections as the polymer is driven through the redox transition (38). These data and those from ESR experiments (39) can be processed in a manner analogous to a cyclic voltammogram (indeed, the shapes are similar in the two cases). It is important to make the distinction, however, that the former are chemistry and molecular specific whereas a current measurement as in cyclic voltammetry is not (38).

Cathodic photocurrents have been observed in experiments similar to those shown in Figure 3 for polyaniline films illuminated by UV-vis light (40). Earlier photoelectrochemical data on this material, some of which seem to be unreliable because of the presence of artifacts resulting from local heating, also have been reviewed (40). The mechanism of the observed photoeffects, unlike in the case of the inorganic semiconductors described earlier, remains unclear. We must establish whether the photocurrents are attributable to initial electron-hole pair generation or to the migration, along the polymer chain, of a partially localized molecular exciton (40).

Conducting polymer thin films are a subset of polymer-modified electrodes (41). These materials present many opportunities for combined electrochemistry-spectroscopy experiments. In particular, clever variations in the synthetic strategy and molecular architecture could be used to build the optical probes into the polymer network (42).

Future perspectives

The addition of spectroscopy to "conventional" techniques can provide a new dimension to the information content from electrochemical systems. Although we have highlighted primarily the compositional issues in this article, the electrode surface structure and interphase can also be key factors in dictating the course of an electrochemical reaction. Given the developments in the preparation of ordered electrode surfaces and the spatial resolution now possible with tunneling spectroscopies and microscopy (43, 44), we can expect to see a spurt of activity in structural aspects in the near future. We believe this trend will complement the implementation of new spectroscopic probes within an electrochemical framework, allowing us to refine existing methodologies and improve the quality of compositional data from electrochemical systems.

The research at The University of Texas at Arlington was supported in part by grants from the National Science Foundation, the Defense Advanced Research Projects Agency (contract monitored by the Office of Naval Research), and the Texas Higher Education Coordinating Board (Advanced Technology and Energy Research Applications Programs). We also acknowledge the support of the Consejo Nacional de Investigaciones Científicas y Técnicas in Argentina.

References

- (1) "In Situ Characterization of Electrochemical Processes"; Publication NMAB 438-3; National Academy Press: Washington, DC, 1987.
- (2) Peter, L. M. *Chem. Rev.* **1990**, *90*, 753.
- (3) Bewick, A.; Pons, S. In *Advances in Infrared and Raman Spectroscopy*; Clark, R. J. H.; Hester, R. E., Eds.; Wiley-Heyden: London, 1985; Vol. 12, pp. 1-63.
- (4) *Spectroelectrochemistry: Theory and Practice*; Gale, R. J., Ed.; Plenum: New York, 1988.
- (5) *Applications of Fourier Transform Raman Spectroscopy—II*, *Spectrochim. Acta Part A*; Hendra, P. J., Ed.; **1991**, *47A*; special volume.
- (6) Parsons, R. *Chem. Rev.* **1990**, *90*, 813.
- (7) Fleischmann, M.; Hendra, P. J.; McQuillan, A. J. *Chem. Phys. Lett.* **1974**, *26*, 163.
- (8) McCreery, R. L.; Packard, R. T. *Anal. Chem.* **1989**, *61*, 775 A.
- (9) Hubbard, A. T. *Chem. Rev.* **1988**, *88*, 633.
- (10) Bard, A. J.; Faulkner, L. F. *Electrochemical Methods*; John Wiley and Sons: New York, 1980; Chapter 14.
- (11) Jang, G.-W.; Tsai, E. W.; Rajeshwar, K. J. *Electrochem. Soc.* **1987**, *134*, 2377.
- (12) Jang, G.-W.; Tsai, E. W.; Rajeshwar, K. J. *Electroanal. Chem.* **1989**, *263*, 383.
- (13) Ho, Y.-H.; Basak, S.; Tsai, E. W.; Rajeshwar, K. J. *Chem. Soc. Chem. Commun.* **1989**, 1078.
- (14) Richards, J. A.; Evans, D. H. *Anal. Chem.* **1975**, *47*, 964.
- (15) Bruckenstein, S.; Gadde, R. M. *J. Am. Chem. Soc.* **1971**, *93*, 5941.
- (16) Rajeshwar, K. *Adv. Mater.* **1992**, *4*, 23.
- (17) Mishra, K. K.; Rajeshwar, K. J. *Electroanal. Chem.* **1989**, *273*, 169.
- (18) Krishnan, V.; Ham, D.; Mishra, K. K.; Rajeshwar, K. J. *Electrochem. Soc.* **1992**, *139*, 23.
- (19) Wei, C.; Rajeshwar, K.; Alavi, K.; Pathak, R. N.; Wang, L. T. *Appl. Phys. Lett.*, in press.
- (20) Gerischer, H. *Corros. Sci.* **1990**, *31*, 81.
- (21) O'Grady, W. E. *J. Electrochem. Soc.* **1990**, *127*, 555.
- (22) Gui, J.; Devine, T. M. *J. Electrochem. Soc.* **1991**, *138*, 1376.
- (23) Lezna, R. O.; de Tacconi, N. R.; Arvia, A. J. *J. Electroanal. Chem.* **1990**, *283*, 319.
- (24) Juanto, S.; Lezna, R. O.; de Tacconi, N. R.; Arvia, A. J. Presented at the 42nd ISE Meeting, Montreux, Switzerland, Aug. 1991.
- (25) Ham, D.; Son, Y.; Mishra, K. K.; Rajeshwar, K. J. *Electroanal. Chem.* **1991**, *310*, 417.
- (26) Lezna, R. O.; de Tacconi, N. R.; Arvia, A. J. *J. Electroanal. Chem.* **1988**, *255*, 251.
- (27) Son, Y.; de Tacconi, N. R.; Rajeshwar, K., unpublished results.
- (28) Clark, J. H.; Jones, C. W. *Inorg. Chim. Acta* **1991**, *179*, 41.

- (29) Lezna, R. O.; de Tacconi, N. R.; Hahn, F.; Arvia, A. J. *J. Electroanal. Chem.* **1991**, 306, 259.
 (30) Corn, R. M. *Anal. Chem.* **1991**, 63, 285 A.
 (31) Beden, B.; Lamy, C.; de Tacconi, N. R.; Arvia, A. J. *Electrochim. Acta* **1990**, 35, 691.
 (32) Beden, B.; Hahn, F.; Lamy, C.; Léger, J.-M.; de Tacconi, N. R.; Lezna, R. O.; Arvia, A. J. *J. Electroanal. Chem.* **1989**, 261, 401.
 (33) Kunimatsu, K.; Lezna, R. O.; Enyo, M. *J. Electroanal. Chem.* **1989**, 258, 115.
 (34) Yau, S.-L.; Gao, X.; Chang, S.-C.; Schardt, B. C.; Weaver, M. J. *J. Am. Chem. Soc.* **1991**, 113, 6049.
 (35) Kanatzidis, M. G. *Chem. Eng. News* **1990**, Dec. 3, 36.
 (36) Krishna, V.; Ho, Y.-H.; Basak, S.; Rajeshwar, K. *J. Am. Chem. Soc.* **1991**, 113, 3325.
 (37) Zhong, C.; Doblhofer, K. *Synth. Met.* **1990**, 38, 117.
 (38) Son, Y.; Rajeshwar, K. *J. Chem. Soc. Faraday Trans.*, in press.
 (39) Oudard, J. F.; Allendoerfer, R. D.; Osteryoung, R. A. *J. Electroanal. Chem.* **1988**, 241, 231.
 (40) Kalaji, M.; Nyholm, L.; Peter, L. M.; Rudge, A. J. *J. Electroanal. Chem.* **1991**, 310, 113.
 (41) Chidsey, C.E.D.; Murray, R. W. *Science* **1986**, 231, 25.
 (42) Kaneko, M.; Wöhrlé, D. In *Advances in Polymer Science* 84; Cantow, H.-J., Ed.; Springer-Verlag: Berlin, Heidelberg, 1988; p. 141.
 (43) Kolb, D. M. *Ber. Bunsen Ges. Phys. Chem.* **1988**, 92, 1175.

- (44) Chang, S.-C.; Weaver, M. J. *J. Phys. Chem.* **1991**, 95, 5391.

Suggested reading

- Gerischer, H. *Angew. Chem. Int. Ed. Engl.* **1983**, 27, 63.
 Chazulviél, J.-N. *Electrochim. Acta* **1988**, 33, 461.
Spectroscopic and Diffraction Techniques in Interfacial Electrochemistry; Gutiérrez, C.; Meléndres, C., Eds.; Kluwer Academic Publishers: Dordrecht, The Netherlands, 1990.
Electrochemical Interfaces; Abruña, H., Ed.; VCH: New York, 1991.
Comprehensive Chemical Kinetics; Compton, R. C.; Hammett, A., Eds.; Elsevier: Amsterdam, The Netherlands, 1989; Vol. 29.
Physical Methods of Chemistry; Rossiter, B. W.; Hamilton, J. E., Eds.; Wiley: New York, 1986; Vol. II.

the faculty at UT, he received postdoctoral training at St. Francis Xavier University in Nova Scotia and at Colorado State University. His research interests include conducting polymer and semiconductor electrochemistry, photoelectrochemistry, and thermal analysis methods development.



Norma R. de Tacconi received her Ph.D. in physical chemistry from La Plata National University, Argentina. Her research efforts are directed toward the optical characterization of electrochemical interfaces using *in situ* UV-vis and IR spectroscopies.

Reynaldo O. Lezna received his Ph.D. in physical chemistry from La Plata National University, Argentina. His research interests include the application of *in situ* optical methods to the study of the electrochemical interface.



Krishnan Rajeshwar received his Ph.D. in chemistry in 1974 from the Indian Institute of Science, Bangalore. Before joining

The Coleman Model 35 Spectrophotometer is economical and provides superior photometric accuracy and linearity. The Model 35 features a multi-functional digital display, a high energy quartz-halogen light source and maintains an excellent signal-to-noise ratio.

CIRCLE 14



The 3D HPLC System combines the three most effective detection modes - UV, fluorescence and conductivity - for both simultaneous or individual analyses - in one, inexpensive unit. The complete system includes the pump, injector, cartridge column, recorder, and the patented trifunctional detector.

CIRCLE 15

The BACHARACH Quality Advantage



With over 80 years of experience and a strong reputation for manufacturing high quality, economical detection, testing and measuring equipment for environmental, quality control and education applications...BACHARACH has become the source for high performance laboratory equipment.

The BACHARACH Analytical Group combines engineering innovations with analytical market experience to create a complete product line that also includes - the Mercury System which combines instruments, computer software and accessories-as well as the 51Ca Flame Photometer.



BACHARACH

Bacharach Analytical Group • 625 Alpha Drive • Pittsburgh, PA 15238 • (412) 963-2107 • Fax (412) 963-2091

Practical Sub-Micron Particle Size Analysis...

**New for
92**



Size range 1 - 5000nm.
Concentrations up to 50%
Choice of laser system
Proven PCS Technology
EASY software

Malvern Instruments, long acknowledged as leaders in particle size measurement by the Photon Correlation Spectroscopy (PCS) technique, now have three **Autosizer** Systems which offer a practical approach to sub-micron particle size analysis.

The **Autosizer** range is flexible enough for use in both highly automated routine QC Laboratories, technically demanding research environments, as well as for on-line process plant applications

For more information, contact Malvern now....

Malvern Instruments Inc
10 Southville Rd. Southborough, MA 01772
Tel. (508)480 0800 Fax.(508)460 9692

MALVERN
INSTRUMENTS
The Practical Approach

CIRCLE 92 ON READER SERVICE CARD

Ion Chromatography Products Guide



NEW for '92!

Columns
Eluants
Standards
Starter Kits
Sample Handling
Fittings
Accessories
Instrumentation

Request Alltech
Bulletin #217!

**Includes Column Selection Guide
and Many Applications!**

Alltech

Alltech Associates, Inc.
2051 Waukegan Road Deerfield, IL 60015
Phone: 1-800-255-8324 Fax: 708-948-1078

CIRCLE 3 ON READER SERVICE CARD

442 A • ANALYTICAL CHEMISTRY, VOL. 64, NO. 7, APRIL 1, 1992

Trends in Chemical Consulting

Restructuring in the chemical industry has created a wealth of opportunities for consultants. Companies are now more willing to seek outside help than in the past as they recognize the value of experienced specialists.

But what constitutes the efficient use of a consultant? And is consulting for you? *Trends in Chemical Consulting* explores these issues through contributions from chemical consultants, those who have used the services of a consultant, and participants in cooperative arrangements. Presentations focus on those considerations specific to consulting relationships between scientific professionals.

Chemists, chemical engineers, and other scientific professionals in support areas to the chemical industry will find this an indispensable resource of information on chemical consulting.

Contents

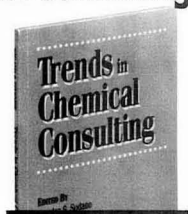
• Consulting to the Chemical Industry • Industrial Expectations for Consultants and Consulting Services • Understanding, Selecting, Managing, and Compensating Consultants • An Academic Perspective on Consulting • University-Industrial Relationships • Accessing Federal Laboratories Know-How • What Consulting Practices Look Like • Defining and Marketing Your Consulting Specialty • Opportunities for Retired Chemists • Using Consultants to Interpret Regulatory Initiatives • Major Chemical Company Retirees as Consultants and Market Developers • Robotic Servicing on the Space Station Freedom • Consultation in Sensory Evaluation • Chemical Information Consultants

Charles S. Sudano and David M. Sturmer, *Editors*

174 pages ('991) Paperbound
ISBN 0-8412-2106-5
\$29.95

Order from: American Chemical Society, Distribution Office, Dept. 11
1155 Sixteenth St., N.W., Washington, DC 20036

or CALL TOLL FREE **800-227-5558**
(in Washington, D.C. 872-4363) and use your credit card!



MEETINGS

1992 Gordon Research Conferences

The Gordon Research Conferences are designed to extend the frontiers of science by fostering a free and informal exchange of ideas among those actively involved in chemistry research or related fields. At each conference, meetings are held in the morning and evening, Monday through Friday, with the exception of Friday evening. The afternoons are available for recreation, reading, or participation in discussion groups.

To promote discussion and to protect individual rights, no information presented at the conferences can be used without the specific authorization of the individual making the contribution. Recording of lectures and photographing of slides also are prohibited.

The unique concept of the conferences was established by Neil Gordon of Johns Hopkins University in 1931. Gordon foresaw the importance of establishing direct communication between scientists while removing the distractions at larger meetings.

This year, 14 conferences are of particular interest to analytical chemists: analytical chemistry, atomic and molecular interactions, bioelectrochemistry, corrosion—aqueous, electron spectroscopy, lasers in medicine and biology, magnetic resonance in biology and medicine, multiphoton processes, optical phenomena in glass, photoacoustic and photothermal phenomena, physical electrochemistry, separation and purification, statistics in chemistry and chemical engineering, and vibrational spectroscopy. Technical programs for these conferences follow.

The fixed fee for resident participants is \$440, which covers registration, room (double occupancy), and meals. The \$400 fee for nonresident conferees covers registration and meals. The \$350 guest fee includes

room and meals only. If registration cards with advance payment are postmarked at least three weeks before the conference, fees are discounted \$50.

Additional information can be obtained from Alexander Cruickshank, Gordon Research Conferences, Gordon Research Center, University of Rhode Island, Kingston, RI 02881-0801 (401-783-4011 or -3372; fax 401-783-7644). From June 2 to Aug. 21, Cruickshank can be reached at Colby-Sawyer College, New London, NH 03257 (603-526-2870; fax 603-526-4717).

Analytical Chemistry

New Hampton School
New Hampton, NH
I. M. Warner, *Chair*
L. D. Fothman, *Vice Chair*

AUGUST 3-7

M. Soriaga, *discussion leader*
Cathodic Reduction of Adsorbates:
Mechanism and Analytical Applications. J. Osteryoung

Surface Analysis by Scanning Electrochemical Microscopy. A. J. Bard

R. Roberts, *discussion leader*
Surface Studies with Ion Beams and Lasers. N. Winograd

In Situ X-ray Absorption and Scattering Studies of Adlayers at Metal-Electrolyte Interfaces. J. G. Gordon

W. May, *discussion leader*
Assessing Carcinogenic Risks. M. W. Pariza
Suggestions for Filling Gaps in Identifying Trace Organics in the Environment. W. T. Donaldson

G. Patonay, *discussion leader*
Frontiers in Trace Element Analysis. J. W. Mitchell

Strategies and Techniques in Ultratrace Analysis of Ubiquitous Organic Pollutants in Clean (Ocean) Samples. C. S. Giam

W. Hinze, *discussion leader*
New Approaches to Chiral Recognition and Separation. D. Armstrong
HPLC Chiral Stationary Phases Based on Immobilized Biopolymers: Enantioselective Tools for Analytical Chemistry and Biochemistry. I. Wainer

L. B. McGown, *discussion leader*
Thermal Lens Circular Dichroism Detection for Liquid Chromatographic Enantiomeric Separations. C. D. Tran
Applications of Time-Resolved Chiroptical Luminescence Spectroscopy in Studies of Excited-State Chiral Dynamics and Intermolecular Chiral Discriminations. F. S. Richardson

M. Wirth, *discussion leader*
Surface Raman Spectroscopy on Metal Surfaces. J. Pemberton
Spectroscopy. R. N. Zare

H. Blount, *discussion leader*
Archaeological Dating of Rock Paintings. M. Rowe

J. Robinson, *discussion leader*
FT-MS Characterization of Normal and Modified Oligonucleotides. M. Buchanan
High-Speed DNA Sequencing. L. M. Smith

Multiphoton Processes

Colby-Sawyer College
New London, NH
T. Baer, *Chair*
R. Compton, *Vice Chair*

JUNE 8-12

MEETINGS

E. Grant, *discussion leader*
Laser-Induced Diffraction Spectroscopy. D. Chandler
Picosecond Pump-Probe Studies of Cluster Reactions. J. Syage
State-Selected Multiphoton Chemistry on the Ground Potential Surface. T. Rizzo

A. Giusti, *discussion leader*
Time-Dependent Calculations of Dressed Molecules in Intense Laser Fields. A. Bandrauk

K. Welge, *discussion leader*
Competition between Above-Threshold Ionization and Harmonic Generation. S. Allendorf
Nonperturbable Behavior of Multielectron Atoms in Strong Fields. X. Tang
Multielectron Dissociative Ionization of Small Molecules in Intense Laser Fields. C. Cornaggia

W. T. Hill, *discussion leader*
Stability of Atoms in Intense Laser Fields. P. Bucksbaum
Molecular Photoionization in Strong Fields. H. P. Helm

J. Miller, *discussion leader*
Coherent Laser Control in Resonant-Enhanced Multiphoton Ionization. R. Gordon
Interfering Optical Interactions. D. Elliot
New Developments in Two-Photon Lasers. D. Gauthier

S. Colson, *discussion leader*
Multielectron Dissociative Ionization in Intense Laser Fields. L. J. Frasinski

E. Eyller, *discussion leader*
Dynamics of Excited States of Polyatomic Species. D. Gauyacq
High ν Rydberg States and Ion Pair Formation in Molecular Hydrogen. S. Pratt
Femtosecond Spectra of Molecules and Metal Clusters. G. Gerber

J. Weisshaar, *discussion leader*
When Radicals See the Light K. deLange
Multiphoton Ionization and Detachment from Atoms. S. Berry

K. Mueller-Dethlefs, *discussion leader*
Angular Distributions of Multiphoton-Detached Electrons from Halogen Anions. C. Blondel
Time-Resolved ZEKE Photoelectron Spectroscopy. J. Kree
Threshold Ionization Spectroscopy with and without Electrons. P. Johnson

Photoacoustic and Photothermal Phenomena

Colby—Sawyer College
 New London, NH
 G. Diebold, *Chair*
 H. Coufal, J. Murphy, *Vice Chairs*

JUNE 8–12

P. Korpiun, *discussion leader*
Heat Diffusion in Various Situations: From Fractals to Neural Networks. C. Boccaro
Heat Pulse Propagation and Phonon Imaging. J. Wolfe
Physical Fundamentals of Thermal Wave Science. A. Mandelis
 V. Gusev, *discussion leader*
Recent Developments in Modeling of Laser Ultrasound. J. Spicer
Applications of Laser Ultrasound. C. Scruby

J. Thoen, *discussion leader*
Control of Interfaces in Composite Materials and in Ceramics at the Micronic Scale with the Photothermal Microscope. F. Lepoutre
Transient Thermal Gratings and Their Applications. M. Fayer

D. Bicanic, *discussion leader*
Recent Developments in Generation and Detection of Surface Acoustic Waves. P. Hess
Electrical Transducers for Measurements of Thermal and Acoustic Transients. W. Arnold

K. Wickramasinghe, *discussion leader*
Photothermal Detection of Microwave Absorption for the Characterization of Local Properties in Magnetic Materials. J. Peizl
Video IR Thermal Wave Imaging. R. Thorias

A. Tam, *discussion leader*
Photothermal Methods for the Analysis of Thin Polymer Films. J. Power
Spectroscopic Applications of Photothermal Beam Deflection. E. Eyring

D. Cahen, *discussion leader*
Thermal and Plasma Waves in Semiconductors: From Linear to Nonlinear Behavior. D. Fournier
Photopyroelectric Theory, Applications, and the State of the Art. C. Christofides

H. Coufal, *discussion leader*
Photothermal Applications to Semiconductors. A. Rosencauig

R. Palmer, *discussion leader*
Laser-Induced Surface Desorption. E. Matthias
Pulsed Photothermal Radiometry of Tissue. S. Prah

Optical Phenomena in Glass

Tilton School
 Tilton, NH
 M. J. Weber, *Chair*
 D. E. Day, *Vice Chair*

JUNE 29–JULY 3

R. H. Stolen, *discussion leader*
Photoinduced Second Harmonic Generation in Glass. D. M. Krol
Large Second-Order Nonlinearities in Silica. S. R. Brueck
Mechanisms for Second Harmonic Generation in Glass: Some Answers, More Quest ones. D. Z. Anderson

P. C. Taylor, *discussion leader*
Optically Induced Phenomena in Chalcogenide Glasses. S. R. Elliott
Origin of Photostructural Changes in Chalcogenide Glasses. H. Fritzsche

D. W. Hall, *discussion leader*
Rare-Earth-Doped Glass Fiber Lasers and Amplifiers. D. N. Payne
Effects of Glass Composition on the Optical Transitions of Rare-Earth-Doped Glass. W. J. Miniscalco
Time-Resolved, Laser-Induced Refractive Index Changes in Rare-Earth-Doped Glasses: From Femtoseconds to Months. R. C. Powell

R. A. Weeks, *discussion leader*
Mechanism and Application of Cross Luminescence (Auger Effect Free Luminescence) in Silica Glass. K. Nagasawa
Hydrogen-Associated Defect Influence on Color Center Generation in Fused Silica. A. R. Siffert

D. R. Uhlmann, *discussion leader*
Quantum-Size Effects and Optical Nonlinearity in Glasses Doped with Semiconductor Clusters. J. H. Simmons
Laser and Nonlinear Properties of Sol Gel Glass. R. Reisfeld
Novel Gradient Index Glasses. D. T. Moore

A. Polman, *discussion leader*
Optical and Structural Properties of Erbium-Implanted Silica. J. M. Poate
Optical and Materials Properties of Copper-Implanted Silica. R. H. Magruder, III

G. H. Sigel, *discussion leader*
Photosensitive Properties of Optical Fiber Waveguides and Novel Planar Glass Structures. K. O. Hill
Photoinduced Phase Gratings in Glass Optical Communication Fibers. V. Mizrahi
Dynamics of Phase Grating Formation in Optical Fibers. J. E. Sipe

N. Kreidl, *discussion leader*
Optics and Glass: A Historical Glimpse. A. R. Cooper

W. M. Yen, *discussion leader*
Photon Echoes in Glass Fibers. Y. Silberberg
Spectral Hole Burning in Inorganic Glasses. R. M. Macfarlane
Laser Spectroscopy and Scattering in Xerogels. G. Boulon

Lasers in Medicine and Biology

Colby—Sawyer College
 New London, NH
 C. Puliafito, M. Van Gemert, *Co-Chairs*

JULY 6–10

Optical Imaging of Disease

Fluorescence Imaging To Guide Laser Angiosurgery. M. Feld
Fluorescence and Transillumination Imaging. S. Svanberg
Interferometric Imaging. J. G. Fujimoto

Interstitial Photocoagulation/Hyperthermia

Optical and Tissue Modeling. S. Jacques
Medical Systems and Image Control. B. Wilson

Photodynamic Therapy

Clinical Issues and New Agents. A. R. Oseroff
New Photosensitizers. J. Levy
TR Domain Photosensitizers. B. Henderson
Biophysics of Port Wine Stain Treatment. M. Van Gemert

Cardiology

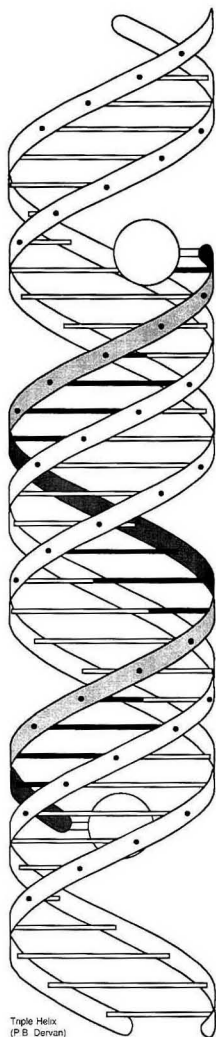
Current Problems of PTCA and Alternative Approaches. L. I. Deckelbaum
Biologic Effects of Holmium-Excimer Ablation. G. Abela
Laser Balloon Angioplasty and the Application of Bioprotective Materials. J. R. Spears
Wavelength-Dependent Effects. J. M. Isner
Photodynamic Therapy for Restenosis. G. M. LaMuraglia

Ophthalmic Lasers

Excimer Laser Corneal Surgery. M. MacDonald
Short-Pulsed Photocoagulation. R. Birngruber
IR Lasers. J.-M. Parel

Dental Laser Applications

Effects of Nd:YAG and CO₂ Laser Applications on Tooth Vitality. S. Kim



Triple Helix
(P.B. Demian)

For innovative solutions to your research problems...

Science *Innovation* '92

New Techniques and Instruments in Biomedical Research

21–25 July 1992 ♦ San Francisco

Sponsored by *Science* Magazine and the
American Association for the Advancement of Science

Science Innovation is the most comprehensive presentation of new biomedical research techniques and instruments available in a single meeting. This annual event is unique in that it focuses on the research *process* rather than on results. Speakers will detail their methodologies and explain how you can adapt their techniques to solve problems in your own area of research.

As a participant, you'll attend plenary sessions by world-renowned scientists on the current status and future potential of the cutting-edge techniques they have developed. You'll also discuss specific applications of problem-solving techniques in any of 24 advanced technology workshops led by top research scientists. You can examine relevant technologies on display in the exhibition and arrange for their implementation in your lab. In addition, you can share your own research in technique-focused poster sessions and seek out new career opportunities in the employment exchange.

If you are a bench scientist, research manager, engineer, professor, or student and are doing biomedical research in a university, industry, or government lab; a research hospital; or a biotech institute, you can't afford to miss **Science Innovation '92**.

For more information about the scientific program, the exhibition, or the contributed paper sessions, use the coupon below or call 202-326-6450.

Confirmed Plenary Speakers: Steven Block ♦ Mario Capecchi ♦ C. Thomas Caskey ♦ Steven Chu ♦ Peter Dervan ♦ Richard Ernst ♦ Stephen Fodor ♦ Robert Goldberg ♦ Joseph Goldstein ♦ Paul Hansma ♦ Curtis Harris ♦ Leroy Hood ♦ Harder McConnell ♦ Fred McLafferty ♦ Carver Mead ♦ George Smith ♦ Richard Voss ♦ Irving Weissman ♦ Savio Woo ♦ Richard Zare

Advanced Technology Workshops: DNA Sequencing ♦ DNA Amplification ♦ Nonisotopic Detection ♦ Information Analysis ♦ Gene Mapping ♦ Gene Therapy ♦ Gene Transfer ♦ Innovations in Crop Production ♦ Protein Structure Determination ♦ Immunological Techniques ♦ Gene Expression ♦ Brain Research ♦ Microscopy ♦ Fluorescent In-situ Hybridization ♦ Mass Spectrometry ♦ Chemical and Structural NMR ♦ DNA Forensics ♦ Oncogene and Suppressor Techniques ♦ Drug Targeting and Delivery ♦ Biomedical Imaging ♦ Optical Tweezers ♦ Field-flow Fractionation ♦ Chromatography ♦ Electrophoresis

Yes! I'd like to learn more about **Science Innovation '92**.

- ☐ Please send me details about the scientific program.
☐ I'm interested in exhibiting. Please send an exhibit prospectus.
☐ I'm interested in presenting a poster. Please send me details.

Name

Institution

Address

City/state

Zip Phone

Mail to: AAAS Meetings, 1333 H Street, NW, Washington, DC 20005 USA. (Phone: 202-326-6450; Fax: 202-289-4021)

E1

CIRCLE 1 ON READER SERVICE CARD

MEETINGS

New Laser Technology and Safety

Current Safety Issues. D. Sliney
New Technologies. T. Deutsch

Electron Spectroscopy

Brewster Academy
Wolfeboro, NH
W. Eberhardt, *Chair*
D. M. Hanson, *Vice Chair*

JULY 13-17

Electronic Structure and Magnetism of Thin Films

D. Pierce, *discussion leader*
Spin-Polarized Photoemission of Thin-Metal Films. P. D. Johnson
Magnetic X-ray Circular Dichroism. G. Schütz
Theory of Magnetism in Thin Films of 4D and 5D Metals. S. Blügel

Molecular Adsorbates on Surfaces

T. E. Madey, *discussion leader*
Core-Induced Dynamics in Surface Molecules. D. Menzel
Soft X-ray Emission Spectroscopy Solids and Surfaces. J. Nordgren
REMPI Studies of Electronically Stimulated Surface Processes. D. R. Jennison

Photoelectron Microscopy

Concepts and Prospects of Photoemission Microscopy. C. Kunz

Spectroscopy of Semiconductors and Interfaces

I. Lindau, *discussion leader*
Surface Photovoltage Effects and Schottky Barrier Measurements. K. Horn
Ballistic Electron Emission Microscopy of Semiconductor Structures. W. J. Kaiser

New Advances in Electron Energy Loss Spectroscopy

E. W. Plummer, *discussion leader*
High-Resolution EELS from Surfaces. H. Ibach
Electron Energy Loss Studies on Oxides. W. Goodman

Spectroscopy of Clusters and Fullerenes

W. Andreoni, *discussion leader*
Photoemission from C_{60} . J. H. Weaver
Theory of C_{60} Superconductivity. M. Schlüter
Studies of Clusters Using Negative-Ion Photodetachment Spectroscopy. D. Neumaier

Photoemission Interference Effects and Electron Holography

J. Pendry, *discussion leader*
Photoelectron Diffraction and Holography. C. Fadley
Adsorbate Structure Determination with Photoelectron Diffraction. P. Woodruff

Coincidence Spectroscopy

J. Eland, *discussion leader*
Energy-Resolved, Auger Electron, Multiple-Ion Coincidence Studies of Molecules. K. Lee
Auger Electron-Photoelectron Coincidence Studies on Atoms. V. Schmidt
Unified Theory of Auger Electron Emission. T. Åberg

High-Resolution Studies of Molecules

K. Kimura, *discussion leader*
High-Resolution Core-Level Spectroscopy of Small Molecules. J. Feldhaus
High-Resolution Core-Level Photoelectron Spectroscopy: Vibrational and Ligand Field Splittings and Inherent Linewidths. M. Bancroft
TBA. S. Pratt

Magnetic Resonance in Biology and Medicine

Tilton School
Tilton, NH
B. J. Gaffney, *Chair*
G. Drobny, *Vice Chair*

JULY 13-17

G. LaMar, *discussion leader*
Magnetic Resonance Studies of 2Fe-2S Ferredoxins. J. L. Markley
NMR Studies of Cytochrome c Peroxidase and Its Redox Complexes. J. D. Saterlee
Cobalt-Substituted Zinc Fingers. J. M. Earg
J. Freed, *discussion leader*
ESEEM Studies of Nickel(III) Model Complexes. J. McCracken
Pulsed EPR Methodology for the Study of Biomolecules. A. Schweiger

G. Drobny, *discussion leader*
Tumor Bioenergetics and MRI of Tumor Edema. G. Steen
Functional Magnetic Resonance Imaging. C. Moonen
The Microphysiometer: A New Tool for the Chemist. H. M. McConnell

Panel

NMR Techniques for Studies of Intermolecular Interactions with Biological Macromolecules. K. Wüthrich
NMR Investigations of Wild-Type and Oncogenic RAS Proteins. S. Campbell-Burk
Multidimensional NMR Studies of Immunosuppressants and Their Binding Proteins. S. Fesik

R. Balaban, *discussion leader*
New Insights into the Pathogenesis of Type II Diabetes Mellitus with NMR. G. I. Shuman
Medical Impact of Diffusion-Perfusion MRI. M. Moseley
Studies of Brain Activation with MRI. B. R. Rosen

P. E. Pfeffer, *discussion leader*
Measuring Internuclear Distances in Protein Complexes by REDOR NMR. J. Scharfer
Pulsed Electron-Nuclear Studies of Electron-Transfer Proteins. H. Thomann

Heteronuclear 2D and 3D NMR Studies of Protein Structure and Dynamics. D. A. Torchia
Recent Advances in NMR Studies of Protein Structure. R. E. Klevit
Spin-Echo Modulation Studies of RAS-p21 Structures. D. Singel

R. R. Vold, *discussion leader*
NMR Structural Studies of Membrane Proteins. S. J. Opella
Site-Directed Spin Label Studies of Structure and Dynamics. W. L. Hubbell

J. Feigon, *discussion leader*
Carbohydrates in Aqueous Solution: NMR and Modeling Studies. L. Lerner

New Approaches to the Assignment of RNA Spectra. P. B. Moore
NMR Studies on Hammerhead RNAs. D. E. Wemmer

Atomic and Molecular Interactions

Colby-Sawyer College
New London, NH
J. J. Valentini, *Chair*
J. Muckerman, *Vice Chair*

JULY 20-24

J. Guest, *discussion leader*
Crossed-Beamed Studies of Radical Reactivities: Dynamic Renner-Teller Effects. K. Liu
Time-Dependent Iterative Schemes of Inversion. R. Kosloff
Stereodynamics of Velocity-Aligned Reactions. J. Simons

J. Hopkins, *discussion leader*
Femtosecond Spectroscopy of Molecular Liquids and Solids. K. Nelson
Variational Transition-State Theory for Reactions in the Condensed Phase. E. Pollak
M. Topp, *discussion leader*
Isomerism and Phase Transitions in van der Waals Clusters. S. Leutwyler
Large Amorphous Ice Clusters: Condensation, Structure, and Adsorbate Dynamics. V. Buch
Rotational and Vibrational Spectroscopy of Molecular Clusters. P. Felker

J. Garvey, *discussion leader*
Photoreactivity of Molecular Clusters. V. Vaidia
Dynamics of Cluster Reactions and Dissociation Following Photoexcitation and Multiphoton Ionization. W. Castleman

P. Aker, *discussion leader*
Laser Chemistry at Liquid Surfaces. K. Eiseenthal
Bouncing Gases off Liquids: Molecular Beam Studies of Energy Transfer and Chemical Reactions at Gas-Liquid Interfaces. G. Nathanson
Interaction-Structure Relationships in the Liquid-Vapor and Liquid-Monolayer Interfaces. S. Rice

D. Lemoine, *discussion leader*
Time-Resolved Probes of Energy Transfer at Surfaces. R. Cavanagh
Quantum Studies of Gas-Metal Sticking. B. Jackson

B. Koplitz, *discussion leader*
Nuclear Symmetry Restrictions in Bimolecular Reactions: A New Kinetic Isotope Effect. G. Gallene
Chemistry near the Zero Energy Limit: Statistics or Dynamics? M. Smith
Collisional Rovibrational Energy Flow in Cold Polyatomics. C. Parmenter

J. Muckerman, *discussion leader*
Solution Reaction Dynamics. K. Wilson

D. Tanner, *discussion leader*
Coherent Phase Control of Unimolecular Processes by Interference between One- and Three-Photon Excitation. R. Gordon
Efficient Laser-Induced Coherent Population Transfer in Atoms and Molecules: The STIRAP Concept and Applications. K. Bergmann
Quantum Dynamics of Atoms in Superintense Laser Fields. T. Uzer

Bioelectrochemistry

Tilton School
Tilton, NH
C. N. Rafferty, *Chair*
E. Neumann, *Vice Chair*

JULY 20–24

Mechanisms of Electric and Magnetic Field Reception in Animals

M. Blank, *discussion leader*
Anatomy of Electrorceptor Systems in Fish.
W. Heiligenberg

Structure and Function of Electrorceptor Systems. H. Zakon
Mechanism of Electric and Magnetic Field Sensitivity in Fish. A. Kalmijn

E. Neumann, *discussion leader*
Electrophysiological Basis of the Sensitivity of Electrorceptors. M. Bennet
Theoretical Limits to the Sensitivity of Electrorceptors. J. Weaver

Electrophysiological Measurements of Electrorceptors and Afferent Fibers. W. Clusin

Physiological Effects of External Electromagnetic Fields on the Nerve. H. Fishman

Sensing of Weak Fields by Modulation of Endogenous Neural Rhythms. H. Wachtel

Recent Evidence and Models Related to a Ferromagnetic Origin for Magnetic Field Sensitivity. J. Kirschvink

Behavioral Studies of Magnetic Field Reception. M. Bitterman

The Search for Magnetite-Based Magnetic Field Receptors and Proposed Models. M. Nesson

Recent Progress in the Electrophysiology of Vision. H. Stieve

Magnetic Field Responses of Visual Receptors of the Blowfly and Salamander. J. Phillips

Magnetic Field Induction of Neural Activity in the Trout. M. Walker

Magnetic Field Stimulation of the Ophthalmic Nerve of the Bobolink. R. Beason
Single-Cell Neural Recordings in Turtles Exposed to Weak Magnetic Fields. K. Lohmann

T. Tenforde, *discussion leader*
Magnetostimulation of Vision. E. Marg

Pineal Responses to Magnetic Fields. R. Reiter
Cooperativity of Light and Magnetic Fields in the Stimulation of the Pineal Gland. J. Olcese

Single-Cell Recordings of the Pineal Gland of the Pigeon Exposed to Switched dc Magnetic Fields. P. Semm

Corrosion—Aqueous

Colby–Sawyer College
New London, NH
D. Macdonald, *Chair*
J. L. Smiazek, *Vice Chair*

JULY 20–24

Novel Surface Analytical Techniques

A. Davenport, *discussion leader*
Comparison of Mass Spectrometric Surface Analysis Techniques. C. Becker
Spectrochemical Techniques in the Study of

Corrosion and Passivation. J. Robinson
Scanning Photoelectrochemical Microscopy. D. Williams

Instability and Chaos in Corrosion Systems

K. Sieadski, *discussion leader*
Fundamentals of Nonlinear Dynamics in Corrosion Systems. A. Markworth
Chaotic Behavior in the Initiation of Localized Corrosion in Metals. S. Sharland

Passivity: An Old Subject Revisited but Still Not Understood

R. Newman, *discussion leader*
Mechanisms of Passivation. B. Baroux
Passivity in Nonequilibrium Alloys. B. Shaw
Fundamental Studies of Interaction of Water and or Oxygen with Metal Surfaces. P. Norton

Fundamental Interactions at Metal–Electrolyte Interfaces

J. D. Sinclair, *discussion leader*
Phase Properties of Water at Interfaces. R. Nuzzo
Emergence of Atomic-Level Electrochemistry. M. Weaver

New Concepts and Techniques in Stress Corrosion Cracking Research

T. Devine, *discussion leader*
Progress in Testing Microscopic Models for Stress Corrosion Cracking. R. Newman
Fracture Reconstruction: A New View of an Old Problem. T. Kobayashi
Electron and Acoustic Probes of Stress Corrosion Cracking Events. W. Gerberich

Scanning Tunneling Microscopy—Corrosion Science at Nanometer Dimensions

H. Isaacs, *discussion leader*
In Situ STM of Corrosion in Silver–Gold Alloys. K. Sieradski
Nanometer-Scale Investigations of Surface Properties. K. Wickramasinghe

Photoelectrochemical Effects

W. Smyrl, *discussion leader*
Alternate Ways of Describing Photoelectrochemical Events. M. Orazem
Measurement and Interpretation of Photoeffects on Passive Films. P. Searson
Photochemical Effects in Nanometer-Scale Surface Phases. A. Goossens

How Extensive Is MIC in the Real World?

D. Pope, *discussion leader*
Mechanisms of MIC. D. White
MIC in Process Industries. D. Dzielwski

Can We Predict Corrosion Damage Functions?

D. D. Macdonald, *discussion leader*
Statistical versus Mechanistic Approaches to Life Prediction. R. Wei
Are Corrosion Predictions Credible? R. Staehle

Statistics in Chemistry and Chemical Engineering

New Hampton School
New Hampton, NH
R. D. DeVaux, *Chair*
R. W. Hoerl, *Vice Chair*

JULY 27–31

S. Wold, *discussion leader*
Multivariate Process Control. J. F. MacGregor
K. Kafadar, *moderator*

B. Hoadley, *discussion leader*
Bayesian Methods for Reliability. A.F.M. Smith
E. I. George, *moderator*

D. B. Rubin, *discussion leader*
Metal Analysis in Science. I. Olkin
D. F. Stroup, *moderator*

J. M. Minor, *discussion leader*
Neural Networks for Chemical Process Control. L. H. Ungar
R. W. Hoerl, *moderator*

A. C. Atkinson, *discussion leader*
Generalized—Generalized Additive Models. T. J. Hastie
D. E. Duffy, *moderator*

N. Kettaneh-Wold, *discussion leader*
Multivariate Methods for Environmental Chemical Analysis. P. K. Hopke
A. Smilde, *moderator*

R. D. DeVaux, *discussion leader*
Moving Regression: Analysis and Design of Experiments. V. V. Fedorov
J. Lucas, *moderator*

J. M. Steele, *discussion leader*
New Directions in Risk Assessment. J. C. Bailar
K. J. Hyver, *moderator*

R. D. Tobias, *discussion leader*
Interactive Statistical Graphics Using the X Windows System. A. Buja
K. J. Bandeen-Roche, *moderator*

Physical Electrochemistry

Colby–Sawyer College
New London, NH
H. D. Abruna, *Chair*
W. E. O'Grady, *Vice Chair*

AUGUST 3–7

H. S. White, *discussion leader*
Scanned Probe Microscopies: Capabilities and Limitations. B. Hamers
Studies of Electrochemical Interfaces with Electron Tunneling Techniques. J. Porter
Atomic Structure and Dynamics of Ordered Metal–Solid Interfaces by STM and IR. M. Weaver

Organic Monolayer Films: Structure, Reactivity, and STM and AFM Studies. M. Porter

L. Blum, *discussion leader*
Water Next to Metallic Surfaces. M. Berkowitz
Superconductivity: A Study from Its Surface. W. Little

Electrochemistry of Superconductors. B. Miller
Theory of Second Harmonic Generation and Its Relevance to Electrochemistry. W. Schmickler

R. Corn, *discussion leader*
Surface X-ray Scattering of Electrochemical Interfaces. M. Toney
Vibrational Spectroscopy at Interfaces. C. Korzeniewski
Use of Synchrotron Radiation in the Far-IR To Study Electrochemical Interfaces. A. Russell
Surface Intercalation Reactions at Semiconductor Surfaces. J. Hupp

MEETINGS

J. S. Facci, *discussion leader*
Studies of Langmuir-Blodgett Films and Liquid Interfaces with X-ray Synchrotron Radiation. J. Als-Nielsen
Photoinduced Electron Transfer in Langmuir-Blodgett Films. M. Fujihira
Long-Distance Electron Transfer in Self-Assembling Monolayers at Electrode Surfaces. C. Chidsey
Redox Chemistry in Mixed Monolayer Films. S. Creager

D. Rolison, *discussion leader*
Electrocrystallization of 1D Materials. M. Ward
Novel Developments in Organic Electrosynthesis. P. Pintauro

Vibrational Spectroscopy

Brewster Academy
Wolfeboro, NH
T. Keiderling, *Chair*
A. Campion, *Vice Chair*

AUGUST 3-7

Ultrafast Processes

W. Woodruff, *discussion leader*
Time-Resolved Optical and Vibrational Spectroscopy of Photochemical Systems. R. Mathies
Femtosecond Vibrational Spectroscopy of Chemical and Biological Reactions. R. Hochstrasser

Resonance Raman, Absorption, Fluorescence, and Electron Transfer Rates: Tying It All Together. A. Myers
Femtosecond Vibrational Spectroscopy of Proteins. J. L. Martin

UV Resonance Raman

N. Ferris, *discussion leader*
Far-UV Resonance Raman Scattering of Mid-sized Molecules. B. Hudson
UV Resonance Raman Scattering of Molecular Structure and Dynamics with Applications to Biological Molecules. S. Asher

Biological Applications (cw IR and Raman)

I. Levin, *discussion leader*
Raman Spectra of Biological Systems on Surfaces. T. Cotton
Quantitative Determination of Conformational Disorder in Biological Membranes by I-T-IR. R. Mendelsohn
Vibrational Studies of Ligands Bound to Proteins. B. Callendar

New Techniques

C. Marcott, *discussion leader*
Vibrational-Raman Optical Activity of Biological Molecules. L. Barron
Near-IR Raman Applications Using a CCD Detector and a Fast Spectrograph. M. Peltier
Raman Microscopy: Possibilities for Cell Studies. J. Greve
Inelastic Neutron Scattering Spectroscopy with a Pulsed Spallation Source. R. Hester

Other Dynamic Processes

B. Chase, *discussion leader*
Study of the Dynamics of the Photoreaction of Bacteriorhodopsin by Time-Resolved FT-IR Spectroscopy. F. Siebert
Ultrafast Electron Transfer in Metal Dimers Using Time-Resolved IR Spectroscopy. B. Dyer

Theoretical Aspects

J. Rabolt, *discussion leader*
Coherent Spectroscopies with Incoherent Light. A. Albrecht
Extreme Anharmonicity in Dynamics of Peptides and Proteins. R. Eiber
Normal-Mode Analysis of Protein Vibrational Spectra. S. Krimm

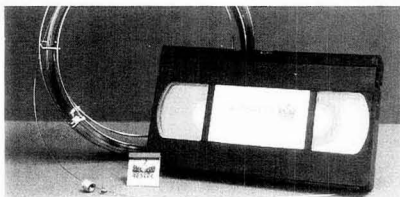
Liquid-State Dynamics

A. Campion, *discussion leader*
Ultrafast Raman Echo Studies of Solvent Vibration Interactions. M. Berg
Femtosecond-to-Millisecond Time-Resolved Spectroscopy of the Liquid State. K. Nelson
Modeling Time-Resolved Stimulated Light Scattering in Liquids. R. Long

Separation and Purification

Colby-Sawyer College
New London, NH
J. D. Sherman, *Chair*
F. Helfferich, *Vice Chair*

Learn Capillary Column Installation From The Experts



Introducing an instructional video that takes the mystery out of capillary column installation and maintenance.

This essential laboratory resource covers:

- carrier gas choice
- instrument preparation
- trouble-free installation
- leak checking
- setting carrier & gas flows
- column conditioning

We guarantee this 45 minute video will be the most useful instructional tool you'll ever see! Cat.#20490, \$149.00

RESTEK CORPORATION

110 Benner Circle, Bellefonte, PA 16823

From Caveman to Chemist Circumstances and Achievements

What was the connection between early chemistry and magic? What was the logic that made alchemists think they could make gold out of lead? Why were gases not recognized until the 17th century? Why did it take 49 years before Avogadro's hypothesis was accepted?

In *From Caveman to Chemist*, author Hugh Salzberg traces the oddities of chemistry, examining cultural and political influences on the ideas of chemists. He follows the evolution of chemistry from the Stone Age beginnings of ceramics and metallurgy, through the rise and decline of alchemy, to the culmination of classical chemistry in the late 19th century.

Chapters 1 through 9 lead from prehistoric technology, through ancient and medieval science to the study of chemicals and reactions that resulted in the 16th century birth of scientific chemistry. Subsequent chapters focus on key chemists such as Sala, Boyle, Black, Lavoisier, Dalton, Berzelius, Laurent, and Arrhenius as they developed the ideas that led to classical chemistry and the concepts of molecules, chemical reactions, homology, valence, and molecular formulas and structures, among others.

Twenty typical illustrations enhance the text. Six timelines and two maps help readers understand the influences of early history on chemistry.

Hugh W. Salzberg

300 pages (1991)

Clothbound: ISBN 0-8412-1786-6

Paperbound: ISBN 0-8412-1787-4

\$24.95

\$14.95

Order from: American Chemical Society, Distribution Office, Dept. 88
1155 Sixteenth St., N.W., Washington, DC 20036

or CALL TOLL FREE **800-227-5558**
(in Washington, D.C. 872-4363) and use your credit card!

CIRCLE 122 ON READER SERVICE CARD

AUGUST 10-14

Molecular Theory and Simulation of Adsorption

P. A. Monson, *discussion leader*
Computer Simulation of Gases Sorbed in Realistic Model Pores. W. A. Steele
Application of Density Functional Theories to Adsorption of Simple Fluid Mixtures. M. L. Rosinberg

Molecular Modeling of Adsorption and Transport in Zeolite Molecular Sieves. D. N. Theodorou

Thermodynamic Theories of Adsorption of Mixtures Based on Molecular Simulations. A. L. Myers

Adsorption Separation

R. L. Albright, *discussion leader*
New Adsorbents for Air Purification. C. Chang, N. N. Li

Pressure Swing Adsorption: The Next Distillation? K. S. Knaebel

Kinetically Controlled PSA Separations: Comparison with Membrane Separations. D. M. Ruthven

Membrane Separation

B. Bikson, *discussion leader*
Olefin Separations in Ion-Exchange Membranes. R. D. Noble
Nanoparticles, Nanocavities, and Nanospace Separation in Ceramic Membranes. M. A. Anderson

Process Models for Control of Separations Processes

J. R. Fair, *discussion leader*
Nonlinear Wave Theory for Dynamics of High-Purity Distillation Columns. Y.-L. Hwang

Dynamic Behavior and Multiple Steady States in Azeotropic Distillation Sequences. M. F. Doherty

Using Tray-to-Tray Models for the Control of Distillation Columns. J. B. Riggs

Use of Steady-State and Dynamic Process Models in the Development of Process Control Strategies: An Industrial Perspective. J. J. Downs

Bioseparation

J. C. Baker, *discussion leader*
Critical Displacer Properties in Protein Displacement Chromatography. S. M. Cramer

Competitive Protein Adsorption in Large-Scale Affinity Chromatography. N.-H. L. Wang

Separation and Focusing Biochemicals in Countercurrent Magnetically Stabilized, Fluidized Bed Adsorption Columns. M. A. Burns

Environmental Applications

New Separation Opportunities in Environmental Applications. G. E. Keller

New Commercial Processes

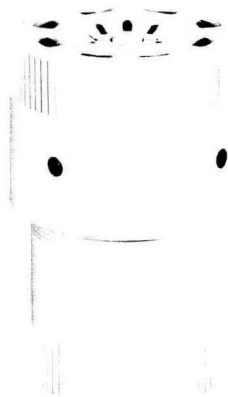
G. L. Hubred, *discussion leader*
Solvent Pulp: Promise and Performance. R. Katzen

Coupling the Separation Technologies into BHP's Resource Processes: The Engineering-Economic Dimensions. G. Rigby

Immunoaffinity Process for Production of Activated Protein C, A New Plasma-Derived Antithrombotic Agent. C. L. Orthner

Microwave Digestion Bombs

In two sizes, 23 ml and 45 ml.



Rapid microwave heating can now be used to speed the treatment of inorganic, organic and biological samples in strong acid or alkali media using Parr Microwave Digestion Bombs. These bombs have a microwave-transparent outer body which encloses an inner Teflon sample holder, allowing microwave energy to be used to develop high internal temperatures and pressures without overheating the outer wall. Samples can be dissolved with heating times of one minute or less with complete safety when the bombs are used as directed. Call or write for Bulletin 4700 for complete technical details.



PARR INSTRUMENT COMPANY

211 Fifty-third Street • Moline, IL 61265 • Telex: 270226
Phone: 309-762-7716 • 800-872-7720 • Fax: 309-762-9453

CIRCLE 108 ON READER SERVICE CARD

ACS Software

High-quality software programs for the personal computer that meet the standards you expect from the ACS

For information about ACS SOFTWARE, call TOLL FREE (800) 227-5558 or write to:

American Chemical Society,
Marketing Communications,
1155 Sixteenth Street, N.W.,
Washington, D.C. 20036

Today's Best Source of Quantitative Numerical Data of Physics and Chemistry JOURNAL OF Physical and Chemical Reference Data

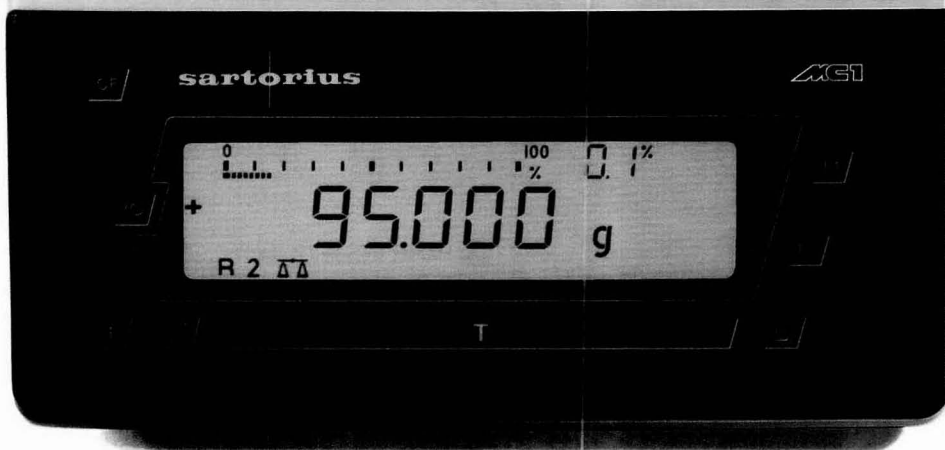
Editor, David R. Lide, Jr.
National Institute of Standards
and Technology

Published BIMONTHLY by the American Chemical Society, the American Institute of Physics, and the National Institute of Standards and Technology, JPCRD provides you with compilations and reviews produced under the National Standard Reference Data System of the National Institute of Standards and Technology.

JPCRD contains recommended values, uncertainty limits, critical commentary on methods of measurement, and full references to the original papers.

Call Toll Free 1-800-333-9511 and charge your order! Outside the U.S. call (614) 447-3776, or write:

American Chemical Society,
Member and Subscriber Services
P.O. Box 3337
Columbus, OH 43210 U.S.A.



From touchdown to full stop in a Sartorius second

Hitting the right mark at the right time is as crucial for precision weighing as it is for precision flying. It requires a careful balance of accuracy and speed.

Time spent waiting for a readout to stabilize can rattle your patience and shake your confidence in the final results. If the digital readout is inconclusive how can you be certain?

Now, the latest top-loading, analytical and semi-micro balances from Sartorius integrate MC 1 technology—a functioning intelligence beyond microprocessors—designed to filter out

noise, vibrations, and other disturbances. This 40 MHz microcomputer is as powerful as most desktop computers. The result is stabilization in *half* the time it would take any competitor's balance.

To land the most accurate results in a Sartorius second, fly right with MC 1 technology.

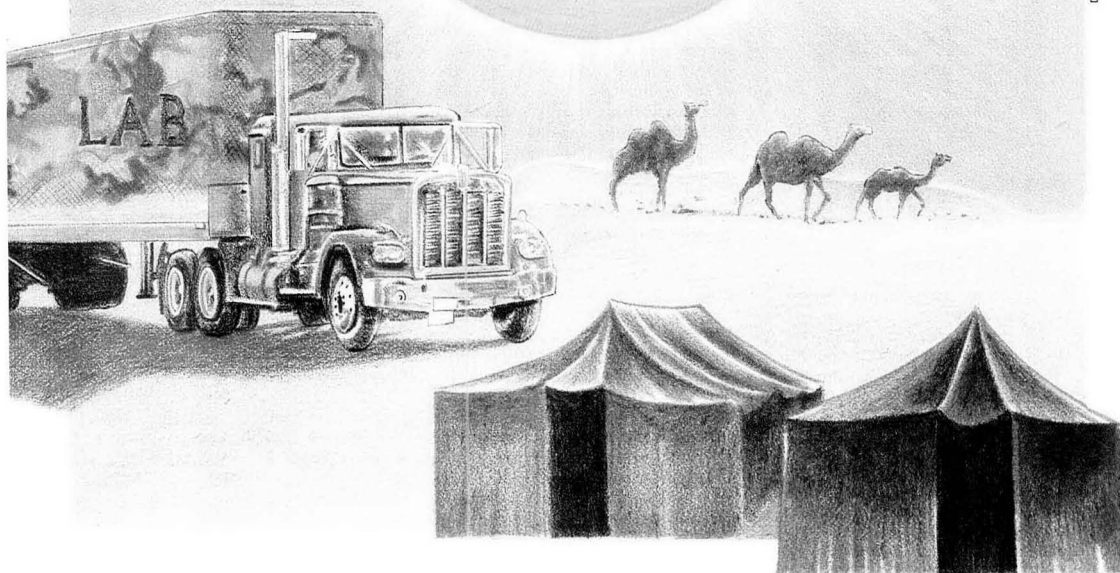
For more information on these balances, call, write or circle the number below.

Sartorius Instruments,
1430 Waukegan Rd., McGaw Park, IL 60085.
Phone: 800-544-3409 FAX: 708-689-2038.

sartorius

Sudden. Smart. Sartorius.

CIRCLE 125 ON READER SERVICE CARD



Have LC Lab, Will Travel

Testing Propellant Stability after Operation Desert Storm

At the conclusion of Operation Desert Storm, one of the problems facing the U.S. Navy was ensuring that unused propellant was safe to ship home after being in the Saudi Arabian desert. Modern gun propellants had never before been used under such severe desert conditions, and there was no way to predict how the propellant might have been affected. Furthermore, the war lasted 100 hours instead of the expected 100 days, and the majority of the gun ammunition sent to the Gulf was not used but instead was stored temporarily in ammunition dumps.

Under normal conditions, the propellant would have been sent to the Naval Surface Warfare Center, Indian Head, MD, to determine the stabilizer content. However, Marine and Navy officials believed that operational readiness would be jeopardized if the propellant were shipped back to the United States before it was tested.

Gail Y. Stine
Propellant Analysis Branch
Indian Head Division, Naval Surface
Warfare Center
Indian Head, MD 20640

I had the opportunity last spring to spend 33 days in the desert analyzing gun propellant using a mobile LC laboratory. As manager of the Propellant Analysis Branch at the Naval Surface Warfare Center, I was given two months to design and implement

FOCUS

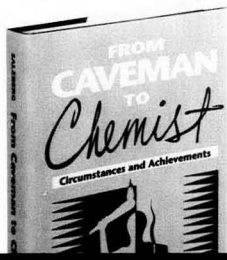
a mobile lab in the desert of Saudi Arabia. Together with Irma Dal-Canton, a physical science technician, we decided what resources would be needed for our journey to Saudi Arabia. Once there, we worked amid severe environmental conditions, including heat and blowing sand, and cultural restrictions against women that limited our freedom of movement.

We set up the lab at an ammunition dump operated by the Marine

Corps near Al Mishad, 60 miles south of the Kuwaiti border. Approximately 70% of the gun propellant that was not used during the war was unloaded there for testing, inventory, and shipment home. We needed to determine whether the propellant could be loaded onto Marine expeditionary ships bound for other missions, shipped home for further tests and storage, or destroyed on site.

All instrumentation, equipment, and consumable supplies had to be purchased and shipped to the site within two months. Planning efforts revolved around the fact that there would be no opportunity to procure spare parts or supplies in that part of the world. In addition, instrumentation and supplies had to be packaged to sustain harsh shipping conditions. The crates of equipment remained on the tarmac at Dhahran airport for 10 days before being transported by truck over unpaved roads 150 miles into the desert.

The lab was set up in one half of a semitrailer equipped with electricity and an air conditioner. The Marines furnished a portable generator to provide electrical power. A fuel truck came by once a day (if we were lucky)



From Caveman to Chemist

Circumstances and Achievements

What was the connection between early chemistry and magic? What was the logic that made alchemists think they could make gold out of lead? Why were gases not recognized until the 17th century? Why did it take 49 years before Avogadro's hypothesis was accepted?

In *From Caveman to Chemist*, author Hugh Salzberg traces the oddities of chemistry, examining cultural and political influences on the ideas of chemists. He follows the evolution of chemistry from the Stone Age beginnings of ceramics and metallurgy, through the rise and decline of alchemy, to the culmination of classical chemistry in the late 19th century.

Chapters 1 through 9 lead from prehistoric technology, through ancient and medieval science to the study of chemicals and reactions that resulted in the 16th century birth of scientific chemistry. Subsequent chapters focus on key chemists such as Sala, Boyle, Black, Lavoisier, Dalton, Berzelius, Laurent, and Arrhenius as they developed the ideas that led to classical chemistry and the concepts of molecules, chemical reactions, homology, valence, and molecular formulas and structures, among others.

Twenty topical illustrations enhance the text. Six timelines and two maps help readers understand the influences of early history on chemistry.

About the Author

Hugh W. Salzberg taught chemistry at the City University of New York for 35 years and offered courses in the history of chemistry over a period of 20 years. *From Caveman to Chemist* reflects his dual passions for chemistry and history and his profound admiration of the great minds that developed the ideas of chemistry.

Hugh W. Salzberg, Editor

300 pages (1991)
Clothbound: ISBN 0-8412-1786-6
\$24.95
Paperbound: ISBN 0-8412-1787-4
\$14.95

O R D E R F R O M

American Chemical Society
Distribution Office, Dept. 68
1155 Sixteenth St., N.W.
Washington, DC 20036

or CALL TOLL FREE

800-227-5558

(in Washington, D.C. 872-4363) and use your credit card!

FOCUS

to refill the generator. A civilian carpenter constructed lab benches, and we unpacked and set up the instruments and equipment. The laboratory was operating within two days of the equipment's arrival at the ammunition dump, and we experienced little downtime because of problems resulting from the harsh shipping conditions.

The propellant analysis involved extraction with acetonitrile followed by filtration using 0.45- μ m filters and subsequent analysis by HPLC (see *Anal. Chem.* **1991**, 63, 475 A). We used a Hewlett-Packard 1050 HPLC system equipped with a quaternary pump, autosampler, and UV detector set at 254 nm. An HP ChemStation was used for data processing and report generation.

Stabilizer and stabilizer degradation products were analyzed and total effective stabilizer determined for each propellant lot analyzed. Based on a comparison of initial stabilizer content and the history of the stabilizer depletion rate for each lot, we were able to decide which lots should be destroyed and which were safe for shipment.

Using an assembly line approach, we extracted and analyzed samples 12 hours a day, seven days a week. Unfortunately, the autosampler could not run unattended overnight because the generator and the fuel supplies were not reliable. Even with this limitation, during a four-week period, we analyzed 450 lots of gun propellant and determined that 15 had below acceptable levels of stabilizer. These lots were destroyed.

Concurrent with our chemical analysis, other members of the Navy's gun propellant surveillance program began to inventory and inspect the packaging conditions of the propellants shipped to the desert. Most of the 15 lots deemed unsafe for shipping had damaged crates that allowed some propellants to be exposed to the environment.

We thus concluded that the propellant lots did not deteriorate as a result of harsh desert conditions unless the packaging container deteriorated or was broken. The propellant was stored in stacks on pallets in the open desert, without any shade or protection, for several months. During winter, temperatures ranged from 40 °F at night to 70 °F during the day; during spring and summer, temperatures rose as high as 115 °F in the shade. We became concerned not so much about the short-term effects (because the data indicated that temperature was not a problem) but about the possible long-term effects of temperature cycling on propellant stability. All propellant stored in the desert has been marked so that it can be closely monitored during future stability testing. We have established a baseline for this monitoring as a result of our on-site desert tests.

Although the environment did not substantially affect the propellant's stability, it did test the endurance of the analysts. The instrumentation was air-conditioned and resided in a reasonably sand-free environment. However, the lodging provided by the Marines posed a real challenge for two women civilians. We lived in a



Sleeping quarters during our stay in Saudi Arabia. The Marine encampment consisted of rows of tents with sand dunes bulldozed around them.

tent in a temporary base camp where there were three women Marines and more than 200 male Marines. It was difficult to keep clean and wash clothes using bottled water. On most days the smoke from the burning Kuwaiti oil fields blotted out the sun and kept temperatures down to 80 °F, although during daylight hours it could get so dark from the smoke that flashlights were required. When the wind shifted and the sun came out, temperatures soared to above 115 °F. Dust storms occurred frequently and coated everything with a fine powder similar to talc, unlike the coarse sand to which most Americans are accustomed. Not only were the flies tenacious, but occasionally scorpions, poisonous spiders, and vipers tried to make their home in our belongings.

Because of the cultural restrictions imposed on women, we were forbidden to drive or to be unescorted in public, and our clothing had to completely cover our arms and legs. We overcame these restrictions by wearing Marine uniforms in public and prevailing upon the male Marines and civilians to act as our chauffeurs.

Under the harsh environmental conditions it was difficult to keep the sand out of the lab area. We vacuumed the computer every few hours in an effort to keep it clean. Sand clogged the LC pumps, and we faced the dilemma of whether to open the pumps to clean them, risking the introduction of even more sand and grit. Brownouts were frequent, and the computer and the data station malfunctioned when temperatures inside the trailer reached 90 °F.

It became imperative to learn how to operate and maintain the generator. Temperature control was the greatest problem. When the sun came out from behind the smoke, it baked the metal trailer, and inside temperatures rose to close to 100 °F despite air conditioning. This problem was mitigated by using camouflage netting over the entire trailer and operating equipment during the coolest time of day.

In the end we were able to analyze the propellant and enable the Marines to load their expeditionary ships in record time. By employing a mobile lab in the desert, we proved that it is feasible to deploy a similar mobile lab elsewhere in the world.

We have designed a mobile lab that will begin operating in late spring. This lab will be used to test the stability of gun propellants stored at various naval bases around the world. Results generated from this new facility will reduce military response times and logistical problems and at the same time increase the operational readiness of our armed forces.



Gail Y. Stine is an analytical chemist for the Indian Head Division of the Naval Surface Warfare Center (NSWC) where she manages the Propellant Analysis Branch. She received an M.S. degree in analytical chemistry from Georgetown University and has been employed by the NSWC since 1985. She is currently developing new chromatographic methods and techniques to further characterize propellants and explosives.

The Best Instruments In The World

for absolute macromolecular characterization.

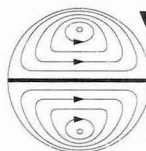
OUR DAWN® instruments will measure the absolute molecular weight of your polymers directly and easily. Couple our systems to your *existing* GPC/SEC line and you'll be determining absolute weights, sizes and distributions without having to rely on polymer standards, column calibration, "universal" constants, or flow rate effects.

You can even determine branching ratios, molecular sizes, and conformations in minutes—without making any assumptions. The DAWNs can also be used to observe polymerization and kinetics *as they occur*, or for immediate quality control "fingerprinting" of complex polymer solutions.

Please contact us for a complete literature package. It won't take us long to delight you with the best service, support—and instruments—in the world!



Call us at
805-963-5904
for FREE literature!



**Wyatt
Technology
CORPORATION**

802 East Cota Street • Santa Barbara, CA 93103
Telephone: (805) 963-5904 • FAX (805) 965-4898

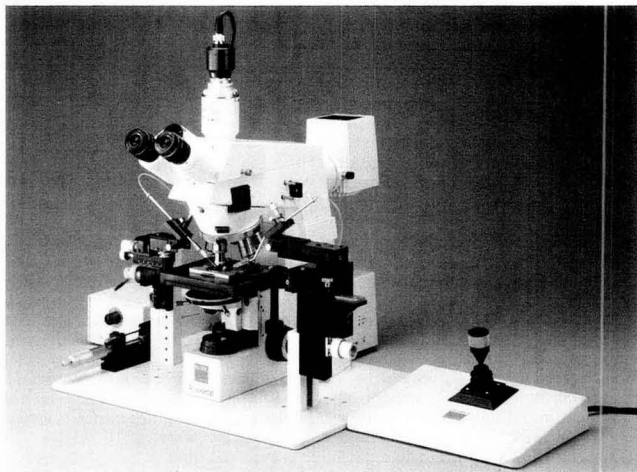
Please visit us at FASEB Booth #2104 and ACS Booth #1425

© 1991, Wyatt Technology Corporation. All rights reserved.

CIRCLE 150 ON READER SERVICE CARD

ANALYTICAL CHEMISTRY, VOL. 64, NO. 7, APRIL 1, 1992 • 455 A

NEW PRODUCTS



Axioskop FS, a fixed-stage microscope, features smooth movement of the microscope tube via an internal counterbalance mechanism. The microscope is suited for biological, materials science, and QC applications. Carl Zeiss

404

Instrumentation

Spectrophotometer. Series 3000 UV-vis scanning spectrophotometers feature a 2-nm optical bandwidth over the 190–1000-nm range and scan speeds ranging from 30 to 4000 nm/min. Automatic calibration of wavelength also is included. Cecil

401

Electrophoresis. Ministaltic pump produces pulse-free liquid flow rates from 10 to 1600 mL/min using a single pump head. It is designed for gel formation and circulation, buffer circulation, and temperature control during electrophoresis procedures. Manostat

402

Water system. EASYpure ultrapure system provides water for HPLC, AA, and GC/MS applications. The system uses reverse osmosis, deionized, or distilled water as the feed source. Barnstead/Thermolyne

403

Water purification. Mega-Pure water purification stills are constructed of Pyrex, Vycor, or Teflon to

minimize contamination. The stills remove most dissolved solids as well as all pyrogens and biological impurities from tap and pretreated water, thereby meeting USP XXII standards. Cole-Parmer Instrument

405

LC. LC-10AD pump, equipped with microvolume plungers, a high-speed plunger drive, and automatic pulse suppression, provides pulse-free solvent delivery. The plunger and pump are completely aligned when the pump head is installed. Shimadzu Scientific Instruments

406

Hg detection. Series 520 mercury sampler provides exact worker exposure as a time-weighted average. Detection of Hg at, above, or below the levels stipulated by NIOSH and OSHA can be achieved. No sampling pump is required. SKC

407

FT-IR. FTS 25PC FT-IR spectrometer, equipped with a PC data system, features computer-selectable resolutions to 0.5 cm^{-1} , an air-bearing Michelson interferometer, a water-

cooled source, and a computer-controlled source aperture. Bio-Rad

408

Controller. Series 4850 controllers can be programmed to monitor and control all functions in a chemical reactor system—including heating, cooling, ramp, and soak programs—and stirring speeds, safety procedures, and data logging. Parr Instrument

409

Oxygen analysis. TMO2D oxygen analyzer combines the thermoparamagnetic technology of the TMO2 oxygen transmitter with the features of a microprocessor-based electronic display. The TMO2 compensates for variation in background gas composition; the electronic display controls solenoid valves for automatic calibration at preset time intervals. Panametrics

410

Evaporator. RotoStill evaporators, available as 50- and 100-L units, are designed for process applications that require safe handling and distillation of large volumes of flammable solvents. Safety-coated borosilicate glass provides maximum protection. Schott Process Systems

411

Temperature control. DC-25 dual-temperature circulator provides heating and cooling simultaneously and is designed for use with the One-Step extractor/concentrator. The cooling loop provides temperature control from -5°C to 35°C for condensing, and the heating loop from ambient temperature to 150°C for extractions. Neslab

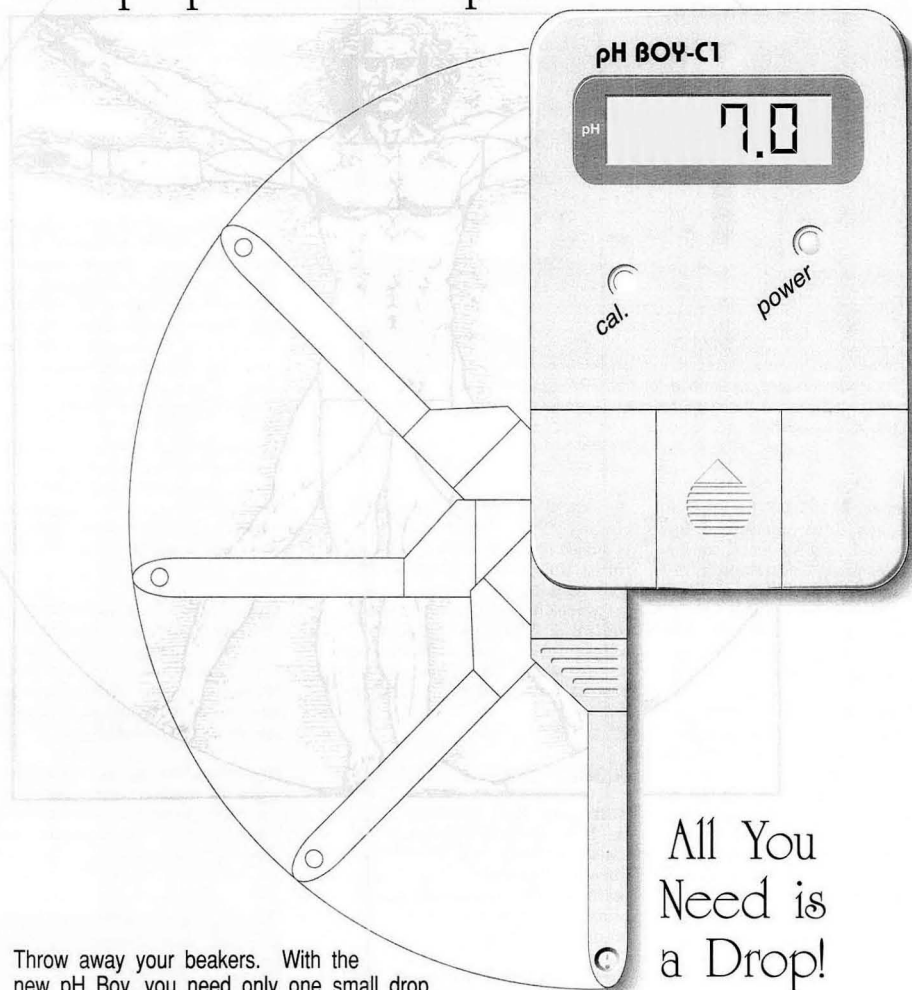
412

FT-IR. In situ process monitoring system, based on FT-IR emission and transmission spectroscopies, features customized optics for beam control, automated subsecond sequential scanning, and a 10-m cell for extractive concentration measurements. Advanced Fuel Research

413

For more information, please circle the appropriate numbers on one of our Readers' Service Cards.

Keep pH in Proportion



Throw away your beakers. With the new pH Boy, you need only one small drop of liquid to determine pH. This solid-state, ISFET (Ion Sensitive Field Effect Transistor) device eliminates the need for fragile glass electrodes. The pH probe folds neatly into a meter case sized like a pocket calculator. The portable pH Boy can be carried in a shirt pocket. It is powered by commonly available batteries which are conserved by an automatic shut-off feature.

Each pH Boy includes a fabric carrying case and calibration standards in convenient plastic dropper bottles.

All You
Need is
a Drop!

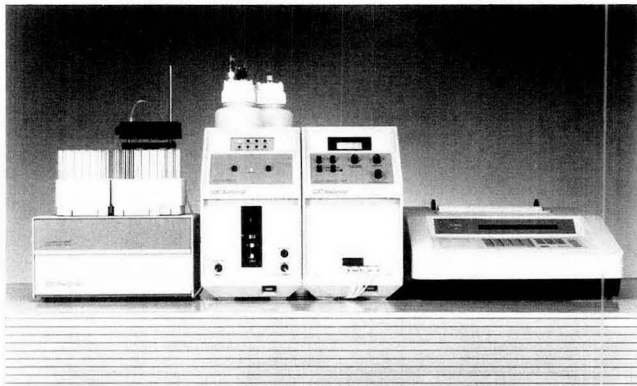
Helping Scientists Do Science.

BAS
Bioanalytical
Systems, Inc

USA 2701 Kent Avenue, West Lafayette, IN 47906, PH (317) 463-4527, FAX (317) 497-1102
Europe Fruithoflaan, 18, B-2500 Lier (KH) Belgium, PH (32) 3 482 1376, FAX (32) 3 482 4636

CIRCLE 17 ON READER SERVICE CARD

NEW PRODUCTS



Mercury analysis system, optimized for the EPA-approved cold vapor method, allows the determination of mercury down to 1-ppt levels with typical precision of < 2% RSD. LDC Analytical

418

Spray dryer. Model GS-31 organic solvent spray dryer, designed for flammable and toxic solvents, can be used for pilot plant testing and in research laboratories. The apparatus features a closed system that circulates nitrogen gas to spray, dry, collect sample, and recover solvent in an inert atmosphere. Yamato

414

X-ray diffraction. D 5000 HR polycrystalline diffractometer determines crystalline structure, layer orientation and thickness, chemical composition, and bond lengths of single- or multilayer thin films. The system incorporates a 4-bounce incident beam monochromator and reduction gearing to achieve accurate resolution at a minimum step size of 0.002° for theta and 2-theta drives. Siemens

415

Surface analysis. Model 7000 TOF-SIMS system is designed for organic surface characterization. The analyzer's wide mass range and a 10-kV postacceleration detector provide enhanced sensitivity for high masses. Perkin Elmer

416

Software

DNA. DNAscan software for Master-Scan-II systems generates the base sequence from autoradiograms or other DNA sequencing gel images. The software operates under Microsoft Windows. Scanalytics

417

Chromatography. Version 3.0 of Expert Ease software, designed for a

variety of separation processes including HPLC, GPC, IC, CE, and GC, is suited for high-throughput laboratories that require large-scale system control and networking. The software offers calibration weighting, control of HP5890 GC and GC 7673 autosamplers, and additional external events for the Satellite interface. Waters Chromatography Division

419

Manufacturers' Literature

Software. Bulletin 3251 discusses the MYCROADVANTAGE PC workstation software and its ability to reduce configuration time, increase plant security and workstation flexibility, and improve operator performance. 8 pp. Moore

420

Environmental analyses. *Meeting the Challenges of Environmental Analysis* includes information on the analysis of toxic industrial solvents, pesticides, metals, and volatile organic chemicals. Solutions to complex environmental problems, from sample cleanup to compound identification and confirmation, are presented. Varian

421

Superconductivity. Technical literature covers a variety of topics, including the automation of low-resistance measurements and resistance measurements on high-temperature superconductors. Three different high-temperature superconductor measurement and test systems are outlined. Keithley

422

Wall chart. "OSHA Concentration Limits for Gases" wall chart lists approximately 700 compounds that have established OSHA-permissible exposure limits. The chart incorporates changes cited in the U.S. Code of Federal Regulations (CFR 29, Part 1910). Foxboro

423

Catalogs

Chromatography. Catalog features more than 6900 products from 40 manufacturers. Technical information is highlighted in chart format to facilitate selection of HPLC fittings, autosampler vials, septa sizes, and TLC paper. Solid-phase extraction techniques, column guides, and more than 300 chromatograms are included. Scientific Products

424

Microwave. Catalog of microwave heating products features a line of power packs (2450 and 915 MHz), instrumentation and waveguide accessories and components, and microwave applicators. Cober Electronics

425

Chemicals. Catalog features biochemicals, organic compounds, and diagnostic reagents. Bioactive peptides, immunochemicals, electrophoresis reagents, environmental standards, and protein analysis reagents are included. Sigma

426

Proteins. Catalog describes chromatography products and techniques for the isolation and purification of proteins, peptides, and nucleic acids. The Nest Group

427



LI-610 generates and maintains an exact dew point in a controlled air stream. It is designed for field calibrations of humidity sensors and H₂O IR gas analyzers. LI-COR

428

NUPRO Valves and Filters for Analytical Applications

NUPRO Valves and Filters offer these design and performance choices:

- **End Connections:** SWAGELOK® Tube Fittings, NPT, Tube Stub, Weld, CAJON VCO® & VCR®
- **Service Ratings:** vacuum to 6000 psi; temperatures to 900°F

STOCKED FOR IMMEDIATE
DELIVERY BY AUTHORIZED SALES
AND SERVICE REPRESENTATIVES.
Nupro Company, 4800 East 345th St.,
Willoughby, OH 44094



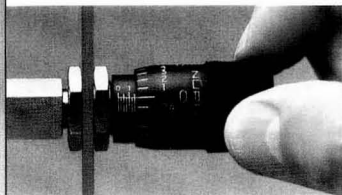
SWAGELOK® — TM Crawford Fitting Company
CAJON VCO® & VCR® — TM Olson Company
© 1992 Swagelok Co. all rights reserved N-55



METERING

Valves for precise flow control in laboratory and instrument systems

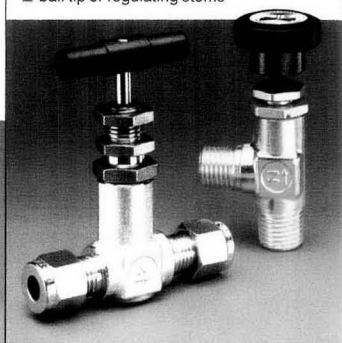
- accurate, repeatable flow adjustment with no initial surge
- compact, low dead space
- stem threads removed from system



SHUT OFF

Compact valves for reliable flow regulation and shut off

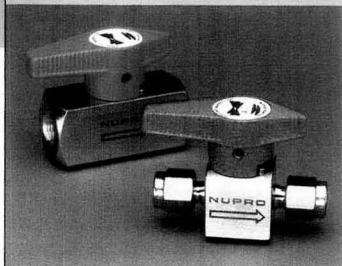
- stem threads removed from system fluid
- compact designs
- ball tip or regulating stems



FILTRATION

Inline and tee type filters to protect instruments by removing hard particle contamination from fluid lines

- choice of sintered and wire mesh elements from 0.5 to 440 microns
- compact designs
- all metal construction

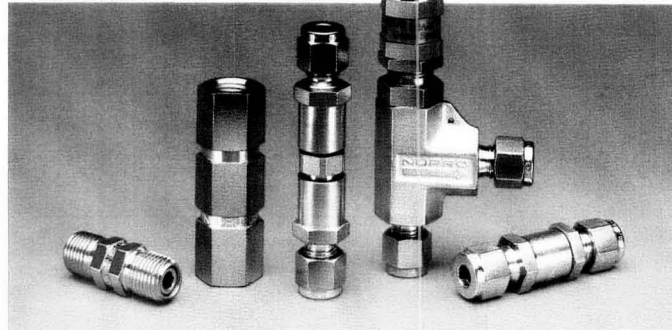


- quick-acting, 1/4 turn
- full flow
- easy maintenance

CHECK & RELIEF

Relief valves open at pre-set pressure; check valves allow unidirectional flow control

- cracking pressures 1/3 to 6000 psi
- smooth floating poppet
- positive back stop



CIRCLE 96 ON READER SERVICE CARD

ANALYTICAL CHEMISTRY, VOL. 64, NO. 7, APRIL 1, 1992 • 459 A

LABORATORY SERVICE CENTER

NMR ANALYSIS

Multinuclear Multifield
Liquid or Solid State
GLP Compliance
Spectral Data Services, Inc.
818 Pioneer, Champaign, IL 61820
(217) 352-7084 Fax (217) 352-9748

FREE DATA, FAST

To quickly amass data on all of the products you need, consult the Lab Data Service section on our *Analytical Chemistry* reader reply card insert.

LABORATORY SERVICE CENTER

(Equipment, Materials, Services, instruments for Leasing), Maximum space — 4 inches per advertisement. Column width, 2-3/16"; two column width, 4-9/16". Artwork accepted. No combination of directory rates with ROP advertising. Rates based on number of inches used within 12 months from first date of first insertion.

Per inch: 1" — \$185; 12" — \$130;
24" — \$175; 36" — \$170; 48" — \$165.

CALL OR WRITE JANE GATENBY

ANALYTICAL CHEMISTRY

1599 Post Road East
P.O. Box 231
Westport, CT 06881
203-256-8211
FAX: 203-256-8175

HELP WANTED ADS

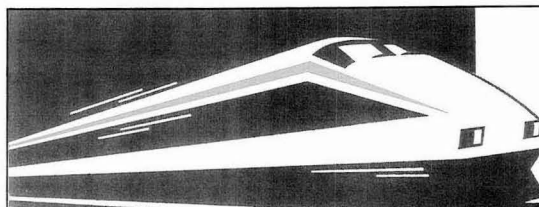
ROP display at ROP rates. Rate based on number of insertions within contract year. Cannot be combined for frequency.

Unit	1-TI	6-TI	12-TI
1" (25 mm)	\$210	\$190	\$180
	24-TI	48-TI	72-TI
	\$170	\$160	\$150

CALL OR WRITE JANE GATENBY

ANALYTICAL CHEMISTRY

1599 Post Road East
P.O. Box 231
Westport, CT 06881
203-256-8211
FAX: 203-256-8175



STN Express®: the fast
track to searching
scientific databases



Easy connection to STN®

Step aboard STN Express® (for the IBM® AT and PS/2 and Apple® Macintosh), the software that will quickly log you on to STN International® and help you prepare your questions *offline*, before online charges are incurred. Then you can upload and execute your search and produce *print-quality output of both text and graphics*.

Easy structure searching

You can draw structures freehand or with templates or venture into molecular modeling. Once you've defined the structure the way you pictured it, *search for it among the 10 million structure diagrams in the CAS Registry file*. Was there a match? If so, that's a valuable piece of information. No match? Knowing that could be *invaluable*.

Let STN Express introduce you to online searching and STN International. They'll take you searching where you've never been before.

YES! Please send me the FREE STN Express evaluation package.

Name

Position

Address

Phone

STN International, c/o CAS, Marketing, Dept 33392, P.O. Box 3012, Columbus, Ohio, 43210-0012
FOR FASTER SERVICE call 614-447-3731, 800-933-4350, or FAX this completed coupon to 614-447-3713.

INDEX TO ADVERTISERS IN THIS ISSUE

CIRCLE INQUIRY NO.	ADVERTISERS	PAGE NO.
3.....	*Alltech Associates, Inc. Chromad	442A
1.....	American Association for the Advancement of Science	447A
5.....	Analytical Products Group, Inc.	413A
14, 15.....	*Bacharach Analytical Group	441A
17.....	Bioanalytical Systems, Inc. Kissinger Advertising Associates	457A
30.....	Digital Equipment Corporation	418A
	Mullen	
40.....	*Fisher Scientific	IFC
	Tech-Ad Associates	
64.....	*Isco, Inc. Farneaux Associates	439A
72.....	Kimble/Kontes	438A
	Lab-Ad Associates	
80.....	Leco Corporation	OBC
92.....	Malvern Instruments Ltd.	442A
85.....	*Mattson Instruments, Inc. Fourier Court Advertising	414A
90.....	*Metrohm, Ltd. Ecknauer + Schoch Werbeagentur ASW	424A
87.....	*Mettler Instrument Corporation	433A
	Gilbert, Whitney & Johns, Inc.	
146.....	*Millipore/Waters Chromatography	437A
	Lehman Millet Incorporated	
98.....	*National Institute of Standards & Technology	438A
94.....	*Nicolet Analytical Instruments	420A
96.....	*Nupro Company/A Swagelok Company	459A
	Falls Advertising Company	
104.....	O.I. Analytical	422A
108.....	*Parr Instrument Company	451A
	Stobie Brace Marketing Communications	
110, 111.....	*Perkin-Elmer Corporation	435A
	Keiler Advertising	
122.....	*Restek Corporation	450A
125.....	*Sartorius Instruments	452A
	Dunlop, Schultz & Associates	
140.....	*Valco Instruments Company, Inc.	416A
	Technical Advertising Associates	
142.....	*Varian	426A
	Lanig Associates	
146.....	Waters Chromatography, Div. of Millipore ..	437A
	Lehman Millet Incorporated	

CIRCLE INQUIRY NO.	ADVERTISERS	PAGE NO.
148.....	Whatman	428A
150.....	*Wyatt Technology Corporation	455A

Directory section, see page 460A.
* See ad in ACS Laboratory Guide.

Advertising Management for the American Chemical Society Publications

CENTCOM, LTD.

President

James A. Byrne

Executive Vice President

Benjamin W. Jones

Robert L. Voepel, Vice President

Joseph P. Stenza, Production Director

1599 Post Road East
P.O. Box 231
Westport, Connecticut 06881-0231
(Area Code 203) 256-8211
Telex No. 643310
Fax No. 203-256-8175

ADVERTISING SALES MANAGER

Bruce E. Poorman

ADVERTISING PRODUCTION MANAGER

Jane F. Gatenby

SALES REPRESENTATIVES

Philadelphia, PA. CENTCOM, LTD. GSB Building, Suite 405, 1 Belmont Ave., Bala Cynwyd, PA. 19004. Telephone: 215-667-9666, FAX: 215-667-9353

New York/New Jersey Dean A. Baldwin, John F. Raftery, CENTCOM, LTD., Schoolhouse Plaza, 720 King Georges Post Road, Fords, NJ 08863, Telephone: 908-738-8200, FAX: 908-738-6128

Westport, CT/Boston, MA. Edward M. Black, CENTCOM, LTD., 1599 Post Road East, P.O. Box 231, Westport, CT 06881-0231. Telephone: 203-256-8211, Telex 643310, FAX: 203-256-8175

Cleveland, OH./Atlanta, GA. Bruce E. Poorman, CENTCOM, LTD., 325 Front St., Suite 2, Berea, OH 44017. Telephone: 216-234-1333, FAX: 216-234-3425

Chicago, IL./Houston, TX. Michael J. Pak, CENTCOM, LTD., 540 Frontage Rd., Northfield, Ill. 60093. Telephone: 708-441-6383, FAX: 708-441-6382

West Coast/Denver, CO. Paul M. Butts, Jay S. Francis, CENTCOM, LTD., Suite 808, 2672 Bayshore Parkway, Mountain View, CA 94043. Telephone: 415-969-4604, FAX: 415-969-2104

United Kingdom, Scandinavia and Europe (Except: Germany, Switzerland, Austria) Malcolm Thiele, Technomedia Ltd., Wood Cottage, Shurlock Row, Reading RG10 0QE, Berkshire, England. Telephone: 0734-343302, Telex #848800, FAX: 0734-343848

France, Belgium, The Netherlands, Spain, and Italy Yvonne Melcher, Bel Air Building 331A, 58 Rue Pottier, 78150, Le Chesnay, France. Telephone: (1)34-62-00-03, FAX: (1)34-62-95-07

Germany, Switzerland, Austria InterMedia Partners, GmbH, Katernberger Strasse 247, 5600 Wuppertal #1, Germany. Telephone: (0202) 711091, FAX: (0202) 712431

Tokyo, Japan Sumio Oka, International Media Representatives Ltd., 1-11-5-502, Tamazutsumi, Setagaya-ku, Tokyo 158 Japan. Telephone: 502-0656, Telex #22633, FAX: 5706-7349

Asia (Except Japan) Bruce E. Poorman, CENTCOM, LTD., 325 Front St., Suite 2, Berea, OH 44017. Telephone: 216-234-1333, FAX: 216-234-3425

South America Bruce E. Poorman, CENTCOM, LTD., 325 Front St., Suite 2, Berea, OH 44017. Telephone: 216-234-1333, FAX: 216-234-3425

Gain Hands-on Experience in MS!

**Enroll today in this intensive short course offered by the
American Chemical Society—**

Mass Spectrometry Principles and Practice

Michigan State University • East Lansing, MI

Only Session in 1992!

June 15-19, 1992

In Just 3½ Days, You'll Learn:

- How to Interpret Mass Spectral Data.
- Which Compounds are Amendable to Various MS Techniques.
- How to Introduce Samples, Collect Data by Scanning, and Process Data with a Data System.
- How to Search on MSD and ITD Data Systems and on Terminals Connected to the Chemical Information Service in Washington, D.C.
- How to Tune a Mass Spectrometer, Maintain it, Introduce Samples, Collect Data by Scanning, and Process Data with a Data System.
- How to Operate a Variety of Benchtop GC/MS, Spectrometers; Each Will Be Equipped with an Integrated Data System.
- AND MUCH, MUCH MORE!

Register Today!

Enrollment in this exceptionally popular course is limited to just 24 participants per session. To register, phone the Continuing Education Short Course Office at (800) 227-5558 or (202) 872-4508. Or, for additional information, mail in the coupon.

The Instructors

Jack T. Watson (Course Director), Professor of Biochemistry and Chemistry, Michigan State University, is an expert in quantitative techniques and methodology of GC/MS.

Plus . . . J. F. Holland, C. C. Sweeley, C. G. Enke, M. Micke, J. Allison, D. A. Gage, and M. Davenport

American Chemical Society
Dept. of Continuing Education
Meeting Code MAS9206
1155 Sixteenth Street, N.W.
Washington, D.C. 20036

YES! Please send me a free brochure describing *Mass Spectrometry: Principles and Practice*, to be held June 15-19, 1992, at Michigan State University, East Lansing, MI.

Name _____

Title _____

Organization _____

Address _____

City, State, Zip _____



Rapid Functional Group Characterization of Gas Chromatography/Fourier Transform Infrared Spectra by a Principal Components Analysis Based Expert System

Erik J. Hasenoeherl, Jonathan H. Perkins,[†] and Peter R. Griffiths*

Department of Chemistry and Idaho Center for Hazardous Waste Remediation Research, University of Idaho, Moscow, Idaho 83843

A procedure for the on-line characterization of compounds eluting from a gas chromatograph (GC) by automated interpretation of their vapor-phase infrared (IR) spectra is described. Principal components analysis (PCA) is applied to a training set containing two classes of appropriately scaled vapor-phase infrared library spectra. A sigmoid (discriminant) function is applied to the results of the PCA. The presence of a given functionality in an unknown spectrum is determined by projection of the unknown spectrum onto the factors defined by the PCA and assigning the projected unknown a discrimination score. The product of the discrimination score and the Gram-Schmidt reconstructed chromatogram can be plotted as a chromatographic trace emulating a functional group selective detector. Examples are shown for chemical classes such as alcohols, carboxylic acids, ketones, and aldehydes. A study of the results of baseline correcting the spectra before projection has been completed. Much more accurate results are obtained after baseline correction has been applied.

INTRODUCTION

Fourier transform infrared (FT-IR) spectrometry is a powerful technique for elucidating the structure of nanogram quantities of organic compounds. When combined with a gas chromatographic separation, FT-IR yields structural information about volatile and semivolatile components of a complex mixture to a minimum identifiable quantity of about 5 ng for polar compounds using a light-pipe detector. However, the unequivocal assignment of the molecular structure of each component from its GC/FT-IR spectrum can be difficult and/or time consuming for two primary reasons. First, infrared reference spectra of the majority of compounds that are amenable to separation by GC do not exist in current vapor-phase spectral libraries. Second, the resolution of capillary gas chromatography is such that a given sample may be shown to contain several hundred components; the identity of each GC peak by either of the two most commonly applied on-line spectroscopic techniques (IR and mass spectrometry) cannot be thoroughly evaluated by an expert spectroscopist

simply because the time required would be prohibitive.

Three procedures for analyzing GC/FT-IR data are currently in common use.¹ In order of selectivity they involve the construction of chromatograms using the Gram-Schmidt vector orthogonalization algorithm,^{2,3} the construction of wavelength-selective chromatograms by integrating the absorbance across a defined spectral window,⁴ and spectral library searching.^{5,7}

In the Gram-Schmidt (GS) vector orthogonalization algorithm, a basis set of several interferograms is collected while only the carrier gas is passing through the light-pipe. This basis set is then removed from each interferogram collected during the GC run. The length of the residual vector remaining after the basis set has been removed from each interferogram measured during the separation gives the chromatographic signal. GS reconstructions can rapidly indicate whether or not any IR active species is present in the light pipe. The magnitude of the residual is approximately proportional to the quantity of sample injected;⁸ however, GS chromatograms give no information as to the chemical structure of each component.

Wavelength-selective chromatograms provide more specific information than Gram-Schmidt chromatograms. Wavelength-selective chromatograms are calculated by integrating the absorbance over one or more specified regions of the IR spectrum that usually correspond to characteristic vibrations of the functional groups of interest. The selectivity of this approach is not particularly high, however. For example, integrating the spectrum between about 1850 and 1650 cm^{-1} will indicate those compounds containing a carbonyl group, but will not generally permit compounds that contain a ketone, carboxylic acid, aldehyde, or ester functionality to be distinguished, nor will integrating the spectrum between 3500 and 3700 cm^{-1} allow an alcohol to be distinguished from a carboxylic acid.

An alternative approach to this calculation of functional group specific chromatograms was described by Wieboldt et al.,⁹ who showed that it is possible to correlate the interferogram of an unknown compound with a synthetic interferogram generated from characteristic vibrational frequencies of the functional group of interest. The sum of the zero-point correlations for each component as it elutes from a chromatograph is then plotted as a chromatographic trace. Their system shows promise for the simultaneous determination of several functionalities. Unfortunately, the incorporation of

*To whom correspondence should be sent.

[†]Present address: Mobile Research and Development Corp., Paulsboro Research Laboratory, Paulsboro, NJ 08066.

a new functionality requires the work of an expert spectroscopist to synthesize the appropriate interferogram. Furthermore, the selection of those spectral bands to be deemed characteristic of a given functionality is also left up to the expert.

To obtain more specific structural information about an unknown analyte from its GC/IR spectrum than a selective wavelength chromatogram provides, the measured spectra may be searched against a library of vapor-phase infrared reference spectra. Comparison of an unknown spectrum with the spectral library is usually accomplished with a Euclidian distance operator. Library searching typically yields reliable results if the unknown spectrum is contained within the spectral library, provided that the signal-to-noise ratio of the spectrum is sufficiently high and the structure of the analyte is not too similar to that of the next best match. Library searching has several drawbacks, however. First, each library spectrum must be compared directly with each unknown spectrum, making library searching a time-consuming procedure. As a result, library searching against extensive databases has not been implemented as an on-line technique. Finally, library searching is guaranteed to give an erroneous result if the spectrum of the unknown is not contained within the spectral library.

This paper describes an approach by which functional and structural information can be extracted rapidly and on-line in a GC analysis with a specificity that is intermediate between that of integrated absorbance chromatograms and library searching. The approach used is similar to that taken in the expert system for characterizing molecular structures through principal components analysis (PCA) that we have recently described.^{10,11} This technique classifies the structure of compounds through their vapor-phase IR spectra. The presence of a specific functional group (such as ketone, carboxylic acid, ester, aldehyde, or alcohol) or structural unit (such as amphetamine, cocaine, or barbiturate) can be recognized using this approach. The rules by which structures can be classified are generated from the protocol established in our previous papers.^{10,11} After determining whether or not the analyte contains the functional group(s) of interest, the information is plotted in the form of a chromatogram that only shows peaks assignable to components with the functional groups of interest. Development of rules to classify new functional groups can be generated easily with minimal knowledge of IR spectrometry.

THEORY

Classification of vapor-phase IR spectra using this PCA-based expert system has been described previously^{10,11} and will only be summarized briefly in this paper. To obtain structural information from gas chromatograms of multicomponent samples using a PCA-based expert system it is necessary to first build an expert system rule. Rule building is accomplished by the following six steps:

- (1) A small training set is selected. In our work, this training set included 25 IR spectra of compounds that contain the structural group of interest and 25 IR spectra of compounds that do not contain this structural group.
- (2) The spectra in the training set are autoscaled by subtracting the mean value at each wavelength from each wavelength in every training set spectrum. Then every mean-centered spectrum is variance-scaled by dividing the each wavelength by the square root of the sums of squares (SQSS) spectrum of the training set.
- (3) The training set spectra are feature weighted by scaling the data such that those vibrational modes that provide the greatest variance between the categories are enhanced.
- (4) A principal components analysis is then performed on the scaled training set.

(5) A large number of library spectra is projected onto the training set.

(6) To determine a classification line for the training set, the results from the PCA are classified by a simplex-optimized sigmoid function:^{12,13}

$$y = \frac{1}{1 + \exp((\mathbf{u}\mathbf{b} - d)/T)} \quad (1)$$

where u is the projected principal component scores of the training set (dimension P), \mathbf{b} is a vector of coefficients, d is an offset, T is the sigmoid temperature, and y is the estimated sample identification score. The form of the function depends upon the dimension of the score space (P). The decision surface has the dimension $P - 1$. Optimization of \mathbf{b} , d , and T is accomplished by a simplex routine to minimize the sums of squares error between the y values and the true class values. With one principal component the decision is made about a point. In two dimensions the decision is made about a line; in three dimensions the decision is made about a plane; and so on. The vector of coefficients, \mathbf{b} , is orthogonal to the subspace defined by the decision surface; \mathbf{b} defines the surface orientation. The value, d , defines the location along the direction, \mathbf{b} , at which the decision lies. The temperature term, T , expresses the uncertainty of the classification. A small value of T defines a sharp transition and hence a good separation, while a large value of T defines a slow transition and hence, a poor separation.

An unknown spectrum can then be assigned a discrimination score based upon its projected principal component scores. The discrimination score can be calculated from the sigmoid function (eq 1). The values \mathbf{b} , d , and T are given by the simplex optimization procedure. u is the projected PC score for a given unknown spectrum; y is the discrimination score. The discrimination score represents a probability that the unknown spectrum belongs to a specific class. For a two class system, C_1 and C_2 , a discrimination score close to unity indicates that the unknown spectrum is highly correlated to class C_1 and has a very low correlation to class C_2 . An unknown is assigned to class C_1 if $y > 0.50$, and it is assigned to class C_2 if $y \leq 0.50$.

The above six steps are completed prior to performing a chromatographic run, and the results can be incorporated into the GC/IR data acquisition program. Rules to classify new functional groups or substructure classes can be developed automatically by a personal computer. For example, if it is determined that the significant components of a mixture all contain the NH_2 functionality, a computer can then be utilized to search (either by name or Wiswesser line notation) a spectral database for all of the NH_2 -containing species and randomly choose 25 for a training set. All of the necessary scaling can be performed by the computer. The only user intervention necessary to create a new rule is determining which functional group or substructure is significant.

Each spectrum collected is projected onto the principal components defined by the PCA expert system rule. Since the absorbances of species eluting from a GC column are typically much lower than the absorbances found in the vapor-phase library spectra from which the training sets are built, normalization of both training set and unknown spectra is necessary. Harrington and Isenhour have investigated the use of two well-known methods of normalizing spectra to improve the results of library searching.¹⁴ The first involves normalizing to unit vector length. The unit vector length, l , of an IR spectrum is calculated as

$$l = \left[\sum_{k=1}^n x_k^2 \right]^{1/2} \quad (2)$$

where x_k is the absorbance of the k th point in the IR spectrum

and n is the number of resolution elements in the spectrum. To normalize a spectrum, each absorbance is divided by l . The alternative normalization procedure involves scaling the spectrum so that the peak absorbance of the most intense band is set to unity by dividing each absorbance by the maximum absorbance within the spectrum. Both of these methods have been tested to determine which permits the lower error rate with functionally specific chromatograms.

Once the spectrum of the unknown has been normalized to either unit vector length or unit maximum absorbance, it is scaled to the training set data by first subtracting the mean spectrum of the training set, then dividing by the SQSS spectrum of the training set, and finally, multiplying by the feature weight spectrum of the training set. The projected score is calculated by simply taking the dot product between the unknown scaled spectrum and the appropriate loading vector and dividing by the singular value. The result of scaling to the training set data, projecting onto the pertinent PC's, and assigning a discrimination score can be combined into one final "classification" vector. This allows the discrimination score for an unknown spectrum to be determined simply by calculating the dot product between the unknown spectrum and the combined vectors. Combining these into one step reduces the computation time considerably.

At each time, t , along the chromatogram, values of the product

$$x_t = G_t y_t \quad (3)$$

may be calculated, where G_t is the Gram-Schmidt intensity at time t in the reconstructed chromatogram and y_t is the discrimination score corresponding to the IF spectrum at time t in the chromatogram. Since this process represents a functional group specific chromatogram, we have dubbed chromatograms computed in this manner FGS chromatograms.

Consider a plot of the discrimination score vs retention time for a case when the training set score is optimized to identify alcohols. The discrimination score is always approximately 1 or 0 (i.e. the sigmoid has a low temperature) if the training set is well separated. When no compound is eluting (chromatographic baseline), the measured spectrum is, theoretically, pure noise, and the discrimination score should randomly flip between 0 and 1 at each digitized retention time. In a case where the discrimination is not perfect, for example, when the unknown PC score falls very close to the classification line or when the temperature is high (i.e. the training set is overlapped), the score will not necessarily be 1 or 0 if an alcohol or nonalcohol, respectively, is eluting. In either case, the trace of the discrimination score vs time is indicative of the confidence that a specific class of compound is eluting and is not indicative of the amount. When a compound is present in the light pipe, the projected score of a spectrum obtained at that point is no longer random. Ideally, the principal component scores should move toward the "true score" of the unknown and remain constant for the duration of the peak. The "true score" of an unknown is the projected score for the unknown given low noise and no baseline errors. Since the discrimination score is obtained directly from the projected factor score, it should also remain constant across the peak.

The Gram-Schmidt reconstructed chromatogram is a measure of the concentration of an analyte present in the light pipe at a given time. When calculating the functional group specific chromatograms, the discrimination score is a measure of the certainty that an unknown spectrum belongs to a given class of compounds. Thus, the intensity of a peak in the FGS chromatogram is neither a measure of the concentration nor the certainty that the component belongs to a given class, but is the product of the two. The certainty, however, can be easily ascertained in the form of a chromatogram simply by plotting

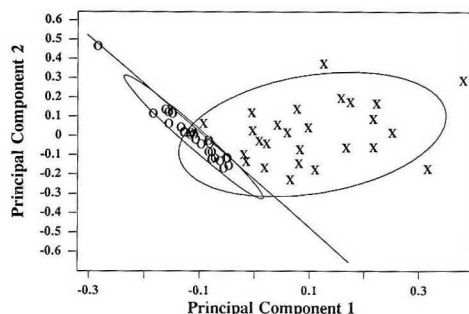


Figure 1. Scatter plot of the first two principal components of the training set for the classification of the spectra of alcohols (X) and non-alcohols (O). The ellipses containing 90% of each distribution are plotted. The solid line is the sigmoid classification line.

the discrimination score when the Gram-Schmidt intensity exceeds a minimum value.

EXPERIMENTAL SECTION

The GC separation shown in this paper was performed on a 30-m-long, 250- μ m-i.d. capillary column coated with a 0.25- μ m-thick layer of DB-23 (50% cyanopropyl, 50% methyl polysiloxane) stationary phase (J & W Scientific, Folsom, CA). The column was installed in a Model 5890 GC (Hewlett-Packard, Palo Alto, CA), and the spectra were obtained using a Hewlett-Packard IRD GC/FT-IR interface; 1.0- μ L aliquots of each sample were injected using a splitless injector.

The IR spectra used in the training sets were extracted from the Sadtler Vapor-Phase IR Library (Sadtler Research Division of Bio-Rad, Philadelphia, PA). Each spectrum was "deresolved" (reduced in size) by removing three out of every four data points. After deresolution the 420 data points between 4000 and 760 cm^{-1} were used to build the training set. Baseline correction of the IR spectra obtained after chromatographic separation was performed using LabCalc (Galactic Industries Corp., Salem, NH). All expert system routines were written in either Turbo C or Turbo Pascal (Borland Int. Scotts Valley, CA). The results were analyzed using Lotus 123 (Lotus Development Corp., Cambridge, MA).

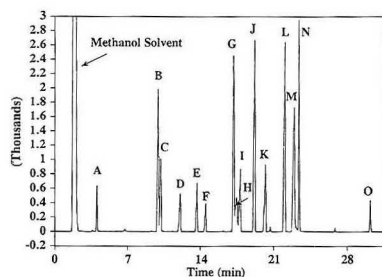
RESULTS AND DISCUSSION

Prior to chromatographic separation, the functional group classification for alcohols and carbonyl compounds (acids, aldehydes, ketones, and esters) was optimized in a similar manner to that described in refs 10 and 11. Alcohols were classified by selecting 25 alcohols and 25 non-alcohols from the Sadtler Vapor-Phase IR Library. The training data were normalized to unit vector length, autoscaled, and feature weighted, and a PCA was performed. The first two principal component (PC) scores from the training set were used in the sigmoid-optimized classification. Figure 1 shows the results of this classification. The 25 spectra in the training set were deemed adequate for analysis by the sigmoid algorithm. The large ellipses are set to encompass 90% of the volume of a normal distribution fit to the data. The classification line is drawn to show where the sigmoid value is 0.5. The temperature of the sigmoid is very low, $T = 1.26 \times 10^{-4}$, which is evident since both classes are well separated. The classification structure used for carbonyl-containing compounds was the same as that described in ref 11.

A 1.0- μ L aliquot of a methanol solution containing the 15 compounds listed in Table I was injected into the chromatograph. Of the 15 compounds, nine contained a carbonyl functionality, five were alcohols, and one contained neither functionality. The resulting Gram-Schmidt chromatogram is shown in Figure 2. The peaks are labeled A through O, and the amounts injected are given in Table I.

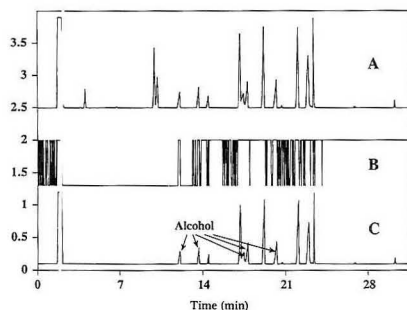
Table I. Compounds and Amounts Injected into the Gas Chromatograph for Use in the Generation of FGS Chromatograms

peak	amount injected, ng	compound	retention time, min
A	122	3-pentanone	4.0
B	144	cyclohexanone	9.8
C	128	heptaldehyde	10.1
D	122	1-hexanol	12.0
E	144	cyclohexanol	13.6
F	167	1-bromooctane	14.4
G	156	benzaldehyde	17.1
H	124	1-nonanol	17.4
I	124	1-octanol	17.7
J	124	2,5-hexanedione	19.1
K	124	2-nonanol	20.1
L	146	3,5-dimethyl-2-cyclohex-1-one	22.0
M	138	heptanoic acid	22.9
N	100	phthalic acid methyl ester	23.2
O	140	1,2-benzenedicarboxaldehyde	30.2

**Figure 2.** Gram-Schmidt reconstructed chromatogram depicting the separation of the compounds listed in Table I. The peaks are labeled A through O.

To calculate a FGS chromatogram, each spectrum was transferred from the Hewlett-Packard IRD Chemstation to an IBM-compatible personal computer using the Galactic Industries IRD integer format file importer. The configuration of the HP IRD was matched to the specifications at which the library spectra were obtained. The spectra were then simply reduced to 420 data points by dropping 3 out of every 4 points. For the alcohol FGS chromatogram, the resulting spectra were normalized to unit vector length, scaled to the training set data, projected onto PC 1 and 2, and assigned a discrimination score. The latter three steps were combined into one final "classification" vector. The discrimination score for each spectrum along the chromatogram is shown in Figure 3B. Because the sigmoid temperature is low, most discrimination scores assigned to unknown spectra are very close to either 1 or 0 (see Figure 3B). The closer a score is to 0, the more sure the discriminant is that the spectrum is not an alcohol, and the closer the value of a score is to 1 the more likely that the unknown is an alcohol. Since the scores of alcohols and non-alcohols in the training set are well separated, the sigmoid classification function classifies the training set spectra with excellent accuracy.

The result of multiplying the Gram-Schmidt reconstructed chromatogram (Figure 3A) and the discrimination score (Figure 3B) is illustrated in Figure 3C. Ideally, only those peaks that are due to alcohols are evident in this chromatogram. However, Figure 3C shows several peaks attributed to compounds that do not contain the OH functionality. This result is caused by negative-sloping IR baselines. A general trend can be seen in the discrimination scores over the time period of the chromatogram. At the beginning of the chro-

**Figure 3.** (A) Gram-Schmidt reconstructed chromatogram. (B) Discrimination score trace for the alcohol classification. (C) Alcohol FGS chromatogram.

matogram the discrimination scores of chromatographic baseline regions tend to be random. As the experiment proceeds the discrimination scores become all 0, then become random again, and finally for the last few minutes they are equal to 1. The IR spectra corresponding to the respective discrimination scores show an analogous trend. Initially, the spectral baseline is flat and centered at zero absorbance. As the oven temperature rises during temperature programming, the spectral baselines begin to show a slope. By the end of the program, the baseline exhibited a severe negative slope with the absorbance at 4000 cm^{-1} always being positive until about 2000 cm^{-1} .

When the baseline of IR spectra obtained after chromatographic separation is skewed due to the effect of temperature programming, source drift, and other instrumental variations, the results of a FGS chromatogram appear to be inaccurate. In order to obtain accurate FGS chromatogram results, the spectral baseline must be as flat as possible and centered at zero. This is critical in cases where the band most indicative of a particular functional group is weak, such as the O-H stretch of an alcohol. An IR baseline with a positive offset above 3000 cm^{-1} equal to or greater than the intensity of a given O-H stretch will cause that spectrum to be classified as an alcohol even though there is no indication of any peak in that region. Furthermore, an alcohol giving rise to a negative absorbance value in the measured spectrum at the maximum of the OH band because of a poor baseline will not be classified as such. This effect is not as prevalent when bands that are most characteristic of a given functional group are very intense, such as the $\nu(\text{C}=\text{O})$ mode of a carboxylic acid, since baseline errors of this magnitude are rare. Baseline correction has proven useful for improving the accuracy of predicting the structure of unknowns searched against a library of vapor-phase IR spectra.¹⁵ Therefore, baseline correction was performed on each spectrum before the FGS chromatograms were generated. Two methods of baseline correction were investigated: (1) a five-point linear baseline correction, (2) subtraction of an average IR baseline obtained by averaging two spectra collected on either side of the chromatographic peak. For comparison a third FGS chromatogram was generated with no baseline correction.

Figure 4 illustrates the effect of baseline correction upon the alcohol FGS chromatogram. The previous alcohol FGS chromatogram without baseline correction is shown in Figure 4A. Figures 4B and 4C depict the FGS chromatograms when a five-point linear baseline correction and baseline subtraction is applied to the spectra, respectively. Figures 4B and 4C show a dramatic improvement in their selectivity compared to the case when no baseline correction was performed; only peaks corresponding to components which have the alcohol func-

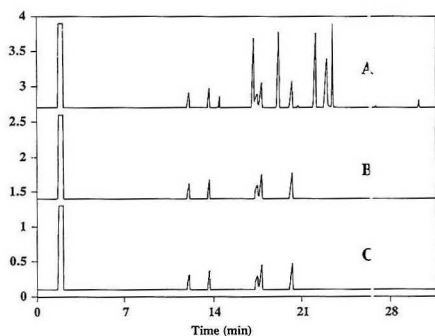


Figure 4. Alcohol FGS chromatogram (A) with no baseline correction, (B) with a five-point baseline correction, and (C) after correcting for baseline by averaging two spectra on either side of a chromatographic peak from the spectra across the peak.

tionality are present in these traces. While Figure 4 illustrates that the best results are obtained after baseline correction, the ideal case would require no correction since baseline correction is time consuming, often subjective, and an optimized protocol for baseline-correcting IR spectra has not been determined. For this work, baselines were corrected by subtracting the baseline that was obtained from the average of two spectra acquired from each side of the chromatographic peak. Although this protocol yielded the most reproducible baselines, it has several drawbacks. Firstly, it is impossible to implement in real time since it requires a priori information as to chromatographic peak location. Secondly, it is computationally more intensive since a routine must be implemented to determine objectively what constitutes a peak. Although somewhat more subjective, the five-point baseline correction (using points at 4000, 3200, 1820, 1650, and 770 cm^{-1} for the categories being studied) can be executed in realtime, and produces results comparable to those using the baseline subtraction method.

The increased specificity of the FGS chromatogram technique sometimes leads to enhanced chromatographic resolution. For example, peaks G, H, and I (Figure 2) are somewhat overlapped in the Gram-Schmidt chromatogram. However, in the two baseline-corrected alcohol FGS chromatograms (Figure 4, parts B and C), peak G is absent as this component is not an alcohol. The absence of this peak means that the leading edge of peak H rises from the baseline of the chromatogram.

A similar FGS chromatogram was constructed to respond only to those components that contain the carbonyl functionality. The pretreatment of spectra for the calculation of FGS chromatograms of carbonyl compounds differs in one respect with the corresponding pretreatment for alcohols. In order to obtain the best classification of the carbonyl training set, the spectra were scaled to unit absorbance rather than to unit vector length. The reason for normalizing the spectra in this way is related to the fact that the $\nu(\text{C}=\text{O})$ vibration is the most intense feature in the spectrum of almost all carbonyl-containing compounds. Scaling the spectra so that the most characteristic band has unit absorbance should only be beneficial when a band that is characteristic of the functional group of interest has a high absorptivity. Our results are in agreement with the results obtained by Harrington and Isenhour for library searching.¹⁴

The carbonyl FGS chromatogram obtained by multiplying the Gram-Schmidt reconstructed chromatogram (Figure 5A) by the discrimination score (Figure 5B) is shown in Figure 5C. No baseline correction was performed. The chromatogram displays only peaks that are due to components of the

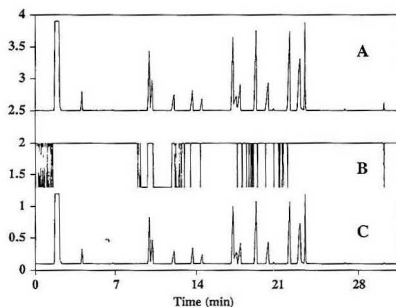


Figure 5. (A) Gram-Schmidt reconstructed chromatogram. (B) Discrimination score trace for the carbonyl classification. (C) Carbonyl FGS chromatogram.

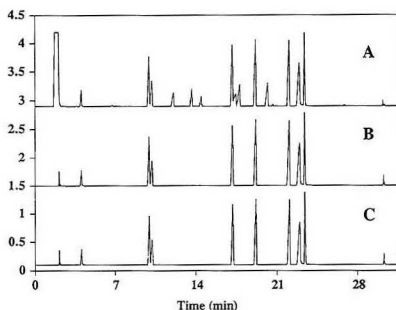


Figure 6. Carbonyl FGS chromatogram (A) with no baseline correction, (B) with a five-point baseline correction, and (C) after correcting for baseline by subtracting the average of two spectra on either side of the chromatographic peak.

mixture which contain the carbonyl functionality; not all carbonyl-containing peaks are present in this trace, however. Figure 6 shows the improved results after baseline correction. Again, both correction routines improve the results in a similar manner. After baseline correction all peaks attributed to compounds containing the carbonyl functionality are present in the FGS chromatogram. As a result of this investigation, it appears that baseline correction should always be applied prior to calculating the discrimination score, as errors may occur with spectra demonstrating low signal-to-noise ratio or spectra of components whose concentrations are near the detection limits.

The certainty that an unknown peak belongs to a specific class can be established from the discrimination score for each unknown spectrum. Since the spectra obtained in baseline regions of the chromatogram contain no information about the molecular structure of an eluting component, the spectra and corresponding discrimination scores are unimportant in determining to which class a component belongs and are discarded for the certainty determination. In this example, any Gram-Schmidt value < 30 automatically resulted in the discrimination score being set to 0. Figure 7B illustrates the certainty that a specific component contains the carbonyl functionality. All of the components that contain the carbonyl functionality show a discrimination value of 1 and all other peaks show a value of 0 because of the exceptional separation of the carbonyl training set.

The carbonyl functionality may be present in many different structural forms within a molecule (e.g. ketone, aldehyde, acid, and ester), and these structural forms are relatively easy to classify by the PCA-based expert system that we have previously described.¹¹ FGS chromatograms can be

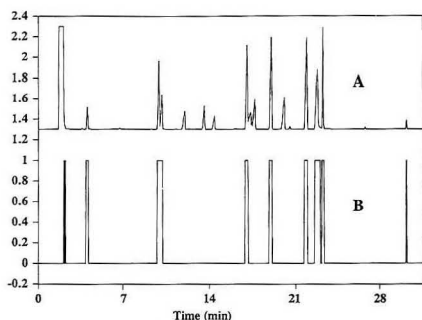


Figure 7. (A) Plot of the Gram-Schmidt chromatogram. (B) Plot of the certainties that an unknown component contains the carbonyl functionality. A value of 1 corresponds to a large certainty that an unknown is a carbonyl and a value of 0 corresponds to a large certainty that an unknown does not contain the carbonyl functionality.

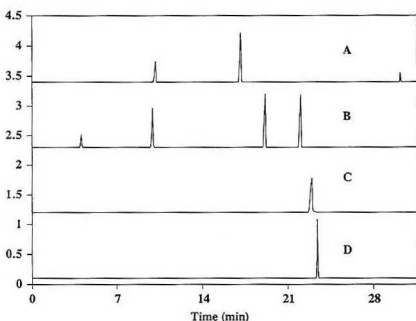


Figure 8. (A) Aldehyde FGS chromatogram. (B) Ketone FGS chromatogram. (C) Carboxylic acid FGS chromatogram. (D) Ester FGS chromatogram.

generated for several of these carbonyl functionalities using the tree structure for these classifications that is described in detail in ref 11. Figure 8 illustrates the FGS chromatogram traces for aldehydes (Figure 8A), ketones (Figure 8B), carboxylic acids (Figure 8C), and esters (Figure 8D). A similar FGS chromatogram could be generated to show even more specific structural information, such as the type of ester functionality or the α -substitution of an aldehyde, ketone, or ester. The spectra used for these traces were baseline-corrected using the average baseline subtraction method described above. The results shown in Figure 8 represents a marked improvement over selective-wavelength chromatograms, since in relatively few cases can a selective-wavelength chromatogram distinguish between different types of carbonyl functionalities. Similarly, a selective wavelength chromatogram is not readily able to distinguish between a component

that contains the alcohol functionality and an acid moiety. In several places increased chromatographic resolution due to the selectivity of this technique can be demonstrated, e.g. for peaks G and H in Figures 4C and 6C.

In summary, a technique has been demonstrated that can rapidly determine the functional groups present in a gas chromatographic trace. This approach has several advantages over current means of on-line analysis of specific functional groups by GC/FT-IR, as it is more specific than selective wavelength chromatograms and faster than library searching. Although the specificity of FGS chromatograms is somewhat less than that of library searching, no library can be sufficiently comprehensive to represent all possible species. New rules can be implemented by relatively inexperienced users and requires only the use of a personal computer and the appropriate IR library spectra.

Calculating chromatograms in this way could have several advantages. For example, those GC peaks that are not relevant to particular analytical problem could be recognized immediately, thus allowing an expert spectroscopist to spend more time identifying the peaks that are of interest. In addition, the availability of an expert system with the capability of classifying GC eluents according to their functional and structural constituents would allow a technician to make simple spectral assignments of each component for which a GC/FT-IR spectrum had been obtained, again freeing up the expert to concentrate on the more important components. Thus we believe that this technique will prove to be a useful and practical means of increasing the specificity of chromatograms obtained by GC/FT-IR.

ACKNOWLEDGMENT

We wish to gratefully acknowledge Hewlett-Packard Corp. for the generous donation of an HP-IRD detection system.

REFERENCES

- (1) White, R. *Chromatography/Fourier Transform Infrared Spectroscopy and its Applications*; Dekker: New York, 1990.
- (2) de Haseth, J. A.; Isenhour, T. L. *Anal. Chem.* **1977**, *49*, 1977-1981.
- (3) Owens, P. M.; Lam, R. B.; Isenhour, T. L. *Anal. Chem.* **1982**, *54*, 2344-2347.
- (4) Coffey, P.; Mattson, D. R.; Wright, J. C. *Am. Lab.* **1978**, *5* (10), 126-132.
- (5) Lowry, S. R.; Huppler, D. A. *Anal. Chem.* **1981**, *53*, 889-893.
- (6) Sebesta, R. W.; Johnson, G. G., Jr. *Anal. Chem.* **1972**, *44*, 260-265.
- (7) Erley, D. S. *Appl. Spectrosc.* **1971**, *25*, 200-202.
- (8) Sparks, D. T.; Lam, R. B.; Isenhour, T. L. *Anal. Chem.* **1982**, *54*, 1922-1926.
- (9) Wieboldt, R. C.; Hohne, B. A.; Isenhour, T. L. *Appl. Spectrosc.* **1980**, *34*, 7-14.
- (10) Perkins, J. H.; Hasenoehtl, E. J.; Griffiths, P. R. *Anal. Chem.* **1991**, *63*, 1738-1747.
- (11) Hasenoehtl, E. J.; Perkins, J. H.; Griffiths, P. R. *Anal. Chem.* In press.
- (12) Harrington, P. B. *J. Chromatogr.* **1991**, *5*, 467-468.
- (13) Perkins, J. H.; Hasenoehtl, E. J.; Griffiths, P. R. *J. Chromatogr. Intel. Lab. Sys.* In press.
- (14) Harrington, P. B.; Isenhour, T. L. *Appl. Spectrosc.* **1987**, *41*, 1298-1302.
- (15) Sherman, J. W.; de Haseth, J. A.; Cameron, D. G. *Appl. Spectrosc.* **1989**, *43*, 1311-1316.

RECEIVED for review September 1, 1991. Accepted January 2, 1992.

Determination of Amino Acids by Capillary Zone Electrophoresis Based on Semiconductor Laser Fluorescence Detection

Toshiyuki Higashijima, Tetsuhiro Fuchigami, Totaro Imasaka,* and Nobuhiko Ishibashi

Faculty of Engineering, Kyushu University, Hakozaki, Fukuoka 812, Japan

Chlorophyll is fluorescent in the deep-red region and is determined by semiconductor laser fluorometry after its separation with capillary zone electrophoresis. The separation efficiency is several hundred thousand in the theoretical plate. Methylene blue is used as a chromophore in indirect fluorometry. The detection limit achieved is 1-pmol levels. A new labeling reagent is synthesized, which consists of a thiazine chromophore for fluorescence detection and a succinimidyl ester for combination with an amino acid. The labeled amino acids are clearly resolved by capillary zone electrophoresis, the detection limit being 10-pmol levels. Amino acids are further labeled with a visible dye such as fluorescein isothiocyanate (FITC) or 7-(diethylamino)coumarin-3-carboxylic acid succinimidyl ester (DCCS), and are detected with visible semiconductor laser fluorometry using second harmonic emission (415 nm) of the near-infrared semiconductor laser. The detection limit achieved is ~100-amol levels.

A laser is currently used in analytical spectroscopy and has provided an ultrasensitive means in trace analysis.¹ Detection of single atoms, ions, or molecules has already been demonstrated by laser spectroscopy. However, its practical application is quite limited except for Raman spectroscopy. This is believed to be due to the cost of the laser, but lifetime and maintenance problems are more serious in commercialization of the instrument. Until now, only a few analytical instruments have been commercialized using a laser, e.g., a HeNe laser for measurement of light scattering. More recently, an air-cooled argon ion laser is used for determination of amino acids after labeling them with 7-chloro-4-nitrobenzoxadiazole (NBD) or fluorescein isothiocyanate (FITC) and separation by high-performance liquid chromatography (HPLC).²

A semiconductor laser is developed for use in a compact disk, a laser printer, and a bar-code reader. It is less expensive than a conventional light source such as a xenon arc lamp, and the lifetime exceeds 10 000 h. Then, a semiconductor laser can be used in a commercial analytical instrument without any maintenance for more than 1 year. The application of the semiconductor laser to analytical spectroscopy has been reviewed elsewhere.^{3,4} Particularly, fluorescence spectrometry is sensitive and has been used in determination of biological molecules such as metabolites, enzymes, and proteins.⁵⁻⁸

When an 1-kW xenon arc lamp is used as a light source and the spectral bandwidth of a monochromator is adjusted to 20–40 nm, the radiant photon flux exceeds 10 mW. This is comparable to the output power of the semiconductor laser (3–40 mW) manufactured by mass production technology. Thus a semiconductor laser is advantageous only when good beam focusing capability and monochromaticity are successfully used. For example, a laser fluorometric detector combined with HPLC gives high sensitivity due to a small

detector volume required and to a sharp-cut-off optical filter for efficient fluorescence collection and scattered light rejection.^{9,9} However, a microliter detection volume currently used in HPLC is still too large for best use of the laser; since the laser beam can be easily focused down to a submicron spot, the detection volume can be minimized to nanoliter or even to picoliter levels if necessary.

Recently, capillary zone electrophoresis has gained its importance. This is due to applicability to many biological substances and ultrahigh resolution in sample separation. Unfortunately, the path length in on-column detection is ~50 μm , so that the detection limit achieved by absorption spectrometry is restricted to 10^{-5} M levels.¹⁰ Contrarily, laser fluorometry is quite advantageous for ultrasensitive detection of samples because of good focusing capability and monochromaticity of the laser. In the extreme case, only a few thousand amino acids labeled with FITC have been detected using an argon ion laser.¹¹⁻¹³ Electrokinetic separation and fluorescence detection of chiral amino acids are further demonstrated with copper(II)-aspartame support electrolyte.^{14,15}

A semiconductor laser is well-matched to capillary zone electrophoresis with respect to a price and a dimension of the instrument; an argon ion laser has a large output power in the visible region, but the dimension and the price sometimes exceed those of the instrument in capillary zone electrophoresis. Furthermore, semiconductor laser fluorometry in the near-infrared or deep-red region provides low background fluorescence, and then the sample is possibly determined at lower levels especially for a real sample containing many contaminants fluorescent in the visible region. There are many compounds fluorescent in the near-infrared and deep-red regions.^{16,17} However, no fluorescence reagent useful for capillary electrophoresis based on indirect fluorometry has been reported so far, though a few near-infrared dyes are already used in HPLC/indirect fluorometry.^{18,20} It is noted that adsorption of the reagent to the separation column is more serious in capillary electrophoresis due to strong negative charges at the capillary surface. Moreover, a labeling reagent of biological molecules has seldom been developed at the present stage.^{16,17} Then, a new labeling reagent is desired for application of semiconductor laser fluorometry to capillary zone electrophoresis. Though the fundamental wavelength of the semiconductor laser commercially available is limited to 660–850 nm, the frequency-doubled output of the semiconductor laser has been used as a light source in analytical spectroscopy such as an optical fiber sensor system or molecular fluorescence spectrometry.^{21,22} However, full performance in focusing capability and monochromaticity of the laser has not yet been utilized.

In this study we first demonstrate capillary zone electrophoresis based on semiconductor laser fluorometry. First, chlorophyll is separated by capillary zone electrophoresis and is detected by 670-nm semiconductor laser fluorometry. Secondly, methylene blue is used as a fluorophore in indirect spectrometry, in which a capillary with a alkylsilane-derivatized surface is used to reduce adsorption of methylene blue.

* Author to whom correspondence should be addressed.

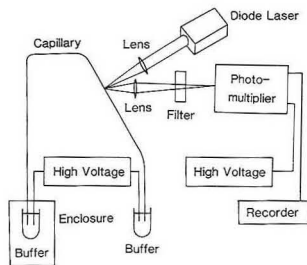


Figure 1. Block diagram of experimental apparatus for capillary zone electrophoresis combined with semiconductor laser fluorometry.

Thirdly, we synthesize a new labeling reagent with a thiazine chromophore fluorescent in the deep-red region and with a succinimidyl ester to bind with an amino acid. In fact, this reagent is applied to capillary zone electrophoresis of amino acids. Finally, a blue semiconductor laser emitting second harmonic wave (415 nm) is used for excitation of the separated amino acids labeled with visible dyes.

EXPERIMENTAL SECTION

Apparatus. A block diagram of the experimental apparatus is shown in Figure 1. The sample was injected into a capillary (Polymicro Technology, 50- μ m i.d., 375- μ m o.d., 60-cm long) by a siphon method. The injection volume was determined to be 1 nL, according to the method reported in ref 23. A high potential is applied between platinum electrodes immersed in the buffer solutions by a high-voltage power supply (Kansai Electric, KTS-30K01, 0–30 kV, 100 μ A). The sample migrates from a positive to negative (ground) potential. The system is enclosed by a Plexiglass box with a safety interlock. A semiconductor laser (ILEE Laser Innovation, LDA02, 670 nm, 2 mW) emitting at 670 nm is focused by a quartz lens (focal length, 25 mm) onto the capillary at which a polyimide coating is burned off by a flame. Fluorescence from a sample is collected by an objective lens for a microscope (Olympus, LWD MSPlan 50, \times 50, NA = 0.6) and is measured by a photomultiplier (EMI, 9558QB) after passing it through interference and color filters (Melles Griot, 03FV024 and 03FCG109). A blue semiconductor laser (Matsushita Electric Industrial Co., IMSO0820-04, 50 μ W, 415 nm, linewidth 3 nm, beam divergence 1°, linearly polarized) consists of a near-infrared semiconductor laser (830 nm), a waveguide of LiNbO₃, a collimating lens, and a power supply (R&K Co., LDA-8502S, 850 MHz). The body of the laser is 8-cm long, 2-cm wide, 2-cm high. In this case, the laser beam is more tightly focused by a pair of quartz lenses (focal length, 10 and 20 mm). A color filter (Toshiba, V-Y45) is used for isolation of fluorescence. The positions of the focusing lens and the capillary are carefully aligned by adjusting the fluorescence image to the pinhole image projected by irradiating the pinhole with a lamp placed behind.²⁴ The fluorescence signal is amplified 100 times by a commercial amplifier (NF Circuit Design Block, LI-75A) and is measured by a strip chart recorder (Hitachi 056).

Reagents. Chlorophyll, a nonrefined mixture of chlorophyll, was purchased from Tokyo Kasei. The content of total chlorophyll is specified to be 0.5% by a manufacturer. Fluorescent dyes of methylene blue and Azur B were obtained from Wako Pure Chemical and of oxazine 750 and rhodamine 800 from Lambda Physik. For synthesis of a labeling reagent, mercaptoacetic acid (Wako Pure Chemical), *N,N'*-dicyclohexylcarbodiimide (DCC, Kishida Chemical), and *N*-(ϵ -maleimidocaproyloxy)succinimide (EMCS, Dojindo Laboratories) were used. Labeling reagents of FITC (isomer-I) and 7-(diethylamino)coumarin-3-carboxylic acid succinimidyl ester (DCCS) fluorescent in the visible region were supplied from Dojindo Laboratories and Molecular Probes, respectively. Amino acids were obtained from Ajinomoto General Foods.

Synthesis of Labeling Reagent. The procedure for synthesis of a labeling reagent is shown in Figure 2. Ethanol solutions of Azur B (10^{-3} M), mercaptoacetic acid (5×10^{-2} M), and DCC (5

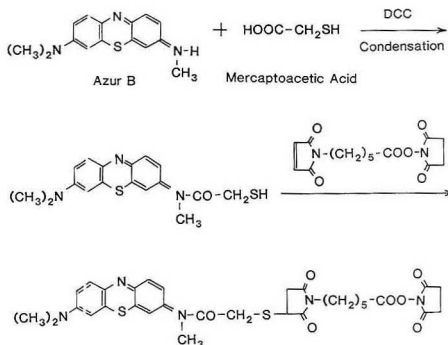


Figure 2. Scheme for organic synthesis of labeling reagent.

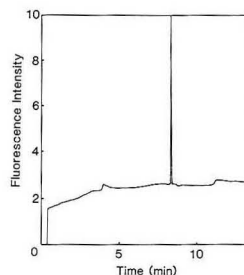


Figure 3. Electropherogram for chlorophyll (100 fmol). The sample was dissolved in pure water. The pH of the carrier solution was adjusted to 6 by a phosphate buffer (60 mM).

$\times 10^{-2}$ M) were mixed with a molar ratio of 1:50:50. The solution was reacted at room temperature during a day by mixing it with a magnetic stirrer. The product was dried by a rotary evaporator. The methanol solution of equimolar EMCS (10^{-4} M) was added and reacted at room temperature during day. This solution was used for labeling amino acids without reagent purification.

Sample Preparation. Amino acid (0.1 M, 0.1 mL) was reacted overnight with the synthesized reagent (10^{-4} M, 2 mL); the time period necessary to complete the reaction may be 0.5–2 h. In order to label amino acids with a visible dye (DCCS), the sample dissolved in the carbonate buffer (pH 11, 20 mM) was mixed during a day with the ethanol solution containing DCCS, their final concentrations being adjusted to 2×10^{-5} and 2×10^{-4} M, respectively. This sample solution was diluted stepwise before measurements.

RESULTS AND DISCUSSION

Determination of Chlorophyll. Several forms of chlorophyll, e.g. chlorophyll a, are known to be fluorescent in the deep-red region.²⁵ Then, chlorophyll is measured to check performance of the instrument developed in this study. A sharp electropherogram is observed as shown in Figure 3, giving a theoretical plate of several hundred thousand. Thus it is confirmed that the present capillary zone electrophoresis combined with semiconductor laser fluorometry is useful in direct determination of water-soluble compounds fluorescent in the deep-red region.

Indirect Fluorometry. Indirect spectrometry has a potential to be used in practical analysis, since all the chemical species are measured without any labeling procedure.¹⁰ In order to find a fluorescent dye suitable for indirect fluorometry, three dyes fluorescent in the deep-red region are injected into a capillary. The electropherograms obtained are shown in Figure 4. All the signal peaks are seriously broadened. This is probably due to strong adsorption of the

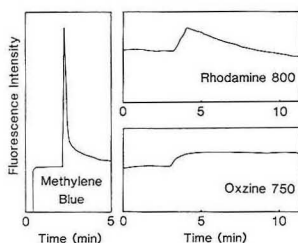


Figure 4. Electropherograms for dyes (100 fmol) fluorescent in deep-red region. The pH of the carrier solution was adjusted to 6 by a phosphate buffer (60 mM). The voltage and current were 25 kV and 80 μ A, respectively.

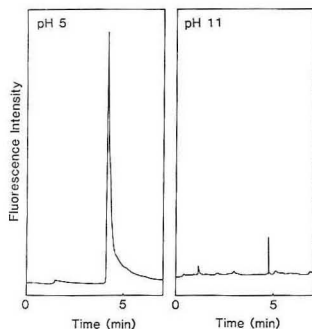


Figure 5. Effect of pH on electropherogram of methylene blue (100 fmol). The pH of the carrier solution was adjusted to 5 by a phosphate buffer (60 mM) or to 11 by a carbonate buffer (20 mM).

dyes to the capillary surface, since the dye molecules are positively charged and the capillary surface is negatively charged by dissociation of the proton from the silanol group. Methylene blue gives the narrowest peak among these dyes, which might be due to a high solubility of methylene blue in an aqueous solution.¹⁶ So, the effect of pH is further investigated for methylene blue, as shown in Figure 5. Adsorption is substantially reduced at higher pH, and a sharp signal peak is observed in the electropherogram though the fluorescence intensity is substantially decreased. The reason is unknown at present, but methylene blue might be negatively charged and is less fluorescent at this pH. The detection limit was 400 amol at pH 5 and was about 1 order of magnitude poorer at pH 11.

Unfortunately, all amino acids are almost completely dissociated to negatively-charged ions at pH 11, and it seems to be difficult to separate amino acids at such high pH. Thus the capillary conventionally used was replaced with one whose surface is alkylsilane-derivatized. In this case, most of the active sites to adsorb chemical species are end-capped, but the electroosmotic flow is still sufficient to drive the solution to a negative potential.²⁶ Capillary electrophoresis of amino acids using methylene blue as an indirect fluorophore is demonstrated in Figure 6. Glycine and proline are clearly separated and detected. Broad bands appearing at 4–8 min in the electropherogram are reproducible, and they probably originate from contaminants included in the sample solution. The detection limit in this approach is ~ 1 pmol. The variation of the fluorescence intensity for 10^{-5} M methylene blue solution in the capillary was 8×10^{-4} (time constant, 1 s), the dynamic reserve being 1300. However, the variation of the output power of the semiconductor laser was 2×10^{-5} , when it was stabilized by feedback control. Therefore, the detection limit might be substantially improved by optimization of the

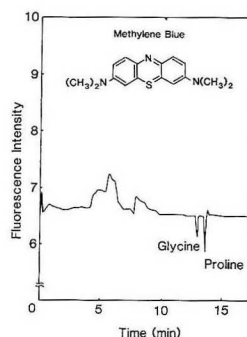


Figure 6. Indirect fluorometry of amino acids (10 pmol) measured by flowing methylene blue (10 μ M) as fluorescence reagent. The pH of the carrier solution was adjusted to 3.8 by a citrate buffer (10 mM). The voltage and current were 20 kV and 5 μ A, respectively.

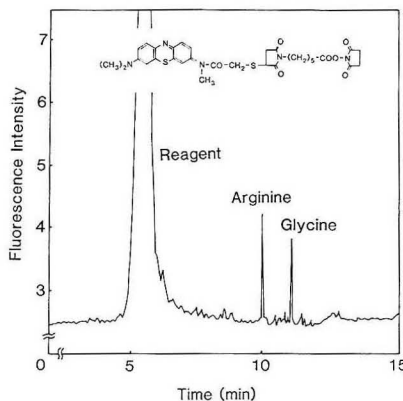


Figure 7. Electropherogram for amino acids (100 pmol) labeled with newly synthesized dye consisting of Azur B chromophore and succinimidyl ester. The pH of the carrier solution was adjusted to 5 by a phosphate buffer (60 mM). The voltage and current were 20 kV and 62 μ A, respectively.

experimental conditions in the future, e.g. by changing the concentration of the dye and the pH of the carrier solution and by using a more efficient optical filter and a vibrationally-isolated optical table. The development of a negatively-charged dye might be important to reduce adsorption of the dye at the capillary surface. Addition of a surfactant^{26,27} or an organic solvent²⁸ changes surface structure and separation mode, so that it may be possible to reduce adsorption of methylene blue to the capillary surface.

Determination Using a Labeling Reagent. More sensitive detection of amino acids may be performed by labeling them with a fluorescent dye. However, no labeling reagent fluorescent in the deep-red region has been so far developed. The electropherogram obtained by labeling amino acids with a new labeling reagent synthesized in this study is shown in Figure 7. A strong peak at 6 min originates from the reagent blank, probably due to nonreacted chemicals or side-reaction products. Arginine and glycine are clearly separated and detected by semiconductor laser fluorimetry. The detection limit is 10-pmol levels, at present. In this preliminary work the labeling reagent synthesized has not been purified, since it requires additional time and skill. Moreover, the reaction yield might be rather low under present nonoptimized conditions. Thus it will be necessary to synthesize a new and pure labeling reagent in the future, which is more soluble in aqueous

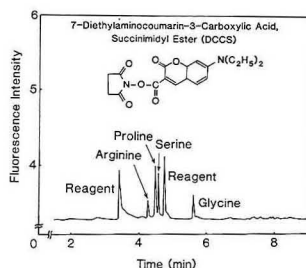


Figure 8. Electropherogram for amino acids (1 fmol each) labeled with a visible dye (DCCS). The pH of the carrier solution was adjusted to 9 by a carbonate buffer (5 mM). The voltage and current were 20 kV and 4 μ A, respectively.

solution and is more fluorescent in the deep-red region. Such an effort is now concentrated by several companies manufacturing chemical reagents.

Visible Fluorometry Using a Blue Semiconductor Laser. Many efficient labeling reagents are already available in the visible region, e.g. at around 415 nm, which corresponds to the emitting wavelength of the blue semiconductor laser. The experiment was performed for two candidates, i.e. FITC and DCCS. A reagent of FITC is widely used for labeling amino acids. Then, this labeling reagent is first applied to capillary zone electrophoresis/blue semiconductor laser fluorometry to check performance of the present analytical instrument. Complete separation of labeled amino acids, e.g. arginine, proline, serine, glycine, was readily demonstrated, as reported by detecting them with an argon ion laser.¹¹ The detection limit was ~ 2 fmol. However, the absorption maximum of FITC is located at around 490 nm, and the excitation efficiency at 415 nm is only several percent in comparison with that at the absorption maximum. Therefore, DCCS (absorption maximum 437 nm, excitation efficiency 66%) is applied for more sensitive detection. The electropherogram obtained is shown in Figure 8. All amino acids measured are separated in 6 min. The detection limit estimated is ~ 100 amol, which is already much lower than the detection limit (femtomole levels) obtained by a commercial HPLC system using a combination of an air-cooled argon ion laser and a labeling reagent of NBD or FITC.² It is noted that a blue semiconductor laser with an output power of 40 mW

is already developed,³⁰ so that the sensitivity in the present method will be substantially improved in the future.

ACKNOWLEDGMENT

This research is supported by Grants-in-Aids for Scientific Research from the Ministry of Education of Japan, from Steel Industry Foundation for the Advancement of Environmental Protection Technology (SEPT), and from Nakatani Electronic Measuring Technology Association of Japan.

REFERENCES

- (1) Imasaka, T.; Ishibashi, N. *Prog. Quant. Electron.* **1990**, *14*, 131.
- (2) Tosoh, Model LF-8010, reported in *HLC MAILGRAM*, **1991**, *53* (6), 5.
- (3) Imasaka, T.; Ishibashi, N. *Anal. Chem.* **1990**, *62*, 363A.
- (4) Lawrenz, J.; Niemax, K. *Spectrochim. Acta, Part B* **1989**, *44*, 155.
- (5) Sauda, K.; Imasaka, T.; Ishibashi, N. *Anal. Chem.* **1988**, *58*, 2649.
- (6) Imasaka, T.; Okazaki, T.; Ishibashi, N. *Anal. Chim. Acta* **1988**, *208*, 325.
- (7) Imasaka, T.; Nakagawa, H.; Okazaki, T.; Ishibashi, N. *Anal. Chem.* **1990**, *62*, 240A.
- (8) Imasaka, T.; Fuchigami, T.; Ishibashi, N. *Anal. Sci.* **1991**, *7*, 491.
- (9) Sauda, K.; Imasaka, T.; Ishibashi, N. *Anal. Chim. Acta* **1988**, *187*, 353.
- (10) Yeung, E. S.; Kuhr, W. G. *Anal. Chem.* **1991**, *63*, 275A.
- (11) Cheng, Y. F.; Dovichi, N. J. *Science* **1988**, *242*, 562.
- (12) Wu, S.; Dovichi, N. J. *J. Chromatogr.* **1989**, *480*, 141.
- (13) Hernandez, L.; Escalona, J.; Joshi, N.; Guzman, N. *J. Chromatogr.* **1991**, *559*, 183.
- (14) Gassmann, E.; Kuo, J. E.; Zare, R. N. *Science* **1985**, *230*, 813.
- (15) Gozel, P.; Gassmann, E.; Michelsen, H.; Zare, R. N. *Anal. Chem.* **1987**, *59*, 44.
- (16) Imasaka, T.; Tsukamoto, A.; Ishibashi, N. *Anal. Chem.* **1989**, *61*, 2285.
- (17) Patonay, G.; Antoine, M. D. *Anal. Chem.* **1991**, *63*, 321A.
- (18) Folestad, S.; Ahlberg, H. *International Symposium on Column Liquid Chromatography*, Stockholm, June 26–30, 1989.
- (19) Kawazumi, H.; Nishimura, H.; Ogawa, T. *Annual Meeting of The Japan Society for Analytical Chemistry*, Yokohama, November 21–23, 1991.
- (20) Lehotay, S. J.; Pless, A. M.; Winefordner, J. D. *Anal. Sci.* **1991**, *7*, 863.
- (21) Okazaki, T.; Imasaka, T.; Ishibashi, N. *Anal. Chim. Acta* **1988**, *209*, 327.
- (22) Imasaka, T.; Hiraiwa, T.; Ishibashi, N. *Mikrochim. Acta* **1989**, *II*, 225.
- (23) Burton, D. E.; Sepaniak, M. J.; Maskarinec, M. P. *J. Chromatogr. Sci.* **1989**, *24*, 347.
- (24) Dovichi, N. J., Alberta University, private communication, September 1990.
- (25) Yoshitake, Y.; Tanino, M.; Morishige, K.; Shigematsu, T.; Nishikawa, Y. *Bunseki Kagaku* **1989**, *38*, 182.
- (26) Towns, J. K.; Regnier, F. E. *Anal. Chem.* **1991**, *63*, 1126.
- (27) Towns, J. K.; Regnier, F. E. *J. Chromatogr.* **1990**, *516*, 69.
- (28) Balchunas, A. T.; Sepaniak, M. J. *Anal. Chem.* **1987**, *59*, 1466.
- (29) Roach, M. C.; Gozel, P.; Zare, R. N. *J. Chromatogr.* **1988**, *426*, 129.
- (30) Kozlovsky, W. J.; Lenth, W.; Latta, E. E.; Moser, A.; Bona, G. L. *Appl. Phys. Lett.* **1990**, *56*, 2291.

RECEIVED for review August 16, 1991. Accepted January 8, 1992.

Drug Release Profiles of Ophthalmic Formulations. 1. Instrumentation

Larry E. Stevens, Paul J. Missel, and John C. Lang*

Alcon Laboratories, Inc., 6201 South Freeway, Fort Worth, Texas 76134

An experimental method is described for measuring time-release profiles of drugs from various ophthalmic dosage forms. This *in vitro* method is carried out under conditions nearly representative of those observed *in vivo*. Specifically, we have reproduced *in vitro* the small volume and the slow exchange rate of the human precorneal tear reservoir. Volumes on the order of 8–30 μL are achievable. The concentration of drug downstream from the sample reservoir is analyzed nearly continuously and the entire release profiles are appropriate for modeling. This analytical system has been used to study drug release kinetics from controlled release formulations such as gels and suspensions. The method is compared with alternative techniques.

INTRODUCTION

Traditional methods for measuring the time-release profile of drugs from sustained release dosage forms, optimized to simulate dissolution in the gastrointestinal tract, are often unsuitable for ophthalmic dosage forms. Typically, large reservoirs (500–1000 mL) are utilized, as recommended in the United States Pharmacopeia.¹ For many dissolution studies, reservoir volume is an important parameter which influences and sometimes governs the rate of release. Therefore, it is important, when performing release experiments, to choose volumes representative of those found *in vivo*. For ophthalmic applications, this volume is only 7–10 μL , often smaller than the volume of the dosage form.²

In vitro release studies for ophthalmic dosage forms have used receptor volumes ranging from 1 to 100 mL. Often, the volume used is not stated; one infers it to be large.^{3–8} For example, a recent study used the USP rotating basket procedure with a buffer reservoir of 100 mL.⁹ Some studies employed a reduced volume of 4–6 mL of solution.^{10–12} Other important features determining rate of drug release are composition of the receptor solution and manner in which fluid is exchanged. In some studies, fluid is not exchanged, and drug concentration is monitored directly by UV spectrophotometry^{7,8} or fluorescence¹⁰ or sampled and analyzed by HPLC⁹ or other methods.⁹ In other studies, fluid is completely exchanged at discrete intervals.^{11,12} *In vivo*, tear fluid is continually exchanged at a rate of about 0.7 $\mu\text{L min}^{-1}$, which represents a turnover rate of about 9% min^{-1} . In only one study was fluid exchanged continually through a flow cell,¹³ however, the cell volume (500 μL) and exchange rate (250 $\mu\text{L min}^{-1}$) were orders of magnitude greater than those observed *in vivo*. Such large volumes have been used in an effort to provide excellent sink conditions for diffusive systems. However, drug release from a device residing in a cul-de-sac may be far from this idealized state, even in the absence of adsorption-desorption phenomena expected with ocular tissues.

Recent studies of transcorneal transport implicitly acknowledge the significance of the small volumes of the pre-

corneal space.^{14,15} While these are realistic *ex vivo* approaches to investigate transport, the specific techniques serve only as cumbersome alternatives for evaluating vehicles.

We describe a new controlled release analytical system (CRAS) for characterizing those found *in vivo*. The reservoir volume was typically 8–30 μL . Buffer was continuously exchanged at a flow rate of 1 $\mu\text{L min}^{-1}$, typically. Drug concentration in the eluent was monitored continuously by UV spectrophotometry. This technique provides an *in vitro* system, that, except for specific—primarily tissue—losses, closely approximates the fluid dynamics of a uniform human precorneal tear reservoir.

In this paper we describe specialized apparatus and techniques used to simulate release expected under physiological conditions. We explore characteristic differences for a variety of ophthalmic vehicles and devices, where time-release profiles are sensitive functions of reservoir volume, eluent flow rate, and the matrix itself. We contrast our analytical technique with more conventional approaches. In particular, we quantify consequences of variation in system parameters, of both our and USP methods, on measured release kinetics. Data and analysis indicate bulk conventional methods introduce ambiguity of sufficient magnitude to question their appropriateness for ophthalmic application; this ambiguity is removed in our CRAS method by adopting only parameters representative of those occurring physiologically. Certainly, the quantitative relevance of the method waits direct comparison with *in vivo* kinetics, the topic of a subsequent publication.¹⁶

EXPERIMENTAL SECTION

Reagents. Levobetaxolol ((-)-1-[2-(cyclopropylmethoxy)ethyl]-3-(isopropylamino)-2-propanol, Laboratories D'Etudes Et De Recherches Synthelabo, Paris, France) free base and hydrochloride, (*R,S*)-betaxolol (also from Synthelabo), apraclonidine hydrochloride (2-[(4-amino-2,6-dichlorophenyl)imino]imidazolidine hydrochloride, Chemische Institut Schaefer, Oberwil, Switzerland), HEZ (6-(hydroxyethoxy)benzothiazole-2-sulfonamide, Organix Inc., Woburn, MA), resin (polystyrene-sulfonic acid, Alcon), and hydroxypropyl methylcellulose (Dow) were used as received. The eluents and all buffers were prepared with purified, deionized water (approximately 18 M Ω cm), adjusted to pH 7.4, and then filtered and degassed by using a Millipore solvent filtration apparatus equipped with 0.45- μm Nylon 66 membranes. Two eluents were used, one a phosphate-buffered saline and the second a tear substitute. Eluent 1 was prepared with 8.3 mM dibasic sodium phosphate, 11.9 mM monobasic potassium phosphate, and 128.3 mM sodium chloride. Eluent 2, the tear substitute,^{17–19} contained 116.4 mM sodium chloride, 18.9 mM potassium chloride, 0.44 mM calcium chloride, 26 mM sodium carbonate, and 0.8 mM monobasic sodium phosphate. The three drug standard solutions contained 0.291 mM betaxolol hydrochloride, 0.355 mM apraclonidine hydrochloride, or 0.365 mM HEZ; each was prepared with the appropriate eluent.

Drug and resin compositions for formulations A–I are presented in Table I. Ophthalmic gels (Xanthan gum, Kelco, San Diego, CA; locust bean gum, RL-200, Hercules, Wilmington, DE) A–D were cylindrical gels with a length of 8.0 mm and a diameter of 1.7 mm. Formulations E–G were not cast into any particular shape but were polymorphous. The gel matrix entrapped an ion-exchange resin, except for formulation G, which had no resin. Two ophthalmic suspensions were examined.

*To whom correspondence should be addressed.

Table I. Drug^a and Resin^b Compositions of Gel Formulations

formulation	gels				polymorphous			suspension	
	A	B	C	D	E	F	G	H	I
levobetaxolol (R,S)-betaxolol	16.3	19.5	39				16.3		16.3
apraclonidine				73		40.8			
HEZ							73		73
resin	19.3	169	253	316	105.3	140		17.6	

^aDrug concentrations are in mM. ^bResin concentrations are in mequiv/L (resin was measured to be 3.51 mequiv/g).

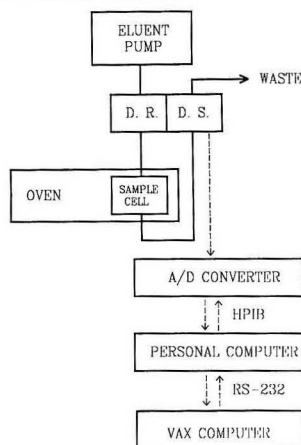


Figure 1. Schematic diagram of the instrument components used in the CRAS. DR/DS indicate the two optical paths of the detector, reference, and sample.

Formulation H contained levobetaxolol hydrochloride and resin in a vehicle containing mannitol for adjusting osmolality. Formulation I contained HEZ as 1- μ m particles in a vehicle containing sodium chloride for adjusting osmolality. The osmolality of suspensions H and I were adjusted to 300 mOsm. The viscosity of suspension I was adjusted to 15 cP with hydroxypropyl methylcellulose.

CRAS Instrumentation. The experimental arrangement is shown schematically in Figure 1. A syringe pump, constructed with saline-resistant Nitronic 50 stainless steel (ISCO Model No. LC 2600), was used to deliver eluent at a rate of 1.0 μ L min⁻¹. The use of a syringe pump was required in order to eliminate pulsations characteristic of reciprocating pumps when operated at this low flow rate. The variable-wavelength ultraviolet-visible detector (Spectra-Physics Model No. 8450) was equipped with a 1- μ L volume (3-mm path length) detector cell. PEEK (polyether ether ketone) HPLC tubing (0.007-in. i.d.) was used from the sample cell to the detector reference inlet. The eluent flowed through the reference side of the detector cell, through the sample cell, and returned through the sample side of the detector cell. The sample cell was housed in an HPLC column oven (FIAtron TC-50) and was maintained at 35 °C. A manual injector equipped with a 20- μ L sample loop (Valco CW6) replaced the sample cell when a system calibration was performed. Drug concentrations were quantified by digitizing the analog output of the detector with a programmable multimeter (Hewlett-Packard Model No. HP3478A). The digitized information was transferred through an HP-IB IEEE-48 interface to a personal computer (American Research Corp.) equipped with a math coprocessor (Intel 8087) and a 20 Mbyte hard disk drive. The data were transferred to and analyzed by a VAX 8600 computer (Digital Equipment Corp.).

Software. Data collection was accomplished using a PC program written in QUICKBASIC (Microsoft, version 4.5) that

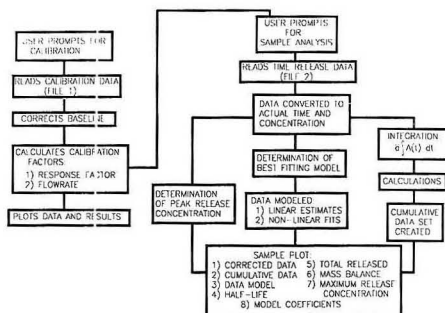


Figure 2. Flowchart describing the calibration and data analysis procedure for CFAS concentration-time profiles.

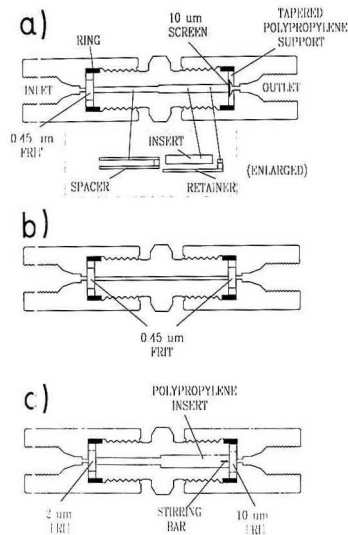


Figure 3. Schematic diagram of the sample flow cells used in the CRAS: (a) sample cell A used for integral gels; (b) sample cell B used for suspensions; (c) sample cell C used for simple solutions.

monitored real time data acquisition, collected at time intervals based on an exponential algorithm. Data transfer from the PC to the VAX was done using Kermit.²⁰ A second program written in SAS²¹ was used to determine the calibration constants, to integrate the amount of drug released, and to model release from samples using nonlinear regression analysis.²² A schematic diagram, presented in Figure 2, describes this program. The program prompts the user for necessary parameters and constants and produces a graphical presentation of corrected data with the coefficients for the mathematical model and other calculated parameters (cf. Data Acquisition and Analysis).

Sample Cell. Precolumns (Upchurch Scientific, Inc., Oak Harbor, WA Part No. C-130B) were modified to specialize the cells for different types of samples (Figure 3). Sample cell A was used for the rigid cylindrical gels (Figure 3a). Its inner diameter was bored to a dimension of 2.5 mm for a depth of 10 mm. This allowed for swelling of the gels while still maintaining reduced residual volume. The sample was retained within the cell by a stainless steel mesh exit screen (1-cm diameter, 10- μ m pore size, Waters Associates, Milford, MA, Part No. 25696), mounted on a polypropylene support with a tapered exit hole designed to reduce volume, mixing, and plugging. In addition to the sample, the cell contains a spacer upstream and a retainer downstream.

Both are 1.8-mm o.d. and 1.0-mm i.d. and fabricated from polypropylene. The spacer has two legs connected by a ring; it is oriented within the unmodified inlet with the ring toward the outlet. This practically eliminated back-flow or mixing into the inlet side (the remaining 2.0-mm i.d. \times 10-mm length) of the cell. The retainer was constructed with a single leg attached to a ring; the ring faces the exit port. The retainer resided in contact with the gel and helped ensure a constant, nonpulsatile eluent flow around the sample. The final reservoir volume, subtracting the volume of the gel sample and retainer, was reduced to 15–30 μ L, close to that of human eyes.

Sample cell B (Figure 3b) was used for suspensions and consisted of a polypropylene precolumn (Upchurch Part No. C-128) with an inner diameter of 1.0 mm, with a length of 10 mm. The reservoir volume of this cell was 15.7 μ L. Insertion of small polytetrafluoroethylene (PTFE) washers prevented most small particles from passing around the stainless steel frits (0.45- μ m pore size). In isolated instances we also supplemented the frits with additional hydrophilic filter membranes (0.2- μ m pore size). These retained some of the smaller submicron particles. However, for most pharmaceutical suspensions this was not necessary.

Sample cell C (Figure 3c) was used for simple drug solutions and consisted of a modified precolumn similar to cell A, only its diameter was enlarged to 3 mm for a depth of 10 mm. This reservoir volume was then reduced to 8 μ L by means of a cylindrical plastic (Nylon 66) insert with a rectangular cavity. A magnetic stirring bar enabled continuous mixing of eluent within the cavity. This *in vitro* dilution corresponds to the clearance by tears, *in vivo*.

Procedure. Calibration of the system was accomplished by flow injection analysis. A 20- μ L aliquot of standard was injected. Drug standard dissolved in eluent was injected onto the system using a manual injector in place of the sample cell. Concentrations of about 100 mg/mL were used for betaxolol, apraclonidine and HEZ; precise absorbance values were obtained at wavelengths of 280 nm for betaxolol, 298 nm for apraclonidine, and 330 nm for HEZ; absorptive coefficients were 1.002, 0.535, and 0.219 (mg/mL)/AU, respectively.

Sample analysis was accomplished after replacing the injector with a sample cell (without altering the flow rate) and allowing the system to reequilibrate for 1 h. Following this, the outlet end of the cell was disconnected from the detector and opened, and sample was inserted. For the analysis of a gel, sample cell A was used with the spacer and retainer; the retainer being inserted following the sample. Sample cell B was used with suspensions, which were injected so as to displace the eluent totally from the cell. Solutions were analyzed using sample cell C, where the solution was injected so as to totally displace the eluent, followed by the addition of a small stirring bar. The cell was then closed and reconnected to the detector, which was reset to zero, and data acquisition initiated. Drug dilution or elution decay times typically range from 0.5 to 8 h for the gel and suspension samples while the decay times for solutions were close to 10 min.

Shaking Basket Procedure. Preformed gel samples were weighed in 100 mesh stainless steel baskets (VanKel Industries T-1045-30, Edison, NJ). At time zero, the baskets were placed in 1.5-oz. glass jars (Scientific Products B7454-1) containing 10.0 \pm 0.1 mL of buffer (eluent 1). The jars were capped and placed in a shaker (Lab-line 3535), which was operated at room temperature with a shaking frequency of 2.5 Hz. At subsequent specified times, the baskets containing the gels were withdrawn from the jars and placed in new jars containing fresh buffer. This resulted in a complete exchange of 10 mL of buffer at each time point. Each aliquot was measured for drug concentration by HPLC, and the cumulative percent released was calculated on the basis of the amount of drug in the formulation. The results from four samples were averaged to produce each data point.

HPLC Procedure for Betaxolol. Analysis of betaxolol concentrations, which ranged from 0.05 to 50 μ g/mL, was accomplished by HPLC. This system consisted of an autosampler (Waters WISP, Model 712), a pump (Waters model 510), a data processor (Waters Model 840), and an ultraviolet spectrophotometer (Waters Model 940) operated at 222 nm. A silica column (Rainin Instrument Co., Microsorb), 150 mm length \times 4.5 mm i.d., with a particle size of 5 μ m was used. The mobile phase consisted of 70% acetonitrile and 30% 5 mM sodium phosphate

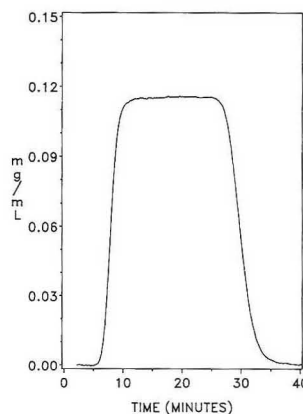


Figure 4. Example of calibration data for the CRAS system for betaxolol.

in water at pH 7.0. The injected volume was 20 μ L, and the flow rate was 1 mL min⁻¹.

This procedure was used in order to measure low concentrations of betaxolol (a drug with an amine functional group). The silica column provided a single separation mechanism, unlike many reversed-phase columns which when used with amines have competing mechanisms and, as a result, are not typically able to measure concentrations below 1 μ g/mL. A betaxolol standard curve (absorbance versus concentration) usually gave $r^2 = 0.999$ with an intercept of zero. A 1.5% CV for 1 μ g/mL of betaxolol was observed for a new column, with precision decreasing slightly to ~3% CV after about 500 injections. This method, even though utilizing a silica column with an aqueous mobile phase, has a column life sufficiently long to be practical. The retention time was about 6 min.

Equilibration Procedure. Gel samples with Betaxolol (formulation D) were weighed in 4-mL screwcap HPLC vials (Kimble 60810G). Five replicates were obtained for each receptor volume examined. Various volumes of phosphate-buffered saline (eluent 1) ranging from 0.2 to 3.0 mL were added to the vials; these were then capped with Teflon septa and placed on the shaker operating at 2.5 Hz. The sample eluted from each gel was analyzed for betaxolol content by HPLC after shaking continuously for 72 h. The percent of drug released was calculated for each sample independently on the basis of the mass of each gel. The samples were analyzed again after shaking an additional 150 h and were found to give identical results, suggesting that the experiment had indeed reached equilibrium after 72 h. The drug content of unsoaked gels was also measured and found to be within 2% of its expected value.

DATA ACQUISITION AND ANALYSIS

Calibration. The most accurate and reliable method of calibrating this system was found to be by injection of a standard which totally displaced the eluent from a portion of tubing; this resulted in plug flow. The plug of standard created a nearly rectangular pulse for calibration (Figure 4) with the maximum absorbance (A_{max}) being the value at the top of the plateau. The following description of the calibration serves to indicate the simplicity and generality of the method.

The computation of both detector response, \bar{a} , and flow rate as functions of observables A_{max} , injected volume, V , duration of pulse, T , and concentration of standard, c_0 , proceed simply. The absorbance, $A(t)$, as a function of time, follows a linear response:

$$\bar{a} = c(t)/A(t) = c_0/A_{max} \quad (1)$$

where $c(t)$ is concentration as a function of time. Thus, as long as the detector response reaches a plateau, \bar{a} can be

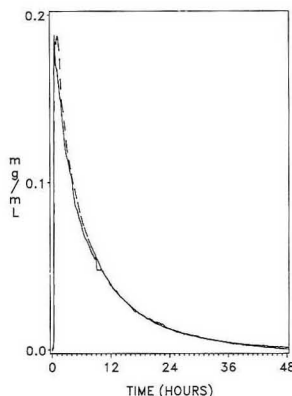


Figure 5. Reproducibility of CRAS time-release profiles (polymorphous formulation E): (—) first experiment; (---) second experiment.

calculated. The flow rate, \dot{V} , can be determined by integrating the absorbance with time; let I be this integral:

$$I = \int_0^T A(t) dt \quad (2)$$

This allows one to define the flow of an idealized rectangular pulse of equivalent mass and define that equivalent pulse duration, T , in principle for any shape pulse so long as it achieves a detectable plateau:

$$A(t) = A_{\max} \quad (3)$$

In this approximation to the integral

$$I = A_{\max} T \quad (4)$$

where T is the duration of the pulse. The flow rate then can be calculated as

$$\dot{V} = V/T = VA_{\max}/I \quad (5)$$

In this way the flow rate can be calculated from the known injection volume of standard dissolved in eluent, the measured absorbance plateau, and the integral of the absorbance. The technique has been shown to be accurate and precise; it is especially valuable at low flow rates.

Data Handling. An advantage of this system over more traditional methods of monitoring drug release by basket and dissolution techniques, is the virtually continuous monitoring of drug release. It was found that a logarithmic collection routine was suitable for most applications since often drug release can be represented as an exponential or multiple exponential process. These combined factors provide sufficient sensitivity to enable accurate detection of subtle responses to modifications in vehicle design, drug concentration, and mechanism of release, mechanisms which can be modeled mathematically.

There are two programs integral to the CRAS experiment. The first is a BASIC program, resident in the PC, used for data acquisition and real-time display. The second, resident on a VAX, analyzes the data sets stored by the first.

The BASIC program orchestrates collection of two data sets per experiment, the calibration run (file 1) and the formulation- and time-dependent drug release (file 2). The program controls the multimeter and instantly displays its digitized information. An example of a typical display of absorbance versus time is shown in Figure 5; one observes its trace formed in real time. This presentation facilitates early detection of experimental problems and permits aborting a run when a

Table II. Influence of Random Noise on Parameters Deduced from Simulated CRAS Data

P	0.0	0.001	0.005	0.02	0.05
E_1	0.50	0.50	0.49	0.48	0.45
E_2	2.05	2.08	1.76	1.44	0.83
D_1	0.10	0.10	0.10	0.09	0.08
D_2	2.01	2.02	1.90	1.71	1.21
D_3	3.96	3.94	4.17	4.47	7.60

problem occurs. By prompting the user for input parameters and constants, such as those measured during calibration, the program has all the information required to create output files needed by the second program when it scales the absorbance and flow rate to provide absolute concentration as a function of time.

Logarithmic sampling was used in order to provide absorbance decrements of approximately equal magnitude for these exponentially decaying response functions. As a simple approximation for logarithmic time sampling we allowed the interval between samples to increase linearly with sample number. The minimum and maximum intervals between samples were set to 3 s, corresponding to the beginning of a run, and 300 s, corresponding to the end of a run. The number of samples measured for short runs was 1000 data points. For runs longer than 42 h, the number of samples was extended, consistent with the constraint of a maximum interval of 300 s. The spacing of time samples beyond 42 h was equal to the maximum spacing. It is because of the high density of points that the entire data curves appear to be continuous.

The VAX program analyzes the two datasets stored by the first program. A flow diagram of this program, which uses SAS software, is shown in Figure 2. First, the calibration data set is processed (file 1) to obtain the detector response factor and eluent flow rate (see eqs 1–5). Next, the time-release data set (file 2) is analyzed. The data are corrected for baseline drift, concentration response factor, and flow rate, in order to provide determinations of absolute concentration versus time. The data are modeled using several variants of routines capable of resolution into multiple exponential components; these are reported as a curve representing the theoretical simulation of the data. The data can be represented using the following multiple exponential forms:

$$C = A_1 e^{-B_1 t} + A_2 e^{-B_2 t} - (A_1 + A_2) e^{-B_3 t} \quad (6a)$$

$$C = A_1 e^{-B_1 t} - A_1 e^{-B_2 t} \quad (6b)$$

Equation 6b is a simplified form of (6a) in which A_2 has been set to zero. The constraint on the prefactors is required by the boundary condition that at the initial time the concentration is zero.

In order to establish the stability of the fitting procedure above to sample noise, the following function was used to generate artificial CRAS data:

$$C(t) = E_1 e^{-D_1 t} + E_2 e^{-D_2 t} - (E_1 + E_2) e^{-D_3 t} + Pr \quad (7)$$

where r is a random number with a mean of zero and a standard deviation of unity and P is a prefactor ranging from $0 < P < 0.05$. Typical sets of input values of the E 's and D 's were

$$\begin{aligned} E_1 &= 0.5 & D_1 &= 0.1 \\ E_2 &= 2.0 & D_2 &= 2.0 \\ D_3 &= 4.0 \end{aligned} \quad (8)$$

The influence of P on the values of the E 's and D 's deduced from the noise-transformed data using the same fitting procedure as for actual data is shown in Table II. A repre-

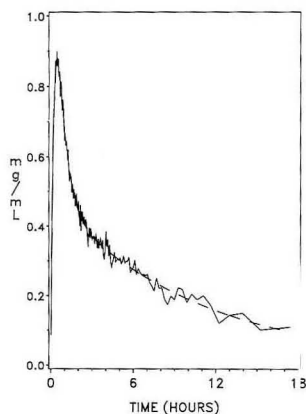


Figure 6. Influence of noise on theoretical CRAS concentration-time profiles: (—) simulated noise using eq 7 with a P value of 0.02; (---) fit to eq 6a. See Table II for fit parameters.

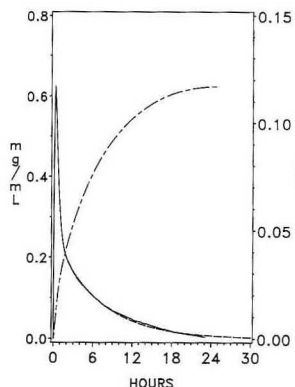


Figure 7. Results from analysis program for a CRAS concentration-time profile: (—) actual data for gel formulation B; (---) fit to eq 6a; (---) cumulative release profile. The total drug dose was 0.115 mg of betaxolol.

Table III. Values of Parameters Fit to Eq 6

formulation	A	B	C	F	H
A_1	0.30	0.26	0.39	0.24	1.36
A_2	0.68	1.44	1.22	0.43	
B_1	0.29	0.15	0.11	0.23	1.54
B_2	1.03	2.67	1.95	2.01	
B_3	11.34	6.01	5.37	82.5	26.2
RMSE	0.031	0.008	0.013	0.019	0.044

sentative plot for a value of $P = 0.02$ is shown in Figure 6. From Table II, it is apparent that E_1 and D_1 are least influenced by noise in the data and that for values of P up to 0.05, they are accurately deduced from the fit. Estimates of the other parameters are accurate for P values below 0.005; however, these parameters are less important for determining the long-term time-release behavior. This demonstrates the fitting procedure is satisfactorily stable when P (or equivalently the root mean square error, RMSE) is less than ~0.05. Our typical results, e.g. Figure 7, give RMSE's in the range ~0.01–0.02 (see also Table III), satisfying the criterion established numerically. Those data sets not satisfying the criterion infrequently occur, usually as the result of sample

Table IV. Parameter Values from Various Runs of Formulation E (Eq 6a)

trial	first	second	third
A_1	0.114 ± 0.008	0.107 ± 0.007	0.50 ± 0.02
A_2	0.107 ± 0.007	0.092 ± 0.006	
B_1	0.093 ± 0.005	0.090 ± 0.004	0.31 ± 0.02
B_2	0.40 ± 0.04	0.39 ± 0.03	
B_3	8.1 ± 0.3	12.1 ± 0.4	4.5 ± 0.5
RMSE	0.003	0.003	0.022

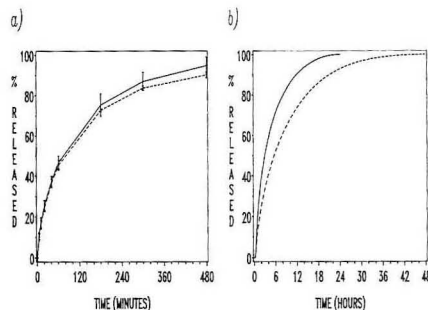


Figure 8. Cumulative time-release profiles for gel formulations: (—) gel formulation B with a drug to resin ratio of 0.125; (---) gel formulation C with a drug to resin ratio of 0.167; (a) shaking basket experiment; (b) CRAS.

inhomogeneities or loading anomalies, and must be discarded.

Reproducibility and Accuracy. In Figure 5, the reproducibility of the system is illustrated graphically. These are two concentration-time profiles produced from separate runs using formulation E. The mean differences between these is less than 3%. In Figure 7, we present a CRAS release profile on formulation B. Plotted are the concentration-time profile (solid line), a modeled multiexponential fit (dotted line), and the integration of the concentration-time profile (dashed line). At times, the fit is so good on the one hand and the number of data points is so large that it is difficult in a plot of both to distinguish between model and experiment. We typically found that the integrated concentration agreed to within 5% of the predicted amounts. This indicates not only the reproducibility but also the accuracy of this technique in determining drug release, the maximum concentrations, and the total amount released.

An example of the reproducibility in the values of parameters deduced by fitting to eq 6 is shown in Table IV, which compares the values of parameters deduced from three separate experiments for formulation E. The first two experiments are those which appear in the overlay of Figure 5. The values deduced are in reasonable agreement for the first two experiments, which showed an RMSE of 0.003. The fit of the third experiment to eq 6a was not in good agreement, and thus eq 6b was used. This run appeared to be flawed, as corroborated by its higher RMSE of 0.022.

A high degree of accuracy in the drug elimination kinetics for solutions (sample cell C) was also shown by a simple solution having a dilution "release" decay time of about 7 min, approximating the tear decay time of an average human eye.²³

RESULTS AND DISCUSSION

Discrete vs Continuous Sampling. The shaking basket method is similar to some published studies in which the dosage form is periodically transferred to fresh aliquots of buffer (4–6 mL) which are later analyzed for drug.^{10–12} This technique differs from the CRAS in using discrete, noncontinuous eluent exchange and a much larger reservoir volume.

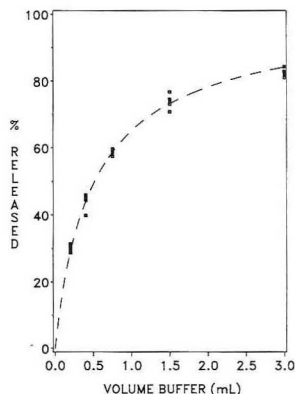


Figure 9. Equilibrium experiment showing percent of drug released after gels (formulation D) were equilibrated in various volumes of eluent 1 for 72 h. The theoretical curve (---) is predicted from Langmuir adsorption (eq 9).

We compare the ability of the two techniques to distinguish between different formulations such as B and C. A comparison of the cumulative time-release profiles from these two techniques can be seen in Figure 8. In the left panel are shown the results from a shaking basket experiment for two gel formulations (B and C); in the right are CRAS data for the same two formulations. In each case the cumulative time-release profile is plotted. In the shaking basket experiment, 50% of the drug is released in about 1 h, and little difference in the time-release profile for the two formulations is observable. However, in the CRAS experiment, the drug decay time is 3–6 times longer and there is a large difference between the cumulative time-release profiles for the two formulations. The drug decay time is about 3 h for formulation B and about 6 h for formulation C. Thus, the CRAS technique can be used to discern differences in time-release profiles obscured by more conventional methods which use much larger reservoir volumes.

By contrast, we find that for shaking basket experiments, the time-release profile depends strongly upon the receptor volume and the frequency of exchange. The equilibrium experiment (Figure 9) shows how receptor volume dramatically influences the amount of drug released at equilibrium in the absence of eluent exchange. Only 30% of drug is released for a 200- μ L receptor volume, which is still about 25 times greater than the residual tear volume in the human cul-de-sac.

This phenomenon, controlling the release profile in shaking basket experiments, can be modeled. Letting M be the fraction of drug released on equilibrating a reservoir of volume V_F with entrapped drug in volume V_I , R be the ratio of rate constants characterizing the rate of release from resin to the rate being bound (here treated as a fit parameter), and S be the initial ratio of concentration of adsorption sites available to concentration of adsorption sites occupied, then the following equation (Appendix, eq A-9) can be used to indicate the dependence of the amount of drug released on the volume of the reservoir into which it is placed, V_F :

$$M = \frac{S}{2} \left\{ \left(1 + R \frac{V_F}{V_I} - \frac{1}{S} \right) + \left[\left(1 + R \frac{V_F}{V_I} - \frac{1}{S} \right)^2 + \frac{4RV_F}{SV_I} \right]^{1/2} \right\} \quad (9)$$

This equation assumes simple Langmuir-type adsorption.²⁴

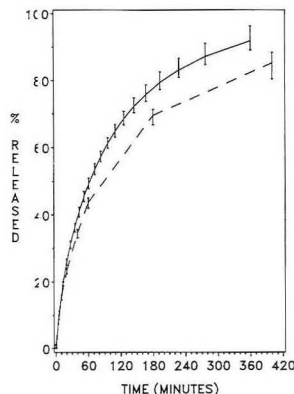


Figure 10. Influence of the frequency of discrete exchange of the receptor solution for the shaking basket experiment using gels (formulation D). The lines connect mean values of the experimental points.

The theoretical curve in Figure 9 was generated using this equation, adjusting only one parameter R for best fit; the fit is well within experimental error, with a predicted R value of 0.0306 ± 0.0035 . Equation 9 predicts that only 1.7% of the drug should be released in a hypothetical physiologic volume of 7.5 μ L. It is for this reason that the standard type of analysis is inadequate. Thus, the volume of the receptor solution used in typical *in vitro* release experiments is far too large to provide realistic estimates of drug release from these systems.

One expects the frequency of exchange also to play an important role in determining drug release rates. This is demonstrated experimentally by the data in Figure 10, where distinct release rates are observed simply by changing the frequency of exchange. In the Appendix we derive the scalloped time-release profile that would be generated from discrete exchange of buffer for systems which exhibit Langmuir adsorption. The time dependence for such a situation can be represented by the following product of multiple exponentials (see Appendix):

$$M_N(T) = \left[\frac{k_1/V_I}{\left(\frac{k_1}{V_I} + \frac{k_2}{V_F} \right)} \right] \left[1 - e^{-(k_1/V_I + k_2/V_F)(T_N - T_{N-1})} \right] \times \prod_{n=1}^{N-1} \left\{ 1 - \left[\frac{k_1/V_I}{\left(\frac{k_1}{V_I} + \frac{k_2}{V_F} \right)} \right] \left[1 - e^{-(k_1/V_I + k_2/V_F)(T_n - T_{n-1})} \right] \right\} \quad (10)$$

where $T_{N-1} \leq T \leq T_N$. Each successive scallop corresponds to another function; the function M_N might better be written $M_N(T, T_1, \dots, T_{N-1})$. Equation 10 was used to generate the theoretical scalloped time-release profiles appearing in Figure 11. Shown are hypothetical release profiles which would result theoretically if the same dosage form were examined in the shaking basket experiment, contrasting frequent versus infrequent exchange of buffer. The shaking basket approach does not provide a continuous release profile but, as Figure 11 suggests, rather represents the splicing together of separate equilibrium experiments. The overall time dependence is greatly influenced by the frequency of exchange. One would also expect there to be differences in release profiles between experiments which have discrete versus continuous exchange of eluent.

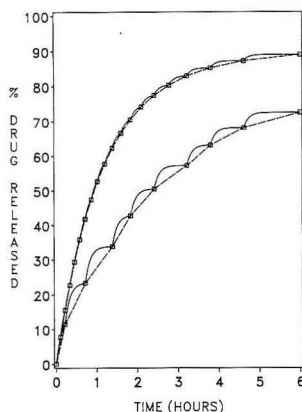


Figure 11. Hypothetical influence of altering the receptor exchange frequency on the cumulative release profile. Scalloped curves (—) are generated from the theory in the appendix; dashed lines merely connect junction points, mimicking the shape of experimental plots (Figure 10).

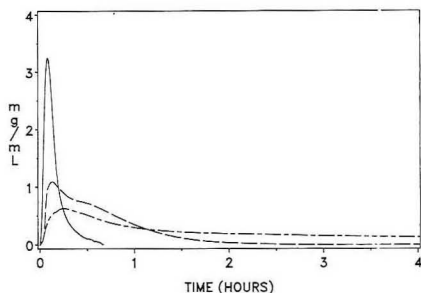


Figure 12. Comparison of time-release profiles from three different preparations of betaxolol: (—) drug solution representing marketed product (sample cell C); (---) suspension formulation H (sample cell B); (- - -) gel formulation B (sample cell A).

Sample-Dependent Release Kinetics. The results presented in this section are intended to survey the utility of the CRAS technique, and not to explore exhaustively all of the variables used, nor the subtlety involved in formulating for controlling drug release. Nonetheless, several prominent features are apparent and the results appear both general and suggestive of the complexity of multicomponent formulations.

In Figure 12 we present dilution or elution profiles for several drugs from sample matrices ranging over simple solutions, suspensions, and integral ophthalmic gels. These differences in formulation, as would be expected, produce widely varying release profiles. In Figure 12, we compare time-release profiles for three different formulations of the β blocker betaxolol: (1) a simple solution (sample cell C); (2) a suspension using ion-exchange resin (sample cell B); (3) a drug-laden resin suspended in a rigid gel (sample cell A).

The briefest profile results from the simple solution where displacement is controlled by drug diffusion into the exchanging eluent within the sample reservoir. This results in rapid dumping, an effect exhibited by the solid curve in Figure 12; it represents the behavior expected for a marketed product (BETOPTIC, 0.56% Betaxolol HCl solution). Time release is essentially complete in $1/2$ h. [Since direct measurement of the marketed product (5000 ppm betaxolol) would have overloaded the detector, a solution of much lower concentration (115 ppm) was used. The absorbance readings were

multiplied by a factor f representing the difference in concentration between the two solutions and also taking into account the dilution which takes place when a 30- μ L drop is mixed with the 7.5- μ L resident tear volume. Thus, the factor f was $f = (5000/115)(30/37.5) = 34.78$.]

The use of an ion-exchange resin in a simple 1:1 drug:resin (weight:weight) suspension sustains drug release over a 2-h period and reduces the maximum drug concentration in the eluent (a precorneal fluid composition) to 30% of that of the solution. The gel formulation, at a lower drug:resin ratio, extends time release beyond 4 h and reduces the maximum concentration further, to only 20% of that of the solution. This suggests that such sustained release formulations should reduce side effects.

The system is sensitive to small changes in formulation, such as a change in concentration of ion-exchange resin. This can be observed from Table III where, for example, the exponents correlated with the long-term exposure (B_1) are smaller for the formulation (B) with the greater amount of resin (relative to A). This corresponds to a longer decay time for formulation B, since the decay time is the inverse of the exponent. This is consistent with the notion that additional binding sites should slow the rate of drug release from the vehicle.

On the other hand, additional complexity of these systems is revealed by comparing the results for formulations B and C. Formulation C has both more drug and more resin than B, but the ratio of drug to resin is increased. If only the intensive variables were important, one might expect the release to be faster from formulation C. The data, and the decay constants derived from them, indicate the release is slower. Clearly, extensive properties are important in these small systems. Perhaps the amount of resin is in part regulating the rate of ion transport from the eluent required for exchange and drug release from resin. Figure 8b also illustrates this response to a higher drug:resin ratio; Figure 8a suggests this effect is independent of reservoir volume.

Equations 6a,b were used to fit data for CRAS time release profiles. In Figure 7, we show a fit to eq 6a from the CRAS experiment shown. The fit is almost exact. We find that two exponents are sufficient to describe release profiles for systems in which little excess of resin was used, such as formulation E (27% excess resin with respect to the dibasic drug apraclonidine) and formulation H (8% excess). For formulations B-F, in which a 3-7-fold excess of resin was present, eq 6a clearly provided the better fit. Values of the parameters fit from eqs 6a,b are summarized in Table III.

It can be shown that eq 6a is consistent with a three-compartment model for the gel (two compartments) and the reservoir (the third compartment) with first-order transfer of material between compartments.¹⁶ Drug release from such a system would be biexponential. Similarly, eq 6b is consistent with a two-compartment model for the total system, one for the dosage form and one for the reservoir. Probably the single most important parameter describing the drug decay time is the exponent corresponding to the slowest process, B_1 . From Table I we see that B_1 , the inverse of the characteristic time for release, decreases as resin concentration increases.

The time-release profiles for suspensions of a sparingly soluble drug are quite different, as observed from Figure 13, where we have shown concentration-time profiles for both a suspension and polymorphous gel formulation of HEZ. The initial small response spike appears to be caused by the presence of a solution saturated with the drug and possibly a solubilizing effect from formulation excipient. This is then followed by simple dissolution at a constant rate, adequate to maintain a steady-state concentration near saturation, as the drug continues to dissolve in the constantly diluting eluent.

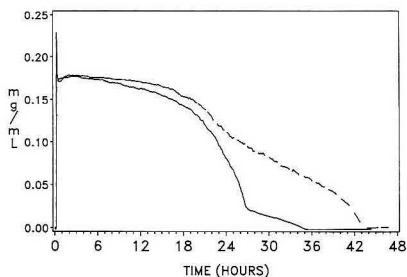


Figure 13. Concentration-time profile from a suspension of a sparingly-soluble drug in the CRAS: (—) HEZ suspension formulation I; (---) HEZ polymorphous gel formulation G.

As the drug is expended, the slope decreases more steeply, indicating the sensitive dependence of release on concentration of particles and particle geometry. Formulations with higher drug content produce longer release times but concentrations still limited by solubility. Suspensions, unlike gels that are retained within the cul-de-sac, are being expelled from the eye continuously. Therefore when suspensions in this model are studied, a further correction allowing for this elimination need be included.

CONCLUSION

The CRAS is a powerful *in vitro* technique for measuring time-release profiles of ophthalmic dosage forms under conditions closely simulating those prevailing in precorneal tear fluid. Because of its automated data sampling, the time-release profile can be monitored simply, reproducibly, continuously, and with great detail. Simultaneous and distinct mechanisms of release can be evaluated by observing multiple exponential profiles, a characteristic not detected with less precise techniques.

It is expected that these more sensitive results will be of significance *in vivo*, that they are both real and relevant therapeutically.¹⁶ For example, the CRAS technique revealed greater dependence of release profiles on composition than did the shaking basket method, in which rates are distorted by imposition of unrealistic boundary conditions, a consequence of unphysiological receptor volumes. The importance of small receptor volume was confirmed unambiguously by equilibrium experiments conducted as a function of volume and explained analytically.

Of practical significance, it was observed that the kinetics of elution from suspensions and gels could be distinguished, each unique in the CRAS analysis due to separate physicochemical factors governing release. These are expected to be manifested *in vivo*.¹⁶ Even in those instances where *in vivo* and CRAS observations may conflict, the discrepancy may be a useful indicator of modified physiological processes, which otherwise might be undetected.

ACKNOWLEDGMENT

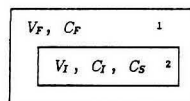
Thanks are due to David Untrecht and Alvin Michaelis for assisting in the development of data-transfer procedures. The capable assistance of Janet Hill-Aiello in formulating gel samples and in obtaining both shaking basket and CRAS time-release profiles is appreciated. Work done by Richard A. Justice in the development of the HPLC method is also appreciated. We appreciate the critical review of the manuscript by Barbara Piper. We also thank Drs. E. R. Cooper, D. F. Hager, B. M. York, and V. J. Rajadhyaksha for their support of this project.

APPENDIX

Theory of Volume Dependence of Release. These re-

sults apply to systems permitted to achieve equilibrium. The models assume Langmuir adsorption of drug to adsorption sites. The model is appropriate for investigating release patterns predicted from a shaking basket type of experiment described in the Results and Discussion.

The following diagram defines the parameters used in the model:



Here we have two homogeneous compartments consisting of the dosage form (compartment 2), envisioned to be an integral gel in this analysis, of volume V_I and having time-dependent drug concentration C_I immersed in a volume V_F of receptor solution (compartment 1) having drug concentration C_F , also time-dependent. The dosage form is imagined to have a concentration C_S of binding sites for drug. For this simple model, the tacit assumption is that all of the drug in compartment 2 is bound.

We presume a Langmuir model²⁴ for the adsorption of drug to binding sites found in the gel, the primary tenet of which is the notion of a finite number of adsorption sites to which an adsorbate can remain in equilibrium. In our notation, we can set the rate of increase in the number of free drug molecules equal to the difference between desorption and recombination at the binding sites in compartment 2. Mathematically, this can be represented by

$$V_F \frac{dC_F}{dt} = k_1 C_I - k_2 C_F \left(1 - \frac{C_I}{C_S} \right) \quad (\text{A-1})$$

This describes the first-order process of drug release and recombination of drug with saturable gel binding sites, where the rate of recombination is controlled by both concentration of free drug and the fraction of available, or unbound, sites. This rate gives rise to the second term. At equilibrium, $dC_F/dt = 0$, so

$$k_1 C_I = k_2 C_F \left(1 - \frac{C_I}{C_S} \right) \quad (\text{A-2})$$

Conservation of drug, assuming its stability, requires the loss of drug from compartment 2 to equal the amount gained by compartment 1:

$$V_I(C_I^\circ - C_I) = V_F C_F \quad (\text{A-3})$$

On replacing C_I in eq A-2 by this last expression

$$\left(\frac{V_F C_F}{V_I C_I^\circ} \right)^2 + \left(\frac{V_F k_1 C_S}{V_I k_2 C_I^\circ} + \frac{C_S}{C_I^\circ} - 1 \right) \left(\frac{V_F C_F}{V_I C_I^\circ} \right) - \frac{k_1 V_F C_S}{k_2 V_I C_I^\circ} = 0 \quad (\text{A-4})$$

Defining the parameter M , the fraction of drug released from gel, as

$$M = \frac{V_F C_F}{V_I C_I^\circ} \quad (\text{A-5})$$

and defining two parameters R and S as

$$R = \frac{k_1}{k_2} \quad (\text{A-6})$$

$$S = \frac{C_S}{C_1^0} \quad (\text{A-7})$$

allows simplification of eq A-4:

$$M^2 + \left[\left(\frac{V_F}{V_I} R + 1 \right) S - 1 \right] M - \frac{V_F}{V_I} R S = 0 \quad (\text{A-8})$$

Only the positive root of this quadratic equation is meaningful:

$$M = \frac{1}{2} \left\{ - \left[\left(1 + R \frac{V_F}{V_I} \right) S - 1 \right] + \left[\left[\left(1 + R \frac{V_F}{V_I} \right) S - 1 \right]^2 + \frac{4 R V_F S}{V_I} \right]^{1/2} \right\} \quad (\text{A-9})$$

Equation A-9 was fit to the data of Figure 9 using SAS procedure NLIN,²¹ using R as a single adjustable parameter, which was found to be 0.0306 ± 0.0005 . The parameter S is factored out to produce the more symmetric eq 9 of the text.

Time Dependence and Solvent Exchange (Langmuir Model). We now solve for the time dependence of drug concentration in each compartment, after placing a drug-laden gel in a buffer aliquot of volume V_F , and consider the influence of successive discrete exchanges. Consider the complement to eq A-1 for the gel compartment:

$$V_I \frac{dC_I}{dt} = -k_1 C_I + k_2 C_F \left(1 - \frac{C_I}{C_S} \right) \quad (\text{A-10})$$

In what follows, we linearize eq A-10 for simplicity:

$$V_I \frac{dC_I}{dt} \approx -k_1 C_I + k_2 C_F \quad (\text{A-11})$$

Using the constraint of the conservation of drug between compartments (eq A-3), eq A-11 becomes

$$V_I \frac{dC_I}{dt} \approx -k_1 C_I + k_2 \frac{V_I}{V_F} (C_1^0 - C_I) \quad (\text{A-12})$$

Dividing by V_I and regrouping terms, we obtain

$$\frac{dC_I}{dt} \approx - \left(\frac{k_1}{V_I} + \frac{k_2}{V_F} \right) C_I + \frac{k_2}{V_F} C_1^0 \quad (\text{A-13})$$

The solution of this linear first-order differential equation satisfying the boundary condition requiring $C_I(0) = C_1^0$ is

$$C_I(t) = \frac{C_1^0}{\left(\frac{k_1}{V_I} + \frac{k_2}{V_F} \right)} \left[\frac{k_2}{V_F} + \frac{k_1}{V_I} e^{-[(k_1/V_I) + (k_2/V_F)]t} \right] \quad (\text{A-14})$$

and the corresponding equation for the compartment for free drug satisfying the boundary condition $C_F(0) = 0$ is

$$C_F(t) = \frac{V_I}{V_F} C_1^0 \left[\frac{k_1/V_I}{\left(\frac{k_1}{V_I} + \frac{k_2}{V_F} \right)} \right] [1 - e^{-[(k_1/V_I) + (k_2/V_F)]t}] \quad (\text{A-15})$$

Note, these solutions, despite the linearization, satisfy the conservation eq A-3 at all times.

Next, at $t = T_1$, the buffer is exchanged. The experiment begins over again, only now a different value of C_1^0 is used— $C_1^0 = C_1(T_1)$ —for the initial bound concentration. For a series of installations at times T_1, T_2, \dots, T_N , we obtain the following product:

$$C_F(T_N) = \frac{V_I}{V_F} C_1^0 \left[\frac{k_1/V_I}{\left(\frac{k_1}{V_I} + \frac{k_2}{V_F} \right)} \right] [1 - e^{-[(k_1/V_I) + (k_2/V_F)](T_N - T_{N-1})}] \times \prod_{n=1}^{N-1} \left\{ 1 - \left[\frac{k_1/V_I}{\left(\frac{k_1}{V_I} + \frac{k_2}{V_F} \right)} \right] [1 - e^{-[(k_1/V_I) + (k_2/V_F)](T_n - T_{n-1})}] \right\} \quad (\text{A-16})$$

The definition of M (eq A-5) can easily be used to obtain the cumulative fraction of drug released, as expressed in eq 10 in the text.

Registry No. HEZ, 95599-36-3; levobetaxolol, 93221-48-8; (R,S)-betaxolol, 87896-30-8; apraclonidine hydrochloride, 73218-79-8; polystyrenesulfonic acid, 50851-57-5.

REFERENCES

- (1) *United States Pharmacopeia*, XXI, and *National Formulary*, XVI, United States Pharmacopeial Convention, Rockville, MD, 1985; Standard Procedure (722), pp 1243–1246.
- (2) Chrai, S. S.; Patton, T. F.; Mehta, A.; Robinson, J. R. *J. Pharm. Sci.* **1973**, *62*, 1112–1121.
- (3) Shell, J. W.; Baker, R. W. *Ann. Ophthalmol.* **1974**, 1037–1045.
- (4) Dohlman, C. H.; Pavan-Langston, D.; Rose, J. *Ann. Ophthalmol.* **1972**, 823–832.
- (5) Allansmith, M. R.; Lee, J. R.; McClellan, B. H.; Dohlman, C. H. *Trans.—Am. Acad. Ophthalmol. Otolaryngol., Sect. Ophthalmol.* **1975**, *79*, OP128–136.
- (6) Ticho, U.; Blumenthal, M.; Zonis, S.; Gal, A.; Blank, I.; Mazor, Z. W. *Br. J. Ophthalmol.* **1979**, *63*, 45–47; *Ann. Ophthalmol.* **1979**, 555–561.
- (7) Gale, R.; Chandrasekaran, S. K.; Swanson, D.; Wright, J. J. *Membr. Sci.* **1980**, *7*, 319–331.
- (8) Meslard, J. C.; Subira, F.; Bunel, C.; Vairon, J. P. *Polym. Prepr.* **1989**, *30*, 488–489.
- (9) Bawa, R.; Coffey, S.; Nandu, M. *Polym. Prepr.* **1989**, *30*, 486–487.
- (10) Waltman, S. R.; Kaufman, H. E. *Invest. Ophthalmol.* **1970**, *9*, 250–255.
- (11) Leaders, F. E.; Hecht, G.; Van Hoose, M.; Kellogg, M. *Ann. Ophthalmol.* **1973**, 513–522.
- (12) Miyazaki, S.; Ishii, K.; Takada, M. *Chem. Pharm. Bull.* **1982**, *30*, 3405–3407.
- (13) Grass, G. M.; Cobby, J.; Makoid, M. C. *J. Pharm. Sci.* **1984**, *73*, 618–621.
- (14) Krohn, D. L.; Breitfelder, J. M. *Invest. Ophthalmol.* **1974**, *13*, 313–316.
- (15) Richman, J. B.; Tang-Liu, D. D.-S. *J. Pharm. Sci.* **1990**, *79*, 153–157.
- (16) L. E. Stevens, P. J. Missel, and J. C. Lang, unpublished work.
- (17) Thaysen, J. H.; Thorn, N. A. *Am. J. Physiol.* **1954**, *178*, 160–164.
- (18) Bachman, W. G.; Wilson, G. *Invest. Ophthalmol. Visual Sci.* **1985**, *26*, 1484–1488.
- (19) Rismondo, V.; Osgood, T. B.; Leering, P.; Hattenhauer, M. G.; Ubels, J. L.; Edelhauser, H. F. *CLAO J.* **1989**, *15*, 222–8.
- (20) Center for Computing Activities, Columbia University, New York, NY 10027.
- (21) SAS Institute, SAS Circle, Box 8000, Cary, NC 27511.
- (22) The DUD (Doesn't Use Derivatives) method was generally used.
- (23) Lee, V. H. L.; Robinson, J. R. *J. Ocul. Pharmacol.* **1986**, *2*, 67–108.
- (24) Daniels, F.; Alberty, R. A. *Physical Chemistry*; J. Wiley & Sons: New York, 1961; pp 609–610.

RECEIVED for review September 4, 1991. Revised manuscript received January 7, 1992. Accepted January 10, 1992.

Determination of Selenium by Inductively Coupled Plasma Mass Spectrometry Utilizing a New Hydride Generation Sample Introduction System

Wayne T. Buckley,* James J. Budac,[†] and David V. Godfrey

Agriculture Canada Research Station, P.O. Box 1000, Agassiz, British Columbia, Canada V0M 1A0

Karen M. Koenig[‡]

Department of Animal Science, University of British Columbia, Vancouver, British Columbia, Canada V6T 1Z4

An inductively coupled plasma mass spectrometer with a newly designed continuous flow hydride generator was used for the determination of Se in biological materials. The design of the hydride generator was important in minimizing interference from HCl and in maximizing analytical sensitivity. Two sample preparation procedures incorporating either 3.8 or 7.2 M HCl in the final sample solutions were compared. Interference from Cu was eliminated by the addition of 0.2 M NaI to the sodium borohydride solution (3.8 M method) or by maintaining a high concentration of HCl in the sample solution (7.2 M method). The 3.8 M method had the advantage of minimizing exposure of expensive equipment to corrosive HCl fumes, whereas the 7.2 M method did not contaminate equipment with I and had no measurable sample-to-sample cross-contamination. In practice, cross-contamination from sample to sample in both methods was negligible during analysis. An important factor in minimizing cross-contamination from sample to sample was the elimination of the air bubble normally entrained between samples. Determination of isotopic tracer enrichment was linear from 0 to 320% enrichment, which provided a broad range for isotope dilution analysis. A detection limit of 6.4 pg of Se was observed under optimum conditions, whereas a detection limit of 1.3 ng of Se was found for routine analysis of 1-g samples of plant material. Selenium was accurately determined by isotope dilution analysis in a variety of biological reference materials.

INTRODUCTION

Numerous methods for Se determination in biological materials have been developed since the discovery of Se as an essential nutrient for animals. The most commonly used techniques appear to be fluorimetry, electrothermal atomization atomic absorption spectrophotometry (AAS), hydride generation AAS, neutron activation, X-ray fluorescence, and proton-induced X-ray emission.¹ Inductively coupled plasma mass spectrometry (ICPMS) has potential as an important technique for Se analysis, but it has yet to be fully explored. While sample introduction by nebulization is limited by lack of sensitivity,² Buckley et al.,³ Powell et al.,⁴ and Janghorbani and Ting⁵ have found that ICPMS coupled with hydride generation appears to be a promising technique.

Hydride generation is an ideal sample introduction method for ICPMS because it separates volatile analytes from the

sample matrix and solution reagents. With nebulization of the sample solution, molecular ions of the same nominal mass/charge as the analyte ions may be derived from the sample matrix, reagents, water, and carrier gas and interfere with determination of the analyte. Formation of most interfering molecular ions is precluded with hydride generation simply because the precursors do not reach the plasma torch. In preliminary work with hydride generation ICPMS it became apparent that variations in hydride generator design could have a profound effect on analytical sensitivity for Se. Several modifications to continuous flow hydride generators were explored, and presented here is a design which yielded a substantial improvement in sensitivity to Se compared to previous reports.^{2,4}

Transition metal interference with Se hydride generation can significantly reduce analytical sensitivity.³ We have found this to be important with biological samples in which variations in Cu concentration can have a substantial effect. Vujan and Leung⁶ described a method of reducing chemical interference through the formation of stable chlorocomplexes of interfering elements in 7.5 M HCl. Although effective, this technique appears to have been used infrequently and we have tested its application for hydride generation ICPMS determination of Se. Agterdenbos and Bax⁷ explained the mechanism of action of transition metal interference when they discovered that the effect of Cu²⁺ in the sample solution was to enhance the decomposition of tetrahydroborate, resulting in lower selenium hydride formation. They also found that iodide catalyzed the formation of hydrogen selenide, allowing complete conversion of Se to hydrogen selenide even in the presence of interfering metal ions.⁸ In the present work the iodide catalysis reaction has been adapted to hydride generation ICPMS determination of Se.

There is considerable practical advantage in having a single method of analysis for a variety of sample types. Techniques were developed which are suitable for plant as well as animal material and permit analysis of fluids (e.g., milk and plasma) as well as solids. Two sample preparation procedures, each suitable for a variety of biological matrices, are reported here along with details of hydride generation and ICPMS techniques.

EXPERIMENTAL SECTION

Inductively Coupled Plasma Mass Spectrometer. An ICPMS (Elan Model 250, Sciex, Thornhill, Ontario, Canada) was used with the standard nebulizer and spray chamber removed. A Sciex-type long torch was positioned relative to the load coil as recommended by the manufacturer, although, in the absence of the spray chamber, a simple, shop-built device was required to fix it in position. The torch and load coil were positioned as determined by the original machine design. Argon gas flows were controlled with Model 5850C mass flow controllers and a Model

*To whom correspondence should be addressed.

[†]Current address: Refinery Process Technology, Inco Ltd., Thompson, Manitoba, Canada R8N 1P3.

[‡]Current address: Agriculture Canada Research Station, P.O. Box 3000 Main, Lethbridge, Alberta, Canada T1J 4B1.

Table I. ICPMS Operating Parameters

parameter	value	comments
ion mode	positive	
quadrupole rod offset	-2.0 V	
E1 lens	-16.3 V	Elan 250 lens setting: 80
P lens	-12.2 V	Elan 250 lens setting: 20
S2 lens	-6.5 V	Elan 250 lens setting: 80
ICP incident power	1.0 kW	
Ar flow rates:		
plasma	12.0 L/min	
auxiliary ^a	~1.5 L/min	adjusted for maximum signal with minimum reflected power (<5 W)
injector (hydride generator) ^b	~1.5 L/min	adjusted for maximum signal with minimum background
resolution (manual) ^c	0.85-0.95 amu	valleys next to ⁷⁷ Se adjusted to 10% or less of ⁷⁷ Se peak height
mass calibration ^d	<i>m/z</i> 76, 77, 78, 82 ^e	calibrated for analyzed isotopes
B lens ^e	3.6-4.6 V	adjusted to yield 20 000 counts/s at <i>m/z</i> 78 for 2 ng Se/mL; Elan 250 lens setting: 35-45
ion intensity measurement:		
measurements per peak	1	
time per measurement	7 ms	
number of cycles	3000	3 repetitions of 1000 cycles each

^{a-c}Parameters adjusted at the beginning of each day are listed in order of adjustment. ^dAtomic mass units. ^eMass to charge ratio.

separator due to production of H₂ gas. Finally, ICPMS operating parameters were optimized before switching the sample line to the autosampler.

Optimization of ICPMS. The ICPMS operating parameters are listed in Table I. All ICPMS parameters were adjusted to give a maximum signal with a solution of 2 ng Se/mL, then the B lens was attenuated so that the expected maximum signal for the samples would not exceed 150 000 counts/s. A count rate attenuated to 20 000 counts/s at mass/charge 78 while analyzing 2 ng Se/mL normally was optimal. There appeared to be no advantage in exceeding this count rate, while, on the other hand, count rates in excess of 150 000 counts/s for samples may reduce the detector life. Even after attenuating the signal, adequate sensitivity for analysis of low-Se samples was available.

Analysis of Data. Ion intensities (counts/s) were used to calculate the ratio of mass of enriched stable isotope to mass of natural Se (Tracer Trace Mass Ratio, TTMR) or 100 × TTMR (Tracer Trace Mass Percentage, TTMP). The tracer was defined as the enriched mixture of isotopes purchased from the supplier (the tracer was not a pure nuclide). The calculations are described elsewhere¹¹ and were performed with the aid of a computer program. The quantity of Se in the original sample was readily calculated from TTMP

$$\text{mass of Se} = \frac{100 \times \text{mass of tracer}}{\text{TTMP}}$$

Instrumental bias was removed by correcting ion intensity ratios of enriched samples for the bias measured with natural abundance Se (after correcting for the blank) according to the following equation:

$$\text{corrected ratio} = \text{uncorrected ratio} \times \frac{\text{true natural ratio}}{\text{measured natural ratio}}$$

Evaluation of Analytical Method. A number of factors affecting the sensitivity and reliability of isotope dilution analysis of Se were examined. These included the sample digestion temperature; the position of the hydride outlet tube in the phase separator; the concentration of HCl in the sample solution; the addition of NaI to the NaBH₄ solution; the reduction of Se⁶⁺ to Se⁴⁺ after sample decomposition; and memory, or cross-contamination, between samples. The latter study included an examination of the effect of an air bubble entrained between samples as well as quantitation of sample-to-sample cross-contamination.

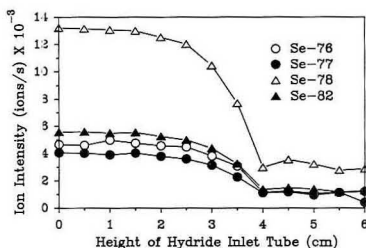


Figure 2. Effect of height of sample inlet tube in the phase separator (glass Y) on ion intensity observed for Se isotopes. See Figure 1 for interpretation of inlet height.

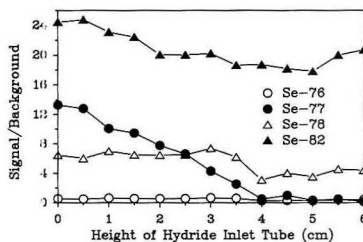


Figure 3. Effect of height of sample inlet tube in the phase separator (glass Y) on signal/background ratio observed for Se isotopes. See Figure 1 for interpretation of inlet height.

The accuracy of Se analysis in biological materials was determined by analysis of reference materials.

RESULTS AND DISCUSSION

Digestion Temperature. It was found that a minimum temperature was required during digestion before the watch glasses were removed from the beakers, otherwise recovery of Se was poor (data not shown). The minimum requirement was 30 min at the 115 °C surface temperature on a Lindberg hotplate (Model H-2, Lindberg, Watertown, WI), which yielded temperatures in the digests of 107 ± 7.6 °C (mean ± SD, *n* = 31). It appears that a minimum temperature was required to oxidize volatile forms of Se to a nonvolatile form (probably selenate) before fumes were allowed to escape freely. While the watch glasses were present they acted as condensers.

Hydride Generator. The effect of the hydride inlet tube position in the phase separator on the intensity of four Se isotopes was investigated with the 7.2 M HCl method. Positioning the inlet tube near the bottom of the stem of the Y yielded over three times the Se signal intensity compared to a position in the upper part of the Y (Figure 2). The effect of the position of the inlet tube on signal/background ratio varied among the isotopes examined (Figure 3). The effect was greatest for ⁷⁷Se and included an increase in the background intensity as the height of the inlet tube was raised. The liquid-and-gas mixture was expelled with sufficient force from the hydride inlet tube that an aerosol, which would contain a high concentration of HCl, probably was formed. It appeared that the aerosol did not travel from the bottom to the top of the stem of the Y, whereas aerosol formed in the top of the Y was picked up by the Ar carrier gas. The additional HCl from entrained aerosol appeared to yield sufficient ⁴⁰Ar³⁷Cl⁺ so as to increase the background intensity at *m/z* 77. Thus, it appeared that the addition of HCl from an aerosol was the main factor in the change in analytical sensitivity seen in Figure 2.

Interference from Copper. Vijan and Leung⁵ found that interference from metal ions, including Cu²⁺, Ni²⁺, and Fe³⁺,

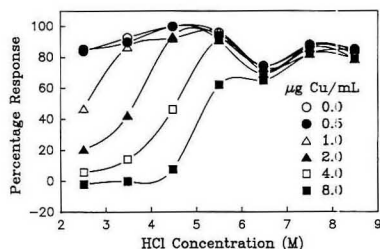


Figure 4. Relationship between Cu and HCl concentrations in the sample solution and the ^{82}Se signal observed for 20 ng Se/mL by hydride generation/ICPMS.

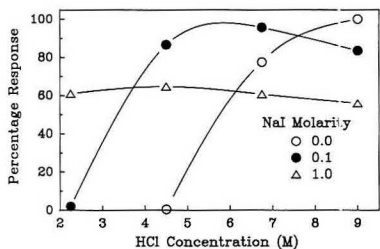


Figure 5. Effect of addition of NaI to the NaBH_4 solution on the ^{82}Se signal observed for 2 ng Se/mL in the presence of 8 μg Cu/mL determined by hydride generation/ICPMS.

in generation of SeH_2 could be eliminated by the formation of stable chlorocomplexes of the interfering ions in 7.5 M HCl. We evaluated this approach by varying the HCl concentration added to final sample solutions from 2.5 to 8.5 M in the presence of 0 to 8 μg Cu/mL (Figure 4). These solutions were prepared with the same quantity of MgO which would be present after ashing real samples. Since MgO is hydrolyzed by HCl, the total Cl^- concentration was greater than the HCl concentration and varied from 4.0 to 10.0 M. The highest concentration of Cu, 8 $\mu\text{g}/\text{mL}$, in the sample solution was what would be expected from analysis of livers of ruminants suffering from chronic Cu toxicity, which is the highest Cu concentration we expect to encounter in biological samples. There appeared to be substantial interference from Cu at HCl concentrations less than 6.5 M and no interference at 7.5 M or higher (Figure 4), which agrees with the results of Vijan and Leung⁵. Vijan and Leung⁵ also found that reduction of Se^{6+} to Se^{4+} occurred spontaneously at room temperature in HCl concentrations greater than 4.5 M and appeared to go to completion at 6.5 M HCl. This is an advantage because Se must be reduced to the tetravalent state before hydride generation. We confirmed that high HCl concentration eliminated the need for an additional procedure, such as boiling, in order to reduce Se^{6+} to Se^{4+} . An HCl concentration of 7.2 M (corrected for hydrolysis of MgO) was selected for routine analysis. However, the production of HCl fumes from samples presented a corrosion problem for the ICPMS instrumentation. Although we set up special ventilation to handle the fumes, some corrosion still developed over a period of about a year. It was concluded that a lower concentration of HCl was required to prevent further damage in the future.

In a kinetic study of trace metal interferences in the formation of SeH_2 , Agterdenbos and Bax⁶ found that iodide catalyzed the reaction between borohydride and Se^{4+} , thereby reducing metal ion interference. We compared 0, 0.1, and 1.0 M NaI added to the NaBH_4 solution and found that a concentration between 0.1 and 1.0 M should be satisfactory for minimizing interference from Cu at low HCl concentrations

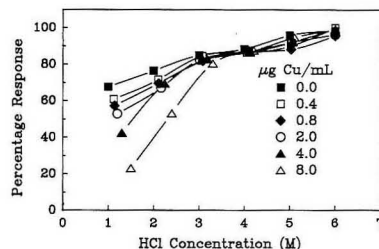


Figure 6. Relationship between Cu and HCl concentrations in the sample solution and the ^{82}Se signal observed for 2 ng Se/mL when 0.2 M NaI was added to the NaBH_4 solution.

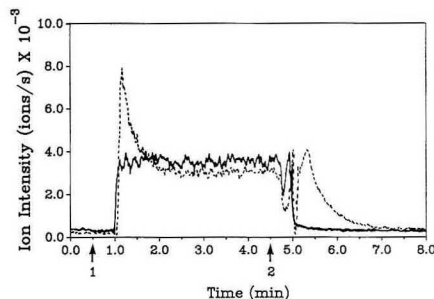


Figure 7. Effect of an air bubble in the sample intake line on signal stability and memory in ^{82}Se determination. At arrow 1, the sample inlet line was switched from 7.2 M HCl to 2.0 ng Se/mL in 7.2 M HCl. At arrow 2 the inlet line was switched back to 7.2 M HCl. The time taken to switch between solutions was about 0.1 s (solid line; 0.002-mL air bubble) or 4 s (broken line; 0.07-mL air bubble).

(Figure 5). Using 0.2 M NaI in the NaBH_4 solution there was little interference from Cu on SeH_2 generation between 3.0 and 6.0 M HCl (Figure 6). An HCl concentration of 3.8 M was selected for routine analyses when 0.2 M NaI was included in the NaBH_4 solution. A 1-min period of high HCl concentration during sample preparation was found to be adequate to reduce Se^{6+} to Se^{4+} before diluting to a final concentration of 3.8 M.

Memory Effects. Janghorbani and Ting² reported that 3.5 min was required to reduce signal intensity to 3.3% of its original value for Se after switching from 0.010 μg Se/mL to 10 M HCl in an ICPMS/hydride generator system, and about 10 min was required for the signal to decrease to 1.2% of its original value.²

We investigated the effect of entrained air in the sample inlet line on the memory effect by omitting the debubbler from the hydride generation apparatus (see Figure 1). About 1 min (excluding the 30-s lag due to the length of the sample inlet tube) was required for the signal to decrease to background level after rapid manual switching from 2 ng Se/mL to a blank solution (both solutions contained 7.2 M HCl) during which an insignificant air bubble (about 0.002 mL) was entrained (solid line, Figure 7). However, the time increased to at least 3.5 min when a larger air bubble (about 0.07 mL, equal to that obtained with the autosampler) was entrained (broken line, Figure 7). Furthermore, the larger air bubble appeared to cause a release of Se from the tubing or phase separator as indicated by the peaks at 1.2 and 5.4 min. A black deposit which slowly built up at the point of mixing the sample and NaBH_4 solutions and in the bottom of the phase separator may have been the source of Se released by the air bubble. The release of Se by an air bubble, though, was not consistent. In another test with an 0.07-mL air bubble (not shown) the

Table II. Evaluation of Cross-Contamination (Memory) in Isotope Dilution Analysis of Se Using Enriched ^{76}Se as the Tracer^a

tracer	tracer enrichment (TTMP ^b)	
	3.8 M HCl	7.2 M HCl
-	0.070	-0.420
-	0.021	0.104
-	-0.036	0.064
-	-0.023	-0.060
-	-0.032	0.312
+	161.367	224.212
-	0.729	0.208
+	161.070	224.155
-	0.931	0.579
+	161.674	221.880
-	0.879	0.571
+	161.045	222.652
-	1.014	-0.016
+	161.226	216.685
-	0.910	0.096
Means without Added Tracer		
1st set of five	0.000 ^c	0.000
2nd set of five	0.893 ^d	0.288
SE ($n = 5$)	0.036	0.121

^a Analyses were performed in the order listed within columns. The total time from the start of one sample to the start of the next sample for 3.8 M HCl was 5.4 ± 0.04 min (mean \pm SD; autosampler in use) and for 7.2 M HCl was 5.2 ± 0.94 min (manual sample changing). Ion intensity measurements required 2.1 min, leaving a mean of 3.1 or 3.3 min for HCl wash and prerinse with the next sample. ^b TTMP is defined in the text. ^{c-d} Means in the same column followed by different letters are significantly different ($P < 0.05$).

Table III. Calibration Sets for Isotope Dilution Analysis of Se

calibration sets (range of TTMP values) ^a	enriched tracer	slope	intercept	correlation coefficient	natural abundance Se (ng/L) ^b
3.8 M HCl					
0-160	^{76}Se	1.013 ^c	-0.109	1.000	4.0
0-20	^{82}Se	1.033 ^c	-0.073	1.000	2.0-8.0
0-80	^{82}Se	1.043	-0.370	0.9996	0.5-4.0
0-320	^{82}Se	1.059	-1.868	0.9972	0.13-4.0
0-1280	^{82}Se	1.459 ^d	-101 ^d	0.9826	0.03-4.0
7.2 M HCl					
0-163	^{76}Se	0.969 ^c	-0.632	0.9999	8.0

^a Five equally spaced TTMP values in each range. TTMP is defined in the text. ^b When a range is shown for natural abundance Se, variations in TTMP were obtained by maintaining the quantity of tracer constant and varying the quantity of natural abundance Se. ^c Slope determined by linear regression was significantly different from 1.0 ($P < 0.05$). No intercept was found to be significantly different from 0.0 ($P \geq 0.05$). ^d Curvilinear relationship.

peak at 1.2 min did not appear while the peak and 5.4 min was over twice the size as in Figure 7. Janghorbani and Ting² did not mention the effect of air, so it may be possible that entrained air contributed to the memory effect they reported.

Sample-to-sample cross-contamination was measured by alternately analyzing solutions of natural Se and enriched Se. A range of enrichment from zero (TTMP = 0) to the maximum expected during isotope dilution analysis (TTMP = 150-250) was tested. Both the 3.8 M HCl and the 7.2 M HCl sample preparation methods were evaluated (Table II). Sample changing was performed without entraining an air bubble in the sample line, which was achieved by utilizing a debubbler in conjunction with the autosampler (3.8 M HCl) or an injection valve in conjunction with manual sample changing (7.2 M HCl). Significant ($P < 0.05$) cross-contamination which increased enrichment by 0.6% of that of the previous sample occurred with the 3.8 M HCl method, whereas no measurable ($P \geq 0.05$) cross-contamination occurred with the 7.2 M HCl procedure. For most applications the observed memory in the 3.8 M HCl method would be negligible; however, slightly better accuracy may be possible with the 7.2 M HCl procedure.

Detection Limits. Two types of detection limits were determined. These are the absolute detection limit for Se in pure solution and the practical detection limit for real sample analysis by isotope dilution. The first provided a comparison of the sensitivity of the analytical method with other methods of Se analysis. The second type of detection limit was useful for routine analysis.

Detection limit is defined as three times the SD obtained from analysis of samples with very low or negligible concentration of analyte. The absolute detection limit for Se, determined by repeated analysis ($n = 10$) of a pure solution of 10 pg Se (natural abundance)/mL in 3.8 M HCl, was 1.4 pg/mL when monitoring ^{82}Se and 5.8 pg/mL when monitoring ^{76}Se . At a solution flow rate of 1.8 mL/min, a sample prerinse time of 90 s and an analysis time of 63 s, these values are equivalent to 6.4 and 27 pg Se, respectively. The B lens was optimized for this detection limit determination, rather than adjusting it to attenuate the signal as described above. Janghorbani and Ting² reported a detection limit of 600 pg of Se for both ^{76}Se and ^{82}Se using the same model of ICPMS but with a commercial hydride generator. Although a number of parameters differed between these two studies, one notable observation is that 50 mL of sample solution was required by the commercial hydride generator and about 2.5 mL by the generator described here.

Ten samples of orchardgrass hay (0.94-0.98 g of dry matter) were prepared and analyzed using the 3.8 M HCl method. The tracer for isotope dilution analysis consisted of 1.00 ng of enriched ^{82}Se . A mean (\pm SD) TTMP of 9.42 ± 0.382 was

Table IV. Determination of Se (Mean \pm SD) in Biological Reference Materials^a

sample	accepted value ^b	method and enriched tracer		
		3.8 M HCl, ^{82}Se	3.8 M HCl, ^{76}Se	7.2 M HCl, ^{76}Se
AC/USDA 132F corn stalk	0.016 (0.008)	0.0122 \pm 0.0004		
BOWEN kale	0.134 (0.0204)	0.122 \pm 0.001		
IAEA A-2 dried blood	0.59 (0.14)	0.600 \pm 0.002	0.637 \pm 0.002	
IAEA A-11 milk powder	0.0339 (0.0072)	0.0292 \pm 0.0008	0.0310 \pm 0.0002	0.032 \pm .004
NIST 1568 rice flour	0.4 (0.1)	0.327 \pm 0.004	0.353 \pm 0.004	
NIST 1572 citrus leaves	0.025 ^c			0.028 \pm 0.002
NIST 1577 bovine liver	1.1 (0.1)	1.11 \pm 0.01	1.18 \pm 0.00	1.16 \pm 0.01
NIST 8419 bovine serum	0.016 (0.002)			0.016 \pm 0.001

^a All values in $\mu\text{g/g}$ dry matter. Each value listed under ^{76}Se is a mean of three determinations performed on the same day. Each value listed under ^{82}Se is a mean of three to ten determinations performed on 2-5 days. Abbreviations: AC/USDA = Agriculture Canada/U.S. Dept. Agriculture; BOWEN = H. J. M. Bowen, Univ. Reading, U.K.; IAEA = International Atomic Energy Agency, Austria; NIST = National Institute of Standards and Technology. ^b Uncertainty calculated by issuing agency in parentheses. ^c Noncertified value, estimate of uncertainty not provided.

obtained. Mean (\pm SD) Se concentration was 10.6 ± 0.44 ng/g dry matter, which indicates a practical detection limit ($3 \times$ SD) for plant materials of 1.3 ng of Se in samples of about 1 g. The ICPMS analyses were performed on the same day.

Isotope Enrichment Calibration Sets. Calibration sets covering a broad range of tracer enrichment were prepared in order to define the linear range of enrichment for isotope dilution analysis. In some sets the quantity of tracer was maintained constant while the quantity of natural Se was reduced so as to mimic isotope dilution analysis of samples of unknown, but very low, Se content. Acceptable linearity up to 320 TTMP was found (Table III), which would be consistent with 3.1 ng of analyte in a sample with 10 ng of tracer (enriched ^{76}Se in this case).

Analysis of Biological Reference Materials. Stable isotope dilution analysis using either enriched ^{76}Se or ^{82}Se as the tracer and either the 7.2 M HCl or the 3.8 M HCl sample preparation methods provided quantitative analysis in good agreement with accepted values for biological reference materials (Table IV). The determinations were successful with a wide range of Se concentrations and a variety of sample matrices, which indicates that the method has a broad range of applications in biological studies.

ACKNOWLEDGMENT

Appreciation is extended to E. G. Wilson for her technical assistance throughout this work. This material was presented

in part by W.T.B. at the 6th International Symposium on Trace Elements in Man and Animals, Pacific Grove, CA, 1987, and by J.J.B. at the 4th International Symposium on Uses of Selenium and Tellurium, Banff, AB, 1989. Contribution no. 453 from the Agriculture Canada Research Station, Agassiz.

Registry No. Se, 7782-49-2; BH_4Na , 16940-66-2.

REFERENCES

- (1) Tölg, G. In *Trace Element Analytical Chemistry in Medicine and Biology*; Brätter, P., Schramel, P., Eds.; Walter de Gruyter: New York, 1984; Vol. 3, pp 95-125.
- (2) Janghorbani, M.; Ting, B. T. G. *Anal. Chem.* **1989**, *61*, 701-708.
- (3) Buckley, W. T.; Godfrey, D. V.; Koenig, K. M.; Shelford, J. A. In *Trace Elements in Man and Animals 6*; Hurley, L. S., Keen, C. L., Lönnnerdal, B., Rucker, R. B., Eds.; Plenum Press: New York, 1988; pp 329-330.
- (4) Powell, M. J.; Boomer, D. W.; McVickers, R. J. *Anal. Chem.* **1986**, *58*, 2864-2867.
- (5) Vijan, P. N.; Leung, D. *Anal. Chim. Acta* **1980**, *120*, 141-146.
- (6) Agterdenbos, J.; Bax, D. *Anal. Chim. Acta* **1986**, *188*, 127-135.
- (7) Su, K. W. M.; Berman, S. S. *Talanta* **1984**, *33*, 1010-1012.
- (8) Poole, C. F.; Evans, N. J.; Wibberley, D. G. *J. Chromatogr.* **1977**, *136*, 73-83.
- (9) Thompson, M.; Walsh, J. N. *A Handbook of Inductively Coupled Plasma Spectrometry*; Blackie & Sons Ltd.: Glasgow, 1983; Chapter 6.
- (10) Hwang, J. D.; Guenther, G. D.; Diomigardi, J. P. *Anal. Chem.* **1989**, *61*, 285.
- (11) Buckley, W. T. *Proc. Nutr. Soc.* **1988**, *47*, 407-416.

RECEIVED for review September 4, 1991. Accepted January 2, 1992.

Simultaneous Determination of Mixtures by Kinetic Analysis of General-Order Reactions

Israel Schechter

Max-Planck-Institut für Quantenoptik, D-8045 Garching, Germany

A new error-compensating algorithm for kinetic determinations of dual-component mixtures without prior knowledge of reaction orders and rate constants is developed and evaluated. The algorithm is primarily evaluated for the quantification of the chemical components, but its ability to determine reaction orders and rate constants is demonstrated as well. The method is applicable for determination of concentrations, rate constants, and reaction orders in a wide range, but there are several limitations and restrictions that are pointed out. The algorithm fails for reaction order of exactly unity; however, an extension to include this singular point is described. Simulated data with Gaussian noise are used to evaluate the effects of the various parameters involved in this problem.

INTRODUCTION

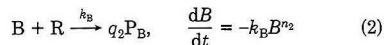
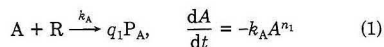
A broad view of the role of kinetics in analytical chemistry has been recently presented, and the importance of simultaneous multicomponent determinations has been pointed out.¹ The principle is to use the difference in the kinetic behavior of the various components in order to determine their initial concentration in a mixture. Such regular kinetic methods have been extensively used for simultaneous determinations of both reactants and catalysts.²⁻⁴ Some of the methods are single-point determinations (e.g., ref 10) and some are multipoint

determinations, which can reduce the errors.^{1,2,21} All these methods assume some prior knowledge of the kinetic characteristics of the various reactions involved, e.g., reaction orders or rate constants. Examples of these methods include multicomponents with first-order reaction,^{2,5,6,8,23} first and zero order,^{7,22} and parallel first and zero order.⁸ A related subject that is equivalent to the first-order case is the extensively studied subject of analysis of multicomponent fluorescence decay kinetics (e.g., refs 11-13).

In this paper we evaluate a method that needs no prior knowledge of reaction orders or reaction rates. The reaction orders may be noninteger numbers which means that the chemical mechanisms need not be completely known. This problem is somewhat complex (it involves 15 variables), and we restrict this paper to dual-component mixtures, although further research on systems of more components is possible.

Kinetic determinations of single compounds without complete knowledge of reaction order or rate constants are well established, and extensively used (e.g., refs 1, 2, 14-16). The kinetic determinations of a monocomponent system of general reaction order and unknown rate constant has been profoundly evaluated.¹⁵ Our study is based on this research, and we extend it to the multicomponent cases. (Mathematically, it means doubling the dimensionality of the problem.)

The system of interest consists of the following reactions and rate equations:



where A and B are the components in the mixture that are to be determined, R is a general reactant (one, many, or none), k_A and k_B are the (unknown) rate constants, n_1 and n_2 are the (unknown) reaction orders (may be nonintegers), and q_1 and q_2 account for the reactions stoichiometry.

The algorithm for the determination of A and B is described in the following. For its evaluation, many (ca. 100 000) simulated experiments have been carried out. Such an experiment consists of producing artificial data with a given Gaussian noise and then using the algorithm in order to recover the initial parameters (concentrations, rate constants, and reaction orders). The reconstruction ability of the algorithm is evaluated as a function of many variables, such as the range of the parameters, the noise level, the initial estimation of the parameters, time range of the experimental data, and other factors.

MATHEMATICAL DESCRIPTION

The kinetic system is described by eqs 1 and 2. Let A_0 and B_0 be the initial concentration of A and B, respectively. The concentrations at time t are given by¹⁷

$$A(t) = [k_A(n_1 - 1)t + A_0^{(1-n_1)}]^{1/(1-n_1)} \quad (3)$$

$$B(t) = [k_B(n_2 - 1)t + B_0^{(1-n_2)}]^{1/(1-n_2)} \quad (4)$$

Let $\alpha(x)$ be the detector sensitivity factor to compound x in the mixture. The signal is assumed to be linearly dependent on the concentrations. In case of spectroscopic detection $\alpha(x)$ is the molar absorbance times the cell path. (In the following we shall refer to spectroscopic detection, although the algorithm is general in this respect). The observed signal at time t , is

$$\begin{aligned} Y(t) &= \alpha(A)A(t) + \alpha(B)B(t) + \\ &\quad \alpha(P_A)P_A(t) + \alpha(P_B)P_B(t) + \text{background} \\ &= [\alpha(A) - q_1\alpha(P_A)]A(t) + [\alpha(B) - q_2\alpha(P_B)]B(t) + \\ &\quad \text{constant} \quad (5) \\ &= \beta_1 A_t + \beta_2 B_t + r \end{aligned}$$

Here, β is a constant proportionality factor and r is a constant, defined by eq 5. The constant r may include other unknown time-independent absorptions. In the suggested algorithm eq 5 is to be fitted to the experimental data by using a modified Levenberg-Marquardt method^{18,19} in order to solve the nonlinear least-square problem. Kalman-Filter could have been used as well, but the Marquardt method has been found to be somewhat better in the case of zero-order reactions.²² In this procedure the following function is to be minimized:

$$\xi = \sum [Y_{\text{exp}} - Y(A_0, k_A, n_1, B_0, k_B, n_2)]^2 \quad (6)$$

and the six unknown parameters of Y are to be found.

Several functional forms of A_t and B_t have been tested for convergence of the algorithm:

$$\text{eqs 3 and 4} \quad (7)$$

$$C(t) = (u_1 t + u_2)^{u_3} \quad (8)$$

$$C(t) = (u_1 t + u_2)^{1/u_3} \quad (9)$$

where $C(t)$ is the concentration of A or B at time t ,

$$u_1 = -k(1 - n), \quad u_2 = C_0^{1-n}, \quad u'_3 = (1 - n)^{-1}, \quad u_3 = (1 - n)$$

The last form is the one used in ref 15 for the monocomponent system. The various forms use different sets of variables; thus

ξ changes differently as a function of them. In other words, the various sets of variables form different response multidimensional surfaces for the minimization process. The best results were obtained by the functional form of eq 9. This is in agreement with the results obtained for the monocomponent system.

Another modification that has been found to be useful for low concentrations is based on the equality¹⁰ (for $f > 0$)

$$[k(n-1)t + C_0^{(1-n)}]^{1/(1-n)} = \frac{1}{f} [f^{1-n} k(n-1)t + (C_0 f)^{(1-n)}]^{1/(1-n)} \quad (10)$$

Best results are obtained for concentrations which are not too far from unity. One of the reasons for this effect, as will be shown later is the diminishing of the signals' Jacobian at too low concentrations, which causes a huge magnification of the noises. Thus, one can use eq 10 to scale the readings so that the concentration (in units of f^{-1}) will be shifted to the safe range. Thus f serves for shifting the function to a range in the parameter space where the carried noise is lower and it should be used in case of convergence problems.

Finally, applying transformations 9 and 10 gives the functional form that has been used in the least-square procedure:

$$Y(t) = \frac{\beta_1}{f_1} (v_1 t + v_2)^{1/v_3} + \frac{\beta_2}{f_2} (w_1 t + w_2)^{1/w_3} + r \quad (11)$$

$$v_1 \equiv k_1(n_1 - 1), \quad k_1 \equiv f_1^{1-n_1} k_A$$

$$v_2 \equiv (A_0 f_1)^{1-n_1}$$

$$v_3 \equiv (1 - n_1)$$

$$w_1 \equiv k_2(n_2 - 1), \quad k_2 \equiv f_2^{1-n_2} k_B$$

$$w_2 \equiv (B_0 f_2)^{1-n_2}$$

$$w_3 \equiv (1 - n_2)$$

The Jacobian of $Y(t)$ in respect to the new variables is

$$\begin{aligned} \frac{\partial Y}{\partial v_1} &= \frac{\beta_1}{f_1 v_3} (v_1 t + v_2)^{(1-v_3)/v_3 t} \\ \frac{\partial Y}{\partial v_2} &= \frac{1}{t} \frac{\partial Y}{\partial v_1} \end{aligned}$$

$$\frac{\partial Y}{\partial v_3} = \frac{-\beta_1}{f_1 v_3^2} (v_1 t + v_2)^{1/v_3} \ln(v_1 t + v_2)$$

$$\frac{\partial Y}{\partial w_1} = \frac{\beta_2}{f_2 w_3} (w_1 t + w_2)^{(1-w_3)/w_3 t}$$

$$\frac{\partial Y}{\partial w_2} = \frac{1}{t} \frac{\partial Y}{\partial w_1}$$

$$\frac{\partial Y}{\partial w_3} = \frac{-\beta_2}{f_2 w_3^2} (w_1 t + w_2)^{1/w_3} \ln(w_1 t + w_2) \quad (12)$$

Equations 11 and 12, with $f = 1$, are the specific equations used in the fitting process. As a result, the best values of v_1 , v_2 , v_3 and w_1 , w_2 , w_3 were obtained. The parameters of interest (concentrations, rate constants, and reaction orders) are simply calculated by eq 11.

An interesting mathematical point is the existence range of the function that describes the signal. $C_0^{1-n} - k(1-n)t$ must be positive but for $n < 1$ it may become negative. For each set of parameters there is a time when the reaction is over, and after that we should impose this factor to remain zero, otherwise eq 11 is not well defined. However, the real values of the parameters are not known to us, and during the minimization of the least squares we may reach domains in the

parameter space where the function (and the Jacobian) are constantly zero, by that definition. This may cause convergence problems mainly in cases of very low reaction order. Therefore, whenever one of the reaction orders is expected to be low, it is recommended to define a large step size to let the computer algorithm escape from such domains.

Another problem is the singular point at unity reaction order. The function¹¹ and the Jacobian¹² are not defined at this point. However, it has been found that reaction orders that are very close to unity, but not exactly unity, may be treated as well by this algorithm. If necessary, the case of unity reaction order can be included in the algorithm, in a way described in the following. However, the price is that one must work with the regular variables (C_0 , n , k), thus losing some accuracy of the results. For this set of variables there is a way to switch to the corresponding $n = 1$ function and Jacobian in the very close vicinity to unity, such that the global function is well defined and smooth enough for the convergence process:

$$\begin{aligned} \beta[k(n-1)t + C_0^{1-n}]^{1/(1-n)} &\rightarrow \beta C_0 e^{-kt} \\ \frac{\partial Y}{\partial k} &= -\beta C_0^n t \rightarrow -\beta C_0 e^{-kt} t \\ \frac{\partial Y}{\partial A_0} &= \beta C_0^n A_0^{-n} \rightarrow \beta e^{-kt} \end{aligned} \quad (13)$$

$\partial Y / \partial n = 0$ is also to be imposed. Plots of the functions show the smooth pass to $n = 1$ case. This procedure cannot be carried out with the other set of variables (eq 11) since the Jacobian (eq 12) approaches the singularity point in different ways when coming from the positive or negative v_3 and w_3 . Moreover, as will be shown later, this effect causes an increase in the errors of the determinations when the initial estimate of the reaction order is less than unity and the real value is greater than unity (and vice versa).

EXPERIMENTAL SECTION

The computer codes for producing the synthetic data, for reconstructing the initial parameters, and for analyzing the results were written in FORTRAN77. An IBM 3090 computer was used, with VS-FORTRAN version 2 compiler. A computer experiment is initiated by determining the values of "real" parameters A_0 , k_1 , n_1 , B_0 , k_2 , n_2 , and the values of the initial estimation of these parameters. Then the experimental conditions have to be specified, e.g., the standard deviation of the readings, the number of readings, and the time schedule of the readings. The synthetic data are produced and the algorithm is applied in order to reconstruct the initial parameters. An output of such an experiment consists of the recovered values and the six errors corresponding to the recovery of the six initial parameters.

In order to systematically evaluate the efficiency of the algorithm, numerous such experiments must be carried out. Moreover, the six results have to be presented as a function of all 15 parameters. In practice, we have restricted each computer run to study of only two variables, since only a function of two variables can be easily presented. Most of the possible combinations have been studied, but only the most interesting results will be presented here.

Figure 1 presents several examples of the signal as a function of time. The task of the algorithm is essentially to resolve the two functions, $\beta_1 A_t$ and $\beta_2 B_t$, out of the experimental points.

RESULTS

The Error Weighting Functions. First, the weighting functions that carry the error from the reading to the results are examined. Viewing these functions can point out special domains in variables space that are more probable to cause larger errors in the determinations. It should be emphasized that the algorithm has an error-correcting ability based on using more data points than variables. Thus, the real accuracy achieved is expected to be better than predicted by the weight

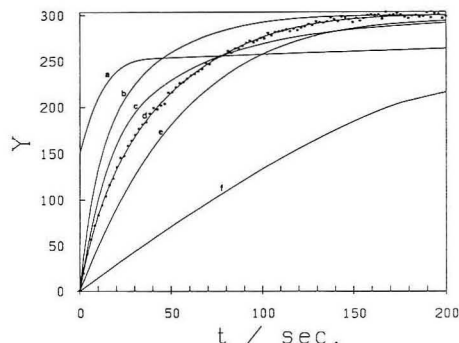


Figure 1. Examples of the signal as a function of time for various parameters: (a) $A_0 = 0.5$, $B_0 = 1.0$, $\sigma_1 = 1.25$, $\sigma_2 = 0.75$, $k_1 = 0.002$, $k_2 = 0.08$, $\beta_1 = \beta_2 = -100$, $r = 300$. (b) $A_0 = 2.0$, $B_0 = 1.0$, $\sigma_1 = 1.25$, $\sigma_2 = 0.75$, $k_1 = 0.08$, $k_2 = 0.02$. (c) $A_0 = 1.0$, $B_0 = 2.0$, $\sigma_1 = 0.75$, $\sigma_2 = 1.25$, $k_1 = 0.08$, $k_2 = 0.02$. (d) $A_0 = 1.0$, $B_0 = 2.0$, $\sigma_1 = 1.25$, $\sigma_2 = 0.75$, $k_1 = 0.08$, $k_2 = 0.02$. (e) $A_0 = 1.0$, $B_0 = 2.0$, $\sigma_1 = 1.25$, $\sigma_2 = 0.75$, $k_1 = 0.02$, $k_2 = 0.02$. (f) $A_0 = 1.0$, $B_0 = 2.0$, $\sigma_1 = 0.3$, $\sigma_2 = 0.5$, $k_1 = 0.008$, $k_2 = 0.005$. A superimposed noise of ca. 0.5% (circles) is shown for curve d.

functions. Nevertheless, singularities and extremes in the weight functions must be manifested in the error of the determinations. The weight functions (for the reaction of A) are

$$\beta_1 \frac{\partial A_0}{\partial Y} = \left(\frac{A_t}{A_0} \right)^{-n} \quad (14)$$

$$-\beta_1 \frac{\partial k_1}{\partial Y} = \frac{1}{t} A_t^{-n} \quad (15)$$

$$\beta_1 \frac{\partial n_1}{\partial Y} = \frac{1 - n_1}{A_t^n (k_1 t - A_0^{1-n_1} \ln A_0) + A_t \ln A_t} \quad (16)$$

where $A_t = [k_1(n_1 - 1)t + A_0^{1-n_1}]^{1/(1-n_1)}$. Similar equations are for the reaction of B.

In Figure 2 these equations are presented as a function of various variables. It may be deduced from Figure 2a, which represents eq 14, that higher errors are introduced to the concentration determination by data originating from the end of the reaction, especially at high-order reactions. Additionally, the error introduced to the determination of the rate constant mainly comes from the beginning of the reaction, and partially from the end of reaction, in the high-order cases (Figure 2b). From our experience, the determination of reaction orders is the most difficult one, for the reasons seen in Figure 2c. In this case errors are introduced not only at the beginning of the reaction but also at later times that depend on the reaction order itself.

Effect of Signal Noise and Number of Data Points. In principle, plots of the error in the determination of all variables (A_0 , B_0 , n_1 , n_2 , k_1 , k_2) should be presented as a function of the standard deviation of the readings and the number of readings (at several times after the reaction has started). Whenever possible, only representative plots will be given and the rest will be just described.

Figure 3a shows the error in the determination of B as resulted from 1600 computer experiments. Such sets of experiments have been carried out at various values of the parameters, and this figure is a representative one. The Gaussian noise has been produced by the Box-Muller method, which provides normally distributed deviates with zero mean and unit variance. In these experiments the noise level has been varied from 0 to 0.1 and the number of readings from 10 to

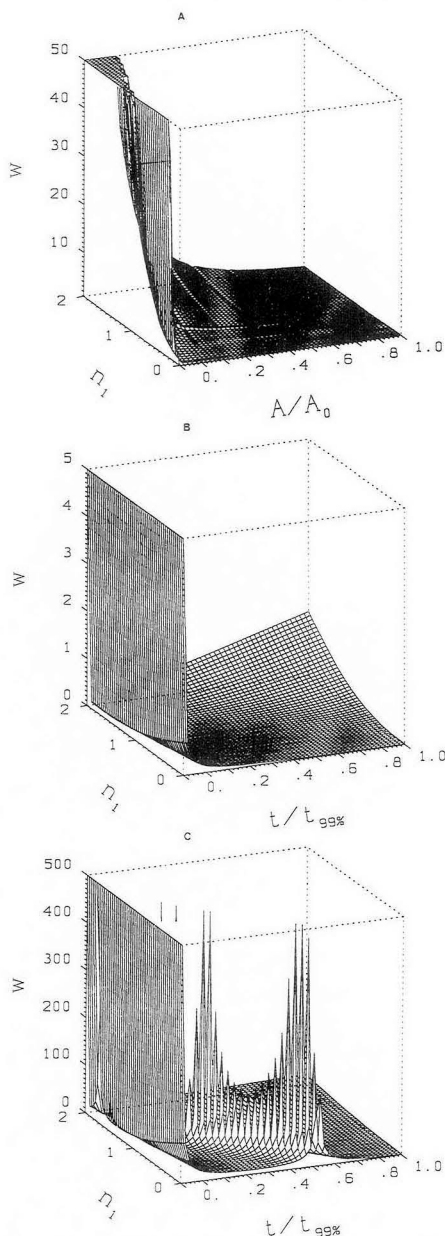


Figure 2. The weight function which carries the noise to the various parameters that are to be determined. (A) The parameter A_0 : w , which is a function of time, is presented as a function of the general variable A/A_0 . (B) The parameter k_1 : Note the increase in the function at high reaction orders, during the informative life-time of the reaction, which is manifested in the results of the determinations ($k_1 = 0.02$, $A_0 = 1.5$). (C) The parameter n_1 : Note the high values of w , compared to A and B. The high values and the internal structure make the reaction order sometimes difficult to determine ($k_1 = 0.02$, $A_0 = 1.5$).

166. The readings have been taken at equal intervals from $t = 0$ to $t = 205$ s. (Usually better results are achieved when randomizing the time intervals between the readings.) For most of the experiments an error of less than 2% has been achieved. Higher errors, up to 10%, have been achieved with less than 18 readings. Essentially, increasing the number of readings over 25 does not improve the recovery.

The errors in the determination of k_2 , obtained in the same set of experiments are lower (ca. 1.5%), even when using only 10 readings. The accuracy of the determination of n_2 is very similar to that of k_2 . Generally, the errors in the determination of variables of group A (A_0 , k_1 , and n_1) are similar to the corresponding variables of group B (B_0 , k_2 , and n_2); however somewhat higher.

In order to test the ability of the algorithm, similar experiments have been carried out at much higher noise levels as well. The error in the determination of B_0 (as resulted from 2601 experiments, averaged over various number of readings) is presented in Figure 3b. Also in this case, the errors in the determination of the rate constants and reaction orders have been lower than in the determination of the concentrations.

Effects of Measurements' Schedule. There are three main questions regarding the times of the measurements, in the reactions scale: What is the effect of a delay in starting the measurements, the effect of stopping the measurements before the reaction has ended, and the effect of mismatch between the measured time and the real time in the chemical system. The principle is that the measurements must be carried out during the most informative period of the reaction's life.

Figure 4a shows the effect of the time of starting the measurements. The error in the determination of A and of B is presented as a function of the start time, in internal units. (τ is the time that takes A to fall down to 0.5% of its initial value). Obviously, one must not start the measurements too late, but it is interesting to note that the main effect is on the determination of A and much less on B. The reason is that at these particular rate constants and reaction orders, A falls down faster than B (Figure 1) so that during the same time delay more information is lost about A than about B.

Figure 4b shows the effect of the termination of the measurements on the accuracy of the determinations. Also in this case, the errors are low, provided that the measurements have not been stopped before the informative time has passed ($t_f > 0.4\tau$). (This period for the reactions of Figure 1 is about 110 s. During this time ca. 85% of the reaction has been completed.) The error as a function of the termination time has two minima, before $t_f/\tau \sim 0.4$, which has just been mentioned. The first is a minima at $t_f/\tau \sim 0.05$ and the second at $t_f/\tau \sim 0.21$. The second minima is manifested here as a shoulder but has been clearly observed in experiments with lower noise levels. These times correspond approximately to the inverse of the rate constants of the two reactions.

In a real experiment, unlike a computer experiment, there may be difficulties in determining the exact instant when the reaction has started. In fast reactions this problem is caused by the duration of the mixing process. Therefore, although times are measured with high accuracy, there might be a mismatch between the measured times and the real times in the reactions' scale. The effect of such a mismatch is presented in Figure 4c. A small mismatch causes much larger errors than a big one does. Therefore, it is recommended to add a constant to the measured times whenever there is a doubt about the real starting instant.

Effect of Spectroscopic Characteristics (Detector's Sensitivity). There are four components in this system that vary as a function of time, and the detector's sensitivity to each component may be different. In spectroscopic deter-

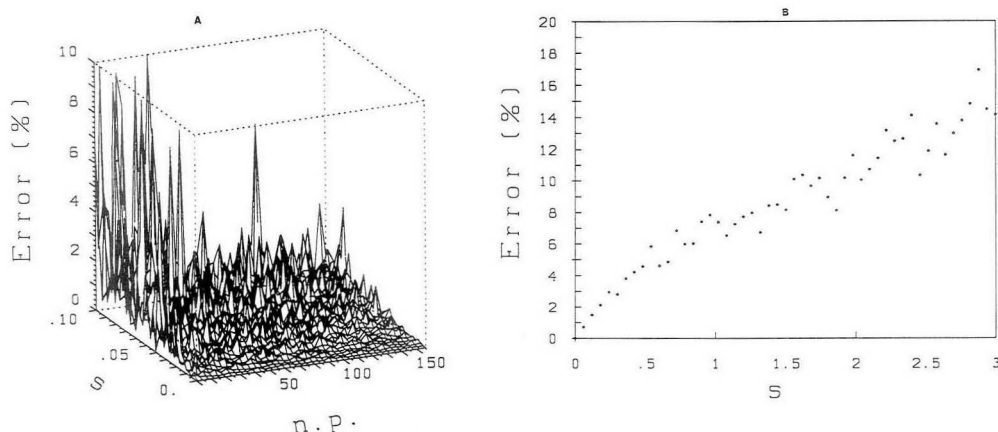


Figure 3. The effect of the number of data points and of noise level (standard deviation) on the determinations of the concentration (A). Higher range of noise level (at 100 points) is presented in B. The spiky shape of the surface in A (due to unaveraged data) may provide information on the variance of the error as well ($k_1 = 0.08$, $k_2 = 0.02$, $A_0 = 1.1$, $B_0 = 1.9$, $\sigma_1 = 1.25$, $\sigma_2 = 0.75$, $t_i = 205$, $\beta_1 = \beta_2 = -100$, $r = 300$).

minations, one has some control over these factors by choosing a proper wavelength where the measurements are carried out. Therefore, it is of importance to study this effect in order to find conditions for best determinations. Equation 5 shows how all these factors determine β_1 , β_2 , and r , which are time independent. r includes the background signal that may come from the instruments or from other components present in the mixture and do not participate in the reactions.

In a series of experiments carried out at various noise levels, r has been varied from zero to ten times the maximal clean signal, and no influence has been observed on the accuracy of the determinations. Thus, the algorithm is not affected by a constant background.

The constants β_1 and β_2 , as defined in eq 5, are the difference between the detector's sensitivity with respect to the reactants and its sensitivity with respect to the products. Obviously, one should prefer high values for these constants in order to get the information out of the reaction change. In a usual case, β_1 will be different from β_2 , thus the question of how this difference affects the accuracy of the determinations is of interest and has been studied. Figure 5a presents the error in the determination of A as a function of the ratio β_2/β_1 for various noise levels. A large increase in the error has been observed for ratios over ~ 50 . It is interesting to note that even at $\beta_2 = 0$ the determination of A can be carried out, which means that the algorithm, as it is, can be applied to kinetic determinations of single compounds in a general order reaction system (a problem that has been already studied¹⁵). This feature has also been checked in another series of experiments where β_2/β_1 has been varied in the range 0–0.2. As expected, the error in the determinations of B obtained from the same sets of experiments increases at very low β_2/β_1 .

The other unknowns that have been determined, namely the reaction orders and rate constants, have been affected by both extremes. For example, Figure 5b shows the error in n_2 which is similar to its group member B but with additional errors that stem from the error in A. The error in k_2 behaves in a similar way, and the error in n_1 and k_1 is mainly like the error in A, with some additional contribution from the error in B. The reason for this characteristic is probably the mixed working variables that are used in the minimization process.

The limitation that β_2/β_1 should be roughly in the range of $1/50$ to 50 does not impose a severe restriction on the applicability of the algorithm, as usually such conditions can be easily accomplished.

The Range of the Parameters. In this section the ranges of the parameters that can be handled by the algorithm are considered.

Range of the Rate Constants. Both rate constants have been varied from 0.01 to 2.01, in a series of 1681 experiments, and the results are presented in Figure 6. The error in the determination of A is presented in Figure 6a. The recovery is good for most of the parameters' value, except of two regimes: The first is characterized by extremely high ratio of k_1/k_2 (150–200). Similar results have been obtained for the determination of B; however, the high error regime has been at high k_2/k_1 . The explanation is that in these cases the compound with the higher rate constant disappears much faster than the other one, and most of the measurements are taken after the informative part of its reaction has passed. However, this is not a real problem, because in these extreme cases the reactions take place on two different time scales, so they may be treated separately. The algorithm of a single general-order reaction may be applied, although they take place in a mixture. The plots of the error in k_1 and in n_1 look similar, in the sense that these two regimes of relatively high error are present, although the errors caused by the high ratio of k_1/k_2 are smaller (Figure 6b). Correspondingly, the plots describing the error in B, k_2 , and n_2 show a regime of high error at high k_2/k_1 .

The second domain is the k_1 – k_2 space that results high errors is characterized by such values of rate-constants that make the fall-off of the functions A_i and B_i look very similar. For each set of values of the reaction orders there are values of the rate constants such that the functions A_i and B_i look similar. In another set of experiments the orders of the two reactions have been set equal and the domain of the higher errors has been found exactly along the line $k_1 = k_2$, as expected.

Range of Reaction Orders. The reaction orders have been varied in a wide range, and it has been found that the algorithm converges almost within no severe limitations for values characterizing ordinary chemical systems. As discussed previously, the current version of the algorithm is not defined for $n = 1$, so at this singular point high errors are found. (As already mentioned, it is possible to extend the algorithm to include $n = 1$, but with the price of losing some accuracy.) Besides $n = 1$, quite high errors have been detected when both reaction orders are high, so lower accuracy is to be expected in this regime. These errors can be explained by the high

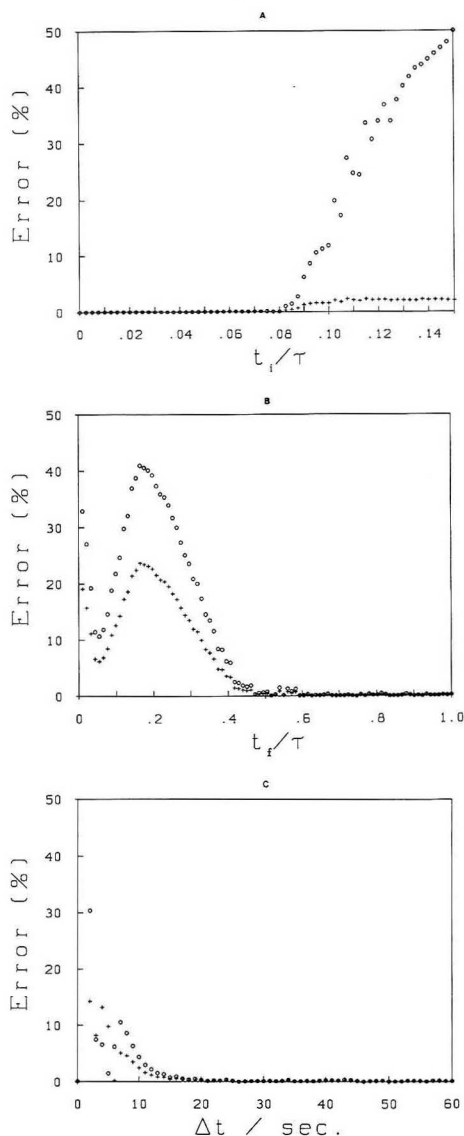


Figure 4. The effect of the time range of the measurements. (A) The time of starting the measurements. (B) The time of terminating the measurements. (C) The effect of a mismatch between the measured time and the real time. (C): The error in the determination of B. +: The error in the determination of A.

contribution of the signal noise, as discussed in the section on the error-weighting function. Figure 7 presents the errors found in k_2 . All the other plots for the other variables look similar. Here, the error at $n = 1$ has been truncated to 20% so the region of high reaction orders can be viewed.

Range of Concentrations. As has already been mentioned in the mathematical description, the concentration units can be scaled in order to bring the concentrations into the range

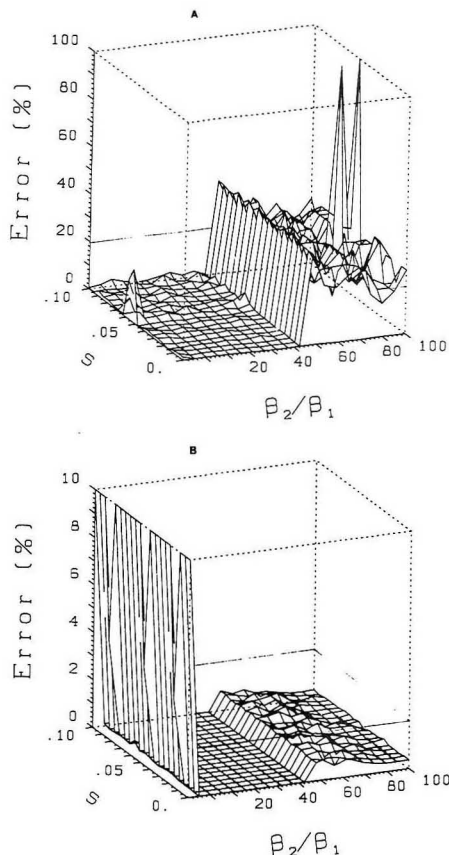


Figure 5. The effect of the detector's sensitivity ratio on the error at several noise levels (standard deviation). (A) Determination of A. (B) Determination of n_2 .

where the algorithm converges best. Moreover, the ratio of A to B can also be controlled by assigning different values to f_1 and f_2 in eq 11. Nevertheless, there are not real degrees of freedom because a problem of immoderate value of the concentrations ratio is thus being transferred to the rate constants space. However, in case of convergence problems, one still can maneuver between these two spaces (concentrations and rate constants). Therefore, study of the effect of concentration range is needed, in addition to the rate constant range. Figure 8a presents the error in n_1 , where the two concentrations have been varied from 0.01 to 3, and Figure 8b presents the error in B where the concentrations have been in the range of 1–100. This figure represent the whole sets of variables that have been studied.

When referring to the "A" group (A_0, n_1, k_1), a low A/B ratio may cause high errors, while in the "B" group (B_0, n_2, k_2), a low B/A ratio may cause this effect. Moreover, very high values of the concentrations (as well as very low values) result a statistical increase in the average error (in both groups of variables).

Effect of the Initial Estimations. The algorithm requires an initial estimation of the six parameters ($A_0^0, B_0^0, n_1^0, n_2^0, k_1^0, k_2^0$). As the initial estimation is better, the minimization of

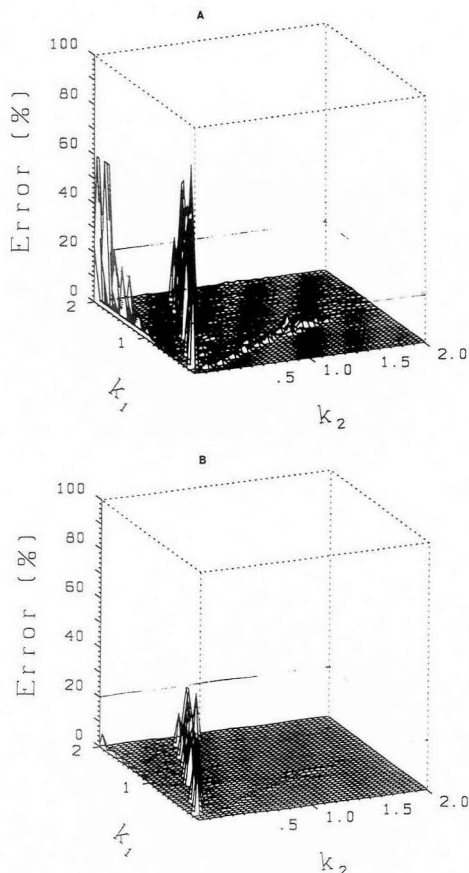


Figure 6. The effect of the range of the rate constants. (A) Determination of A. (B) Determination of B. ($A_0 = B_0 = 1.5$, $n_1 = 0.75$, $n_2 = 1.25$, $\beta_1 = -160$, $\beta_2 = -100$, $r = 300$. The standard deviation of the readings has been 0.1. t_r has been calculated so that A falls to 0.5% of its initial value.)

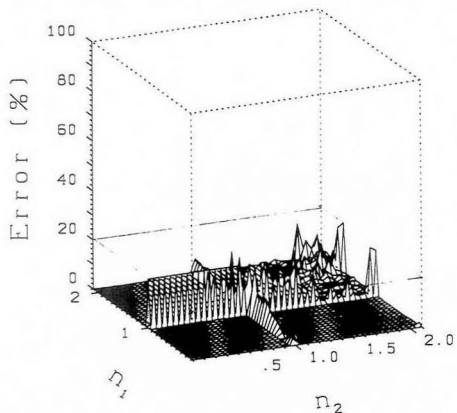


Figure 7. The error in the determination of k_2 as a function of the two reaction orders. Note the probability of high errors when both reaction orders are high.

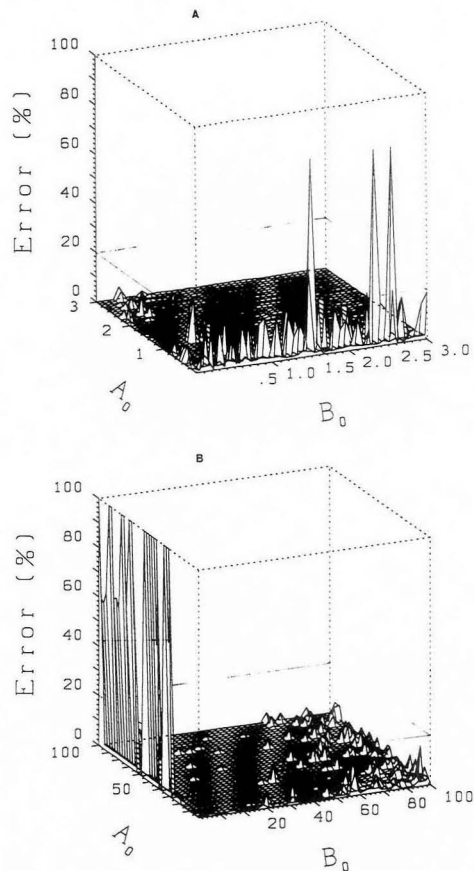


Figure 8. The effect of the range of the concentrations on the determination of n_1 (A). Similar results have been obtained for k_1 and A_0 . Determination of B (B): Similar results have been obtained for k_2 and n_2 .

the least square is faster and the final results may be better. The previous sections were focused on the effect of other parameters so the initial estimates were generated by a Gaussian deviate (ca. 50%) from the real values. This section describes the effect of the initial estimates on the ultimate results of the determination.

In order to study how good the initial estimation of the concentrations should be, ca. 1600 experiments have been carried out, where the concentrations have been varied from almost 0 to 10. For each value of the concentration (A_0), the initial estimate (A_0^0) has been varied in the same range. When studying the determination of parameters from group B, (B_0 , n_2 , k_2), the recovery has been found to be excellent for the whole range of A_0/A_0^0 except for $A_0/A_0^0 > \sim 200$. For the determinations of variables of group B, good results have been obtained even for $A_0/A_0^0 \sim 0.005$. However, in the same experiments (where the ratio A_0/A_0^0 has been varied) good recoveries of group A variables required both $A_0/A_0^0 < \sim 200$ and $A_0/A_0^0 > \sim 0.005$. Even at these two limits better results have been obtained for determination of reaction orders and rate constants than for concentrations, which suggests an iterative process that could be applied in cases of extremely poor initial estimation of the concentrations.

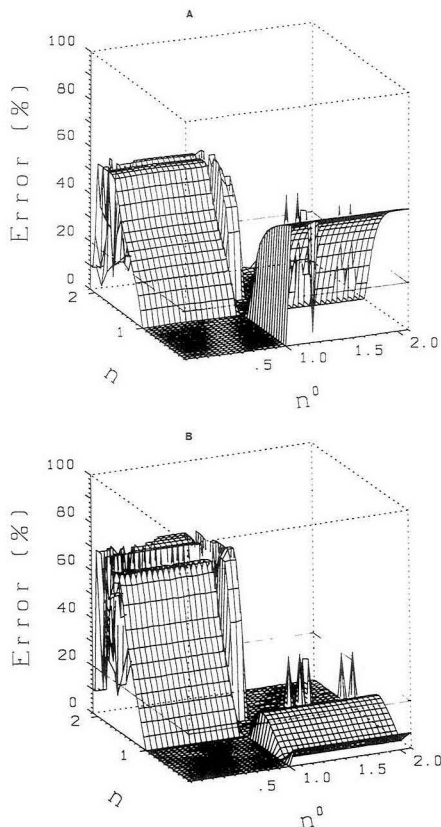


Figure 9. The errors in the determination of A (A) and of k , (B) as a function of the reaction orders and their initial estimates.

Similar experiments have been done for the study of the effect of initial rate constant estimation. The error always increases at too low values of k^0 ($k^0/k < 0.02$). Therefore, in case of doubt, it is recommended to use a high value as an initial estimate of the rate-constant.

The initial estimate of the reaction-order is somewhat problematic, because of the singularity at $n = 1$. The Jacobian (eq 12) is proportional to $1/(1 - n)$, and its value near the singular point is positive for $n < 1$ and negative for $n > 1$. Consequently, the error in the determinations increases when $n > 1$ and its initial estimate, $n^0 < 1$, and vice versa. Figure 9a illustrates that for good results, the initial estimate of the reaction order should be on the same side as the real value, regarding to unity. (The error has not been shown at $n = 1$.) In this figure the error in the concentration that belongs to the same group as the reaction orders has been represented, however, the errors of the other group are somewhat lower but with the same characteristics.

The error in the rate constant for $n < 1$ is much less sensitive to the estimate of n , but for $n > 1$ it is even more sensitive than the error in the concentrations (Figure 9b). The determination of the reaction order exhibits a different behavior. In this case the error is extremely high for $n < 1$ and $n^0 > 1$, but not so sensitive for $n > 1$ and $n^0 < 1$.

A general feature characterizing all determinations is that excellent results are obtained whenever n^0 is on the same side

of unity as n , and $n^0 > n$ for $n > 1$. In other words, even when the real reaction order is known to be somewhat higher than unity, it is better to use a value of n^0 much larger than unity and let the algorithm converge to the real value.

DISCUSSION

The proposed algorithm has been found to work in a wide range of the parameters. However, some limitations have been pointed out. It may be applied to kinetic determination of dual mixtures when very little knowledge on the chemical reactions is available. In some complicated cases, the overall reaction orders may depend on the specific conditions (pH, temperature), thus this is the only possible way to perform the analysis. The proven ability of the algorithm to converge even with data collected before the completion of reactions implies the application of the method to cases where equilibrium is achieved after too long time. The other extreme cases of fast reactions usually suffer from difficulties in the determination of the starting instant of the reaction. However, as previously demonstrated, the algorithm can compensate for a constant error in the time measurements.

Since our work may be considered as an extension of the monocomponent case,¹⁵ a comparison to that system is required. It should be noted that these two methods have different purposes (kinetic determination of one component and simultaneous determination of mixtures), as well as the fact that they face different mathematical problems (3-dimensional and 6-dimensional minimization). But the kinetic description of a single component is the same and the numerical process is based on the same Marquardt least-square fit. In general, some of the characteristics of the monocomponent system have been observed also in this system. However, there are some differences. No restriction has been found for reaction orders of zero, and in the vicinity to zero, as was found in ref 15. At $n = 0$ eqs 3 and 4 describe a zero-order process, namely $C_i = C_{i0} - kt$, as well as the Jacobian (eq 12). Since our method can be applied to a monocomponent system as well, this dissimilarity can only be explained in different accuracy of the computers used in these studies. Our results in the vicinity of $n = 1$ are similar to the monocomponent case; however, our suggested way of including the unity order reactions in this algorithm may be applied to the monocomponent system as well.

Reference 15 implies a large effect of mismatch between the real starting point of the reaction and the measured one, especially on the determination of the concentration. This is in contrast to our findings that the effect is present at small delays only, and it is quite equal for all the parameters (concentrations, reaction orders, and rate constants).

A more profound comparison is not possible since this study covers more variables than provided in ref 15. Moreover, although the systems are similar, they are far from being identical and no complete agreement is expected.

A rather different approach to kinetic determinations has been based on numerical integration of the differential equations.²⁰ This approach is mainly used for kinetic modeling but also for chemical determinations. Thus, results on the general-order reactions may be obtained by this method as well. A comparison to such results would be of interest.

This study is focused on simultaneous determinations of only two components, because of the principle questions rising in such determinations, where the reaction orders and the rate constants are unknown. However, further research on extension of the algorithm to more components, as well as developing algorithms that consider information obtained at several wavelengths, is planned.

REFERENCES

- (1) Pardue, H. L. *Anal. Chem.* **1990**, *237*, 207.
- (2) Fitzpatrick, C. P.; Pardue, H. L. *Anal. Chem.* **1989**, *61*, 2551.

- (3) Mottola, H. A. *Kinetic Aspects of Analytical Chemistry*; Wiley: New York, 1988.
- (4) Mark, H. B., Jr.; Rechnitz, G. A. *Kinetics in Analytical Chemistry*; Interscience: New York, 1968.
- (5) Ridder, G. M.; Margerum, D. W. *Anal. Chem.* **1977**, *49*, 2090.
- (6) Brown, P. B.; Lewis, K. O. *Ann. Clin. Biochem.* **1980**, *17*, 192.
- (7) Weiser, W. E.; Pardue, H. L. *Anal. Chem.* **1986**, *58*, 2523.
- (8) Harner, R. S.; Pardue, H. L. *Anal. Chim. Acta* **1981**, *127*, 23.
- (9) Abe, S.; Saito, T.; Suda, M. *Anal. Chim. Acta* **1986**, *181*, 203.
- (10) Ballesteros, L.; Perez-Bendito, D. *Anal. Chim. Acta* **1986**, *182*, 213.
- (11) Eaton, D. F. *Pure Appl. Chem.*, **1990**, *62*, 1631.
- (12) Drew, J.; Szabo, A. G.; Morand, P.; Smith, T. A.; Ghiggino, K. P. *J. Chem. Soc., Faraday Trans. 2*, **1990**, *86*, 3853.
- (13) Bajzar, Z.; Sharp, J. C.; Sedarous, S. S.; Prendergast, F. G. *Eur. Biophys. J.* **1990**, *18*, 101.
- (14) Schechter, I. *Anal. Chem.* **1991**, *63*, 1303.
- (15) Larsson, J. A.; Pardue, H. L. *Anal. Chim. Acta* **1989**, *224*, 289.
- (16) Laios, I.; Fast, D. M.; Pardue, H. L. *Anal. Chim. Acta* **1986**, *180*, 429.
- (17) Benson, S. W. *The Foundations of Chemical Kinetics*; McGraw-Hill: New York, 1960.
- (18) Levenberg, K. Q. *Appl. Math.* **1944**, *2*, 164.
- (19) Marquardt, D. *SIAM J. Appl. Math.* **1963**, *11*, 431.
- (20) Havel, J.; Gonzalez, J. L. *Scr. Fac. Sci. Nat. Univ. Purk. Brun.* **1989**, *19*, 183.
- (21) Mottola, H. L.; Mark, H. B., Jr. *Anal. Chem.* **1984**, *56*, 96R.
- (22) Rutan, S. C.; Fitzpatrick, C. P.; Skoug, J. W.; Weiser, W. E.; Pardue, H. L. *Anal. Chim. Acta* **1989**, *224*, 243.
- (23) Wentzell, P. D.; Karayannis, M. I.; Crouch, S. R. *Anal. Chim. Acta* **1989**, *224*, 263.

RECEIVED for review October 21, 1991. Accepted December 31, 1991.

Preconcentration of Trace Rare-Earth Elements in Seawater by Complexation with Bis(2-ethylhexyl) Hydrogen Phosphate and 2-Ethylhexyl Dihydrogen Phosphate Adsorbed on a C₁₈ Cartridge and Determination by Inductively Coupled Plasma Mass Spectrometry

Mohammad B. Shabani,* Tasuku Akagi, and Akimasa Masuda

Department of Chemistry, Faculty of Science, The University of Tokyo, Hongo, Tokyo 113, Japan

A rapid and reliable sample preconcentration method with minimum time-consumption and labor has been developed to separate rare-earth elements (REEs) from seawater for the measurement by inductively coupled plasma mass spectrometry (ICPMS). The method involves adsorption of a mixture of bis(2-ethylhexyl) hydrogen phosphate (HDEHP) and 2-ethylhexyl dihydrogen phosphate (H₂MEHP) onto a C₁₈ cartridge. By passage of seawater samples through the C₁₈ cartridge, quantitative complexation of REEs with adsorbed complexing agent took place and almost all matrix elements passed through to the drain. The REEs are then removed from the adsorbed complexing agent with an acid eluent. This technique used an eight-channel peristaltic pump for sample processing. Eight 1-L samples of seawater at flow rates of 20 mL/min were preconcentrated within 1 h. This method permitted large enrichment factors of 200–1000-fold to be attained while providing almost matrix-free concentrate suitable for ICPMS analysis. The total contamination determined for the whole process was much less than 1% of the amount of REEs in 1 L of seawater. The average precisions for all REEs after four replicate preconcentrations of 1000 and 5000 mL of the same seawater to final measurement solutions of 5 mL were calculated to be 2.72% and 1.04%, respectively. The parameters which were evaluated for the optimum experimental conditions include pH of the sample, amount of complexing agent loaded on the C₁₈ cartridge, flow rate of the sample, volume of seawater, and concentration and volume of the acid for elution. Since there is no standard seawater sample for REEs, in order to evaluate the precision and accuracy of this novel technique, the analytical results obtained by this method were compared with those obtained by ICPMS coupled with solvent extraction concentrations and neutron activation analysis (NAA) after Chelex 100 concentrations.

INTRODUCTION

Inductively coupled plasma mass spectrometry (ICPMS) has been used successfully for direct determination of rare-earth elements (REEs) in geological materials.^{1–7} However, application to the determination of REEs in seawater remains limited. The major restriction comes from the extremely low levels of these elements which are below the detection limits of the instrument. Another limitation is due to the high matrix concentrations of approximately 3.5%, present in seawater which is not compatible with the sampling system of ICPMS. Therefore, the analysis of REEs in seawater requires preconcentration and matrix separation in order to eliminate matrix elements and increase the concentration factor above the instrument detection limits prior to analysis by ICPMS.

Preconcentration techniques are currently used for REE determination in seawater before isotope dilution mass spectrometry (IDMS) and neutron activation analysis (NAA).^{8–16} By far the most widely used preconcentration technique is based upon the coprecipitation of REEs with Fe followed by cation-exchange chromatography and determination with IDMS.^{8–14} The coprecipitation technique suffers from several limitations, which include nonquantitative recovery (quantitative recovery can be only established by the addition of spike isotopes) and additional necessary procedures for removal of Mg, Ca, and Fe. This will increase sample manipulation and contamination of blanks. In addition, the coprecipitation technique cannot be easily automated. Another technique recently used for REE preconcentration in seawater is chelating ion-exchange resin, Chelex-100.^{15–18} Although this technique has been successfully employed in seawater analysis by NAA,^{14,15} it also has serious drawbacks. These include time-consumption (the recovery of REEs is strongly limited by flow rates of 1–3 mL/min) and removal of calcium and magnesium prior to elution of the REEs, requiring careful washing with ammonium acetate¹⁹ or additional

cation- and anion-exchange chromatography before instrumental determination.^{14,15} All these will increase sample manipulation and contamination of blanks. Coprecipitation and Chelex-100 techniques are not suitable preconcentration techniques for ICPMS determination of REEs in seawater.

A reliable method capable of preconcentration of a large number of samples with minimum time-consumption and labor and compatible with high sample throughput of the ICPMS system is strongly desired by the many researchers in the field of oceanography dealing with REE determination.

Recently, we developed a successful technique based on the solvent extraction and back-extraction preconcentration of REEs in seawater and determination with ICPMS,²⁰ where REEs were concentrated 200 times with almost all matrix elements separated. Although this method has several advantages over conventional methods in simplicity, rapidity, and small blank, there are still some problems with this technique. These problems are time-consuming procedures of the prewashing of the solvent extraction apparatus and purification of the reagents and solvents and limited preconcentration factor. In another study we developed an on-line two-stage solvent extraction and back-extraction and the method made possible rapid preconcentration of REEs in geological samples and synthetic seawater.²¹ With this method, under optimum conditions, an enrichment factor of 10 was obtained for synthetic seawater. However, for application to real seawater samples, higher enrichment factors were found to be necessary because of the extremely low levels of REEs present in seawater (below the detection limits of the instrument).

In the last several years, a number of researchers have developed preconcentration methods based upon the reversed-phase adsorption of complexed metals onto a small column²²⁻²⁵ or immobilization of complexing agents on substrate for concentration of metal ions on it.²⁶⁻³¹ These methods have been applied to several determinations of transition elements in seawater and other natural samples. None of the above mentioned methods have been used for the preconcentration of REEs in seawater.

In an attempt to overcome the several limitations of the other preconcentration techniques, we have developed a new method which involved adsorption of a mixture of bis(2-ethylhexyl) hydrogen phosphate (HDEHP) and 2-ethylhexyl dihydrogen phosphate (H₂MEHP) onto a Sep-Pak C₁₈ cartridge (C₁₈). These complexing agents offer several advantages and have proven to be a particularly useful material for sample preparation, matrix isolation, and preconcentration of trace REEs in seawater by solvent extraction techniques.²⁰ Because of the high molecular weight of HDEHP and its water insolubility, it strongly adsorbs onto hydrophobic substrates like C₁₈ and no leaching of the complexing agent or metal complexes occurs under preconcentration conditions. The process of preconcentration is simple, requires very few reagents, and minimizes the contamination of blanks. Unlike Chelex-100 and 8-hydroxyquinoline no buffer or additional reagents are necessary and preconcentration is possible in acidic solutions.

This study has attained rapid chemical separation, less contamination of blanks, and improvement of the enrichment factor necessary for high-precision measurements.

EXPERIMENTAL SECTION

Instrumentation. The inductively coupled plasma mass spectrometer used for this work was the VG Plasma Quad (VG Elemental, Winsford, U.K.). The nebulizer used was standard concentric glass in conjunction with a water-cooled spray chamber. Details of the operating conditions and data collection parameters are given in Table I. A Gilson eight-channel peristaltic pump (Gilson Minipulse 2) was used for sample pretreatment.

Reagents. The Sep-Pak C₁₈ cartridges (Part No. 51910) were purchased from the Waters Division of Millipore Corp., and all

Table I. Instrument Operation Conditions

Plasma Conditions	
forward power	1.35 kW
reflected power	<5 W
cooling flow	13 L/min
auxiliary flow	1.1 L/min
nebulizer flow	0.75 L/min
Sampling Conditions	
sampling aperture diameter	1.2 mm
skimmer diameter	1.0 mm
load coil aperture distance	10 mm
Nebulizer	
nebulizer type standard concentric solution	0.4 mL/min
uptake rate controlled by peristaltic pump	
Data Acquisition	
dwell time	160 μ s
no. of scans	600
no. of channels	1024
measurement time	98 s
scanning mass	m/z 109-179

were washed before use by passing 10 mL of 6 M high-purity hydrochloric acid through the peristaltic pump, followed by 5 mL of subboiling distilled water. The cleaned C₁₈ cartridges were then stored in a plastic bag until loading of complexing agent.

The mixture of 65% bis(2-ethylhexyl) hydrogen phosphate and 35% 2-ethylhexyl dihydrogen phosphate was purchased from Tokyo Kasei Co. Ltd. and used as received. The ultrapure HCl and HNO₃ were purchased from Wako Pure Chemical Industries Ltd. The acids and water were further purified in our laboratory by subboiling distillation as described previously.²⁰

Seawater Samples. The S₁ seawater was collected in June 1989, from latitude 35°40'22" N and longitude 133°3'33" E, Japan Sea, near the Shimane prefecture (depth 1 m from the surface). The S₂ seawater was collected in Feb 1991, from latitude 33°17'3" N and longitude 134°13'1" E, Pacific Ocean near the Kochi prefecture (2.7 km off the shore, depth 320 m from the surface). After collection the seawater samples were acidified to pH 1.5 with HCl.

Synthetic Seawater. Synthetic seawater solution was prepared from high-purity chloride salts of sodium, potassium, magnesium, and calcium and subboiling distilled water. The final solution contained 10 560 mg/L sodium, 1270 mg/L magnesium, 400 mg/L calcium, 380 mg/L potassium, and 100 mg/L of each REE. This solution had the same matrix as a seawater sample, acidified with hydrochloric acid to different pH values for preconcentration and matrix separation studies.

Standard. The standard solutions of each REE were prepared by dissolving their high-purity oxides. The REE stock solution, which contained all REEs at the same concentration, was then diluted to 5 ng/mL of each element with water. After addition of Cd internal standard, 50 ng/mL, the standard prepared in this manner had a final acid concentration of 3% v/v HNO₃. Cd was used as an internal standard because it was not concentrated as a condition of this study.

Procedure of Adsorption of Complexing Agents onto Sep-Pak C₁₈ Cartridges. The precleaned C₁₈ cartridges were loaded with a mixture of HDEHP and H₂MEHP using a Pasteur pipet and with sucking by peristaltic pump. Different amounts of complexing agents were adsorbed onto the C₁₈ cartridge depending on the type and amount of sample used. The C₁₈ cartridge prepared in this manner was stored in a plastic bag until just before using. No further conditioning is necessary.

Preconcentration Procedures. All of the sampling and preconcentration procedures were performed in a clean laboratory prior to analysis of the trace REEs. The preconcentration system consisted of a Gilson eight-channel peristaltic pump, with eight Tygon pump tubes connected to C₁₈ cartridges which had previously adsorbed a 200- or 300-mg mixture of HDEHP and H₂MEHP. After connection of the C₁₈ cartridges, no prior conditioning of C₁₈ was necessary for the preconcentration of the REEs. The pH of each seawater sample before preconcentration was adjusted to 3 or 3.5 using a few drop of high-purity ammonia water. Samples of 1000 or 5000 mL were passed through the C₁₈

cartridge, at a flow rate of 20 mL/min. With this procedure all REEs in samples will quantitatively complex with complexing agents adsorbed on C₁₈ cartridges and, at the same time, all of the matrix elements and Ba will pass through to the drain. It should be stressed here that Ba, one of the sources of a troublesome oxide interference element for Sm, Eu, and Gd, is perfectly removed in this process of preconcentration. Following passage of the samples, the cartridges were washed with 5 mL of 0.01 M HCl to remove any remaining matrix elements. The preconcentrated REEs were then eluted by 40 or 50 mL of 6 M HCl at flow rates of 5 mL/min.

The REE concentrates were collected in Teflon beakers, and before the acid solutions were dried, 250 ng of Cd was added as an internal standard. The final solutions containing REEs and the Cd internal standard were then carefully monitored to evaporate the acid solution completely using a hot plate and yet avoid baking the residue. Finally, 1 mL of concentrated HNO₃ was added to each beaker and the beakers were again put on the hot plate. This process removed all remaining HCl and chlorides whose presence would disturb ICPMS determination. This process surely redissolves all REEs in nitric acid. Again, in this process special care must be taken to avoid complete evaporation of the sample, since dissolution of dried sample in a small amount of solution is quite difficult. The last few drops of remaining HNO₃ containing REEs and Cd internal standard were then diluted with water to a total volume of 5 mL. Under these conditions solutions of 3% v/v HNO₃ and approximately 200- or 1000-fold preconcentration of seawater were obtained before introduction to ICPMS.

Measurements. Quantitative analyses were performed by using the scanning mode of data acquisition. The scan conditions are summarized in Table I. The following analyses for every sample were applied: first the blank was measured, then the sample, and at the end, the standard. Five continuous measurements were made on each solution. A 5% v/v HNO₃ solution was used for washing the instrument to remove any contamination and memory effect prior to sample and standard introduction to ICPMS.

RESULTS AND DISCUSSION

Strength of the Adsorption of Complexing Agents onto C₁₈. Adsorption of organic acids on hydrophobic substrates is favored when the pH is low and the acids are in their undissociated form; this is well documented.³²⁻³⁶ Elution of acidic species with aqueous solutions can be accomplished by raising the pH and ionizing the molecule.^{32,36} The special advantage of HDEHP and H₂MEHP over other complexing agents (e.g. 8-hydroxyquinoline, iminodiacetates, dithiocarbamates, and so on) is their strong tendency to be adsorbed by organic substrates at all ranges of pH. In several studies, 8-hydroxyquinoline, dithiocarbamates, and iminodiacetates were used by sorption of metal complexes onto various substrates²²⁻²⁴ or retention of metal ions on immobilized complexes.²⁵⁻³¹ Their characteristics enable them to preconcentrate trace elements in water samples. The problem of HDEHP and H₂MEHP and their metal complexes is that they are water insoluble and cannot be used the same as water-soluble complexes. Immobilization of these complexing agents on a substrate using chemical material may also reduce their complexing ability. Since these complexing agents are present in dimeric or polymeric form with high molecular weights by formation of hydrogen bonding,³⁷ this will make them more insoluble in water at lower pH and enhance their adsorption to hydrophobic substrates such as C₁₈ and Amberlite XAD. The H₂MEHP is slightly soluble in water, especially at higher pH, and is partly removed by passage of seawater; HDEHP is water insoluble and almost all remained at the top of the C₁₈ cartridge after the passage of 5 L of seawater used in this study. A mixture of HDEHP and H₂MEHP or HDEHP alone has the same extraction ability at the working sample pH. In this study a mixture was preferred rather than HDEHP alone because of the lower REE impurities in the mixture comparing with HDEHP alone. Generally, the manufacturer produces

Table II. REE Impurities before Treatment in Sep-Pak C₁₈ Cartridges and Total Preconcentration Procedure Blanks

element	REE impurities, pg ^a	
	C ₁₈ cartridge before treatment	total procedure blank
La	68.9	6.1
Ce	140.0	8.6
Pr	17.7	1.2
Nd	60.2	4.2
Sm	10.4	
Eu	1.7	
Gd	8.2	
Tb	1.2	
Dy	7.6	
Ho	2.0	
Er	4.1	
Tm	0.31	
Yb	4.3	
Lu	0.29	

^a Average REE impurities obtained from pretreatment of eight Sep-Pak C₁₈ cartridges and of eight procedure blanks.

HDEHP from the mixture of HDEHP and H₂MEHP, and for purification additional reagents and containers are used; this will increase the REE contamination. Once HDEHP is contaminated by REEs, it is difficult to remove them.

Impurities of REEs in the C₁₈ Cartridge and Total Procedure Blanks. The REEs are present in seawater at extremely low concentrations. Working with such very low level samples, special care must be taken to reduce contamination problems. This can be done by use of smaller amounts of high-purity reagents and also by development of more practical preconcentration techniques. In the solvent extraction preconcentration technique, an additional process was necessary for lengthy cleaning of the extraction vessels.²⁰ Using a C₁₈ cartridge as a preconcentration technique will completely reduce the possible contamination problems by simply washing with 10 mL of 6 M HCl in less than 1 min. Generally, the C₁₈ cartridges supplied by Millipore contained picogram amounts of REEs. The determination of such small amounts of REE impurities in C₁₈ cartridges before pretreatment and total procedure blanks was difficult. So in this study for more accurate determination of REE impurities in the C₁₈ cartridge and total procedure blanks, eight C₁₈ cartridges were processed and average concentrations were obtained. The cleaning process is very simple, as explained in the Experimental Section. By passage of 10 mL of 6 M HCl, it was possible to remove completely all REE impurities. The total preconcentration procedure blanks were determined by using eight C₁₈ cartridge and carrying out the same procedure as stated in the Experimental Section without use of seawater samples. The results in Table II show the absolute amounts of REE impurities in each C₁₈ cartridge and the total procedure blanks. The results show that the pretreatment of the C₁₈ cartridge is one of the necessary processes before using it for preconcentration of REEs in seawater. It is important to stress here that the total procedure blanks determined are much less than 1% of their amounts in 1000 mL of seawater for all REEs.

Effect of the Amount of the Absorbed Complexing Agents on the C₁₈ Cartridge. According to the manual of the manufacturer, the mean weight of C₁₈ inside each Sep-Pak cartridge is 360 mg. The amount of complexing agents which can be adsorbed onto C₁₈ without passing through was found to be approximately 400 mg. In order to establish the quantitative recovery of REEs from seawater, four different amounts of mixtures of HDEHP and H₂MEHP, 50, 100, 200, and 300 mg, were loaded onto four C₁₈ cartridges. Four 1-L synthetic seawater samples at pH 3.5 were passed through the

Table III. Recovery of Spiked REEs from Different Solutions Using a C₁₈ Cartridge Loaded with 50 mg of Complexing Agents

element	% recovery ^a		
	demineralized water	synthetic seawater	seawater
La	99.6	89.7	88.8
Ce	99.2	99.1	98.7
Pr	99.9	99.1	99.0
Nd	99.1	99.0	98.9
Sm	99.7	99.3	99.2
Eu	98.6	99.5	99.4
Cd	99.7	100.0	99.8
Tb	99.1	99.1	99.3
Dy	98.6	99.7	99.4
Ho	98.3	99.1	99.7
Er	99.3	99.7	99.5
Tm	98.1	99.3	99.6
Yb	98.2	99.9	99.8
Lu	98.1	99.3	99.5

^aThe pH of the all samples was adjusted to 3.5 before preconcentration.

C₁₈ cartridge at a flow rate of 20 mL/min. The results of these experiments showed that in all cases the concentration recovery was higher than 99% for all REEs except for La in the 50- and 100-mg loaded mixture, which were 89.7% and 95.1% respectively.

In another study the recovery of REEs spiked in demineralized water, synthetic seawater, and seawater were examined by loading 50 mg of complexing agents onto C₁₈. As can be seen from the results of Table III, no loss of recovery is shown for demineralized water, but in cases of synthetic seawater and seawater approximately the same percent loss is found for La. The reason for loss of La in synthetic seawater and seawater is due to the presence of matrix elements, especially Ca, which competes with La to a small extent but no Ca will be concentrated in this preconcentration procedure. The distribution coefficient of La is smaller than other REEs. From the results of these experiments one can easily decide that, for preconcentration and determination of REEs in samples which do not have Ca or have a very low Ca concentration (e.g. freshwater, ground water, etc.), 50 mg of complexing agents is enough for quantitative recovery of all REEs. In the cases of seawater of similar solutions, 200 mg or more of complexing agents is necessary for quantitative recovery of all REEs.

In another study, the reuse of a C₁₈ cartridge was tested for its ability to preconcentrate two or more seawater samples. It was found that, for use of the same C₁₈ cartridge three times, no change was observed in recovery of REEs. The use of the C₁₈ cartridge more than three times was not studied since the adsorption of complexing agents is very simple and also a C₁₈ cartridge is not so costly. It is recommended that for preconcentration of such low-level samples, a new C₁₈ cartridge should be used for every sample, so as to offer protection of samples from possible contamination.

Effect of pH on Recovery. The effect of varying the pH of the sample solution on recovery of REEs was studied for 50- and 300-mg amounts of complexing agents loaded on a C₁₈ cartridge. The pH of the sample was varied from 2 to 8. The results, in Table IV, show that the recoveries of La, Ce, Pr, and Nd for pH 2 and 2.85 are nonquantitative and for pH 3.5 and 4.4 only La is nonquantitative. At pHs higher than 5.5, the recovery for all REEs is nonquantitative from synthetic seawater and 50 mg of complexing agents loaded on C₁₈. In the cases of 300 mg of complexing agents, as are shown in Table V, only at pH 2 is La recovery nonquantitative. At pHs higher than 5.5, all the REEs were again recovered poorly. One

Table IV. Percent Recovery^a of REEs from Synthetic Seawater as a Function of pH

element	synthetic seawater pH				
	2	2.85	3.5	4.4	>5.5
La	54.5	65.2	89.7	92.1	88.7
Ce	71.2	90.4	99.1	99.1	91.9
Pr	76.8	94.5	99.1	99.0	88.2
Nd	79.4	96.2	99.0	99.4	87.7
Sm	98.5	99.6	99.3	99.5	87.0
Eu	99.6	99.9	99.5	99.1	86.2
Gd	99.7	100.1	100.0	99.7	86.7
Tb	99.4	100.4	99.1	99.5	85.5
Dy	99.8	99.8	99.7	99.6	86.7
Ho	99.9	99.7	99.1	99.7	86.6
Er	99.6	99.9	99.7	99.6	86.2
Tm	100.2	99.4	99.3	99.8	83.6
Yb	100.4	99.8	99.9	99.3	82.2
Lu	99.9	99.7	99.3	99.5	83.0

^aAmount of complexing agents loaded on C₁₈ cartridges was 50 mg for all cases.

Table V. Percent Recovery^a of REEs from Synthetic Seawater as a Function of pH

element	synthetic seawater pH				
	2	2.85	3.5	4.4	>5.5
La	93.6	99.1	99.8	99.8	87.9
Ce	99.9	99.3	99.9	99.9	83.6
Pr	99.2	99.4	99.8	100.1	85.1
Nd	99.2	99.7	99.9	100.1	85.0
Sm	99.3	99.8	100.2	99.8	81.4
Eu	99.8	99.5	100.3	99.4	81.8
Gd	99.8	99.4	100.6	100.2	82.9
Tb	99.6	99.3	99.9	99.7	81.6
Dy	100.2	99.7	100.2	100.2	82.6
Ho	100.1	99.8	99.8	99.8	82.5
Er	99.8	100.4	100.2	100.1	81.3
Tm	99.7	99.4	99.9	99.9	78.7
Yb	100.4	99.3	99.8	99.8	76.2
Lu	100.4	100.2	99.9	100.1	76.8

^aAmount of complexing agents loaded on C₁₈ cartridges was 300 mg for all cases.

possible explanation for nonquantitative recovery at pHs higher than 5.5 is the dissociation of these complexing agents and as a result the reduction in ability to complex REEs. A similar problem appeared in a solvent extraction study of REEs from these complexing agents.³⁸

Effects of the Flow Rate and Volume of the Sample. The effect of different flow rates of sample solution on the recovery of REEs is studied with 50 and 300 mg of complexing agents loaded on C₁₈ and by passing 1 L of synthetic seawater at a constant pH of 3.5. The flow rates were varied from 5 to 50 mL/min. In the case of 300 mg of complexing agents, quantitative recovery was obtained for all flow rates studied. For 50 mg of complexing agents, only at flow rates of 5 mL/min or less was the recovery of all REEs quantitative. However, at a flow rate higher than 5 mL/min there is a loss in La recovery. As the flow rate increased, the loss of La also increased. The reason for the loss is due to the competition of La with Ca in complexation, since Ca is present in a higher concentration than La in seawater.

The volume of sample solution was varied at a constant flow rate of 20 mL/min and pH 3.5. Two different amounts, 50 and 300 mg, of complexing agents on the C₁₈ cartridge were employed. In the case of 300 mg of complexing agents, there was no change in quantitative recovery of all REEs. However, when 50 mg of complexing agents was used for sample volumes lower than 300 mL, all REEs were recovered quantitatively. At higher volumes of synthetic seawater, the recovery of La

Table VI. Elution Recovery^a of REEs from a C₁₈ Cartridge as a Function of Volume of 6 M HCl

element	volume of acid mL			
	first 5	second 5	third 5	total (5 + 5 + 5)
La	89.0	0.56	0.14	89.7
Ce	98.4	0.62	0.12	99.1
Pr	98.3	0.65	0.11	99.1
Nd	98.2	0.61	0.09	99.0
Sm	98.5	0.76	0.08	99.3
Eu	98.7	0.71	0.14	99.5
Gd	99.2	0.67	0.11	100.0
Tb	98.2	0.82	0.12	99.1
Dy	98.6	1.00	0.09	99.7
Ho	98.0	0.95	0.13	99.1
Er	98.4	1.15	0.12	99.7
Tm	97.7	1.45	0.18	99.3
Yb	97.4	2.10	0.36	99.9
Lu	95.7	2.85	0.75	99.3

^a After concentration of 1000 mL of synthetic seawater on a C₁₈ cartridge containing 50 mg of complexing agents.

Table VII. Elution Recovery^a of REEs from a C₁₈ Cartridge as a Function of Volume of 6 M HCl

element	volume of acid, mL				
	first 10	second 10	third 10	fourth 10	total (10 + 10 + 10 + 10)
La	95.4	4.10	0.34		99.8
Ce	96.9	2.83	0.14		99.9
Pr	96.7	2.58	0.14		99.4
Nd	97.0	2.76	0.16		99.9
Sm	98.1	1.96	0.14		100.2
Eu	98.7	1.47	0.13		100.3
Gd	98.1	2.38	0.13		100.6
Tb	98.3	1.52	0.10		99.9
Dy	98.5	1.60	0.09		100.2
Ho	98.5	1.21	0.11		99.8
Er	98.3	1.76	0.14		100.2
Tm	95.2	4.3	0.38	0.04	99.9
Yb	84.8	12.5	2.10	0.40	99.8
Lu	73.0	18.1	6.85	1.96	99.9

^a After concentration of 1000 mL of synthetic seawater on a C₁₈ cartridge containing 300 mg of complexing agents.

was nonquantitative. As the volume was increased to more than 1000 mL, the recovery of Ce, Pr, and Nd also became nonquantitative. So, in preconcentration of a real seawater sample, the following parameters were used: for 1-L seawater samples, a sample flow rate of 20 mL/min, a sample pH of 3, and 200 mg of complexing agents; for 5-L seawater samples, a sample flow rate of 20 mL/min, a sample pH 3.5, and 300 mg of complexing agents.

Effects of Types, Concentrations, and Volumes of Acids on Elution Recovery. Of the various eluting acids HCl, HClO₄, and HNO₃ tried, HCl was found to be most satisfactory. The effect of concentration of HCl from 2 to 12 M showed that, for lighter REEs, recovery was satisfactory at all concentrations. However, for heavier REEs, especially Tm, Yb, and Lu, it was found that 6 M of acid was the best concentration. At concentrations higher or lower than 6 M, the volume of the acid necessary for quantitative recovery unfavorably increased.

As found in the above studies, HCl with a concentration of 6 M is the most satisfactory for elution recovery. The studies for elution recovery were undertaken with 50- and 300-mg amounts of complexing agents loaded on a C₁₈ cartridge using different volumes of acid after preconcentration of 1 L of synthetic seawater. The results are shown in Tables VI and VII. From the results of Table VI it can be seen that

Table VIII. Reproducibility^a of the Measurements Using Four Separate Preconcentration of 1000 mL of the Same Seawater to 5 mL

element	1	2	3	4	av	% RSD
La	2.50	2.56	2.52	2.51	2.52	1.04
Ce	1.57	1.56	1.59	1.58	1.57	0.82
Pr	0.416	0.421	0.410	0.420	0.417	1.20
Nd	2.14	2.12	2.04	2.11	2.10	2.06
Sm	0.443	0.465	0.446	0.424	0.444	3.77
Eu	0.117	0.124	0.118	0.112	0.118	4.18
Gd	0.762	0.689	0.727	0.692	0.717	4.78
Tb	0.101	0.099	0.095	0.105	0.100	4.16
Dy	0.717	0.724	0.718	0.745	0.726	1.79
Ho	0.217	0.211	0.219	0.210	0.214	2.06
Er	0.687	0.658	0.664	0.654	0.666	2.21
Tm	0.093	0.086	0.087	0.090	0.089	3.35
Yb	0.629	0.614	0.590	0.598	0.608	2.85
Lu	0.107	0.111	0.102	0.105	0.106	3.55

^a Five measurements for each sample.

Table IX. Reproducibility^a of the Measurements Using Four Separate Preconcentrations of 5000 mL of the Same Seawater to 5 mL

element	1	2	3	4	av	% RSD
La	2.53	2.52	2.51	2.54	2.52	0.51
Ce	1.57	1.56	1.57	1.58	1.57	0.52
Pr	0.416	0.418	0.412	0.416	0.415	0.60
Nd	2.16	2.13	2.15	2.10	2.13	1.23
Sm	0.435	0.450	0.441	0.442	0.442	1.39
Eu	0.114	0.119	0.114	0.117	0.116	2.11
Gd	0.726	0.719	0.722	0.712	0.720	0.82
Tb	0.101	0.099	0.098	0.101	0.099	1.53
Dy	0.720	0.719	0.718	0.730	0.722	0.77
Ho	0.216	0.216	0.218	0.214	0.216	0.93
Er	0.669	0.672	0.666	0.665	0.668	0.47
Tm	0.091	0.089	0.090	0.090	0.090	0.90
Yb	0.619	0.614	0.599	0.601	0.608	1.60
Lu	0.108	0.106	0.105	0.107	0.106	1.21

^a Five measurements for each sample.

5 mL of 6 M HCl is sufficient for quantitative recovery, except for some heavy REEs. By using 15 mL of 6 M HCl, perfect recovery of all REEs was possible, except for La. The small amount of losses for La shown in Table VI is related to the concentration process and not to the elution process. In the case of 300 mg of complexing agents, the results of Table VII show that lighter REEs were quantitatively recovered by 20 mL of 6 M HCl whereas for quantitative recovery of all REEs 40 mL was necessary. Therefore, in preconcentration of real seawater, 50 mL of 6 M HCl was used for quantitative elution recovery.

Reproducibility of Preconcentrations of 1000- and 5000-mL Seawater Samples and Matrix Effect. The reliability of the novel preconcentration technique was tested by making two series of four replicate C₁₈ cartridge preconcentrations of 1000 and 5000 mL of the same seawater. A summary of the results along with relative standard deviations for all REEs is presented in Tables VIII and IX. The average relative standard deviations were calculated to be 2.72% and 1.04% for preconcentrations of 1000- and 5000-mL seawater samples, respectively. The relative better precision obtained for 5000 mL of preconcentrated seawater seems to be due to higher ion count rates by ICPMS measurements, as a result of the higher concentration of REEs in the final solutions. This level of precision is very close to that expected for an ICPMS instrumental determination alone without sample manipulation.

Generally, high-precision measurements of REEs are most desirable for researchers working in oceanography and geo-

Table X. Analytical Data (pg/mL) and Precision of Seawater Samples

element	S ₁		S ₂			
	C ₁₈ method mean	ref 20 mean	C ₁₈ method		solvent extraction	
			mean	% RSD	method ^a mean	ref 15 mean
La	3.49	3.41	2.52	1.04	2.55	2.64
Ce	5.03	4.95	1.57	0.82	1.61	2.52
Pr	0.731	0.693	0.417	1.20	0.414	0.42
Nd	3.26	3.25	2.10	2.06	2.14	2.16
Sm	0.670	0.700	0.444	3.77	0.441	0.390
Eu	0.180	0.178	0.118	4.18	0.116	0.117
Gd	0.985	0.979	0.717	4.78	0.710	0.675
Tb	0.17	0.164	0.100	4.16	0.101	0.097
Dy	0.976	0.996	0.726	1.79	0.718	
Ho	0.25	0.255	0.214	2.06	0.217	0.168
Er	0.730	0.714	0.666	2.25	0.659	
Tm	0.105	0.106	0.089	3.55	0.091	0.096
Yb	0.634	0.642	0.608	2.85	0.616	0.638
Lu	0.102	0.104	0.106	3.55	0.109	0.110

^a A 1000-mL aliquot of seawater was preconcentrated by using our previous method.²⁰

chemistry in the study of concentration-depth profiles,^{11,12,15} anomalies in REE distributions,¹⁶ and the tetrad effect.⁸

To test the matrix effect, in the above studies an internal standard, Cd, was added after preconcentrations of 1000 and 5000 mL to control the matrix effect. It was found that no significant matrix correction is necessary for the matrix effect, since almost all matrix elements have been passed to the drain while seawater was passed through the C₁₈ cartridge. The remaining negligible matrix elements could also be removed by washing the C₁₈ cartridge with 5 mL of 0.01 M HCl, as explained in the Experimental Section. With this process the final solutions do not have significant matrix elements and are suitable for ICPMS measurements.

Comparison of Results. Since there is no seawater standard with accurate analytical values for REEs, the accuracy of the technique was checked by comparison with the results obtained by ICPMS coupled with solvent extraction concentrations²⁰ and NAA coupled with Chelex 100 concentrations.¹⁵ It should be noted that the seawater analyzed by the NAA method is not exactly the same sample analyzed here, which was sampled from a similar depth at a different station in the Pacific Ocean at a different occasion. The results of ICPMS coupled with solvent extraction, results of NAA, and results and standard deviations of this study are listed in Table X. Comparison of the data obtained by the present method with those obtained by other methods indicates favorable agreement and lends strong support to the high reliability and validity of the technique developed here. Both ICPMS methods gave a value for Ce that was a bit lower than the value in ref 15, because of the different sampling position and possibly related to the oxidation reactivity of Ce³⁺ to Ce⁴⁺ in seawater.

CONCLUSIONS

Adsorption of a mixture of HDEHP and H₂MEHP onto C₁₈ cartridges provides a rapid, accurate, precise, reliable, and simple technique for the concentration and matrix isolation of trace REEs in seawater. The most attractive feature of the method is its high sample throughput (up to 50 mL/min), and preconcentration of eight 1-L samples in less than 30 min is feasible with a small amount of operator attention.

Preconcentration of trace REEs from 1000 and 5000 mL to 5 mL with matrix-free final solutions (200–1000-fold concentration factors) was obtained, and after determination with ICPMS no significant matrix effect or BaO⁺ interferences were evident, because the distribution coefficients of REEs are much higher than Ba and other matrix elements in seawater. A higher concentration factor is possible by preconcentration

of higher volumes of seawater or by reducing the volume of the final concentrate solutions.

No additional process or preconditioning of complexing agents adsorbed on C₁₈ is necessary before preconcentration of seawater. Since the preconcentration is performed in acidic solutions, no buffer is necessary for controlling the pH.

The mixture of HDEHP and H₂MEHP is a very strong complexing agent and can be used in acidic solution. This has several advantages over other complexing agents which can only be used at higher sample pHs in the presence of a buffer solution. The high distribution coefficients of REEs and their ability to be used in acidic solutions make them very strong complexing agents over the dissolved organic matter present in natural waters.

This approach allows quantitative elution of all REEs from C₁₈ containing 50 and 300 mg of complexing agents using 15 and 40 mL of 6 M HCl. Alternatively, reduction of volumes of eluting acid and direct introduction of concentrate after elution to ICPMS is possible by changing the eluting solvent. This can be done using octyl alcohol and then acid for the elution of REEs and complexing agents from C₁₈ and with collection in a separatory funnel in the same manner as back-extraction previously developed.²⁰

The preconcentration technique developed here can be used for any sample type that is high or very low in matrix, examples are brines, Dead Sea water, freshwater, and demineralized water. The method can be coupled with other instrumental measurement techniques such as ICPAES, IDMS, and NAA.

ACKNOWLEDGMENT

We express sincere thanks to Hiroshi Shimizu for his help and useful discussions during this work. We also express appreciation to Stephen B. Moore and S. K. Sahoo for their critical reading of this manuscript. This work was supported in part by a Grant-in-Aid for Fundamental Scientific Research from the Ministry of Education, Science, and Culture, Japan.

Registry No. H₂O, 7732-18-5; La, 7439-91-0; Ce, 7440-45-1; Pr, 7440-10-0; Nd, 7440-00-8; Sm, 7440-19-9; Eu, 7440-53-1; Gd, 7440-54-2; Tb, 7440-27-9; Dy, 7429-91-6; Ho, 7440-60-0; Er, 7440-52-0; Tm, 7440-30-4; Yb, 7440-64-4; Lu, 7439-94-3.

REFERENCES

- (1) Date, A. R.; Gray, A. L. *Spectrochim. Acta, Part B* 1985, 40B, 115–122.
- (2) Doherty, W.; Vander Voet, A. *Can. J. Spectrosc.* 1985, 30, 135–146.
- (3) Litcher, F. E.; Meier, A. L.; Crook, J. G. *Anal. Chem.* 1987, 59, 1150–1157.
- (4) Longrich, H. P.; Fryer, B. J.; Strong, D. F.; Kantipuly, C. J. *Spectrochim. Acta, Part B* 1987, 42B, 75–92.

- (5) Hirata, T.; Shimizu, H.; Akagi, T.; Masuda, A. *Anal. Sci.* **1988**, *4*, 637-643.
- (6) Jarvis, K. E. *J. Anal. At. Spectrosc.* **1989**, *4*, 563-570.
- (7) Doherty, W. *Spectrochim. Acta, Part B* **1989**, *44B*, 263-280.
- (8) Masuda, A.; Ikeuchi, Y. *Geochem. J.* **1979**, *13*, 19-22.
- (9) Piepgras, D. J.; Wasserburg, G. J.; Dasch, E. J. *Earth Planet. Sci. Lett.* **1979**, *45*, 223-236.
- (10) Piepgras, D. J.; Wasserburg, G. J. *Earth Planet. Sci. Lett.* **1980**, *50*, 128-138.
- (11) Elderfield, H.; Greaves, M. J. *Nature* **1982**, *296*, 214-219.
- (12) Glinkhamer, G.; Elderfield, H.; Hudson, A. *Nature* **1983**, *305*, 185-186.
- (13) Goldberg, E. D.; Koide, M.; Schmitt, R. A.; Smith, R. H. *J. Geophys. Res.* **1963**, *68*, 4209-4217.
- (14) Hodgahl, O. T.; Melson, S.; Bowen, V. T. In *Advances in Chemistry Series*; Baker, R. A., Ed.; American Chemical Society: Washington, DC, 1968; Vol. 73, pp 308-325.
- (15) De Baar, H. J. W.; Bacon, M. P.; Brewer, P. G. *Geochim. Cosmochim. Acta* **1985**, *49*, 1943-1959.
- (16) De Baar, H. J. W.; Brewer, P. G.; Bacon, M. P. *Geochim. Cosmochim. Acta* **1985**, *49*, 1961-1969.
- (17) Greenberg, R. R.; Kingston, H. M. *Anal. Chem.* **1983**, *55*, 1160-1165.
- (18) Riley, J. P.; Taylor, O. *Anal. Chim. Acta* **1968**, *40*, 479-485.
- (19) Kingston, H. M.; Barnes, I. L.; Brady, T. J.; Rains, T. C.; Champ, M. A. *Anal. Chem.* **1978**, *50*, 2084-2070.
- (20) Shabani, M. B.; Akagi, T.; Shimizu, H.; Masuda, A. *Anal. Chem.* **1990**, *62*, 2709-2714.
- (21) Shabani, M. B.; Masuda, A. *Anal. Chem.* **1991**, *63*, 2099-2105.
- (22) Sturgeon, R. E.; Berman, S. S.; Willie, S. N. *Talanta* **1982**, *29*, 167-171.
- (23) King, J. N.; Fritz, J. S. *Anal. Chem.* **1985**, *57*, 1016-1020.
- (24) Taguchi, S.; Yai, T.; Shimada, Y.; Goto, K.; Hara, M. *Talanta* **1983**, *30*, 169-172.
- (25) Van Grieken, R. E.; Vanderborcht, B. M. *Anal. Chem.* **1977**, *49*, 311-316.
- (26) Sugawara, K. F.; Weetall, H. H.; Schucker, G. D. *Anal. Chem.* **1974**, *46*, 489-492.
- (27) Moorhead, E. D.; Davis, P. H. *Anal. Chem.* **1974**, *46*, 1879-1880.
- (28) Jezorek, J. R.; Freiser, H. *Anal. Chem.* **1979**, *51*, 366-373.
- (29) Watanabe, H.; Goto, K.; Taguchi, S.; McLaren, J. W.; Berman, S. S.; Russell, D. S. *Anal. Chem.* **1981**, *53*, 738-739.
- (30) Sturgeon, R. E.; Berman, S. S.; Willie, S. N.; Desaulniers, J. A. H. *Anal. Chem.* **1981**, *53*, 2337-2340.
- (31) McLaren, J. W.; Mykityuk, A. P.; Willie, S. N.; Berman, S. S. *Anal. Chem.* **1985**, *57*, 2907-2911.
- (32) Grieser, M. D.; Pietrzyk, D. J. *Anal. Chem.* **1973**, *45*, 1348-1353.
- (33) Pietrzyk, E. J.; Chu, C. H. *Anal. Chem.* **1977**, *49*, 860-867.
- (34) Pietrzyk, E. J.; Kroeff, E. P.; Rotsch, T. D. *Anal. Chem.* **1978**, *50*, 497-502.
- (35) Aiken, G. R.; Thurman, E. M.; Malcolm, R. L.; Walton, H. F. *Anal. Chem.* **1979**, *51*, 1799-1803.
- (36) Mantoura, R. F. C.; Riley, J. P. *Anal. Chim. Acta* **1975**, *76*, 97-106.
- (37) Peppard, D. F.; Ferraco, J. R.; Mason, G. W. *J. Inorg. Nucl. Chem.* **1958**, *7*, 231-244.
- (38) Shabani, M. B.; Akagi, T.; Shimizu, H.; Masuda, A. Paper presented at the 38th Annual Meeting of the Japan Society for Analytical Chemistry, Oct 1989.

RECEIVED for review October 25, 1991. Accepted January 2, 1992.

Is Plasma Desorption Mass Spectrometry Useful for Small-Molecule Analysis? Fragmentations of the Natural α -Amino Acids

Stephane Bouchonnet, Jean-Pierre Denhez, Yannik Hoppilliard,* and Christine Mauriac

Laboratoire DCMR, Ecole Polytechnique, 91 128 Palaiseau Cedex, France

Plasma desorption mass spectrometry (PDMS) is well suited for studying small solid compounds. This technique combines together the advantages of the "soft" and "energetic" ionization methods: MH^+ ions as well as extensive intense fragmentations are observed. High-resolution measurements, metastable transitions, and labeled ions have made possible an identification of the ions formed. The fragmentation processes demonstrate several structures for the MH^+ ion depending on the protonation site of the molecule; in the case of multifunctional molecules, fragmentation can be induced by a protonation on each basic site. The formation of the immonium ion, the prominent fragment ion, involves a protonation at the α carboxylic group. This ion then decomposes following several reaction processes (as many as four successive fragmentations). Moreover PDMS fragmentations reflect the structures of neutral molecules making it possible to differentiate isomeric species.

INTRODUCTION

Plasma desorption (PD) mass spectrometry introduced by Macfarlane and Torgerson¹ uses the high-energy fragments emitted from the spontaneous fission of ^{252}Cf to desorb and ionize intact large or nonvolatile molecules for mass analysis. The secondary ions are mass-analyzed by their time of flight.

Until now, most of the molecules analyzed with this method have been peptides or proteins in the mass range 3000-30000 Da, but many pharmacological products, drugs, pesticides, and

their metabolites (MW < 1000 Da) are also nonvolatile and thermolabile molecules.

We have been interested to determine if PD mass spectrometry could be useful for analyzing small molecules and for obtaining structural information. We have chosen to study the 20 natural α -amino acids (AAs) because only the PD mass spectra of alanine (Ala) and arginine (Arg) have been explicitly reported.² In the past, free amino acids have been studied by a variety of different ionization methods such as electron impact (EI),³⁻⁶ chemical ionization (CI),⁷⁻¹⁵ field desorption (FD),¹⁶ secondary ion mass spectrometry (SIMS),¹⁷⁻¹⁹ fast atom bombardment (FAB) and CID-FAB,^{20,21} laser mass spectrometry (LMS),²²⁻²⁶ and atmospheric pressure ionization (API).²⁷ Except for CH_3^+ and CID-FAB, only partial data for the AAs are available.

We describe the positive PD mass spectra of the 20 natural AAs. We present results concerning the mode of fragmentation of the ions and structural information deduced from these fragmentations. We then discuss the use of this method to analyze small nonvolatile molecules in general, as compared with other ionization techniques.

EXPERIMENTAL PART

Materials. The 20 α -amino acids glycine (Gly), alanine (Ala), valine (Val), leucine (Leu), isoleucine (Ile), proline (Pro), phenylalanine (Phe), tyrosine (Tyr), tryptophan (Trp), histidine (His), serine (Ser), threonine (Thr), cysteine (Cys), methionine (Met), lysine (Lys), arginine (Arg), aspartic acid (Asp), glutamic acid (Glu), asparagine (Asn), and glutamine (Gln) have been purchased from Sigma Chimie S.a.r.l.

Table I. Plasma Desorption Mass Spectra (Relative Intensities in Italic Type Below m/z Values) of the 20 α -Amino Acids

name	MH	MH - NH ₃	MH - H ₂ O	I	MH - 63 ^a	MH - 64 ^b	I - H ₂	I - R ₁ H or - R ₂ H	I - R ₁ R ₂	74	MH - CO ₂	others								
Gly	76			30			28				32	45								
	60			100			18				6	23	14							
Ala	90			44			42													
	40			100			16			4										
Val	118			72	55		70	56			74	57	43	30	29	28				
	55			100	20		14	16		5	4	11	8	21	15	19				
Leu	132			86			84	70			88	44	43	30						
	87			100			16	18		10	5	55	55	33						
Ile	132			86	69		84	70	56		88	58	57	44	30					
	78			100	20		11	15	24	7	5	9	14	19	49					
Pro	116			70			68				72									
	77			100			21				8									
Phe	166			120	103							119	91	77	65	63	51	50		
	64			100	22					17	13	40	20	11	14	14	10			
Tyr	182	165		136	119						163	147	135	107	91	79	77	51	50	
	89	15		100	9					31	27	5	23	69	15	7	19	24	15	
Trp	205	188		159	142						158	132	130	117	103	77	46			
	17	12		28	5					22	21	20	100	17	5	20	13			
His	156			110							95	83	82	81	69					
	100			46							5	16	23	10	7					
Ser	106		88	60	43	42					62	86	70	44	30					
	100		4	93	30	37				7	11	13	7	37	33					
Thr	120		102	74	56						76	84	57	58						
	100		10	54	49					5	9	6	25	13						
Cys	122	105		76	59						88	87	75	69	46	45	44	43	42	
	100	9		72	23					22	12	13	18	15	15	30	78	39	28	
Met	150	133		104				56			102	75	69	61	45	44				
	88	10		44				69		20	12	10	10	100	29	12				
Lys	147	130		101	84			56			82	70	44	43	42	41	30			
	100	4		17	78			79		25	13	23	27	37	23	52	86			
Arg	175										131	130	100	87	70	73	60	59	44	43
	100									6	3	11	7	19	60	11	37	23	18	61
Asp	134			88		70	86				90	102	69	57	46	44	43	41		
	100			63		59	14			94	17	17	25	58	44	82	82	75		
Glu	148		130	102	85	84		56			104	113	73	71	69	57	55	43	41	
	100		6	74	25	59		75		38	15	18	31	25	32	88	75	98	78	
Asn	133	116		87	70						89	88	60	44	43					
	100	4		45	34					31	8	4	11	35	27					
Gln	147	130		101	84			56			103	102	86	71	69	57	55			
	100	41		20	59			31		13	5	10	13	17	20	34	37			

^a MH - 63 corresponds either to [I - NH₃] or to [MH - NH₃ - CH₂O₂]⁺. ^b MH - 64 corresponds either to [I - H₂O] or to [MH - H₂O - CH₂O₂]⁺.

Sample Preparation. The aqueous solutions of AAs are electrosprayed onto a thin aluminized Mylar foil stretched tight on a sample-holder, using the electrospray sample preparation method.²⁸

The electrosprayed solutions of AAs dissolved in ultrapure water lead to positive PD mass spectra characterized by peaks corresponding to ions of various origins: protons (H⁺), alkali-metal cations (Na⁺ and K⁺), protonated and cationized monomers (MH⁺, MNa⁺, MK⁺), polycationized molecules like [M - H + 2Na]⁺, [M - H + Na + K]⁺, ..., complexed dimers [MHM]⁺, [MNaM]⁺, ..., polymers, and fragment ions.

In order to simplify the spectra and to increase the relative intensities of the peaks corresponding to the amino acids, we have desalted the sample solutions. Under these conditions, K⁺ and MK⁺ totally disappear and Na⁺ and MNa⁺ considerably decrease (except in the case of the dicarboxylic AAs). A 100- μ L aliquot of an aqueous 10⁻² M solution of amino acid is mixed with 100 μ L of 2-propanol. This solution is purified by exchanging alkali-metal cations with a cation-exchange resin in the acidic form, amberlyst-15; 30 μ L of the solution was sprayed.

PD Mass Spectra. The PD mass spectra have been recorded on the time of flight DEPIL-X system constructed at the IPN (Institut de Physique Nucléaire) of Orsay (France), fitted with a ²⁵²Cf source and an electrostatic mirror, designed with axial symmetry. The activity of the source is 10 μ Ci. The acceleration distance is 2 mm, and the distance between the sample and the detector is 710 mm. A voltage V₀ of 10 kV is applied on the sample. Each spectrum is acquired for a 600-s period. The electrostatic mirror can be operated in two modes: to provide velocity focusing to achieve high resolution ($M/\Delta M = 5000$) or as a means for metastable ion analysis.²⁹

Direct Spectra. We will call a "direct spectrum" a spectrum obtained without the mirror. Each direct spectrum is presented as a percentage of the base peak. Each peak intensity is determined by summing the counts from each channel that includes the events for a particular ion. No background subtraction was done. Spectra were calculated using H⁺ = 1.007277 units and Na⁺ = 22.989222 units as mass calibration ions.

The PD mass spectra recorded after sample purification are given as a function of the base peak in Table I. All spectra exhibit peaks at m/z 45, 44, 43, 42, 41, 30, 29, 28, 27, and 18. Intensities of ions below m/z 50 are given only when they are of unusual importance. The direct AA spectra exhibit peaks corresponding to intense MH⁺ ions (most of the time the base peak) as well as abundant fragment ions.

Metastable Ion Studies. The analysis method for metastable ion studies (P⁺ decomposing in the free field region to A⁺ + N) has been extensively described by Della-Negra and Le Beyec.²⁹

When the mirror is active (V = 10.9 kV), it is possible for a decay occurring in flight to register one event due to N in a "neutral spectrum" and one event due to the complementary charged fragment A⁺ in a "reflex spectrum". Many peaks corresponding to metastable ions can exist in the neutral spectrum. For each of them, there is a defined time window. For each time window, a "coincidence spectrum" is related to a specific metastable ion and the comparison between the total ion reflex spectrum and each coincidence spectrum permits a dissection of the parent-fragment relationships to define the connections between the parent ion and sequences fragment ion decays that occur.

Regarding the decomposition pathways, three different cases have been described by Chait and Field.³⁰

(1) The decomposition $P^+ \rightarrow A^+ + N$ occurs within the sample during the passage of a fission fragment or slightly after ($10^{-15} < t < 10^{-9}$ s); then the ionized fragment A^+ will appear as very sharp lines at time t_A in the reflex spectrum.

(2) The decay takes place during the acceleration step for which the time scale t_{acc} depends on the mass and on the acceleration voltage (but typically $10^{-8} < t_{acc} < 10^{-7}$ s). The ion A^+ acquires a lower kinetic energy, which then contributes to a tail and to a background appearing at times larger than t_A .

(3) The metastable ions are those decomposing in the free field region and having a lifetime greater than t_{acc} .

In unimolecular dissociations, the RRKM theory³¹ states that the rate constant k of each possible dissociation of an ion depends only on its internal energy. For the reaction $P^+ \rightarrow A^+ + N$, the classical value of k is given by the equation $k = \nu [(\epsilon - \epsilon^0)^{-1}] / \epsilon$ where ϵ = the P^+ internal energy, ϵ^0 = the critical energy for the reaction, s = the effective number of oscillators, and ν = the frequency factor.

Rearrangement reactions generally have low critical energies and low frequency factors while simple cleavages often have higher critical energies and higher frequency factors. Ions' lifetimes are inversely related to the rates of dissociation. Consequently, an ion that can dissociate either via rearrangement(s) or via simple cleavage reaction(s) dissociates via the rearrangement process(es) at low internal energy (ions having long lifetimes), whereas at high internal energies (ions having short lifetimes), simple cleavages tend to dominate.³²

In summary, the direct spectrum reflects the events occurring in a time shorter than 10^{-9} s (the most energetic processes), while the metastable transitions give the fragmentations corresponding to ions of low internal energy (long lifetime).

Note that the ions in direct PD mass spectra are extracted and accelerated faster than the ions formed in an EI source of a sector mass spectrometer (which are extracted after a residence time roughly equal to 10^{-6} s). Consequently, the direct PD mass spectrum may reflect more rapid fragmentations than those observed in an EI spectrum.

The observed metastable transitions are given in Table II. It must be borne in mind that while metastable transitions may give information on the formation of daughter ions, the same fragment ion may be also generated by other competitive, faster fragmentation(s) with no metastable transition component.

High-Resolution Spectra. To obtain high-resolution mass spectra, the electrostatic mirror works in the reflecting mode: at the entrance of the mirror two grids are used respectively set to $V_1 = 0$ and $V_2 = 2/3 V_0$ while a maximum potential of 12.8 kV is applied at the end of the mirror;³³ the latter must be greater than V_0 applied to the accelerating grid. Typically, $V_0 = 10$ kV is used.

High-resolution measurements have been performed to identify the different ions of protonated valine ($ValH^+$) and valine- d_3 ($Vald_3H^+$) (Table III) and of protonated threonine ($ThrH^+$) (Table IV). The mass accuracy is better than 0.02%.

Desorption Mechanism. The desorption (sputtering) and ionization mechanism (DI) of the molecular ions is "not at all well understood".³⁴ Some years ago, several hypotheses were proposed, reviewed by Pachuda and Cooks.^{35,36} The "ion track model" proposed by Sundqvist et al.³⁷⁻³⁹ centers around electronic rather than thermal effects, involving multiple simultaneous bond breakage events.

Interpretation. In the present work, we intend to investigate the formation of the most characteristic fragment ions observed in the direct PD mass spectra. The fragmentation processes are borne out by comparative criteria, results of the literature, exact mass determinations, deuterium-labeling results, metastable transitions of low internal energy ions, and classical rules of fragmentation in chemical ionization as well as in electron impact. In accordance with the Sundqvist's hypothesis to interpret the intense fragment ions, we favor the mechanisms giving rise to these ions in a minimum of steps. This is in agreement with rapid reactions occurring in the source.

IDENTIFICATION OF THE MAIN FRAGMENTS OF $ValH^+$ AND $ThrH^+$

The main fragmentations of the amino acids are presented for two examples: valine and threonine.

Table II. Metastable Transitions

compd	decomp of ions (units)			
Gly	76 (MH^+)	\rightarrow 30 (I)		
Val	118 (MH^+)	\rightarrow 72 (I)	\rightarrow 55 (I - NH_3)	\rightarrow 29 (I - NH_3 - C_2H_5)
	70 (I - H_2)	\rightarrow 43 (I - H_2 - HCN)		
	56 (I - CH_4)	\rightarrow 28 (I - CH_4 - C_2H_5)		
Leu	132 (MH^+)	\rightarrow 86 (I)	\rightarrow 44 (I - C_3H_5)	
		86 (I)	\rightarrow 30 (I - C_4H_5)	
	88 (MH^+ - CO_2)	\rightarrow 30 (H_2C^+ - NH_2) ⁺		
Ile	132 (MH^+)	\rightarrow 86 (I)	\rightarrow 44 (I - C_3H_5)	
		86 (I)	\rightarrow 30 (I - C_4H_5)	
		86 (I)	\rightarrow 69 (I - NH_3)	\rightarrow 41
Phe	166 (MH^+)	\rightarrow 120 (I)	\rightarrow 103 (I - NH_3)	\rightarrow 79
			103 (I - NH_3)	\rightarrow 77 \rightarrow 51
	91	\rightarrow 65		
Tyr	182 (MH^+)	\rightarrow 165 (MH^+ - NH_3)	\rightarrow 119 (165 - CH_2O_2)	
	182 (MH^+)	\rightarrow 136 (I)	\rightarrow 119 (I - NH_3)	\rightarrow 91 (I - NH_3 - CO)
		136 (I)	\rightarrow 91 (I - NH_3 - CO)	
	107 (Ar - CH_2^+)	\rightarrow 79 and 77		
Trp	205 (MH^+)	\rightarrow 188 (MH^+ - NH_3)		
	159 (I)	\rightarrow 142 (I - NH_3)		
	159 (I)	\rightarrow 132 (I - HCN)		
	159 (I)	\rightarrow 130 (Ar - CH_2^+)	\rightarrow 103	\rightarrow 77 \rightarrow 51
His	156 (MH^+)	\rightarrow 110 (I)	\rightarrow 83	\rightarrow 56 and 42
	156 (MH^+)	\rightarrow 95		
	81	\rightarrow 54 and 57		
	69	\rightarrow 41		
Ser	106 (MH^+)	\rightarrow 88 (MH^+ - H_2O)	\rightarrow 70 (MH^+ - 2 H_2O)	
	106 (MH^+)	\rightarrow 60 (I)	\rightarrow 30 (I - CH_2O)	
		60 (I)	\rightarrow 42 (I - H_2O)	
Thr	120 (MH^+)	\rightarrow 102 (MH^+ - H_2O)	\rightarrow 84 (MH^+ - 2 H_2O)	\rightarrow 57
		102 (MH^+ - H_2O)	\rightarrow 84 (MH^+ - 2 H_2O)	\rightarrow 56 \rightarrow 28
		102 (MH^+ - H_2O)	\rightarrow 56 (102 - 46)	
	120 (MH^+)	\rightarrow 74 (I)	\rightarrow 56 (I - H_2O)	
		74 (I)	\rightarrow 58 (I - CH_4)	\rightarrow 41 and 29
	76 (MH^+ - CO_2)	\rightarrow 58		
Cys	122 (MH^+)	\rightarrow 105 (MH^+ - NH_3)	\rightarrow 87 (105 - H_2O)	\rightarrow 59 (87 - CO)
	122 (MH^+)	\rightarrow 76 (I)	\rightarrow 59 (I - NH_3)	
	88 (MH^+ - H_2S)	\rightarrow 44 (88 - CO_2)	\rightarrow 18 (NH_4^+)	
	88 (MH^+ - H_2S)	\rightarrow 45		
Met	150 (MH^+)	\rightarrow 133 (MH^+ - NH_3)	\rightarrow 61 (H_3C - $SCCH_2$)	
	150 (MH^+)	\rightarrow 104 (I)	\rightarrow 56 (I - CH_3SH)	\rightarrow 28
Lys	147 (MH^+)	\rightarrow 130 (MH^+ - NH_3)		
	147 (MH^+)	\rightarrow 84 (I - NH_3)	\rightarrow 56 (I - NH_3 - C_2H_5)	\rightarrow 28
		84 (I - NH_3)	\rightarrow 30 (H_2C^+ - NH_2)	
	101 (I)	\rightarrow 84 (I - NH_3)		
Arg	175 (MH^+)	\rightarrow 130 (MH^+ - 45)	\rightarrow 70	\rightarrow 43 and 28
		130 (MH^+ - 45)	\rightarrow 87	\rightarrow 59 and 44
	175 (MH^+)	\rightarrow 60	\rightarrow 43 and 18	
Asp	134 (MH^+)	\rightarrow 88 (I)	\rightarrow 70 (I - H_2O)	\rightarrow 43 and 28
		88 (I)	\rightarrow 45	
	74	\rightarrow 46		
	57	\rightarrow 41		
Glu	148 (MH^+)	\rightarrow 130 (MH^+ - H_2O)	\rightarrow 85	\rightarrow 42 and 55
	148 (MH^+)	\rightarrow 130 (MH^+ - H_2O)	\rightarrow 84 (130 - CH_2O_2)	
	148 (MH^+)	\rightarrow 84	\rightarrow 56 and 41	
	148 (MH^+)	\rightarrow 102 (I)	\rightarrow 84 (I - H_2O)	
		102 (I)	\rightarrow 56 (I - CH_2O_2)	\rightarrow 28
	113 (MH^+ - H_2O - NH_3)	\rightarrow 71		

Fragmentation of Protonated Valine (Figure 1). The fragmentation processes of valine are derived from comparison of the normal valine with the valine- d_3 spectra. The composition of each ion was obtained from high-resolution (HR) measurements (Table III). Metastable decompositions are reported in Table II.

Table III. Exact Masses of Valine and Valine- d_8 Ions

Val	MH ⁺	MH ⁺ - CO ₂	I	I - H ₂	I - CH ₃ [*]	I - CH ₄	I - NH ₃	I - H ₂ - HCN	I - NH ₃ - C ₂ H ₂	I - CH ₄ - C ₂ H ₄
<i>m/z</i> exp	118.09	74.09	72.08	70.05	57.05	56.04	55.05	43.05	29.03	28.02
<i>m/z</i> calc	118.086	74.096	72.081	70.065	57.057	56.049	55.054	43.054	29.039	28.018
formula	C ₅ H ₁₂ NO ₂	C ₄ H ₁₂ N	C ₄ H ₁₀ N	C ₄ H ₈ N	C ₃ H ₇ N	C ₃ H ₆ N	C ₄ H ₇	C ₃ H ₇	C ₂ H ₅	CH ₂ N

Val- d_8	MH ⁺	MH ⁺ - CO ₂	I	I - D ₂	I - CD ₃ [*]	I - CD ₄	I - NH ₂ D	I - D ₂ - DCN	I - NH ₂ D - C ₂ D ₂	I - CD ₄ - C ₂ HD ₃
<i>m/z</i> exp	126.14	82.14	80.13	76.09	62.09	60.07	62.09	48.08	34.07	29.03
<i>m/z</i> calc	126.136	82.147	80.131	76.103	62.089	60.075	62.098	48.085	34.07	29.024
formula	C ₅ H ₄ D ₈ NO ₂	C ₄ H ₄ D ₈ N	C ₄ H ₂ D ₈ N	C ₄ H ₂ D ₆ N	C ₃ H ₂ D ₅ N	C ₃ H ₂ D ₄ N	C ₄ D ₇	C ₃ H ₂ D ₅	C ₂ D ₅	CHDN

Table IV. Exact Masses of Threonine

Thr	MH ⁺	MH ⁺ - H ₂ O	MH ⁺ - 2H ₂ O	MH ⁺ - CO ₂	MH ⁺ - CO ₂ - H ₂ O	MH ⁺ - RH	I	I - H ₂ O	I - OH [*]	I - H ₂ O - C ₂ H ₄
<i>m/z</i> exp	120.07	102.06	84.06	76.07	58.06	74.02	74.06	56.06	57.05	28.02
<i>m/z</i> calc	120.066	102.055	84.049	76.076	58.065	74.024	74.060	56.049	57.057	28.018
formula	C ₄ H ₁₀ NO ₃	C ₄ H ₈ NO ₂	C ₃ H ₆ NO	C ₃ H ₁₀ NO	C ₃ H ₈ N	C ₂ H ₄ NO ₂	C ₃ H ₆ NO	C ₃ H ₆ N	C ₃ H ₇ N	CH ₂ N

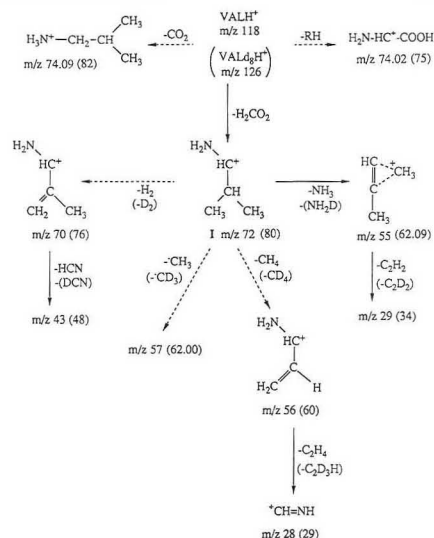
ValH⁺ decomposes to give the *m/z* 72.08 ion (100%) identified as the immonium ion I = [ValH - CH₂O]⁺ and two small ions identified by HR measurements *m/z* 74.09 (4%), [C₄H₁₂N]⁺ (corresponding to the loss of CO₂), and *m/z* 74.00 (5%), H₂N - CH⁺ - COOH (corresponding to the loss of the lateral chain R with a hydrogen atom). These fragment ions are shifted to *m/z* 80 for I, *m/z* 82 for [C₄H₂D₈N]⁺, and *m/z* 75 for the loss of RH in the Val- d_8 spectrum. A metastable transition is associated only with the formation of the immonium ion. As the protonated valine eliminates predominantly CH₂O₂, it can be assumed that the fragmenting molecular ions are principally protonated on the carboxylic function.

Four daughter ions identified by HR measurements arise from the immonium ion (a metastable transition is associated only with the formation of *m/z* 55 from I): (1) *m/z* 70.05 [C₄H₉N]⁺ (18%) shifted to *m/z* 76 [C₄H₂D₈N]⁺ in the Val- d_8 spectrum is obtained by loss of H₂ (α,β elimination) to give the conjugated H₂N - CH⁺ - C(CH₃)=CH₂ cation; (2) *m/z* 56.04 [C₃H₆N]⁺ (16%), shifted to *m/z* 60 [C₃H₂D₅N]⁺ in the Val- d_8 spectrum, corresponds to an α,β loss of CH₄, generating the conjugated carbocation H₂N - CH⁺ - CH=CH₂; (3) *m/z* 55.05 [C₄H₇]⁺ (20%) is obtained by elimination of the α -amino group with a hydrogen atom of the chain; no randomization of the hydrogens occurs prior to fragmentation as the Val- d_8 spectrum exhibits only a peak at *m/z* 62 [C₄D₇]⁺ corresponding to the loss of NH₂D; (4) *m/z* 57.05 [C₃H₇N]⁺ (11%) corresponds to a methyl radical loss.

Subsequent fragmentations of the I daughter ions occur. The [C₄H₉N]⁺ ion (*m/z* 70) decomposes in the field-free region (FFR) to give *m/z* 43. This ion is shifted to *m/z* 48 proceeding from the [C₄H₂D₈N]⁺ ion (*m/z* 76). This comparison implies an HCN elimination. Similarly, the [C₃H₆N]⁺ ion (*m/z* 56) decomposes in the FFR to give the *m/z* 28 ion. The shift to *m/z* 29 from [C₃D₄H₂N]⁺ is consistent with the formation of [CDHN]⁺. The loss of acetylene from [C₄H₇]⁺ (*m/z* 55) or that of DCCD from [C₄D₇]⁺ is observed. The formation of *m/z* 30, H₂N - CH₂, might involve several precursors.

The I formation is in competition with the loss of CO₂ and the formation of H₂N - CH⁺ - COOH, suggesting initial protonation on sites other than COOH. The formation of H₂N - CH⁺ - COOH would correspond formally to the loss of the side chain with a hydrogen of the protonated α -amino group.

Fragmentation of Protonated Threonine (Figure 2). The ions observed on the Thr direct PD mass spectrum have been identified by HR measurements. The exact masses of

Figure 1. Fragmentation modes of ValH⁺ and Val- d_8 H⁺.

the different ions are given in Table IV.

Four ions may correspond to an initial fragmentation of ThrH⁺: *m/z* 102.06 (10%), 76.07 (9%), 74.06 (54%), and 74.02 (5%). The most prominent fragment ion, *m/z* 74.06 (loss of 46 units), is attributed, as previously, to the formation of the immonium ion. The *m/z* 74.02 ion, which was also observed in the Val spectrum, corresponds to the H₂N - CH⁺ - COOH ion. The *m/z* 76 ion (loss of 44 units) is identified again as the loss of CO₂. Metastable transitions are observed for *m/z* 120 (ThrH⁺), giving *m/z* 102 (ThrH⁺ - H₂O) and *m/z* 74 attributed to ThrH⁺ - CH₂O₂ = I.

Concerning *m/z* 102 (loss of 18 units), its exact mass is in agreement with a loss of water. This water elimination has been also observed in CH₂-CI¹⁰ and in CID-FAB²¹ of AAs including a hydroxyl group on the lateral chain. This loss involves an initial protonation on the oxygen atom of the

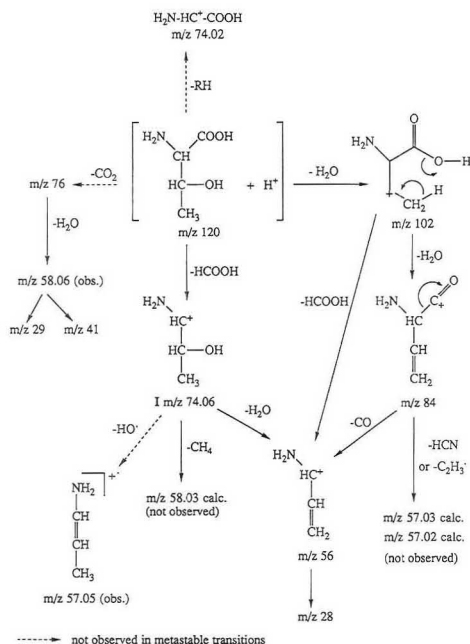


Figure 2. Fragmentation modes of ThrH⁺.

hydroxyl function of the lateral chain. Each primary fragment ion gives subsequent cleavages. The $[\text{MH} - \text{H}_2\text{O}]^+$ ion may decompose in two ways to form m/z 56 $[\text{C}_3\text{H}_6\text{N}]^+$. The first loss of water from MH^+ (m/z 102) is followed by another loss of water (mechanism 1) involving a six-center proton transfer from the methyl group to the remaining hydroxyl function to give m/z 84, eliminating in turn CO to generate $\text{H}_2\text{N}-\text{CH}^+-\text{CH}=\text{CH}_2$ $[\text{C}_3\text{H}_6\text{N}]^+$ (m/z 56). The first loss of water is also followed by an α,β elimination of formic acid leading to $\text{HN}=\text{CH}-\text{CH}^+-\text{CH}_3$ $[\text{C}_3\text{H}_6\text{N}]^+$ (m/z 56) (mechanism 2). Metastable transitions are observed for m/z 102 $\rightarrow m/z$ 84 and m/z 84 $\rightarrow m/z$ 56 and for the direct elimination m/z 102 $\rightarrow m/z$ 56 as well. Ab initio calculations at the MP4/6-31C* + ZPVE level⁴⁰ give an energy difference of 200 kJ between the two $[\text{C}_3\text{H}_6\text{N}]^+$ structures in favor of $\text{H}_2\text{N}-\text{CH}^+-\text{CH}_2$. Both metastable and thermodynamical results give mechanism 1 as the lower energy process.

As previously observed with I(Val), I(Thr) eliminates neutral molecules involving the substituents of the chain, ammonia or radicals. A metastable transition is associated with this water elimination. I(Thr) eliminates a molecule of water and gives the $\text{H}_2\text{N}-\text{CH}^+-\text{CH}=\text{CH}_2$ ion (m/z 56) as discussed above. A loss of H_2 is of very low intensity. The presence of a metastable transition associated with I(Thr) losing 16 units has a subtlety revealed by the HR measurement. The loss of methane would lead to $[\text{C}_3\text{H}_5\text{NO}]^+$ (m/z 58.03) in disagreement with the exact m/z 58.06 found. This latter is attributed to $[\text{C}_3\text{H}_5\text{N}]^+$, corresponding to a water loss from m/z 76 $[\text{MH}-\text{CO}_2]^+$. No ammonia loss is observed from I(Thr). The methyl radical loss observed in the Val spectrum has no correspondence in the Thr spectrum. In counterpart, high-resolution measurements give an ion at m/z 57.05 and a metastable transition corresponding to m/z 84 $[\text{MH}-2\text{H}_2\text{O}]^+$ losing 27 units is observed. The m/z 57 ion may have several origins: fragmentation of $[\text{MH}-2\text{H}_2\text{O}]^+$ either to $\text{HCN} + [\text{C}_3\text{H}_5\text{O}]^+$ (calc m/z 57.033) or to the C_2H_5 radical + $[\text{C}_3\text{H}_5\text{NO}]^{++}$ (calc m/z 57.021); fragmentation of the im-

monium ion either to $\text{NH}_3 + [\text{C}_3\text{H}_6\text{O}]^+$ (calc m/z 57.033) or to $\text{OH} \cdot + [\text{C}_3\text{H}_7\text{N}]^{++}$ (calc m/z 57.057). The formula in agreement with the HR measurements is the radical cation $[\text{C}_3\text{H}_7\text{N}]^{+ \cdot}$. The ions m/z 57 obtained by loss of 27 units from m/z 84 are not observed in the direct spectrum.

Figure 3 shows a comparison between the direct spectrum and the neutral spectrum of the threonine prominent ions, namely m/z 120 (ThrH^+), m/z 102 ($\text{ThrH}^+ - \text{H}_2\text{O}$), and m/z 74 ($\text{I}(\text{Thr})$). In a direct spectrum, which is obtained when the mirror is not active, not only the ions but also the neutrals resulting from “in-flight” fragmenting ions of low internal energy are observed. In a neutral spectrum, which is obtained when the mirror is in operation, only the neutrals are registered. Figure 4 gives the total reflex ion spectrum of threonine and the coincidence spectra with time windows on masses 120, 102, and 74 set on the neutral spectrum. All the ions which are deflected by the mirror are detected to give the total reflex ion spectrum. The reflex spectrum and each coincidence spectrum look very much the same except for the metastable peaks which are much more visible. From the construction parameters of the electrostatic mirror (distances, voltage, ...) it is possible to identify the decays.²⁹

In summary, the similarities between the fragmentation modes of ValH⁺ and ThrH⁺ relate to the formation and fragmentation of the immonium ion, the loss of CO₂, and the formation of the *m/z* 74 ion. A new pathway for MH⁺ fragmentation is observed in the case of ThrH⁺ involving a protonation on the linear chain.

The mechanisms displayed for these amino acids may be extended to interpret the spectra of the other amino acids.

INTERPRETATION OF AA PD MASS SPECTRA

The abundance of the MH^+ ions is 50–100% (except for Trp). MH^+ ions decompose with several processes in competition. Results concerning the initial protonation site (the carboxylic function, the linear chain, or the α -amino group) are presented. Concerning the loss of CO_2 , the initial ionization site is not clearly defined.

A. Fragmentations Deduced from Protonation on the Carboxylic Function. Formation of the Immonium Ion

I. The immonium ion $I = [H_2N-CHR]^+$ (loss of 46 units from MH^+) is observed in all PD mass spectra except arginine. This ion is usually the prominent fragment ion. A metastable transition associated with the loss of $[CH_2O_2]$ is observed in most cases. The protonated amino acids are well-known to lose formally $[CH_2O_2]$.^{2,7-15,17-21} Several mechanisms have been proposed to explain the loss of the carboxylic function from protonated AAs. Meot-Ner and Field⁸ have proposed direct loss of formic acid from a cyclic intermediate, based on studies using butane-Cl. Tsang and Harrison¹⁰ have presented convincing arguments for a concerted two-step process in methane-Cl: the formal loss of formic acid from the protonated AAs would be, to a large extent, the sequential loss of H_2O and CO. The water elimination is triggered by the transfer of a hydrogen atom of the protonated α -amino function to the OH of the α -carboxylic group. A simple bond-breaking mechanism has been assumed for the SIMS spectra of AAs¹⁷ in which the immonium ion arises by loss of $COOH^+$ from the M^{++} parent molecule (i.e. $M - 45$), corresponding to an α rupture in conventional EI spectra.

The lack of random protonation in deuterated acids demonstrated in PDMS,⁴¹ SIMS,⁴² and laser desorption²⁶ implies that intermolecular proton transfer is a likely mechanism for all high-energy solid-state mass spectral techniques. Parker and Hercules²⁶ have proposed in LMS a fragmentation sequence suggested by Tsang and Harrison but after an initial protonation on the hydroxyl group of the carboxylic function. The proposition of Parker and Hercules is in agreement with our results.

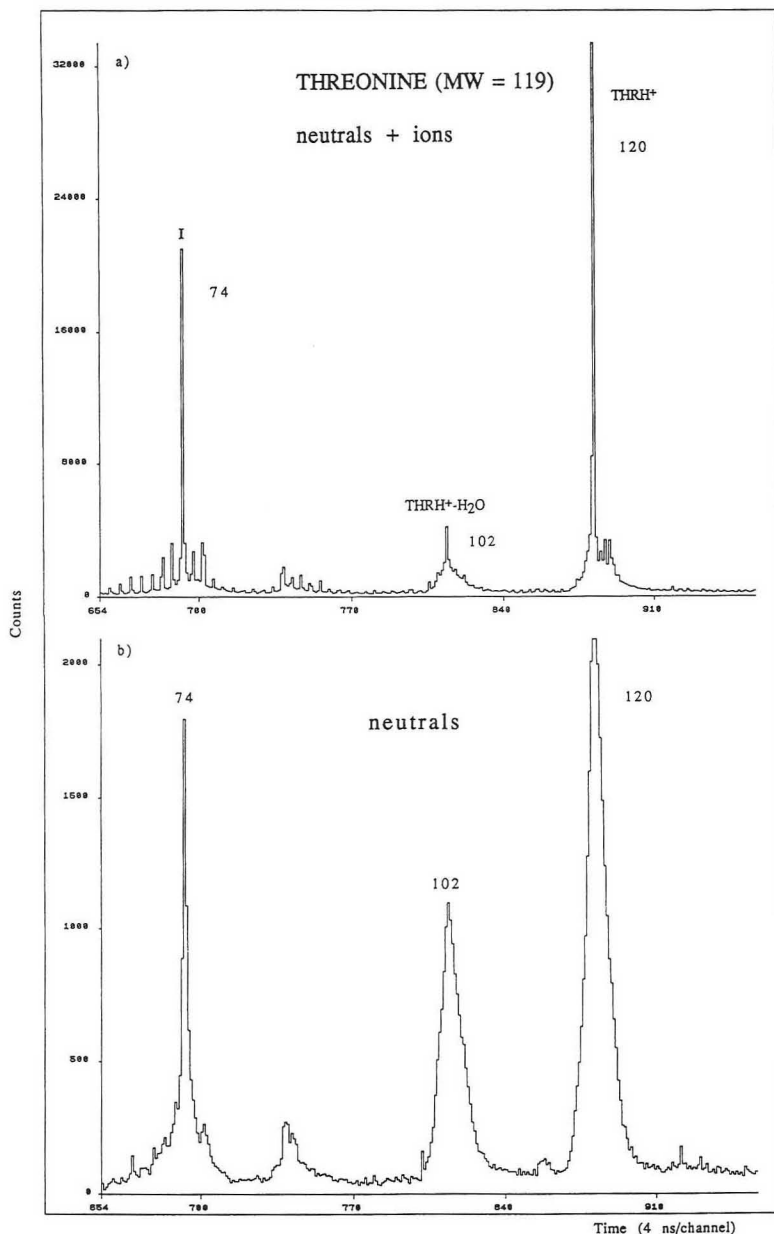


Figure 3. (a) Direct spectrum of the threonine prominent ions. Ions and neutrals resulting from "in-flight" fragmentations are detected when the mirror is not in operation. (b) Neutrals detected only when the mirror is active. The counting time is the same as in (a).

Fragmentation of the Immonium Ion. The immonium ion fragmentations observed for Val and Thr have been investigated in the other AA spectra.

(1) α,β Neutral Molecule Eliminations. α,β eliminations leading to a conjugated carbocation are observed in several AA spectra as an important fragmentation mode of I. If the

side chain is long enough, the saturated molecules eliminated from I are H₂, R₁H (R₁ = CH₃, OH), R₂H (R₂ = CH₃, SCH₃, (CH₂)₂NH₂, COOH), or R₁R₂ (R₁ = CH₃, R₂ = CH₃), depending on the linear-chain constitution (Figure 5, Table V).

The water loss from I(Asp) can also be explained as an α,β elimination involving the OH of the β -carboxylic function (R₂

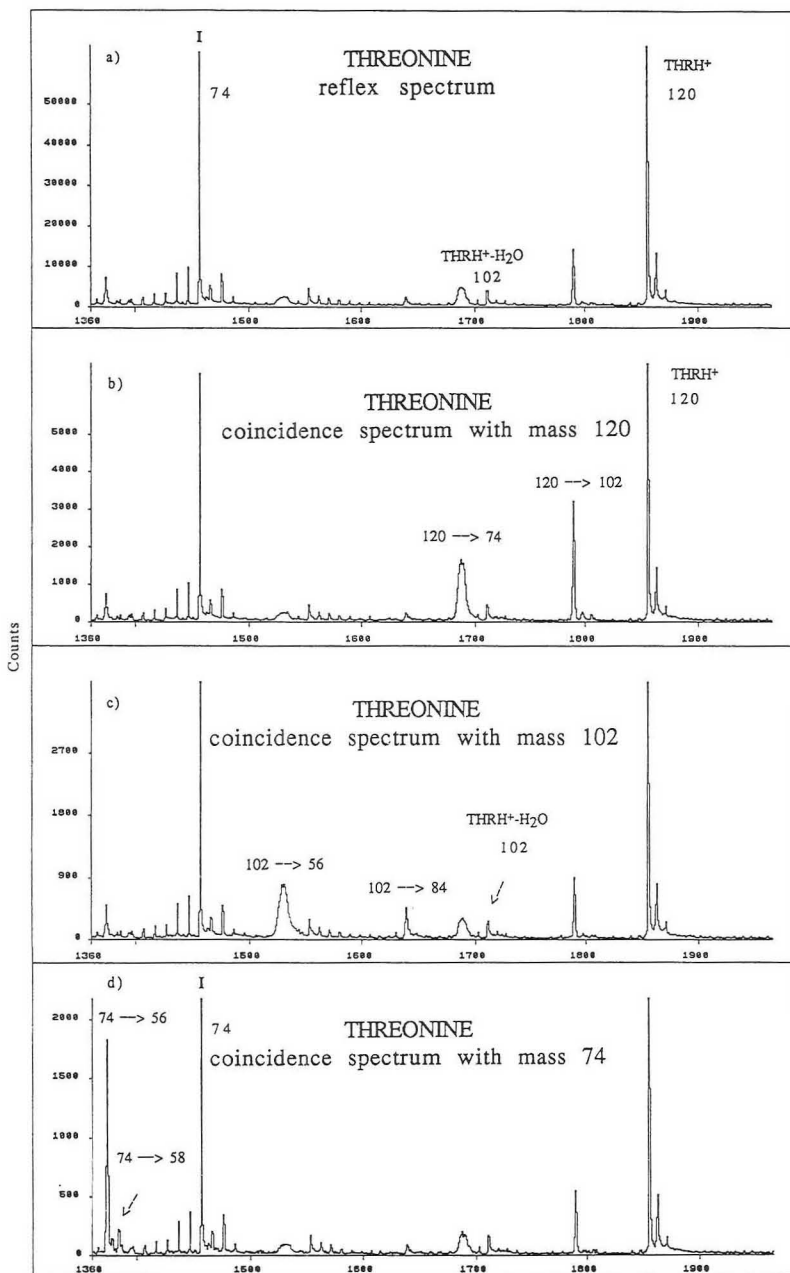


Figure 4. (a) Total reflex ion spectrum of threonine with the mirror active. (b) Coincidence spectrum with the mass window on mass 120 in the neutral spectrum showing "in-flight" fragmentations of ThrH⁺. (c) Coincidence spectrum with a time window on mass 102 (ThrH⁺ - H₂O). (d) Coincidence spectrum with mass 74 showing also "in-flight" fragmentations of the immonium ion.

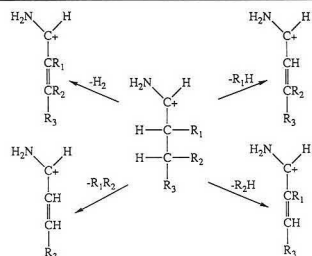
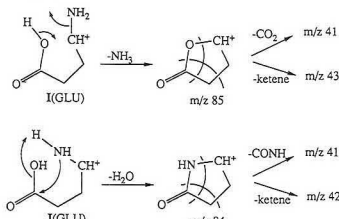
= OH) and a hydrogen atom of the α -carbon atom. The neutral molecule loss seems particularly significant for the neutral amino acids.

(2) *Loss of Ammonia Leading to the [MH - 63]⁺ Ion*. The loss of ammonia is favored by the electron-donating substituents of the chain, leading to a cyclic ion.⁷ I(Ser), I(Glu),

and I(Cys) give respectively m/z 43 (30%), m/z 85 (25%), and m/z 59 (23%). This reaction is in competition with loss of another small molecule favored by the electron-donating effect of the amino group; either loss of water from I(Ser) and I(Glu) (Figure 6), m/z 42 (32%) and m/z 84 (59%), respectively, or loss of SH₂ from I(Cys), m/z 42 (28%).

Table V. Ions Formed from I by α,β Elimination as a Function of the Linear-Chain Substituents

AA	R ₁	R ₂	R ₃	-H ₂	-R ₁ H	-R ₂ H	-R ₁ R ₂
Val	CH ₃	H	H	70	56		
Leu	H	CH ₃	CH ₃	84		70	
Ile	CH ₃	CH ₃	H	84	70		56
Pro	H	H	ring	68		70	
Thr	OH	H	H		56		
Met	H	SCH ₃	H			56	
Lys	H	(CH ₂) ₂ NH ₂	H			56	
Glu	H	COOH	H			56	

Figure 5. α,β elimination from the immonium ion.Figure 6. Competitive eliminations of NH_3 and H_2O from I(Glu).

A similar behavior occurs with the AAs that include an NH_2 group in the lateral chain: the mutual ammonia elimination enhances the $[\text{I} - \text{NH}_3]^+$ intensity, especially in the case of I(Lys) (m/z 84, 78%). In $\text{CH}_3\text{-Cl}$ experiments, m/z 84 has also been explained, using $\alpha^{15}\text{NH}_2$ lysine and $\epsilon^{15}\text{NH}_2$ lysine, in terms of two competitive mechanisms, in two steps, with mutual assistance of the second amino group during the NH_3 elimination. Both processes give rise to the stable pyrrolinium ion.⁷ In agreement with Sundqvist's hypothesis³⁷⁻³⁹ suggesting multiple simultaneous bond breakage events, the mechanism given in Figure 7, which is geometrically favorable, could be proposed to be in competition with pyrrolinium ion formation. This mechanism could have the advantage of explaining the formation of the product ion m/z 56 by simple heterolytic bond cleavage, suggested by the metastable sequential decay path m/z 84 \rightarrow 56.

In the case of the aromatic and of the α -trisubstituted neutral AA immonium ions, the delocalization of the electron-donating substituents favors NH_3 elimination and the formation of a stabilized ion formed with $\text{NH}_2\text{-C=CH}$ bridged with either a methyl or a phenyl ion similar to that proposed by Milne et al.⁷ for the $[\text{TyrH} - \text{NH}_3]^+$ ion formation. The $[\text{I}(\text{Ile}) - \text{NH}_3]^+$ (m/z 69, 20%) ion observed in the direct spectrum of Ile and not in that of Leu is noteworthy since it gives the opportunity to differentiate the isomeric AAs Leu and Ile (Figure 8). The ion corresponding to $[\text{I}(\text{Ile}) - \text{NH}_3]^+$ was observed before as a predominant product ion in the CID-FAB spectrum of I(Ile) and not in that of the isomeric I(Leu),⁴³ but not in the FAB spectra of both AAs.

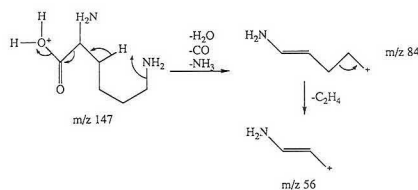
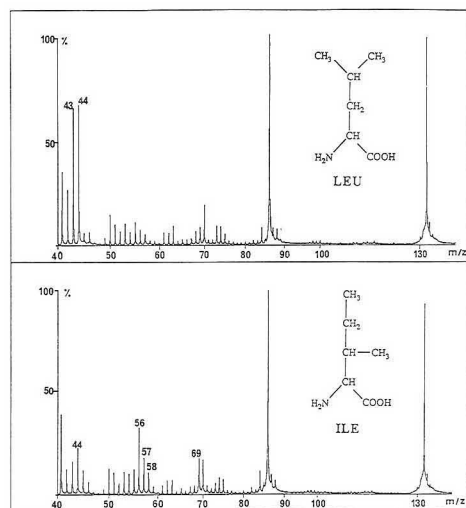
Figure 7. Main fragmentation modes of LysH^+ .

Figure 8. PD mass spectra of Leu and Ile.

(3) *Loss of Radicals.* As observed previously, the loss by a simple bond cleavage of a methyl or hydroxyl radical from I(Val) and I(Thr) gives a radical cation. Similar reactions were investigated with the other AAs. A metastable transition is never associated with a radical loss.

When the immonium ions have the structure $\text{H}_2\text{N}-\text{CH}^+-\text{CH}_2-\text{R}$, two eliminations have to be taken under consideration. The first is the loss of a hydrogen atom, favored in the cases of the aromatic AAs. This elimination gives rise to the formation of a conjugated radical cation $[\text{H}_2\text{N}-\text{CH}=\text{CH}-\text{R}]^{+\bullet}$ (R = an aromatic ring) ($[\text{I}(\text{Phe}) - \text{H}]^{+\bullet}$, m/z 119 (13%), $[\text{I}(\text{Tyr}) - \text{H}]^{+\bullet}$, m/z 135 (23%), and $[\text{I}(\text{Trp}) - \text{H}]^{+\bullet}$, m/z 158 (21%)). The second is the loss of the radical R^\bullet , observed in several spectra, leading to the $[\text{H}_2\text{N}-\text{CH}=\text{CH}_2]^{+\bullet}$ (m/z 43) radical cation (Leu, Lys, Glu, Asp, Asn). Both eliminations in competition are observed in the Cys spectrum ($[\text{I}(\text{Cys}) - \text{H}]^{+\bullet}$, m/z 75 (18%) and m/z 43 (39%)).

In the particular case of I(Leu), m/z 43 (55%) may be either $[\text{H}_2\text{N}-\text{CH}=\text{CH}_2]^{+\bullet}$ (homolytic cleavage) or $[\text{C}_3\text{H}_7]^+$ (heterolytic cleavage). The thermodynamic data favor $[\text{C}_3\text{H}_7]^+$.⁴⁴ This simple heterolytic bond cleavage involving the loss of the neutral $\text{H}_2\text{N}-\text{CH}=\text{CH}_2$ from I to form R^\bullet would also be invoked to explain the formation of $[\text{C}_3\text{H}_5]^+$ (m/z 77, 20%) from I(Phe) and that of $[\text{CH}_3\text{SCH}_2]^+$ (m/z 61, 100%) from I(Met). This is a more plausible formation mechanism for m/z 61, which is especially abundant, than the sequential NH_3 and $\text{H}_2\text{C}=\text{CH}-\text{COOH}$ losses suggested by the metastable transitions.

When the immonium ions have the structure $\text{H}_2\text{N}-\text{CH}^+-\text{CH}(\text{CH}_3)-\text{R}$, the elimination of the radical R^\bullet gives rise to the formation of a significant peak at m/z 57 corresponding

to $[\text{H}_2\text{N}-\text{CH}=\text{CH}-\text{CH}_3]^+$. This ion is observed in the Val, Ile, and Thr spectra. These cleavages have the advantage of differentiating the two isomeric Leu and Ile amino acids. I(Leu) decomposes to m/z 43 while I(Ile) gives rise to m/z 57 (Figure 8). These results are in agreement with those of Aubagnac et al.⁴³ showing the preponderance of the m/z 43 ion in the CID-FAB spectrum of I(Leu) and that of m/z 57 in the CID-FAB spectrum of I(Ile).

Significant ions at m/z 57 are also observed in the Glu and Gln spectra. No metastable transition is associated with the formation and the fragmentation of these ions. It is tempting to suggest the elimination by simple bond cleavage of HCOO^+ and $\text{H}_2\text{N}-\text{CO}^+$ from I(Glu) and I(Gln) ions, respectively, leading to the dicationic $\text{H}_2\text{N}-\text{CH}^+-\text{CH}_2-\text{CH}_2^+$ radical or to its rearranged form $[\text{H}_2\text{N}-\text{CH}=\text{CH}-\text{CH}_3]^+$.

(4) *Other Fragmentations Occurring from I*. In this section other fragmentation modes of I are given, suggested by the metastable transition data.

Aromatic AAs. Some fragmentations of the immonium ions of the aromatic AAs are specific fragmentations of each aromatic ring in electron impact. The metastable I(Trp) ion gives two fragmentations. The first is the loss of 27 units corresponding to the loss of HCN from the indole ring⁴⁵ to give m/z 132 (20%). The second is the loss of 29 units ($\text{H}_2\text{C}=\text{NH}$), generating m/z 130, the base peak in the Trp spectrum. The metastable I(His) ion is the precursor of m/z 83 (loss of 27 units), consistent with the easy loss of HCN from the imidazole ring.⁴⁶

Neutral AAs. A major ion in the Leu spectrum is m/z 44 (Figure 8). The formation of this ion has been rationalized before⁴⁶ as a 1-5 hydrogen-atom transfer from the γ -carbon atom of the chain to the nitrogen atom leading to $[\text{H}_2\text{N}-\text{CH}=\text{CH}_2]^+$ by loss of propene. This pathway is borne out by the presence of m/z 58 ion from I(Ile) formed by the same mechanism. To account for the m/z 44 ion from I(Ile), one must invoke a linear-chain rearrangement prior to ethylene elimination, requiring more time than simple bond rupture. The isomerization constraint leads to an m/z 44 ion of lower intensity for Ile.

Formation of the m/z 30 Ion. An ion at m/z 30 is observed in all the direct AA (except Pro) spectra (m/z 30 = $[\text{H}_2\text{N}-\text{CH}_2]^+$). The formation of this ion implies a hydrogen transfer from the chain to the carbocation.

B. Protonation on the Linear Chain. The fragmentations presented in this section are deduced from a molecular ion protonated on a basic site of the linear chain as already observed for ThrH⁺.

$\text{H}_2\text{N}-\text{CH}(\text{COOH})-\text{CH}_2-\text{R}$ Amino Acids. For comparison purposes it is convenient to divide these compounds in two categories: nonaromatic and aromatic AAs.

(1) *Serine, Cysteine, Aspartic Acid, and Asparagine (Nonaromatic AAs).* The PD mass spectra of these compounds exhibit small ions at m/z 88 and intense ions at m/z 44.

The formation of m/z 88 from Ser and Cys is explained by an initial protonation on R followed by a heterolytic cleavage giving rise to $\text{H}_2\text{N}-\text{CH}(\text{COOH})-\text{CH}_2^+$ (loss of, respectively, H_2O and H_2S). For Asp or Asn protonated on the lateral function, the formation of m/z 88 can be obtained by loss of H_2O or NH_3 rapidly followed by CO elimination (by analogy with I formation). We note that I(Asp) is detected at the same m/z 88 as $[\text{AspH} - \beta\text{-HCOOH}]^+$, consistent with the high-intensity peak observed, but both type m/z 88 ions have different structures.

The peak of high intensity at m/z 44 for these four AAs is explained by a loss of CO_2 from $\text{H}_2\text{N}-\text{CH}(\text{COOH})-\text{CH}_2^+$ accompanied by a hydrogen transfer. The loss of CO_2 from m/z 88 is in competition with the losses of H_2O and H_2 to give

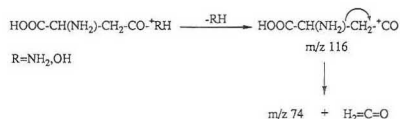


Figure 9. Formation of the m/z 74 ion from AspH⁺ and AsnH⁺: "retro aldol type reaction".

respectively m/z 70 and m/z 86 in the Ser and Asp spectra.

Concerning Asp and Asn, an abundant m/z 74 ion may be explained by a ketene elimination from m/z 116 despite its low intensity. The latter corresponds to a partial elimination of the protonated β function. This mechanism called a "retro aldol type reaction" has been proposed by Milne et al.⁷ to explain the m/z 74 ion (Figure 9) observed in CI spectra of Asn and Asp.^{7,10} In fact the m/z 74 ion is not only observed in Asp and Asn spectra but quasi in all the AA spectra; its formation requires another interpretation, which must be generally applicable (see below: protonation on the amino function).

(2) *Phenylalanine, Tyrosine, Tryptophan, and Histidine (Aromatic AAs).* The fragmentation of the protonated aromatic AAs is dominated by the formation of "benzylic ions" characteristic of the "benzylic rupture" observed in electron impact (Phe (m/z 91, 40%), Tyr (m/z 107, 69%), Trp (m/z 130, 100%), His (m/z 81, 10%)) and by their subsequent classical fragmentations. The benzylic ions are formed from a rapid process (no metastable transition is associated with their formation) while their decompositions are longer lived (observed in metastable ion/neutral coincidence spectra).

When the protonation occurs on the aromatic ring, the benzylic ion formation is obtained by benzylic bond cleavage accompanied by the transfer of the protonating hydrogen in order to eliminate $\text{H}_2\text{N}-\text{CH}_2-\text{COOH}$. The well-known fragmentations of the aromatic ions are observed: m/z 65 and 63 from m/z 91 (Phe), m/z 79 and 77 from m/z 107 (Tyr), m/z 103 (loss of HCN from the ring⁴⁵) from m/z 130 (Trp). The case of histidine is different. This molecule possesses a basic site located on the aromatic ring, able to fix the proton. Consequently, besides the formation of the benzylic ion (m/z 81), a new ion appears at m/z 82, corresponding to the 5-methylimidazole radical ion.

$\text{H}_2\text{N}-\text{CH}(\text{COOH})-\text{CH}_2-\text{CH}_2-\text{R}$ and $\text{H}_2\text{N}-\text{CH}(\text{COOH})-\text{CH}(\text{CH}_3)-\text{R}$ Amino Acids. Threonine, Methionine, Glutamic Acid, and Glutamine. An ion at m/z 102 appears in the spectra of these compounds. This ion corresponds to a loss of H_2O , CH_3SH , $\text{H}_2\text{O} + \text{CO}$, and $\text{NH}_3 + \text{CO}$ from Thr, Met, Glu, and Gln, respectively, after protonation on the linear chain. This ion has the structure A = $\text{H}_2\text{N}-\text{CH}(\text{COOH})-\text{CH}^+-\text{CH}_3$ for Thr and the structure B = $\text{H}_2\text{N}-\text{CH}(\text{COOH})-\text{CH}_2-\text{CH}_2^+$ for Met, Glu, and Gln. Ion B can lose C_2H_4 by simple heterolytic cleavage, giving rise to m/z 74. This mechanism was suggested previously by Tsang and Harrison¹⁰ to explain the origin of the m/z 74 ion from MetH⁺ in CI experiments.

Ions at m/z 85 already encountered in the Glu fragmentation (Figure 6) may be also formed by the mechanism depicted in Figure 10a. The cyclic ion thus formed is a favorable precursor of m/z 55 (m/z 85 losing $\text{CH}_2=\text{O}$). The CH_2O elimination is consistent with the metastable transition m/z 85 \rightarrow m/z 55. A similar mechanism could explain the formation of m/z 55 from GlnH⁺ (Figure 10a).

After the loss of H_2O (NH_3) from GluH⁺ (GlnH⁺), correlated with the donor effect of the remaining carboxylic group, the m/z 130 cyclic ion is proposed as a key precursor for several ions: m/z 71 (NH_3 + ketene eliminations) and m/z 69 obtained by successive eliminations of NH_3 and CO_2 (Glu) or CO_2 and NH_3 (Gln) (Figure 10b).

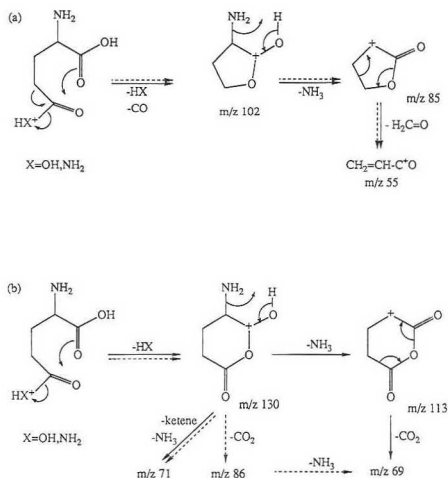


Figure 10. Fragmentations induced by the loss of the substituent chain from GluH⁺ and GlnH⁺.

AAs with Longer Lateral Chains. (1) *Lysine*. The concerted elimination of H₂O, CO, and NH₃ from LysH⁺, giving *m/z* 84 has been interpreted before (Figure 7). As described for ion B, Lys protonated on the δ -amino group can eliminate a molecule of ammonia and then, successively, two molecules of ethylene to form *m/z* 74.

(2) *Arginine*. The spectrum of Arg is very different from those of the other AAs. Several significant peaks are detected in the direct spectrum: MH⁺ and ions at *m/z* 70, 60, 59, and 43. Other small peaks are observed at *m/z* 130, 100, 87, 74, and 73. The absence of the immonium ion is consistent with the main protonation on the guanidyl group. The fragmentation modes of arginine have been the subject of several studies.^{2,20,22}

If we first consider the *m/z* 130 ion, the loss of 45 units from ArgH⁺ (as suggested by metastable transition data) may correspond to three mechanisms: (1) the loss of the radical HCOO[•], leading to [C₅H₁₄N₄]^{•+} (calc *m/z* 130.121), (2) the loss of NH₃ and then of the radical HN=CH[•], giving [C₅H₁₀N₂O₂]^{•+} (calc *m/z* 130.074), or (3) the loss of NH₃ + CO, corresponding to [C₅H₁₂N₃O]^{•+} (calc *m/z* 130.097). The last possibility (3) has been suggested by Zwinselman et al.²⁰ but its formation is difficult to rationalize. The first and second processes both lead to a radical cation. An exact mass (*m/z* 130.107) has been given by Chait et al.,² but the given value is the average between [C₅H₁₄N₄]^{•+} (mechanism 1) and [C₅H₁₀N₂O₂]^{•+} (mechanism 2). In the FFR, the *m/z* 130 ion decomposes into *m/z* 87 and 70 and the *m/z* 87 ion gives rise to the *m/z* 59 ion. If all the fragmenting ArgH⁺ ions are protonated on the guanidyl group, the first mechanism implies a charge-remote fragmentation to give a distonic radical cation: H₂N-CH-(CH₂)₂-NH-C(NH₃⁺)=NH (*m/z* 130). This ion may easily lose H₂N-CH=CH₂ (simple bond cleavage) to give [H₂C[•]-CH₂-NH-C(NH₃⁺)=NH] (*m/z* 87), eliminating in turn either NH₃ to give the *m/z* 70 ion or C₂H₄ to give *m/z* 59. The second process involves the loss of ammonia from the protonated guanidyl group of ArgH⁺ followed, after a hydrogen rearrangement, by that of HN=CH[•] to generate [HN=CH-(CH₂)₂-CH(NH₂)-COOH]^{•+} (*m/z* 130). This *m/z* 130 ion may give rise after two competitive McLafferty rearrangements to [H₂C=C(NH₂)-COOH]^{•+} (*m/z* 87) and [HO-C(OH)=CH-NH₂]^{•+} (*m/z* 73). The *m/z* 70 ion would be generated from *m/z* 87 by loss of the radical [•]OH (simple

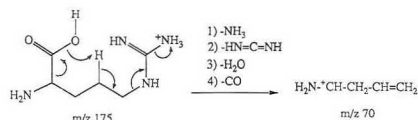


Figure 11. Interpretation of *m/z* 70 in the Arg spectrum by a "concerted mechanism".



Figure 12. Elimination of RH from N-protonated amino acids.

bond cleavage). The high intensity of *m/z* 70, a prominent fragment ion in the Arg spectrum (64%), can also be explained by a concerted mechanism (Figure 11). This last process may be in competition with the ones described above. A mechanism involving the successive losses of CH₅N₃, CO₂, and H₂ from ArgH⁺ was proposed to explain *m/z* 70.² However, a stepwise mechanism in three steps without an intermediate ion is not particularly plausible.

The *m/z* 60 ion (36%) corresponds to [(NH₂)₃C]⁺ (or any isomeric form) formed by transfer of a hydrogen atom from the linear chain to the protonated guanidyl group. The metastable *m/z* 60 ion then fragments into *m/z* 43 (loss of NH₃) or *m/z* 18 [NH₄]⁺.

C. Fragmentations Deduced from Protonation on the α -Amino Function. Simple fragmentation involving the loss of ammonia is rarely, if ever, observed and of low importance, except for Gln. Only seven AAs exhibit an [MH - NH₃]⁺ ion: Tyr, Trp, Cys, Met, Lys, Asn, and Gln. Moreover, for the last three AAs, the formation of this ion seems better explained by involving the NH₂ group of the lateral chain. Several hypotheses may explain the low abundance of [MH - NH₃]⁺. First, the [MH - NH₃]⁺ is unstable and dissociates extremely rapidly to give fragment ions similar to what happens when I is formed from successive losses of H₂O and CO. However, no systematic fragmentation process occurs from [MH - NH₃]⁺. Secondly, an initial protonation on the nitrogen atom of the α -amino group is immediately followed by a hydrogen transfer from the resulting α -NH₃ group to the hydroxyl oxygen atom of the carboxylic function as it has been proposed in CI by Harrison et al.⁷ This mechanism is in variance with Parker and Hercules hypothesis that was previously cited.²⁶ Third, the protonation occurs on α -NH₂ but the protonating hydrogen is eliminated during the primary fragmentation without NH₃ loss and without prior arrangement. The formation of the ion H₂N-CH[•]-COOH at *m/z* 74 (Figure 12) is even more consistent with this mechanism since all the AAs except the cyclic Pro exhibit *m/z* 74. The same fragment is classically observed in the electron impact spectra of amino acids.³⁻⁶ Finally, the protonation may occur on the nitrogen atom but the MH⁺ ion formed does not easily fragment. This mechanism could explain the high MH⁺ intensity in the AA PD mass spectra.

COMPARISON OF PDMS WITH OTHER IONIZATION METHODS GENERATING PROTONATED MOLECULES

The PD mass spectra of the AAs are compared with the available spectra obtained using the following techniques: CI using methane⁷⁻¹⁰ and hydrogen¹⁰ as protonating gas, FAB and CID-FAB ionization,²¹ SIMS,¹⁸ and laser mass spectrometry.²⁴ All these techniques give rise to both quasi molecular MH⁺ and immonium ions. However, the relative intensities of the pseudomolecular ions MH⁺ and of the immonium ion [MH - CH₂O]⁺ as well as the appearance of several other fragment ions are dramatically dependent on the ionization technique.

MH⁺ Ions. To attempt a comparison of the level of ex-

Table VI. Ratio $R = i[I]/i[MH]^+$ for Neutral and Aromatic AA^a

	Gly	Ala	Val	Leu	Pro	Phe	Tyr	Trp
FAB	0.1	0.2	0.4	0.5	0.2	0.7	0.4	0.7
laser	0.9	0.9	0.4	0.4	1.0	1.0	0.6	2.4
SIMS	0.4	0.9	0.2	50	3.7	3.2	1.9	1.0
CH ₃ -CI	2.3	3.3	2.5	1.5	0.7	0.9	1.2	0.5
PDMS	1.7	2.5	1.3	1.3	2.0	2.0	1.4	1.9
H ₂ -CI	100	5	25	25	12.5	17	2.5	3.0

^aThe ratio R cannot be calculated for CID-FAB since MH^+ is the collisioned ion.

citation energy involved during the ionization for each technique, the average abundance of the MH^+ ions of all the available AAs was calculated, normalized to the FAB method: 100% in FAB, 78% in PDMS, 73% in CH₃-CI, 66% in laser, 63% in SIMS, and 16% in H₂-CI. To a first approximation, it could be presumed that the more abundant the MH^+ ion is, the softer is the ionization technique.

Primary Fragmentations of MH^+ . Immonium Ion. The immonium ion I is, most of the time, the main fragment ion observed in mass spectra of protonated AAs. The ratio $R = i[I]/i[MH]^+$ (i being the peak intensity) has been calculated for the amino acids analyzed with all techniques (neutral and aromatic AAs) (Table VI). This ratio R correlates with the MH^+ internal energy; as R becomes larger, so does the internal energy content. Very low values of R are obtained in FAB ionization while high ratios are observed using H₂-CI. On these observations, FAB remains as a soft technique while H₂-CI remains as an energetic technique.

Small-Molecule Eliminations. In competition with the loss of [CH₂O₂] small molecule eliminations also occur.

Ammonia elimination from MH^+ is typically encountered in aromatic, sulfur-containing, amido-substituted, and basic amino acid spectra. This loss is the main fragmentation mode under CID-FAB conditions and to a smaller extent in CH₃-CI experiments.

Water elimination is specific for the AAs having a second hydroxyl group on the lateral chain: alcoholic (Ser, Thr), dicarboxylic (Asp, Glu), and phenolic (Tyr) AAs. Primary water elimination is CID-FAB specific but also observed in CH₃-CI mass spectra.

RSH loss concerns only the sulfur-containing AAs (Cys and Met). Elimination of H₂S leading to m/z 88 is detected with a low intensity in CID-FAB and in PD mass spectra. Concerning methionine, the loss of CH₃SH generates the ion at m/z 102 in CH₃-CI and in PDMS.

Secondary Fragmentations. Fragment ions corresponding to two successive losses of molecules predominate in PD mass spectra as well as in CID-FAB and H₂-CI spectra.

The loss of 63 units, formally $[I - NH_3]^+$, is observed in CID-FAB and PD mass spectra of several AAs in significant abundance. The protonated AAs giving $[MH - 63]^+$ are those which lose NH₃ directly from MH^+ in CID-FAB.

The loss of water is more often observed as a second fragmentation leading formally to $[I - H_2O]^+$ in CID-FAB, H₂-CI, and PD mass spectra of hydroxyl-containing AAs.

CH₃SH elimination is observed as a fragmentation mode of I(Met), leading to an m/z 56 ion of high intensity in H₂-CI and PD mass spectra.

In CID-FAB spectra, ions appear corresponding to successive losses of two small molecules (NH₃ + H₂O, 2H₂O, etc. according to the side chain substitution).

CONCLUSION

When ionized with the less energetic FAB technique, the AAs give only intense peaks corresponding to MH^+ and immonium ions.

In CH₃-CI and CID-FAB experiments, a competition between immonium ion formation and small-molecule elimination occurs. Small-molecule eliminations are much more favored in CID-FAB than in CH₃-CI experiments, suggesting the formation of MH^+ ions of greater internal energy in CID-FAB.

H₂-CI is well-known to be more energetic than CH₃-CI. Under H₂-CI conditions, the MH^+ ion abundance decreases while formation of secondary ions appears. These secondary ions are also observed in CID-FAB and PD mass spectra.

PDMS generates intense MH^+ and immonium ions in addition to many more characteristic secondary ions than any other ionization technique.

In PDMS, the effective interaction volume from the passage of 100-MeV ions through the sample is much greater than that of the other techniques. This energy is diffused rapidly and decreases with distance from impact, which leads to a broad distribution of the internal energy of the ions.³⁶

Consequently, PDMS combines together the advantages of the soft and energetic techniques and is a powerful technique to ionize and analyze small solid molecules.

Registry No. Gly, 56-40-6; Ala, 56-41-7; Val, 72-18-4; Leu, 61-90-5; Ile, 73-32-5; Pro, 147-85-3; Phe, 63-91-2; Tyr, 60-18-4; Trp, 73-22-3; His, 71-00-1; Ser, 56-45-1; Thr, 72-19-5; Cys, 52-90-4; Met, 63-68-3; Lys, 56-87-1; Arg, 74-79-3; Asp, 56-84-8; Glu, 56-86-0; Asn, 70-47-3; Gln, 56-85-9.

REFERENCES

- (1) Togerson, D. F.; Skowronski, R. P.; Macfarlane, R. D. *Biochem. Biophys. Res. Commun.* **1974**, *60*, 616-621.
- (2) Chait, B. T.; Agosta, W. C.; Field, F. H. *Int. J. Mass Spectrom. Ion Phys.* **1981**, *39*, 339-366.
- (3) Biemann, K.; McCloskey, J. A. *J. Am. Chem. Soc.* **1962**, *84*, 3192-3193.
- (4) Junk, G.; Svec, H. *J. Am. Chem. Soc.* **1963**, *85*, 839-845.
- (5) Heyns, K.; Grutzmacher, H.-Fr. *Annalen* **1963**, *667*, 194.
- (6) Vetter, W. In *Biochemical Applications of Mass Spectrometry*; Waller, G. R., Ed.; Wiley: New York, 1972; p 387. *Ibid.*; Wiley: New York, 1980; Suppl. Vol. 1, p 439.
- (7) Milne, G. W. A.; Axenrod, T.; Fales, H. M. *J. Am. Chem. Soc.* **1970**, *92*, 5170-5175.
- (8) Meot-Ner, M.; Field, F. H. *J. Am. Chem. Soc.* **1973**, *95*, 7207-7211.
- (9) Leclercq, P. A.; Desiderio, D. *Org. Mass Spectrom.* **1973**, *7*, 515-533.
- (10) Tsang, C. W.; Harrison, A. G. *J. Am. Chem. Soc.* **1976**, *98*, 1301-1308.
- (11) Hunt, D. F.; Shabanowitz, J.; Botz, F. K.; Brent, D. A. *Anal. Chem.* **1977**, *49*, 1160-1163.
- (12) Beuhler, R. J.; Flannigan, E. L.; Greene, L. J.; Friedman, L. J. *Am. Chem. Soc.* **1974**, *96*, 3990-3999.
- (13) Voigt, D.; Schmidt, J. *Biomed. Mass Spectrom.* **1978**, *5*, 44-46.
- (14) Vairamani, M.; Srinivas, R.; Viswanadha Rao, G. K. *Indian J. Chem., Sect. B* **1988**, *27*, 264-265.
- (15) Eckersley, M.; Bowie, J. H.; Hayes, R. N. *Int. J. Mass Spectrom. Ion Processes* **1989**, *93*, 199-213.
- (16) Winkler, H. U.; Beckey, H. D. *Org. Mass Spectrom.* **1972**, *6*, 655-660.
- (17) Benninghoven, A.; Jaspers, D.; Sichtermann, W. *Appl. Phys.* **1976**, *11*, 35-39.
- (18) Benninghoven, A.; Sichtermann, W. *Anal. Chem.* **1978**, *50*, 1180-1184.
- (19) Liu, L. K.; Busch, K. L.; Cooks, R. G. *Anal. Chem.* **1981**, *53*, 109-113.
- (20) Zwinseelman, J. J.; Nibbering, N. M. M.; Van der Greef, J.; Ten Noever de Brauw, M. C. *Org. Mass Spectrom.* **1983**, *18*, 525-529.
- (21) Kulik, W.; Heerma, W. *Biomed. Mass Spectrom.* **1988**, *15*, 419-427.
- (22) Posthumus, M. A.; Kistemaker, P. G.; Meuzelaar, H. L. C.; Ten Noever de Brauw, M. C. *Anal. Chem.* **1978**, *50*, 985-991.
- (23) Schiller, C.; Kupka, D.; Hillenkamp, F. *Fresenius' Z. Anal. Chem.* **1981**, *308*, 304-308.
- (24) Fan, T. P.; Hardin, E. D.; Vestal, M. L. *Anal. Chem.* **1984**, *56*, 1870-1873.
- (25) Parker, C. D.; Hercules, D. M. *Anal. Chem.* **1985**, *57*, 698-704.
- (26) Parker, C. D.; Hercules, D. M. *Anal. Chem.* **1986**, *58*, 25-30.
- (27) Kambara, H. *Anal. Chem.* **1982**, *54*, 143-146.
- (28) McNeal, C. J.; Macfarlane, R. D.; Thurston, E. L. *Anal. Chem.* **1979**, *51*, 2038-2039.
- (29) Della-Negra, S.; Le Beyec, Y. *Anal. Chem.* **1985**, *57*, 2035-2040.
- (30) Chait, B. T.; Field, F. H. *Int. J. Mass Spectrom. Ion Phys.* **1981**, *41*, 17-29.
- (31) Beynon, J. H.; Gilbert, J. R. *Applications of Transition State Theory to Unimolecular Reactions. An Introduction*; Wiley: New York, 1984.
- (32) Busch, K. L.; Glish, G. L.; McLuckey, S. A. *Mass Spectrometry/Mass Spectrometry—Techniques and Applications of Tandem Mass Spec-*

- metry; VCH Publishers: New York, 1988; p 53-106.
- (33) Brunelle, A. Spectrométrie de masse par temps de vol à multi-sonde de désorption-ionisation (photons UV et particules keV et MeV). Des atomes aux agrégats comme projectiles. Thèse de l'Université Paris Sud, 1990; pp 59-90.
- (34) Burlingame, A. L.; Baillie, T. A.; Derrick, P. J. *Anal. Chem.* **1986**, *58*, 165R-211R.
- (35) Pachuda, S. J.; Cooks, R. G. *Chem. Rev.* **1987**, *87*, 647-669.
- (36) Cooks, R. G.; Busch, K. L. *Int. J. Mass Spectrom. Ion Phys.* **1983**, *53*, 111-124.
- (37) Sundqvist, B.; Hedin, A.; Haakansson, P.; Kamensky, I.; Salehpour, M.; Sawe, G. *Int. J. Mass Spectrom. Ion Processes* **1985**, *65*, 69-89.
- (38) Hedin, A.; Haakansson, P.; Sundqvist, B.; Johnson, R. E. *Phys. Rev. B: Condens. Matter* **1985**, *31*, 1780-1787.
- (39) Sundqvist, B.; Hedin, A.; Haakansson, P.; Salehpour, M.; Sawe, G.; Johnson, R. E. *Nucl. Instrum. Methods Phys. Res., Sect. B* **1986**, *14*, 429-435.
- (40) Bouchoux, G.; Flament, J. P.; Hoppillard, Y.; Tortajada, J.; Flammang, R.; Maquestiau, A. J. *Am. Chem. Soc.* **1989**, *111*, 5560-5567.
- (41) Macfarlane, R. D.; Torgerson, D. F. *Science* **1977**, *191*, 920-925.
- (42) Benninghoven, A. In *Proceedings of Ion Formation from Organic Solids*; Benninghoven, A., Ed.; Springer Series in Chemical Physics; Springer-Verlag: New York, 1983; Vol. 25, pp 64-89.
- (43) Aubagnac, J. L.; El Amrani, B.; Devienne, F. M.; Combarieu, R. *Org. Mass Spectrom.* **1985**, *20*, 428-429.
- (44) I(Leu) gives either $\text{H}_2\text{N}-\text{CH}=\text{CH}_2 + \text{H}_3\text{C}-\text{CH}^+-\text{CH}_3$ by heterolytic simple bond cleavage (A) or $[\text{H}_2\text{N}-\text{CH}=\text{CH}_2]^{*+} + \text{H}_3\text{C}-\dot{\text{C}}\text{H}-\text{CH}_3$ by homolytic cleavage (B).
- (A)
- $$\Delta H^\circ(\text{H}_2\text{C}=\text{CH}-\text{NH}_2) = 29 \text{ kJ}\cdot\text{mol}^{-1}$$
- $$\Delta H^\circ(\text{H}_3\text{C}-\text{CH}^+-\text{CH}_3) = 799 \text{ kJ}\cdot\text{mol}^{-1}$$
- $$\rightarrow E(\text{A}) = 826 \text{ kJ}\cdot\text{mol}^{-1}$$
- (B)
- $$\Delta H^\circ(\text{H}_2\text{C}=\text{CH}-\text{NH}_2)^{*+} = 820 \text{ kJ}\cdot\text{mol}^{-1}$$
- $$\Delta H^\circ(\text{H}_3\text{C}-\dot{\text{C}}\text{H}-\text{CH}_3) = 93 \text{ kJ}\cdot\text{mol}^{-1}$$
- $$\rightarrow E(\text{B}) = 913 \text{ kJ}\cdot\text{mol}^{-1}$$
- ΔH° values are extracted from: Lias, S. G.; Bartmes, J. E.; Lieman, J. F.; Holmes, J. L.; Levin, R. D.; Mallard, W. G. *J. Phys. Chem. Ref. Data* **1988**, *17*, Supp. 1.
- (45) Porter, Q. N. In *Mass Spectrometry of Heterocyclic Compounds*, 2nd ed.; John Wiley and Sons: New York, 1985; pp 555-556.
- (46) Porter, Q. N. In *Mass Spectrometry of Heterocyclic Compounds*, 2nd ed.; John Wiley and Sons: New York, 1985; pp 694-695.

RECEIVED for review July 16, 1991. Accepted December 31, 1991.

Neutral-Ion Correlation Measurements: A Novel Tandem Mass Spectrometry Data Acquisition Mode for Tandem Magnetic Sector/Reflectron Time-of-Flight Instruments

F. H. Strobel, L. M. Preston, K. S. Washburn, and D. H. Russell*

Department of Chemistry, Texas A&M University, College Station, Texas 77843

A new instrument concept for tandem mass spectrometry is described. The instrument consists of a high-performance magnetic sector (Kratos MS-50) as MS-I and a reflectron time-of-flight as MS-II. The instrument concept is compatible with pulsed and continuous ionization sources. This paper describes the basic instrument concept and presents preliminary data for tandem mass spectrometry experiments. This paper emphasizes the use of neutral-ion correlation measurements for obtaining metastable ion and collision-induced dissociation spectra by using a continuous ion source.

INTRODUCTION

Ionization methods for nonvolatile, thermally labile molecules are now sufficiently developed that virtually any class of organic molecule can be produced as an intact ion,¹ and considerable efforts are now focused on developing structural mass spectrometry to a comparable level. Ionization methods such as field-desorption,² plasma desorption,³ fast-atom bombardment (FAB) ionization,⁴ electrospray⁵ ionization (ESI), and matrix-assisted laser desorption⁶ (MALD) ionization have spawned explosive growth in biomolecule mass spectrometry. The advantage of each of these ionization methods is that the dominant ion in the mass spectrum corresponds to the protonated molecule $[\text{M} + \text{H}]^+$ (in the case of ESI multiple-charged ions are produced), metal ion adducts of the molecule, $[\text{M} + \text{Na}]^+$, or the corresponding anion, $[\text{M} - \text{H}]^-$ or $[\text{M} + \text{Na} - 2\text{H}]^-$. A disadvantage of these ionization methods is that very little structural information is obtained from the normal mass spectral data,⁷ and with the exception

of FAB, there is considerable difficulty associated with adapting these methods to tandem mass spectrometry experiments. In the case of ESI, identification of the charge state of collision-induced dissociation product ions is difficult, especially for unknowns,⁸ and MALD ionization is pulsed and not directly compatible with most tandem mass spectrometers. Because ionization methods such as fast-atom bombardment (FAB) or liquid-SIMS are easily adapted to tandem instruments, FAB/tandem mass spectrometry experiments have developed rapidly and are now firmly established as routine structural methods.⁹

The tandem mass spectrometry experiment adds new dimensions to structural characterization studies. First, the $[\text{M} + \text{H}]^+$ ion of the analyte can be separated from impurity ions, and the dissociation reactions of the $[\text{M} + \text{H}]^+$ ion can be examined free of interference ions, assuming the interference ions and analyte ions have different m/z values that can be separated at the working resolution of MS-I. Secondly, changes in the nature of the parent ion, e.g., selecting the $[\text{M} + \text{Na}]^+$ ion rather than the $[\text{M} + \text{H}]^+$ ion, can provide detailed/specific structural information.¹⁰ Thirdly, tandem mass spectrometry facilitates probing of the ions by a range of methods, such as collision-induced dissociation,¹¹ photodissociation,¹² surface-induced dissociation,¹³ and endothermic ion-molecule reactions.¹⁴ Although the kinds of structural information obtained by each of these methods are quite similar, often times there are significant differences in the spectra.

In terms of increasing the sensitivity of mass spectrometry, an important feature of tandem mass spectrometry is the elimination of interference signals, thereby enhancing the

signal-to-noise ratio. For example, background ions that arise from sample impurities or ionization of matrix materials complicate the mass spectrum (due to "chemical noise").¹⁵ The chemical noise in the mass spectrum can be greatly attenuated, if not eliminated entirely, by performing tandem mass spectrometry experiments.¹⁶ In addition, background ions (chemical noise) from the matrix can be reduced further by using pulsed ionization,¹⁷ and pulsed ionization methods are less sensitive to ion yield variation due to the presence of impurities. Although pulsed ionization methods are not normally used with scanning (e.g., magnetic sector or quadrupole) tandem instruments, we recently demonstrated that matrix-assisted laser desorption ionization combined with tandem mass spectrometry can (under ideal conditions) be used for the detection of subfemtomole levels of peptides.¹⁸

On the basis of current or planned work in several laboratories it is quite clear that the next major frontier in structural mass spectrometry involves the maturing of tandem mass spectrometry and the development of greater sensitivity, specifically the improvement in the signal-to-noise ratio, especially in terms of background noise. Several new instrument designs are in the developmental stage, e.g., multisection instruments with spatial array detectors¹⁹ and time-array detectors,²⁰ Fourier transform ion cyclotron resonance (FTICR),²¹ quadrupole ion traps,²² and sophisticated time-of-flight instruments.²³ Each instrument design possesses specific advantages, in terms of operating parameters and range of experiments, but it is too early to evaluate in detail the specific advantages/disadvantages of a particular instrument concept.

This paper introduces a new instrument under development in our laboratory. The instrument incorporates a high-resolution magnetic sector as MS-I (Kratos MS-50)²⁴ and a reflectron time-of-flight (TOF) as MS-II. The instrument design is mechanically simple, operator friendly, and compatible with pulsed ionization methods. In this paper we present the first detailed description of the instrument, but the major focus of the paper is on the use of neutral-ion correlation measurements, a specialized time-of-flight data acquisition mode for obtaining tandem mass spectra. Time-of-flight methods have been used previously for tandem mass spectrometry experiments. For example, Enke and co-workers have described a spectrometer that simultaneously measures momentum (magnetic analyzer) and velocity (time-of-flight) of ions. They demonstrated that this method can be used to acquire normal mass spectra as well as collision-induced dissociation spectra.²⁵ Glish and co-workers developed a tandem quadrupole/time-of-flight instrument and demonstrated the utility of the instrument for tandem mass spectrometry experiments.²⁶ Although the resolution of the tandem quadrupole/TOF instrument was not optimized (the TOF spectra were obtained by using a linear TOF) the reported data are comparable (in terms of resolution) to that obtained with mass-analyzed ion kinetic energy (MIKE) spectrometers. More recently Standing's group used neutral-ion correlation measurements²⁷ to detect ions formed by unimolecular dissociation reactions in the field-free region of a reflectron time-of-flight analyzer. The utility of this method for peptide sequence analysis was demonstrated on an unknown sample of dynorphin.²⁸

The instrument under development in our laboratory differs from the earlier tandem mass spectrometry involving time-of-flight methods in several ways. First, MS-I is a high-performance/high-resolution magnetic sector instrument with an upper mass range limit of 3500 Da at full accelerating potential, and the upper mass limit can be extended by approximately a factor of 2 by reducing the accelerating voltage to 4 kV. Thus, the instrument is well suited for the analysis of modest size biomolecules. Secondly, the reflectron time-

of-flight instrument is designed for high sensitivity and modest mass resolution ($m/\Delta m = 500$ –1500 and 1000–5000 for analyte m/z values of 1000 and 5000, respectively). The reflectron differs from those used on most time-of-flight instruments, e.g., two-stage reflectrons used for high resolution of ions formed by direct ionization in the ion source,²⁹ in that it is designed to focus product ions which are formed by dissociation in a field-free region and therefore have a broad range of kinetic energies. The kinetic energy of the fragment ion is dependent on the ratio of the daughter ion mass to the parent ion mass, e.g., $E_k(m_i) = E_k(m_p)(m_i/m_p)^{1/2}$.³⁰ Other factors contributing to the kinetic energies for a particular fragment ion mass include kinetic energy release,³¹ collisional scattering, and the initial kinetic energy distribution of the parent ion. Finally, the instrument is designed for operation in the tandem mass spectrometry mode with either continuous or pulsed ionization sources. In this regard the instrument is comparable to the new generation four-sector tandem instruments equipped with spatial array detectors; however, it should be noted that the cost of the four-sector tandem instruments with spatial array detectors far exceeds the cost of the two-sector/R-TOF tandem instruments.

EXPERIMENTAL SECTION

A schematic of the tandem magnetic sector (EB)/reflectron time-of-flight (TOF) instrument is shown in Figure 1. The instrument consists of a Kratos MS-50 and a home-built reflectron time-of-flight instrument. The instrument is equipped with a 30-keV Cs⁺ ion gun (Phasor Scientific) that can be operated in a continuous or pulsed mode, an excimer laser (Questek Model 2440) for performing pulsed laser desorption and/or photodissociation, and a Laser Science, Inc., cartridge type N₂ laser (Model VSL 337 and VSL 337ND). Time-of-flight spectra can be obtained by using a time-to-digital converter (TDC) (LeCroy Model 4208 TDC), a 350-MHz digital oscilloscope (LeCroy Model 9450), or a transient recorder (LeCroy Model TR8828D 200-MHz digitizer). All of the TOF data acquisition modules are interfaced to PC/AT computers by using a National Instruments GPIB mainframe card. Event sequences for the various experiments are controlled by an EG&G Princeton Applied Research digital delay generator Model 9650. A bias collision cell and deflector lens are available but are not used in the present work.

The reflectron TOF instrument currently in use has a total flight path of 2 m and the reflection angle is approximately 0°. The advantages of a collinear reflectron are high ion transmission and high mass resolution in comparison to that obtained with larger (5–20°) reflecting angles. The collinear arrangement is also convenient for positioning detectors to detect both neutrals and ions. For example, neutrals formed by metastable ion dissociation reactions, collision-induced dissociation (CID), or photodissociation in the region between MS-I and MS-II are detected by a microchannel plate detector (detector no. 1) positioned behind the reflectron. Ions are detected by the microchannel plate detector (detector no. 2) (25 mm diameter, 32 μ m c-c, 25 μ m diameter pore Chevron detector with 6 mm diameter center hole from Galileo) positioned at the entrance to the reflectron TOF instrument. The reflector is 40 cm in length consisting of 33 electrodes with each electrode having a 7 cm inner diameter. The front plate of the reflectron is a grid with 98% transmission (20 lines/in., copper grid). A linear electric field gradient is produced by a resistor bridge placed in the vacuum system using 1 M Ω \pm 1% glass-encapsulated resistors from Victoreen. The vacuum in the reflectron housing is maintained with a 60 L/s turbo pump (Balzers Model No. TPU 060).

A particular advantage of the neutral-ion correlation experiment is that either continuous or pulsed ionization/excitation can be used for the time-of-flight measurements. For example, dissociation reactions (unimolecular dissociation, collision-induced dissociation, or photodissociation) of the mass-selected M_1^+ ion that occur in the field-free region between MS-I and the reflectron produce a fragment ion (M_2^+) and a neutral (M_3^0). The velocity of M_2^+ and M_3^0 are the same as that of M_1^+ . The neutral fragment will not experience any force due to the reflectron and will strike detector no. 1 and produce a signal. M_2^+ will be decelerated upon

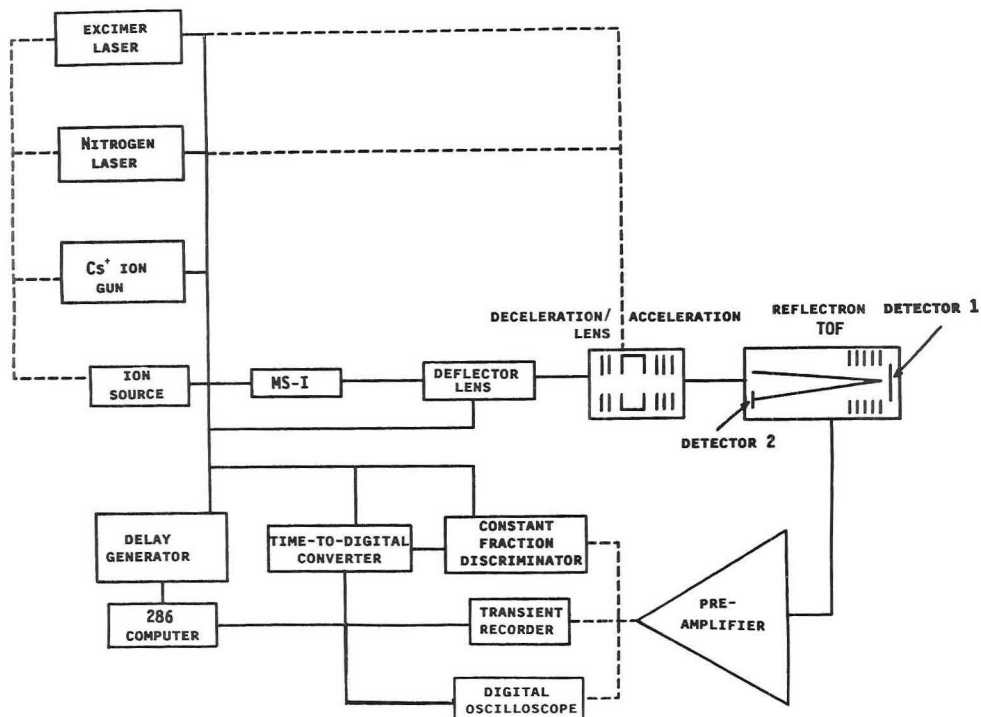


Figure 1. Schematic diagram of the magnetic sector/reflectron time-of-flight mass spectrometer.

entering the reflectron, eventually reaching zero velocity, at which point its direction is reversed. M_2^+ is then reaccelerated back to its initial velocity. Because the initial velocities of the fragment ions are independent of the m/z value, the time that an ion spends in the reflectron depends upon the rate of deceleration and reacceleration. The rate of deceleration/reacceleration is proportional to the m/z of M_2^+ . Therefore, the difference in the arrival time of the neutral and the arrival time of M_2^+ is dependent upon the m/z of the ion.

The neutral-ion correlation experiment can be performed in two ways. The first is to use the neutral signal as the start for the time-of-flight measurement and measure the arrival time for the ion. The second method uses the ion as the start event for the time-of-flight experiment while delaying the signal from the neutral detector. In both modes the time delay between arrival of a neutral at detector no. 1 and the arrival time of the ion at detector no. 2 is used to assign the m/z of the fragment ion. The two methods should give identical spectra; however it has been our experience that the second method yields a better signal-to-noise ratio.

In order to understand the signal-to-noise ratio associated with this experiment, it is necessary to examine the signal and noise components separately. The signal observed in the neutral-ion correlation measurement is the result of a neutral and an ion striking the appropriate detector within a specified time interval. For example, if M_1^+ dissociates to M_2^+ and M_3^0 , M_3^0 striking the neutral detector starts the TOF clock and M_2^+ must arrive at the ion detector within a time interval Δt . Similarly, if the TOF clock is started by M_2^+ striking the ion detector, the delayed signal for M_3^0 must fall within a time interval Δt . Δt is defined by the initial velocity of M_1^+ , the value of M_2^+ , and the dimensions of the reflectron (i.e., the deceleration/reacceleration for M_2^+). Because only one Δt is measured for each start signal, noise and signal are mutually exclusive.

The correlation between the number of false coincidences and

the primary ion count rate for the neutral-ion correlation experiment is the same as that for photoelectron-photoion coincidence spectroscopy.³³ A special requirement of this experiment is the need for a low beam current density (ca. 10^3 – 10^4 ions/s for the M_1^+ ion) in order to eliminate (or minimize) the number of false correlations. There are two major sources of noise associated with neutral-ion correlation measurements: (i) "dark current noise" associated with the detector and (ii) noise associated with the ion beam (M_1^+ ions that penetrate the potential applied to the reflectron and/or neutrals formed by charge-transfer ion-molecule reactions between M_1^+ and the CID target gas, which cause false coincidences). We have found that the signal-to-noise ratio for the EB/R-TOF neutral-ion correlation experiment can be improved by adjusting the potential (E_R) of the reflectron to a value less than the kinetic energy of M_1^+ , e.g., $E_R = 7500$ V for a nominal beam energy of 8 keV. This reduces the beam noise associated with the ion detector but does not overcome beam-related noise associated with the neutral detector. In the Results and Discussion section, we will demonstrate that CID spectra are currently limited by beam-related noise (M_1^+ and charge-transfer neutrals) striking the neutral detector. An instrument modification is currently underway that will improve the signal-to-noise ratio associated with the neutral detector. Another source of beam-related noise is due to sputtering of particles upon impact of M_1^+ , M_2^+ , and M_3^0 with one detector since the sputtered ions are then detected at the opposing detector.³⁴ This source of noise can be minimized if the fronts of the detectors are biased at the same voltage.

In our experiments, the fronts of the detectors are at ground and a positive potential is applied to the backside of the microchannel plates and collection anodes (2000 and 2500 V, respectively). The collection anode is then capacitively coupled to a constant-fraction discriminator (Canberra Model Nos. 2128 and 2126). The output from the constant-fraction discriminators can then be used as inputs to the TDC or to the delay generator.

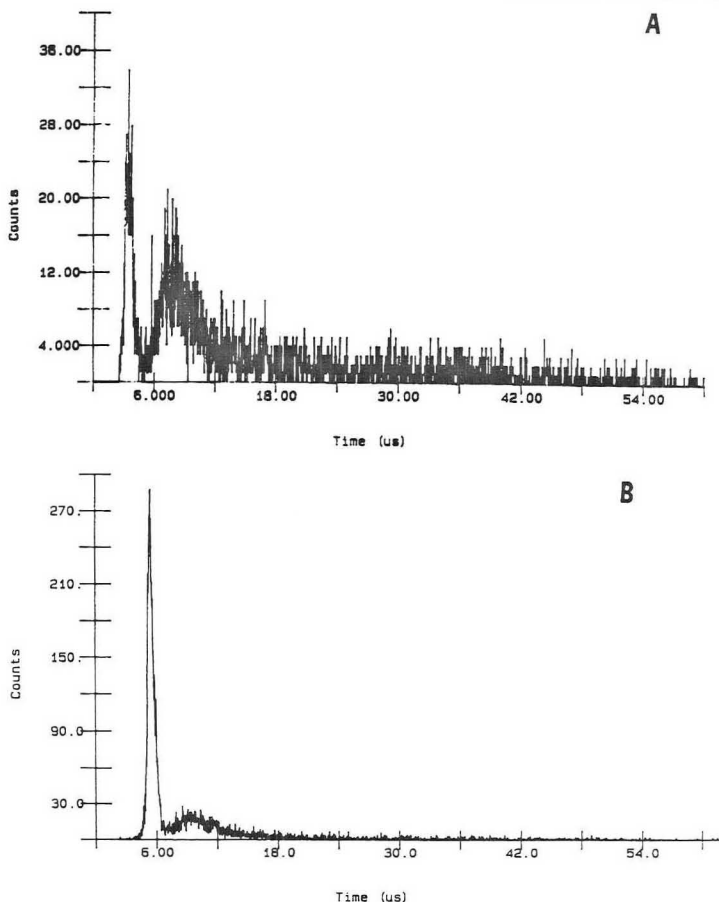


Figure 2. Arrival time distributions of the mass-selected $(M + H)^+$ ion of (A) sinapic acid ($m/z = 225$) and (B) [Aus¹⁶] oxytocin ($m/z = 957$) after a 3-ns laser pulse (337 nm).

The m/z value of the fragment ions are assigned by using eq 1 and 2, where C_1 , C_2 , and C_3 are calibration constants, m_1 is the

$$m/z = A + C_3(1 - A/m_1) \quad (1)$$

$$A = (C_1(t_{\text{ion}} - t_{\text{neutral}})m_1^{1/2} + C_2m_1^{1/2}) \quad (2)$$

parent ion mass, and $t_{\text{ion}} - t_{\text{neutral}}$ is the time difference that is measured by the neutral-ion correlation measurements. A is a theoretical calibration where the first term reflects the time in the reflectron and the second term is used to correct for the fact that the distance from the exit of the reflectron to the ion detector is different from the distance from the entrance of the reflectron to the neutral detector.²⁷ The second term in equation 1 was found empirically by measuring the fragment ions of known compounds, e.g., butylbenzene, metal carbonyls (e.g., $\text{Mn}_2(\text{CO})_{10}$), and glycerol clusters, to fit previously reported mass-to-charge ratios of the fragment ions. Because C_1 reflects the penetration depths of the ions, C_1 will change with the reflectron voltages, therefore, C_1 is calibrated every day with a known compound.

RESULTS AND DISCUSSION

The standard mode of operation for time-of-flight instruments is to form ions by using a pulsed ionization source, e.g., a pulsed Cs^+ ion source or a pulsed laser (for desorption or multiphoton ionization). If the ions are formed with a small

spatial distribution and a narrow kinetic energy distribution, the mass resolution of the time-of-flight measurement is limited by the temporal characteristics of the ionization pulse.³⁵ Thus, ionization pulse durations of 1–3 ns are required for high mass resolution measurements. Although pulse widths of 1–10 ns can be obtained by rastering a conventional Cs^+ ion gun across a small slit,³⁶ this mode of operation requires summing a large number of events (10^4 or greater) to obtain a complete mass spectrum. The requirement of a large number of ionization events presents a major obstacle to performing tandem mass spectrometry by using a pulsed ion source. For example, the efficiency of collision-induced dissociation is quite low ranging from a few percent to 0.1–0.5% for large molecules.³⁷ If we assume a collision-induced dissociation efficiency of 0.1%, then 10^4 primary ions yield 10 fragment ions. Because the number of reaction channels available to the collisionally activated ion is quite large (say 10–15 structurally significant fragment ions are typical for relatively small peptides), it may be necessary to accumulate data from 10^5 – 10^8 ionization events in order to collect a statistically significant data set. If the repetition rate of the ionization source is 10 kHz, a data set of 10^8 events can be obtained in 100 s. However, as the ion yield or collision-induced dissociation efficiency decreases, as is observed for

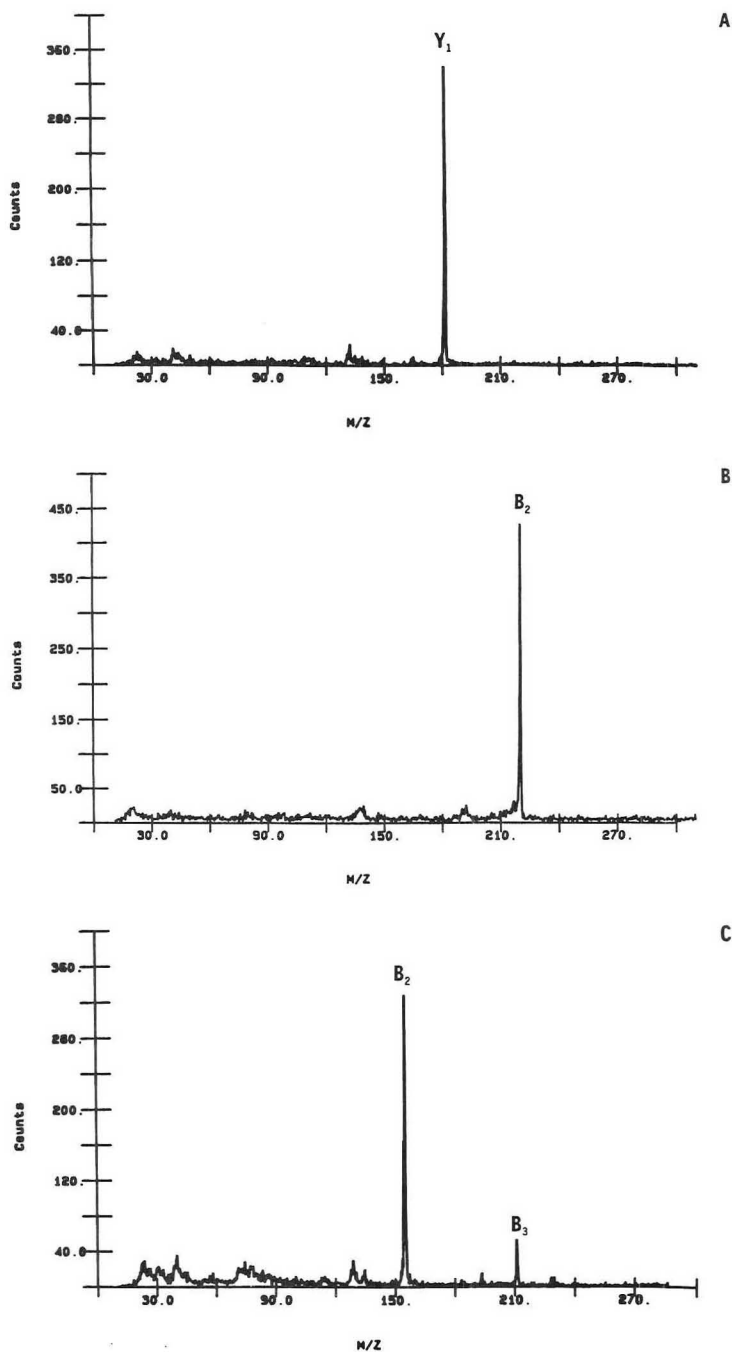


Figure 3. Metastable ion spectra of the $(M + H)^+$ ion of (A) glycine-alanine-tyrosine ($m/z = 310$), (B) glycine-tyrosine-alanine ($m/z = 310$), and (C) glycine-proline-glycine-glycine ($m/z = 287$) obtained by neutral-ion correlation measurements on the EB/R-TOF instrument.

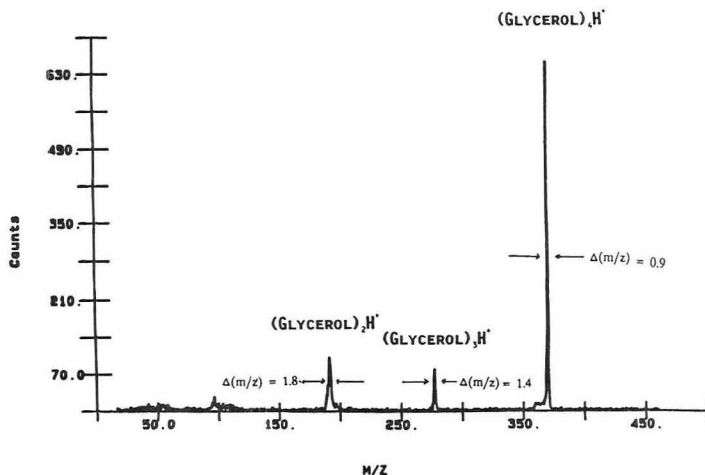


Figure 4. Metastable ion spectrum of $((C_3H_6O_3)_5H^+)$ ($m/z = 461$) obtained by neutral-ion correlation measurements on the EB/R-TOF spectrometer.

increasing molecular weight, the number of events required to collect a statistically significant data set also increases.

An alternative approach to performing measurements with a pulsed ion beam is to form large numbers of ions per ionization pulse and collect the data by using a transient recorder. This is a common mode of operation for matrix-assisted laser desorption where the yield of ions per laser pulse is high; e.g., Standing has reported that approximately 10^4 ions are formed for each laser pulse;³⁸ however, the numbers of ions per laser pulse varies with the laser power density, the type of matrix used, and the matrix-to-analyte ratio. The limitation of this experiment is the high rate of sample consumption and the inherent loss in sensitivity over single ion-counting experiments. The sample consumption rate does not affect acquisition of normal mass spectral data, but this does pose a problem for signal-averaging. In addition, because the efficiency of the activation/dissociation process is low, the transient recorder mode is less effective for acquisition of collision-induced dissociation and/or photodissociation data.

A complicating factor associated with laser desorption ionization, and especially matrix-assisted laser desorption, is the temporal evolution of ions following laser excitation. Figure 2 contains a plot of the ion abundance for the $[M + H]^+$ ion of sinapic acid and oxytocin as a function of time following the laser pulse. The laser pulse width is approximately 3 ns but the arrival time distribution for the $[M + H]^+$ ions is bimodal. One portion of the arrival distribution has a width at half-height of approximately 50 ns, but the total arrival time distribution extends to 50–70 us. Although data such as that shown in Figure 2 are important in terms of the fundamentals of MALD and further studies of this observation are underway, in this paper we want to focus on those factors that directly impact the performance characteristics of the EB/R-TOF instrument. That is, the extended arrival time distribution complicates tandem mass spectrometry experiments with an instrument such as shown in Figure 1 in two ways: (i) the start signal for the time-of-flight experiment is not sufficiently defined for high mass resolution, and (ii) to achieve reasonable mass resolution, it is necessary to pulse the ion beam entering MS-II such that a small slice of the arrival distribution is selected. Although such an experiment achieves the desired result, the sensitivity is reduced because a substantial portion of the ions produced are not analyzed. In order to achieve the desired sensitivity and resolution with

a reflectron TOF instrument, the ions must be formed with an infinitely short pulse (1–10 ns) with at least one ion in each pulse. A low current density ion beam (e.g. 100–10 000 ions/s) can be considered a series of infinitely short pulses that contain one ion of interest. Because the timing of the pulse is not known, two particles (e.g. an ion and a neutral) that strike different detectors can be used to synchronize the time-of-flight clock.³⁹

Figure 3 contains the metastable ion spectra for selected peptides (Gly-Ala-Tyr, Gly-Tyr-Ala, Gly-Pro-Gly-Gly) obtained by using the neutral-ion correlation experiment. In these experiments the ion is used to synchronize the TOF clock and the neutral signal was delayed (see Experimental Section). The metastable ion spectra for the $(M + H)^+$ ions of small peptides are relatively simple, with a single fragment ion typically dominating the spectrum. The major product ions are assigned according to the notation introduced by Roepstorff.⁴⁰

Figure 4 shows the metastable ion spectrum for the glycerol cluster $((C_3H_6O_3)_5H^+)$. Peak widths at half-height for each of the daughter ion signals are indicated. Ions were produced by Cs^+ ion bombardment of neat glycerol. The glycerol clusters may be considered to be simple solvated species.⁴¹ The peak widths of the fragment ions increase as the mass of the daughter ion decreases, e.g., as the ratio m_2^+/m_1^+ decreases. The temporal focusing of the reflectron depends on the penetration depth of the ions into the reflectron. The daughter ions with lower m/z values have lower energy; therefore, the lower m/z ions will not penetrate the reflector as far as the higher mass ions.

Neutral-ion correlation measurements can also be used for acquisition of collision-induced dissociation spectra. The collision-induced dissociation spectrum of the glycerol cluster $((C_3H_6O_3)_5H^+)$ is contained in Figure 5.

By comparison of Figures 4 and 5, it can be seen that the peak widths at half height in the collision-induced dissociation spectra are larger than the peak widths at half height in the metastable ion spectra. The increased peak widths in the collision-induced dissociation spectra can be attributed to the spread of kinetic energies of the M_1^+ ion due to translation energy loss accompanying collisional activation⁴² and the scattering of ions that occur upon kiloelectronvolt collisions. The higher mass daughter ions appear to be less affected by the translational energy losses and scattering. The effect of

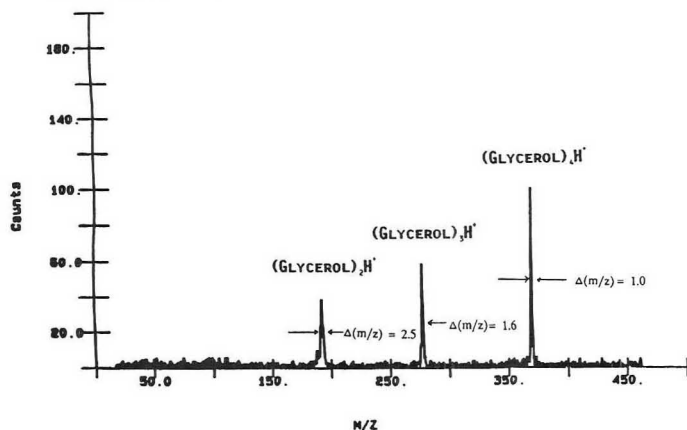


Figure 5. Collision-induced dissociation spectrum of $((C_3H_6O_3)_3H)^+$ ($m/z = 461$) (8 keV, 25% attenuation, He collision gas) obtained by neutral-ion correlation measurements on the EB/R-TOF instrument.

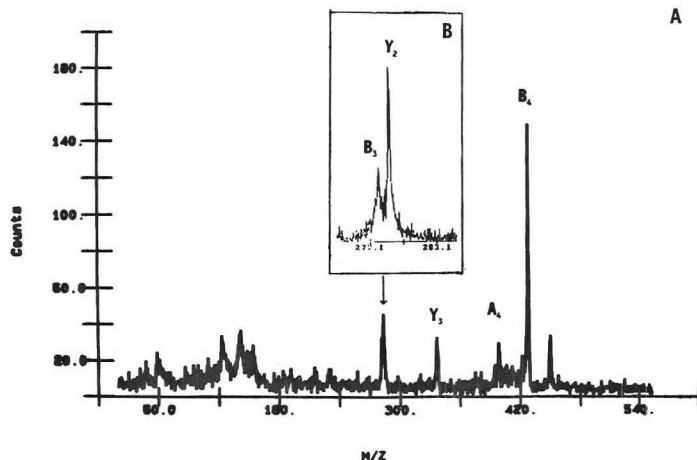


Figure 6. Metastable ion spectrum of leucine enkephalin $(M + H)^+$ ($m/z = 556$) obtained by neutral-ion correlation measurements on the EB/R-TOF spectrometer. (A) Full spectrum with reflectron voltage at 8000 V. (B) Spectrum in the region of m/z 278, 279 with the reflectron voltage at 5000 V.

the penetration can be seen by comparison of the peak widths of the $(\text{glycerol})_4H^+$ and the $(\text{glycerol})_2H^+$ daughter ions in Figures 4 and 5. While the peak widths of the $(\text{glycerol})_4H^+$ daughter ions are approximately equal in Figures 4 and 5, the peak width of the $(\text{glycerol})_2H^+$ peak is 40% larger for the collision-induced dissociation spectra than for the metastable spectra.

To obtain higher resolution on the lower mass daughter ions, the potential on the reflector can be lowered to change the penetration depth of the lower mass daughter ions. Figure 6 contains the metastable spectrum of leucine enkephalin. The largest signal corresponds to the B_4 fragment, but the Y_3 and the B_3 and/or Y_2 fragment ions also are observed.⁴³ The B_3 and Y_2 ($m/z = 278$ and 279) fragment ions are not resolved in this spectrum, but when the reflectron was lowered to 5000 V, the doublet could be resolved (see Figure 6B).^{23b,c}

The spectra in Figures 3-6 illustrate the utility of the neutral-ion correlation experiment for acquisition of tandem mass spectra. However, the signal-to-noise ratio for colli-

sion-induced dissociation spectra acquired in this way is less than that obtained for metastable ion spectra. This limitation can be readily seen by comparing the metastable ion spectrum for Leu enkephalin (Figure 6) with the collision-induced dissociation spectrum contained in Figure 7. The reduction in the signal-to-noise ratio for the collision-induced dissociation spectrum can be attributed to the background noise that is associated with neutralization of the incident ions upon collision with the target gas. For example, Figure 8 shows the arrival time distribution data for $[M + H]^+$ of sinapic acid and the arrival time distribution of the neutrals after the ion beam is attenuated by 25% by the addition of collision gas. Most of the attenuation of the beam can be accounted for by neutrals that are formed by a charge-transfer reaction; whereas, neutrals (and ions) formed by collision-induced dissociation account for less than 1% of the total neutrals. The large number of uncorrelated neutrals produces a significant background noise. Because noise and signal are mutually exclusive (see Experimental Section), the signal-

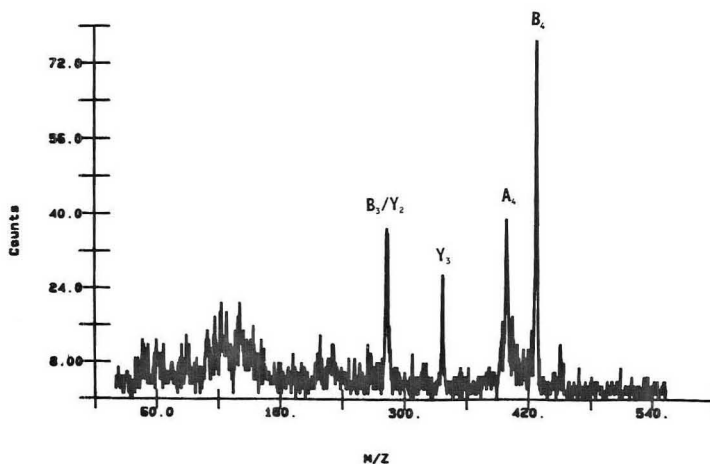


Figure 7. Collision-induced dissociation spectrum of leucine enkephalin ($M + H$) $^+$ ($m/z = 556$) (8 keV, 25% attenuation, He collision gas) obtained by neutral-ion correlation measurements on the EB/R-TOF instrument.

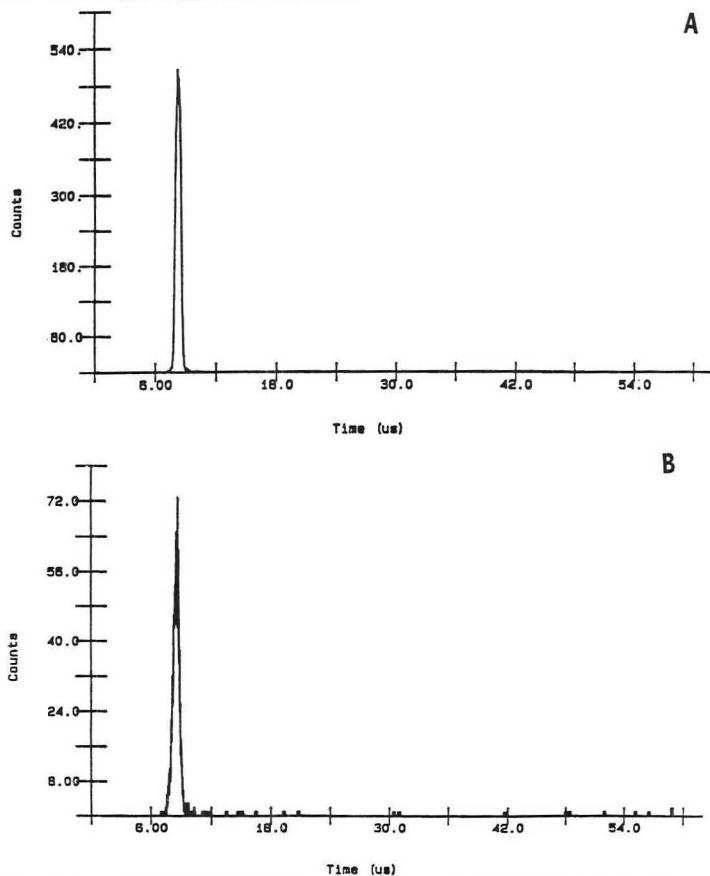


Figure 8. (A) Arrival time distribution without bias applied to the reflectron. Therefore both ions and neutrals of sinapic acid ($M + H$) $^+$ ($m/z = 225$) are detected using the line of sight detector (4-keV collision energy, 25% attenuation, He collision gas). (B) Arrival time distribution with 5-kV bias on the reflectron. Therefore neutral products of collisions of the sinapic acid ($M + H$) $^+$ ($m/z = 225$) ion with the He target gas are detected using the line of sight detector (4-keV collision energy, 25% attenuation, He collision gas).

to-noise ratio for the collision-induced dissociation product ions is reduced. The large numbers of neutrals detected in this experiment have direct bearing on the unresolved issue concerning charge-transfer reactions between kiloelectronvolt translational energy polyatomic ions and neutral target atoms, e.g., the competition between collisional activation and target gas excitation in the collision-induced dissociation experiment.⁴⁴⁻⁴⁸ The neutral species measured in this experiment provides irrefutable evidence for the large cross-sections of endothermic charge-transfer reactions between the incident ion and rare gas target atoms.

The effects of a large background signal on the neutral-ion correlation measurement suggests that activation methods that do not produce significant amounts of neutrals will be best suited for this method. Thus, this measurement should be ideally suited for photodissociation,¹² electron-induced dissociation,⁴⁷ and possibly surface-induced dissociation.¹⁴

CONCLUSIONS

Ion-neutral correlation measurements provide a convenient method for acquiring metastable ion and collision-induced dissociation spectra for ions produced by a continuous ion source in a tandem magnetic sector/reflectron-time-of-flight instrument. Although the signal-to-noise ratio for the collision-induced dissociation data is reduced by random background from charge-transfer reactions, this may be overcome by signal-averaging a large number of dissociation events. Another approach to improving the signal-to-noise ratio is to reduce the background. Background reduction can be accomplished by using a pulse ionization source¹⁷ or by using activation methods that do not contribute excess neutrals, e.g., photodissociation,¹² electron-induced dissociation,⁴⁷ and (possibly) surface-induced dissociation.¹⁴

ACKNOWLEDGMENT

This work is sponsored by the U.S. Department of Energy, Division of Chemical Sciences, Office of Basic Energy Sciences (Grant DE-FG05-85ER-13434) and the U.S. Department of Energy, University Research Instrumentation Program (Grant DE-FG05-89ER75502).

REFERENCES

- Burlingame, A. L.; Millington, D. S.; Norwood, D. L.; Russell, D. H. *Anal. Chem.* **1990**, *62*, 268R. (b) Mass Spectrometry; McCloskey, J. A., Ed.; Abelson, J. N., Simon, M. I., Eds.-in-Chief; Methods in Enzymology; Academic Press: Harcourt, Brace, Jovanovich Publishers: San Diego, CA, 1990; Vol. 193.
- Lattimer, R. P.; Schulten, H. R. *Anal. Chem.* **1989**, *61*, 1201A.
- Haakanson, P.; Sundqvist, B. U. R. *Vacuum* **1989**, *39*, 397.
- Barber, M.; Bordoli, R. S.; Sedgwick, R. D.; Tyler, A. N. *J. Chem. Soc., Chem. Commun.* **1981**, 244.
- Fenn, J. B.; Mann, M.; Meng, C. K.; Wong, S. F.; Whithouse, C. M. *Science* **1989**, *246*, 64.
- Karas, M.; Hillenkamp, F. *Anal. Chem.* **1988**, *60*, 2301.
- Very recent studies have demonstrated that structurally informative fragment ions can be obtained for peptides, but the amount of sample required is quite large. See, for example: Vorst, H. J.; van Tilborg, M. W. E. M.; van Veen, P. A.; Tjaden, U. R.; van der Greef, J. *Rapid Commun. Mass Spectrom.* **1990**, *4*, 202.
- Smith, R. D.; Loo, J. A.; Barings, C. J.; Edmonds, C. G.; Udseth, H. R. *J. Am. Soc. Mass Spectrom.* **1990**, *1*, 53.
- Tomer, K. B. *Mass Spectrom. Rev.* **1989**, *8*, 445.
- (a) Mallis, L. M.; Russell, D. H. *Anal. Chem.* **1986**, *58*, 1076. (b) Russell, D. H.; McGlochin, E. S.; Mallis, L. M. *Anal. Chem.* **1988**, *60*, 1818. (c) Mallis, L. M.; Rauschel, F. M.; Russell, D. H. *Anal. Chem.* **1987**, *59*, 980. (d) Tang, X.; Ens, W.; Standing, K. G.; Westmore, J. B. *Anal. Chem.* **1988**, *60*, 1791. (e) Renner, D.; Spittler, G. *Biochem. Environ. Mass Spectrom.* **1988**, *15*, 75. (f) Grese, R. P.; Cerny, R. L.; Gross, M. L. *J. Am. Chem. Soc.* **1989**, *111*, 2655. (g) Leary, J. A.; Williams, T. D.; Bott, G. *Rapid Commun. Mass Spectrom.* **1989**, *3*, 192. (h) Leary, J. A.; Zhou, Z.; Ogden, S. A.; Williams, T. D. *J. Am. Soc. Mass Spectrom.* **1990**, *1*, 473. (i) Teesch, L. M.; Adams, J. J. *Am. Chem. Soc.* **1990**, *112*, 4110. (j) Teesch, L. M.; Adams, J. J. *Am. Chem. Soc.* **1991**, *113*, 812.
- Cooks, R. G. In *Collision Spectroscopy*; Cooks, R. G., Ed.; Plenum Press: New York, 1978.
- (a) Tecklenburg, R. E., Jr.; Miller, M. N.; Russell, D. H. *J. Am. Chem. Soc.* **1989**, *111*, 1161. (b) Tecklenburg, R. E., Jr.; Russell, D. H. *Mass Spectrom. Rev.* **1990**, *9*, 405. (c) Martin, S. A.; Hill, J. A.; Kittrell, C.; Biemann, K. *J. Am. Soc. Mass Spectrom.* **1990**, *1*, 107.
- (a) Mabud, M. A.; Dekrey, M. J.; Cooks, R. G. *Int. J. Mass Spectrom. Ion Processes* **1985**, *67*, 285. (b) Aberth, W. *Anal. Chem.* **1990**, *62*, 609.
- Orlando, R.; Fenselau, C.; Cotter, R. J. *Anal. Chem.* **1990**, *112*, 5747.
- Caldwell, K. A.; Gross, M. A. Proceedings of the 39th ASMS Conference on Mass Spectrometry and Allied Topics, Nashville, TN, May 19-24, 1991; p 122.
- Cooks, R. G.; Busch, K. L.; Glish, G. L. *Science* **1983**, *222*, 273.
- Tecklenburg, R. E., Jr.; Castro, M. E.; Russell, D. H. *Anal. Chem.* **1989**, *61*, 153. See also: Olthoff, J. K.; Cotter, R. J. *Nucl. Instrum. Methods Phys. Res.* **1987**, *B26*, 566.
- Strobel, F. H.; Solouki, T.; White, M. A.; Russell, D. H. *J. Am. Soc. Mass Spectrom.* **1991**, *2*, 91.
- (a) Hill, J. A.; Biller, J. E.; Martin, S. A.; Biemann, K.; Yoshidome, K.; Sato, K. *Int. J. Mass Spectrom. Ion Processes* **1989**, *92*, 211. (b) Ishihara, M.; Kammei, Y. *Rapid Commun. Mass Spectrom.* **1989**, *3*, 420. (c) Brunnee, C.; Pesch, R.; Schröder, E. *Rapid Commun. Mass Spectrom.* **1990**, *4*, 173.
- (a) Stults, J. T.; Enke, C. G.; Holland, J. F. *Anal. Chem.* **1983**, *55*, 1323. (b) Holland, J. F.; Enke, C. G.; Allison, J.; Stults, J. T.; Pinkston, J. D.; Newcome, B.; Watson, J. T. *Anal. Chem.* **1983**, *55*, 997A. (c) Erickson, E. D.; Enke, C. G.; Holland, J. F.; Watson, J. T. *Anal. Chem.* **1980**, *62*, 1079.
- (a) Russell, D. H. *Mass Spectrom. Rev.* **1986**, *5*, 167. (b) James, C. F.; Wilkins, C. L. *J. Am. Chem. Soc.* **1988**, *110*, 2687. (c) Henry, K. D.; Williams, E. R.; Wang, B. H.; McLafferty, F. W.; Shabanowitz, J.; Hunt, D. F. *Proc. Natl. Acad. Sci. U.S.A.* **1989**, *86*, 9075. (d) Lebrilla, C. B.; Wang, D. T.-S.; Hunter, R. L.; McIver, R. T., Jr. *Anal. Chem.* **1990**, *62*, 878. (e) Henry, K. D.; McLafferty, F. W. *Org. Mass Spectrom.* **1990**, *25*, 490. (f) Marshall, A. G.; Grosshans, P. B. *Anal. Chem.* **1991**, *63*, 215A.
- Cooks, R. G.; Glish, G. L.; McLuckey, S. A.; Kaiser, R. E. *Chem. Eng. News* **1981**, *59* (12, March 25), 26.
- (a) Schey, K.; Cooks, R. G.; Grix, R.; Wolnik, H. *Int. J. Mass Spectrom. Ion Processes* **1987**, *77*, 49. (b) Standing, K. G.; Ens, W.; Tang, X.; Westmore, J. B. In *Mass Spectrometry of Peptides*; Desiderio, D. M., Ed.; CRC Press: Boca Raton, FL, 1991; p 159-170. (c) Tang, X.; Ens, W.; Mayer, F.; Standing, G. *Rapid Commun. Mass Spectrom.* **1989**, *3*, 443-448.
- Evans, S.; Graham, R. *Adv. Mass Spectrom.* **1974**, *6*, 429.
- Stults, J. T.; Enke, C. G.; Holland, J. F. *Anal. Chem.* **1983**, *55*, 1323. (b) Stults, J. T.; Holland, J. F.; Watson, J. T.; Enke, C. G. *Int. J. Mass Spectrom. Ion Processes* **1986**, *71*, 169.
- Glish, G. L.; Goeringer, D. E. *Anal. Chem.* **1984**, *56*, 2291. (b) Glish, G. L.; McLuckey, S. A.; McKown, H. S. *Anal. Instrum.* **1987**, *16*, 191.
- Della-Negra, S.; Le Beyec, Y. *Anal. Chem.* **1985**, *57*, 2035. (b) Tang, X.; Ens, W.; Standing, K. G.; Westmore, J. B. *Anal. Chem.* **1988**, *60*, 1791.
- Proceedings of the 38th ASMS Conference on Mass Spectrometry and Allied Topics, Tucson, AZ, June 3-8, 1990; p 1575.
- Bergmann, T.; Martin, T. P.; Schaber, H. *Rev. Sci. Instrum.* **1990**, *61*, 2592.
- Cooks, R. G.; Beynon, J. H.; Caprioli, R. M.; Lester, G. R. *Metastable Ions*; Elsevier Scientific Publishing: Amsterdam, 1973; p 40.
- Cooks, R. G.; Beynon, J. H.; Caprioli, R. M.; Lester, G. R. *Metastable Ions*; Elsevier Scientific Publishing Co.: New York, 1973; p 104-120.
- Della-Negra, S.; Le Beyec, Y. *Int. J. Mass Spectrom. Ion Processes* **1984**, *61*, 21.
- Eland, J. H. D. *Int. J. Mass Spectrom. Ion Phys.* **1972**, *8*, 143.
- (a) Della-Negra, S.; Le Beyec, Y.; Hakansson, P. *Nucl. Instrum. Methods Phys. Res.* **1985**, *B9*, 103. (b) Robertson, J. B.; Williams, P. In *Advances in Mass Spectrometry*; Kendrick, E., Ed.; Institute of Petroleum: London, 1968; Vol. 4, p 847; (c) McAfee, C. D. Ph.D. Dissertation, Texas A&M University, Department of Chemistry, May 1990.
- Price, D.; Milnes, G. J. *Int. J. Mass Spectrom. Ion Processes* **1990**, *99*, 1. (b) Opsal, R. B.; Owens, K. G.; Reilly, J. P. *Anal. Chem.* **1985**, *57*, 1884.
- (a) Standing, K. G.; Chait, B. T.; Ens, W.; McIntosh, G.; Beavis, R. *Nucl. Instrum. Methods* **1982**, *198*, 33. (b) Hues, S. M.; Colton, R. J.; Wyatt, J. R. *Rev. Sci. Instrum.* **1989**, *60*, 1239.
- Tecklenburg, R. E., Jr.; Castro, M. E.; Russell, D. H. *Anal. Chem.* **1989**, *61*, 153.
- Ens, W.; Mao, Y.; Mayer, F.; Standing, K. G. *Rapid Commun. Mass Spectrom.* **1991**, *5*, 117.
- Torgerson, D. F.; Skowronski, R. P.; Macfarlane, R. D. *Biochem. Biophys. Res. Commun.* **1974**, *60*, 616.
- Roepstorff, P.; Fohlmann, J. *Biomed. Mass Spectrom.* **1984**, *11*, 601.
- Emery, W. B.; Cooks, R. G.; Toren, P. C. *Anal. Chem.* **1986**, *58*, 1218.
- (a) Neuman, G. M.; Derrick, P. J. *Org. Mass Spectrom.* **1984**, *19*, 165. (b) Neuman, G. M.; Shell, M. M.; Derrick, P. J. *Z. Naturforsch., A: Phys.-Phys. Chem., Kosmophys.* **1984**, *39*, 584. (c) Cooks, R. G. In *Collision Spectroscopy*; Cooks, R. G., Ed.; Plenum Press: New York, 1978; pp 357-450.
- Alexander, A. J.; Boyd, R. K. *Int. J. Mass Spectrom. Ion Phys.* **1989**, *90*, 211.
- Bricker, D. L.; Russell, D. H. *J. Am. Chem. Soc.* **1986**, *108*, 6174.
- Alexander, A. J.; Thibault, P.; Boyd, R. K. *J. Am. Chem. Soc.* **1990**, *112*, 2484.
- Hop, C. E. C. A.; Holmes, J. L. *Org. Mass Spectrom.* **1991**, *26*, 476.
- Tajima, S.; Tobita, S.; Ogino, K.; Niwa, Y. *Org. Mass Spectrom.* **1987**, *21*, 236.

Mass Discrimination in Laser Desorption/Fourier Transform Ion Cyclotron Resonance Mass Spectrometry Cation-Attachment Spectra of Polymers

Jeremiah D. Hogan and David A. Laude, Jr.*

Department of Chemistry and Biochemistry, The University of Texas at Austin, Austin, Texas 78712

A mass discrimination effect is demonstrated in laser desorption/ionization (LDI)/Fourier transform ion cyclotron resonance mass spectrometry (FTICR) data for low molecular weight poly(ethylene glycol) (PEG) samples mixed with potassium halide salts. This effect is attributed to factors that influence the relative overlap of gas-phase neutral and ion populations that react to form the cation-attached products detected by FTICR. Specifically, these factors include laser power density and reactant masses which determine velocity distributions, trap potential which serves as an energy filter for detected product ions, and distance between trapped ion cell and desorption site. For example, the number averaged molecular weights, M_n , for PEG-600, PEG-1000, and PEG-1500 samples vary by 7, 10, and 12%, respectively, as the desorption site is displaced over a 10-cm distance from the cell. The polydispersity value for a standard PEG-1000 sample, as determined by vapor-phase osmometry, is achieved at probe distances of 5.4, 7.2, and 8.2 cm, respectively, when different salts, KF, KBr, and KI, are mixed with the polymer. All data are consistent with an ionization mechanism in which a distribution of desorbed low-energy polymer neutrals reacts in the cell with the low-energy tail of a salt adduct population. The well-defined polymer distribution is demonstrated to provide effective time resolution in defining the gas-phase reactions that occur in the FTICR experiment but are not otherwise discernible on the time scale of the detection process.

Mass spectrometry is increasingly used to directly determine the molecular weight and structure of organic polymer distributions without a preliminary chromatographic step to separate the individual oligomeric units.¹⁻¹⁸ This has become possible with the development of ionization techniques that minimize fragmentation and extend the accessible mass range for these typically larger, nonvolatile materials. For example, field desorption (FD),³ plasma desorption (PD),⁶ fast atom bombardment (FAB),⁵ electrohydrodynamic ionization (EH),¹ electrospray ionization (ESI),¹⁶ and laser desorption/ionization (LDI)⁷ all have been applied to assorted polymers to obtain average molecular weight distributions.^{19,20} Of these, LDI is recommended because it is easily interfaced to both time-of-flight (TOF) mass analyzers which are capable of very high mass-to-charge detection¹⁴ and FTICR which offers high mass resolution and accuracy.^{11,13,15,17,18}

Any evaluation of a new mass spectrometric technique for polymer analysis must focus on the extent to which mass discrimination in the molecular weight assignment occurs in each phase of the experiment, including sample volatilization, ionization, mass selection, and detection. Several comparison experiments have been conducted to determine which techniques are most suitable.^{5,7,9,13,15} For example, in studies using low molecular weight poly(ethylenimines) (PEIs), FD, FAB, EH, and LDI/TOF all yielded molecular weight values that were significantly lower than expected.^{5,9,14} These results contrast with LDI/FTICR experiments that yielded data

consistent with reference values.¹³ In general, better results were obtained with low molecular weight poly(ethylene glycols) (PEGs), as EH, FD, LDI/TOF, and LDI/FTICR yielded molecular weight distributions in good agreement with reference values,^{7,13} although FAB again yielded lower than expected results.⁵ Finally, LDI/FTICR comparisons with secondary ion and FAB results for a series of alkoxyated pyrazoles again contrasted the capabilities of LDI with the limitations of FAB.¹⁵ Summarizing, with the few exceptions noted above, EH, FD, LDI/TOF, and LDI/FTICR are demonstrated to be effective alternatives to more traditional methods for determination of molecular weight distributions. In contrast, FAB yields poor quantitative information because of extensive fragmentation and is not recommended.

The conclusion of LDI/FTICR polymer work performed to date is that mass discrimination effects do not occur in either the ion formation, selection, or detection process.^{13,18} However, as a result of our examination of the general mechanism for ion formation and trapping in the infrared LDI/FTICR experiment,²¹⁻²³ we believe that a well-defined mass selectivity effect associated with the gas-phase formation of analyte species does alter the relative ion abundances in LDI/FTICR spectra. This is because in contrast with other infrared LDI mechanisms for ion formation that occur at the desorption surface,^{24,25} the cationization of polymers and other nonvolatile organic molecules involves the gas-phase overlap of neutral and salt ion populations that react to yield a product ion population that is accessible to the mass analyzer.^{26,27} Consequently, if the relative gas-phase evolution of desorbed neutral and ion precursor distribution is altered, then mass discrimination will occur during FTICR trapping of product ions to be detected. Although this effect is transparent in most LDI spectra of organic molecules because a single product ion dominates, quantitative differences should be present in the envelope of product ions used to determine polymer molecular weight distributions.

It should be emphasized that conclusions drawn from LDI/FTICR experiments to be presented do not necessarily extend to LDI/TOF because even for identical LDI and sample conditions, the ion population to be sampled is unlikely to be the same for the two mass analyzers. Several distinctions can be drawn between the two techniques, including the FTICR strong magnetic field that reduces the radial dispersion of the desorbed ion cloud, the different electric fields experienced by the product ions (kilovolt acceleration fields for TOF compared to low-voltage trapping potentials for FTICR), microsecond time scales for TOF detection compared to hundreds of milliseconds for FTICR, and finally, the very different ion source geometries and dimensions. Even though Gross verified that infrared LDI/FTICR cation attachment occurs in the gas phase,²⁷ the qualitative differences often observed between LDI/TOF and LDI/FTICR spectra suggest that different ion formation and selection processes are occurring. In support of this, we have observed that whereas cation attachment in LDI/TOF is assumed to involve the reaction of the bare metal cation such as K^+ or Na^+ with the neutral,²⁶ in the LDI/FTICR experiment an adduct ion from

the salt can be the direct precursor in the reaction.^{22,23}

In work to be presented, low molecular weight PEGs will be evaluated by LDI/FTICR to assess the extent of mass discrimination associated with the gas-phase ionization process. If mass discrimination does occur during ionization, then any parameter that alters the temporal and spatial evolution of either neutral or salt adduct populations would alter the calculated molecular weight. The primary factors involved are those that affect the velocity of reactive species and include laser power density and salt and polymer mass. Even the potential applied to FTICR trap plates will influence polymer distribution if, for example, there is a kinetic energy dependence to the temporal evolution of the precursor ion population. The discrimination effect should be amplified by varying the distance between the trapped ion cell and laser desorption site since the overlap of neutral and performed ion populations of different velocities in the cell will change; a probe mounted fiber optic laser interface developed in our lab is used to control this parameter.²¹

EXPERIMENTAL SECTION

All LDI/FTICR spectra were acquired with instrumentation and procedures described in detail elsewhere.²¹ Briefly, the FTICR spectrometer consists of a 3.0 T superconducting magnet, two cubic trapped ion cells of 5-cm dimension which share a common trap plate, a vacuum chamber that is diffusion-pumped to base pressures in the 10^{-9} Torr range, and a data system and analog electronics from the Nicolet Analytical Instruments FTMS 2000. LDI is accomplished with a Spectra Physics Model DCR-11 Nd:YAG laser capable of 8-ns, 275-mJ pulses at 1064 nm. As much as 30 mJ per pulse of laser light can be transmitted from the laser to the sample through a high-power fiber optic. Unfocused light exiting the fiber creates a 0.9-mm² spot size on the sample probe which calculates to a maximum laser power density of about 3×10^8 W/cm². Both fiber optic and sample probe are housed in a hollow, vacuum-sealed 3/4-in. stainless steel probe that can be translated over a 40-cm distance along the z-axis centerline of the vacuum chamber from the trapped ion cell to a region in the fringing magnetic field.

Samples were prepared by aspirating a potassium halide salt dissolved in a 50/50 mixture by volume of acetone and water onto a spinning stainless steel probe tip, followed by a PEG dissolved in methylene chloride. PEG-600, PEG-1000, and PEG-1500 samples (Polyscientific Inc.) were obtained with polydispersity values, M_w/M_n , certified from vapor-phase osmometry at 1.05, 1.09, and 1.05, respectively. Samples were dried in a vacuum oven, positioned on the fiber optic probe assembly, and inserted in the FTICR vacuum chamber. Spectra were acquired when pressures returned to the low 10^{-8} Torr range. Unless otherwise stated, standard parameters for the LDI/FTICR experiment are as follows. FTICR spectra resulted from a single laser firing on fresh sample with an estimated power density of 3×10^8 W/cm². Product ions were trapped and detected without transfer in the source-trapped ion cell that was continuously maintained at 2.0 V. A 1-s delay permitted the return to base pressures. During this time, K⁺ ions were ejected to minimize space charge effects. A 2.66-MHz broadband linear frequency sweep was applied at the rate of 3200 Hz/ μ s to excite the cyclotron motion of the ions for detection. Direct observation of an 800-kHz window with 32K data yielded spectra with resolution of 600 at mass 1000. Shot to shot reproducibility for identical experimental parameters was excellent, with less than 2% variation in the calculation of average molecular weight. This, combined with the ability to obtain several hundred laser shots on a fresh sample for each sample preparation, gave the required reproducibility when varying experimental parameters.

Transients were base-line corrected and sine bell apodized, an equivalent number of zeros was appended to the data set, and a magnitude mode Fourier transform was performed. Data was then processed to obtain number-average (M_n) and weight-average (M_w) molecular weights as well as the polydispersity (M_w/M_n) of the sample.^{19,20} Several schemes for extracting and processing numerical data were evaluated. These included using peak heights, peak areas as determined from an Extrel software in-

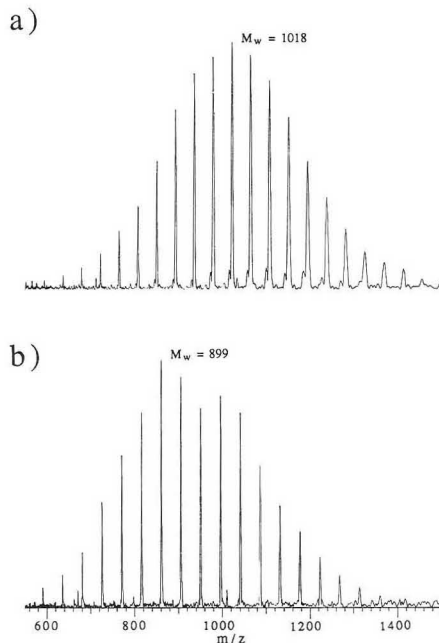


Figure 1. LDI/FTICR spectra of PEG-1000: (a) polymer mixed with KBr, probe sample tip positioned 4 cm from the trapped ion cell, laser power density set to 7×10^7 W/cm², and trap potential of 1.5 V to yield $M_w = 1018$, $M_n = 997$, and $M_w/M_n = 1.02$; (b) polymer mixed with KF, probe sample tip positioned 14 cm from the cell, laser power density at 3×10^8 W/cm², and trap potential of 2.0 V to yield $M_w = 899$, $M_n = 804$, and $M_w/M_n = 1.12$.

tegration routine, and peak areas determined by simple triangulation. All yielded essentially identical results for several sets of PEG-1000 spectra. Given this, and because the relative rather than absolute variation in average molecular weight was of greatest concern here, peak heights were used to process the data.

It was of interest to determine the magnitude of the mass discrimination effect as a function of systematically varied experimental parameters. For example, variable laser power density experiments were performed over the threshold range from 1×10^7 W/cm² to 3×10^8 W/cm². Variable trapping potential data was performed over a 1–3-V range; outside this narrow trapping window, signal magnitudes were either too low or reproducibility was poor. The probe-mounted interface permitted the sample to be displaced from within 1 mm of the trapped ion cell to a 15-cm distance from the cell with both good S/N and spectral reproducibility achieved. Beyond a 15-cm distance from the cell, S/N diminished rapidly.

RESULTS AND DISCUSSION

M_n , M_w , and M_w/M_n values were obtained from LDI/FTICR spectra of PEG/salt mixtures under different conditions. The results are compiled in Table I and will be displayed graphically in several figures to emphasize important trends. What the tabulated data clearly indicate are systematic variations in M_w , as much as 8%, M_n , as much as 14%, and M_w/M_n , as much as 6%. These variations are a function of polymer size, type of salt, laser power density, trapping potential, and probe position change. For example, the two spectra of PEG-1000 in Figure 1 are for data collected under ordinary, but different LDI/FTICR conditions, which nevertheless exhibit large differences molecular weight distributions. As will be discussed, the spectrum in Figure 1a was

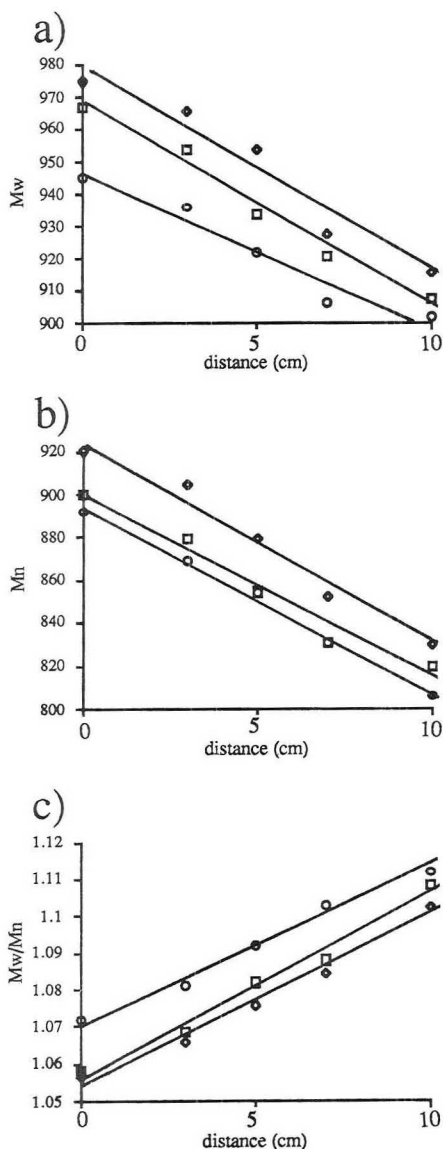


Figure 2. Sample probe displacement profiles of (a) M_w values; (b) M_n values; (c) M_w/M_n values extracted from LDI/FTICR spectra of PEG-1000 mixed with KF, O; KBr, □; and KI, ◇. For all data, a 2.0-V trap potential and 3×10^8 W/cm² laser power density was used.

acquired with conditions that favored detection of the higher oligomers, including the use of a lower trap potential and a lower molecular weight salt; calculated M_w , M_n , and M_w/M_n values were 1018, 997, and 1.02, respectively. In contrast, Figure 1b was acquired under conditions that favored detection of low-mass oligomers, including the use of a larger trap potential and a larger molecular weight salt; calculated M_w , M_n , and M_w/M_n values were 899, 804, and 1.12, respectively. From vapor-phase osmometry, the standard M_w/M_n value of 1.09 lies between these two extremes. The balance

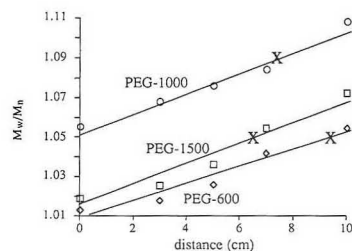


Figure 3. Probe displacement profiles demonstrate the variation in polydispersity for various polymer/KBr samples (PEG-1000, O; PEG-1500, □; PEG-600, ◇) as distance between sample probe tip and trapped ion cell increases. Data are for a 3×10^8 W/cm² laser power density and 2-V trap potentials. The M_w/M_n from osmometry data is noted by X and corresponds to optimum distances of 9.4, 7.3, and 6.5 cm for the PEG-600, PEG-1000, and PEG-1500, respectively.

of the paper will demonstrate that the differences in the data are consistent with selective trapping of ions formed in the LDI/FTICR experiment.

Figure 2 presents probe-displacement for PEG-1000 with different salts. In Figures 2a and 2b both M_w and M_n decrease as desorption occurs at increasing distances from the cell. In Figure 2c polydispersity is observed to increase with probe displacement, evidently because M_n decreases at a faster rate than M_w . The choice of salt also appears to influence the values for M_w , M_n , and M_w/M_n that are obtained. The general trend is that for any particular probe displacement, the larger the molecular weight of the potassium halide salt that is used, the larger the calculated average molecular weight and the lower the polydispersity for the polymer. Thus for these data at a 2.0-V trap potential and laser power density of 3×10^8 W/cm², the reference M_w/M_n value of 1.09 is obtained at optimum probe displacements of 5.4, 7.2, and 8.2 cm for KF, KBr, and KI, respectively.

Presented in Figure 3 are results from additional probe displacement studies in which LDI/FTICR spectra are acquired for KBr mixed with PEG-600, PEG-1000, PEG-1500. Again, as in Figure 2, for polymers of different average size the polydispersity data increase linearly with increasing probe displacement. The validity of the data in Figure 3 is supported by independent determinations of polydispersity for each of the PEGs; in each case these independent values are bounded in the LDI/FTICR probe displacement results and suggest optimum positions of 9.4, 7.2, and 8.2 cm for PEG-600, PEG-1000, and PEG-1500, respectively. The trend to reduced probe displacement for polymers of larger size indicates that LDI/FTICR analyses of larger polymers performed by other groups with the probe adjacent to the cell are decreasingly subject to this type of mass discrimination.

Data in Figure 4 indicate that both laser power density and FTICR trap potential introduce a systematic bias in the determination of average molecular weight and polydispersity data. In Figure 4a, as laser power density increases, polydispersity increases. The trends are similar at two probe positions, although as would be expected from the data in Figures 2 and 3, larger polydispersity values are obtained with increased probe displacement. In neither profile is the reference polydispersity value of 1.09 for the PEG-1000 sample reached, but this is expected because as the data in Figure 3 indicate, at the maximum laser power of 3×10^8 W/cm² achieved with this interface, even greater probe displacement would be necessary.

The trend indicated in Figure 4b is that as trapping potential increases, polydispersity increases. The correlation of this parameter with mass discrimination is important because in contrast with power density and probe position which

Table I. Comparison of PEG M_w , M_n , and Polydispersity Values from LDI/FTICR Mass Spectrometry

salt	polymer	trapping potential, V	laser power, W/cm ²	probe distance, cm	M_w	M_n	M_w/M_n
KBr	PEG-600	2	3×10^8	4	573	565	1.014
				7	568	555	1.023
				9	560	542	1.033
				11	548	523	1.048
KBr	PEG-1000	2	3×10^8	14	534	501	1.066
				0	958	909	1.051
				4	945	892	1.059
				7	933	868	1.075
KBr	PEG-1500	2	3×10^8	9	923	850	1.086
				11	909	830	1.095
				14	899	804	1.118
				4	1488	1458	1.021
KF	PEG-1000	2	3×10^8	7	1481	1442	1.027
				9	1464	1412	1.037
				11	1452	1376	1.055
				14	1449	1350	1.073
KI	PEG-1000	2	3×10^8	4	967	900	1.074
				7	952	877	1.086
				9	933	851	1.096
				11	921	829	1.111
KBr	PEG-1000	1	3×10^8	14	904	814	1.123
				4	974	919	1.060
				7	964	900	1.071
				9	950	878	1.082
KBr	PEG-1000	2	3×10^7	11	928	849	1.093
				14	914	823	1.111
				0	993	949	1.046
				2	981	928	1.057
KBr	PEG-1000	1	3×10^8	3	973	911	1.069
				4	986	942	1.047
				2	985	926	1.064
				3	965	889	1.084
KBr	PEG-1000	2	3×10^7	0	1007	985	1.022
				8×10^8	989	959	1.031
				3×10^8	967	925	1.045
				3×10^7	1018	994	1.024
KBr	PEG-1000	2	3×10^8	5	998	965	1.034
				8×10^8	979	932	1.050

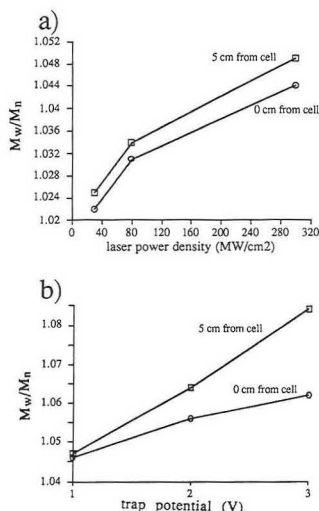


Figure 4. Profiles of polydispersity values extracted from LDI/FTICR spectra of PEG-1000/KBr. (a) Laser power is varied for spectra acquired with 2.0-V trap potential and sample probe positioned 0 cm (O) and 5 cm (□) from the trapped ion cell. (b) Trap potential is varied for spectra acquired with laser power density at 3×10^8 W/cm² and sample probe positioned 0 cm (O) and 5 cm (□) from the cell.

are less likely to be altered in standard LDI/FTICR experiments, the trap potential is routinely varied. Typically, low trap potentials are desired to simplify calibration and reduce space charge because fewer ions reside in the cell and radial trapping electric fields are reduced. Higher trapping potentials are often used to improve S/N by increasing the number of ions trapped in the deeper potential well. For the LDI/FTICR data presented here, only a narrow range of trapping potentials were effective in generating good quality polymer spectra. The two volt range used in Figure 4b contrasts with the ability to use very wide ranges of trap potentials with other types of ionization and attests to the delicate balance of ionization and trapping conditions necessary to generate desired cation-attachment products.

Mechanism for Mass Discrimination. It is well established that the cation-attachment process leading to formation of $(M + K)^+$ products shown in mass spectra in Figure 1 occurs in the gas phase.²⁶ We have further shown that the chemistry leading to formation of product ions detected by FTICR occurs in the trapped ion cell and involves the potassium salt adduct of the form $[K_x X_{x-1}]^+$ rather than K^+ .^{22,23} The comparison double resonance LDI/FTICR spectra in Figure 5 verify these aspects of the ion formation and trapping process. Shown in Figure 5a is a spectrum acquired from the mixture of PEG-1000/KBr with K^+ continuously ejected from the trapped ion cell. If K^+ was a precursor to this reaction occurring in the cell, then the abundant polymer envelope consisting of K^+ -attached oligomers would not be observed. However, this result does not rule out the possibility that chemistry involving K^+ occurs outside the cell with products subsequently pene-

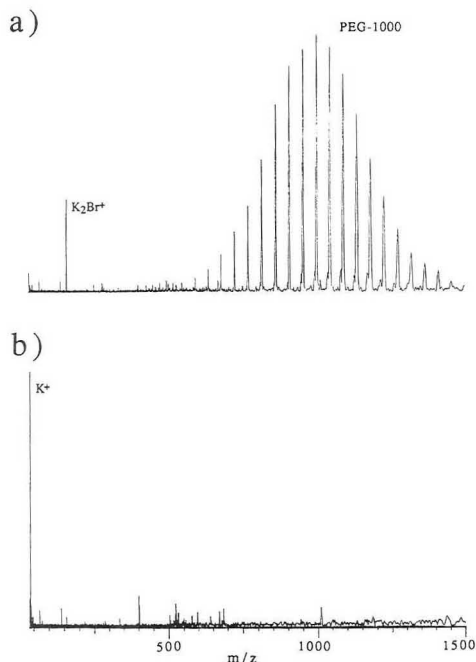


Figure 5. LDI/FTICR spectra of PEG-1000/KBr sample acquired at 3×10^8 W/cm² laser power density, 2.0-V trap potential, and sample probe tip positioned 4 cm from the cell. (a) Spectrum acquired with K^+ continuously ejected during the laser pulse and delay before excitation. (b) Spectrum acquired with K_2Br^+ continuously ejected during the laser pulse and delay before excitation.

trating the trapping electric field. However, the spectrum in Figure 5b acquired after continuous ejection of K_2Br^+ does discount this possibility and verifies two important features of cation-attachment reactions in the FTICR. First, the complete absence of polymer-related ions in Figure 5b indicates that K_2Br^+ is the exclusive precursor to $(M + K)^+$ formation. Second, the fact that ejection of the adduct is effective only inside the trapped ion cell excludes the possibility that external ion formation is of consequence to the FTICR experiment.

The double resonance experiments producing the data in Figure 5 have been reproduced for many organic samples, with probe displacement of up to 35 cm from the cell. The idea of gas-phase populations of neutrals and salt ions traversing such distances is in contrast with TOF experiments in which cation attachment occurs within a few millimeters of the entrance to the flight tube. The difference is likely due to the strong radial confining nature of FTICR magnetic field. A second distinctive feature of the LDI/FTICR experiment is that a salt adduct is the precursor to the cation-attachment process. Again, these data contrast with TOF work in which the precursor ion is assumed to be the bare cation. Variable trapping potential studies on LDI of pure salts provide insight into the distinction between the TOF and FTICR experiments. As is shown in Figure 6, the distribution of desorbed K^+ for each salt is much more energetic than the corresponding adduct. Thus in contrast with TOF, FTICR is disposed to select against K^+ attachment products at the typical trap potentials used for infrared LDI experiments. Moreover, in experiments in which the probe is increasingly displaced from the cell, the attachment of neutrals to K^+ in the cell is disfavored because the larger molecular weight

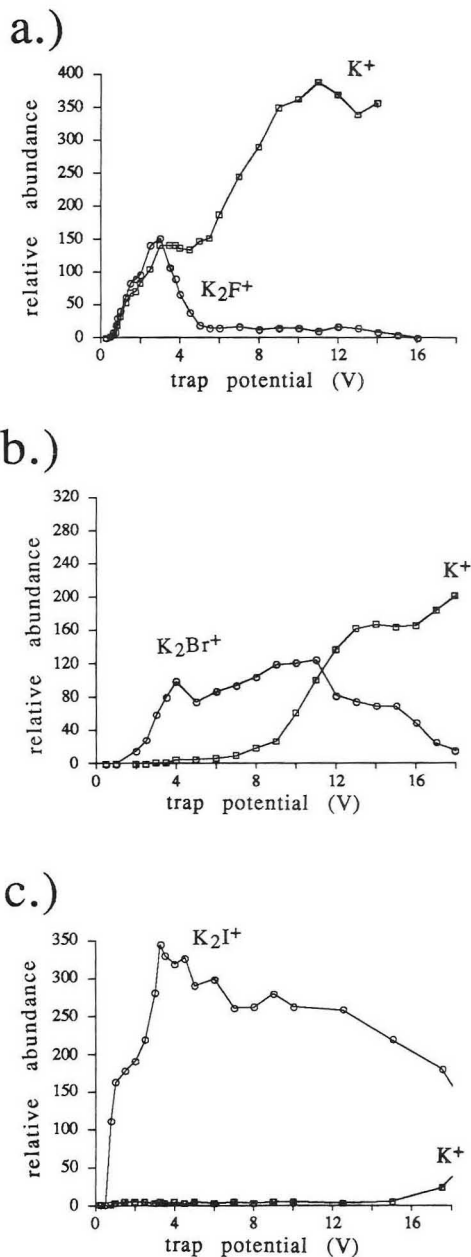


Figure 6. Profiles of LDI/FTICR signal intensities for K^+ (\square) and the adduct, K_2X^+ (\circ) of pure salts acquired at 3×10^8 W/cm² and 2.0 V trap potentials. Profiles are for (a) KF, (b) KBr, and (c) KI.

neutrals would require enormous kinetic energies to achieve velocities that would ensure concurrent arrival in the cell with K^+ . Time-resolved studies of the LDI process indicate that K^+ is actually desorbed before the neutral, which makes the overlap of K^+ and neutral populations in the FTICR experiment even less likely.²⁸ An alternative explanation for K^+

reactivity in the FTICR experiment involves the arrival and trapping of K^+ in the cell, with subsequent reaction with later arriving neutrals. However, this process is contradicted by double-resonance experiments which indicate $(M + K)^+$ is formed in the absence of K^+ in the cell.

A mechanism is now suggested for cation attachment in the LDI/FTICR experiment that is consistent with both the double resonance experiments and the profiles in Figures 2-4. The data suggest that any aspect of the LDI/FTICR experiment that alters the time evolution of polymer and K_2X^+ distributions should alter the relative abundance of ions detected by FTICR. However, whereas this is difficult to evaluate from LDI/FTICR spectra of most pure materials which yields a single spectral peak, the broad, well-defined mass envelope of polymer ions provides an excellent calibration of the extent of change in the evolution of gas-phase reactants. Before presenting our suggestion for the evolution of the LDI process, an obvious alternative is considered. If salt adducts are desorbed from the sample prior to the neutrals, then it is possible that the adducts are trapped and later react with neutrals. This mechanism is similar to the one proposed for K^+ earlier, but in this case, it is supported by the double resonance data. However, this mechanism still conflicts with the data in Figures 2-4 because it would require an invariance of detected polymer distributions to changes in experiment parameters.

As an alternative mechanism, we believe the data are consistent with near simultaneous evolution of broad envelopes of both intact neutrals and salt adduct ions. As the polymer distribution evolves in the gas phase, lower mass oligomers concentrate at the leading edge of the distribution and larger oligomers concentrate at the trailing edge of the distribution. Also, as the data in Figure 5 indicate, the desorbed adduct ion population is not monoenergetic, and if there is a time-dependence to the desorption event, then later adducts are desorbed with decreasing kinetic energy and the adduct distribution increasingly exhibits a high-energy leading edge and low-energy tail. It is the relative overlap of these two evolving distributions in the trapped ion cell that is responsible for the mass discrimination observed. Consistency of the data in Figures 2-4 with this mechanism is now considered.

All probe displacement data exhibit a decrease in M_w and M_n as the distance between cell and probe increases. This is explained by assuming that an increased path length allows increasing overlap in the cell of the low energy tail of the salt adduct distribution with the lower mass, leading edge of the polymer distribution. This also explains the increase in polydispersity with probe displacement. Because the low mass ions preferentially undergo cationization, the increased number of low mass oligomers represented will enhance M_n over M_w , with a consequent increase in polydispersity.

The choice of salt will influence the distribution in two ways. First, the mass difference requires that for ions of equal kinetic energy, the lower mass ion will assume a higher velocity, for example, a value that is 45% higher in the case of K_2F^+ and K_2I^+ . Thus, low mass adduct ions with higher velocities would preferentially encounter the lower mass leading edge of the polymer distribution, which again enhances M_n and therefore increases M_w/M_n . The relative decrease in M_n and increase in the polydispersity in order $KI > KBr > KF$ is supported in Figure 2. However it is difficult to quantitate the results because as shown in Figure 6, each salt adduct exhibits a different kinetic energy profile. In general, the larger salt adducts exhibit a larger average kinetic energy profile than K_2F^+ which would tend to offset the mass difference in defining the relative overlap of ion and neutral profiles.

Profiles in Figure 3 indicate that the size of the polymer also influences the selection of experimental parameters. As

the polymer size increase, the optimum position for laser desorption is observed to decrease. This is consistent with the proposed mechanism because if the kinetic energy of the neutral PEGs is constant, then the average velocity of the population decreases and in order to effectively overlap with the appropriate region of the higher velocity adduct population, the probe must be positioned closer to the cell.

As shown in Figure 4a, laser power density is important in defining the geometry and energy characteristics of the desorbed plasma and therefore will influence the polymer distribution. As power density increases, the neutral polymer population is unlikely to achieve a velocity increase that is equal to the lower mass adduct ions. Consequently, overlap of the adduct with the low mass front edge of the polymer distribution will be enhanced and M_n will decrease. The model is supported by the data in Figure 4a which indicate that increasing the power density increases the polydispersity calculated for the polymer. These data are important because they demonstrate that the traditional interface for LDI/FTICR, in which the probe and cell are closely positioned, is still capable of exhibiting discrimination even when TOF effects on the neutral polymer population are small. Finally, the profiles in Figure 4b indicate that calculated polydispersity increases with trapping potential. This is also consistent with the model because an increased trap potential favors selection of higher velocity adducts that will overlap with the leading edge of the neutral polymer distribution. Consistent with the data are decreases in M_n and corresponding increases in polydispersity. These data support the argument for a time dependence to the kinetic energy distribution of the adduct population.

In summarizing these results, it is important to adopt a pragmatic perspective in evaluating LDI/FTICR for molecular weight determination or small organic polymers. Although the data support arguments for a mass selection process associated with ion formation and trapping, they also verify that for a wide range of experimental conditions, the technique yields highly reproducible results that are within a few percent of actual values. Such results compare favorably with the reproducibility and accuracy achieved with other mass spectrometry techniques. The data also indicate that selectivity in ion trapping is most severe for lower molecular weight polymers desorbed adjacent to the cell, and that as the size of the polymer increases, the discrimination effect decreases. However, the data do indicate that it is inappropriate to assume average molecular weight values can be determined absolutely, to any better than 5-10%, given the large number of variables that contribute to the effect. Primary standards would be required to calibrate instrument parameters for each different type of polymer to be analyzed if improved accuracy was necessary.

ACKNOWLEDGMENT

This work is supported by the Welch Foundation (F-1138), the Arnold and Mabel Beckman Foundation, and the National Science Foundation (CHE9013384 and CHE9057097).

Registry No. PEG, 25322-68-3; KBr, 7758-02-3; KF, 7789-23-3; KI, 7681-11-0.

REFERENCES

- (1) Lai, S.-T.; Chan, K. W.; Cook, K. D. *Macromolecules* **1980**, *13*, 953-956.
- (2) Lattimer, R. P.; Harmon, D. J.; Hansen, G.E. *Anal. Chem.* **1980**, *52*, 1808-1811.
- (3) Lattimer, R. P.; Hansen, G. E. *Macromolecules* **1981**, *14*, 776-780.
- (4) Chan, K. W. S.; Cook, K. D. *Org. Mass Spectrom.* **1983**, *18*, 423-425.
- (5) Lattimer, R. P. *Int. J. Mass Spec. Ion Proc.* **1983/1984**, *55*, 221-232.
- (6) Chait, B.T.; Shuping, J.; Field, F. H. *Int. J. Mass Spec. Ion Proc.* **1984**, *58*, 121-137.

- (7) Mattern, D. E.; Hercules, D. M. *Anal. Chem.* **1985**, *57*, 2041-2046.
- (8) Callahan, J. H.; Cook, K. D. 32nd Annual Conference on Mass Spectrometry and Allied Topics, San Antonio, TX, May 1984; Abstr. 552-553.
- (9) Lattimer, R. P.; Schulten, H. R. 33rd Annual Conference on Mass Spectrometry and Allied Topics, San Diego, CA, May 1985; Abstr. 409-410.
- (10) Schulten, H. R.; Lattimer, R. P. *Mass Spectrom. Rev.* **1984**, *3*, 231-315.
- (11) Brown, E. C.; Kovacic, P.; Wilkie, C. A.; Cody, R. B., Jr.; Kinsinger, J. A. *J. Polym. Sci., Polym. Lett. Ed.* **1985**, *23*, 453-463.
- (12) Lattimer, R. P.; Harris, R. E.; Schulten, H. R. *Rubber Chem. Technol.* **1985**, *58*, 577-621.
- (13) Brown, R. S.; Weil, D. A.; Wilkins, C. L. *Macromolecules* **1986**, *19*, 1255-1260.
- (14) Cotter, R. J.; Honovich, J. P.; Olthoff, J. K.; Lattimer, R. P. *Macromolecules* **1986**, *19*, 2996-3001.
- (15) Nuwaysir, L. M.; Wilkins, C. L. *Anal. Chem.* **1988**, *60*, 279-282.
- (16) Wong, S. F.; Meng, C. K.; Fenn, J. B. *J. Phys. Chem.* **1988**, *92*, 548-550.
- (17) Brenna, J. T. In *Microbeam Analysis*; Russell, P. E., Ed.; San Francisco Press, Inc.: San Francisco, 1989; pp 306-310.
- (18) Liang, Z.; Marshall, A. G.; Westmoreland, D. G. *Anal. Chem.* **1991**, *63*, 815-818.
- (19) Bikales, N. B. *Characterization of Polymers*; Wiley Interscience: New York, 1971; pp 55-57.
- (20) Slade, Jr., P. E., Ed. *Polymer Molecular Weights. Techniques of Polymer Evaluation*; Marcel Dekker: New York, 1975; Parts I and II, Vol. 4.
- (21) Hogan, J. D.; Beu, S. V.; Majidi, V.; Laude, D. A., Jr. *Anal. Chem.* **1991**, *63*, 1452-1457.
- (22) Hogan, J. D.; Laude, D. A., Jr. *Anal. Chem.* **1991**, *63*, 2105-2109.
- (23) Hogan, J. D.; Laude, D. A., Jr. *J. Am. Soc. Mass Spectrom.*, in press.
- (24) McCrery, D. A.; Ledford, E. B., Jr.; Gross, M. L. *Anal. Chem.* **1982**, *54*, 1435-1437.
- (25) Vertes, A.; DeWolf, M.; Juhasz, Gijbels, R. *Anal. Chem.* **1989**, *61*, 1029-1035.
- (26) Van Der Peijl, G. J. Q.; Haverkamp, J.; Kistemaker, P. G. *Int. J. Mass Spectrom. Ion Phys.* **1982**, *42*, 125-141.
- (27) Chiarelli, M. P.; Gross, M. L. *Int. J. Mass Spectrom. Ion Proc.* **1987**, *78*, 37-52.
- (28) Van Breemen, R. B.; Snow, M.; Cotter, R. J. *Int. J. Mass Spectrom. Ion Proc.* **1983**, *49*, 35-50.

RECEIVED for review September 30, 1991. Accepted December 31, 1991.

Pulsed Sample Introduction Interface for Combining Flow Injection Analysis with Multiphoton Ionization Time-of-Flight Mass Spectrometry

Alan P. L. Wang and Liang Li*

Department of Chemistry, University of Alberta, Edmonton, Alberta, Canada T6G 2G2

A pulsed sample introduction (PSI) interface is developed to combine flow injection analysis with a time-of-flight mass spectrometer. In PSI, sample molecules carried by a liquid carrier such as methanol at a flow rate of 0.5 mL/min are vaporized by passing through a heated capillary tube and then through a sample vaporizer of a high-temperature pulsed nozzle. The resulting sample vapors are introduced into the mass spectrometer in a pulsed form and ionized by laser-induced multiphoton ionization. The applicability of this interface for the detection of volatile and nonvolatile compounds is studied. It is found that a variety of chemicals including molecules with environmental or biological significance can be studied by this method. Preliminary studies of the performance of this interface are reported. It is shown that reproducible results from repeated injection of the same concentration of samples can be readily obtained. The average relative standard deviation is in the range 4-8%. No memory effects and severe peak tailing are found with this PSI interface. The detection limits of the present technique are compound dependent. For aniline, tryptamine, and indole-3-acetic acid, the detection limits are found to be 3, 4, and 140 ng, respectively. Excellent linearity over 2 orders of magnitude of analytical range can be obtained for quantitation. It is also shown that cluster formation during the supersonic expansion is not a major problem in this technique.

INTRODUCTION

Laser-induced multiphoton ionization has been shown to be a powerful method for the generation of ions in mass spectrometry.¹ With a tunable laser such as a dye laser system, both supersonic jet spectroscopy (SJS) and multiphoton ionization (MPI) mass spectrometry can be performed for chemical analysis. It has been demonstrated that a two-di-

mensional detection scheme based on the wavelength spectrum and mass spectrum can be uniquely used for molecular detection and structural analysis.²⁻⁶ Recently, in an attempt to extend both methods for the studies of biological chemicals, a number of novel sample desorption/vaporization techniques have been developed. These include laser desorption,⁷⁻¹⁰ fast atom bombardment,¹¹ and pulsed rapid heating.¹² In addition, supercritical fluid and high-pressure liquid injection have also been developed to introduce thermally labile and nonvolatile molecules into a time-of-flight mass spectrometer (TOFMS) for SJS and MPI.^{13,14}

However, for real sample analysis, it is often necessary to separate the complex mixture prior to the sample injection into a mass spectrometer. Thus, there is a great deal of interest to combine chromatography techniques such as high-performance liquid chromatography (HPLC) with a mass spectrometer for on-line detection and quantitation. The great challenge here is to develop suitable interfaces for introducing the liquid flow into the mass spectrometer without significant compromise in the operating conditions of either the HPLC system or the mass spectrometer. In the last two decades or so, several on-line interfaces have been developed for LC/MS with varying degrees of success.¹⁵⁻²⁴ Many excellent reviews on the development and applications of LC/MS can be found in the literature.²⁵ To our best knowledge, however, no suitable LC interfaces have yet been developed for SJS and MPI mass spectrometry.

There are some reports on the studies of combining HPLC or liquid injection into a supersonic jet with laser-induced fluorescence spectroscopy for molecular detection.^{26,27} Unfortunately, those interfaces are generally not suitable for laser ionization work. This is because a TOFMS, commonly used in laser ionization work, must be operated at the pressure less than 10⁻⁵ Torr whereas in the SJS/fluorescence detection experiments the pressure can be in the range 0.02-0.005 Torr.¹ In related work, Lubman and co-workers have developed an

interface for supercritical fluid injection into a supersonic beam mass spectrometer.^{13,14} Although this interface may not be suitable for HPLC experiments, their work provides valuable information for the future development of LC/MPI mass spectrometry in terms of mass spectrometer system designing and the general applicability of the MPI technique.

Here we report an interface to introduce the liquid flow into a time-of-flight mass spectrometer with MPI. Although the ultimate goal of this research is to develop a convenient interface for combining conventional HPLC with a TOFMS, this report is mainly focused on the development of fluid injection analysis (FIA)^{28,29} with SJS and MPI mass spectrometry. It should be noted that for the simplest FIA system, such as the one used here, one can view the flow injection analyzer as a HPLC system without a column. The operating conditions for its interface to a TOFMS are similar to those introducing the effluent of HPLC to a mass spectrometer. Thus, the study of FIA/TOF mass spectrometry would provide some information on the performance of the interface for the future work of LC/TOF mass spectrometry. In addition, there are several advantages of using FIA for SJS and MPI. FIA has the capability of introducing small-volume samples into the system in a rapid, precise way.²⁸ As demonstrated here, quantitation, which is not an easy task in desorption/MPI techniques,¹² can be readily performed with FIA. Using FIA, there is also a potential to automate the sample injection process. Moreover, it is possible to perform on-line sample derivatization²⁸ such as the addition of an absorption center to a molecule of interest. This unique feature should prove useful for MPI in the detection of molecules that possess no absorption centers at the chosen wavelength.

The interface described here differs from most reported LC/MS interfaces in which the sample molecules are introduced continuously into a quadrupole or sector mass spectrometer.¹⁵⁻²⁵ In light of the fact that a TOFMS detects ions in a discrete manner, continuous sample introduction into a TOFMS will reduce the sample utilization efficiency. Thus, the work described here utilizes a pulsed sample introduction (PSI) interface to introduce the sample vapor into the TOFMS in a pulsed form. Compared with a continuous sample introduction technique, PSI allows us to use a much larger diameter orifice to introduce a larger amount of sample vapor in a short pulse into the mass spectrometer without overloading the pumping system.

This PSI interface consists of two major parts: a heated capillary tube and a high-temperature pulsed nozzle. In the experiment, sample and liquid carrier are transported through a heated capillary tube to form aerosol droplets. These aerosols are entrained into the sample vaporizer of the nozzle where the sample is thermally vaporized. The nozzle allows the vapor to be injected into the TOFMS at a repetition rate determined by the ionization source.

In this paper, a time-of-flight mass spectrometer designed for combining FIA and HPLC with SJS and MPI is first described. The design and preliminary work on the performance of the PSI interface are then reported. This work is intended to demonstrate the feasibilities of the interface for combining FIA with SJS and MPI. No attempt is made to examine the effect(s) of every individual experimental parameter on the performance of the system.

EXPERIMENTAL SECTION

Figure 1 shows the schematic diagram of the experimental setup of flow injection analysis with SJS and MPI mass spectrometry. It consists of a linear time-of-flight mass spectrometer mounted vertically in a six-port cross pumped by a 6-in. diffusion pump (Varian Associated, Inc., Lexington, MA). The 1-m-long flight tube is differentially pumped by a 4-in. diffusion pump (Varian).

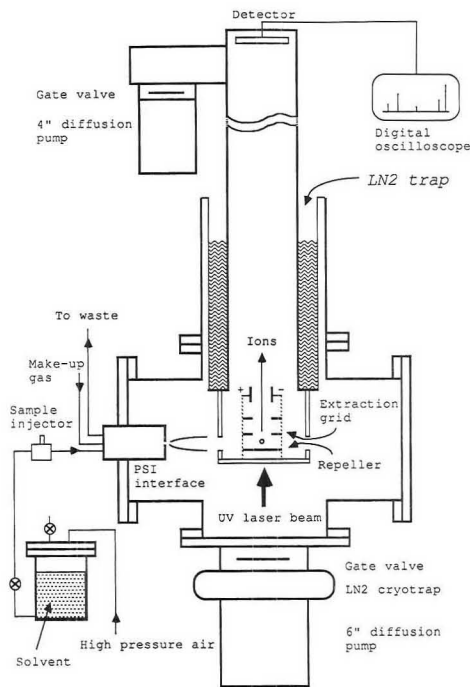


Figure 1. Schematic of the linear time-of-flight mass spectrometer for flow injection analysis.

A liquid nitrogen (LN2) trap assembly is used to cool part of the flight tube and the entire acceleration lens assembly (see Figure 1). The trap was manufactured by R. M. Jordan Co. (Grass Valley, CA) to our specifications. All other vacuum components were constructed in-house.

The use of a LN₂ trap results in significant reduction of background signals and the vacuum pressure. Without LN₂ being filled in the trap, the pressure is normally at 5×10^{-7} Torr in the detector region when the nozzle is off. However, when the nozzle is open, the pressure rises to 2×10^{-5} Torr. After the LN₂ trap is filled, the pressures are 1×10^{-7} Torr with the nozzle off and 1.5×10^{-7} Torr with the nozzle on. It is found that this reduction of the vacuum pressure increases the ion signal intensity. In addition, it allows us to use higher voltages for ion acceleration without any problems such as arcing. It should be noted that when the system is continuously being operated, a full tank in the LN₂ trap (about 4 L) can last for about 5 h without refilling.

The ionization laser source is a 266-nm laser beam from a frequency-quadrupled Nd:YAG laser (GCR-3, Spectra-Physics, Mountain View, CA). The laser is operated at a repetition rate of 10 Hz. A combination of a concave and a convex lens is generally used to produce a beam 2–3 mm in diameter for ionization. The ions generated by the laser beam are extracted to the acceleration region and then are accelerated to the drift tube. Voltages up to 15 kV can be applied to both the repeller and the extraction grid through high-voltage vacuum feedthroughs (Ceramaseal, New Lebanon, NY). The power supplies are from Spellman High Voltage Electronics (Model RH5R20PN60, Plainville, NY). In general, the voltage applied to the extraction grid is about 500–1500 V less than the repeller voltage. This combination of voltage settings gives optimal sensitivity and mass resolution. The ions are detected by a microchannel plate detector (Galleo Electro-Optics Corp., Sturbridge, MA). The mass spectrum is recorded by a LeCroy 9400A digital oscilloscope. Data are then stored in an IBM-compatible 386SX PC for processing. The mass resolution of this system is typically about 300.

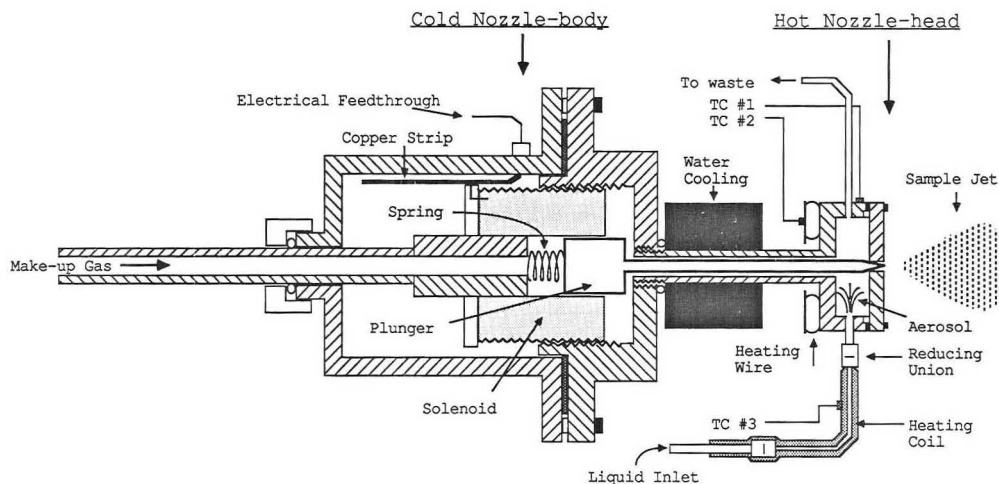


Figure 2. Schematic of the design of the pulsed sample introduction interface. Drawing is not to scale. The dimensions of the major components are given in the text.

The schematic diagram of the pulsed sample introduction interface is shown in Figure 2. This PSI interface consists of two important parts. One is the heated capillary tube in which the liquid flow is converted into aerosol droplets and/or super-saturated vapor. These aerosols are then expanded into the sample vaporizer for complete desolvation and vaporization. The heated capillary tube is a 5-cm-long, $1/16$ -in.-o.d. and 0.010-in.-i.d. stainless-steel tubing wrapped with a Nichrome 60 heating coil (Pelican Wire Co., Naples, FL). The sample vaporizer is part of the nozzle head of a high-temperature pulsed nozzle. This nozzle is designed to be used for flow injection analysis based on the earlier version of the high-temperature pulsed nozzle used for SJS reported by Li and Lubman.³⁰ It consists of two components, i.e., the nozzle body and the nozzle head, separated by a water cooling system.³⁰ The cold nozzle body contains a solenoid, which is used to drive a plunger for introducing the sample vapor to the mass spectrometer in a pulsed form. The nozzle head is heated during the operation for sample vaporization.

The current design of the nozzle body is similar to the one reported by Li and Lubman. It consists of a solenoid, a spring, and a plunger (see cold nozzle-body in Figure 2). The solenoid is a modified automobile fuel injection valve (Bosch, Part No. 0280150035, purchased from a local auto-parts store). The dimension of the solenoid is 25 mm in diameter and 32 mm in length. The electric feedthrough used to provide the current for driving the solenoid is constructed of Vespel that is threaded so that it screws into the stainless-steel body. A stainless-steel rod is epoxied into the Vespel using "Torr Seal" (Varian). A copper strip screwed on the rod is used to contact the lead of the solenoid. The power supply for driving this solenoid is similar to that reported.³¹ It can generate a 400-V pulse with a duration of ~ 35 μ s. In this experiment, a 100-V pulse is used to drive the solenoid.

The plunger is made of a long stainless-steel needle (1.5 mm in diameter and 55 mm in length) which screws into a steel base for magnetic attraction. The other end of the needle forms a metal-to-metal seal against the orifice. During the operation, a voltage is applied to the solenoid to generate a magnetic field that attracts the plunger away from the orifice to form a jet. When the power is off, the spring pushes the plunger against the orifice to make a seal. The leakage from the seal is negligible compared with the gas emitted per pulse. The sample pulse width is measured to be about 750- μ s fwhm.

The hot nozzle head contains a sample vaporizer, an aerosol inlet, and an outlet to waste. The sample vaporizer is heated by a coil of thermocouple heating wire (Phillips Electronic Instruments, Norcross, GA). A stainless-steel plate with a 500- μ m-diameter orifice is sealed to the nozzle head using a copper gasket and knife-edge seal. The dimension of the inner area of the nozzle

head in which aerosol expansion and vaporization takes place is 25 mm in diameter and 8 mm in length.

Three type-K thermocouples (TCs) are used to monitor the temperatures of the interface at different regions. In the studies reported here, the temperature of the nozzle front (TC #1 in Figure 2) is 425 °C. The temperature near the heating wire (TC #2) is 600 °C. The temperature of the heating coil (TC #3) is ~ 200 °C. The reading of this temperature depends on the position of the TC. In this experiment, TC #3 is located about 5 cm away from the nozzle head.

The FIA system consists of a pump driven by compressed gas, a metering valve for flow rate adjustment, and a sample injector (Rheodyne Model 7125 with a 20- μ L injection loop). Sample and carrier liquid are pumped to the PSI interface through a $1/16$ -in.-o.d. and 0.040-in.-i.d. stainless steel tubing. In this experiment, methanol is used as the carrier liquid with a flow rate of 0.5 mL/min. The flow rate is determined by measuring the volume of methanol consumed in a given time period. All samples are freshly made by using methanol as the solvent. All chemicals were purchased from Aldrich Chemical Co., Milwaukee, WI, or Sigma Chemical Co., St. Louis, MO, and used without further purification.

RESULTS AND DISCUSSION

Applicability of the Interface. Table I lists the compounds studied by this FIA with MPI time-of-flight mass spectrometry. The ionization laser beam is at 266 nm with its power density of $\sim (1-2) \times 10^8$ W/cm². The reason for choosing these compounds to demonstrate the applicability of this interface is mainly because they have been extensively studied by MPI in this laboratory with various vaporization/desorption techniques for sample introduction in a TOFMS. We have not yet tried other solvents for our interface. Throughout this study the experimental conditions are kept the same. The temperature of the heated capillary tube is 200 °C, and the temperature near the nozzle orifice is 425 °C. A makeup gas of CO₂ is used and its flow rate is optimized to be ~ 40 mL/min. The use of the makeup gas prevents sample and liquid carrier condensation which may occur due to their feedback from the nozzle's hot head to its cold body. It also provides a means of sweeping the sample and liquid carrier vapors out of the sample vaporizer rapidly, resulting in sharp peaks with less tailing (see below and Figure 4).

Figure 3 shows some typical MPI mass spectra of molecules studied by this FIA/MPI mass spectrometry. All peaks shown

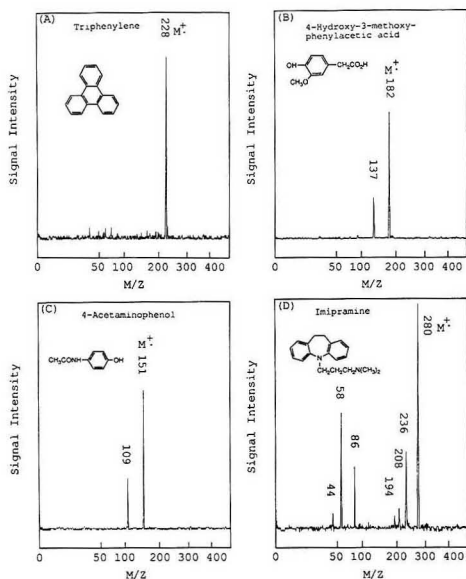


Figure 3. MPI mass spectra of (A) triphenylene, (B) 4-hydroxy-3-methoxyphenylacetic acid (homovanillic acid), (C) 4-acetaminophenol, and (D) imipramine. The ionization laser beam was at 266 nm with its power density $\sim 1 \times 10^6$ W/cm².

in Figure 3 are from the molecular ions and their fragments. No background signals are observed. One of the key results is that molecular ions are observed for most compounds studied. In general, no thermal-decomposed products are detected. The lack of thermal decomposition in this study can be attributed to the fact that the sample molecules are rapidly vaporized in the sample vaporizer. Moreover, the probability for the sample to make contact with the inner wall of the vaporizer is minimized due to the presence of large quantity of hot methanol vapor, resulting in the reduction of catalysis action of the metal surface.³² However, for anthranilic acid, as shown in Table I, only the thermally decomposed product is observed. This indicates that for thermally very labile compounds this interface involving rapid heating may still cause decomposition.

It should also be noted from Table I that this interface is capable of introducing both volatile and nonvolatile sample molecules into a TOFMS. The ability of the system to also detect highly volatile species is an important aspect of this interface technique. For nonvolatiles which can be dissolved in methanol, compounds with melting points as high as 325 °C (DL-tyrosine) can be transported into the mass spectrometer using the PSI interface. Work is planned to investigate the use of other liquid carriers and solvents for FIA/TOF mass spectrometry. The use of other carriers and solvents will extend the applicability of PSI to a wide range of important chemicals such as small peptides.

Precision and Memory Effects. Figure 4 illustrates a series of repeated injections of different concentrations of indole-3-acetic acid. In this experiment, the molecular ion intensity is monitored and integrated by a boxcar integrator. The averaged signal is recorded on a chart recorder to produce a flowgram. As Figure 4 shows, for five injections at each concentration, the peak areas are quite reproducible. The relative standard deviation (RSD) for each set of peaks is shown above these peaks in the figure. The key parameters

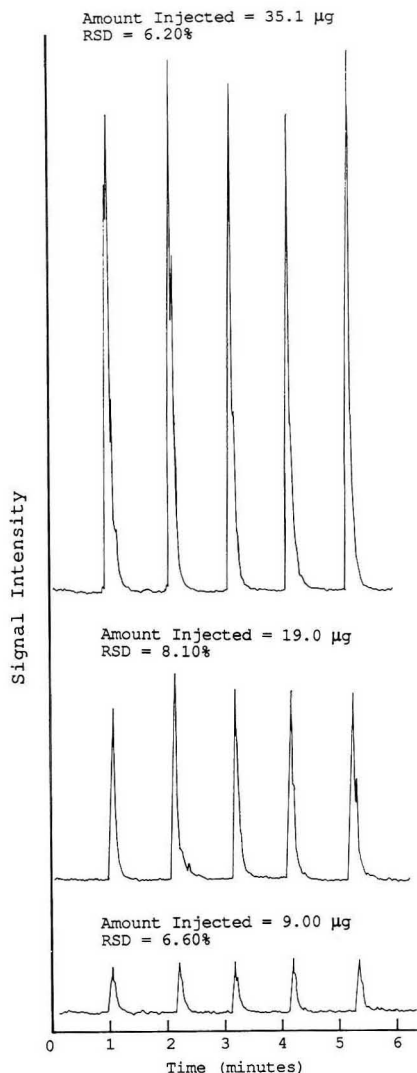


Figure 4. Flowgrams for repeated injections of different concentrations of indole-3-acetic acid.

needed to be optimized to achieve reproducible results are the flow rate and the temperature of the heated capillary tube. For this work, the temperature of the tube is optimized at 200 °C and the flow rate is 0.5 mL/min. We find that reproducible results can also be obtained for other compounds using the same experimental parameters as those used for indole-3-acetic acid. The average RSD is in the range 4–8%. However, the RSD increases to about 10–20% when the amount of the sample injected is close to the detection limit. Although the reproducibility of the present system is sufficient for many analytical applications, it can be further improved by (1) using a better solvent delivery system to regulate the flow rate more precisely, (2) using feedback control power supplies to control the heat of the interface, and (3) using electronic integration

Table I. Compounds Studied by FIA/MPI Mass Spectrometry with the PSI Interface

compd	MW	MP, °C	major ions, <i>m/z</i> (% rel int)
(a) PAHs			
2-methylanthracene	192	204–206	192 (100)
9,10-dimethylanthracene	206	182–184	206 (100)
2-chloroanthracene	212	221–223	212 (100)
9-chloroanthracene	212	100–101	212 (100), 178 (99)
1-aminoanthracene	193	114–118	193 (100), 165 (36), 139 (10), 63 (16), 51 (7), 39 (13), 27 (4)
2-methylnaphthalene	142	34–36	142 (100), 115 (7), 63 (7), 51 (3), 39 (5)
triphenylene	228	197–200	228 (100)
carbazole	167	245–247	167 (100)
anthranilic acid	137	144–148	93 (100)
(b) Pineal Indoles			
tryptophan	204	289–290	204 (100), 130 (47)
melatonin	232	116–118	232 (100), 174 (41), 160 (53)
5-methoxytryptamine	190	121–123	190 (100), 160 (84), 117 (9), 30 (22)
6-methoxytryptamine	190	146–147	190 (100), 160 (49), 117 (8), 30 (20)
harmaline	214	232–234	214 (100)
5-hydroxyindole-3-acetic acid	191	161–164	191 (100), 146 (32)
tryptophol	161	59	161 (100), 130 (43), 103 (12), 77 (22), 51 (17)
(c) Catecholamines			
DL-tyrosine	181	325	181 (100), 137 (5), 107 (35)
tyramine	137	161–163	137 (100), 30 (63)
octopamine ^a	153	169–171	153 (69), 123 (100), 30 (54)
synephrine	167	187	167 (24), 123 (8), 44 (100)
phenylephrine ^a	167	143–145	167 (7), 123 (2), 44 (100)
metanephrine ^a	197	175	197 (21), 153 (9), 44 (100)
norephedrine ^a	151	174–176	151 (2), 107 (3), 77 (2), 44 (100)
L-dopa	197	195	197 (100), 137 (17), 123 (24)
hydrocinnamic acid	150	47–49	150 (100)
vanillic acid	168	210–213	168 (100)
4-hydroxy-3-methoxyphenylacetic acid	182	142–145	182 (100), 137 (33)
3,4-dihydroxyphenylacetic acid	168	127–130	168 (100), 146 (71)
4-hydroxy-3-methoxymandelic acid	198	132–134	198 (100), 153 (5), 65 (14)
3-hydroxy-4-methoxymandelic acid	198	132–134	198 (100), 153 (5), 65 (9)
homovanillyl alcohol	168	40–42	168 (100), 137 (31)
(d) Neuroleptic Drugs			
desipramine ^a	266	214	266 (100), 208 (17), 194 (15), 72 (20), 58 (17), 44 (32)
promazine ^a	284	181	284 (23), 86 (8), 58 (100), 44 (6)
chlorpromazine ^a	318	194–196	318 (20), 274 (3), 86 (9), 58 (100), 44 (9)
imipramine ^a	280	174–175	280 (100), 236 (34), 208 (9), 194 (6), 86 (28), 58 (52), 44 (7)
(e) Volatile Molecules			
phenol	94	43	94 (100), 65 (10), 39 (8)
3-ethylphenol	122	<i>b</i>	122 (100), 107 (48), 77 (14), 51 (4), 39 (6), 27 (12)
4-propylphenol	136	22	136 (100), 107 (88), 77 (10), 27 (10)
2- <i>sec</i> -butylphenol	150	16	150 (94), 121 (100), 107 (3), 91 (3), 77 (14), 51 (10), 39 (5), 27 (6)
1-benzylpiperazine	176	<i>b</i>	176 (100)
2-isopropylaniline	135	<i>b</i>	135 (100), 120 (57), 103 (4), 77 (7), 51 (4), 39 (3), 27 (3)
<i>o</i> -anisidine	123	6	123 (100), 108 (31), 80 (15), 51 (8), 39 (4), 27 (8)
<i>o</i> -cresol	108	31	108 (100), 91 (7), 77 (10), 27 (10)

^aHCl salt. ^bLiquid.

(instead of a chart recorder) with digital filtering or other noise reduction methods.

Memory effects of the interface are also investigated. This is studied by making a blank injection after an injection of indole-3-acetic acid. Different concentrations of samples are used. In all cases, no peaks are detected in the blank injections, which indicates that there are no memory effects associated with this PSI interface.

Figure 4 also illustrates that no severe peak broadening and peak tailing are observed at the experimental conditions used. The peak width in terms of time is about 10 s at fwhm. At a flow rate of 0.5 mL/min, this will correspond to a sample volume of 83 μ L. This indicates that peak broadening is observed, since we only inject 20 μ L of sample. The extent of interface contribution to this broadening is unknown at present, as the carrier transport tube also introduces peak broadening. However, one would expect that peak broadening does occur in this interface, since a large volume change takes place when sample and liquid carrier are vaporized. It takes

finite time for the sample vapor to exit the sample vaporizer, resulting in a small tailing in the detected peak as shown in Figure 4. Nevertheless, this tailing is not so severe, compared with other interfacing techniques.³³ The fact that no memory effects and no severe tailing are observed in this interface for FIA/MPI leads us to conclude that it seems feasible to combine HPLC with a TOFMS by using this PSI interface.

Sensitivity and Quantitation. Although the overall sample transmission efficiency for the PSI interface is unknown, the detection limits for several compounds are measured. It is found that for the current system the detection limits are compound dependent. For instance, the detection limits at a signal-to-noise ratio of 2 are 3 ng for aniline (bp 184 °C), 140 ng for indole-3-acetic acid (mp 165–169 °C), and 4 ng for tryptamine (mp 114–119 °C). Although these three compounds have different volatility, it appears that the sensitivity of this technique very much depends on only the ionization efficiency for these three compounds. This is because, in the MPI studies of indole-3-acetic acid and trypt-

amine with the use of laser desorption or FAB for sample vaporization, the calibration curves of the molecular ion intensity vs concentration are similar to that observed here. Aniline has a very high ionization efficiency (~25%).³⁴ Thus, the detection limit for this compound is lower. However, for chemicals with very low volatility, the sensitivity of the technique may not just depend on the ionization efficiency. Other parameters such as vaporization efficiency are expected to play an important role. Further work is needed to illustrate the effect of various individual parameters on the sensitivity of the system.

The ability to perform quantitation without the use of any internal standards is an important feature of this FIA/MPI method. For tryptamine, a linear calibration curve at concentrations ranging from 7.8 to 1000 ng can be obtained with the use of high laser power and high acceleration voltages. When the total amount of tryptamine injected is above 2 µg, molecular ion signal becomes very broad though, indicating that the signal is saturated with the electric detection system used here. However, by decreasing the laser power and acceleration voltages, signal saturation can be eliminated. On the other hand, decreasing the laser power and voltages reduces the detection sensitivity for the lower concentration samples. It is found that a linear response over 2 orders of magnitude (from 250 ng to 32 µg) can again be obtained for tryptamine by using low laser power and low acceleration voltages. Thus, it can be concluded that (1) with a fixed laser power and acceleration voltages, 2 orders of magnitude of linearity can be achieved for quantitations and (2) by proper selection of the laser power and/or acceleration voltages, the linear region can be changed to a different concentration range.

As indicated before, the lower vacuum pressure achieved in the system due to the aid of a LN₂ trap allows us to apply higher voltages for ion acceleration without causing problems such as arcing. We find that by using 12.5 kV for ion acceleration instead of 5 kV, signals can be generally enhanced about 5–10 times for the compounds studied.

Clustering. Cluster formation is very likely during the supersonic jet expansion.³⁵ This is particularly true in the cases where polar solvents are used. Solvents such as methanol and water can interact with sample molecules strongly to form clusters. Cluster formation will reduce the molecular ion peak intensity. In some cases such as the analysis of a mixture, peaks from the cluster ions will also make the molecular ion peak assignment difficult. Thus, for analytical applications, cluster ions are usually undesirable. Fortunately, in this experimental setup, we normally do not observe a significant amount of clusters, as illustrated in Figure 3. The reason for this is believed to be related to the fact that the temperature of the sample vaporizer of the nozzle is very high. It is known that the reduction of the nozzle temperature energetically favors the formation of clusters while heating the nozzle can reduce the population of clusters.³⁶

In the cases where we do observe the cluster ions, the variation of the delay time (Δt) between the nozzle opening and the ionization laser pulse can eliminate the cluster ion peaks in the MPI mass spectrum. The cluster ions are not detected when the delay time is set properly so that the laser beam intersects the front portion of the sample pulse. This portion of the molecular beam does not contain a significant amount of clusters. This finding is consistent with the results reported by Pang and Lubman³⁷ where a supercritical NH₃ fluid is used for sample delivery.

CONCLUSION

We have developed a pulsed sample introduction interface for combining FIA with a TOFMS. It is demonstrated that this PSI interface can be used to introduce a variety of volatile and nonvolatile molecules into a TOFMS for MPI studies.

In most cases, thermal decomposition is not observed. It is also shown that reproducible results can be readily obtained with PSI. No memory effects are found, and no severe peak tailing is observed. The detection limits of the present system are compound dependent. The detection limits are found to be 3, 4, and 140 ng for aniline, tryptamine, and indole-3-acetic acid, respectively. It is found that excellent linearity over 2 orders of magnitude analytical range can be obtained for the compounds studied. Another important issue, i.e., clustering, which is unique to the supersonic jet expansion, is studied. It is found that clustering is not a major problem for this interface. For most compounds studied, significant amounts of cluster ions are not observed in MPI mass spectra. In the cases where clusters do form, these clusters are found to be formed in the back portion of the sample pulse. Thus, the proper adjustment of the delay time between the nozzle opening and laser pulse allows one to ionize the parent molecules only.

The next stage of the development of this PSI interface is to use this interface to combine HPLC with a TOFMS. Many important parameters which may affect the performance of the interface will be studied in detail. These include the type of solvent and its flow rate, the temperatures of the heated capillary tube and the sample vaporizer, the type of makeup gas and its flow rate, and the diameter and length of the heated capillary tube. In addition, the capability of this interface for supersonic jet spectroscopy will be investigated. In fact, jet-cooled spectra of aniline, fluorene, and indole-3-acetic acid have been obtained with this technique. Detailed studies are underway and will be reported elsewhere.

ACKNOWLEDGMENT

L.L. thanks the staff of the Department of Chemistry, University of Alberta, for help in setting up the instruments and accessories in this work. This work was supported by the University Central Research Fund and the Department of Chemistry, University of Alberta. Additional funding was provided by the Alberta Environmental Research Trust and the Natural Sciences and Engineering Research Council of Canada.

REFERENCES

- (1) See for example: Lubman, D. M. *Mass Spectrom. Rev.* **1988**, *7*, 535–554 and 559–592 and references cited therein.
- (2) Hayes, J. M. *Chem. Rev.* **1987**, *87*, 745 and references cited therein.
- (3) Syage, J. A.; Wessell, J. E. *Appl. Spectrosc. Rev.* **1988**, *24*, 1.
- (4) Amirav, A.; Even, U.; Jortner, J. *Anal. Chem.* **1982**, *54*, 1666.
- (5) Sin, C. H.; Tembreull, R.; Lubman, D. M. *Anal. Chem.* **1984**, *56*, 2776.
- (6) Imasaka, T.; Shigezumi, T.; Ishibashi, N. *Anal. Chem.* **1986**, *58*, 2152.
- (7) Tembreull, R.; Lubman, D. M. *Anal. Chem.* **1986**, *58*, 1299.
- (8) Li, L.; Lubman, D. M. *Anal. Chem.* **1988**, *60*, 2591.
- (9) Grotemeyer, J.; Schlag, E. W. *Angew. Chem., Int. Ed. Engl.* **1988**, *27*, 447 and references therein.
- (10) de Vries, M. S.; Hunziker, H. E.; Wandt, H. R. In *Lasers and Mass Spectrometry*; Lubman, D. M., Ed.; Oxford: New York, 1990; Chapter 17, pp 383–401.
- (11) Li, L.; Hogg, A. M.; Wang, A. P.; Zhang, J. Y.; Nagra, D. S. *Anal. Chem.* **1991**, *63*, 974.
- (12) Nagra, D. S.; Zhang, J. Y.; Li, L. *Anal. Chem.* **1991**, *63*, 2188.
- (13) Sin, C. H.; Pang, H. M.; Lubman, D. M.; Zorn, J. C. *Anal. Chem.* **1986**, *58*, 487.
- (14) Pang, H. M.; Sin, C. H.; Lubman, D. M. *Appl. Spectrosc.* **1988**, *42*, 1200.
- (15) Scott, R.; Scott, C.; Munroe, M.; Hess, J. Jr. *J. Chromatogr.* **1974**, *99*, 395.
- (16) Tal'Rose, V.; Karpov, G.; Gordoetshii, I.; Skurat, V. Russ. *J. Phys. Chem.* **1968**, *42*, 1658.
- (17) Baldwin, M.; McLafferty, F. *Org. Mass Spectrom.* **1973**, *7*, 111.
- (18) Henion, J. D. *Anal. Chem.* **1978**, *50*, 1687.
- (19) Blakley, C. R.; Vestal, M. L. *Anal. Chem.* **1983**, *55*, 750.
- (20) Willoughby, R. C.; Browner, R. F. *Anal. Chem.* **1984**, *56*, 2626.
- (21) Carroll, D. I.; Dzidic, I.; Stillwell, R. N.; Haeghele, K. D.; Horning, E. C. *Anal. Chem.* **1975**, *47*, 2369.
- (22) Thomson, B. A.; Iribarne, J. V.; Dzidic, P. J. *Anal. Chem.* **1982**, *54*, 2219.
- (23) Whitehouse, C. M.; Dreyer, R. N.; Yamashita, M.; Fenn, J. B. *Anal. Chem.* **1985**, *57*, 675.
- (24) Caprioli, R. M.; Fan, T.; Cottrell, J. S. *Anal. Chem.* **1986**, *58*, 2949.

- (25) See for example: (a) Crowther, J. B.; Covey, T. R.; Henion, J. D. In *Detectors for Liquid Chromatography*; Yeung, E. S., Ed.; John Wiley & Sons: 1986, New York; Chapter 8, pp 292-330. (b) *Liquid Chromatography/Mass Spectrometry, Applications in Agricultural, Pharmaceutical, and Environmental Chemistry*; Brown, M. A., Ed.; American Chemical Society: Washington, DC, 1990.
- (26) Imasaka, T.; Yamaga, N.; Ishibashi, N. *Anal. Chem.* **1987**, *59*, 419.
- (27) Anderson, B. D.; Johnston, M. V. *Appl. Spectrosc.* **1987**, *41*, 1358.
- (28) Ruzickica, J.; Christian, G. D. *Analyst* **1990**, *115*, 475 and references cited therein.
- (29) Stewart, K. K. *Anal. Chem.* **1983**, *55*, 931A.
- (30) Li, L.; Lubman, D. M. *Rev. Sci. Instrum.* **1989**, *60*, 499.
- (31) Sin, C. H.; Pang, H. M.; Lubman, D. M. *Anal. Instrumen.* **1988**, *17*, 87.
- (32) Beuhler, R. J.; Flanagan, E.; Greene, L. J.; Friedman, L. *Biochem. Biophys. Res. Commun.* **1972**, *46*, 1082.
- (33) Vestal, M. L.; Winn, D. H.; Vestal, C. H.; Wilkes, J. G. In *Liquid Chromatography/Mass Spectrometry, Applications in Agricultural, Pharmaceutical, and Environmental Chemistry*; Brown, M. A., Ed.; American Chemical Society: Washington, DC, 1990; Chapter 14, pp 215-231.
- (34) Boesl, U.; Neusser, H. J.; Schlag, E. W. *Chem. Phys.* **1981**, *55*, 193.
- (35) See for example: Levy, D. H.; Wharton, L.; Smalley, R. E. In *Chemical and Biochemical Applications of Lasers*; Moore, C. B., Ed.; Academic: New York, 1977; Vol. II, pp 1-41.
- (36) Bartell, L. S. *J. Phys. Chem.* **1990**, *94*, 5102.
- (37) Pang, H. M.; Lubman, D. M. *Rev. Sci. Instrum.* **1988**, *59*, 2460.

RECEIVED for review October 3, 1991. Accepted January 6, 1992.

Quadrupole Mass Spectrometry in Combination with Lithium Ion Attachment for Sampling at Atmospheric Pressure: Possible Coupling to Supercritical Fluid Chromatography

Toshihiro Fujii

National Institute for Environmental Studies, Tsukuba, Ibaraki 305, Japan

A novel device has been developed which permits sampling at atmospheric pressure followed by soft ionization mass spectrometry. Sample gases are introduced through a small aperture at atmospheric pressure into an ionization reaction chamber containing a lithium ion emitter. In this ionization reaction chamber, lithium ion attachment to the molecule takes place. The ionized adduct is detected by a quadrupole mass spectrometer. With this instrument incorporating soft ionization, it should be possible at atmospheric pressure to detect any chemical species, including radical intermediates, on a real time basis. In addition, the coupling to a supercritical fluid, gas, and liquid chromatograph is feasible.

INTRODUCTION

The real time analysis of quantities of constituents in ambient air is a common analytical challenge. For example, the complexity of the volatile organic mixtures found airborne in indoor environments, from a variety of sources including tobacco smoke and paint, presents special difficulties in obtaining meaningful data.

Mass spectrometry with a sensitive ionization method is a suitable choice, since mass spectrometric analysis is essential for the identification and quantitation of these intricate organic mixtures.

Several approaches have been made. One approach is to introduce an air sample into the mass spectrometer with an electron impact (EI) ionization source through the leak.¹ The conventional method of ionization, standard 70-eV electron impact, is vulnerable to the presence of oxygen, since the ion source filament tends to oxidize rapidly and burn out. Furthermore, EI ionization causes extensive fragmentation of components entering the ion source, producing an overlapping of fragment and molecular ion signals. This makes identification of individual compounds extremely difficult, especially, when several complex compounds coevolve.

The former problem has been partially overcome in the past by using a membrane² that permeates certain organic compounds. However, there are limitations imposed by the

membranes; that is, many polar or reactive compounds are incompatible.

One type of chemical ionization (CI), referred to as atmospheric pressure ionization (API) has been used successfully³⁻⁶ for the ionization and subsequent MS analysis of chemicals in the ambient environment. API has proven to be extremely sensitive for certain organics. However, identification of a particular compound is highly speculative and, in addition, the problem of chemical interference cannot be avoided.

Recently, McLuckey et al.⁷ proposed a new approach of direct sampling of air for the determination of trace organic compounds in ambient air. This approach is based on the establishment of a glow discharge⁸ in ambient air drawn into a region of reduced pressure. The ion source is simple, rugged, and relatively maintenance-free, exhibits a very short memory, and is extremely sensitive for compounds with high proton affinity, high electron affinities, high gas-phase acidities, and/or low ionization energies. A detection limit of 1-2 ppt and a linear dynamic range of at least 6 orders magnitude are reported for 2,4,6-trinitrotoluene.

Hodges and Beauchamp^{9,10} described a technique for obtaining mass spectra consisting solely of quasi-molecular ions formed by addition of Li⁺ ions to the sample molecules. This demonstrated that alkali-metal ion CI mass spectrometry is a useful addition to the field of analytical mass spectrometry. Potassium ion CI was also used to ionize certain compounds selectively in a mass spectrometer source.¹¹ More recently, the study was extended to determine the ultimate sensitivity of Li⁺ ion CI mass spectrometry.¹²

The cationization appears to have a unique set for atmospheric monitorings. In general, cationized molecules are more stable than radical molecule ions or protonated molecules. The fragmentation of the polar molecules resulting from cationization by alkali-metal ions (alkali-metal ion attachment) has a higher activation energy than does splitting off functional groups after protonation.¹³ Cationization is, therefore, potentially useful for the determination of molecular weights. Cationization occurs primarily through ion attachment reactions. When this takes place in a region of reduced pressure with ambient air, this ionization may be proven to be especially

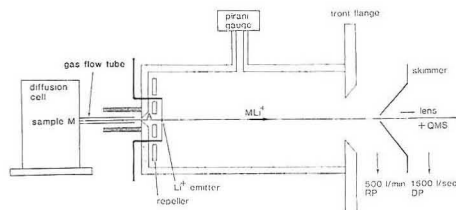


Figure 1. Schematic of the ionization chamber which allows the ambient air through aperture A. The chamber is fixed on a front flange which has been hollowed out in the center with a 20-mm hole.

sensitive for a variety of heteroatom-containing organic molecules.

The objectives of this study are to construct a mass spectrometric system for sampling ambient air at atmospheric pressure. This system is based upon the establishment of an alkali-metal ion attachment reaction in a region of reduced pressure with ambient air. Reported and discussed are (1) an optimized Li ion source with its operation and characters, (2) experimental conditions, and (3) possible applications to SFC.

EXPERIMENTAL SECTION

All experiments were performed with a modification of the apparatus specially prepared by the Shimadzu Corp. for an atmospheric pressure ionization mass spectrometer¹⁴ with a lithium ion emitter.

The schemes involves in the sampling at atmospheric pressure can be illustrated in Figure 1. It shows a drawing of a Li⁺ ion attachment reaction chamber (ionization chamber) into which a stream of gas from ambient air is directed. The ionization chamber (IC) is fixed to the vacuum envelope, housing a quadrupole mass spectrometer.

The IC constructed for this work was a modification of the previously reported lithium ion source (LIS) for lithium ion chemical ionization mass spectrometry.¹² The IC consists of a lithium ion emitter, reaction region and repeller. Lithium ions are emitted from the lithium ion emitter, which is a small mineral bead (about 2 mm in diameter) fused to a 0.1-mm-diameter Pt-filament wire. The bead is prepared with a thoroughly ground mixture of Li₂O:Al₂O₃:SiO₂ in a 1:1:1 molar ratio for Li⁺ alkali-metal ions.¹⁵ Primary ions are produced in the carrier gas by heating the bead. The filament power was kept less than 1 W to reduce heating effects. The repeller electrode is made of a 15-mm-diameter stainless steel disk, which is 2 mm behind the bead. The repeller voltage was maintained at the same potential as the emitter.

The bead is placed 10 mm from the aperture. The reaction region is a cylindrical tube (i.d., 60 mm) with the lithium ion emitter centered within the chamber. The IC can be heated to 250 °C and connected to a 500 L/min rotary pump to maintain ion-molecule reaction conditions by changing the pumping speed or replacing the aperture with a center hole of a certain diameter. To reduce the pumping speed, a valve is situated in the line to rotary pump. This allows the pressure in the source to be elevated.

Several different ambient gases have been studied which were drawn through aperture A. For instance, when aperture A with its diameter of 0.4 mm is used, the ambient air is sampled at a rate of roughly 530 mL/min. Under these conditions, the pressure in the ionization chamber is 1.1 Torr, as measured with a pirani gauge (WP-01, ULVAC, Tokyo) connected into the IC. The accessible pressure range was determined by the ability to sustain the ion attachment reaction.

The adduct ions of sample gas from the IC impinges on the skimmer, in the tip of which a 1-mm-diameter orifice was drilled. No potential was applied to the skimmer.

The details of a quadrupole mass spectrometer (QMS) with the vacuum system and the focus system ahead of the mass analyzer have been described previously.¹²

The diffusion cell method¹⁶ has been used to facilitate sampling. The characterization study of the present system was carried out

with reference compounds through a gas flow tube. The gas flow tube was built from 3-mm-i.d. Pyrex and was ca. 60 cm long. This tube could be moved up to aperture A.

For volatile samples, the diffusion tube¹⁷ or permeation tube (laboratory-made of Teflon)¹⁸ was used to prepare sample concentrations. Diffusion tubes (D-10, D-20, D-30, Gastec, Tokyo) with apertures of 2.5, 5, and 8 mm, respectively, and a length of 10 cm were used to create concentration samples by flowing the carrier gas over the diffusion tube enclosed in a diffusion cell (a stainless steel housing). The prepared samples passed through the glass tubing into the aperture of the present system. Provided the diffusion tube was used, the sample was further diluted to a concentration that is estimated to be on the order of 10⁻⁸ ppt on the basis of the dilution factor of the flows. For involatile samples, such as naphthalene, a small quantity of the solid is placed in a vial which is in the diffusion cell. Vapors above the solid are carried into the gas flow tube.

The calibration curve data for toluene were obtained by the combined use of the diffusion and permeation tubes, showing the linear response range over the chosen range of 3.0 × 10⁻¹¹ to 4.1 × 10⁻⁸ g/s.

RESULTS AND DISCUSSION

Lithium Ion Intensity. The maximum emission current of Li⁺ ions was measured around 6 × 10⁻⁷ A, as the air gas flow of 530 mL/min passed through the ionization chamber at 1.1 Torr, the emitter current was 3.2 A, and the ion multiplier gain was 3.8 × 10³. At a fixed pressure, the Li⁺ current increases linearly, or nearly so, with the emitter current over the pressure range 0.2–1.2 Torr.

Ionization Chamber. Ionization in the IC is initiated by formation of lithium ions on the emitter. A successful method for obtaining lithium ion cationization mass spectra must provide means for binding the lithium ion to the sample molecule (M). (M + Li)⁺ complexes are formed by termolecular association reactions. The ionic products observed are a reflection of association reaction rates.

The formation of an adduct ion is commonly assumed to be a three-body process, in which a neutral molecule collides with an ion-molecule complex, removing an amount of energy and stabilizing the (M + Li)⁺ complex. On the basis of this model, the cationization process would be suitable in a high-pressure environment, since the main-component gas molecules serve as the third body in the analyte addition reaction with alkali-metal ions.

Sensitivity Considerations. For lithium ion association with most organic molecules, bimolecular kinetics was observed with the pressure in the IC at greater than 1 Torr. Therefore, the sensitivity can be evaluated by using the following equations:¹⁹

$$\ln [Li^+]/[Li^+]_0 = -Qkl/3.14r_0^2v_0^2 \quad (1)$$

$$[(M + Li)^+] = [Li^+]_0 - [Li^+] \quad (2)$$

where [Li⁺]₀ is the concentration of Li⁺ prior to the introduction of the sample gas M, *l* (11 cm) is the length of the reaction path, *r*₀ (3.0 cm) is the radius of the reaction chamber, *v*₀ (216 cm/s) is the average gas flow velocity, and *Q* (particle/s) is the rate of introduction of M.

Assuming that (i) *k*, the effective bimolecular rate constant²⁰ of the termolecular reaction in the 1-Torr buffer gas environment, is 1 × 10⁻⁹ cm³/(molecule s), (ii) the fraction of ions transmitted from source to detector is 1 × 10⁻³, based on a factor of 0.1 for the ion lens and 0.01 for the mass analyzer, and (iii) the Li⁺ ion density [Li⁺]₀ in an ionization chamber, is 4.2 × 10⁶ ions/cm³, as estimated by the previous treatment,¹² the sensitivity expressed in A/(g/s) can be calculated as approximately 2.9 × 10⁻⁴ A/(g/s) for the case of the 1-bromopropane introduction rate of 1 × 10⁻¹⁰ g/s.

Figure 2 shows three mass spectra around *m/z* 7, 25, and 129, respectively, in which the primary ions, Li⁺ and H₂O⁺Li⁺ and the Li⁺ attachment ion, C₃H₇BrLi⁺ are monitored. The

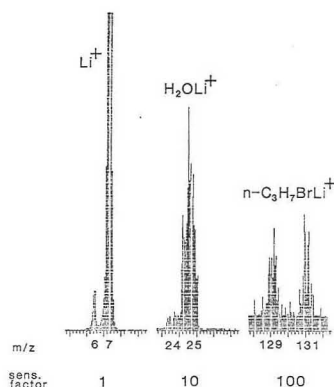


Figure 2. Spectrum obtained from 1-bromopropane samples, showing $n\text{-C}_3\text{H}_7\text{BrLi}^+$ ($m/z = 129$ and 131). Samples were introduced through the diffusion cell at the rate of 1.5×10^{-10} g/s.

Table I. Minimum Detectable Amount (mda) and Detectable Concentration (v/v) in Air for a Number of Compounds

compd	mda, g/s	detectable concn, ppt (v/v)
toluene	8.3×10^{-12}	130
1-bromopropane	4.5×10^{-12}	52
naphthalene	7.9×10^{-12}	91
trichloroethylene	4.8×10^{-12}	54
D-camphor	1.2×10^{-11}	120

1-bromopropane sample, diluted by 1000 mL/min of cylinder air, is introduced at a rate of 1.5×10^{-10} g/s from the permeation tube at 25°C . The measurement of the adduct ion yielded a value of 2.5×10^{-10} A, which is the output of the ion multiplier with the gain at 3.8×10^3 . This current corresponds to 6.6×10^{-14} A. Thus, the sensitivity is 4.4×10^{-4} A/(g/s). In comparison with the calculated sensitivity, a slightly better sensitivity has been actually demonstrated; confirming the essentially correct nature of the previous estimate of the effective bimolecular rate constant.

Taking the actual noise level of the system as the ultimate limitation on minimum detectable sample size, we can estimate the minimum detectable amount (mda). The mda is calculated to be 4.5×10^{-12} g/s on the assumption that the capability of the ion detection system in the electrometer, at the signal to noise ratio of 3, is around 2×10^{-15} A. These sensitivity calculations were supported with the linear calibration curves over the chosen range of 1.1×10^{-9} to 6.2×10^{-11} g/s derived from the 1-bromopropane sample.

The mda is obtained as 4.5×10^{-12} g/s (5.2×10^{-8} mL/min at 25°C), as the 1-bromopropane compound enters the IC, diluted by 1000 mL/min of air. Therefore the detectable concentration is calculated to be 52 ppt (v/v).

The 1-bromopropane example is given to show the mda and detectability possible with this system in the optimal case. We have measured a similar performance for four other compounds, whose results are listed in Table I. Compounds with high Li^+ affinity are readily detected at low levels.

Background Mass Spectra. When the nitrogen gas from the cylinder passed through the diffusion cell to the mass spectrometer, the background mass spectrum generally showed an abundant H_2OLi^+ as well as other ions with a low intensity peak at m/z 35, 51, 67, and 83. The mass spectrum was obtained at repeller voltages of 200 V. The scan time was 5 s and the scanning mass range was 5–150 amu. H_2OLi^+ is

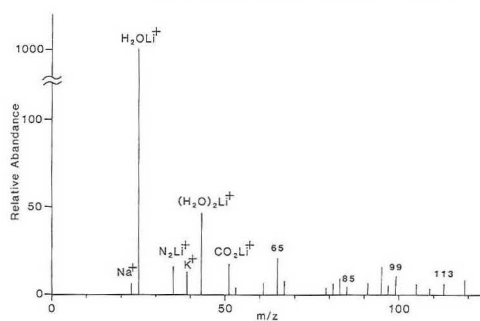


Figure 3. Mass spectrum produced from laboratory air.

probably derived from the ever-present water in the nitrogen carrier gas. m/z 35 and 51 may be assigned to N_2Li^+ and CO_2Li^+ , respectively. The peaks m/z 67 and 83 are persistent. They have yet to be assigned. Presumably, the limit of detectability is determined mainly by the impurity content (Na^+ , K^+ , Rb^+ , Cs^+) of the emitter bead.

Mass Spectrum of Laboratory Air. Using the pulse-counting system, the accumulated laboratory-air mass spectrum was obtained in the 100 recurrent multiscanning mode of the multichannel analyzer.¹⁴ The scan time was 5 s, and the scanning mass range was 5–150 amu. Consistent mass spectra were obtained (Figure 3). The major ions are $(\text{H}_2\text{O})_n\text{Li}^+$, where $n = 1$ –5. The distribution of these ions can vary dramatically with relative humidity. In comparison to our work, it was also observed (in the work of McCluckey,⁷ where a glow discharge was produced from ambient air at 0.54 Torr) that the ions are $(\text{H}_2\text{O})_n\text{H}^+$, where $n = 1$ –5, and larger water clusters under any conditions have never been observed. Our experiments showed the same n numbers.

The appearance of alkali-metal ion contaminations at m/z 23, 39, 41, 85, and 87 hinges on the heating condition. Their distribution primarily depends on the conditioning temperature and time. Practically, the Na^+ , K^+ , and Rb^+ ions can be reduced to a negligible size after weeks of heating.

The remainder of other peaks, m/z 35, 39, 51, 53, 65, 67, 79, 81, 83, 85, 91, 95, 99, 105, 109, 113, and 119, are caused by major components in the laboratory air. Unfortunately, the limited resolution of the mass spectrometer and the lack of reference spectrum do not allow a clear interpretation of this spectrum. However, some peaks can be assumed. m/z 35 (N_2Li^+), 39 (O_2Li^+), and 51 (CO_2Li^+) may be assigned as adduct ions due to the major component of ambient air. The m/z 65 peak is due to Li^+ attached to acetone, attributable to the presence of acetone used frequently as the solvent in the room, while m/z 85, 99, and 113 may be $\text{C}_6\text{H}_6\text{Li}^+$, $\text{C}_7\text{H}_8\text{Li}^+$, and $\text{C}_8\text{H}_{10}\text{Li}^+$, respectively.

Simulation of SFC/MS Combination. Supercritical fluid chromatography/mass spectrometry (SFC/MS) has been growing for the efficient separation and characterization of mixtures not amenable to gas chromatography, establishing this new technique as an excellent complement to GC and HPLC methods.² Since superfluids are simply dense pressurized gases, considerable flexibility exists for SFC/MS interfacing.^{22,23} The direct fluid injection approach is currently the simplest and most widely used approach to SFC/MS. It is based upon the rapid expansion of the supercritical fluid mobile phase into a low-pressure region where ionization can occur.

Since proper conditions produce a gas after expansion, conventional mass spectrometric ionization methods are readily adapted. Both electron impact and chemical ionization have been explored with SFC interfacing. An advantage of

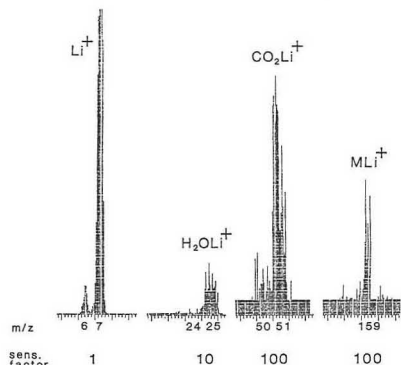


Figure 4. Spectrum obtained from d-camphor diluted by 1000 mL/min of CO_2 .

SFC/MS with small-diameter capillary columns is that the flow rates are sufficiently low, so that any CI reagent gas may be used. However, truly useful SFC/MS instrumentation must address problems related to sample injection methods and quantitation. Nearly all earlier capillary SFC work with small-diameter capillaries has used split injection techniques, which can have low reproducibility and result in constraints on sample size due to the often limited solubility in the solvent. This is further complicated by the relatively small size²⁴ typically required to avoid overloading such columns (typically ca. 1–10 ng/component for 50- μm -i.d. columns with a 0.25- μm film thickness).

As an attempted solution to these limitations, an alternative high flow rate SFC/MS interface is desirable with the aim of (1) operation at high fluid flow rates, (2) improved sensitivity, and (3) allowing operational convenience. Variations upon this approach can be implemented using the present system.

The SFC/MS combination was simulated by employing the diffusion cell through which the CO_2 gas flows over the sample at the rate of 1000 mL/min, similar to previous sensitivity experiments. There is no limitation to the flow rate; high flow rates can be readily accommodated by not changing any experimental conditions. This approach, which makes the sensitivity higher, provides relatively high capacity introduction to the mass spectrometer.

The performance for d-camphor (M) is demonstrated in Figure 4, which shows a selected ion spectrum at the sample introduction rate of 5.3×10^{-9} g/s. A significant amount of CO_2Li^+ ions is observed in the spectrum, but it is not crucial.

CONCLUSION

This study has demonstrated quadrupole mass spectrometry employing lithium ion attachment for sampling at at-

mospheric pressure. This system has exhibited the following features: (1) the ability to accept high capacity sample introduction, to operate in atmospheric pressures, and to allow easy coupling of various sample introduction sources to the mass spectrometric analysis; (2) an opportunity for real time detection of any chemical species, including the radical intermediates;²⁵ (3) the ability to identify compounds easily due to analysis of a generation of ions that does not fragment.

The thermogravimetry (TG)/mass spectrometry with sampling inlet at atmospheric pressure seems to be interesting.²⁶ The compatibility of TG (a predominantly atmospheric pressure technique with a TG effluent at a 2–3 L/min stream of nitrogen or zero air carrier) with the present system permits an interface that is easily coupled and decoupled. This combination may exhibit the following features: excellent temporal correspondence between TG and mass spectral data and the ability to identify and resolve complex coevolving products.

ACKNOWLEDGMENT

I thank H. Jimba and M. Ogura for their many contributions to the development of the sampling system.

REFERENCES

- (1) Evans, J. E.; Arnold, J. T. *Environ. Sci. Technol.* **1975**, *9*, 1134.
- (2) Woldsing, S.; Owens, G.; Woolford, D. C. *Science* **1966**, *153*, 885.
- (3) Horning, E. C.; Horning, M. G.; Carroll, D. I.; Dzidic, I.; Stillwell, R. N. *Anal. Chem.* **1973**, *45*, 936.
- (4) Carroll, D. I.; Dzidic, I.; Horning, E. C.; Stillwell, R. N. *Appl. Spectrosc. Rev.* **1981**, *17*, 337.
- (5) Lane, D. A.; Thomson, B. A.; Lovett, A. M.; Reid, N. M. *Adv. Mass Spectrom.* **1980**, *8*, 1480.
- (6) Ketkar, S. N.; Dulak, J. G.; Fite, W. L.; Buchner, J. D.; Dheandhanoo, S. *Anal. Chem.* **1989**, *61*, 260.
- (7) McLuckey, S. A.; Glish, G. L.; Asano, K. G.; Grant, B. C. *Anal. Chem.* **1988**, *60*, 2220.
- (8) Sofer, I.; Zhu, J.; Lee, H.; Antos, W.; Lubman, D. M. *Appl. Spectrosc.* **1990**, *44*, 1391.
- (9) Staley, R. H.; Beauchamp, J. L. *J. Am. Chem. Soc.* **1975**, *97*, 5920.
- (10) Hodges, R. V.; Beauchamp, J. L. *Anal. Chem.* **1976**, *48*, 825.
- (11) Bombick, D.; Pinkston, J. D.; Allison, J. *Anal. Chem.* **1984**, *56*, 396.
- (12) Fujii, T.; Ogura, M.; Jimba, H. *Anal. Chem.* **1989**, *61*, 1026.
- (13) Schade, U.; Stoll, R.; Rollgen, F. W. *Org. Mass Spectrom.* **1981**, *16*, 441.
- (14) Fujii, T.; Jimba, H.; Arimoto, H. *Anal. Chem.* **1990**, *62*, 107.
- (15) Blewett, J. P.; Jones, E. J. *Phys. Rev.* **1936**, *50*, 464.
- (16) Miguel, A. H.; Natusch, D. F. S. *Anal. Chem.* **1975**, *47*, 1705.
- (17) Altschuler, A. P.; Cohen, I. R. *Anal. Chem.* **1960**, *32*, 802.
- (18) Scoringelli, F. P.; O'Keefe, A. E.; Rosenberg, E.; Bell, J. P. *Anal. Chem.* **1970**, *42*, 871.
- (19) Ferguson, E. E.; Fehsenfeld, F. C.; Schmeltekopf, A. L. *Adv. At. Mol. Phys.* **1961**, *5*, 1.
- (20) Spears, K. G.; Ferguson, E. E. *J. Chem. Phys.* **1973**, *59*, 4174.
- (21) Arpino, P. J.; Cousin, J.; Higgins, J. *Trends Anal. Chem.* **1987**, *6*, 69.
- (22) Fjeldsted, J. C.; Lee, M. L. *Anal. Chem.* **1984**, *56*, 619A.
- (23) Smith, R. D.; Udseth, H. R.; Kalinoski, H. T. *Anal. Chem.* **1984**, *56*, 2971.
- (24) Novotny, M.; Springston, S. R.; Peaden, P. A.; Fjeldsted, J. C.; Lee, M. L. *Anal. Chem.* **1981**, *53*, 407A.
- (25) Fujii, T. *Chem. Phys. Lett.*, in press. We are successfully detecting the C_2H_3 and C_2H_2 radicals formed by the microwave discharge in the gas mixture isobutane/He.
- (26) Prime, R. B.; Shushan, B. *Anal. Chem.* **1989**, *61*, 1195.

RECEIVED for review October 15, 1991. Accepted January 6, 1992.

Capillary Zone Electrophoretic Detection of Biological Thiols and Their S-Nitrosated Derivatives

Jonathan S. Stamler and Joseph Loscalzo*

Department of Medicine, Brigham and Women's Hospital, Brockton/West Roxbury VA Medical Center, Harvard Medical School, Boston, Massachusetts 02115

Reduced thiols (RSH) react with certain oxides of nitrogen to yield S-nitroso thiols (RSNO) possessing smooth muscle relaxant and platelet inhibitory properties. Nitrosated derivatives of the biological thiols—glutathione, cysteine, and homocysteine—have therefore been considered as bioactive intermediates in the metabolism of organic nitrates and the endothelium-derived relaxing factor with properties of nitric oxide. As yet, however, there is no established chemical method for identifying the biological S-nitroso thiols and, consequently, little is known of their distinguishing chemical characteristics or biochemistry. In this study, we demonstrate for the first time a simple, rapid, and reproducible method for separating these thiols from their S-nitrosated derivatives using capillary zone electrophoresis. Cysteine, homocysteine, and glutathione were separated from one another and from their corresponding disulfides in 0.01 M phosphate buffer, pH 2.5, by capillary zone electrophoresis and absorbance detection at 200 nm with measured elution times of 5.92–16.15 min; corresponding S-nitroso thiols were selectively detected at 320 nm and eluted at 2.50–18.20 min. These data support the specificity and reproducibility of this technique for separation and identification of thiols, disulfides, and S-nitroso thiol derivatives.

INTRODUCTION

The fraction of sulfur existing as free sulfhydryl moieties (RSH) in eukaryotic cells largely resides in the low-molecular-weight compounds glutathione, cysteine, and homocysteine.¹ Although these compounds exploit unique aspects of sulfur chemistry to execute various thiol-specific biochemical functions, they share many physical properties and a common chemistry. Indeed, the conversion of reduced thiols to S-nitroso thiols (thionitrites, RSNO) upon treatment with certain oxides of nitrogen is a case in point.² The S-nitrosated biological thiol derivatives are each reactive chemical species possessing innate antiplatelet and vasodilatory properties not manifested by equimolar amounts of thiol and nitric oxide alone.^{3–5} S-nitroso thiols have been proposed as active intermediates in the biochemistry and metabolism of organic nitrates,^{3–5} and interest in these compounds has been recently heightened by the discovery of an endothelium-derived relaxing factor (EDRF) with the identity of nitric oxide (NO) or a closely related oxide of nitrogen.^{6,7} Unfortunately, progress in the area of investigation of the metabolism of the biological S-nitroso thiols has been greatly hindered by the lack of an established method for their separation and identification. Accordingly, little is known of their biochemistry and, as yet, these compounds have not been detected in living tissue.

High performance capillary electrophoresis (HPE) is a relatively new high-resolution electrophoretic technique that separates compounds on the basis of their molecular weight and net charge. The efficiency of this method has already been demonstrated for several small molecules including amino acids and peptides.^{8–10} Very recently, Tsikas and Brunner

reported the separation of conjugated forms of glutathione,¹¹ and Holloway and Battersby have described the resolution of reduced glutathione from its disulfide;¹² these latter observations have been confirmed in alkaline medium.¹³ However, despite the potential promise implicit in this novel methodology, alkaline conditions may be limiting in that they predispose to spontaneous sulfhydryl autooxidation.^{12,14,15} Moreover, these conditions are not conducive to the study of S-nitroso thiols which are exceedingly unstable in alkali, rapidly decomposing to nitric oxide and their corresponding disulfides.⁴ Thus, the objectives of experiments described here were 2-fold. First, to establish alternate (acidic) conditions for detection of reduced thiols; and second, to demonstrate the capillary electrophoretic separation of the biological thiols and their S-nitrosated derivatives. This report describes for the first time a simple and reproducible method for separation of these biologically relevant chemical compounds.

MATERIALS AND METHODS

Chemicals and Solutions. Glutathione, L-cysteine, D,L-homocysteine, homocysteine thiolactone (free base and hydrochloride), cystine, homocystine, bradykinin triacetate, iodoacetamide, and 2-mercaptoethanol were purchased from Sigma Chemical Co. (St. Louis, MO). Glutathione disulfide and N-acetylcysteine were purchased from Aldrich Chemical Co. (Milwaukee, WI). Sodium nitrite was purchased from Fisher Scientific (Fairlawn, NJ).

Apparatus. The isotachopheric analyses were performed on the Bio-Rad HPE-100 capillary electrophoresis system (Bio-Rad, Richmond, CA) fitted with a silica-coated capillary (20 cm × 25 µm). Electrophoretic separations were detected on-line and recorded with a Model 1321 single-pen strip chart recorder (Bio-Rad, Richmond, CA) programmed at a chart speed of 1.0 cm/min with a rise time of 1 s. Samples were injected using Hamilton syringes, and analyses were performed at room temperature.

Sample Preparation. A. S-Nitroso Thiols. S-Nitroso thiols were prepared at 25 °C by reacting equimolar (100 mM) concentrations of reduced thiol with NaNO₂ in 1 N HCl.³ Solutions turned from clear to various shades of red instantaneously, indicating completion of the reaction. The S-nitroso thiols could be identified by visible absorption spectroscopy having characteristic absorption maxima at 320 and 550 nm.^{3,4,16} Owing to the instability of S-nitroso derivatives, fresh samples were made at hourly intervals and stored in 1 N HCl at 4 °C until use. Immediately prior to electrophoresis, S-nitroso thiols were diluted in all cases in 0.01 N HCl, 0.01 M sodium phosphate. For S-nitrosoglutathione, S-nitrosocysteine, and S-nitrosomercaptocysteine, the pH of the sample solution was 2.3, and for S-nitroso-N-acetylcysteine the pH was 5.0. Concentrations of stock solutions were determined by the Saville reaction.¹⁷

B. Thiols, Disulfides, and Thiolactone. Stock solutions of thiols were first prepared by dissolving these compounds in 1 N HCl at a final concentration of 100 mM. Owing to their propensity to autooxidize,^{14,15} even at acidic pH, fresh preparations of thiols were made at hourly intervals, protected from light, and stored on ice at 4 °C until immediately prior to electrophoresis. Samples were then diluted in 0.01 N HCl, 0.01 M sodium phosphate, pH 2.3. Concentrations of the stock solutions were determined by reaction with 5,5'-dithiobis(2-nitrobenzoic acid) (DTNB).¹⁸

Fresh stock solutions of homocysteine thiolactone were prepared daily in warm 1 N HCl, and dilutions in phosphate buffer were

made immediately prior to use as described above for thiols. The expected stability of homocysteine thiolactone in 1 N HCl¹⁹ was confirmed by demonstrating the inaccessibility of the ring sulfur to thiol-disulfide exchange in the reaction with 5,5'-dithiobis(2-nitrobenzoic acid) (DTNB)¹⁸ over a 6-h period; stability was later also confirmed by HPE for up to 48 h.

Similar preparatory steps were taken in the case of disulfide sample preparation, with the single exception that stock solutions in 1 N HCl were immediately diluted in 0.01 N HCl, 0.01 N sodium phosphate, pH 2.3, to avoid the potential electrophilic cleavage of disulfides in more strongly acid media.²⁰ Fresh solutions of disulfides were prepared every 3–4 h and stored on ice at 4 °C until use. Concentrations of stock solutions were determined by failure to react in the Saville reaction (without mercurous ion) and by direct detection of disulfides after sulfitolysis with 2-nitro-5-thiosulfonate (NTSB).²¹

In selected experiments thiols and their sulfides were dissolved in 0.1 M borate, followed by dilutions as necessary for a sample solution in 0.01 M borate, pH 8.0. To minimize spontaneous oxidation of thiols^{14,15} and nucleophilic cleavage of disulfides,²⁰ fresh samples were prepared immediately prior to use.

C. Thiol Derivatization. Carboxyamidation of reduced thiols was performed with a 2.5-fold molar excess of iodoacetamide at neutral pH for 60 min at 37 °C.²² Reaction mixtures were protected from light with the use of aluminum foil. Samples were then diluted into a final sample solution containing 0.01 N HCl, 0.01 M sodium phosphate, pH 2.3.

Electrophoresis. To initiate analyses, the capillary and electrode reservoirs were filled with electrophoresis buffer. This inlet was then flushed with deionized water, and a 10- μ L sample solution was loaded for 9 s at 11 kV. The inlet electrode reservoir was subsequently flushed with electrophoresis buffer and the sample run performed at 11 kV. Equally reproducible electrophoresis was also accomplished using a constant current of 20 μ A. For free zone electrophoresis in phosphate buffer at pH 2.5, the polarity of the internal power supply was set for the migration of cations toward the detector (+ polarity). Conversely, analyses performed in phosphate buffer at pH 5.0 or borate at pH 8.0 utilized negative polarity for the migration of anions. Between analyses the capillary was flushed with separation buffer. Eluted volumes were monitored at 200 nm, and confirmatory evidence of S-nitroso thiol detection was obtained at 320 nm.²³ Optimal sensitivity was achieved at 200 nm. S-Nitroso thiols possess secondary absorbance maxima in the range 320–360 nm^{12,23} and at approximately 550 nm.^{3,15,16} Absorbance at 550 nm was too insensitive to be useful in these analyses; thus, absorbance at 320 nm was chosen for specific S-nitroso thiol detection.

RESULTS

Theoretical Considerations. The general expression relating electrophoretic mobility (μ_e) of peptides to their molecular size and charge can be given as

$$\mu_e = \nu / E = q / (6\pi\eta\bar{R}_h)$$

where μ_e is the electrophoretic mobility, ν is the migration velocity, E is the electric field strength, q is the solute charge, η is the solvent viscosity, and \bar{R}_h is the mean Stoke's (hydrodynamic) radius of the peptide. Grossman and colleagues²⁴ have pointed out the complexities involved in accurate calculations of electrophoretic mobility (μ_e) by this equation owing to the complicated effects of hydration and the conformational state of the analyte in the case of \bar{R}_h and the effects of the electrical double layer, solvent concentration and composition, and solvent association with analyte in the case of q . Nevertheless, in dealing with simple molecules that do not exhibit notable intramolecular interactions under a given set of solvent conditions, this equation may provide a useful estimate of relative electrophoretic mobility that may be derived from a calculation of charge-to-mass ratio (=effective charge). The calculated net charges of homocysteine, cysteine, and glutathione^{25,26} at pH 2.3 are 0.44, 0.27, and 0.35, respectively. Effective charge calculations predict the electrophoretic mobility of homocysteine > cysteine > glutathione.

Table I. Migration Times As Predicted from Effective Charge (q/m) of Selected Biological Thiols and Their S-Nitrosated Derivatives^a

	q	q/m	t_p	t_m (mean \pm SD)
homocysteine	0.44	0.0033	std	5.92 \pm 0.15
cysteine	0.27	0.0022	8.80	8.34 \pm 0.12
glutathione	0.35	0.0011	16.93	16.15 \pm 0.30
S-nitrosohomocysteine	0.44	0.0027	7.20	7.74 \pm 0.18
S-nitrocysteine	0.27	0.0018	11.03	12.14 \pm 0.50
S-nitroglutathione	0.35	0.0010	18.55	18.20 \pm 0.37

^a q is the charge and was calculated at an assumed pH of 2.3; m is the mass for which molecular weight was substituted in calculations of effective charge; t_p is the predicted migration time based on the homocysteine standard (std) in minutes (where $t_p = t_{m, \text{homocysteine}} [q/m]_{\text{homocysteine}} / [q/m]_p$), while t_m is the corresponding measured migration time (mean \pm SD, $n = 3-8$).

On the basis of the observed elution of homocysteine at 5.92 \pm 0.15 min (vide infra), the predicted migration times (t_p) of the other thiols and their S-nitrosated derivatives have been calculated (Table I) and show an excellent concordance with the observed migration times (t_m) ($R = 0.9919$, $P = 0.0001$).

Thiols and Their Oxidized Derivatives. Figure 1A–D provides representative electropherograms of homocysteine (A), cysteine (B), glutathione (C), and N-acetylcysteine (D). The latter thiol, a minor metabolite of cysteine, has received a great deal of attention in the context of nitrate metabolism and is included in our analysis for this reason. N-Acetylcysteine does not elute under the same conditions as the other biological thiols (Figure 1D), presumably as a result of the neutralizing influence of the negatively charged acetyl group on the effective charge of the molecule at pH 2.3. Commercially available glutathione provides another notable exception in that it elutes as two fully resolved peaks (Figure 1C), the smaller of which (peak a) corresponds to contaminant glutathione disulfide. According to the concentration-response data of Table III, this particular preparation of reduced glutathione contained approximately 10% glutathione disulfide, a value that was confirmed with the DTNB reaction.

The migration of relevant homodisulfides is illustrated in Figure 2. Distinct differences in migration are apparent, allowing for clear differentiation among disulfides in solutions containing several of these compounds (cf. Figure 3 below). The peak of homocysteine is also fully resolved from those of its disulfide and thiolactone derivatives, the latter forming spontaneously from the reduced thiol under acidic conditions.^{27,28} In contrast, free zone capillary electrophoresis cannot accurately separate cysteine from cystine under these conditions. Derivatization of cysteine by methods including carboxyamidation ($t_m = 11.0$ min, $n = 2$) (data not shown) and S-nitrosation (vide infra), however, provides a simple means of achieving this separation.

The reproducibility of HPE in the above analysis is evidenced by the small standard deviations in migration times for the biological thiols and their oxidized derivatives (Table II). In addition, excellent linearity is demonstrated in plots of peak height vs concentration with correlation coefficients ≥ 0.99 in each case (Table III). An example of the applicability of this method to analysis of a variety of disulfides is shown in Figure 3, in which electrophoresis was performed of a mixture of equimolar amounts of homocysteine, cysteine, and glutathione disulfide. The electropherogram demonstrates four peaks corresponding in their electrophoretic mobilities to those of reduced glutathione, cysteine, and homocysteine, with an additional unidentified peak noted at 11.9 min. Peak heights for homocysteine and reduced glutathione account for 61% and 65% of the injected sample disulfides, respectively, suggesting that the unknown peak is glutathione-homo-

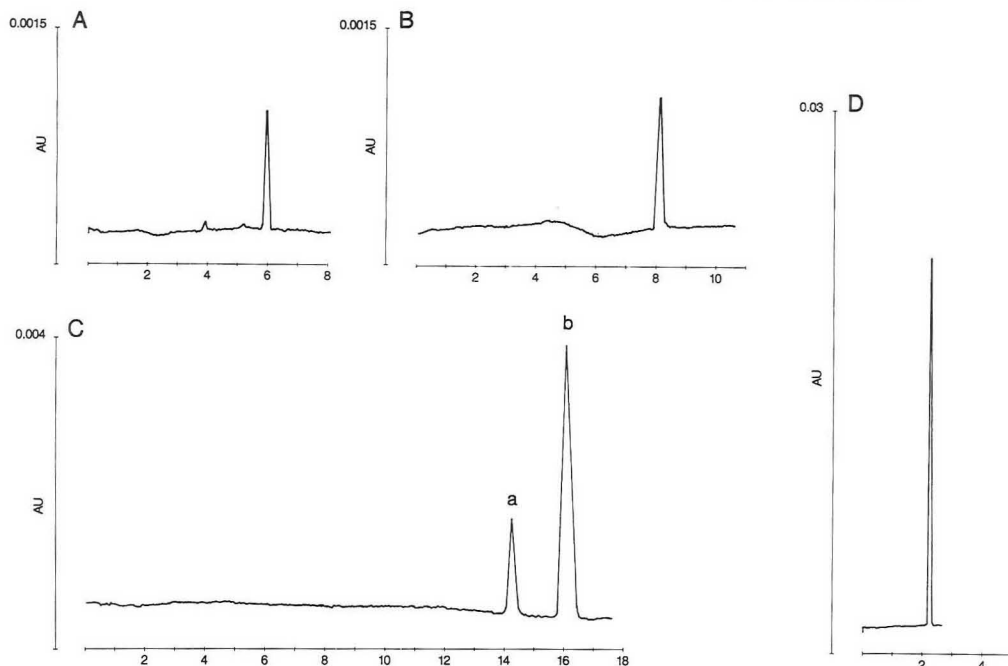


Figure 1. Electropherograms of biological thiols: (A) homocysteine (250 μ M); (B) cysteine (500 μ M); (C) glutathione (500 μ M). Reduced glutathione elutes as two fully resolved peaks with the earlier peak (a) corresponding to glutathione disulfide and the later peak (b) to reduced glutathione. (D) Electropherogram of *N*-acetylcysteine (500 μ M). Conditions (A–C): sample buffer, 0.01 M sodium phosphate, 0.01 N HCl, pH 2.3; positive polarity at 11 kV; absorbance, 200 nm. Conditions (D): sample buffer, 0.01 sodium phosphate, 0.01 N HCl, pH 5.0; negative polarity at 11 kV; absorbance, 200 nm.

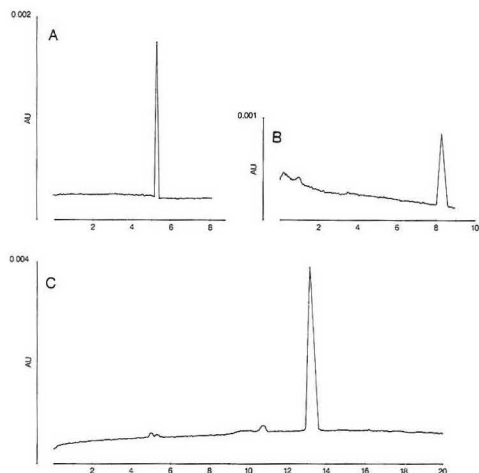


Figure 2. Electropherograms of disulfides: (A) homocysteine (250 μ M); (B) cystine (250 μ M); (C) glutathione disulfide (250 μ M). Conditions: sample buffer, 0.01 M sodium phosphate 0.01 N HCl, pH 2.3; positive polarity at 11 kV; absorbance, 200 nm.

cysteine disulfide. This contention is supported by the estimated migration time of 10.6 min for glutathione-homocysteine disulfide, based on a calculation of effective charge using the pK_s of the individual thiols.

***S*-Nitroso Thiols.** The electropherograms of *S*-nitroso-homocysteine, *S*-nitrosocysteine, *S*-nitrosglutathione, and

Table II. Migration Times of Biological Thiols, Oxidized Derivatives, and *S*-Nitroso Thiols

	t_m^a (mean \pm SD)
homocysteine	5.92 \pm 0.15
homocysteine	5.20 \pm 0.10
homocysteine thiolactone (free base)	2.53 \pm 0.08
homocysteine thiolactone (hydrochloride)	1.65 \pm 0.06
cysteine	8.34 \pm 0.12
cystine	8.30 \pm 0.04
glutathione	16.15 \pm 0.30
glutathione disulfide	13.40 \pm 0.34
<i>N</i> -acetylcysteine ^b	2.42 \pm 0.06
<i>S</i> -nitrosohomocysteine	7.74 \pm 0.18
<i>S</i> -nitrosocysteine	12.14 \pm 0.5
<i>S</i> -nitrosglutathione	18.20 \pm 0.37
<i>S</i> -nitroso- <i>N</i> -acetylcysteine ^b	2.50 \pm 0.06

^a Migration times (t_m mean \pm SD) in minutes are based on $n = 5$ –8. Under these conditions a bradykinin standard eluted at $t_m = 2.70 \pm 0.03$ min. Electrophoretic mobility ($\text{cm}^2/(\text{s/V})$) can be related to t_m by the relationship $\mu_e = L^2/tV = 5.39 \times 10^{-4}/t_m$ substituting $L_d L_i$ for L^2 where L_d is the length of the capillary from sample injection site to detector and L_i is the full capillary length.

^b Conditions for *N*-acetylcysteine and *S*-nitroso-*N*-acetylcysteine were exceptional (see text for details).

S-nitroso-*N*-acetylcysteine are displayed in Figure 4A–D. Confirmatory evidence for the detection of these *S*-nitroso thiol adducts was provided by monitoring absorbance at 320 nm (Figure 5). Reduced thiols and their disulfides were not detectable at this wavelength. As predicted above (Table I), the *S*-nitrosated derivatives exhibit slower electrophoretic mobilities than their corresponding thiols (Table II). It is again noteworthy that the conditions for electrophoresis of

Table III. Linearity of Peak Height vs Concentration of Thiols, Oxidized Derivatives, and *S*-Nitroso Thiols

	linear eq	corr coeff (<i>R</i>)
homocysteine	$Y = 2.98X - 0.0000016$	1.000
homocystine	$Y = 1.74X + 0.000014$	0.999
homocysteine thiolactone	$Y = 11.6X - 0.000014$	0.999
cysteine	$Y = 47.3X + 0.00032$	0.998
cystine	$Y = 4.90X + 0.000036$	0.990
glutathione	$Y = 3.60X + 0.000025$	0.999
glutathione disulfide	$Y = 10.3X + 0.000065$	0.995
<i>N</i> -acetylcysteine	$Y = 6.36X + 0.000062$	0.996
<i>S</i> -nitrosohomocysteine	$Y = 3.07X - 0.0000059$	0.999
<i>S</i> -nitrosocysteine	$Y = 6.44X + 0.000041$	0.990
<i>S</i> -nitroglutathione	$Y = 9.92X - 0.000039$	0.993
<i>S</i> -nitroso- <i>N</i> -acetylcysteine	$Y = 5.99X + 0.000010$	0.995

^a The *X* value of each equation refers to the concentration of each molecular species (in mol/L) and the *Y* value refers to the peak amplitude in absorbance units (at 200 nm). The slope of each equation is expressed in absorbance units/L/mole, and *Y* intercept in absorbance units.

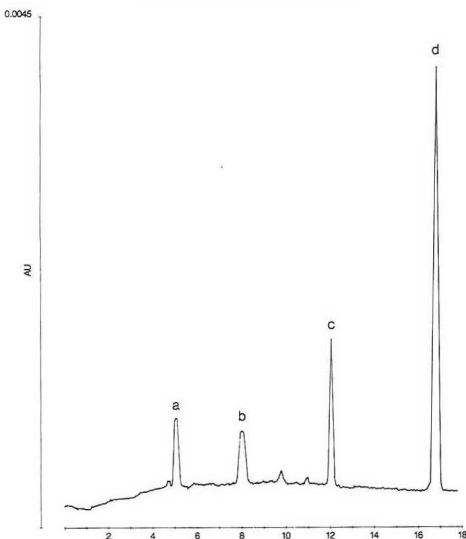


Figure 3. Reactions among disulfides under acidic conditions. Electrophoresis was performed on a sample mixture of equimolar (167 μ M) homocysteine, cystine, and glutathione disulfide. The electropherogram demonstrates four fully resolved peaks corresponding in concentration (cf. Table III) to homocysteine (102 μ M) (peak a), cystine (145 μ M) (peak b), and reduced glutathione (217 μ M) (peak d), with an additional unidentified peak noted at 11.9 min (peak c). On the basis of the quantitative discrepancy between injected and detected solute as well as theoretical predictions, peak c is identified as glutathione-homocysteine mixed disulfide. Thus, the electropherogram implicates the electrophilic cleavage mechanism for mixed disulfide formation under acidic conditions (see text for details). Conditions: sample buffer, 0.01 M sodium phosphate, 0.01 N HCl, pH 2.3; positive polarity at 11 kV; absorbance, 200 nm.

S-nitroso-*N*-acetylcysteine were exceptional (pH 5.0, negative polarity). Linearity in the relationship between peak heights and concentration is again excellent with correlation coefficients ≥ 0.99 (Table III).

In the case of *S*-nitroglutathione, four peaks were detected at 200 nm. The major peak of slowest electrophoretic mobility is identified as the *S*-nitroso thiol on the basis of predicted elution times (Table I), the coincident loss of the peak of

reduced glutathione (Figure 1), and the absorbance of this peak at 320 nm. The minor peak immediately preceding the *S*-nitroso thiol is identified as reduced glutathione on the basis of its migration time and is the result of incomplete nitrosation during synthesis or *S*-nitroso thiol decomposition during electrophoresis. The other two peaks remain unidentified. It is likely, however, that one of these is glutathione disulfide that forms as a result of spontaneous decomposition of the *S*-nitroso thiol¹ as it traverses the capillary. The peak height of *S*-nitroglutathione accounts for $72 \pm 6\%$ ($n = 4$) of the sum of the four peaks, and linearity between the sum total peak height and sample concentration is preserved ($R \geq 0.99$).

The separating power of HPE is further demonstrated in Figure 6A–C in which combinations of two (A) and three (B) thiols have been separated from their *S*-nitrosated derivatives. These electropherograms were generated by mixing equimolar amounts of thiol mixture in 2-fold and 3-fold molar excess, respectively, over sodium nitrite. It is noteworthy that *S*-nitroglutathione and *S*-nitrosohomocysteine form at the expense of *S*-nitrosocysteine.

DISCUSSION

These data reveal that capillary electrophoresis provides a rapid and reproducible method for separating the biological thiols, their oxidized forms (specifically, disulfides and homocysteine thiolactone) and their *S*-nitrosated derivatives. In that many techniques for sulfhydryl purification and separation exist, this method is remarkable for its simplicity, the lack of a requirement for thiol derivatization, and its general applicability. In the case of the biological *S*-nitroso thiols, this is the first report of a reliable method for their separation.

Although the diverse and critical roles of the biological thiols have been appreciated for quite some time, it was not until the early 1980s that Ignarro and co-workers recognized the potent vasodilatory properties of *S*-nitroso thiols and their possible importance as biochemical intermediates in the metabolism of organic nitrates;²⁹ the antiplatelet actions of these chemical species were noted shortly thereafter.⁵ Following the more recent observation that the endothelium-derived relaxing factor (EDRF) of Furchgott and Zawadzki possesses biochemical and chemiluminescent properties of NO,⁶ there has been increasing speculation that *S*-nitroso thiols exist as important biological intermediates in vascular smooth muscle and platelets as well. In fact, one group³⁰ has suggested that the chemical and spectrophotometric properties of EDRF more closely resemble those of *S*-nitrosocysteine than NO. These findings cannot, however, be accepted unconditionally as they are based on an original method for thionitrite synthesis that was not rigorously verified and a novel HPLC technique for separation of cysteine from its *S*-nitrosated derivative that did not convincingly show resolution of these species and was not tested for its reproducibility. Thus, the inadequacies of available techniques for purification and separation of *S*-nitroso thiols have significantly slowed progress in this area and have contributed in large measure to current controversy. Assays for free nitrite³¹ in diazotization reactions with sulfanilic acid in the presence and absence of HgCl₂, the latter reagent facilitating the hydrolysis of the S–NO bond,¹⁷ remain the most popular method in the biomedical literature for the detection of *S*-nitroso thiols. This method is useful in quantitative analyses but cannot elucidate the chemical identity of the parent *S*-nitroso thiol compound and is relatively insensitive.

Reversed-phase high-performance liquid chromatography (RP-HPLC) has been utilized for preparations of organic *S*-nitroso thiols³² and has proven helpful in limited analyses of the biological *S*-nitroso thiols.^{30,33} However, the sample preparation required for this method is a formidable obstacle

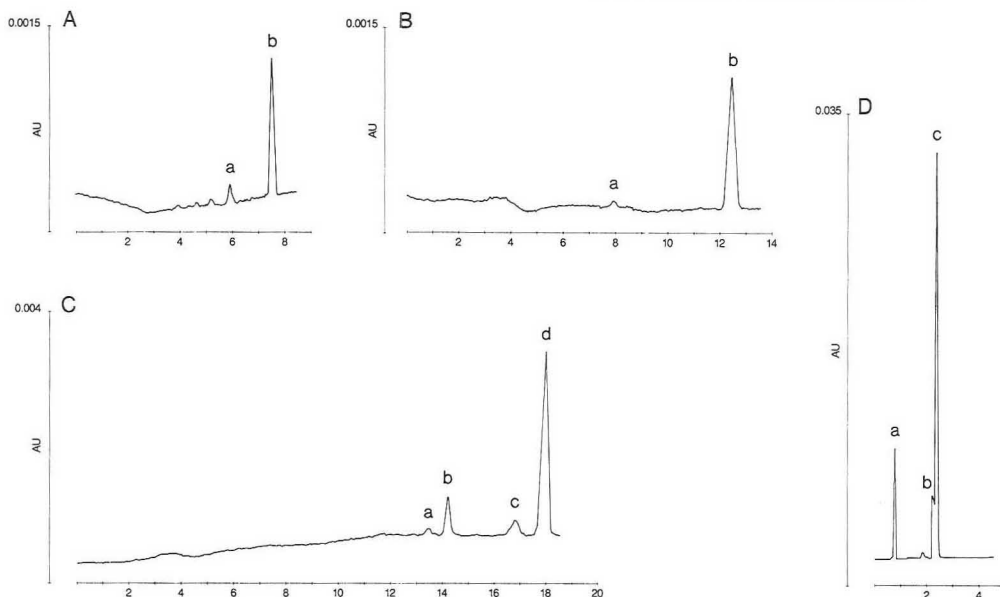


Figure 4. Electropherograms of *S*-nitrosothiols: (A) *S*-nitrosohomocysteine, with 92% conversion of 250 μ M homocysteine (peak a) to *S*-nitrosohomocysteine (299 μ M) (peak b); (B) *S*-nitrosocysteine, with 91% conversion of 250 μ M cysteine (peak a) to *S*-nitrosocysteine (228 μ M) (peak b); (C) *S*-nitrosogluthathione, with 92% conversion of 250 μ M glutathione (peak c) to *S*-nitrosogluthathione (170 μ M) (peak d) and to two additional unidentified peaks (peaks a and b), one of which very likely represents glutathione disulfide resulting from either oxidation of glutathione or decomposition of *S*-nitrosogluthathione (see text for details); (D) *S*-nitroso-*N*-acetylcysteine, with 82% conversion of 500 μ M *N*-acetylcysteine (peak b) to *S*-nitroso-*N*-acetylcysteine (410 μ M) (peak d) (peak a is unidentified; however it most likely represents *N*-acetylcysteine disulfide). *S*-Nitrosation of biological thiols was performed as described in the Materials and Methods, and concentrations were determined from the data of Table III. Conditions (A–C): sample buffer, 0.01 M sodium phosphate, 0.01 N HCl pH 2.3; positive polarity at 11 kV; absorbance, 200 nm. Conditions (D): sample buffer, 0.01 M sodium phosphate, 0.01 N HCl pH 5.0; negative polarity at 11 kV; absorbance, 200 nm.

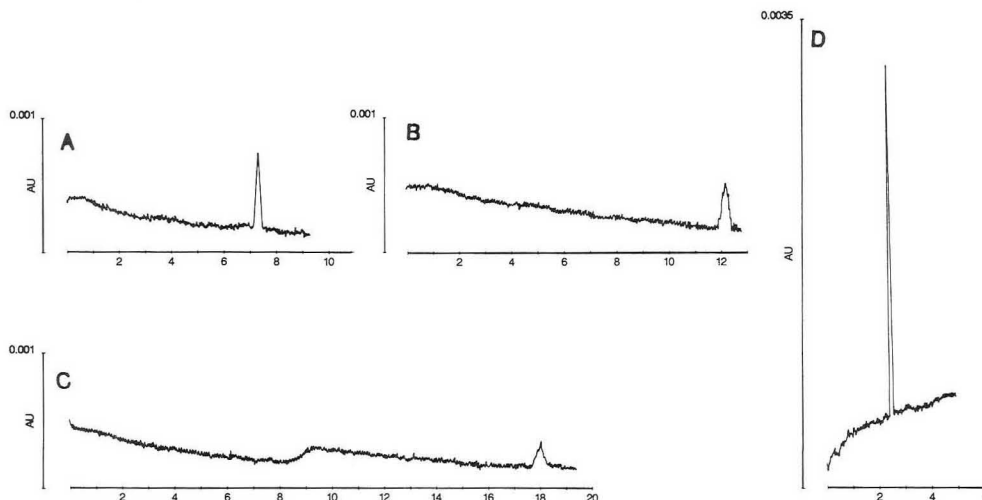


Figure 5. Electropherograms of *S*-nitroso thiols: (A) *S*-nitrosohomocysteine; (B) *S*-nitrosocysteine; (C) *S*-nitrosogluthathione; (D) *S*-nitroso-*N*-acetylcysteine. Details of sample preparation and detection are as presented in the legend in Figure 4, with the exception that the absorbance was measured at 320 nm.

owing to the inherent instability of the S–NO bond. Furthermore, such preparative modification results in sample dilution and may secondarily affect the analyte, thus altering its chemical and biological activity. At this time, these concerns have not been addressed for RP–HPLC detection of the

S-nitroso thiols of interest; and its sensitivity, reproducibility, and separating power have not been established.

HPE is not without a significant shortcoming, namely its lack of sensitivity. Although capable of detecting picomole quantities of *S*-nitroso thiols, its concentration detection limits

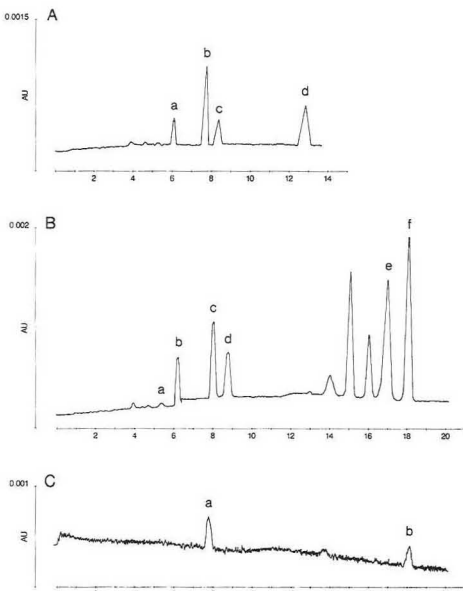


Figure 6. Separations of thiols and their S-nitrosated derivatives, with concentrations determined from the data of Table III. (A) Equimolar (500 μ M) homocysteine and cysteine were exposed to NaNO_2 in a 2:1 molar excess thiol over NaNO_2 . The electropherogram demonstrates preferential S-nitrosation of homocysteine over cysteine (1.5:1). The four fully resolved peaks correspond to homocysteine (peak a) (176 μ M), S-nitrosomethylhomocysteine (peak b) (335 μ M), cysteine (peak c) (295 μ M), and S-nitrosocysteine (peak d) (217 μ M). (B) Equimolar (1 mM) homocysteine, cysteine, and glutathione were exposed to NaNO_2 in a 3:1 molar excess thiol over NaNO_2 . Homocysteine (peak b) (312 μ M), cysteine (peak d) (528 μ M), and glutathione (peak e) (206 μ M) are fully resolved from S-nitrosomethylhomocysteine (peak c) (327 μ M) and S-nitrosoglutathione (peak f) (292 μ M), which form at the expense of S-nitrosocysteine (not detected). The small peak corresponding to homocysteine is also identified (peak a). (C) Capillary electrophoretic detection of the sample in B at 320 nm demonstrates the presence of S-nitrosomethylhomocysteine (peak a) and S-nitrosoglutathione (peak b). Conditions (A–C): sample buffer, 0.01 sodium phosphate, 0.01 N HCl, pH 2.3; positive polarity at 11 kV; absorbance (A, B) 200 nm.

are in the micromolar range. Thus, the current generation of commercial analytical systems is likely to be of limited usefulness for investigations at the cellular level. Similarly, with the exception of glutathione, which is present in micromolar to millimolar concentrations intracellularly, the physiologic concentrations of the other biologic thiols are at the limits of the sensitivity of HPE. Glutathione provides yet another technical problem in that (commercially available) preparations elute as two fully resolved peaks (Figure 1C), an observation that has been suggested by investigators in the area (A. Slivka, personal communication) to be the consequence of significant contamination with glutathione disulfide. The following evidence supports the view that the early minor peak is glutathione disulfide and the major peak is reduced glutathione: (1) the predicted migration times of the disulfide and the reduced thiol on the basis of effective charge calculations are 13.2 and 16.9 min (Table I), respectively, closely corresponding to the observed elution times of the minor ($t_m = 14.2 \pm 0.4$ min, $n = 6$) and major ($t_m = 16.3 \pm 0.4$ min, $n = 6$) peaks; (2) carboxyamidation of glutathione's sulfhydryl group with iodoacetamide leads to the generation of a new peak with a migration time of 18.3 ± 0.3 min, closely ap-

proximating that predicted for a carboxyamidated glutathione conjugate ($t_p = 18.9$ min) (data not shown); (3) the strong reducing conditions engendered by preincubation of glutathione in a 14-fold molar excess of 2-mercaptoethanol (a neutral thiol that will not migrate electrophoretically) for 30 min eliminated the early peak (data not shown); and, most importantly, (4) the observed mobility of purified glutathione disulfide ($t_m = 13.4 \pm 0.3$ min, $n = 6$) closely corresponds to that of the minor peak (Figure 2C).

Another potential problem that arises in the analysis of biologic thiols and their S-nitrosated derivatives is the potential artifactual formation of S-nitroso thiols under conditions of acidic pH. Ignarro and colleagues⁴ showed that S-nitroso thiols can form at pHs as high as 5, but these experiments were conducted at 37 °C. We have analyzed the pH and temperature dependence of the formation of S-nitroso thiols (specifically S-nitroso-L-cysteine from 50 mM NaNO_2 and 50 mM L-cysteine) at pH 5.0 and found that no more than 4.7% of L-cysteine is converted to S-nitroso-L-cysteine by 20 min when working at 4 °C. Thus, by working at low temperatures and less acidic pH, the artifactual formation of S-nitroso thiols can be limited. Furthermore, in the preparation of protein-containing biologic specimens, precipitation of protein with acetone or ether is to be preferred over acid.

The simplicity and rapidity of HPE suggests that it may find its place among the more powerful spectrophotometric³⁴ and fluorometric³⁵ assays for thiol detection as a complementary tool in instances where sensitivity is not a limiting factor. In such cases, separations under acidic conditions are preferable as specificity is improved. The availability and successful application of thermo-optical absorbance,⁹ electrochemical detection,³⁶ and indirect fluorescence emission⁹ to electrophoretic techniques promises to lower the detection limits of this modality significantly, thereby obviating the one major limitation of the method at the present time.

ACKNOWLEDGMENT

We thank Nancy Beattie and Stephanie Tribuna for superb secretarial support. This work was supported by NIH Grants HL40411 and HL43344, by a Grant-in-Aid from the American Heart Association with funds contributed in part by its Massachusetts Affiliate, and by a grant from Glaxo, Inc. J.S.S. is the recipient of a National Research Fellowship Award from the NIH (F32 HL08177); J.L. is the recipient of a Research Career Development Award from the NIH (K04 HL02273).

REFERENCES

- Jocelyn, P. C. *Biochemistry of the SH Group*; Academic Press: London/New York, 1972; pp 1–46.
- Oae, S.; Shinham, K. *Org. Prep. Proced. Int.* **1983**, *15*, 165–198.
- Loscalzo, J. J. *Clin. Invest.* **1985**, *76*, 703–708.
- Ignarro, L. J.; Lipton, H.; Edwards, J. C.; Baricos, W. H.; Hyman, A. L.; Kadowitz, P. J.; Gruetter, C. A. *J. Pharmacol. Exp. Ther.* **1981**, *218*, 739–749.
- Mellon, B. T.; Ignarro, L. J.; Myers, C. B.; Ohlstein, E. H.; Ballot, B. A.; Hyman, A. L.; Kadowitz, P. J. *Mol. Pharmacol.* **1983**, *23*, 653–664.
- Palmer, R. M. J.; Ferrige, A. G.; Moncada, S. *Nature (London)* **1987**, *327*, 1020–1022.
- Ignarro, L. J.; Buga, G. M.; Wood, K. S.; Byrns, R. E.; Chandhuri, G. *Proc. Natl. Acad. Sci. U.S.A.* **1987**, *84*, 9265–9268.
- Kahr, W. G.; Yeung, E. S. *Anal. Chem.* **1988**, *60*, 1832–1834.
- Yu, M.; Dovichi, N. J. *Anal. Chem.* **1989**, *61*, 37–40.
- Grossman, P. D.; Wilson, K. J.; Petrie, G.; Lauer, H. H. *Anal. Biochem.* **1988**, *173*, 265–270.
- Tskas, D.; Brunner, G. J. *Chromatogr.* **1989**, *470*, 191–199.
- Holloway, C. J.; Battersby, R. V. *Analytical and Preparative Isotachophoresis*; Walter de Gruyter: Berlin/New York, 1984; pp 193–196.
- Biorad Laboratories, Application No. 1, 1990.
- Hopkins, F. G. *J. Biol. Chem.* **1929**, *84*, 266–320.
- Jocelyn, P. C. *Biochemistry of the SH Group*; Academic Press: London/New York, 1972; pp 95.
- Ignarro, L. J.; Edwards, J. C.; Gruetter, D. Y.; Barry, B. K.; Gruetter, C. A. *FEBS Lett.* **1980**, *11*, 275–278.
- Saville, B. *Analyst* **1958**, *83*, 670–672.
- Ellman, G. L. *Arch. Biochem. Biophys.* **1959**, *82*, 70–77.
- Riegel, B.; du Vigneaud, V. J. *Biol. Chem.* **1935**, *112*, 149–154.
- Jocelyn, P. C. *Biochemistry of the SH Group*; Academic Press: London/New York, 1972; pp 117–136.

- (21) Thannhauser, T. W.; Konishi, Y.; Sheraga, H. A. *Anal. Biochem.* **1984**, *138*, 181-186.
- (22) Smythe, C. V. *J. Biol. Chem.* **1936**, *114*, 601-608.
- (23) Jocelyn, P. C. In *Methods in Enzymology*; Jacoby, W. B., Griffith, O., Eds.; Academic Press: New York, 1987; Vol. 143, pp 63-66.
- (24) Grossman, P. D.; Colburn, J. C.; Lauer, H. H. *Anal. Biochem.* **1989**, *179*, 28-33.
- (25) Pirie, N. W.; Pinhey, K. G. *J. Biol. Chem.* **1929**, *84*, 321-333.
- (26) *Handbook of Biochemistry and Molecular Biology*; CRC Press: Boca Raton, FL, 1982.
- (27) Rodgers, G. M.; Kane, W. H. *J. Clin. Invest.* **1986**, *77*, 1909-1916.
- (28) McCully, K. S.; Carvalho, A. C. A. *Res. Commun. Chem. Pathol. Pharmacol.* **1987**, *56*, 349-360.
- (29) Ignarro, L. J.; Barry, B. K.; Gruetter, D. Y.; Edwards, J. C.; Ohlstein, F. O.; Gruetter, C. A.; Baricos W. H. *Biochem. Biophys. Res. Commun.* **1980**, *94*, 93-100.
- (30) Myers, P. R.; Minor, R. L., Jr.; Guerra, R., Jr.; Bates, J. N.; Harrison, D. G. *Nature* **1990**, *345*, 161-163.
- (31) Snell, F. D.; Snell, C. T. *Colorimetric Methods of Analysis*, 3rd ed.; D. Van Nostrand Co.: New York, 1949; pp 804.
- (32) Oae, S.; Kim, Y. H.; Fukushima, D.; Shinham, K. J. *Chem. Soc.* **1978**, *38*, 913-917.
- (33) Fung, H.-L.; Chong, S.; Kowaluk, K.; Hough, K.; Kakemi, M. *J. Pharmacol. Exp. Ther.* **1988**, *246*, 524-530.
- (34) Jocelyn, P. C. *Methods in Enzymology*; Jacoby, W. B., Griffith, O., Eds.; Academic Press: New York, 1987; Vol. 143, pp 44-67.
- (35) Jocelyn, P. C. *Methods in Enzymology*; Jacoby, W. B., Griffith, O., Eds.; Academic Press: New York, 1987; Vol. 143, pp 67-75.
- (36) Banks, P. J. *Natl. Inst. Health Res.* **1990**, *2*, 87-89.

RECEIVED for review June 11, 1991. Accepted January 2, 1992.

Microscopic Order as a Function of Surface Coverage in Alkyl-Modified Silicas: Spin Probe Studies

Paul B. Wright, Edward Lamb, John G. Dorsey,[†] and Robert G. Kooser*

Department of Chemistry, Knox College, Galesburg, Illinois 61401

The chemically modified surface plays an important role in retention in reversed-phase liquid chromatography. One surface factor that might affect retention is solute expulsion due to partial ordering of the grafted chains at sufficiently high grafting densities. This study has shown by the use of the electron paramagnetic resonance technique of spin probing that spectroscopic evidence exists for an increase in molecular order of the bonded octadecyl phase as a function of grafting density. The spin probe, DOXYL-cholesterol, shows significant increase in the order parameter, S , as a function of increased surface coverage. In addition, DOXYL-cholesterol undergoes a decrease in rotational freedom and an increase in rotational anisotropy as the grafting density increases.

INTRODUCTION

Knowledge of the molecular mechanism of retention in reversed-phase liquid chromatography (RPLC) is important for the design of separation procedures and for the fundamental understanding of the chemistry of solvated heterogeneous surfaces. Recently, theoretical studies by Dill¹ have indicated that, for small solute molecules, the partitioning of solute between the stationary and mobile phases should be the operable mechanism in RPLC. This theory along with other possible theories have been reviewed by Dorsey and Dill.² In Dill's work² there are two driving forces that affect chromatographic retention: (i) the free energy difference between the interaction of the solute with molecular neighbors in the stationary and mobile phases as measured by binary interaction constants and (ii) the partial ordering of the bonded stationary phase which at sufficiently high grafting densities causes expulsion of the solute from the stationary phase. The chromatographic consequence of driving force ii is the prediction that the thermodynamic partition coefficient, K , for small nonpolar molecules between the mobile and stationary phases should increase linearly with bonded-phase surface

coverage until a maximum is reached at a coverage of about $2.7 \mu\text{mol}/\text{m}^2$ at which point a decrease occurs with further increase in coverage. This prediction was found to be experimentally true in the work of Sentell and Dorsey³ where partition coefficients of naphthalene were shown to increase linearly with surface coverage of octadecyl alkyl chains until a density of $3.1 \mu\text{mol}/\text{m}^2$ was reached, after which point the K value decreased. The inference from this study is that the increased chain ordering caused this decrease.

Spectroscopic techniques have been extremely useful in characterizing and understanding bonded surfaces, exemplified by the fluorescent techniques of Lochmüller and associates.⁴⁻⁷ For instance, there is partial spectroscopic evidence for some degree of chain ordering from ^{13}C NMR studies⁸⁻¹⁰ that have shown there is a motional gradient among the carbon atoms in a bonded chain with those nearest the surface as the most hindered. No spectroscopic studies have been conducted on the effects of chain ordering as a function of surface coverage, however.

A viable method for the study of molecular order is the spin probe technique in which paramagnetic molecules are intercalated into a medium and the electron paramagnetic resonance (EPR) spectrum is studied as a function of medium modification. The spin probe technique has been very useful in membrane and polymer studies and has been reviewed several times.¹¹⁻¹⁸ It has been applied to RPLC phases to determine surface solvation and solute-surface interactions.^{17,18} Ordering information of the host phase comes about from the rotational effects on the probe by the host which, in turn, affect the EPR spectral shape and line widths. Line width analysis in the fast motional regime (rotational rates greater than about 10^9 s^{-1}) using the fast motional theory of Freed and co-workers^{19,20} can yield a mean rotational correlation time, τ , and rotational anisotropy factor, N , that can demonstrate motional constraints that the host medium places on the probes and thereby indicate how the probe is constrained geometrically by the host. Another common indicator of molecular order is the order parameter, S , which is calculated from the differences in magnetic field values of certain EPR spectral features and the single crystal hyperfine coupling tensor components.²¹ In the motional domain observed for

[†] Department of Chemistry University of Cincinnati, Cincinnati, OH 45221-0172.

spin probes, the order parameter is a measure of motional order of the probe²¹ and runs from zero, perfectly disordered motion, to unity, perfectly ordered; the order of the probe motion reflects directly the order of the host.

We report here the first spin probe study of molecular order as a function of grafting density in octadecyl alkyl modified silicas, and the results confirm the earlier inferences of Sentell and Dorsey³ and corroborate the theory of Dill.¹

EXPERIMENTAL SECTION

Materials. The spin probes 2,2,6,6-tetramethyl-1-piperidinyloxy (TEMPO) and *N*-oxy-4,4-dimethylspiro[oxazolidine-5 α -cholestane] (CSL) were purchased from Aldrich Chemical (Milwaukee, WI) and used as received. The organic solvents, methanol (MeOH) and acetonitrile (ACN), were reagent grade and were purchased from Fisher Scientific (Chicago, IL). Doubly deionized water was used. Before use, the solvents were filtered through 0.2- μ m membrane filters (Alltech Associates, Deerfield, IL). All mixed solvents were made up on a volume/volume basis and were thoroughly degassed with nitrogen to exclude oxygen before EPR examination. The alkyl bonded phases were synthesized and characterized as previously described³ and were identical to those samples used in the partition coefficient study.³

EPR Measurements. EPR spectra were taken on a modified Varian V-4500 EPR spectrometer with 6-in. magnet equipped with a MicroNow (Chicago, IL) modified bridge and a Stanford Research Systems (Palo Alto, CA) SR-565 lock-in amplifier. Data acquisition and reduction was done using LabCalc (Galactic Enterprises, Salem, NH) software on a 386 computer. The magnetic field modulation frequency was 100 kHz, and the usual precautions were taken to avoid microwave saturation and field modulation distortions. The magnetic field sweep was calibrated using the known coupling constants of either *p*-benzosemiquinone ion (0.2368 mT²²) in alkaline ethanol solution or TEMPO in CCl₄ (1.535 mT²³). The coupling constants were uncertain to ± 0.008 mT; line widths to ± 0.002 mT.

All experiments with the spin probes in contact with the alkyl-modified silicas were done in a dynamic "steady state" mode. A column consisting of $1/8$ -in.-o.d. Tefzel tubing (Upchurch, Oak Harbor, WA) held rigid by a $1/8$ -in.-i.d. glass tube was connected on either end with unions (Upchurch Model P-614) to $1/16$ -in. PEEK tubing (Upchurch); one end of the PEEK tubing was attached to a Spectra Physics (San Jose, CA) IsoChrom solvent delivery pump. The column was dry-packed with the stationary phase and held in the column by a frit ($1/16$ in., Alltech, Model 720005) in the exit end of the column. The column was inserted into the cavity and held in place with aqueous flat cell holders on the Varian TE102 cavity. All experiments were done by pumping the degassed mobile phase of given composition containing the spin probe (concentration of 0.1 mM or less) through the column in the spectrometer, and observations were done when the column was under flow conditions. The entire solvent delivery Teflon tubing was encased in $1/2$ -in.-i.d. plastic tubing in order to provide a nitrogen gas sheath to prevent reincorporation of oxygen into the solvent. All columns were "conditioned" with the mobile phase/probe solution for at least 0.5 h before observation. Flow rates ranged from 0.1 to 0.5 mL/min.

EPR parameters for probes in the absence of the bonded phases were determined by degassing a probe solution with nitrogen and transferring the solution in a nitrogen atmosphere in a glovebox to a 1.5-mm capillary tube for EPR observations.

Rotational correlation time analysis was done using the fast tumbling theory of Freed and co-workers.^{19,20} In the fast tumbling regime, the line width can be expressed as a quadratic function of the nitrogen hyperfine index number, *m*.

$$\delta = A + Bm + Cm^2 \quad (1)$$

The values of *A*, *B*, and *C* were taken from line widths corrected for inhomogeneous broadening using the method of Bales²⁴ by measuring the width of the central line and the amplitudes of the high- and low-field lines, allowing for the more precise determination of the high- and low-field lines. The calculation of the rotational properties requires the knowledge of the *g* and hyperfine tensor components for the probe. The magnetic parameters for CSL were taken from Meirovitch and Freed,²⁵ and the hyperfine

Table I. EPR Spectral Parameters for TEMPO in Different Bonded Surface Coverages

probe/coverage, $\mu\text{mol}/\text{m}^2/\text{solvent}$	a_N , mT	line heights ^a		center line width, mT ^b
		low field	high field	
TEMPO/1.74/MeOH	1.590	0.969	0.961	0.131
3.48/MeOH	1.577	0.967	0.956	0.132
1.74/50-50 MeOH-water	1.603	0.942	0.779	0.132
3.48/50-50 MeOH-water	1.597	0.938	0.798	0.136

^a Relative to the central line as 1.000. ^b Uncorrected for inhomogeneous broadening.

components were corrected for solvent polarity by multiplying each by the ratio of the isotropic coupling constant in contact with the bonded surface to the literature value.²⁵ The rotational correlation times were calculated separately from the *B* and *C* terms following the method of Polnaszek et al.²⁶ in order to establish the preferred direction of probe rotation. If the rotational motion is isotropic, the τ_B and τ_C values are the same; if the values are unequal, they establish the preferred direction of rotation in the molecular axis system. The values of the mean rotational correlation time, τ , and the rotational anisotropy, *N*, were obtained by an iterative convergence method (*N* is the ratio of the molecular symmetry axis rate of rotation to the perpendicular axes rate; hence for isotropic rotation, *N* is unity and, if *N* is greater than unity, the molecular symmetry axis is the fast axis). Approximate correlation times were first obtained by solving for their values in the fast tumbling line width equations without nonsecular and pseudosecular terms²⁰ as given in²

$$B = 0.103\omega_0[\Delta g\Delta a\tau_0 + 3\delta g\delta a\tau_2]$$

$$C = 1.13 \times 10^7[(\Delta a)^2\tau_0 + (\delta a)^2\tau_2]$$

$$\tau = [2\tau_2(\tau_0)^2/(3\tau_0 - \tau_2)]^{1/2}$$

$$N = [3\tau_0 - \tau_2]/[2\tau_2\tau_0] \quad (2)$$

where *B*, *C*, and hyperfine terms are in milliteslas; $\Delta a = a_z - 0.5(a_x + a_y)$ and $\delta a = 0.5(a_x - a_y)$ with similar definitions for the *g*-value terms (axes refer to the molecular system¹¹). Then these initial, but approximate, correlation time values were placed into the nonsecular terms of the full line width expressions (without the pseudosecular terms which are negligible in this motional domain) for *B* and *C*.²⁷ The full equations²⁰ were then solved for τ_0 and τ_2 , these new approximate values were resubstituted into the nonsecular terms of the full equations, and new values for the correlation times were found until no further change in the correlation times were found.

The order parameter, *S*, was calculated by method II of Hayes and Griffith,²⁸ corrected for the approximate location of the spectral peaks using the method of Gaffney.²⁹

RESULTS AND DISCUSSION

A small nearly spherical spin probe (TEMPO) was first investigated for its rotational hindrance in the presence of two RPLC phases of different coverages. Previous studies¹⁷ have established that the EPR signals seen under the dynamic conditions used here are from the probe partitioned into the stationary phase. Furthermore, we have established that small molecules like TEMPO are excellent probes of surface solvation.^{17,18} For the TEMPO probes interacting with bonded silicas of various coverages, the coupling constants and line width and amplitude values are given in Table I. The coupling constant, a measure of the interaction between the nitrogen nuclear spin and unpaired electron in the NO bond, is sensitive to the polarity of the solvent in the neighborhood of the probe;^{23,30} the greater the polarity of the solvent medium, the greater the coupling constant. In addition, the slower the rotational motion, the broader are the line widths (center line width) and, for a given rotational rate, changes in the spectral peak height ratios are an indication of changes in spatial restrictions of the host medium on rotational motion

Table II. EPR Spectral Features for the Cholestane Spin Probe Interacting with Solvated Bonded Octadecylsilicas of Various Surface Coverages

surface coverage, $\mu\text{mol}/\text{m}^2$	solvent	a_N , mT	center line width, mT ^b	line heights ^a		order param	rel integrated intens
				low field	high field		
free in soln	MeOH	1.535	0.261	0.978	0.941	0.071	
1.74	MeOH	1.520	0.278	0.733	0.489	0.093	1.0
2.72	MeOH	1.523	0.286	0.703	0.437	0.103	1.1
3.48	MeOH	1.534	0.315	0.611	0.328	0.127	4.5
free in soln	ACN	1.501	0.237	0.982	0.970	0.067	
1.74	ACN	1.486	0.275	0.752	0.504	0.068	1.0
2.72	ACN	1.492	0.284	0.738	0.482	0.076	1.4
3.48	ACN	1.489	0.311	0.636	0.391	0.129	1.2

^aRelative to the center peak height as 1.000. ^bUncorrected for inhomogeneous broadening.

of the probe: the greater the peak height decreases, the greater the restriction, i.e. rotational anisotropy. The data show that there are only small variations in both coupling constants and line widths; careful inspection does show slight, but significant, variations in the coupling constants for TEMPO, decreasing with increased surface coverage in pure methanol solvent. This is indicative of a less polar probe environment at the higher grafting density that is probably due to a slight decrease in the extent of solvation of the bonded surface since it is to be expected that the polar methanol molecules would be less likely to penetrate the more densely covered surface. This is consistent with the observations of Cole and Dorsey³¹ who found that reequilibration times after an elution gradient followed the same curve as the partition coefficients for small solute molecules in octadecyl phases.³ This effect is the result of decreased surface solvation at high grafting densities.

The line widths for the TEMPO probe show no significant variation with either coverage or change in the solvent from pure methanol to 50–50 methanol–water. The fact that little in the way of rotationally dependent spectral changes are seen as a function of grafting density for this probe should not be surprising as TEMPO is a small, approximately spherical molecule and would be expected to have little rotational sensitivity to increased surface order. The changes from pure methanol to 50–50 methanol–water do show increased rotational anisotropy in both coverages which is the result of increased chain stiffening in the presence of the water.^{17,18}

The cholestane spin probe is of a different character than the piperidinyloxy probes as it is a large, rather "flat" molecule (see Figure 1), and it should exhibit significantly different intercalation behavior. An important feature is that the paramagnetic center, the dimethylxazolidine-*N*-oxyl (DOXYL) group, is bonded to the cholestane moiety so that the y magnetic axis of the nitroxide group is oriented parallel to rotational axis (z') of the host molecule.²¹ Because the shape of this molecule is approximately cylindrical, the rotation of the probe is anisotropic with the fast axis parallel to the long axis of the molecule (z').²⁵ The studies of the spectral features of CSL as a function of surface coverage in two different solvents are given in Table II, and typical spectra are shown in Figures 2 and 3. Keep in mind that the spectra in the presence of the chemically modified phase are from probe molecules in contact with the bonded medium and are not those seen from the superposition of two signals, one in the solvent and the other from the intercalated probe¹⁷ as often seen in membrane studies.^{11,13,14} In order to establish the spectral effects as due to the interaction of the probe with bonded octadecyl phase rather than the silica surface, a similar experiment was run using unmodified silica and results, as shown in Figure 2, clearly indicate it is the presence of the bonded phase that is responsible for the spectral changes seen.

The insertion behavior of CSL is expected to be different than the small TEMPO-like probes; hence the coupling con-

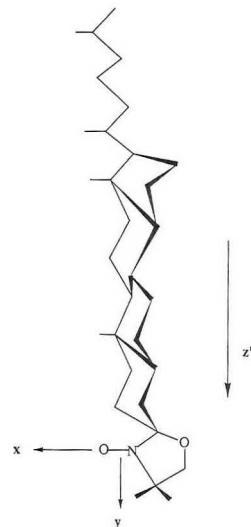


Figure 1. 3-Doxyl-5- α -cholestane spin label showing the orientation of the magnetic axes with respect to the symmetry axis of the molecule. The magnetic y axis is parallel to the z' symmetry axis.

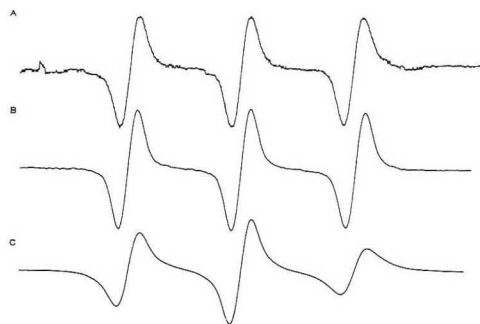
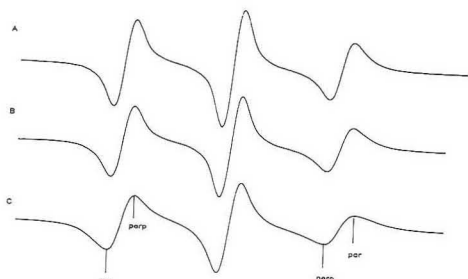


Figure 2. EPR spectra of the cholestane spin probe in various environments: (A) probe free in methanol solution; (B) probe in methanol flowing through a unmodified silica column; (C) probe in methanol flowing through a column packed with octadecyl RPLC phase at a coverage of $3.48 \mu\text{mol}/\text{m}^2$. Note the similarities of (A) and (B) showing that the silica surface is not causing the spectral shifts seen.

stants contain different information. It is known that when CSL is intercalated into membranes, the DOXYL group is found in the polar headgroup region of the membrane.³²

Table III. Line Width Values and Correlation Times for the Cholestane Spin Probe Interacting with Octadecyl-Modified Silicas of Different Surface Coverages

surface coverage, $\mu\text{mol}/\text{m}^2$	solvent	B , mT	C , mT	$10^{-10}\tau_B$, s	$10^{-10}\tau_C$, s	τ_C/τ_B
1.74	MeOH	-0.0120	0.0441	1.5	5.3	3.6
2.72	MeOH	-0.0130	0.0496	1.6	6.0	3.7
3.48	MeOH	-0.0179	0.0736	2.2	8.9	4.0
1.74	ACN	-0.0141	0.0448	1.8	5.7	3.2
2.72	ACN	-0.0171	0.0523	2.2	6.7	3.0
3.48	ACN	-0.0296	0.0824	3.8	10	2.7

**Figure 3.** Cholestane spin probe in methanol flowing through the column with RPLC phases of different coverages: (A) 1.74 $\mu\text{mol}/\text{m}^2$; (B) 2.72 $\mu\text{mol}/\text{m}^2$; (C) 3.48 $\mu\text{mol}/\text{m}^2$. The lines on (C) indicate the features used to evaluate the order parameter; the parallel component is the difference between the points marked "par", and the perpendicular difference between the points marked "perp". Note the progressive broadening of the high- and low-field lines as coverage increases.

Because of this, it is highly likely that the large nonpolar cholestane part of the probe is in the hydrocarbon region and the DOXYL moiety is near or in the solvent-bonded phase interface. The coupling constant patterns shed only some light on changes in the bonded phase. A slight increase to pure solvent values for CSL is seen in methanol solvent, indicative of partial expulsion of the probe into the solvent region at high bonding density. As in methanol, the coupling constant of CSL in acetonitrile is lower in the presence of the bonded phase, indicating the lower medium polarity in the reversed phase. Little change in the coupling constants with coverage is seen in acetonitrile, reflecting the greater amount of acetonitrile in the stationary phase for a given volume fraction of solvent than methanol.^{33,34}

In contrast, the line widths and line shapes show some remarkable changes. The width of the central line of the three-line coupling pattern is broader in the presence of the modified surface, as has been seen in other probe-RPLC phases,^{17,18} and is indicative of rotational hindrance from intercalation of the probe into the octadecyl-modified surface. The emergent pattern in both acetonitrile and methanol is that the line width increases monotonically with increasing surface coverage and, at the same time, the low- and high-field lines broaden, as indicated by their decreased amplitudes (see Figure 3). The changes result from decreased rotational mobility and an increase in the rotational anisotropy, both effects that would be expected if there were an increase in microscopic order in the bonded phase. This inference finds truth in the changes seen in S , the order parameter, as displayed in Table II. In both acetonitrile and methanol solutions, the order parameter increases as coverage increases and is direct evidence of an increase in RPLC order as predicted by the experimental work of Sentell and Dorsey.³

Further evidence of the role of increased surface coverage in the modification of the rotational motion of the probe can be gotten from a detailed line width analysis. Following

Table IV. Correlation Times and Rotational Anisotropy Factors for the Cholestane Spin Probe as a Function of Octadecyl-Modified Silica Coverage

surface coverage, $\mu\text{mol}/\text{m}^2$	solvent	$10^{-10}\tau$, s	N
1.74	MeOH	3	32
2.72	MeOH	3.6	35
3.48	MeOH	4.9	43
1.72	ACN	3.9	25
2.72	ACN	4.7	22
3.48	ACN	6.7	13

Polnaszek et al.,²⁶ we have calculated correlation times separately from the line width B and C terms and display the results in Table III. These correlation times in Table III are not the true rotational correlation times, but they contain motional information. If τ_C is greater than τ_B , the fast motional axis is along the magnetic y or z axes (see Figure 1), but because of the geometry of CSL, we can eliminate the z axis case. It should not be a surprise that the y axis is the fast axis because of the CSL geometry.

It might be argued that the spectral changes observed in Table II are from effects due to an increase in the intercalated probe concentration as the coverage increases.³⁵ Since the double integral of the derivative EPR spectrum gives a value proportional to the spin concentration, we have given the relative integrated intensities in Table II. The values are relative to the smallest intensity in contact with a given solvent, and no comparisons between solvents are possible because the precautions to remove changing instrumental factors when solvents are changed were not taken.³⁶ Keeping in mind the relatively high uncertainty of spin concentration determinations, an inspection of the data shows that there is an increase of 4–5-fold in the methanol case while acetonitrile reveals almost no variation. Since the order parameter in both solvents increases dramatically with coverage, the trends show that changing probe concentration with coverage is not the source of the order effects.

A more detailed motional analysis can be done by solving the fast motional equations for B and C for the values of τ and N using the iterative method explained in the Experimental Section. Table IV shows the results of these calculations. The rotational correlation times are uniformly slower for acetonitrile than methanol at all coverages, an indication of the greater surface solvation³⁴ and increased microviscosity in the acetonitrile-solvated bonded phase. Both solvents also show an increase in the correlation time as coverage increases, indicating an inhibition in rotation at higher bonding densities. The values of N show that rotational anisotropy increases in methanol solvation but decreases in acetonitrile. The picture that comes from these data is that increased bonding density impedes rotation. The fact that the N value trend in acetonitrile is opposite to that in methanol and opposite to naive expectations reinforces the anomalous role that acetonitrile plays in RPLC.³⁷ Recent work by Rowlen and Harris³⁸ focused on the structure of water-acetonitrile mixtures with emphasis on chromatographic implications. They found that in aqueous

solutions acetonitrile associates with itself and the character of the associated species varies with solvent composition. It is this variation and the unique interaction that each species has with solutes and the stationary phase that give acetonitrile its chromatographic character.³⁸ In this study, the mobile-phase composition is fixed, but the stationary phase varies. It is possible that the nature of associated acetonitrile in the stationary phase will change as the bonding density changes and this will cause the character of the solvated phase to change. The Rowlen and Harris study³⁸ involved a hydrogen-bonding solvent, so the detailed conclusions drawn there are not obviously applicable to acetonitrile-hydrocarbon mixtures. Additionally, work in this laboratory with six-carbon dimethylloxazolidine-*N*-oxyl-labeled silicas³⁹ has reinforced the anomalous behavior of acetonitrile-solvated phases. In this study, the temperature dependence of the rotational correlation time of methanol- and acetonitrile-solvated bonded silicas of intermediate coverage gave rise to a good Arrhenius fit. While the activation energy for rotation in acetonitrile phases was slightly lower than methanol (10 versus 13 kJ/mol), the frequency factor was much larger (5.9×10^{-12} s versus 1.1×10^{-12} s). This indicates that while the energy barrier to rotational activation is lower in the better solvated acetonitrile phase, the entropy of activation for rotation is less favorable.

The EPR results above argue strongly for the increase in molecular order with an increase in surface coverage. The most direct evidence comes from the increase in both solvents of the order parameter as a function of increased RPLC phase coverage. In addition, line width analysis indicates a substantial degree of rotational hindrance as a function of increased coverage, a result consistent with more densely packed alkyl chains. The fact that, in methanol, the rotational anisotropy factor increases with coverages argues for a more ordered environment while the results in acetonitrile remain anomalous in character with its chromatographic behavior.

ACKNOWLEDGMENT

We are grateful for support for this work from NSF Grant CHE-8921987, the Educational Committee of the E. I. du Pont de Nemours Co., and The Dow Chemical Co. Foundation. Acknowledgment is also made to the donors of the Petroleum Research Fund, administered by the American Chemical Society, in partial support of this research. J.G.D. gratefully acknowledges support from AFOSR 91-0254.

REFERENCES

- (1) Dill, K. A. *J. Phys. Chem.* **1987**, *91*, 1980.
- (2) Dorsey, J. G.; Dill, K. A. *Chem. Rev.* **1989**, *89*, 331.

- (3) Sentell, K. B.; Dorsey, J. G. *Anal. Chem.* **1989**, *61*, 930.
- (4) Lochmüller, C. H.; Marshall, D. B.; Wilder, D. R. *Anal. Chim. Acta* **1981**, *130*, 31.
- (5) Lochmüller, C. H.; Marshall, D. B.; Harris, J. M. *Anal. Chim. Acta* **1981**, *131*, 263.
- (6) Lochmüller, C. H.; Colburn, A. S.; Hunnicutt, M. L.; Harris, J. M. *Anal. Chem.* **1983**, *55*, 1344.
- (7) Lochmüller, C. H.; Colburn, A. S.; Hunnicutt, M. L.; Harris, J. M. *J. Am. Chem. Soc.* **1984**, *106*, 4077.
- (8) Gilpin, R. K. *J. Chromatogr. Sci.* **1984**, *22*, 371.
- (9) Gilpin, R. K.; Gangoda, M. E. *J. Chromatogr.* **1983**, *21*, 352.
- (10) Sindorf, D. W.; Maciel, G. E. *J. Am. Chem. Soc.* **1983**, *105*, 1848.
- (11) *Spin Labeling: Theory and Applications*; Berliner, L. J., Ed.; Academic Press: New York, 1976.
- (12) *Molecular Motion in Polymers by ESR*; Boyer, R. F.; Keinath, S. E., Eds.; MMI Press Symposium, Vol. 1; Harwood Academic Press: New York, 1980.
- (13) *EPR and Advanced EPR Studies of Biological Systems*; Dalton, L. R., Ed.; CRC Press: Boca Raton, FL, 1985.
- (14) *Methods for Studying Membrane Fluidity*; Aloia, R. C.; Curtin, C. C.; Gordon, L. M., Eds.; Alan R. Liss: New York, 1988.
- (15) *Spin Labeling: Theory and Applications, Biological Magnetic Resonance*; Berliner, L. J.; Reuben, J., Eds.; Plenum Press: New York, 1989; Vol. 8.
- (16) *Advanced EPR Techniques: Applications in Biology and Biochemistry*; Hoff, A. J., Ed.; Elsevier: Amsterdam, 1989.
- (17) Miller, C.; Dadoo, R.; Kooser, R. G.; Gorse, J. J. *Chromatogr.* **1988**, *458*, 255.
- (18) Miller, C.; Joo, C.; Roh, S.; Gorse, J.; Kooser, R. G. In *Chemically Modified Oxide Surfaces*; Leyden, D. E., Collins, W. T., Eds.; Proceedings of Chemically Modified Surfaces Symposium; Gordon and Breach: New York, 1990; pp 251-268.
- (19) Freed, J. H. *J. Chem. Phys.* **1964**, *41*, 2077.
- (20) Goldman, S. A.; Bruno, G. V.; Polnaszek, C. F.; Freed, J. H. *J. Chem. Phys.* **1972**, *56*, 716.
- (21) Griffith, O. H.; Jost, P. J. Reference 11, pp 453-523.
- (22) Venkataraman, B.; Fraenkel, G. K. *J. Chem. Phys.* **1955**, *23*, 588.
- (23) Windle, J. J. *J. Magn. Reson.* **1981**, *45*, 432.
- (24) Bales, B. L. Reference 15, pp 77-130.
- (25) Meirovitch, E.; Freed, J. H. *J. Phys. Chem.* **1984**, *88*, 4995.
- (26) Polnaszek, C. F.; Scheirer, S.; Butler, K. W.; Smith, I. C. P. *J. Am. Chem. Soc.* **1978**, *100*, 8223.
- (27) The nonsecular terms in the width expressions appear as $(1/[1 + (\omega_0\tau)^2])$ (see ref 20) and are the reason that the equations for the width as a function of correlation time cannot be solved exactly for the correlation times.
- (28) Reference 21, p 463.
- (29) Gaffney, B. J. Reference 11, Appendix IV.
- (30) Zager, S. A.; Freed, J. H. *J. Chem. Phys.* **1982**, *77*, 3344.
- (31) Cole, L. A.; Dorsey, J. G. *Anal. Chem.* **1990**, *62*, 16.
- (32) Kozle, P.; Dammers, A. J.; Van Ginkel, G.; Levine, Y. K. *Biochim. Biophys. Acta* **1984**, *777*, 297.
- (33) Yonker, C. R.; Zwier, T. A.; Burke, M. F. *J. Chromatogr.* **1982**, *241*, 269.
- (34) McCormick, R. M.; Karger, B. L. *Anal. Chem.* **1980**, *52*, 2249.
- (35) We would like to thank a reviewer for pointing out this possible interpretation.
- (36) *Operational Considerations with the V-4532 Dual Sample Cavity*; Publication No. 87-214-002; Varian Associates: Palo Alto, CA.
- (37) Raymond, D.; Chung, G. N.; Mayer, J. M.; Testa, B. J. *Chromatogr.* **1987**, *391*, 97.
- (38) Rowlen, K. L.; Harris, J. M. *Anal. Chem.* **1991**, *63*, 964.
- (39) Unpublished work.

RECEIVED for review July 26, 1991. Accepted January 10, 1992.

Separation and Molecular Weight Distribution of Anionic and Cationic Water-Soluble Polymers by Flow Field-Flow Fractionation

Maria Anna Benincasa and J. Calvin Giddings*

Field-Flow Fractionation Research Center, Department of Chemistry, University of Utah, Salt Lake City, Utah 84112

A broad study is reported here on the retention and separation of anionic polystyrenesulfonate (PSS) and cationic polyvinylpyridine (PVP) water-soluble polymers by flow field-flow fractionation (FFF) using a thin hydrophobic polypropylene membrane as the accumulation wall of the FFF channel. As background, the general role and impact of polymer adsorption in size exclusion chromatography and in flow FFF are compared. Adsorption at the accumulation wall in FFF systems is described, and explanations for its self-limitation and nonobtrusion are supported by experimental data. The retention and separation of PSS and PVP standards in the molecular weight range 6500–690 000 and 28 000–240 000, respectively, are shown to be generally consistent with theory. Molecular weight distribution curves obtained for the PVP polymers by different flow FFF runs and by thermal FFF are found to be consistent. Weight and number average molecular weights and their ratios are determined for both polymer types. Overloading studies show unexpectedly improved selectivity with low (submicrogram) loading.

INTRODUCTION

Because of the steadily widening base of industrial and pharmaceutical applications of water-soluble polymers (WSPs), the characterization of these polymeric materials has become an activity of major analytical importance.^{1,2} One of the most difficult challenges in the analysis of WSPs is the characterization of molecular weight or chain length distribution. The principal methodology used for this purpose is size exclusion chromatography (SEC). This method, however, is subject to perturbations caused by the interaction of the polymers with, or in many cases adsorption to, the support matrix.^{3–6} These interactions are particularly troublesome for charged (especially positively charged or cationic) WSPs, or polyelectrolytes, which are of major practical importance.

Polymer-support interactions have a magnified effect in SEC because, by the very nature of the SEC process, polymer molecules must partition into pores that are only slightly larger than the molecule, thus requiring that the polymer spend a considerable fraction of its time in close proximity to the solid walls of the porous support matrix.^{7,8} Because of this forced proximity and the ensuing tendency to experience interactive effects in SEC, and in addition because polymers of higher molecular weight are subject to shear degradation in the complex flow space of packed SEC beds,⁹ it is useful to further develop alternate methods less prone to these complications for determining the molecular weight distribution of WSPs. One promising alternative is field-flow fractionation (FFF).

FFF is a broad family of methods widely applicable to macromolecules, colloids, and particles.^{10–14} In these chro-

matographic-like methods, an external field is applied across the face of a thin ribbonlike channel in a direction perpendicular to the principal axis of flow. The external field forces components of different mass or size into different streamlines that travel at unequal velocities, thus leading to the separation and differential elution of the components.

Among the fields and associated driving forces potentially applicable to WSPs are crossflow, sedimentation, thermal, and electrical.^{10–13} The most promising of these is crossflow (leading to the subtechnique of flow FFF), as will be described more fully in this paper. Flow FFF is more universally applicable to different polymer compositions and types (including cationic, anionic, and neutral) as well as to a broader range of molecular weights (from a few hundred to a very high but indeterminate upper limit extending into the millions) than the other FFF techniques. Several earlier papers from this laboratory have described the application of flow FFF to synthetic anionic WSPs.^{15,16} The present paper describes further advances in this area, including the fractionation of cationic polyelectrolytes and the acquisition and intercomparison of polydispersity and molecular weight distribution data for both cationic and anionic WSPs. We also report the utilization of a new polypropylene membrane to enhance the performance of flow FFF.

An essential element of most forms of flow FFF is a permeable membrane that serves as the accumulation wall of the thin channel.^{12,15,16} This membrane accommodates the passage of the crossflow stream, consisting of a secondary flow of liquid (superimposed on the primary axial channel flow) that serves as the perpendicular driving force of the flow FFF process. Particles and/or polymers are driven toward the membrane wall by this crossflow. The pores of the membrane must reject these solutes so that they remain confined in the channel and can be swept differentially along the channel axis by the primary or axial flow stream. Ideally, the membrane will be flat and smooth, thus allowing the precise construction of thin uniform channels.

In this paper we report the use of a thin (25- μm) isotactic polypropylene membrane produced by Hoechst-Celanese for the flow FFF of polyelectrolytes. These thin robust membranes are smooth and relatively incompressible and thus permit the construction of channels of well-defined dimensions. With these membranes, we are able to routinely use channels of 254- μm thickness (in some cases much thinner), a common goal for the thickness dimension of channels used in many forms of FFF. Most earlier channels were relatively thick, generally in the range 380–510 μm , in order to accommodate membranes (primarily cellulose acetate and polyether sulfone) having excessive surface texture.^{15,16} The expansion of these membranes into part of the channel space led to uncertainties in the channel thickness, a difficulty compounded by the fact that the void volume V^0 of a flow FFF channel cannot generally be measured as the elution volume of a void peak because true void peaks rarely appear in flow FFF. (We have measured void volumes here in terms of the breakthrough volume of a high molecular weight component

* Corresponding author.

swept through the channel at high velocity without crossflow; this breakthrough volume is $2/3 V_0$.)

Another factor that must be considered in membrane selection for flow FFF is the avoidance of "pathological" interactions between the solute and the membrane. As in SEC, it is important to avoid such interactions, particularly those that perturb the retention of the polymer or lead to significant sample losses through adsorption. In contrast to SEC, where virtually any kind of interaction (repulsive or attractive) will have one or both of these effects, in flow FFF many types of interactions (even strong ones) are acceptable and are likely to cause no adverse effects, as will be explained below.

The interaction of polymers with membranes (and their interfaces) has been studied by a number of workers.¹⁷⁻¹⁹ These interactions depend upon various properties of the polymer, the solvent, and the membrane material. These properties include the polarity, polarizability, and charge density of the various media. Isotactic polypropylene is nonpolar and thus has a zero value of the polar component of the solubility parameter; the dispersion component is intermediate in level.¹⁷ It carries essentially no electrical charge. Because of these characteristics, the principal interaction of a polymer with a polypropylene membrane in a highly polar medium will be hydrophobic in nature. The extent of this interaction will, of course, depend on the nature and number of hydrophobic groups in the polymer.

It is possible, depending upon the nature of the polymer, that hydrophobic interactions could lead to the adsorption of a monolayer of polymer on the polypropylene membrane surface. Providing this monolayer does not block the pores and significantly impede fluid flow, no pathological effects are expected after the monolayer is deposited. If, for example, a cationic polymer is adsorbed, the membrane surface will become positively charged as a result of this adsorption and it will electrostatically repel any subsequent cationic polymers that approach the surface. If the polymer is neutral, it is likely that steric repulsion^{2,17,18,20} will prevent other polymers from penetrating up to the polypropylene surface.

A major difference between SEC and flow FFF is that limited (e.g., monolayer) adsorption is expected to have pathological effects in the first case but not in the second. Since the pore size in SEC is the same order of magnitude as the molecular size, an adsorbed polymer monolayer will significantly increase the exclusion of polymers from the pores, thus altering retention. In addition, because the surface area of an SEC support is large, monolayer adsorption will entail considerable sample loss. Consequently, such adsorption is highly undesirable in SEC. In flow FFF, on the other hand, the exclusion of polymer from a thin layer in the immediate vicinity of the membrane will normally have little effect on retention. For polyelectrolytes, the repulsion will extend only a few times the double layer thickness into the solution, leading to a thin region from which polymers will be excluded of typical dimensions from 1 to 50 nm, depending upon the ionic strength. However, since the typical mean elevation of retained components in FFF channels is several micrometers, a distance that is large compared to the thickness of the excluded layer, the disturbance of retention will generally be negligible.

The above arguments suggest that the adsorption of a monolayer of sample material onto the membrane will have only slight effects on retention, which can in most cases be further reduced by increases in ionic strength. Furthermore, because of the low surface area of the planar membrane wall, monolayer adsorption would not be expected to significantly deplete polymer from injected samples, except initially. For example, a monolayer whose thickness, if condensed, is 20 Å, adsorbed on a channel surface of 50 cm² (close to our present

membrane area), would occupy a condensed volume of only 10⁻² μL, consisting of about 10 μg of sample material. Such a monolayer could easily be deposited by using a small amount of the polymer (as estimated above) in a conditioning run (see later).

By way of generalization, the above arguments would suggest that it is immaterial whether polymer tends to adsorb onto the membrane or not as long as flow through the pores can be maintained. Ideally, there would be no adsorption, but even in the presence of strong interactions, polymer adsorption should be self-limiting because of the above-mentioned electrostatic and steric repulsion effects. At worst, a few micrograms of polymer would be needed to condition the surface. Care would be needed in switching from one polymer type to another (e.g., from cationic to anionic samples) because strong attractive interactions between the different polymer types would lead to the buildup of additional polymer layers, eventually interfering with flow. Thus as long as the solution of the sample polymer is thermodynamically stable (a condition that excludes unduly strong interactions between neighboring polymer molecules), it should be possible to operate flow FFF successfully with any type of polymer and any type of membrane. If this point of view proves mainly correct, the primary advantage of the polypropylene membrane used for polymer analysis may relate to its desirable physical characteristics.

By way of further generalization, the above conclusions should apply to polymer analysis in any kind of FFF system including thermal FFF. Again, it should be immaterial whether a thin layer of polymer (even up to several monolayers) adsorbs or not. Unfortunately, such is not the case for particle analysis where even a monolayer of deposited particles might consume a considerable amount of sample material. In addition, the adsorption of larger particles would perturb the channel wall texture. In these cases it might be beneficial to graft or adsorb a polymer layer onto the surface beforehand, which would tend to repel approaching particles through steric repulsion.

One important factor that must be considered in the fractionation of high molecular weight polyelectrolytes is the possible overloading of the separation system. In general, long-chain molecules are subject to considerable entanglement even at low mass concentration levels,^{21,22} thus making retention times and elution profiles dependent on concentration. Ideally, results should be reported that have been extrapolated to zero concentration, but this is not always feasible. Overloading effects are likely amplified for polyelectrolytes (as compared to neutral polymers) because charge repulsion will lead to additional chain expansion and an increasing penetration of chain segments into regions occupied by other polymer molecules. The enhancement of overloading by the introduction of charge into the polymer is expected to be greatest at low ionic strengths.¹⁵

The experiments reported below are carried out using nonprogrammed symmetrical flow FFF. Although we have developed and demonstrated the use of programming in flow FFF in two different studies,^{16,23} programming was not necessary here to cover the approximately 100-fold molecular weight range of polymers utilized. Furthermore, programming invariably complicates the interpretation of results because conditions vary during the run and thus performance is difficult to correlate with basic operating parameters, such as field strength.

Symmetrical flow FFF, in which a crossflow stream of carrier enters one permeable wall and exits another, is used in this investigation, as in most previous studies of flow FFF done in this laboratory. This system provides a more versatile flow control and a simplifying absence of gradients as com-

pared to asymmetrical flow FFF, a variant first developed by Wahlund and Giddings.²⁴

THEORY

The theory of component retention in FFF in general, and in flow FFF in particular, has been developed and discussed in a number of places.^{11,12,16,25} These theoretical developments give a general equation for retention time t_r expressed as follows

$$\frac{t_r}{t^0} = \frac{1}{6\lambda[\coth(1/2\lambda) - 2\lambda]} \quad (1)$$

where t^0 is the void time (the emergence time of a nonretained component) and λ is the retention parameter, a term that depends upon the properties of the species to be separated. The physicochemical properties upon which λ depends vary with the applied field. In sedimentation FFF, λ depends upon effective particle mass. In thermal FFF it depends upon the thermal diffusion factor and in electrical FFF it depends upon the electrical charge of the analyte species.^{10,11} In flow FFF λ is given by^{11,25}

$$\lambda = D/Uw \quad (2)$$

where D is the diffusion coefficient of the solute particle or polymer, U is the velocity of crossflow, and w is the channel thickness. Polymers of different chain length have different D and thus λ values, thereby establishing differential retention (i.e., separation) as expressed by the variation of t_r with λ in eq 1.

Since retention is controlled by D , it is useful to express D in terms of molecular weight M . For linear random coil polymers, the appropriate relationship is^{21,26,27}

$$D = AM^{-b} \quad (3)$$

where A and b are constants for a given polymer type in a designated solution. The exponent b is 0.5 in a θ solvent and is typically ~ 0.55 – 0.6 in a good solvent. For polyelectrolytes, for which the polymer chain can be expanded by the mutual repulsion of backbone charges, random coil behavior is expected only in strong electrolyte solutions.^{26,28}

The value of D can also be related to the Stokes diameter d_s of the polymer by the Stokes-Einstein equation²⁶

$$D = kT/3\pi\eta d_s \quad (4)$$

where k is the Boltzmann constant, T the temperature, and η the viscosity.

The substitution of eq 3 into eq 2 yields

$$\lambda = AM^{-b}/Uw \quad (5)$$

It is instructive to examine the case in which the crossflow velocity U in eq 5 is sufficiently high that $\lambda \ll 1$. Under these circumstances the right-hand side of eq 1 reduces to $1/6\lambda$ and we get the simplified retention equation^{11,25}

$$t_r/t^0 = 1/6\lambda \quad (6)$$

When the λ from eq 5 is substituted into eq 6, we get

$$t_r/t^0 = UwM^b/6A \quad (7)$$

Thus t_r is predicted to increase with M^b where b is 0.5 or higher depending on polymer conformation.^{21,26} Clearly, the magnitude of t_r can be modulated by varying U . By using the expressions $U = \dot{V}_c/bL$, $t^0 = V^0/\dot{V}_c$, and $V^0 = bLw$, we get the simple retention time equation

$$t_r = \frac{w^2 M^b}{6A} \frac{\dot{V}_c}{\dot{V}} \quad (8)$$

This equation relates t_r directly to M and to the two flow rates, \dot{V}_c for the crossflow and \dot{V} for the channel flow, used to control the separation. Other parameters utilized in the

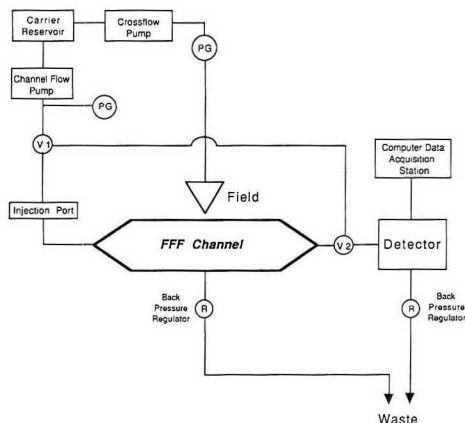


Figure 1. Schematic diagram of the arrangement of instrumental components of the flow FFF system: V = valve, PG = pressure gauge.

derivation are channel length L , breadth b , and void volume V^0 . Equations for plate height and resolution can be found in ref 16.

EXPERIMENTAL SECTION

Apparatus and Procedure. The flow FFF system used in this study is schematically represented in Figure 1. The channel was constructed in much the same manner as previously described,²⁹ except for the membrane. The Celgard 2400 isotactic polypropylene membrane utilized here was obtained from Hoechst-Celanese (Charlotte, NC). For this membrane the nominal pore width is given as 50 nm but the effective pore size is listed as 20 nm. A strip of this membrane was laid on the bottom wall of the disassembled channel, and the oversized portions were taped to the sides of the channel. Care was taken that the membrane film did not undergo uneven stretching. For this purpose the taping was carried out all along the sides of the channel and the holes in the membrane needed to accommodate the bolts were cut after the membrane was in place. Subsequently the membrane was wetted with a few milliliters of isopropyl alcohol which penetrated through the pores of the membrane and made the film, previously opaque due to the scattering of light, transparent. Finally, the channel was assembled and the carrier flow started.

Two HPLC pumps were used to drive two streams of identical carrier, one longitudinally through the channel and a second (the crossflow) across the channel and through the membrane and supporting frits. In order to minimize band broadening, the sample was initially accumulated onto the bottom wall (accumulation wall) by stopping the axial flow and allowing only the crossflow to act on the components. This stopflow procedure³⁰ was achieved by diverting the axial flow into the detector by switching the two synchronized solenoid valves V_1 and V_2 . During this relaxation period the sample components achieve different equilibrium positions on the basis of their unequal diffusion coefficients. The separation is then initiated when the longitudinal flow is resumed.

The flow FFF channel described here has a tip-to-tip length of 27.65 cm, a breadth of 2.0 cm, and a thickness of 0.0254 cm. The channel void volume measured with a protein probe yielded a value of 1.27 mL, which is also the geometrical volume. The axial flow rate set on an HPLC Model 110B pump from Beckman Instruments (Berkeley, CA) was measured at both the inlet and outlet of the channel. In case differences in values were registered, the outlet flow rate was adjusted to the value of that measured at the inlet by using two variable back-pressure regulators from Optimize Technologies (Bend, OR) placed at the detector and crossflow outlets (see Figure 1). This procedure ensured the absence of velocity gradients along the channel due to differences

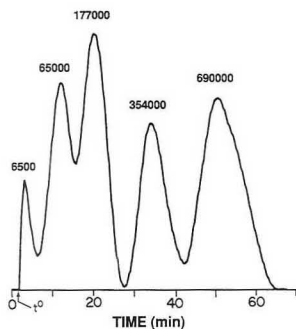


Figure 2. Fractogram of mixture of 5 μg each of polystyrenesulfonate (PSS) polymers of the five different nominal molecular weights shown in the figure. Flow rates of Tris buffer are $\dot{V} = 0.77$ and $\dot{V}_c = 1.35$ mL/min. Detection is at 254-nm wavelength.

in the inlet and outlet flow rates.

The crossflow was generated by a Spectraphysics (San Jose, CA) Isochron LC pump. The steadiness of the pressure drop generated by crossflow through the frits and the membrane was checked first in the absence and then in the presence of the channel flow. When differences in flow were registered, the two black-pressure regulators were adjusted in such a way that the pressure drop was constant.

The detection was provided by a Shimadzu (Kyoto, Japan) Model SPD-6A variable-wavelength detector equipped with an 8- μL cell, set at 254 nm and at an attenuation of 0.005–0.01 AUFS. The response time was typically 0.5 s. All operations were carried out at ambient laboratory temperatures, 24–25 $^{\circ}\text{C}$.

The thermal FFF system used here for complimentary measurements is of conventional design as reported previously from this laboratory³¹ and as can be found in the Model T100 instrument from FFFractionation (Salt Lake City, UT). For this channel the tip-to-tip length is 41.7 cm, the breadth is 2.0 cm, and the thickness is 0.0076 cm. The void volume is 0.72 mL. The detector is an Applied Biosystems (Ramsey, NJ) Model 757 variable-wavelength detector. The pump used with this system is the same Spectraphysics unit described above for the flow FFF system. For all the thermal FFF runs a stopflow procedure was employed with a typical stopflow time of 30 s. The solvent, tetrahydrofuran, used as carrier and solubilizing medium for the samples, was ultrafiltered and degassed prior to use.

Reagents and Samples. The carrier liquids used in the flow FFF work were all aqueous solutions prepared from distilled and deionized water. The primary carrier medium used for the separation of the polystyrenesulfonate samples was a 0.05 M solution of Tris- HNO_3 buffer at pH 8.6 containing 0.02% (w/w) NaN_3 as a bactericide. The ionic strength $I = 0.0079$ M. Subsequently, a 0.0065 M Na_2SO_4 solution ($I = 0.0195$ M) was employed. For the separation of the poly(2-vinylpyridine) samples a 0.01 M HNO_3 solution at pH 2, with the same amount of sodium azide, was used. Here the ionic strength is 0.013 M.

The samples were injected directly into the channel with a microsyringe through a septum port placed in a tee-union in the axial flow line and allowed to relax under the field only for the time (typically about 1 min) corresponding to that needed by the crossflow to displace one channel volume. Injection volumes, on the order of a few microliters, contained microgram amounts of polymer or, for some experiments, nanogram amounts. The anionic samples consisted of narrow molecular weight distributions of polystyrenesulfonate or PSS (as the sodium salts) with nominal molecular weights M of 4000, 6500, 16000, 65000, 88000, 177000, 354000, and 690000. (The molecular weight refers to the polystyrenesulfonate chain and does not include the mass contribution of Na^+ counterions.) These were provided by Pressure Chemical Co. (Pittsburgh, PA). The cationic samples, poly(2-vinylpyridine) or PVP, with nominal $M = 28000$ and 110000, were obtained from Polysciences (Warrington, PA), while the sample with $M = 240000$ was provided by Dr. Thomas Mourey of Eastman Kodak (Rochester, NY). All the samples were dissolved in their carrier

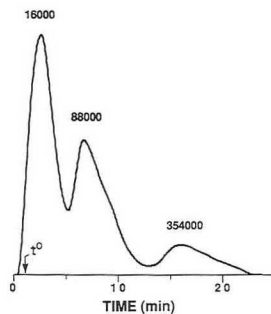


Figure 3. Fractogram of three PSS polymers of indicated nominal molecular weights. The amount of each polymer injected is 7 μg . Flow rates are $\dot{V} = 1.05$ and $\dot{V}_c = 1.23$ mL/min. Detection is at 254 nm.

solution (at concentrations ranging from 0.05 to 0.5 g/L) prior to injection.

RESULTS AND DISCUSSION

Polymer Fractionation. Figure 2 shows the elution profile (fractogram) of a sample consisting of a mixture of 5 μg each of the sodium salts of polystyrenesulfonate of molecular weights 6500, 65000, 177000, 354000, and 690000. This figure shows that the separation of these five anionic WSPs, spanning a molecular weight range of 100-fold, is completed at a reasonable level of resolution in a time of 1 h. Baseline resolution is approached for the higher molecular weight components.

Higher fractionating speed can be gained by adjusting the flow rates (specifically by increasing \dot{V} and/or decreasing \dot{V}_c) of the two participating flow streams (see eq 8). The fractogram presented in Figure 3 illustrates a higher speed run on a sample containing 7 μg each of the three different PSS polymers identified by molecular weight in the figure. The run is essentially complete in about 20 min. While this separation speed is greater than that realized previously^{15,16} for synthetic water-soluble polymers, additional gains can undoubtedly be made with further optimization.

Some retention anomalies were observed in our studies of PSS separation in the Tris buffer. (These were largely eliminated in subsequent studies—reported below—in a Na_2SO_4 buffer.) Retention times sometimes differed for identical runs, and they failed to follow theory closely when conditions were changed. For example, on the basis of the observed $t_r = 33$ min of the PSS 354000 peak in Figure 2, the t_r for this peak in Figure 3, according to eq 8, should be 22 min. The actual $t_r \approx 16.5$ min, a considerable discrepancy. Despite this anomaly with absolute t_r values, the relative positions of peaks remained relatively invariant. All other WSP–electrolyte systems studied (below) provided much better consistency.

The flow FFF system exhibits a capability for the fractionation of cationic as well as anionic polyelectrolytes. Figure 4 shows the fractionation of ~ 1 μg each of the three PVP samples eluted in the HNO_3 carrier at pH 2.0 with $\dot{V} = 1.07$ and $\dot{V}_c = 1.49$ mL/min. This separation was achieved by utilizing a different sheet of the polypropylene membrane whose subsequent use was confined to these cationic materials. The separation is satisfactory despite the contribution of polydispersity to band broadening. In fact, a preliminary estimate of polydispersity can be made on the basis of the width of the observed peak profiles.

It has been shown that polydispersity alone will contribute an amount σ_p^2 to the peak variance (in the time units) approximated by³²

$$(\sigma_p/t_r)^2 = S_M^2(\mu - 1) \quad (9)$$

where $\mu = M_w/M_n$ represents the polymer polydispersity and

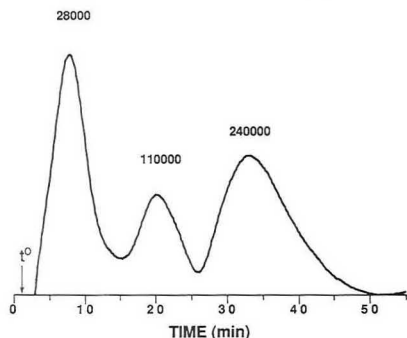


Figure 4. Fractogram of three poly(2-vinylpyridine) or PVP polymers of indicated nominal molecular weights. The amounts of polymer injected are 0.3, 0.7, and 2.0 μg , respectively, for polymers of increasing molecular weight. Flow rates are $\dot{V} = 1.07$ and $\dot{V}_c = 1.49$ mL/min. Detection is at 254 nm.

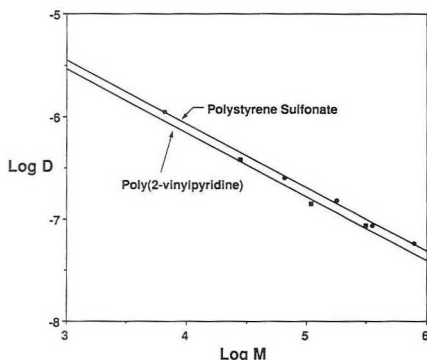


Figure 5. Plots of the logarithm of the diffusion coefficient D (cm^2/s) versus the logarithm of molecular weight M obtained from the fractograms in Figures 2 (PSS) and 4 (PVP).

S_M is the mass selectivity, ~ 0.62 in the present case (see below). Since the peaks of Figure 4 are observed to have $(\sigma_p/t_r) \sim 0.15\text{--}0.3$, the application of eq 9 suggests that the polydispersities are as low as $\mu \sim 1.06\text{--}1.25$. (They may be lower depending on the contribution of the channel to band broadening.) This subject will be examined below by more exact means. However, we note generally that the high resolving power of FFF affords a systematic means of extending the measurement of polydispersity down to extremely narrow samples for which μ is as low as ≈ 1.003 .³²

In order to examine the consistency of the observed retention and that described by theory, values of λ were calculated for the measured retention time t_r of each peak maximum using eq 1 and converted to a diffusion coefficient using eq 2. The relationship represented by eq 3 was examined by plotting the logarithm of D against the logarithm of M . Such a plot is shown in Figure 5 for both the PSS peaks separated in Figure 2 and the PVP peaks resolved in Figure 4. Both of these plots yield reasonably straight lines. The absolute values of the slopes (equal to mass selectivity S_M) are 0.62 in both cases, a value consistent with those reported in our earlier work¹⁶ and the expectations of random-coil behavior.^{26,27}

Molecular Weight Distribution. The diffusion coefficient plot of Figure 5 provides the calibration constants A and b of eq 3. These constants, when used in conjunction with

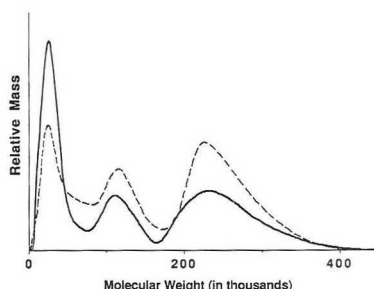


Figure 6. Comparison of the molecular weight distribution curves for different mixtures of PVP polymers acquired under different flow conditions: solid line (derived from Figure 4), $\dot{V} = 1.07$ and $\dot{V}_c = 1.49$ mL/min; broken line, $\dot{V} = 0.85$ and $\dot{V}_c = 1.47$ mL/min.

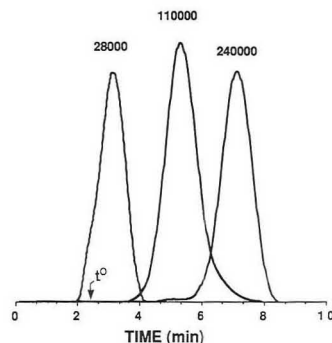


Figure 7. Thermal FFF fractograms of three PVP polymers with THF as the liquid carrier. Conditions are $\dot{V} = 0.32$ mL/min and $\Delta T = 70$ $^\circ\text{C}$. Detector wavelength = 254 nm.

eqs 1 and 2, establish a relationship between retention time t_r and molecular weight M . With this relationship in place, a variant of our normal software can be used to obtain molecular weight distribution (MWD) curves. The self-consistency of the results can, in principle, be tested by comparing such distribution curves obtained under different experimental conditions. Figure 6 shows a comparison of two MWD curves obtained from different mixtures of the three PVP polymers. The solid line is the distribution obtained from the fractogram of Figure 4. The broken line is from another fractogram obtained with $\dot{V} = 0.85$ and $\dot{V}_c = 1.47$ mL/min. The injected amounts in the latter run were not carefully controlled, so the comparison of peak heights and areas are not meaningful. However, peak positions, widths, and even shapes are in good agreement. The reasonable consistency between these distribution curves supports the thesis that flow FFF is an effective method for generating meaningful molecular weight distribution curves. This matter will be scrutinized at greater length below.

Comparison with Thermal FFF. Many water-soluble polymers will dissolve in polar organic solvents. In this case they can be effectively analyzed by thermal FFF, in which a temperature gradient rather than a crossflow serves as the perpendicular driving force.¹⁰⁻¹⁴ A comparison of the results then provides an additional check on the validity of the parameters obtained by flow FFF.

In order to carry out this part of the study, the PVP samples were dissolved in tetrahydrofuran (THF) and subjected to thermal FFF using a THF carrier flowing at 0.32 mL/min and a temperature drop ΔT of 70 $^\circ\text{C}$. A sample load of 0.5 μg of

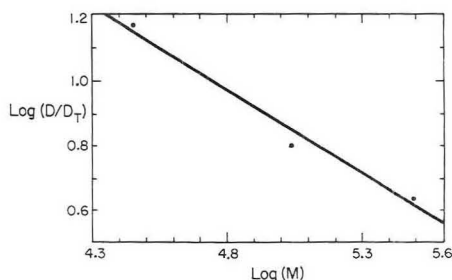


Figure 8. log-log plot of D/D_T (K) versus M for the PVP polymer components shown in the fractogram of Figure 7. The value of D_T can be assumed constant.

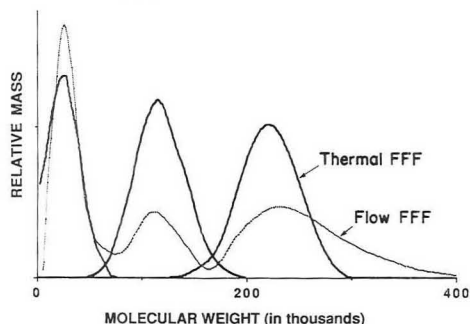


Figure 9. Comparison of MWD curves of three individual PVP polymers using thermal FFF (obtained from Figure 7) and of a mixture of the three polymers using flow FFF (from Figure 4).

each polymer component was injected with separate runs made for each polymer. Figure 7 shows the superposition of the resulting fractograms. Although the elution time scale is different from that observed for the flow FFF fractogram of the PVP mixture because conditions are not equivalent, the relative spacing and resolution of peaks bears a close resemblance to that observed for the flow FFF fractogram displayed in Figure 4. This resemblance lends support to one of the basic objectives of FFF, namely that the fractograms represent the distribution of polymers and not system or operating anomalies. We note that if both systems are operating properly, a close correspondence of fractograms is not unexpected because for thermal FFF $\lambda = D/D_T \Delta T$ where the thermal diffusion coefficient D_T is constant for polymers of a given composition.³¹ Thus for a given field strength ΔT , λ is proportional to D just as it is for flow FFF (see eq 2). Since D is given by eq 3, a plot of the logarithm of $\lambda \Delta T = D/D_T$ versus the logarithm of molecular weight M should yield a straight line. Such a plot, shown in Figure 8, is virtually identical in appearance to the logarithmic plot based on flow FFF retention measurements and shown in Figure 5. However, the slopes are slightly different: -0.51 and -0.62 for the thermal and flow FFF plots, respectively. This probably reflects the difference in solvent properties and thus in solvent-polymer interactions. The nearly equal deviation of the three experimental points (corresponding to the three polymers) from the straight line in the two plots suggests that the molecular weight provided for one or more of the polymers may be in error.

As before, based on the appropriate logarithmic calibration plot, in this case shown in Figure 8, molecular weight distributions were obtained. In Figure 9, the three MWD curves obtained by thermal FFF for the three PVP polymers are shown. These curves are compared with the MWD of the

Table I. Molecular Weight Averages and Polydispersities of Three PVP Polymers Measured Both by Flow FFF and Thermal FFF

method	M_p	M_w	M_n	$\mu = M_w/M_n$
Nominal $M = 28\,000$				
flow FFF	26 100	30 600	24 500	1.25
thermal FFF	26 300	28 700	19 900	1.44
Nominal $M = 110\,000$				
flow FFF	111 500	115 500	110 000	1.05
thermal FFF	113 200	136 000	127 500	1.07
Nominal $M = 240\,000$				
flow FFF	233 400	252 300	241 300	1.05
thermal FFF	221 600	221 150	217 700	1.02

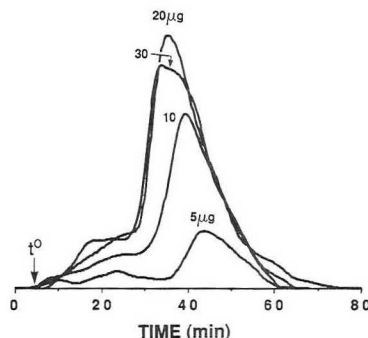


Figure 10. Fractograms of $M = 690\,000$ PSS showing effect of sample load on elution pattern and peak retention. $\dot{V} = 0.30$ and $\dot{V}_c = 0.50$ mL/min.

polymer mixture obtained from the flow FFF fractogram of Figure 4. Once again, the injected quantities (and thus relative peak areas) differ in the two cases. Nonetheless, the comparison of the distribution curves in the figure shows reasonable consistency, especially in view of the fact that two entirely different FFF techniques utilizing two different solvents (aqueous and nonaqueous) were used for the analysis.

The MWD curves shown in Figure 9 can be used to compute molecular weight averages and polydispersities for the three PVP polymers. (For flow FFF, the single MWD curve must be broken into three component parts, leading to some error.) The results are compiled in Table I. The results are reasonably consistent with the expectation based on peak width analysis (above) that most $\mu = M_w/M_n$ values should fall in the approximate range 1.06–1.25. Most remarkable is the finding based on thermal FFF of $\mu = 1.02$ for the $M = 240\,000$ PVP. Since actual polydispersities tend to be lower than the values measured because of system band broadening, this result suggests that this polymer is unexpectedly narrow in distribution.

Overloading. As noted above, the propensity for chain entanglement (and viscosity modification) in solutions of high molecular weight polymers suggests that overloading effects may readily arise. This tendency can be countered by reducing sample loads, which often requires that detector sensitivity be improved.

A preliminary study of overloading has been carried out to better delineate the effects of sample size. The polystyrenesulfonate polymers in the Tris buffer were used for this work. Figure 10 shows the superposition of eluted peaks of the 690 000 molecular weight PSS polymer for sample loads ranging from 5 to 30 μg . The figure shows that there is a tendency for the high-load peaks to elute earlier than those generated by small sample loads. This result, although con-

Table II. Stokes Diameters d_s (nm) of Various Polymers Obtained from Eq 4^a

polymer (<i>M</i>)	electrolyte			
	HNO ₃	Tris	Na ₂ SO ₄	1 M NaCl
PSS (6500)		2.9		
PSS (65 000)		12	18	
PSS (177 000)		21	40	
PSS (354 000)		36	79	23
PSS (690 000)		53	131	43
PVP (28 000)	14			
PVP (110 000)	37			
PVP (240 000)	61			

^aThe D values are acquired from retention measurements using eqs 1 and 2.

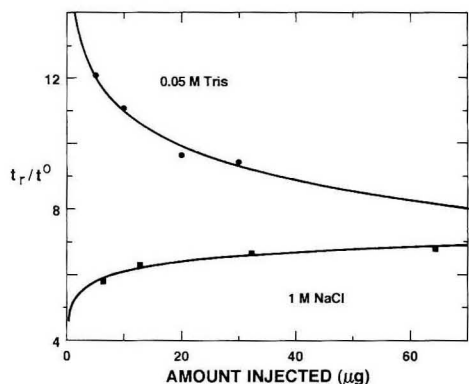


Figure 11. Plot of relative retention time t_r/t^0 of 690 000 PS polymer peak against sample load in 1 M NaCl and in usual Tris buffer of ionic strength 0.0079 M. Flow rates are $\dot{V} = 0.30$ and $\dot{V}_c = 0.50$ mL/min for Tris and $\dot{V} = 0.32$ and $\dot{V}_c = 0.45$ mL/min for 1 M NaCl.

sistent with earlier work,¹⁵ is unlike that expected for chain entanglement and viscosity effects; the latter generally lead to an increase in retention time with increasing sample load.²² The opposite trend—an inverse correlation between retention time and sample load—has been observed for charged colloids subject to mutual electrostatic repulsion.³³ It is possible that both entanglement and electrostatic repulsion effects influence the course of overloading for polyelectrolytes. The relative importance of the two is likely to be determined by the ratio of the Stokes diameter d_s (or some other appropriate molecular dimension) and the double-layer thickness, which is controlled by the ionic strength. (Molecular dimensions such as d_s are also influenced by ionic strength.) For the ionic strength (0.0079 M) used in the present experiments, the double-layer thickness (Debye length) is 3.4 nm. The distance is comparable to the Stokes diameter of the very small polymers but considerably less than that of the large polymers (see Table II).

The possibility that the electrolyte concentration influences overloading was further investigated by conducting overloading experiments in 1 M NaCl solutions where the double-layer thickness is reduced to ~ 0.3 nm. Figure 11, in which the relative peak retention time t_r/t^0 is plotted against sample load in two different electrolyte solutions, shows that PSS ($M = 690\,000$) behaves more like uncharged polymers at high ionic strength, with t_r tending to increase with load.²² The opposite is true in the Tris buffer, as noted earlier. (Figure 11 is intended only to show overloading trends; the relative values of t_r/t^0 are not meaningful because the flow conditions are

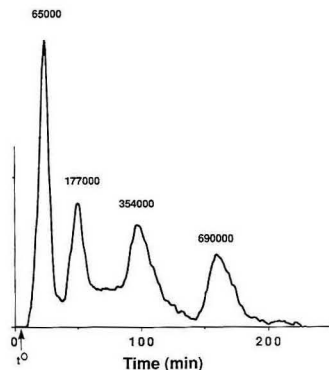


Figure 12. Fractogram for low-load PSS injection in 0.0065 M Na₂SO₄. Sample amounts are 94, 120, 138, and 188 ng, respectively, for the four peaks from left to right. Flow rates are $\dot{V} = 0.30$ and $\dot{V}_c = 0.85$ mL/min.

different.) An earlier study using 0.1 M KCl confirmed that t_r varies less rapidly with load at higher as compared to lower salt concentration, but it did not show a reversal of trend (t_r increasing with load) as observed here.¹⁵

More data are obviously needed to establish an overloading mechanism and, in particular, to see if the mechanism may be dependent upon ionic strength and molecular dimensions as suggested above. If so, it might be found that overloading effects in a given molecular weight range can be minimized by a careful choice of ionic strength.

In order to test the behavior of the system at the lowest possible sample load, we reduced sample amounts below the microgram level to the lowest detectable quantities. In this case, the carrier electrolyte was 0.0065 M Na₂SO₄; sodium azide was excluded from the carrier. In order to operate at lower sample loads, the detector wavelength was changed from 254 to 200 nm for signal enhancement. Figure 12 shows a fractogram of a mixture of PSS polymers obtained with injected sample amounts ranging from 94 ng ($M = 65\,000$) to 188 ng ($M = 690\,000$). The run was carried out at flow rates of $\dot{V} = 0.30$ and $\dot{V}_c = 0.85$ mL/min. The resolution is obviously higher than that displayed in Figure 2. The resolution may have changed because of the altered run conditions or because of the reduced concentration.

According to theory,¹⁶ the resolution between any two peaks in Figure 12, given equal selectivity and diffusivity, should be 1.25 times the resolution level displayed in Figure 2. (This factor is controlled by flow rates according to $(\dot{V}_c^3/\dot{V})^{1/2}$.) However, an interesting observation in comparing the two fractograms is that the selectivity displayed in Figure 12 is higher than that found in Figure 2, thus enhancing resolution. The selectivity can be equated to the absolute value of the slope (also equal to b) of the log D versus log M plot and, as shown by Figure 5, has the value of 0.62 for the fractogram of Figure 2. On the other hand, the slope of the log D versus log M plot (not shown) constructed for Figure 12 has the value of -0.84 , giving a selectivity of 0.84. However, the apparent D values, in absolute terms, are smaller in Na₂SO₄. This is reflected in the substantially larger Stokes diameters found for PSS polymers in Na₂SO₄ as compared to those in Tris (see Table II); the opposite effect is expected on the basis of charge-induced chain expansion. This anomalously enhanced selectivity and reduced diffusivity may be a consequence of reduced sample loading, but it may be influenced to some extent by the variation in electrolyte composition between the two runs. This subject requires further investigation.

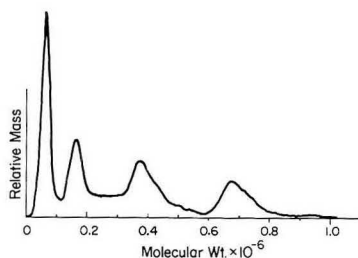


Figure 13. Molecular weight distribution of the mixture of PSS standards from the fractogram of Figure 12.

Table III. Weight and Number Averages (and Their Ratio) for PSS Polymer Standards Deduced from Flow FFF Fractograms

nominal M	M_w	M_n	$\mu = M_w/M_n$
65 000	64 300	56 900	1.15
88 000	90 400	80 400	1.13
177 000	160 300	146 400	1.09
354 000	364 900	355 300	1.03

Because Figure 12 displays higher resolution for PSS polymers than Figure 2, the conditions of the former are preferred to obtain molecular weight distribution (MWD) curves for PSS. Figure 13 gives the MWD curve of the polymer mixture shown fractionated in Figure 12. Additional experiments were carried out under the same conditions to characterize the individual polymer fractions. Software was applied to get weight and number averages. These numbers and their ratio μ (reflecting polydispersity) are reported in Table III. The actual μ values should be somewhat lower than those reported because of band broadening. Hence the values are reasonably consistent with the supplier's specifications: $\mu < 1.1$. We note that the polydispersity measured for the $M = 354\,000$ PSS, $\mu < 1.03$, is quite low, reflecting both the narrowness of the polymer MWD and the high resolving power necessary for flow FFF to discern that narrowness. The measurement of μ for a narrow MWD PVP polymer using thermal FFF was discussed in connection with Table I.³²

Relative Recovery. An interesting observation stemming from this work is that the effective hydrodynamic diameter (the Stokes diameter d_s) of many of the polymers used here is less than the width (given by the manufacturer as 50 nm) of the slitlike pores of the polypropylene membrane. Table II shows three different sets of values of the Stokes diameters of the various PSS polymers based on the diffusion coefficients deduced from the fractograms of Figures 2 (see Figure 5) and 12, along with the 1 M NaCl fractogram (not shown), and the utilization of eq 4. The d_s values for PVP based on Figure 4 are also shown. This table shows that d_s for the polystyrenesulfonate with $M = 6500$ is ~ 3 nm, about 1 order of magnitude smaller than the pore width. In principle, this and other low- M polymers should be driven through the membrane by crossflow and, accordingly, should not be recovered and detected at the channel outlet. The fact that these polymers are both retained and detected suggests that there is a repulsive interaction between the membrane and the charged polymeric species. This interaction may be generated, as suggested earlier, by the adsorption of a small amount of polymer onto the membrane, which would then serve to repel, through Coulombic interactions, polymers approaching to within a few double-layer thicknesses of the membrane surface and its adsorbed layer.

The adsorption-repulsion mechanism is further supported by conditioning observations. With each new membrane in-

stalled (consisting of ~ 15 installations over 30 months), the first two or so injections (usually 5–10 μg each) of either PSS or PVP produced no peaks, after which normal elution occurred. The apparent adsorption was irreversible in that no reconditioning was necessary after prolonged periods (days to weeks) of continuous-flow operation without polymer injection. After 100–200 injections, the peak profiles gradually degenerated, possibly due to slow ongoing adsorption with the partial blockage of some pores. However, the pressure drop over the membrane changed very little over this time.

In this study we did not make quantitative measurements of the fraction of injected polymer recovered at the outlet. However, some of the peak area measurements provide evidence on relative recovery factors. For example, the peak areas in Figure 10 ($M = 690\,000$ PSS) were found to be roughly proportional to sample load. However, some of our fractograms exhibit anomalies. For example, equal amounts of each polymer component were used for the runs shown in Figures 2 and 3, yet the peak areas are not equal. In Figure 2 some low- M polymer appears to be lost while in Figure 3 the high- M polymer has a reduced peak area. (Sample preparation errors may be responsible for much of the discrepancy.) In Figures 4 and 12, where the high- M peaks have been more heavily loaded, areas are not perfectly proportional to load, suggesting some loss of high- M polymer. More recent studies, however, show that peak areas are proportional to load and do not differ substantially with changes in M . More work is clearly called for to thoroughly characterize sample recovery and to understand the underlying physicochemical phenomena.

We note that the validity of the molecular weight distribution curves derived from either flow FFF or size exclusion chromatography data is dependent on the equal fractional recovery of components of all molecular weights.

CONCLUSIONS

This study demonstrates the applicability of flow FFF to the fractionation and characterization of both anionic and cationic polyelectrolytes over a broad molecular weight range using the same hydrophobic polypropylene membrane material. Specifically, the separation and molecular weight characterization of water-soluble polystyrenesulfonates of molecular weights ranging from 6500 to 690 000 and of poly-(2-vinylpyridine) from 28 000 to 240 000 have been achieved by flow FFF in an analysis time of less than 1 h. Results from thermal FFF have been used to corroborate the molecular weight distribution curves obtained for the PVP polymers. For either polyanions or polycations, the elution sequence, selectivity, and separation agree in broad outline with theory under a wide range of conditions. We have examined other phenomena, especially overloading and recovery, and have found some anomalies along with tentative mechanistic explanations. A great deal more work is needed to fully elucidate these phenomena and thus pave the way for the further optimization of flow FFF as applied to these important classes of polymers.

ACKNOWLEDGMENT

We are grateful to Hoechst-Celanese for providing the polypropylene membrane and to Tom Mourey of Eastman Kodak and Lawrence J. Rosen of Pressure Chemical for providing samples. This work was produced under Grant CHE-9102321 from the National Science Foundation. Supplementary support was provided by the industrially sponsored Technology Transfer Program of the Field-Flow Fractionation Research Center.

GLOSSARY

A	constant defined by DM^b , eq 3
b	exponent in diffusion expression, eq 3
b	channel breadth

D	diffusion coefficient
d_s	Stokes diameter
k	Boltzmann constant
M	molecular weight
T	absolute temperature
t^0	void time
t_r	retention time
U	crossflow velocity
\bar{V}	flow rate of channel stream
\bar{V}_s	flow rate of crossflow stream
V^0	void volume
w	channel thickness
Greek Characters	
η	viscosity
σ_p^2	variance due to polydispersity
λ	retention parameter

Registry No. Isotactic polypropylene (homopolymer), 25085-53-4.

REFERENCES

- (1) Bekturov, E. A.; Bakauova, Z. Zh. *Synthetic Water-Soluble Polymers in Solution*; Huethig & Wepf: Basel, 1986.
- (2) Molyneux, P. *Water-Soluble Synthetic Polymers: Properties and Behavior*; CRC Press: Boca Raton, FL, 1984; Vols. I and II.
- (3) Dubin, P. L.; Principi, J. M. *Macromolecules* **1989**, *22*, 1891.
- (4) Rollings, J. E.; Bose, A.; Caruthers, J. M.; Tsao, G. T.; Okos, M. R. In *Polymer Characterization*; Craver, C. D., Ed.; Advances in Chemistry Series 203; American Chemical Society: Washington, DC, 1983; Chapter 18.
- (5) Soria, V.; Campos, A.; García, R.; Parets, M. J. *J. Liq. Chromatogr.* **1990**, *13*, 1785-1808.
- (6) Giddings, J. C. In *Advances in Chromatography*; Giddings, J. C., Grushka, E.; Cazes, J.; Brown, P. R., Eds.; Marcel Dekker: New York, 1982; Vol. 20, Chapter 6.
- (7) Giddings, J. C. *J. Chromatogr.* **1976**, *125*, 3-16.
- (8) Giddings, J. C.; Kucera, E.; Russell, C. P.; Myers, M. N. *J. Phys. Chem.* **1968**, *72*, 4397-4408.
- (9) Barth, H. G.; Carlin, F. J., Jr. *J. Liq. Chromatogr.* **1984**, *7*, 1717-1738.
- (10) Giddings, J. C. *Anal. Chem.* **1981**, *53*, 1170A-1175A.
- (11) Giddings, J. C. *Sep. Sci. Technol.* **1984**, *19*, 831-847.
- (12) Giddings, J. C. *Chem. Eng. News* **1988**, *66*, 34-45.
- (13) Caldwell, K. D. *Anal. Chem.* **1988**, *60*, 959A-971A.
- (14) Giddings, J. C. *J. Chromatogr.* **1989**, *470*, 327-335.
- (15) Giddings, J. C.; Lin, G. C.; Myers, M. N. *J. Liq. Chromatogr.* **1978**, *1*, 1-20.
- (16) Wahlund, K.-G.; Winegarner, H. S.; Caldwell, K. D.; Giddings, J. C. *Anal. Chem.* **1986**, *58*, 573-578.
- (17) Sourirajan, S.; Matsuura, T. *Reverse Osmosis/Ultrafiltration Process Principles*; National Research Council Canada Publications: Ottawa, 1985.
- (18) Goddard, E. D.; Vincent, B. *Polymer Adsorption and Dispersion Stability*; ACS Symposium Series 240; American Chemical Society: Washington, DC, 1984.
- (19) Danielli, J. F.; Rosenberg, M. D.; Cadenhead, D. A. *Progress in Surface and Membrane Science*; Academic Press: New York and London, 1971; Vol. 4.
- (20) Napper, D. H. *Polymeric Stabilization of Colloidal Dispersions*; Academic Press: New York, 1983.
- (21) de Gennes, P.-G. *Scaling Concepts in Polymer Physics*; Cornell University Press: Ithaca, NY, 1979.
- (22) Caldwell, K. D.; Brimhall, S. L.; Gao, Y.; Giddings, J. C. *J. Appl. Polym. Sci.* **1988**, *36*, 703-719.
- (23) Ratanathanawongs, S. K.; Giddings, J. C. *Anal. Chem.* **1992**, *64*, 6-15.
- (24) Wahlund, K.-G.; Giddings, J. C. *Anal. Chem.* **1987**, *59*, 1332-1339.
- (25) Giddings, J. C.; Yang, F. J.; Myers, M. N. *Anal. Chem.* **1976**, *48*, 1126-1132.
- (26) Tanford, C. *Physical Chemistry of Macromolecules*; Wiley: New York, 1961.
- (27) Flory, P. J. *Principles of Polymer Chemistry*; Cornell University Press: Ithaca, NY, 1953.
- (28) Morawetz, H. *Macromolecules in Solution*; John Wiley & Sons: New York, 1965.
- (29) Giddings, J. C.; Chen, X.; Wahlund, K.-G. *Anal. Chem.* **1987**, *59*, 1957-1962.
- (30) Yang, F. J.; Myers, M. N.; Giddings, J. C. *Anal. Chem.* **1977**, *49*, 659-662.
- (31) Schimpf, M. E.; Giddings, J. C. *Macromolecules* **1987**, *20*, 1561-1563.
- (32) Schimpf, M. E.; Myers, M. N.; Giddings, J. C. *J. Appl. Polym. Sci.* **1987**, *33*, 1170.
- (33) Hansen, M. E.; Giddings, J. C.; Beckett, R. J. *Colloid Interface Sci.* **1989**, *132*, 300-312.

RECEIVED for review August 5, 1991. Accepted January 2, 1992.

Migration Behavior of Inorganic Anions in Micellar Electrokinetic Capillary Chromatography Using a Cationic Surfactant

Takashi Kaneta, Shunitz Tanaka, Mitsuhiro Taga,* and Hitoshi Yoshida

Department of Chemistry, Faculty of Science, Hokkaido University, Kita-ku, Sapporo 060, Japan

The interactions between inorganic anions and a cationic surfactant were investigated using micellar electrokinetic capillary chromatography (MECC). Using cetyltrimethylammonium chloride (CTAC) as a cationic surfactant, the effective electrophoretic mobilities of inorganic anions decreased due to two processes. The first was the ion association equilibria with a monomeric surfactant below the critical micellar concentration (cmc) and the other was partitioning into the micelle above the cmc. Fundamental equations for migration of ionic species in MECC were derived using the effective electrophoretic mobility as an electrochemical parameter. Ion association constants of inorganic anions with cationic surfactant and distribution coefficients into the micelle were estimated on the basis of these equations.

INTRODUCTION

Micellar electrokinetic capillary chromatography (MECC),

which was first introduced by Terabe et al.,^{1,2} is an electrokinetic separation technique for electrically neutral solutes. The separation mechanism is based upon the differential partitioning of analytes between an electroosmotically pumped aqueous mobile phase and an electrophoretically retarded micellar pseudophase. Because of its high efficiency and resolving power, MECC provides excellent separations of many neutral substances, for example, the separation of phenylthiohydantoin-amino acids,³ aromatic sulfides,⁴ and so on.^{5,6} Also, there are some applications of MECC to ionic species, for example, catecholamines^{7,8} and water-soluble vitamins.^{9,10} Terabe et al. investigated the migrating behavior of anionic species in MECC using an anionic surfactant, sodium dodecylsulfate (SDS), and reported that anionic species were rarely retained in the anionic micelle. However, ionic species exhibit a strong interaction with a surfactant having the opposite charge and are retained in its micelle.¹⁰ Although the unique separation selectivity for anionic species can be expected to be achieved by MECC using a cationic surfactant, there are no reports on the migration behavior of anions in a cationic surfactant system.

On the other hand, in order to investigate the interaction between ionic species and a charged surfactant in detail, it is essential to derive fundamental equations which represent the migration of ionic species in MECC. Recently, Ghowsi et al. reported a theoretical study for MECC based on electrochemical parameters.¹¹ However, only neutral species were discussed in their work. Terabe et al. investigated the migration behavior of ionic species in an anionic micellar solution,^{3,12} but only the capacity factors for ionic species were reported.

In this paper, fundamental study of the migration behavior of inorganic anions in the presence of a cationic surfactant was carried out by MECC using a cationic surfactant, cetyltrimethylammonium chloride (CTAC). An interesting separation selectivity and a high resolution based on the interaction between anionic species and a cationic surfactant were observed in this migrating system. To investigate the interaction with cationic surfactant in detail, fundamental equations representing the migration of anionic species were derived. By using an effective electrophoretic mobility as an electrochemical parameter, the influences of electroosmotic velocity could be eliminated. On the basis of the derived equations, the capacity factors for inorganic anions were calculated and the ion association constants with monomeric surfactant and the distribution coefficients into the micelle were estimated.

THEORY

The net electrophoretic velocity of ionic species, v_{ep} , and the electroosmotic velocity, v_{eo} , in an electric field, E , are given as

$$v_{ep} = \mu_{ep}E \quad (1)$$

$$v_{eo} = \mu_{eo}E \quad (2)$$

where μ_{ep} and μ_{eo} are the electrophoretic and the electroosmotic mobilities, respectively. The observed migration velocity of an ionic species, v_{ob} , is the summation of them

$$v_{ob} = v_{ep} + v_{eo} = (\mu_{ep} + \mu_{eo})E \quad (3)$$

In the presence of a cationic surfactant, the electrophoretic velocity of an anion will be influenced either by ion association below the critical micellar concentration (cmc) or by partitioning into the micelle above the cmc. The ion association constant between a monovalent anion and a cationic surfactant, K_{IA} , is defined as

$$K_{IA} = \frac{[AC]}{[A^-][C^+]} \quad (4)$$

where $[A^-]$ is the concentration of the free anion, $[C^+]$ is the concentration of the free cationic surfactant, and $[AC]$ is the concentration of the associated anion with the cationic surfactant. In light of the fact that the free anion migrates at v_{ep} and the associated anion migrates at v_{eo} because it has no charge, the observed migration velocity below the cmc, v_{ob} , is represented with v_{ep} and v_{eo} as

$$v_{ob} = \frac{n_{A^-}}{n_{A^-} + n_{AC}}(v_{ep} + v_{eo}) + \frac{n_{AC}}{n_{A^-} + n_{AC}}v_{eo} \quad (5)$$

where n_{A^-} and n_{AC} are the total moles of the free and the associated anions, respectively. Under the approximate assumption that $[C^+]$ is equal to the bulk concentration of the cationic surfactant, C_{sf} , eq 4 is rewritten as

$$\frac{[AC]}{[A^-]} = \frac{n_{AC}}{n_{A^-}} = K_{IA}C_{sf} \quad (6)$$

By substituting eq 6 into eq 5, we obtain

$$v_{ob} = \frac{1}{1 + K_{IA}C_{sf}}(v_{ep} + v_{eo}) + \frac{K_{IA}C_{sf}}{1 + K_{IA}C_{sf}}v_{eo} \quad (7)$$

The effective electrophoretic velocity, v_{eff} , and the effective electrophoretic mobility, μ_{eff} , for an ionic species can be defined as

$$v_{eff} = \frac{n_{A^-}}{n_{A^-} + n_{AC}}v_{ep} \quad (8)$$

$$\mu_{eff} = \frac{n_{A^-}}{n_{A^-} + n_{AC}}\mu_{ep} \quad (9)$$

The observed migration velocity, v_{ob} , can also be represented with v_{eff} and μ_{eff} as

$$v_{ob} = v_{eff} + v_{eo} = (\mu_{eff} + \mu_{eo})E \quad (10)$$

By substituting eq 10 into eq 7, we can obtain

$$\frac{1}{v_{eff}} = \frac{K_{IA}}{v_{ep}}C_{sf} + \frac{1}{v_{ep}} \quad (11)$$

Equation 11 can also be rewritten by using the effective electrophoretic mobility as

$$\frac{1}{\mu_{eff}} = \frac{K_{IA}}{\mu_{ep}}C_{sf} + \frac{1}{\mu_{ep}} \quad (12)$$

Equation 12 shows that the plots of $1/\mu_{eff}$ vs C_{sf} give linear relationships below the cmc, and the ion association constant between the anion and the surfactant can be obtained from the slope and the intercept.

The concentration of the monomeric surfactant above the cmc is constant and is the same as that of the solution at the cmc.¹³ Therefore, the effective electrophoretic velocity and mobility of anion in the aqueous solution above the cmc will be also constant and the same as the electrophoretic velocity, $v_{eff(cmc)}$, and mobility, $\mu_{eff(cmc)}$, at the cmc, respectively. On the other hand, the electrophoretic velocity of the anion incorporated in the micelle can be assumed to be the same as that of the micelle, v_{mc} . Then, v_{ob} in the solution above the cmc will be presented as

$$v_{ob} = \frac{n_{aq}}{n_{aq} + n_{mc}}(v_{eff(cmc)} + v_{eo}) + \frac{n_{mc}}{n_{aq} + n_{mc}}(v_{mc} + v_{eo}) \quad (13)$$

where n_{aq} and n_{mc} are the total moles of the anions in the aqueous phase and in the micelle, respectively. In the case of a neutral solute the electrophoretic velocity is zero, and v_{ob} is given by

$$v_{ob} = \frac{n_{aq}}{n_{aq} + n_{mc}}v_{eo} + \frac{n_{mc}}{n_{aq} + n_{mc}}(v_{mc} + v_{eo}) \quad (14)$$

By using the capacity factor, $k' = n_{mc}/n_{aq}$, eq 13 can be shown as

$$v_{ob} = \frac{1}{1 + k'}(v_{eff(cmc)} + v_{eo}) + \frac{k'}{1 + k'}(v_{mc} + v_{eo}) \quad (15)$$

By rearrangement of eq 15 using the effective electrophoretic velocity and mobility, k' can be expressed as

$$k' = \frac{v_{eff(cmc)} - v_{eff}}{v_{eff} - v_{mc}} = \frac{\mu_{eff(cmc)} - \mu_{eff}}{\mu_{eff} - \mu_{mc}} \quad (16)$$

Equation 16 also shows that the relation between the effective electrophoretic velocity and capacity factor is not affected by the electroosmotic velocity. The capacity factor for a neutral species can be given as follows because the electrophoretic velocity for neutral species in aqueous phase is zero

$$k' = \frac{-\mu_{\text{eff}}}{\mu_{\text{eff}} - \mu_{\text{mc}}} \quad (17)$$

The relationship between k' and the distribution coefficient, K , can be approximated as follows²

$$k' = K\bar{v}(C_{\text{st}} - \text{cmc}) \quad (18)$$

where \bar{v} is the partial specific volume. Then the distribution coefficient for an inorganic anion can be determined from plotting k' obtained by eq 16 as a function of C_{st} .

EXPERIMENTAL SECTION

Apparatus. An experimental equipment for capillary electrophoresis was built according to the literature.^{1,14} Fused-silica capillary tubes with 50 μm i.d. \times 500 mm, were obtained from Gasukuro Kogyo (Tokyo, Japan). A high-voltage power supply, a Model HCZE-30PNO.25 (Matsusada Precision Devices, Shiga, Japan) was used for applying the voltage. A variable-wavelength absorbance detector, a Model CV⁴ (ISCO, Inc., Lincoln, NE), was utilized to measure the absorbance at 210 nm. The detection was carried out by measuring the absorbance on the column at a position 20 cm from the positive end of the capillary tube. A new capillary was flushed with 0.1 M potassium hydroxide solution overnight before use. After rinsing with water, the capillary was filled with a buffer solution without CTAC and stood for 1 h. Then the capillary was filled with an operating buffer containing CTAC. A sample was injected by moving the injection end of the capillary to the sample reservoir and raising it above the other end for 5 s. The injection volume was about 0.6 nL for the injection time of 5 s. The electroosmotic velocities of the bulk solution and the electrophoretic velocities of micelles were evaluated from the measurement of the methanol peak, which is insoluble in the micellar phase, and the Sudan III peak, which is completely soluble in it, respectively.^{3,15} The mixture of 4 mM bromide and bromate, 2 mM iodide and iodate, and 1 mM nitrate in Sudan III-saturated methanol was used as a sample to investigate the migration behavior of these anions. The directions of both electroosmotic flow and electrophoretic migration of the CTAC micelle were the opposite of those in SDS solution. The direction of the electroosmotic flow was from the cathode to the anode, and that of the electrophoretic migration of the CTAC micelle was from anode to cathode. The direction migrating from cathode to anode was defined to be positive in this paper.

Materials. All reagents were of analytical grade and used without further purification. Cetyltrimethylammonium chloride (CTAC) was obtained from Wako pure chemicals (Osaka, Japan). Standard solutions of inorganic anions were prepared by dissolving potassium salts with water. The background electrolyte solution was prepared as follows: the required amounts of CTAC were dissolved with water, and then 1.0 mL of 1 M potassium dihydrogen phosphate was added to the solution. The pH of the solution was then adjusted to 7.0 by adding 1 M tris(hydroxymethyl)aminomethane (Tris); finally, the solution was diluted to 50 mL.

RESULTS AND DISCUSSION

If the inorganic anions have some interaction with a cationic surfactant, the migration behavior of ionic species in the solution containing surfactant will be different from that in a buffer solution which is used in capillary zone electrophoresis. Chromatograms of the mixture of several inorganic anions in the CTAC solution at the various concentrations are shown in Figure 1. The elution order in Figure 1A, where the CTAC concentration is below the cmc (cmc = 1.0 mM), is bromide < nitrate < bromate = iodide < iodate. This order is in accord with the order of their molar conductivities (bromide (78.4 S cm² mol⁻¹), nitrate (71.4 S cm² mol⁻¹), bromate (55.8 S cm² mol⁻¹), iodide (76.9 S cm² mol⁻¹), iodate (41.0 S cm² mol⁻¹) at 25 °C¹⁶), that is, their absolute mobilities except for iodide ion. Iodide ion is retarded largely by ion association equilibria with a monomeric surfactant even below the cmc. The unique separation selectivity was observed in the micellar solution as shown in Figure 1C. The elution order, iodate < bromate < bromide < nitrate < iodide, is completely

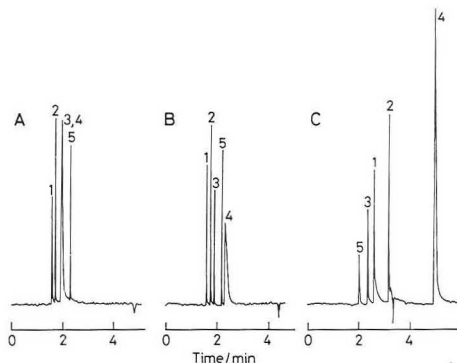


Figure 1. Chromatograms of inorganic anions at various concentrations of CTAC: (A) 0.2 mM; (B) 1.0 mM; (C) 25 mM. Key: (1) bromide, (2) nitrate, (3) bromate, (4) iodide, (5) iodate. Conditions: buffer, 20 mM phosphate-Tris buffer, pH 7.0; applied voltage, 15 kV; temperature, 22 °C. The apparent migration velocities (mm s⁻¹) are (A) $v_{\text{Br}} = 3.23$, $v_{\text{NO}_3} = 2.98$, $v_{\text{BrO}_3} = 2.62$, $v_{\text{I}} = 2.62$, $v_{\text{IO}_3} = 2.20$, $v_{\text{eo}} = 1.07$, (B) $v_{\text{Br}} = 3.13$, $v_{\text{NO}_3} = 2.86$, $v_{\text{BrO}_3} = 2.63$, $v_{\text{I}} = 2.14$, $v_{\text{IO}_3} = 2.27$, $v_{\text{eo}} = 1.14$, and (C) $v_{\text{Br}} = 1.91$, $v_{\text{NO}_3} = 1.57$, $v_{\text{BrO}_3} = 2.12$, $v_{\text{I}} = 1.00$, $v_{\text{IO}_3} = 2.48$, $v_{\text{eo}} = 1.51$.

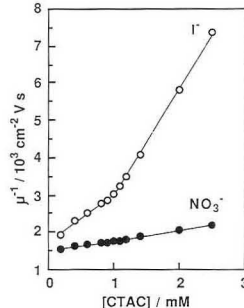


Figure 2. Dependence of the reciprocal of the effective mobility of iodide and nitrate on the concentrations of CTAC. Conditions are given in Figure 1.

different from that below the cmc.

In order to investigate the interaction between inorganic anions and a cationic surfactant by MECC, the effect of CTAC concentrations on the mobilities of inorganic anions should be examined. However, the electroosmotic mobility varied depending on the CTAC concentration and preconditioning of capillary, and it has a poor reproducibility. Then the observed migration velocity cannot be used to evaluate a true influence due to interaction between anionic species and a cationic surfactant. On the other hand, the use of effective electrophoretic mobilities of inorganic anions enabled the evaluation of the interaction without influences of the electroosmotic mobility as described above. It is predicted from eq 12 that $1/\mu_{\text{eff}}$ is in proportion to C_{st} and the slope and intercept give the association constant. Actually, the plots of $1/\mu_{\text{eff}}$ vs C_{st} below the cmc show the linearity as shown in Figure 2. The intercepts indicate the mobilities in the buffer solution without CTAC. The order of the values is in accord with the absolute mobilities except for iodide. The ion association constants for various inorganic anions calculated from the slopes and the intercepts are summarized in Table I. The ion association constant of iodate is not shown in this table because the slope was a negative value. This is due to the very weak interaction of iodate with CTAC. The slope

Table I. Ion Association Constants of Inorganic Anions

solute	ion assocn const/M ⁻¹	solute	ion assocn const/M ⁻¹
bromide	93	nitrate	140
bromate	38	iodide	760

for iodate is really very small, and the value is near zero. The anion selectivity order found on this study is iodide > nitrate > bromide > bromate > iodate. This order is similar to the selectivity order of typical ion interaction chromatography (IIC) with tetraalkylammonium salts.^{17,18} Though the separation mechanism of IIC is not simple, the anion selectivity order can be considered the order of the interaction between the tetraalkylammonium ions and anions. Ito et al. have reported the separation of inorganic anions by IIC with cetyltrimethylammonium, and their results are also in accordance with ours.¹⁹

The plot of $1/\mu_{\text{eff}}$ vs C_{st} for the iodide ion in Figure 2 can be divided into two lines below and above 1 mM. The inflection point seems to give the cmc of CTAC under this experimental condition. The CTAC concentration at the reflection point agrees with a literature value of the cmc.²⁰ Above the cmc, the effective mobilities of inorganic anions decreases due to partitioning to the micelle according to the eq 16. If eq 16 is solved for $1/\mu_{\text{eff}}$, the resulting equation is

$$\frac{1}{\mu_{\text{eff}}} = \frac{1 + k'}{k'\mu_{\text{mc}} + \mu_{\text{eff(cmc)}}} \quad (19)$$

The linearity for iodide above the cmc can be explained as follows. At near the cmc, k' is much smaller than unity so that we can consider $k'\mu_{\text{mc}} \ll \mu_{\text{eff(cmc)}}$. Thus, the denominator is approximately equal to a constant value, $\mu_{\text{eff(cmc)}}$, and as result $1/\mu_{\text{eff}}$ is in proportion to k' , that is, C_{st} . When the CTAC concentration is fairly beyond the cmc, the approximation used above does not apply. The relationship between $1/\mu_{\text{eff}}$ and k' is no longer linear but follows eq 19. As k' increases, μ_{eff} decreases to zero (that is, $1/\mu_{\text{eff}}$ will approach infinity) and then becomes negative. For the other inorganic anions, the slopes of $1/\mu_{\text{eff}}$ vs C_{st} plots are so small that the inflection points cannot be found. These results show that the iodide ion will be a useful marker to obtain the cmc under this experimental condition.

We have to know the values of $\mu_{\text{eff(cmc)}}$ for each anion in order to calculate the k' values of inorganic anions. Since the inflection point in Figure 2 can be regarded as the cmc of CTAC under this experimental condition, the effective mobilities of inorganic anions at this point can be used as the electrophoretic mobilities at the cmc, $\mu_{\text{eff(cmc)}}$. The k' values calculated using $\mu_{\text{eff(cmc)}}$ show good linearities against C_{st} . The distribution coefficients estimated from the slopes of the lines are summarized in Table II. The order of distribution coefficients for the inorganic anions in the micelle is iodide > nitrate > bromide > bromate > iodate. These values are much smaller than the values determined by micelle exclusion chromatography,²² and the order bromide > nitrate differs

Table II. Distribution Coefficients of Inorganic Anions^a

solute	distrib coeff	solute	distrib coeff
bromide	180	nitrate	270
bromate	86	iodide	880
		iodate	11

^aThe partial specific volume of CTAC used is the value determined by Armstrong and Stine, 0.977 mL g⁻¹.²¹

from our results. These differences seem to be ascribed to the coexisting ions because the values estimated in this study are virtually the conditional constants in the presence of background ions, such as phosphate and chloride. Okada also reported that foreign ions influence the retention behavior of inorganic anions in micelle exclusion chromatography.²² Mullins et al. have reported that the order of distribution coefficients in a 10 mM phosphate buffer solution, whose experimental condition is relatively similar to ours, is nitrate > bromide in micelle chromatography.²³ This order is in agreement with our results.

MECC using cationic surfactant not only shows the interesting separation selectivity for monovalent inorganic anions but also provides information on the ion association of inorganic anions with a surfactant monomer and the distribution into the cationic micellar phase. The method should be applicable to separation of many organic anions.

REFERENCES

- (1) Terabe, S.; Otsuka, K.; Ichikawa, K.; Tsuchiya, A.; Ando, T. *Anal. Chem.* **1984**, *56*, 111-113.
- (2) Terabe, S.; Otsuka, K.; Ando, T. *Anal. Chem.* **1985**, *57*, 834-841.
- (3) Otsuka, K.; Terabe, S.; Ando, T. *J. Chromatogr.* **1985**, *332*, 219-226.
- (4) Otsuka, K.; Terabe, S.; Ando, T. *Nippon Kagaku Kaishi* **1987**, *7*, 950-955.
- (5) Balchunas, A. T.; Sepaniak, M. J. *Anal. Chem.* **1988**, *60*, 617-621.
- (6) Bushey, M. M.; Jorgenson, J. W. *Anal. Chem.* **1989**, *61*, 491-493.
- (7) Wallingford, R. A.; Ewing, A. G. *Anal. Chem.* **1988**, *60*, 258-263.
- (8) Wallingford, R. A.; Ewing, A. G. *J. Chromatogr.* **1988**, *441*, 299-309.
- (9) Fujiwara, S.; Iwase, S.; Honda, S. *J. Chromatogr.* **1988**, *447*, 133-140.
- (10) Nishi, H.; Tsumagari, N.; Terabe, S. *Anal. Chem.* **1989**, *61*, 2434-2439.
- (11) Ghowsi, K.; Foley, J. P.; Gale, R. J. *Anal. Chem.* **1990**, *62*, 2714-2721.
- (12) Otsuka, K.; Terabe, S.; Ando, T. *J. Chromatogr.* **1985**, *348*, 39-47.
- (13) Berthod, A.; Girard, I.; Gonnet, C. *Anal. Chem.* **1986**, *58*, 1356-1358.
- (14) Jorgenson, J. W.; Lukacs, K. D. *Anal. Chem.* **1981**, *53*, 1298-1302.
- (15) Burton, D. E.; Sepaniak, M. J.; Maskarinec, M. P. *J. Chromatogr. Sci.* **1987**, *25*, 514-518.
- (16) Dobos, D. *Electrochemical Data*; Elsevier: Amsterdam, Oxford, New York, 1975.
- (17) Cassidy, R. M.; Elchuk, S. *Anal. Chem.* **1982**, *54*, 1558-1563.
- (18) Iskandarani, Z.; Pietrzyk, D. J. *Anal. Chem.* **1982**, *54*, 2427-2431.
- (19) Ito, K.; Ariyoshi, Y.; Tanabiki, F.; Sunahara, H. *Anal. Chem.* **1991**, *63*, 273-276.
- (20) Rosen, M. J. *Surfactants and Interfacial Phenomena*; Wiley: New York, 1978.
- (21) Armstrong, D. W.; Stine, G. Y. *J. Am. Chem. Soc.* **1983**, *105*, 2962-2964.
- (22) Okada, T. *Anal. Chem.* **1988**, *60*, 1511-1516.
- (23) Mullins, F. G. P.; Kirkbright, G. F. *Analyst (London)* **1984**, *109*, 1217-1221.

RECEIVED for review August 5, 1991. Accepted January 15, 1992.

Combined Supercritical Fluid Extraction/Solid-Phase Extraction with Octadecylsilane Cartridges as a Sample Preparation Technique for the Ultratrace Analysis of a Drug Metabolite in Plasma

Hanjia Liu, Linda M. Cooper, Douglas E. Raynie, J. David Pinkston, and Kenneth R. Wehmeyer*

The Procter & Gamble Company, Miami Valley Laboratories, P.O. Box 398707, Cincinnati, Ohio 45239-8707

Supercritical fluid extraction was coupled with solid-phase extraction using octadecylsilane cartridges for the selective isolation of ultratrace levels of a drug metabolite, mebeverine alcohol, from plasma. Plasma was directly applied to the extraction cartridge, the cartridge was washed to remove protein and then extracted under supercritical conditions using CO₂/5% methanol. The effluent from the extraction cell was bubbled through a small volume of 2-propanol to trap the extracted mebeverine alcohol. The effects of extraction pressure and temperature on analyte recovery were examined. The absolute recovery, selectivity, precision, and accuracy of the combined supercritical fluid extraction/solid-phase extraction approach were compared to those of conventional solid-phase extraction using gas chromatography/mass spectrometry in the selected-ion monitoring mode. Mebeverine alcohol was used as a model compound, and dog plasma was employed as the biological matrix for these studies.

INTRODUCTION

The rapid and accurate measurement of ultratrace levels of drugs and their metabolites in biological fluids plays a major role in the pharmaceutical development process. The measurement of plasma levels of drugs and metabolites provides information for mechanism of action and pharmacology and toxicology studies, as well as for clinical development efforts of drug substances.¹ Many ultratrace analysis techniques are based on chromatographic methods and usually require some form of sample preparation prior to analysis. The sample preparation step may be required to remove potential endogenous interferences and proteins. In addition, a sample concentration step is often required to raise the signal-to-noise level for the analyte to a value sufficient for accurate quantification.

Liquid-liquid extraction (LLE) and more recently solid-phase extraction (SPE) have been used extensively as sample preparation methods.² Although widely employed, LLE techniques have a number of potential disadvantages including the formation of emulsions, lack of totally automated instrumentation, and disposal issues around organic solvents. SPE has seen increasing use as a sample preparation technique.^{2,3} SPE offers a number of attractive features including the availability of automated instrumentation and a high degree of selectivity in analyte isolation. However, for ultratrace analysis the collected SPE effluent must be removed prior to analysis. This solvent removal is a time-consuming step, often requiring hours or overnight conditions to reach dryness. Additionally, SPE still involves the use of large quantities of organic solvents, which results in significant purchase and disposal costs.

Recent studies have shown that the use of supercritical fluids as an extraction medium provides a powerful alternative

to traditional extraction methods.^{4,5} Supercritical fluids can provide increased extraction efficiencies and give at least 1 order-of-magnitude increase in the rate of extraction. The solvent strength of the supercritical fluid can be easily controlled by adjusting extraction pressure or temperature. Also, the supercritical fluid can be easily removed following extraction. The most commonly used supercritical fluid, CO₂, is cost effective from both an acquisition and disposal point of view.

To date, most published supercritical fluid extraction (SFE) work has been done on solid or semisolid sample matrices.⁴ A small number of reports have dealt with the direct SFE of liquid matrices. Taylor and Hedrick^{6,7} extracted tripropylidene, phenol, and phosphonate from aqueous solutions by directly passing a supercritical fluid through the matrix. Ong and co-workers⁸ extracted high levels of cholesterol from a plasma matrix directly with a supercritical fluid. An alternative approach for liquid aqueous matrices would be to remove the water before sample extraction with the supercritical fluid. Several approaches have been taken to remove water from sample matrices including freeze-drying the sample⁹ and using an adsorbent like anhydrous sodium sulfate.¹⁰ Additionally, Niessen et al. have used an on-line cartridge precolumn packed with XAD-2 resin to isolate an analyte from plasma prior to analysis by supercritical fluid chromatography.¹¹

We report a new approach for the extraction of drugs at ultratrace levels from plasma which combines SFE with SPE using octadecylsilane (ODS) cartridges. The SFE/SPE procedure is similar to SPE except that a supercritical fluid is used to elute the analyte from the cartridges. The use of a supercritical fluid eliminates the time-consuming task of solvent removal incurred when conventional SPE is used for sample preparation in ultratrace analysis. Mebeverine alcohol (MEBOH; see Figure 1), a metabolite of the antispasmodic drug mebeverine, was used as a model compound for these studies. The effect of extraction temperature and pressure on the recovery of MEBOH during SFE/SPE was examined to determine optimal extraction conditions. The selectivity, accuracy, and precision of SFE/SPE relative to conventional SPE were examined over a MEBOH concentration range from 10 to 250 ng/mL using a stable-isotope-based gas chromatography/mass spectrometry (GC/MS) method with selected-ion monitoring (SIM) for MEBOH analysis.

EXPERIMENTAL SECTION

Chemicals. Distilled/deionized water was from a Barnstead Nanopure II system (Dubuque, IA). Methanol (MEOH; HPLC Grade), 2-propanol (HPLC Grade), and formic acid (Reagent Grade) were from J. T. Baker, Phillipsburg, NJ. Octane (99%+) and triethylamine (TEA; 99%) were from Aldrich Chemical, Milwaukee, WI. Dimethylhexylamine (DMHA; Purum Grade) was from Fluka Chemical Corp., Ronkonkoma, NY. The derivatizing reagent, *N,O*-bis(trimethylsilyl)trifluoroacetamide (BSTFA) was from Pierce, Rockford, IL. Mebeverine alcohol and deuterium-labeled mebeverine alcohol (MEBOH-d₄; see Figure 1) were synthesized at Procter & Gamble, Miami Valley Labo-

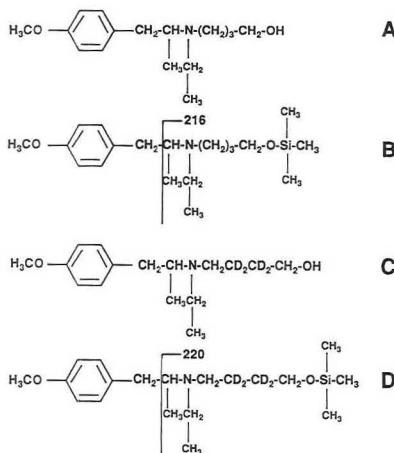


Figure 1. Structure of (A) mebeverine alcohol (MEBOH), (B) trimethylsilyl (TMS) derivative of MEBOH, (C) internal standard, mebeverine-*d*₄ alcohol (MEBOH-*d*₄), and (D) TMS derivative of MEBOH-*d*₄. The position of the ¹⁴C label is shown by the asterisk on the MEBOH structure. The ions used for selected-ion monitoring during the GC/MS analysis are indicated for the TMS derivatives.

atories. [¹⁴C]Mebeverine alcohol ([¹⁴C]MEBOH) was obtained from [¹⁴C]mebeverine (109 μ Ci/mg) by alkaline hydrolysis, as described previously.¹² Dog plasma was obtained from Pel-Freez, Rogers, AR. SFC-grade CO₂ and SFC-grade CO₂ with 5% MEOH modifier were purchased from Scott Specialty Gases, Plumsteadville, PA.

SFE/SPE Recovery Studies. Dog plasma (1.0 mL), containing 0.1 mL of TEA or DMHA, was spiked with [¹⁴C]MEBOH (10, 50, or 250 ng/mL). The plasma was applied to ODS cartridges (J. T. Baker, 3 mL, 500 mg), previously conditioned with 5 mL of MEOH followed by 5 mL of water/MEOH (95/5, v/v), at a flow rate of approximately 2 mL/min. The ODS cartridges were then washed with 5 mL of water/MEOH (95/5, v/v). In some cases, the cartridges were given an additional wash with 5 mL of water/MEOH (60/40, v/v). The cartridges were then blown dry with N₂. The ODS packing was then removed from the cartridges and carefully transferred into 1-mL extraction vessels (Suprex, Pittsburgh, PA). Each vessel was placed in a Suprex SFE/50 extraction system with a fused-silica capillary restrictor (50 cm \times 25 μ m i.d.). The end of the restrictor was placed into a test tube (16 mm \times 100 mm) containing 4 mL of 2-propanol at room temperature to trap the eluted [¹⁴C]MEBOH. Both CO₂ and CO₂/5% MEOH were used as supercritical fluids.

Extraction temperature, pressure, and time were varied to determine their effect on the recovery of [¹⁴C]MEBOH. The extent of the extraction was determined by counting the 2-propanol solutions on a Packard Model 2000CA liquid scintillation analyzer (Packard Tri-Carb, Downers Grove, IL). SFE/SPE recovery was directly compared to an equivalent standard solution. Additionally, SFE/SPE recovery of [¹⁴C]MEBOH was examined without the use of amine modifiers in the plasma. Recovery was also examined when TEA was added directly to the ODS material prior to SFE/SPE, rather than added to the plasma prior to SFE/SPE. The use of a 100-mg polymeric-based octadecyl packing as the solid-phase material (Polysorb MP-1 Columns, Interaction Chemicals, Mountain View, CA) was also examined.

SFE/SPE Selectivity, Accuracy, and Precision Studies. Blank plasma, blank plasma spiked with internal standard (MEBOH-*d*₄, 50 ng/mL), and blank plasma spiked with internal standard (50 ng/mL) and MEBOH (10, 50, or 250 ng/mL) were prepared. TEA (0.1 mL) was added to 1.0-mL aliquots of each plasma sample, and the samples (1.1 mL) were applied to ODS cartridges. The cartridges were washed and dried, and the ODS packing was transferred to the SFE extraction cells as described above. The SFE/SPE extraction was performed using CO₂/5%

MEOH at 350 atm and 40 $^{\circ}$ C for 10 min with a liquid flow rate of 0.3 mL/min. The effluent from the restrictor was passed through 4 mL of 2-propanol at room temperature to trap the extracted MEBOH and MEBOH-*d*₄. After completion of the extraction, the 2-propanol was blown to dryness under N₂. The residue was derivatized with 0.2 mL of BSTFA at 60 $^{\circ}$ C for 15 min. The BSTFA was removed under N₂, and the resulting residue was reconstituted in 0.1 mL of octane. The reconstituted sample was analyzed by GC/MS analysis as described below.

Solid-Phase Extraction Conditions. Solid-phase extraction was done using 3-mL syringe-barrel cartridges containing 500 mg of ODS (J. T. Baker). The cartridges were conditioned with 5 mL of MEOH followed by 5 mL of water/MEOH (95/5, v/v). Blank plasma, blank plasma spiked with MEBOH-*d*₄ (50 ng/mL), and blank plasma spiked with MEBOH-*d*₄ (50 ng/mL) and MEBOH (10, 50, and 250 ng/mL) were applied to ODS cartridges. The total sample volume was 1.0 mL in each of these cases. The cartridges were then washed sequentially with 5 mL of water/MEOH (95/5, v/v) and water/MEOH (60/40, v/v). In some instances, the second wash (water/MEOH, 60/40) was omitted. The cartridges were then eluted using 5 mL of water/MEOH/TEA/formic acid (10/90/0.5/0.32, v/v/v/v). The purpose of TEA was to block active silanol sites, and that of formic acid was to reduce the ionization of acidic silanol groups on the ODS surface.¹² The effluent was collected and taken to dryness on a Speed Vac concentrator (Savant, Farmingdale, NY). The residue was then derivatized with 0.2 mL of BSTFA as described above and reconstituted with 0.1 mL of octane. The reconstituted sample was then analyzed by GC/MS analysis as described below.

GC/MS Analysis. Briefly, the GC conditions involved a 0.5- μ L splitless injection (1.0 min) onto a Hewlett-Packard (HP; Avondale, PA) Ultra-2 column (30 m \times 0.20 mm i.d., 0.11- μ m film). A thermal program involving an initial oven temperature of 75 $^{\circ}$ C for 1 min followed by a thermal ramp to 300 $^{\circ}$ C at 25 $^{\circ}$ C/min was used to elute MEBOH and MEBOH-*d*₄. The injection port and GC/MS transfer line were held at 225 and 290 $^{\circ}$ C, respectively. MEBOH and MEBOH-*d*₄ were detected using SIM at *m/z* 216.0 and 220.0, respectively (see Figure 1). The GC/MS system was composed of a HP Model 5890A GC system equipped with a HP Model 7673A autosampler and a HP Model 5971A mass-selective detector. MEBOH standard solutions covering a concentration range from 2 to 500 ng/mL were prepared in MEOH. The standards (1.0 mL) were pipetted into test tubes containing 50 ng of MEBOH-*d*₄, and the MEOH was removed under N₂. The standards were derivatized with BSTFA and reconstituted as described above. Standard curves were obtained by plotting the peak area ratio (peak area MEBOH/peak area MEBOH-*d*₄) versus concentration of MEBOH. The concentration of MEBOH in plasma samples was determined from the peak area ratio obtained from the sample by extrapolation from the linear regression curve.

RESULTS AND DISCUSSION

Optimization of MEBOH Recovery. [¹⁴C]MEBOH was used to examine the absolute recovery of the SFE/SPE and conventional SPE approaches. A high recovery of the analyte from the sample preparation step is desirable, although the use of a stable-isotope internal standard (MEBOH-*d*₄) should correct for any loss of MEBOH. For both SFE/SPE and SPE, recovery of [¹⁴C]MEBOH was poor without the addition of an amine modifier due to silanol interactions between MEBOH and the silica. The recovery of [¹⁴C]MEBOH (50 ng/mL) by SFE/SPE (350 atm and 40 or 80 $^{\circ}$ C for 20 min) was less than 1% without the addition of an amine modifier (TEA or DMHA) using either CO₂ or CO₂/5% MEOH as the supercritical fluid. Subsequent extraction of the ODS packing material demonstrated that the unextracted [¹⁴C]MEBOH was still on the packing.

It is common practice in the reversed-phase HPLC of basic compounds to mask the active silanol groups by adding a tertiary amine to the mobile phase. Two tertiary amines, TEA and DMHA, were investigated to determine their effect on SFE/SPE recovery of [¹⁴C]MEBOH. The SFE/SPE recovery of [¹⁴C]MEBOH from the ODS packing using plasma samples containing TEA or DMHA with CO₂/5% MEOH as the su-

Table I. Absolute Recovery of [^{14}C]MEBOH^{a,b}

[^{14}C]MEBOH concn, ng/mL	SFE/SPE % recovery		SPE % recovery
	TEA	DMHA	
10.0	70.2 \pm 5.6	80.3 \pm 2.2	101.3 \pm 1.1
50.0	87.9 \pm 3.7	95.2 \pm 3.0	100.2 \pm 3.0
250	85.7 \pm 1.0	95.5 \pm 5.0	100.6 \pm 1.5

^a Errors are standard deviations based on triplicate measurements. ^b SFE/SPE conditions: supercritical fluid = CO_2 /MEOH (95/5), pressure = 350 atm, temperature = 40 °C, liquid flow rate = 0.3 mL/min, and extraction time = 10 min.

percritical fluid is shown in Table I. The addition of the amine modifiers to the plasma resulted in good recovery of [^{14}C]MEBOH (70–95%) for spiked plasma concentrations from 10 to 250 ng/mL. However, when pure CO_2 was used as the supercritical fluid, recoveries of [^{14}C]MEBOH were less than 3%. Therefore, only CO_2 /5% MEOH was used in subsequent studies.

The addition of DMHA gave a better recovery of [^{14}C]MEBOH than TEA (Table I). The greater recovery obtained with DMHA may be due to less loss of DMHA during the N_2 drying step that precedes the SFE/SPE extraction. It was also found that similar recoveries were obtained if TEA was added to the packing immediately before SFE extraction rather than into the plasma. However, all the packing may not be exposed to the modifier during the extraction without an initial static extraction step. The possible loss of extracted [^{14}C]MEBOH due to poor trapping or aerosol formation was studied by total counting of the radioactivity. Experimental results showed that the sum of the radioactivity in the trapping solvent and that left on the ODS packing virtually accounted for 100% of the radioactivity added to the sample. Therefore, the loss due to poor trapping is minimal.

The recovery of [^{14}C]MEBOH at the 10 ng/mL level using either TEA or DMHA was lower than obtained at higher spiked concentrations (Table I). The lower recovery at the 10 ng/mL level may be due to the inability of the supercritical fluid to overcome strong silanol interactions. An alternative approach for the plasma analysis would be to use a non-silica-based support in the extraction cartridge to avoid the strong silanol interactions. A preliminary study with a polymeric-based support containing octadecyl groups as the solid-phase material gave quantitative recovery (100%) by SFE/SPE without the use of an amine modifier. Further investigations of this material are in progress.

The recovery of [^{14}C]MEBOH from the SPE extraction using an eluent containing 0.5% TEA is shown in Table I. Quantitative recovery of [^{14}C]MEBOH was obtained for all plasma concentration levels (10–250 ng/mL). The greater recovery of [^{14}C]MEBOH by SPE relative to SFE/SPE is probably due to the water/methanol eluent being a stronger solvent than the supercritical fluid for desorbing the adsorbed MEBOH from the ODS surface. The standard deviations for triplicate extractions by SPE and SFE/SPE procedures are comparable.

The time profile for the SFE/SPE of [^{14}C]MEBOH in TEA spiked plasma from the ODS packing was studied by collecting the supercritical effluent from the cartridge in a series of 5-min intervals. The SFE/SPE recovery of [^{14}C]MEBOH versus time, for extraction at 350 atm and 40 °C with a liquid flow rate of 0.3 mL/min, is shown in Figure 2. The extraction reached a plateau in less than 10 min under these conditions. To ensure complete extraction, however, a 10-min extraction time was used for all subsequent studies.

The effect of pressure and temperature on the cumulative recovery of [^{14}C]MEBOH by SFE/SPE was also examined by collecting the effluent from a single extraction cell for 10

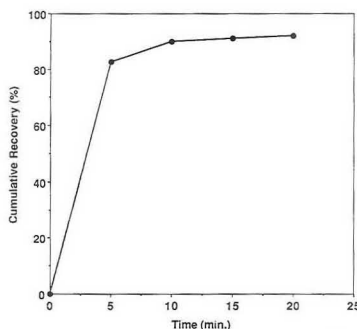


Figure 2. Cumulative SFE/SPE cumulative recovery of [^{14}C]MEBOH from plasma samples applied to ODS cartridges and extracted with CO_2 /5% MEOH in the presence of an amine modifier (TEA) versus time.

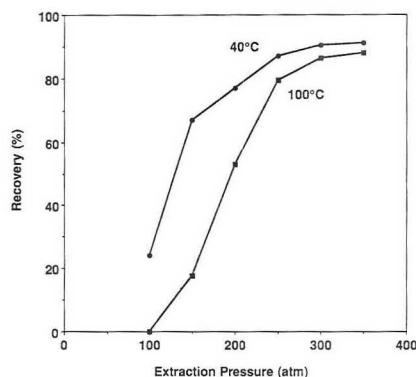


Figure 3. SFE/SPE recovery of [^{14}C]MEBOH from plasma samples applied to ODS cartridges and extracted with CO_2 /5% MEOH as a function of temperature and pressure.

min as the pressure was varied at constant temperature (Figure 3). At 40 °C, recovery of [^{14}C]MEBOH increases with increasing pressure and reaches a constant value (~87%) around 300 atm. Increasing the extraction temperature from 40 to 100 °C decreased the recovery of [^{14}C]MEBOH over the pressure range studied. The lower recovery is likely due to the decrease in the supercritical fluid density at the elevated temperature. It is possible that higher temperatures and pressures might result in improved recovery of [^{14}C]MEBOH; however, cell leakage prevented these parameters from being evaluated. Therefore, optimal SFE/SPE conditions for MEBOH involved the use of supercritical CO_2 /5% MEOH at 350 atm and 40 °C with a 10-min collection interval.

SFE/SPE Selectivity. The selectivity of SFE/SPE relative to conventional SPE was examined using a GC/MS method with SIM for the detection of MEBOH (m/z 216.0) and MEBOH- d_4 (m/z 220.0). Blank plasma, blank plasma spiked with internal standard (50 ng/mL), and blank plasma spiked with both MEBOH- d_4 (50 ng/mL) and MEBOH (10 ng/mL) were prepared for analysis by the SFE/SPE and SPE methods. For SFE/SPE, the plasma samples (1.0 mL) were spiked with 0.1 mL of TEA prior to extraction. Two different wash conditions were used for the ODS cartridges prior to the elution step by the supercritical fluid (SFE/SPE) or the organic/aqueous solvent (SPE). In one case, the ODS cartridge was washed with water/MEOH (95/5, v/v) after the appli-

Table II. Analysis of MEOH in Plasma Samples^{a,b}

[MEOH], ng/mL	found [MEOH], ng/mL				% recovery mean (% RSD)
	1	2	3	mean ± SD	
	SFE/SPE				
10.0	10.2	10.1	10.0	10.1 ± 0.1	101.0 (1.0)
50.0	47.7	47.8	47.9	47.8 ± 0.1	95.6 (0.2)
250.0	226.2	226.9	230.0	227.7 ± 2.0	91.1 (0.9)
	SPE				
10.0	9.75	9.99	9.87	9.87 ± 0.12	98.7 (1.2)
50.0	47.6	49.4	51.3	49.4 ± 1.8	98.8 (3.6)
250.0	238.9	234.2	236.2	236.5 ± 2.3	94.6 (1.0)

^aErrors are standard deviations based on triplicate sample preparations and analysis. ^bSFE/SPE conditions: supercritical fluid = CO₂/MEOH (95/5), pressure = 350 atm, temperature = 40 °C, liquid flow rate = 0.3 mL/min, and extraction time = 10 min.

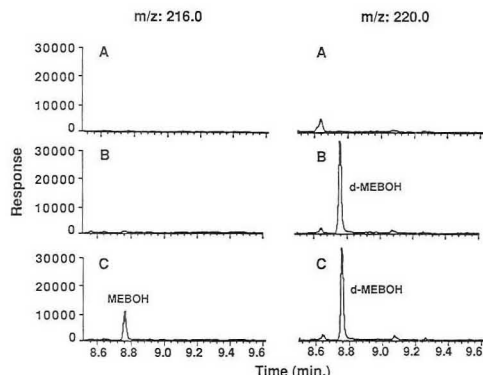


Figure 4. Selected-ion chromatograms (m/z 216.0 and 220.0) for the SFE/SPE of MEOH from (A) blank dog plasma, (B) blank dog plasma spiked with internal standard (MEBOH- d_4 , 50 ng/mL), and (C) blank dog plasma spiked with MEBOH- d_4 (50 ng/mL) and MEBOH (10 ng/mL).

cation of the plasma sample. In the other case, the ODS cartridge was given an additional wash with water/MEOH (60/40, v/v).

Typical SIM chromatograms obtained for samples prepared by SFE/SPE and SPE using the water/methanol (95/5) wash before elution are shown in Figures 4 and 5, respectively. Both approaches allowed interference-free detection of MEBOH and MEBOH- d_4 . However, the SIM chromatogram for the SPE approach contained several closely eluting peaks which were absent from the SFE/SPE approach. If the additional water/MEOH (60/40) wash was used, the selectivity of the SPE approach improved and was equivalent to that obtained by SFE/SPE. Apparently, the intermediate wash with water/MEOH (60/40) removes some materials that are extractable with the SPE elution solvent but not extractable with the supercritical fluid. These results demonstrate the potential of SFE/SPE to provide different, and perhaps complementary, selectivities to those obtained with conventional SPE. DMHA was found to contain impurities which produced interferences in the GC/MS analysis by SPE and SFE/SPE.

SFE/SPE Accuracy and Precision. The accuracy and precision of the SFE/SPE and conventional SPE approach were compared for the analysis of dog plasma (1.0 mL) spiked with MEBOH over a concentration range from 10 to 250 ng/mL. The results of the GC/MS analysis for triplicate SFE/SPE sample preparations of the spiked dog plasma are shown Table II. The recovery of MEBOH relative to MEBOH- d_4 from plasma by SFE/SPE ranged from 91.1 to 101.0% with RSD values of 1% or less for triplicate sample preparations. The recovery of MEBOH relative to MEBOH- d_4 from the plasma by the SPE method ranged from

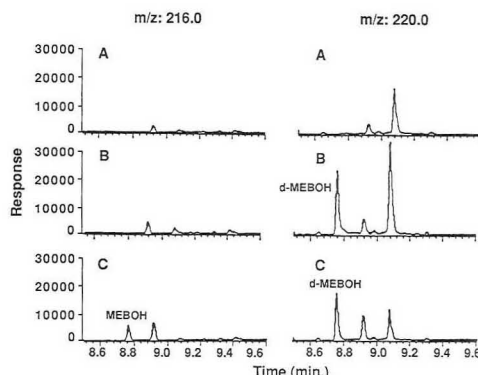


Figure 5. Selected-ion chromatograms (m/z 216.0 and 220.0) for the solid-phase extraction of MEOH from dog plasma: (A) blank plasma, (B) blank plasma spiked with internal standard (MEBOH- d_4 , 50 ng/mL), and (C) blank plasma spiked with MEBOH- d_4 (50 ng/mL) and MEBOH (10 ng/mL).

94.6 to 98.8% with RSD values of 3.6% or less (Table II). The SFE/SPE and SPE sample preparation approaches demonstrated comparable accuracy and precision for the analysis of MEBOH.

CONCLUSIONS

Although the SFE/SPE approach described in this work is clearly in a development stage, there are a number of potentially attractive aspects to this mode of sample preparation for the analysis of drugs in biological fluids. The removal of the supercritical fluid is very facile whereas the removal of the organic/aqueous eluent from SPE is often a very time-intensive step. The selectivity of the SFE extraction can be varied easily by changing the pressure and/or temperature conditions of the extraction and thereby changing the solvating power of the supercritical fluid. The selective partitioning of the analyte with the ODS packing coupled with the ability to vary the solvating power of the supercritical fluid by controlling pressure results in a powerful and selective new approach to sample preparation. Additionally, the SFE/SPE approach minimizes the cost associated with the use and disposal of organic solvents.

Future areas of investigation will involve further examination of polymeric octadecyl materials, the direct use of the SPE cartridges without the removal of the packing material, and investigations into the effect of drying time and the effect of the composition and volume of the trapping solvent.

ACKNOWLEDGMENT

The technical assistance of T. E. Delaney is gratefully appreciated.

REFERENCES

- (1) Yacobi, A.; Skelly, J. P.; Batra, V. K. *Toxicokinetics and New Drug Development*; Pergamon Press: New York, 1989.
- (2) Lin, C. K. *Trends Anal. Chem.* 1988, 7, 340-345.
- (3) Poole, S. K.; Dean, T. A.; Oudsema, J. W.; Poole, C. F. *Anal. Chim. Acta* 1990, 236, 3-42.
- (4) Hawthorne, S. B. *Anal. Chem.* 1990, 62, 633A-642A.
- (5) King, J. W. *J. Chromatogr. Sci.* 1989, 27, 355-364.
- (6) Hedrick, J. L.; Taylor, L. T. *J. High Resolut. Chromatogr.* 1990, 13, 312-316.
- (7) Hedrick, J. L.; Taylor, L. T. *Anal. Chem.* 1989, 61, 1986-1988.
- (8) Ong, C. P.; Ong, H. M.; Li, S. F. Y.; Lee, H. K. *J. Microcolumn Sep.* 1990, 2, 69-73.
- (9) Ndiomu, D. P.; Simpson, C. F. *Anal. Chim. Acta* 1988, 213, 237-243.
- (10) Nam, K. S.; Kapila, S.; Yanders, A. F.; Puri, R. K. *Chemosphere* 1990, 20, 873-880.
- (11) Niessen, W. M. A.; Bergers, P. J. M.; Tjaden, U. R.; Van Der Greef, J. *J. Chromatogr.* 1988, 454, 243-251.
- (12) Stadalius, M. A.; Berus, J. S.; Snyder, L. R. *LC-GC* 1988, 6, 494-500.

RECEIVED for review October 3, 1991. Accepted January 2, 1992.

Intravenous Microdialysis Sampling in Awake, Freely-Moving Rats

Martin Telting-Diaz, Dennis O. Scott, and Craig E. Lunte*

Department of Chemistry, The University of Kansas, Lawrence, Kansas 66045

Intravenous microdialysis sampling in the awake, freely-moving rat for the determination of free drug concentrations in blood is described. Intravenous microdialysis was performed with a nonmetallic, flexible dialysis probe. The pharmacokinetics of theophylline were determined using both microdialysis sampling and collection of whole blood following an iv dose. There was no difference in the half-life of elimination of theophylline determined by microdialysis, 4.4 ± 0.4 h, and whole blood sampling, 4.5 ± 0.7 h. The kinetics of elimination were affected by removing blood samples and by using anesthesia. The half-life of elimination was 4.4 ± 0.4 h when using simultaneous microdialysis and whole-blood sampling and only 3.0 ± 0.4 h using microdialysis alone. The half-life of elimination was 17.0 ± 7.1 h in chloral hydrate anesthetized rats. Microdialysis samples were continuously collected for over 7 h without fluid loss using a single experimental animal. Microdialysis sampling directly assesses the free drug concentration in blood. The extent of theophylline binding to blood proteins was determined in vitro in rat plasma and rat whole blood using both ultrafiltration and microdialysis. Theophylline was $(47.3 \pm 1.3)\%$ bound in rat plasma and $(52.2 \pm 1.6)\%$ bound in rat whole blood. Microdialysis sampling is a powerful tool for pharmacokinetic studies, providing accurate and precise pharmacokinetic data.

INTRODUCTION

In vivo microdialysis has been demonstrated to be a powerful tool to continuously sample the blood and tissue of animals for metabolic and pharmacokinetic experiments.¹⁻⁶ Experiments outside the central nervous system have been limited to anesthetized animals typically because of the rigid design of the microdialysis probes commonly employed. For neurochemical experiments the rigid probe can be used in awake, freely-moving animals because it can be secured to the skull.⁶⁻⁹ In other tissues, the integrity of the microdialysis probe system is often compromised when the animal moves. Alternative designs of microdialysis probes that are flexible have been described.¹⁰⁻¹³ The use of a flexible microdialysis probe overcomes the limitations of rigid probes and permits

experiments to be performed in all parts of a freely-moving animal.

This report describes the application of in vivo microdialysis perfusion to the determination of the pharmacokinetics of theophylline in awake, freely-moving rats. It is well established that anesthetics can have a pronounced effect on the observed pharmacokinetics of drugs.¹⁴ The ability to use microdialysis sampling for pharmacokinetic determinations in awake, freely-moving rats greatly improves the relevance of the data obtained. In addition, microdialysis sampling directly provides the concentration of unbound drug in the blood relative to the total concentration determined from whole blood samples. It is generally considered that the unbound concentration is the pharmacologically more relevant.¹⁵ When binding is accounted for microdialysis sampling gives equivalent results to whole blood sampling.

EXPERIMENTAL SECTION

Chemicals. Theophylline was purchased from Sigma Chemical Company (St. Louis, MO). HPLC-grade acetonitrile was obtained from Fisher Scientific (Fair Lawn, NJ). All other chemicals were reagent grade or better and were used as received.

Apparatus. Dialysis System. Microdialysis sampling was performed using a CMA/100 microinjection pump from Bioanalytical Systems, Inc./CMA (West Lafayette, IN) coupled to a microdialysis probe inserted into the jugular vein of the experimental animal. The perfusion medium was pumped through the probes at a flow rate of 1 μ L/min for all experiments. Microdialysis samples were collected by a CMA/200 refrigerated fraction collector.

Chromatographic System. The liquid chromatographic system consisted of a BAS PM-60 pump, an SPD-6A variable wavelength UV-vis absorbance detector with a microbore cell (Shimadzu Scientific Instruments, Inc., Columbia, MD), and a Rheodyne 7125 injection valve with a 5- μ L sample loop. Separation was achieved using a Brownlee 5 μ m ODS (1-mm \times 15-cm) column and a flow rate of 50 μ L/min. For all experiments the UV detector was operated at 270 nm.

Microdialysis Probe. The flexible microdialysis probe was similar to those described previously.¹⁰⁻¹³ The probe was constructed as shown in Figure 1 by inserting two pieces of fused silica tubing, 75- μ m i.d. and 147- μ m o.d. (Polymicro Technologies Inc., Phoenix, AZ), into a 5-mm length of polyethylene tubing, 0.28-mm i.d. and 0.61-mm o.d. One of the pieces of fused silica was inserted into but not through the polyethylene tubing. The other piece

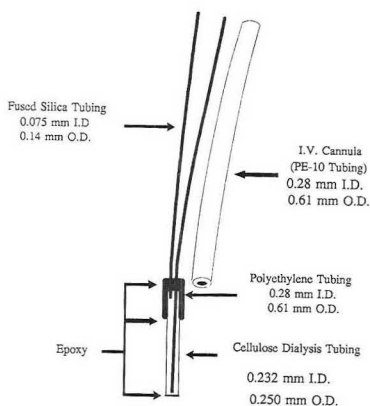


Figure 1. Schematic diagram of the flexible microdialysis probe and parallel iv cannula.

of fused silica was inserted through the polyethylene tubing such that 5 mm was exposed. The exposed piece of fused silica tubing was covered with the dialysis fiber which was then attached to the polyethylene tubing with epoxy (Devcon, Danvers, MA). The other end of the dialysis fiber was sealed with the epoxy. Regenerated cellulose dialysis fibers with a 232- μ m i.d. and 250- μ m o.d. and a molecular weight cut-off of 5000 were used (Dow Chemical Corporation, Midland, MI).

Microdialysis Probe Characterization. To determine the in vivo concentration of theophylline giving rise to the concentration detected in the perfusion medium, it is necessary to know the recovery of the dialysis probe. The recovery is defined as the ratio of the analyte concentration determined in the dialysate to the actual concentration of the analyte in the sample. Recoveries were determined in rat whole blood, rat plasma, and pH 7.4 Ringer's solution consisting of 155 mM NaCl, 5.5 mM KCl, and 2.3 mM CaCl_2 . All experiments were performed in a thermostated shaker bath to both maintain the temperature at 37 °C and provide the hydrodynamic system to model flowing blood. The free drug concentration in the whole-blood and plasma samples was determined by ultrafiltration. There was no difference in the recoveries from the different matrices when binding of theophylline to blood proteins was taken into account and was consistent with previous reports.¹⁰ The average recovery of theophylline for all probes used in these experiments was $(24.2 \pm 1.8)\%$. The recovery of each dialysis probe was determined both before and after implantation. The recovery determined after the implantation was used to calculate in vivo concentrations although the two recoveries never differed by more than 5% relative.

Protein Binding. Because microdialysis only samples the free drug in blood, the extent of binding of the drug to blood proteins must be known to compare results from microdialysis to those from whole blood.¹⁶ The extent of binding of theophylline to rat blood proteins was determined by ultrafiltration using both whole blood and plasma. Ultrafiltration was performed with an MPS-1 micropartition system with a YMT-membrane filter (Amicon, Lexington, MA). Samples of both EDTA-treated rat whole blood and rat plasma were spiked with known concentrations of theophylline and equilibrated for 1 h at 37 °C. The free fraction was then separated by ultrafiltration and analyzed by liquid chromatography.

In Vivo Pharmacokinetic Experiments. Four to five month old Sprague-Dawley rats weighing approximately 400 g were used. Rats were anesthetized with the inhalation anesthetic isoflurane. Isoflurane was chosen because it has a very short duration of action. The rat is typically fully recovered in less than 30 min after the administration of isoflurane is stopped. For experiments in anesthetized animals, the rat was initially anesthetized with isoflurane but then given a 400 mg/kg ip dose of chloral hydrate. After 2 h, maintenance doses of 200 mg/kg chloral hydrate were given every hour by iv administration.

A small incision through the skin was made at the back of the neck and on the right shoulder. The jugular vein was exposed and a small nick made into the vein. The microdialysis probe and a cannula were inserted through this nick, and the probe and cannula were threaded through the vein to a region near the heart (ca. 2.5 cm). The cannula was backed-off 5 mm from the dialysis membrane. The jugular vein was then ligated. The inlet and outlet tubing of the dialysis probe and the cannula tubing were then threaded under the skin and out the incision on the back of the neck. Both incisions were closed with surgical staples and the rat was placed in a flexible jacket that covered both incisions and supported the placement of the dialysis probe. The rat was then attached to the awake animal system (CMA/BAS) with a stiff wire attached to a collar on the rat and to a counterbalanced arm attached to the animal container. The counterbalanced arm also had a two-channel liquid swivel through which the dialysis probe was attached to the perfusion pump and fraction collector. The liquid swivel allows the animal full motion without the tubing becoming entwined and kinked.

To validate the microdialysis sampling technique, whole-blood samples were simultaneously collected. This was done through a cannula implanted along with the dialysis probe. A 100- μ L sample of whole blood was collected every 30 min for the first hour then once every hour. The whole-blood sample was centrifuged for 10 min; 40 μ L of the resulting plasma was treated with an equal volume of 0.7 M perchloric acid to precipitate proteins and centrifuged for 10 min. The supernatant was injected into the chromatographic system.

Pharmacokinetic experiments were performed by perfusing the implanted probe with a Ringer's solution at a perfusion rate of 1 μ L/min. Samples were continuously collected over 10-min intervals. Dialysis samples were diluted with Ringer's solution as needed to keep the concentration in the range of calibration. Blanks were collected for at least 1 h following insertion of the microdialysis probes. No chromatographic interferences were observed in the blanks. The animal was then dosed with theophylline (15 mg/kg) in 0.5 mL of Ringer's solution iv at 37 °C. Dialysis samples were collected for 6–7 h after dosing. The in vivo concentration of theophylline was calculated by determining the concentration in the dialysate from a standard curve and then accounting for the recovery of the microdialysis probe.

Microdialysis is a continuous sampling technique, therefore each sample represents the average concentration of analyte in the blood during the sampling interval. This is compared to taking discrete blood samples that represent the concentration in the blood only at the time of sampling. Because of the continuous sampling, microdialysis is an integrating technique that is less prone to fluctuations than an instantaneous sampling technique. Pharmacokinetic parameter calculations are also simplified. For example, area-under-the-curve (AUC) calculations are performed by summing the product of the concentration (μ g/mL), perfusion rate (mL/min), and sample interval (min) for all samples instead of interpolating between points with the trapezoidal rule.

Pharmacokinetic Calculations. Terminal half-lives of free theophylline were estimated by fitting an equation of the form

$$C(t) = A \exp(-\alpha t) + B \exp(-\beta t) \quad (1)$$

using a nonlinear least-squares fit. The first term in eq 1 describes the distribution phase following an iv bolus injection of theophylline where α is the distribution rate constant. The second term describes the elimination phase where β is the elimination rate constant. The half-life of elimination can be determined from the elimination rate constant (β). The concentration in the blood at the time of injection (C_0) can be calculated by adding the terms A and B.

The AUC values for blood sampling were estimated using the linear trapezoidal rule and were extrapolated to infinity by adding C_n/β , where C_n is the concentration of the last measurement. For the microdialysis data, the AUC was estimated by summing the products of the measured concentrations and the collection time interval with the addition of C_n/β (eq 2). Noncompartmental

$$\text{AUC} = \sum_0^n C_n \Delta t + \frac{C_n}{\beta} \quad (2)$$

analysis was used to obtain the total body clearance of theophylline

Table I. Binding of Theophylline to Blood Protein^a

	theophylline concentration		
	1 $\mu\text{g/mL}$	10 $\mu\text{g/mL}$	20 $\mu\text{g/mL}$
plasma			
microdialysis	47.7 \pm 2.7	48.4 \pm 3.6	45.9 \pm 4.5
ultrafiltration	47.5 \pm 2.6	50.1 \pm 2.9	52.2 \pm 3.3
whole blood			
microdialysis	53.8 \pm 4.6	52.1 \pm 3.0	50.7 \pm 6.7
ultrafiltration	49.9 \pm 2.8	53.0 \pm 7.0	54.6 \pm 5.0

^a $n = 3$.Table II. Recovery of Theophylline by Microdialysis^a

	theophylline concentration		
	1 $\mu\text{g/mL}$	10 $\mu\text{g/mL}$	20 $\mu\text{g/mL}$
Ringer's	24.4 \pm 1.9	24.9 \pm 2.2	21.7 \pm 1.7
plasma	26.6 \pm 3.0	25.6 \pm 5.1	22.6 \pm 4.7
whole blood	22.4 \pm 3.2	22.4 \pm 4.5	21.1 \pm 6.3

^a $n = 3$.

(C_1 = dose/AUC) and the volume of distribution ($V_d = C_1/\beta$). The mean residence time (MRT) was calculated by dividing the AUMC (first moment of the area under the curve) by the AUC. All results are expressed as the mean \pm standard deviation.

RESULTS AND DISCUSSION

Probe Calibration and Protein Binding. The extent of theophylline binding to blood proteins is listed in Table I. The percent bound is independent of the concentration of theophylline in the range studied. Theophylline was found to be (52.2 \pm 1.6)% bound in rat whole blood and (47.7 \pm 0.8)% bound in rat plasma. This is in good agreement with previous results using human plasma.¹⁷ The whole blood value was used in subsequent comparisons of microdialysis samples to whole-blood samples.

The recovery of the microdialysis probe was determined in whole blood, plasma, and Ringer's solution over the concentration range needed for the pharmacokinetic experiments. The recovery results are tabulated in Table II. The recovery is independent of the concentration and the matrix for these experiments. Based on these results, subsequent probes were only calibrated using the Ringer's solution.

Intravenous Microdialysis Sampling. Typical chromatograms of blood dialysate obtained by in vivo sampling are shown in Figure 2. In vivo dialysis samples were directly injected into the chromatograph. The blank sample was run at the most sensitive detector gain setting used to determine if any endogenous interferences occur at high gain. As can be seen (Figure 2A), no interferences occur in the blanks obtained prior to dosing of the animal with theophylline.

The whole-blood samples were more difficult to analyze, requiring protein precipitation and removal before injection into the chromatographic system. These samples exhibited more potential interferences in the blanks relative to the dialysis samples (Figure 3). Fortunately, none of these endogenous compounds interfered with the determination of theophylline with this separation. For comparison, the whole-blood samples of Figure 3 correspond in time to the dialysis samples of Figure 2.

Pharmacokinetic Comparison to Whole-Blood Samples. Microdialysis sampling was validated by simultaneously collecting blood samples. Pharmacokinetic curves obtained by the two methods were identical (Figure 4) when the samples were taken simultaneously and binding of theophylline to blood proteins is taken into account. Also shown in Figure 5 is a semi-log plot for the microdialysis sampling data clearly showing the fast distribution phase followed by the slower

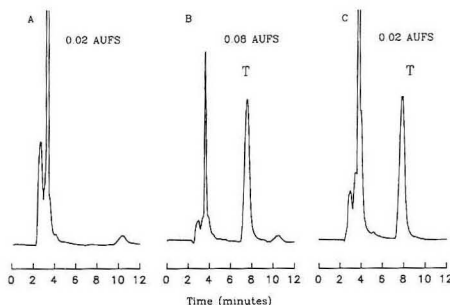


Figure 2. Typical chromatograms of iv microdialysis samples: (A) blank prior to dosing, (B) 30 min after a 15 mg/kg iv dose of theophylline, (C) 300 min after a 15 mg/kg iv dose.

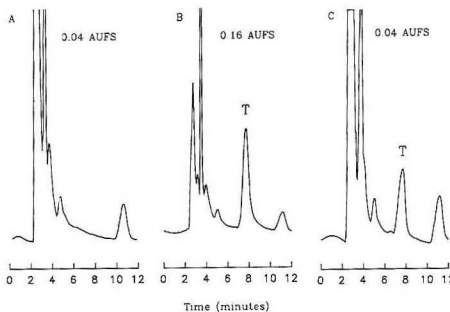


Figure 3. Typical chromatograms of iv whole-blood samples: (A) blank prior to dosing, (B) 30 min after a 15 mg/kg iv dose of theophylline, (C) 300 min after a 15 mg/kg iv dose.

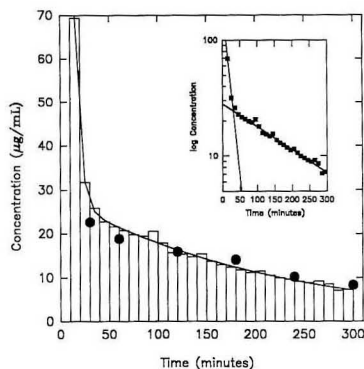


Figure 4. Concentration-versus-time profile for a 15 mg/kg iv dose of theophylline in the awake, freely-moving rat. The bars represent the microdialysis samples and the circles represent the whole-blood samples. The concentration of theophylline in whole blood is corrected for protein binding. Shown in the inset is a plot of log concentration-versus-time using the microdialysis sampling data.

elimination phase. The pharmacokinetic parameters extracted from the data are listed in Table III. The results for the whole blood are in good agreement with previously reported values.¹⁸ The values for whole blood sampling and simultaneous microdialysis sampling show no statistical difference. The half-life of elimination determined from microdialysis samples

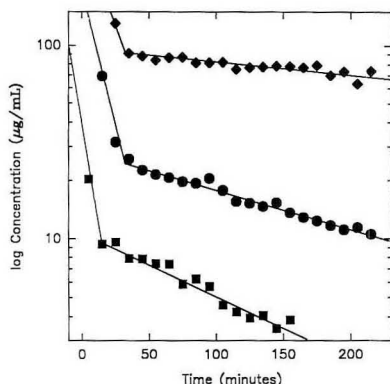


Figure 5. Semi-log presentation of the concentration-versus-time profile for 15 mg/kg iv doses of theophylline in rats determined using microdialysis sampling. Awake animal without blood sampling (■); awake animal with simultaneous blood sampling (●); anesthetized animal (◆).

Table III. Pharmacokinetic Parameters for Theophylline-Dosed iv at 15 mg/kg^a

	microdialysis sampling		blood sampling ^b
	w/o blood sampling	w/ blood sampling	
$t_{1/2}$ distribution, min	3.6 ± 2.2	5.2 ± 1.3	7.8 ± 4.1
$t_{1/2}$ elimination, h	3.0 ± 0.4	4.4 ± 0.7	4.4 ± 0.4
MRT, h	2.5 ± 0.6	2.8 ± 0.8	2.9 ± 0.8
AUC, µg min/mL	3525 ± 1414	5616 ± 1614	6135 ± 1267
V_d , L	1.2 ± 0.4	1.1 ± 0.3	1.1 ± 0.3
$C_{1/2}$, mL/min	4.7 ± 1.9	2.9 ± 0.7	2.5 ± 0.5

^a $n = 3$. ^b Data corrected for protein binding; values reflect unbound theophyllin concentration.

was 4.4 ± 0.4 h ($n = 3$) and from whole-blood samples was 4.5 ± 0.7 h ($n = 3$). However, when microdialysis was performed alone a half-life of only 3.0 ± 0.4 h ($n = 3$) was found. This half-life is statistically different from the half-life with blood sampling, $p < 0.004$. In addition, when only microdialysis sampling is performed the AUC and clearance are significantly different while the MRT and V_d are the same relative to simultaneous blood sampling. It has been reported previously that the pharmacokinetics can be affected by blood sampling because of resulting changes in blood volume. These data indicate that microdialysis sampling eliminates such perturbations because no net fluid is removed even with continuous sampling for several hours.

Effect of Anesthesia. The pharmacokinetics of theophylline are also greatly affected by the use of anesthesia during the pharmacokinetic experiment. This is shown in Table IV where the pharmacokinetic parameters obtained by microdialysis sampling in awake, freely-moving rats are compared to those in anesthetized rats. All parameters affected by the rate of metabolism are dramatically different in the anesthetized rat whereas the rate of distribution, which depends predominantly on blood flow, is unchanged. That the half-life of elimination more than quadruples is an indication that the anesthetic is inhibiting the metabolic enzymes of the liver. The effect of experimental conditions on the pharmacokinetics of theophylline in rats as determined by microdialysis sampling is shown graphically in Figure 5. Using the semi-log presentation of the concentration-versus-time curve, the slope of the lines is proportional to the rate of that phase. As can be seen, the initial rapid distribution phase is the same

Table IV. Pharmacokinetics of Theophylline (15 mg/kg iv) in Awake and Anesthetized Rats^a

	awake	anesthetized
$t_{1/2}$ distribution, min	3.6 ± 2.2	2.4 ± 0.6
$t_{1/2}$ elimination, h	3.0 ± 0.4	17.0 ± 7.1
MRT, h	2.5 ± 0.6	24.6 ± 1.1
AUC, µg min/L	3523 ± 1414	32626 ± 8084
V_d , L	1.2 ± 0.4	0.15 ± 0.03
$C_{1/2}$, mL/min	4.7 ± 1.9	0.10 ± 0.02

^a $n = 3$.

in all cases. However, the elimination phase varies considerably depending upon both whether the animal is anesthetized and whether blood samples are drawn simultaneously with the microdialysis.

CONCLUSIONS

Microdialysis offers several advantages for pharmacokinetic studies. The temporal resolution is much higher than for other methods. While 10-min intervals were used for these experiments, shorter times are easily achieved if needed. Since no blood is drawn, a large number of samples can be collected from a single animal without loss of fluid volume. Simultaneous sampling can be achieved using multiple dialysis probes. This provides the ability to monitor pharmacokinetics at multiple sites in a single animal. Because complete pharmacokinetic curves can be obtained for several organs using a single experimental animal, overall fewer animals will be necessary to obtain data on a given drug. Microdialysis samples only the free fraction of the drug in blood. In addition, microdialysis coupled to collection of whole blood samples provides a technique to determine the degree of drug binding in vivo during a pharmacokinetic experiment. The major limitation of microdialysis sampling is the small sample volumes obtained. The sample volume, perfusion rate, recovery, and sampling interval are all interrelated. Slow perfusion rates provide higher recoveries but smaller samples per unit time. Therefore the detection method must be sufficient to directly determine the lowest drug concentration necessary.

ACKNOWLEDGMENT

We wish to acknowledge the Center for Bioanalytical Research at The University of Kansas, Bioanalytical Systems, Inc., and Merck, Sharpe & Dohme for partial financial support of this work. D.O.S. acknowledges the financial assistance of the Procter & Gamble Co. through the P&G Bioanalytical Fellowship at The University of Kansas.

REFERENCES

- (1) Scott, D. O.; Sorenson, L. R.; Lunte, C. E. *J. Chromatogr.* **1990**, *506*, 461-469.
- (2) Scott, D. O.; Sorenson, L. R.; Steele, K. L.; Puckett, D. L.; Lunte, C. E. *Pharm. Res.* **1991**, *8*, 389-392.
- (3) Steele, K. L.; Scott, D. O.; Lunte, C. E. *Anal. Chim. Acta* **1991**, *246*, 181-186.
- (4) Lunte, C. E.; Scott, D. O.; Kissinger, P. T. *Anal. Chem.* **1991**, *63*, 773A-780A.
- (5) Caprioli, R. M.; Lin, S. *Proc. Natl. Acad. Sci. U.S.A.* **1990**, *87*, 240-243.
- (6) Menacherry, S. D.; Justice, J. B. *Anal. Chem.* **1990**, *62*, 597-601.
- (7) Ungerstedt, U. *Measurement of Neurotransmitter Release In Vivo*; Marsden, C. A., Ed.; Wiley-Interscience: Chichester, 1984; pp 81-105.
- (8) Ungerstedt, U.; Forster, C.; Herrera-Marschitz, M.; Hoffman, I.; Jungnell, U.; Tossman, U.; Zetterstrom, T. *Neurosci. Lett. (Suppl.)* **1992**, *10*, 493.
- (9) Sandberg, M.; Lindstrom, S. *J. Neurosci. Methods* **1983**, *9*, 65-74.
- (10) Wages, S. A.; Church, W. H.; Justice, J. B., Jr. *Jr. Anal. Chem.* **1986**, *58*, 1649-1656.
- (11) Church, W. H.; Justice, J. B., Jr. *Jr. Anal. Chem.* **1987**, *59*, 712-716.
- (12) Pettit, H. O.; Pan, H. T.; Parsons, L. H.; Justice, J. B., Jr. *J. Neurochem.* **1990**, *55*, 798-804.
- (13) Pan, H. T.; Menacherry, S.; Justice, J. B., Jr. *J. Neurochem.* **1991**, *56*, 1299-1306.

- (14) Mather, L. E.; Runciman, W. B.; Isley, A. H. *Reg. Anaesth.* **1982**, 7 (suppl 4), S24-S33.
(15) Benet, L. Z.; Mitchell, J. R.; Sheiner, L. B. *The Pharmacological Basis of Therapeutics*, 8th ed.; Gilman, A. G., Rall, T. W., Nies, A. S., Taylor, P., Eds.; Pergamon Press: New York, 1991; p 12.
(16) Herrera, A. M.; Scott, D. O.; Lunte, C. E. *Pharm. Res.* **1990**, 7, 1077-1081.

- (17) Ogilvie, R. I. *Clin. Pharm.* **1978**, 3, 267-293.
(18) Fruncillo, R. J.; Digregorio, G. J. *J. Pharm. Sci.* **1984**, 73, 1117-1121.

RECEIVED for review October 14, 1991. Accepted January 2, 1992.

Parts-per-Trillion Determination of Trihalomethanes in Water by Purge-and-Trap Gas Chromatography with Electron Capture Detection

Louis Lépine* and Jean-François Archambault

Institut de recherche d'Hydro-Québec, 1800 montée Sainte-Julie, Varennes, Québec, Canada J3X 1S1

A gas chromatographic method using a purge-and-trap concentrator and electron capture detection to monitor trihalomethanes (THMs) at the low parts-per-billion (ppb) and the parts-per-trillion (ppt) levels is described in this paper. The method shows good linearity over 4 orders of magnitude with a detection limit between 0.01 and 0.05 ppt for each THM normally found after chlorination: chloroform, bromodichloromethane, dibromochloromethane, and bromoform. Special procedures, for sample handling and the preparation of blank water and analytical standards, required at such a low concentration, are also discussed. The analytical method has been successfully applied in the analysis of samples taken at different points of the water treatment plant of Hydro-Québec's Gentilly 2 nuclear power station. Analysis of samples taken after chlorination and demineralization revealed the formation of all four THMs and other unidentified halogenated volatile compounds. Chloroform and bromodichloromethane were found at the low ppb level, while dibromochloromethane and bromoform were present at the ppt level.

INTRODUCTION

Nuclear and fossil-fueled power plants generally have their own water treatment unit, similar to those used to produce municipal drinking water, which includes a chlorine-disinfection step that is known to produce trihalomethanes (THMs). The far most common THM in chlorinated water is chloroform (CHCl_3), although lower concentrations of brominated THMs such as bromodichloromethane (CHBrCl_2), dibromochloromethane (CHBr_2Cl), and bromoform (CHBr_3) are often detected.¹⁻³ The iodine-containing compounds reported by a few workers^{4,5} are not usually found. These molecules are not likely to be removed by the demineralization system and are therefore introduced into the steam-generation cycle where the water is heated at temperatures reaching 260 °C or more. At Hydro-Québec's Gentilly 2 nuclear power plant, a 685 MW CANDU-PHW (CANadian Deuterium Uranium-Pressurized Heavy Water), abnormally high chloride concentrations have been observed in steam-generator blowdown and found to be related to the THM level in the makeup water.⁶ A recent study conducted in our laboratories on the thermal stability of chloroform confirmed the latter's rapid degradation to produce three Cl^- ions.⁷ It is believed that other

THMs will follow the same degradation mechanism to yield the corresponding acid (HCl , HBr) and subsequently increase the bromide and chloride level.⁸ This is of great concern to the nuclear industry because of the known corrosive effect of chloride on structural components. Owing to the concentrating factor involved in steam generators for nonvolatile species such as chloride, even a small amount of THMs in the makeup water can result in chloride concentrations exceeding the limit for safe system operation.

The vast majority of methods used for THM analysis are designed for quality control of drinking water. Their analytical range is limited to parts per billion (ppb), in compliance with the 100 ppb total THM maximum contaminant level prescribed in the USEPA Safe Drinking Water Act. The particular application to the nuclear plant operation called for a more sensitive technique to analyze samples with individual THM concentrations in the low-ppb or even in the parts-per-trillion (ppt) range and, in our study on thermal degradation,⁷ to monitor their residual concentration in the low-ppt range.

Gas chromatography with electron capture detection (ECD) is an attractive method for THM analysis since it offers a wide linear dynamic range and is the most sensitive method available for halogenated organic compounds. To a certain extent, it is specific to organohalides, which means the latter can be discriminated from a complex background. However, this detector cannot tolerate a large quantity of water and, although direct aqueous injection with solvent bypass has been reported,⁹ a preextraction step is generally performed. Three different approaches have been considered: liquid-liquid extraction,¹⁰⁻¹² headspace sampling,¹²⁻¹⁴ and purge-and-trap.¹⁵ Comparison studies^{12,16} have shown that even with ECD detection, liquid-liquid extraction and headspace sampling are limited to the ppb range; these methods are also subjected to airborne or solvent contamination, often giving high blank values.

The purge-and-trap technique is free from these problems because it uses an inert gas to extract THMs from water and the sample, once introduced, is never in contact with the atmosphere. The concentrating factor obtained by trapping the analytes selectively on an adsorbent material allows analysis of very low-concentration samples. This paper describes the analytical method developed for ultratrace analysis of the four THMs of interest in water samples, using a purge-and-trap concentrator coupled to a gas chromatograph

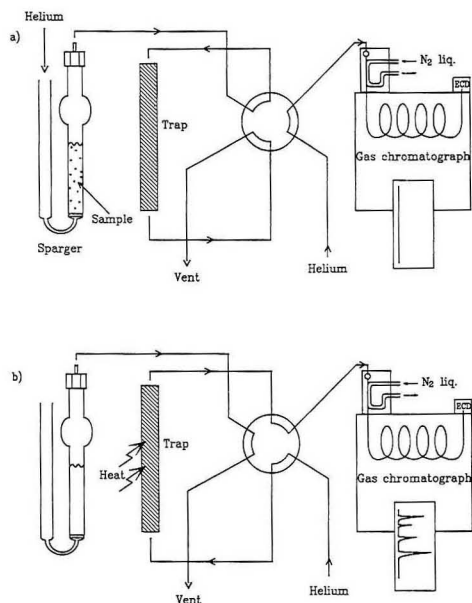


Figure 1. Instrumental setup for purge-and-trap GC-ECD analysis: (a) purge mode; (b) desorb and injection modes.

with ECD detection. It also discusses the precautions necessary to avoid contamination or loss of analytes at such a low concentration.

EXPERIMENTAL SECTION

Chemicals. Chloroform 99.7% was obtained from Anachemia Ltd., bromoform >99% from Aldrich Chemical Co., and bromodichloromethane >98% and dibromochloromethane >98% from Fluka Chemical Corp. Primary standard solutions of the four THMs were made in methanol 99.8% from Anachemia. The

helium gas was UHP grade (99.999%).

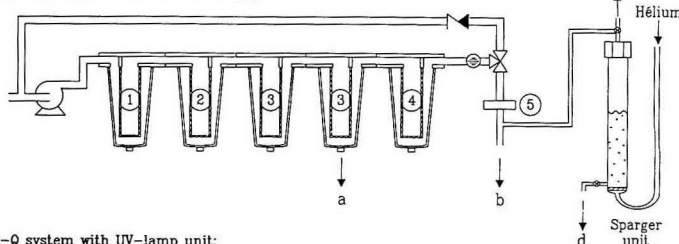
Equipment. The analyses were done on a Hewlett Packard 5890A gas chromatograph equipped with an electron capture detector. A LSC-2000 purge-and-trap system and a cryogenic interface Model 2530, both from Tekmar Co., were used to extract the THMs from the water and inject them into the gas chromatograph. Figure 1 shows the instrumental setup. The cryogenic interface kept at -120°C with liquid nitrogen was added to refocus the analytes at the head of the capillary column during desorption, and thus eliminated the loss of resolution caused by diffusion in the transfer line or by slowly desorbing analytes. Chromatography begins by rapidly heating the cryogenic trap.

Water Quality. The water used to prepare standard solutions was city water passed through two purification units. The in-house primary treatment system comprised a water softener, an activated charcoal column, a $5\text{-}\mu\text{m}$ filter, two reverse-osmosis units, two ion-exchange mixed-bed columns, and a $0.22\text{-}\mu\text{m}$ filter. The secondary purification system consisted of a Milli-Q system from Millipore Corp. equipped with a Milli-Guard filter, an activated carbon cartridge, two ion-exchange mixed-bed cartridges, an Organex-Q cartridge (which contains an organic removal material, proprietary of Millipore Corp.), and a $0.22\text{-}\mu\text{m}$ filter. Two additional treatments, shown on Figure 2, have been tested in an effort to obtain perfectly clean blank water. Water passed through the Milli-Q unit was further sparged with helium for at least 16 h in a 4-L glass container equipped with a glass frit at the bottom and kept under helium pressure until needed. Secondly, an ultraviolet water purifier (Millipore Corp. XP module) was installed between the Organex-Q cartridge and the $0.22\text{-}\mu\text{m}$ filter. The quality of the blank water prepared these different ways is described in the Results and Discussion.

Sampling, Standard Preparation, and Operating Precautions. The risk of contamination at every step of the analytical protocol is always a great concern when working at the ultratrace level. Special precautions are needed, in addition to good laboratory practices. The sampling vials must be filled to the brim, without any headspace, to avoid contamination from the atmosphere at the sampling station and loss of analyte from the water before analysis. Sodium thiosulfate is also added in the vials before sampling in order to neutralize excess chlorine present in chlorinated-water samples. The samples should be stored at 4°C and analyzed within 48 h.

Work with chlorinated solvents should be avoided in the laboratory. All glassware used in the preparation of ppt level

Milli-Q system with helium-spurge unit:



Milli-Q system with UV-lamp unit:

- ① Milli-Guard filter
- ② Activated carbon
- ③ Ion-exchange mixed bed
- ④ Organex-Q
- ⑤ $0.22\text{ }\mu\text{m}$ filter

Figure 2. Secondary polishing unit used to prepare blank water. a-d indicate sample collection points.

Table I. Instrumental Conditions

Purge and Trap			
purge gas	helium at 40 mL/min		
injection volume	5 mL		
sparger	5-mL frit		
trap	100% Tenax (Tekmar trap no. 1)		
program	purge	8 min	<30 °C ^a
	dry purge	4 min	<30 °C ^a
	capillary cooldown		<30 °C ^a -120 °C ^b
	desorb preheat		175 °C ^a -120 °C ^b
	desorb	4 min	180 °C ^a -120 °C ^b
	inject	0.75 min	180 °C ^a 200 °C ^b
	bake	8 min	225 °C ^a
	Gas Chromatograph		
analytical column	HP-5; 30 m × 0.53 mm × 0.88 μm (5% diphenyl and 95% dimethylpolysiloxane)		
gas: column	helium at 2.7 mL/min		
ECD makeup	5% methane, 95% argon at 32 mL/min		
oven program	30 °C for 5 min		
	30-80 °C at 10 °C/min		
	80-180 °C at 20 °C/min		
	180 °C for 2 min		

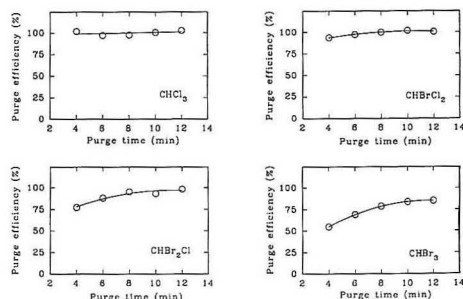
^aTenax trap. ^bCryogenic interface.

Figure 3. Purge time optimization for the four THMs.

standards should be checked with blank water prior to first use, specially marked, and never used for other applications. The standards at or below the ppb level are prepared daily by successive dilution of a 1000 ppm stock solution in methanol. A 1 ppm secondary standard in water can be used but should be changed on a weekly basis. The standard solutions should be kept at 4 °C in vials with no or minimal headspace.

The purge-and-trap unit also requires special attention. The Tenax trap must be conditioned by a 15-min bake every morning, followed by a blank run to verify the cleanliness of the system. Before the sample is introduced, the sparger is purged for at least 2 min with the drain on. This allows both sides of the sparger to be flushed with clean helium.

RESULTS AND DISCUSSION

Optimization of the Purge-and-Trap Technique. The instrumental conditions are detailed in Table I. A Tenax trap was chosen because this material does not adsorb water and has good adsorption/desorption characteristics for the THMs. Standard purge-and-trap parameters were used, except for the purge and dry purge times which have been optimized. The purge time is the most critical parameter of all and was optimized separately for each of the four THMs, as shown in Figure 3. Chloroform is the most volatile of the four and is completely purged after only 4 min. Bromodichloromethane and dibromochloromethane take 8 min to reach their maximum purge efficiency while bromoform, the least purgeable of the four, takes 10 min. In view of these results, a purge

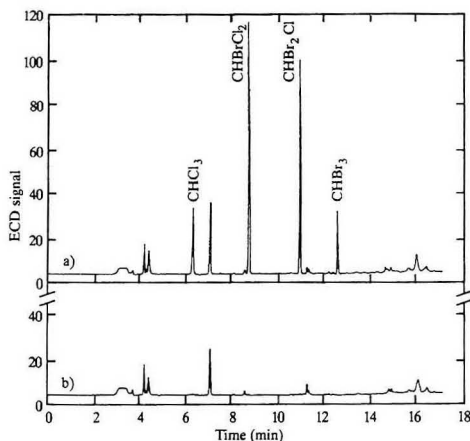


Figure 4. Typical chromatograms: (a) 100 ppt mixed standard solution of the four THMs; (b) blank water.

Table II. Performance of the Analytical Method

	CHCl ₃	CHBr ₂ Cl ₂	CHBr ₂ Cl	CHBr ₃
purge efficiency, %	100	99.7	95.2	78.6
detn limit, ^a ppt	0.05	0.01	0.02	0.05
sensitivity (relative to CHCl ₃)	1	3.2	2.3	0.8
% RSD ^b				
at 1 ppt	2.7	2.4	4.5	4.4
at 100 ppt	1.8	2.1	1.7	0.8
at 10000 ppt	1.4	0.6	0.6	0.3

^a Concentration is equivalent to a peak height 3 times the baseline noise. ^b Relative standard deviation for three consecutive injections.

time of 8 min was selected as a good compromise between analysis time and sensitivity. A dry purge of 4 min, where dry helium flows through the trap, was found to be enough to remove excess water. With these parameters, the total analysis time, including trap cooldown, is approximately 30 min.

Optimization of the Gas Chromatography Technique. The gas chromatograph parameters are also detailed in Table I. The oven temperature program was optimized to obtain the highest possible resolution between the four peaks of interest and any common contaminant found in blank water. Figure 4 shows a chromatogram of a 100 ppt standard solution of the four THMs compared with a blank water run. The unidentified peaks present in both chromatograms are attributed to contaminants that are hard to avoid at such a low level. For example, the peak at 7 min has been identified as 1,1,1-trichloroethane, a solvent frequently used in the mechanical shop one floor below the laboratory and present at trace levels in the atmosphere. However, the four THM peaks of interest are completely absent in the blank water run and are well separated from these contaminants in the chromatogram of the standard solution.

Performance of the Method. Table II presents the performance of the method for the four THMs. The purge efficiency was determined by multiple purges of a mixed standard. The purge is almost complete for all compounds, with the exception of bromoform, which is the least volatile. These results are comparable to values obtained by other workers.¹⁷ The detection limits, also presented in this table, are better than those obtained by any published method

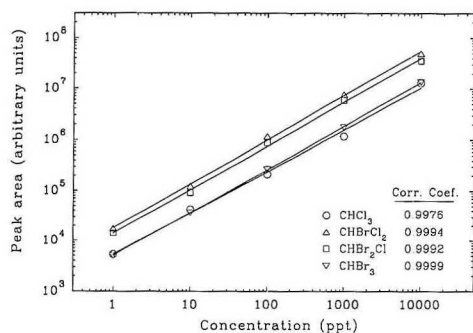


Figure 5. Linear dynamic range of the analytical method.

known to us. The highest sensitivity is obtained for bromodichloromethane and dibromochloromethane and is caused by the greater response of the ECD detector for bromine than for chlorine. The lower response for bromoform can be explained by a lower purge efficiency. The precision, expressed as the relative standard deviation (RSD), is very good, even at 1 ppt. The calibration curves presented in Figure 5 shows a linear dynamic range covering 4 orders of magnitude, from 1 ppt up to 10 ppb, beyond which the ECD detector saturates rapidly, especially for bromodichloromethane and dibromochloromethane. Higher-concentration samples can nevertheless be analyzed by injecting smaller amounts or a diluted sample.

Analysis of Blank Water Prepared by Different Approaches. Samples were taken at different steps of the Milli-Q water purification unit and after additional polishing treatments (indicated by a-d in Figure 2) and analyzed in triplicate. Typical chromatograms are shown in Figure 6. The first chromatogram shows numerous peaks present in the water before the Organex-Q cartridge. Among them are

Table III. Triplicate Analysis of Blank Water^a

	CHCl ₃	CHBrCl ₂	CHBr ₂ Cl	CHBr ₃
Milli-Q water before	36.3 (2.7)	0.5 (1.8)	0.1 (17)	nd
Organex-Q cartridge				
Milli-Q water after	81.0 (0.3)	0.8 (0.5)	0.2 (7.0)	nd
Organex-Q cartridge				
Milli-Q water after	187.4 (1.2)	1.0 (2.4)	0.3 (4.5)	nd
Organex-Q cartridge				
plus UV lamp				
Milli-Q water after	3.3 (2.4)	0.1 (1.8)	0.1 (5.5)	nd
Organex-Q cartridge				
plus helium sparge				

^aConcentrations expressed in ppt, RSD (%) in parentheses.
^bnd: not detected.

chloroform and bromodichloromethane, two of the four THMs of interest, and the 1,1,1-trichloroethane peak at 7 min. The group of peaks between 3 and 4.5 min have not been positively identified but are believed to contain Freons or other light halogenated hydrocarbons. The addition of an Organex-Q cartridge to the standard Milli-Q unit reduced the peaks at the end of the chromatogram related to heavier compounds but had little or no effect on the other peaks. Adding the UV lamp after the Organex-Q cartridge slightly increased most of the peaks in the area of interest, including the THM peaks. We believe these organohalogenes are produced by the degradation of heavier molecules by the UV radiation. Alternatively, the use of an overnight helium sparge on water taken after the Organex-Q cartridge significantly reduced most of the peaks and almost completely eliminated the THMs. The average concentrations and RSD values for these triplicate analysis are presented in Table III, which shows that even at these very low concentrations, the precision is very good.

Field Samples Analysis. The purge-and-trap-GC-ECD method was used to monitor the THM content in water samples collected at Hydro-Québec's Gentilly 2 plant located on the St. Lawrence River. Raw water is taken from the river

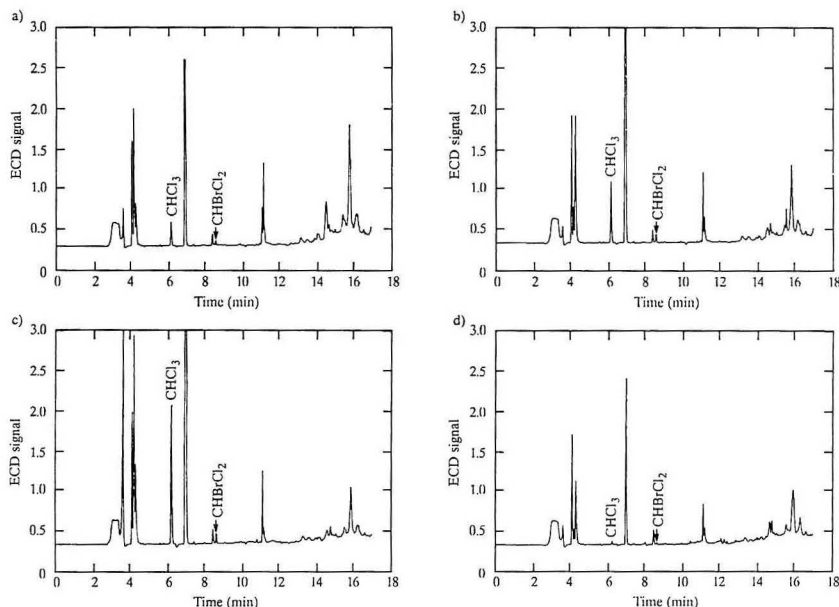


Figure 6. Chromatograms of blank water obtained by different treatments: (a) Milli-Q without Organex-Q; (b) Milli-Q with Organex-Q; (c) Milli-Q with Organex-Q plus UV lamp; (d) Milli-Q with Organex-Q plus helium sparge.

Table IV. Typical Analysis of Gentilly 2 Water Samples^a

	CHCl ₃	CHBrCl ₂	CHBr ₂ Cl	CHBr ₃
raw water	0.023	0.001	0.001	0.010
after chlorination	4.1	2.8	1.2	0.22
after demineralization	4.9	1.4	0.65	0.088

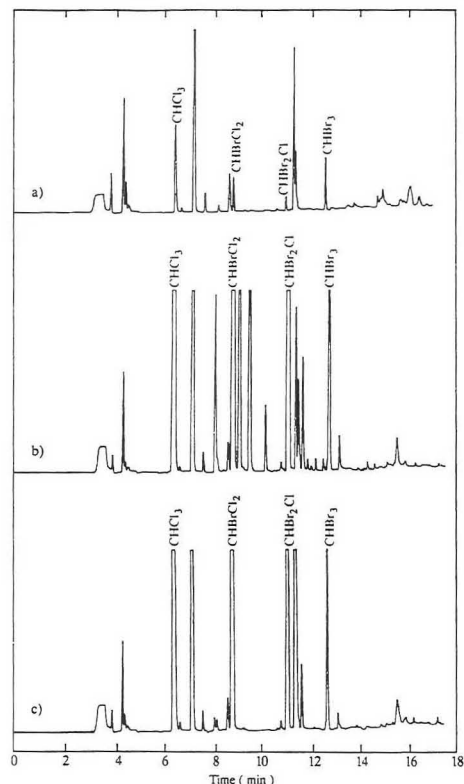
^a Concentrations expressed in ppb.

Figure 7. Typical chromatograms of Gentilly 2 water samples (same scale for all): (a) raw water; (b) after chlorination; (c) after demineralization.

and treated by flocculation, chlorination, and filtration. This pretreated water is stored in the clear-water well and later passed through ion-exchange mixed-bed columns to serve as makeup in the steam-condensate cycle. In the past, makeup water and samples from the clear-water well were analyzed by other laboratories using less sensitive techniques. They reported only the presence of chloroform and bromodi-

chloromethane above their detection limit of 1 µg/L. Table IV presents typical results obtained using the present technique. The four THMs were detected at different degrees in all locations. The most abundant is always chloroform, with decreasing concentrations of bromodichloromethane, dibromochloromethane, and bromoform. Analyses of raw-water samples show very minimal traces of the four THMs, which confirms that the THMs found in the makeup water are generated during the chlorination process. Numerous other compounds formed during chlorination were also detected, as shown on the chromatograms presented in Figure 7. It has not been possible to positively identify them but, considering the relative specificity of the ECD detector for the halogenated compounds, they are probably of this class of molecules.

ACKNOWLEDGMENT

The support provided by Yücel Dündar and Richard Laporte at Hydro-Québec's Gentilly 2 nuclear power station is gratefully acknowledged. Thanks also go to Roland Gilbert for constructive discussions of the results and Lorenzo Ouellet for his technical assistance. A special word of thanks must go to Lesley Kelley-Régnier for her assistance in the preparation of the manuscript. We are grateful to the Natural Sciences and Engineering Research Council of Canada for an Industrial Research Fellowship awarded to the principal author to perform this work.

Registry No. CHCl₃, 67-66-3; CHBrCl₂, 75-27-4; CHBr₂Cl, 124-48-1; CHBr₃, 75-25-2; water, 7732-18-5.

REFERENCES

- (1) Symons, J. M.; Bellar, T. A.; Carswell, J. K.; DeMarco, J.; Kropp, K. L.; Roback, G. G.; Seeger, D. R.; Slocum, C. J.; Smith, B. L.; Stevens, A. A. *J. Am. Water Works Assoc.* **1975**, *67*, 634-647.
- (2) Williams, D. T.; Otson, R.; Bothwell, D.; Murphy, K. L.; Robertson, J. L. *Environ. Sci. Res.* **1978**, *16*, 503-512.
- (3) Otson, R.; Williams, D. T.; Bothwell, D. *J. Assoc. Off. Anal. Chem.* **1982**, *65*, 1370-1374.
- (4) Glaze, W. H.; Henderson, J. E.; Smith, G. *Water Chlorination: Environmental Impact and Health Effects*; Ann Arbor Science: Ann Arbor, MI, 1978; Vol. 1, pp 139-159.
- (5) Thomas, R. F.; Weisner, M. J.; Brass, H. J. *Water Chlorination: Environmental Impact and Health Effects*; Ann Arbor Science: Ann Arbor, MI, 1980; Vol. 3, pp 161-168.
- (6) Laporte, R.; Dündar, Y. Gentilly 2 power plant, 1987. (Unpublished work).
- (7) Lépine, L.; Gilbert, R.; Ouellet, L. Submitted for publication in *Can. J. Chem. Eng.*
- (8) Pallino, G. F.; Miller, M. R.; Sawochka, S. G. *Proc. Am. Power Conf.* **1985**, 1076-1082.
- (9) Pfander, F. K.; Jonas, R. B.; Stevens, A. A.; Moore, L.; Hass, J. R. *Environ. Sci. Technol.* **1978**, *12*, 438-441.
- (10) Otson, R.; Williams, D. T. *J. Chromatogr.* **1981**, *212*, 187-197.
- (11) Norin, H.; Renberg, L. *Water Res.* **1980**, *14*, 1397-1402.
- (12) Castello, G.; Gerbino, T.; Kanitz, S. *J. Chromatogr.* **1986**, *351*, 165-175.
- (13) Kolb, B.; Auer, M.; Pospisil, P. *J. Chromatogr.* **1983**, *279*, 341-348.
- (14) Comba, M. E.; Kaiser, K. L. E. *Int. J. Environ. Anal. Chem.* **1983**, *16*, 17-31.
- (15) Hu, H. C.; Weiner, P. H. *J. Chromatogr. Sci.* **1980**, *18*, 333-342.
- (16) Otson, R.; Williams, D. T.; Bothwell, P. D. *Environ. Sci. Technol.* **1979**, *13*, 936-939.
- (17) Westendorf, R. Tekmar application manual. Tekmar application note B011587; Tekmar Co.: Cincinnati, OH, 1987.

RECEIVED for review October 31, 1991. Accepted January 2, 1992.

Selective Sorption and Column Concentration of Alkali-Metal Cations by Carboxylic Acid Resins with Dibenzo-14-crown-4 Subunits and Their Acyclic Polyether Analogues

Takashi Hayashita,[†] Joung Hae Lee,[‡] Matthew G. Hankins, Jong Chan Lee, Jong Seung Kim, John M. Knobeloch, and Richard A. Bartsch*

Department of Chemistry and Biochemistry, Texas Tech University, Lubbock, Texas 79409-1061

Alkali-metal cation sorption from aqueous and aqueous methanolic solutions and column concentration of alkali-metal cations from dilute aqueous solutions by carboxylic acid resins containing dibenzo-14-crown-4 units and their acyclic polyether analogues have been investigated. The crown ether carboxylic acid resins exhibit enhanced sorption selectivity over the acyclic polyether resins. Good sorption selectivity for Li^+ and Na^+ was obtained with a cyclic polyether resin in which the carboxylic acid group is positioned over the crown ether ring. For column concentration of alkali-metal cations from dilute aqueous solutions, gradient elution of the sorbed metal ions from the resin with the carboxylic acid group positioned over the crown ether cavity gave selective column concentration of Li^+ and Na^+ .

INTRODUCTION

Synthetic macrocyclic multidentate ligands, such as crown ethers, have been utilized extensively for the separation of alkali-metal and alkaline-earth-metal cations, as well as some transition-metal ions from their solutions.¹⁻³ Of particular importance is the size recognition ability of the cyclic ligands for different metal ions. Efficient complexation of a metal ion by a crown ether is facilitated by a good fit of the cation within the polyether cavity.²

Polymerization of such macrocyclic ligands or their immobilization on support materials is important to the development of continuous separation processes and alleviation of the toxicity of some macrocyclic complexing agents.^{4,5} In recent studies, the polyether carboxylic acid resins 1-3 (Figure 1), which contain both ion-exchange and cyclic or acyclic polyether binding sites for metal ions, were synthesized⁶ and their alkali-metal and alkaline-earth-metal cation sorption behaviors evaluated.⁶⁻⁸ It was found that both the cyclic or acyclic nature of the polyether unit and the positioning of the pendent carboxylic acid group with respect to the polyether unit played an important role in metal ion recognition. Good sorption selectivity for Na^+ was observed only for dibenzo-16-crown-5 carboxylic acid resin 2 in which the carboxylic acid function is positioned over the polyether cavity. Selective column concentration of Na^+ from a dilute aqueous solution of alkali-metal cations was achieved with resin 2.⁹

To probe the effect of crown ether ring size and further examine the influence of carboxylic acid group positioning relative to the polyether subunit, new acyclic polyether carboxylic acid resin 4 and crown ether carboxylic acid resins 5 and 6 have now been prepared and their alkali-metal cation sorption and column concentration behaviors investigated. From comparison of the results for previously-examined resins

1 and 2, which have dibenzo-16-crown-5 rings, with those for new resins 5 and 6, which have dibenzo-14-crown-4 rings, the effect of crown ether ring size can be assessed. Similarly, by comparison of the results for resins 3 with 4 and 5 with 6, the influence of positioning of the carboxylic acid group relative to the polyether unit can be examined more completely.

EXPERIMENTAL SECTION

Apparatus. The apparatus was the same as that reported previously⁶⁻⁹ with the addition of a Bio-Rad Model 2110 fraction collector for the column concentration study. To prevent metal contamination, all glassware was soaked in 5% HNO_3 solution for 24 h and rinsed with distilled, deionized water before use.

Reagents. Sources of inorganic reagents were the same as those reported previously.⁶⁻⁹ Purified water was prepared by passing distilled water through three Barnstead D8922 combination cartridges in series. *sym*-Hydroxydibenzo-14-crown-4 and *sym*-dibenzo-14-crown-4-oxoacetic acid were prepared by the reported methods.¹⁰⁻¹² *sym*-Ketodibenzo-14-crown-4 (8) was produced by heating *sym*-gem-dihydroxydibenzo-14-crown-4 in a vacuum oven.¹³ 1,3-Bis(*o*-methoxyphenoxy)-2-propanol and resin 3 were synthesized by the reported procedures.⁶

Preparation of *sym*-(Hydroxy)(propyl)dibenzo-14-crown-4 (9). To 1.16 g (48 mmol) of magnesium turnings in 40 mL of THF was added 2.96 g (24 mmol) of 1-bromopropane, and the mixture was refluxed until most of the magnesium had been consumed. To the cooled mixture was added 3.78 g (12 mmol) of 8 in 82 mL of THF over a 15-min period, and the mixture was refluxed for 2 h. After cooling, 60 mL of 5% aqueous NH_4Cl was added and the mixture was stirred for 1.5 h. The THF was evaporated in vacuo, and the residue was extracted with Et_2O (4 × 30 mL). The combined Et_2O layers were dried over MgSO_4 and evaporated to give a white solid which was purified by chromatography on alumina with Et_2O then $\text{EtOAc}/\text{Et}_2\text{O}$ (1:9) as eluents to afford 1.98 g (46%) of 9 as a white solid with mp 121-122 °C: IR (deposit from CDCl_3 solution on a NaCl plate) 3548 (OH), 1254, 1119 (CO) cm^{-1} ; ^1H NMR (CDCl_3) δ 0.97 (t, 3), 1.40-1.75 (m, 4), 2.10-2.45 (m, 2), 2.73 (br s, 1), 3.95-4.40 (m, 8), 6.80-7.00 (m, 8). Anal. Calcd for $\text{C}_{21}\text{H}_{28}\text{O}_5$: C, 70.37; H, 7.31. Found: C, 70.57; H, 7.44.

Preparation of *sym*-(Propyl)dibenzo-14-crown-4-oxoacetic Acid (10). To 0.45 g (60% dispersion in mineral oil, 110 mmol) of NaH under nitrogen was added 1.00 g (2.8 mmol) of 9 in 50 mL of THF. After 0.5 h, a solution of 0.91 g (6.5 mmol) of bromoacetic acid in 10 mL of THF was added dropwise. After being stirred for 2 h at room temperature, the mixture was refluxed overnight. The excess NaH was destroyed by careful addition of ice, and the THF was evaporated in vacuo. The residue was acidified to pH 1 with concentrated HCl, and 250 mL of CH_2Cl_2 was added. After shaking, the CH_2Cl_2 layer was separated and the aqueous layer was extracted with CH_2Cl_2 (3 × 20 mL). The combined CH_2Cl_2 layers were washed with 5% HCl, dried over MgSO_4 , and evaporated in vacuo to give a gold oil which was passed through a 1-in. bed of alumina using MeOH/EtOAc (1:10) as eluent. The solvents were evaporated from the eluate in vacuo, the pH of the residue was adjusted to 1 with concentrated HCl, and CHCl_3 was added. After shaking, the CHCl_3 layer was separated, washed with water, dried over MgSO_4 , and evaporated in vacuo to give 0.97 g (83%) of 10 as a thick, yellowish oil: IR (deposit from a CDCl_3 solution on a NaCl plate) 3375 (COOH), 1740 (C=O), 1255, 1119 (CO) cm^{-1} ; ^1H NMR (CDCl_3) δ 1.00 (t,

[†]Permanent address: Department of Chemistry, Saga University, 1 Honjo-machi, Saga 840 Japan.

[‡]Permanent address: Korea Research Institute of Standards and Science, Taejeok Science Town, Taejeon 305-606, Republic of Korea.

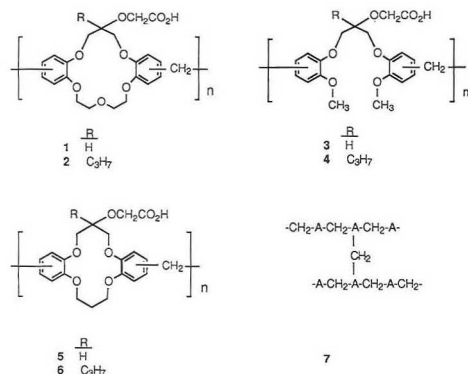


Figure 1. Structures of the polyether carboxylic acid resins.

3), 1.35–1.65 (m, 2), 1.65–1.90 (m, 2), 2.10–2.60 (m, 2), 4.00–4.40 (m, 8), 4.45 (s, 2), 6.80–7.00 (m, 8), 8.10 (br s, 1). Anal. Calcd for $C_{23}H_{28}O_7 \cdot 0.3CHCl_3$: C, 61.87; H, 6.31. Found: C, 61.72; H, 6.32.

Preparation of 1,3-Bis(*o*-methoxyphenoxy)-2-propanone (11). To 100 mL of CH_2Cl_2 was added 7.43 g (34 mmol) of pyridinium chlorochromate,¹⁴ 1.88 g (23 mmol) of anhydrous NaOAc, 40 g of $MgSO_4$, and 7.00 g (23 mmol) of 1,3-bis(*o*-methoxyphenoxy)-2-propanol, and the mixture was stirred for 2 days at room temperature under nitrogen. The mixture was filtered through a bed of Florisil which was subsequently washed with three 30-mL portions of CH_2Cl_2 . The filtrate and washings were evaporated in vacuo to afford a yellow oil which was purified by chromatography on silica gel with hexane/EtOAc (8:1) as eluent to give 3.98 g (57%) of a white solid with mp 69–71 °C. IR (deposit from CH_2Cl_2 solution on a NaCl plate) 1742 (C=O) cm^{-1} ; 1H NMR ($CDCl_3$) δ 3.87 (s, 6), 4.96 (s, 4), 6.84–7.01 (m, 8). Anal. Calcd for $C_{17}H_{18}O_5$: C, 67.54; H, 6.00. Found: C, 67.67; H, 6.05.

Preparation of 2-[(*o*-Methoxyphenoxy)methyl]-1-(*o*-methoxyphenoxy)-2-pentanol (12). To 0.46 g (20 mmol) of magnesium turnings in 100 mL of THF under nitrogen was added 2.44 (20 mmol) of 1-bromopropane, and the mixture was refluxed until the magnesium turnings disappeared. The solution was cooled to 0 °C and 3.00 g (10 mmol) of 11 in 15 mL of THF was added. The reaction mixture was refluxed for 5 h and cooled to 0 °C. After slow addition of 20 mL of 5% aqueous NH_4Cl , the THF was evaporated in vacuo. To the residue were added EtOAc and water (100 mL of each). After shaking, the EtOAc layer was separated and washed with saturated aqueous $NaHCO_3$ (30 mL) and then with brine (30 mL). After drying over $MgSO_4$, the solvent was evaporated in vacuo to give 3.18 g (93%) of a colorless oil: IR (deposit from CH_2Cl_2 solution on a NaCl plate) 3474 (OH) cm^{-1} ; 1H NMR ($CDCl_3$) δ 0.95 (t, 3), 1.47–1.60 (m, 2), 3.30 (s, 1), 3.80 (s, 6), 3.98–4.17 (AB q, 4), 6.82–6.98 (m, 8). Anal. Calcd for $C_{20}H_{26}O_5 \cdot 0.25H_2O$: C, 68.49; H, 7.55. Found: C, 68.72; H, 7.83.

Preparation of 4,4-Bis[(*o*-methoxyphenoxy)methyl]-3-oxaheptanoic Acid (13). After removal of the mineral oil from 3.61 g (60% dispersion in mineral oil, 27 mmol) of KH with pentane under nitrogen, 3.20 g (9.2 mmol) of 12 in 50 mL of THF was added. The mixture was stirred for 2 h at room temperature, and 1.93 g (13.8 mmol) of bromoacetic acid in 10 mL of THF was added during 1 h. The mixture was stirred for 3 h and ice-water was carefully added to consume the excess KH. The THF was evaporated in vacuo. The residue was extracted with EtOAc (3 \times 30 mL) and then with water (50 mL). The water layer was acidified to pH = 1 with 6 N HCl and extracted with CH_2Cl_2 (3 \times 50 mL). The CH_2Cl_2 layer was dried over $MgSO_4$ and evaporated in vacuo to afford 3.55 g (95%) of 13 as a pale yellow oil: IR (deposit from CH_2Cl_2 solution on a NaCl plate) 2955 (COOH), 1737 (C=O) cm^{-1} ; 1H NMR ($CDCl_3$) δ 0.98 (t, 3), 1.39–1.51 (m, 2), 1.80–1.88 (m, 2), 3.79 (s, 6), 4.09–4.23 (AB q, 4), 4.40 (s, 2), 6.82–7.01 (m, 8). Anal. Calcd for $C_{22}H_{28}O_7$: C, 65.33; H, 6.98. Found: C, 65.04; H, 7.00.

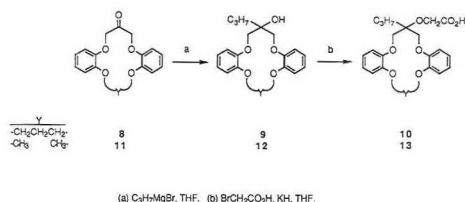


Figure 2. Synthetic routes to compounds 10 and 13.

Preparation of Polyether Carboxylic Acid Resins 4–6. The polyether carboxylic acid resins 4–6 were synthesized by condensation polymerization of the corresponding monomers 13, *sym*-dibenzo-14-crown-4-oxyacetic acid, and 10, respectively, with formaldehyde in formic acid as described in detail previously.⁶ The resins were ground and used in powder form (finer than 100 mesh).

Resin 4, 25% yield: IR (KBr) 3422 (COOH), 1752 (C=O), 1280, 1094 (CO) cm^{-1} . Anal. Calcd for 7: C, 66.49; H, 6.74. Found: C, 66.40; H, 6.51.

Resin 5, 60% yield: IR (KBr) 3448 (COOH), 1735 (C=O), 1278, 1094 (CO) cm^{-1} . Anal. Calcd for 7-0.5H₂O: C, 65.20; H, 5.73. Found: C, 65.02; H, 5.52.

Resin 6, 59% yield: IR (KBr) 3448 (COOH), 1735 (C=O), 1278, 1103 (CO) cm^{-1} . Anal. Calcd for 7: C, 67.43; H, 6.56. Found: C, 67.80; H, 6.37.

Sorption of Alkali-Metal Cations by Resins 3–6. An aqueous solution of the five alkali-metal chlorides with hydroxides for pH adjustment (5.0 mL, 0.10 M in each) and 0.050 g of the resin were shaken for 3.0 h in a 30-mL, pear-shaped flask with a 14/20 joint and a polypropylene stopper at room temperature (21–23 °C) with a Burrell wrist-action shaker. The aqueous phase was filtered with a sintered glass filter funnel (15 mL, medium porosity), and the equilibrium pH of the aqueous phase was measured. The resin was washed with 100 mL of water and dried. Of the dried resin, a 0.020-g sample was shaken with 5.0 mL of 0.10 M HCl for 1.0 h to strip the alkali-metal cations from the resin into an aqueous solution for analysis by ion chromatography after appropriate dilution.

Column Concentration of Alkali-Metal Cations by Resins 3–6. The column concentration procedure was the same as that reported⁹ except that the flow rate was 3.4 mL/min for loading and washing and 0.3 mL/min for stripping. The stripping solutions were collected by 10-drop fractions with a fraction collector and analyzed by ion chromatography after appropriate dilution. After each stripping operation, the volume of the 10-drop fractions (0.25–0.26 mL) was determined with a microsyringe.

RESULTS AND DISCUSSION

Synthesis of New Dibenzo-Polyether Carboxylic Acid Monomers. By a Grignard reaction, *sym*-ketodibenzo-14-crown-4 (8) was converted into the crown ether tertiary alcohol 9 in 46% yield (Figure 2). Reaction of 9 with KH and the bromoacetic acid gave *sym*-(propyl)dibenzo-14-crown-4 (10) in 80% yield. Oxidation of 1,3-bis(*o*-methoxyphenoxy)-2-propanol with pyridinium chlorochromate¹² provided the acyclic dibenzopolyether ketone 11 in 57% yield. A Grignard reaction transformed this ketone into tertiary alcohol 12 in 92% yield, and reaction of 12 with KH and then bromoacetic acid gave a 95% yield of acyclic polyether carboxylic acid 13.

Synthesis of New Polyether Carboxylic Acid Resins. The polyether carboxylic acid resins 4–6 were prepared by condensation polymerization of the corresponding dibenzopolyether monomers with formaldehyde in formic acid. As in an earlier study,⁶ it was observed that the yield was higher for formation of a cyclic polyether carboxylic acid resin than the corresponding acyclic polyether carboxylic acid resin. New resins 4–6 were characterized by IR spectroscopy and by elemental analysis. The structural representations 1–6 imply polymers with no cross-linking. This is most certainly an

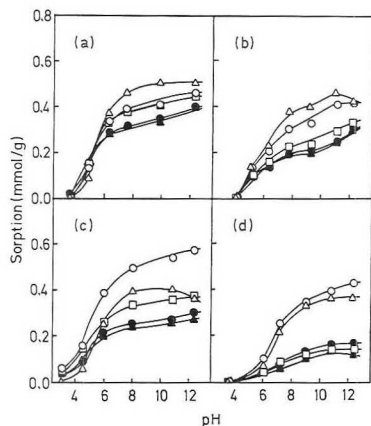


Figure 3. Sorption of alkali-metal cations by the polyether carboxylic acid resins vs the equilibrium pH of the aqueous phase for (a) 3, (b) 4, (c) 5, and (d) 6: (Δ) Li^+ , (○) Na^+ , (□) K^+ , (▲) Rb^+ , (●) Cs^+ .

oversimplification since some level of cross-linking is anticipated.¹⁵ A possible structure for the partially cross-linked resins is given by 7 (Figure 1) in which A is the polyether carboxylic acid unit. In agreement with the results obtained previously for resins 1–3,⁶ the elemental analysis data for the new polyether carboxylic acid resins 4–6 are consistent with this formulation.

Alkali-Metal Cation Sorption by Polyether Carboxylic Acid Resins 3–6. To provide greater relevance to actual metal separation systems, competitive, rather than single species, alkali-metal cation sorption by resins 3–6 was investigated. An aqueous solution (5.0 mL) of the five alkali-metal cations (0.10 M in each) as chlorides and hydroxides was shaken with the resin (0.050 g) for 3 h (even though sorption is probably complete in a matter of minutes⁶). The resin was filtered, washed with water, and dried. Of the dried resin, a weighed portion (0.020 g) was shaken with 5.0 mL of 0.10 M HCl to strip the alkali-metal cations from the resin into an aqueous solution for analysis by ion chromatography. From the ion chromatographic analysis data, the amount of sorbed alkali-metal cations per unit amount of the acid form of the dried resin (millimoles per gram) was calculated. The reproducibility of this alkali-metal cation sorption and stripping procedure for different batches of resin has been demonstrated.⁶ For a given resin, the alkali-metal cation sorption at a specified pH was found to be reproducible within 5% of the stated value.

Data for competitive alkali-metal cation sorption as a function of the equilibrium pH of the aqueous phase of acyclic polyether carboxylic acid resin 4 and the dibenzo-14-crown-4 carboxylic acid resins 5 and 6 are presented in Figure 3b–d, respectively. For comparison, data reported earlier⁶ for acyclic polyether carboxylic acid resin 3 are given in Figure 3a. As would be anticipated for weak acid resins,¹⁶ alkali-metal cation sorption by resins 3–6 is negligible when the aqueous solution pH is ≤ 4 but increases markedly as the pH becomes neutral and then basic.

A commercially available carboxylic acid resin CG-50, a polymethacrylic acid resin, exhibits Li^+ selectivity under basic conditions.⁶ This is attributed to a strong ion-association interaction of the carboxylate anion with Li^+ .¹⁷ Thus the Li^+ sorption selectivities found with acyclic polyether carboxylic resins 3 and 4 (Figure 3a,b, respectively) suggest primary interaction of the alkali-metal cations with the ion-exchange sites.

Table I. Sorption of Alkali-Metal Cations from an Aqueous Solution at pH = 12.5 by Polyether Carboxylic Acids 3–6 and Percent Loading

resin	sorption, mmol/g					% loading
	Li^+	Na^+	K^+	Rb^+	Cs^+	
3	0.50	0.47	0.44	0.40	0.41	83
4	0.42	0.41	0.34	0.30	0.31	73
5	0.37	0.57	0.38	0.27	0.30	74
6	0.37	0.44	0.15	0.12	0.16	73

From an examination of the Corey–Pauling–Kortum (CPK) space-filling models, the cavity diameter of a dibenzo-14-crown-4 ring is estimated to be 1.2–1.5 Å. The ionic diameters of the alkali-metal cations are as follows: Li^+ , 1.20 Å; Na^+ , 1.90 Å; K^+ , 2.66 Å; Rb^+ , 2.96 Å; Cs^+ , 3.38 Å.¹⁸ On the basis of the relationship between the metal ion and dibenzo-14-crown-4 cavity diameters, Li^+ selectivity would be anticipated for crown ether carboxylic acid resins 5 and 6. However resin 5 exhibits Na^+ selectivity and resin 6 shows nearly equal sorption selectivity for Li^+ and Na^+ over the other alkali-metal cations as a group (Figure 3c,d, respectively). The changes in sorption selectivity on going from the acyclic polyether carboxylic acid resins 3 and 4 to the crown ether carboxylic acid resins 5 and 6 are consistent with metal ion–cyclic polyether unit interactions in the latter.

Since Na^+ is too large to fit within the crown ether cavity, the Na^+ selectivity shown by resin 5 suggests the formation of a complex in which the metal ion perches on the crown ether oxygens while associating with one or more of the oxygen atoms in the sidearm. It should be noted that Na^+ selectivity has also been observed in competitive solvent extraction of alkali-metal cations from water into chloroform by 2-[sym-dibenzo-14-crown-4-oxy]decanoic acid.¹⁸ On the basis of results of earlier studies conducted with dibenzo-16-crown-5 carboxylic acid resins,⁶ attachment of a propyl group to the same polyether ring carbon that bears the oxyacetate acid group is expected to help position the carboxylic acid group over the crown ether cavity.¹⁹ Thus the enhancement of Li^+ sorption relative to the other alkali-metal cations in going from crown ether carboxylic acid resin 5 to 6 may be attributed to preorganization of the binding site in 6 which increases recognition of that metal ion which should be best accommodated within the crown ether cavity.

The alkali-metal cation sorptions and loadings for polyether carboxylic acids 3–6 when the equilibrium pH = 12.5 are presented in Table I. The loading is defined as the total alkali-metal cation sorption, as calculated from the total alkali-metal cation concentration in the stripping solution, divided by the ion-exchange capacity, as calculated from the elemental analysis data. The calculated ion-exchange capacities for resins 3–6 are 2.66, 2.39, 2.57, and 2.32 mmol/g, respectively. The loadings vary from 83% for resin 3 to 53% for resin 6. The diminished loading for resin 6 could result from an increase in the hydrophobicity of the resin or from steric hindrance to metal ion sorption by a more rigid structure. To distinguish between these two possibilities, the effect of medium polarity upon the alkali-metal cation sorption²⁰ was investigated.

Influence of Medium Polarity upon Alkali-Metal Cation Sorption by Polyether Carboxylic Acid Resins 3–6. The polarity of the medium from which the alkali-metal cations are sorbed might influence the microenvironment of the resin and thereby affect the selectivity and/or efficiency of metal ion sorption. To probe the influence of medium polarity upon metal ion sorption by polyether resins 3–6, each resin was shaken with aqueous methanolic solutions (10, 20, 40, 60, and 80 volume percent of methanol) which were 0.10 M in each of the five alkali-metal cations as the chlorides and

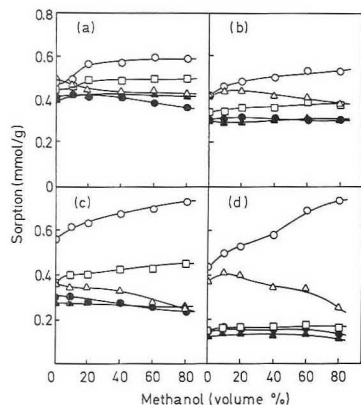


Figure 4. Sorption of alkali-metal cations by the polyether carboxylic acid resins vs methanol percentage in the aqueous methanol solvent at pH 12.5–12.9 for (a) 3, (b) 4, (c) 5, and (d) 6: (Δ) Li⁺, (○) Na⁺, (□) K⁺, (▲) Rb⁺, (●) Cs⁺.

Table II. Sorption of Alkali-Metal Cations from 80% Methanol–20% Water at pH = 12.9 by Polyether Carboxylic Acids 3–6 and Percent Loading

resin	sorption, mmol/g					% loading
	Li ⁺	Na ⁺	K ⁺	Rb ⁺	Cs ⁺	
3	0.44	0.58	0.49	0.40	0.36	86
4	0.38	0.53	0.37	0.30	0.30	79
5	0.25	0.73	0.45	0.26	0.23	75
6	0.26	0.74	0.16	0.11	0.12	60

hydroxides, for which the equilibrium pH values were in the range 12.5–12.9. Under such alkaline conditions, maximum alkali-metal cation sorption is anticipated (Figure 3). The resins were filtered, washed, dried, and stripped as before.

Data for the competitive alkali-metal cation sorptions by resins 4–6 as a function of the methanol content of the medium are presented in Figure 4b–d, respectively. For comparison, data reported earlier for acyclic carboxylic acid resin 3²⁰ are included as Figure 4a. For all four resins, the influence of the methanol content of the medium is similar. Thus with increasing methanol content, the Na⁺ sorption increases, the Li⁺ sorption decreases, while the sorptions of K⁺, Rb⁺, and Cs⁺ remain nearly the same.

It has been proposed that the strong ion associative interaction of Li⁺ with carboxylate anions in ion-exchange resins takes place through the dipole of a water molecule.¹⁷ Also relevant is the X-ray crystal structure of the lithium carboxylate salt of the monomer of resin 5 which has a bridging water molecule between the crown ether-bound Li⁺ and the pendent carboxylate anion.²¹ Thus diminution of such water-mediated sorption of Li⁺ by polyether carboxylic acid resins 3–6 as the methanol content of the medium is enhanced may be rationalized. Such decreases in Li⁺ sorption are coupled with enhanced adsorption of the best sorbed cation Na⁺. It is interesting to note the similarities in Li⁺ and Na⁺ sorption profiles for resins 4 and 6 versus 3 and 5 which suggest that the propyl group also helps to preorganize the binding site in acyclic polyether resin 4, albeit to a lesser degree than in the cyclic polyether resin 6.

In Table II are recorded the alkali-metal cation sorption and loading data for resins 3–6 in 80% methanol–20% water at an equilibrium pH of 12.9. Comparison with the data contained in Table I reveals that the efficiency of alkali-metal

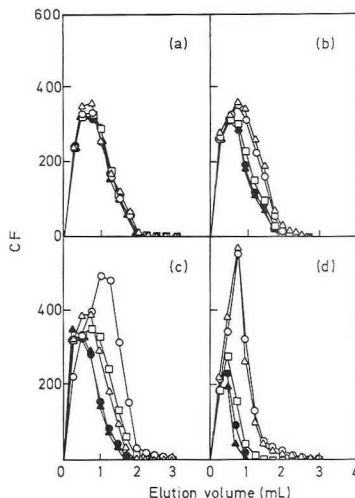


Figure 5. Concentration factors (CF) for alkali-metal cations from a sample solution (1.0 L, pH = 10.4, 6.0×10^{-5} M in each alkali-metal cation) vs. the elution volume of 0.10 M HCl for columns of resins (a) 3, (b) 4, (c) 5, and (d) 6: (Δ) Li⁺, (○) Na⁺, (□) K⁺, (▲) Rb⁺, (●) Cs⁺.

cation sorption exhibits only a very modest increase in loading (1–7%) as the polarity of the medium is decreased by a change from water to 80% methanol–20% water. Thus the lower loading for resin 6 than the other three polyether carboxylic acid resins 3–5 appears to arise from steric hindrance to metal ion sorption by a more rigid structure rather than a more hydrophobic nature of the resin.

Selective Column Concentration of Alkali-Metal Cations by Polyether Carboxylic Acid Resins 3–6. Polyether carboxylic acid resins are potential candidates as stationary phases for selective column concentration of alkali-metal cations from dilute aqueous solution.⁹ Selective column concentration of Na⁺ was achieved with dibenzo-16-crown-5 carboxylic acid resin 2 in which the pendent carboxylic acid group is positioned over the crown ether cavity. The column concentration behavior of polyether carboxylic acid resins 3–6 has now been examined.

An aqueous solution (1.00 L, pH = 10.2) of the five alkali-metal cations (6.00×10^{-5} M each) as the chlorides and hydroxides was eluted through a 0.42-cm-i.d. column of resin (0.10 g) at a flow rate of 3.4 mL/min, and the column was washed with 100 mL of water at the same flow rate. The sorbed alkali-metal cations were then stripped with 0.10 M HCl at a flow rate of 0.3 mL/min, fractions were collected, and the fractions were analyzed by ion chromatography. Profiles for elution of sorbed alkali-metal cations from polyether carboxylic acid resin 3–6 are shown in Figure 5a–d, respectively, in which the concentration factor (CF) is defined as

$$CF = \frac{\text{conc of } M^+ \text{ in the stripping solution}}{\text{initial conc of } M^+ \text{ in the sample solution}} \quad (1)$$

For acyclic polyether carboxylic acid resins 3 and 4, most of the resin-bound alkali-metal cations were eluted in the first 3.0 mL of stripping solution and the maximum CF values are in the range 300–400. No separation of alkali-metal cations during elution was noted for resin 3 (Figure 5a). However for resin 4, the elution of both Li⁺ and Na⁺ is slightly retarded compared with that for the other alkali-metal cations (Figure

Table III. Total Alkali-Metal Cation Sorption and Percent Recovery in Column Concentration by Polyether Carboxylic Acid Resins 3-6

resin	sorption, mmol/g (recovery, %)				
	Li ⁺	Na ⁺	K ⁺	Rb ⁺	Cs ⁺
3	0.24 (40)	0.22 (37)	0.24 (40)	0.22 (37)	0.23 (39)
4	0.28 (46)	0.26 (43)	0.21 (35)	0.18 (30)	0.19 (32)
5	0.25 (42)	0.37 (62)	0.27 (45)	0.18 (30)	0.18 (30)
6	0.24 (40)	0.26 (43)	0.10 (17)	0.07 (11)	0.08 (14)

5b). The elution order for crown ether carboxylic acid resin 5 is Rb⁺, Cs⁺ > Li⁺, K⁺ > Na⁺ with significant retardation of Na⁺ elution and a maximal CF value near 500 (Figure 5c). For crown ether carboxylic acid resin 6 (Figure 5d), the elution order is K⁺, Rb⁺, Cs⁺ > Li⁺, Na⁺ with significant retardation of Li⁺ and Na⁺ elution and maximum CF values approaching 600. The elution retardation orderings are in agreement with the sorption selectivities observed in the batch analysis experiments (see Table I). Thus the same structural features of the resin which produce enhanced sorption through stronger complexation also retard elution of the more tightly bound cations.

The total alkali-metal cation sorptions and percent recoveries are presented in Table III. For resin 6, the recoveries of Li⁺ and Na⁺ were 40 and 43%, respectively, while those for the other alkali-metal cations were in the range 11–17%. Although the sorption levels observed in the column concentration system are lower than those found in the batch sorption system (Table I) due to different pH and sample conditions, the alkali-metal cation sorption selectivities are quite similar. This indicates that the viability of a given column concentration system can be predicted by a batch sorption analysis experiment.

To accentuate the differences between weakly bound and more strongly bound alkali-metal cations, the use of gradient elution was investigated for crown ether carboxylic acid resin 6. The sample solution (1.0 L, pH = 10.4) of five alkali-metal cations (6.00×10^{-5} M in each) was passed through the column of resin 6 and unbound metal ions were removed by washing with water as before. Elution was performed with 1.06 mL of 0.050 M HCl, then 3.2 mL of water, and then 1.0 M HCl. The elution profile is presented in Figure 6. Of the second peak, 84% was comprised of Li⁺ and Na⁺ and the maximum CF values for Li⁺, Na⁺, K⁺, Rb⁺, and Cs⁺ were 605, 712, 104, 35, and 70, respectively. Of the recovered Li⁺ and Na⁺, 46 and 54%, respectively, were in the second peak. Thus selective concentration and separation of both Li⁺ and Na⁺ from the other alkali-metal cations was achieved by gradient elution of sorbed metal ions from crown ether carboxylic acid 6 in which the carboxylic acid group is positioned over the polyether cavity.

CONCLUSIONS

Both the crown ether ring size and positioning of the carboxylic acid group over the polyether ring are important factors for metal ion recognition. Compared with the results for dibenzo-16-crown-5 carboxylic acid resin 2, a substantial difference in alkali-metal cation sorption by the analogous dibenzo-14-crown-4 carboxylic acid resin 6 was observed. The sorption selectivity was found to be considerably better for cyclic polyether resins 5 and 6 than with the corresponding acyclic polyether resins 3 and 4. The sorption selectivity was found to increase in the order resin 3 < resin 4 < resin 5 < resin 6 which demonstrates that structural rigidity improves sorption selectivity of the binding site. Good sorption selectivity for both Li⁺ and Na⁺ was obtained for resin 6 in which the pendent carboxylic acid group is positioned over the crown

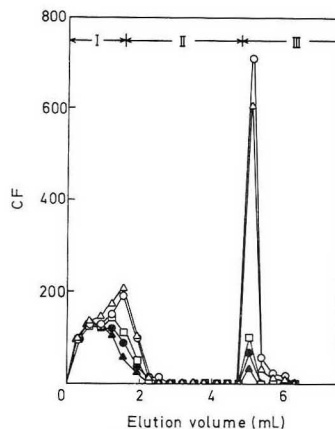


Figure 6. Concentration factors (CF) for alkali-metal cations from a sample solution (1.0 L, pH = 10.4, 6.0×10^{-5} M in each alkali-metal cation) with a column of resin 6 vs the elution volume of (I) 0.05 M HCl, (II) H₂O, and (III) 1.0 M HCl: (Δ) Li⁺, (○) Na⁺, (□) K⁺, (▲) Rb⁺, (●) Cs⁺.

ether cavity. Use of resin 6 as a stationary phase was shown to provide selective concentration of both Li⁺ and Na⁺ from a dilute aqueous solution of five alkali-metal cations.

ACKNOWLEDGMENT

This research was supported by the Division of Chemical Sciences of the Office of Basic Energy Sciences of the U.S. Department of Energy (Grant DE-FG05-88ER13832) and the Advanced Technology Program of the Texas Higher Education Coordinating Board.

REFERENCES

- Pedersen, C. J. *J. Am. Chem. Soc.* **1967**, *89*, 7017–7036.
- Izatt, R. M.; Bradshaw, J. M.; Nielsen, S. A.; Lamb, J. D.; Christensen, J. J.; Sen, D. *Chem. Rev.* **1985**, *65*, 271–339.
- Cation Binding by Macrocycles. Complexation of Cationic Species by Crown Ethers*; Inoue, Y.; Gokel, G. W., Eds.; Marcel Dekker: New York, 1990.
- Hiraoka, M. *Crown Compounds: Their Characteristics and Applications*; Elsevier: New York, 1982; pp 265–272.
- Kimura, K.; Shono, T. *Functional Monomers and Polymers*; Takemoto, K.; Inaki, Y.; Ottenbrite, R. M., Eds.; Marcel Dekker: New York, 1987; pp 349–421.
- Hayashita, T.; Goo, M.-J.; Lee, J. C.; Kim, J. S.; Krzykawski, J.; Bartsch, R. A. *Anal. Chem.* **1990**, *62*, 2283–2287.
- Hayashita, T.; Goo, M.-J.; Kim, J. S.; Bartsch, R. A. *Talanta* **1991**, *38*, 1453–1457.
- Hayashita, T.; Bartsch, R. A. *Anal. Chem.* **1991**, *63*, 1847–1850.
- Hayashita, T.; Lee, J. H.; Chen, S.; Bartsch, R. A. *Anal. Chem.* **1991**, *63*, 1844–1847.
- Heo, G. S.; Bartsch, R. A.; Schlobohm, L. L.; Lee, J. G. *J. Org. Chem.* **1991**, *46*, 3574–3575.
- Bartsch, R. A.; Heo, G. S.; Kang, S. I.; Liu, Y.; Strzelbicki, J. *J. Org. Chem.* **1992**, *47*, 457–460.
- Olsher, U.; Frolow, F.; Bartsch, R. A.; Puglia, M. J.; Shoham, G. *J. Am. Chem. Soc.* **1989**, *111*, 9217–9222.
- Olsher, U.; Frolow, F.; Shoham, G.; Luboch, E.; Yu, Z.-Y.; Bartsch, R. A. *J. Inclusion Phenom. Mol. Recognit. Chem.* **1990**, *9*, 125–135.
- Corey, E. J.; Suggs, J. W. *Tetrahedron Lett.* **1975**, *31*, 2647–2650.
- Blasius, E.; Adrian, W.; Janzen, K.-P.; Kalutke, G. *J. Chromatogr.* **1982**, *47*, 457–460.
- Hefflerich, F. *Ion Exchange*; McGraw-Hill: New York, 1962; p 86.
- Gregor, H. P.; Hamilton, J. J.; Oza, R. J.; Bernstein, F. *J. Phys. Chem.* **1956**, *60*, 263–267.
- Wolkowiak, W.; Charewicz, W. A.; Kang, S. I.; Yang, I.-W.; Puglia, M. J.; Bartsch, R. A. *Anal. Chem.* **1990**, *62*, 2018–2021.
- Bartsch, R. A. *Solvent Extr. Ion Exch.* **1989**, *7*, 829–854.
- Hayashita, T.; Lee, J. H.; Krzykawski, J.; Bartsch, R. A. *Talanta*, in press.
- Shoham, G.; Christianson, D. W.; Bartsch, R. A.; Heo, G. S.; Olsher, U.; Lipscomb, W. N. *J. Am. Chem. Soc.* **1984**, *106*, 1280–1285.

RECEIVED for review November 11, 1991. Accepted January 2, 1992.

CORRESPONDENCE

Continuous Rods of Macroporous Polymer as High-Performance Liquid Chromatography Separation Media

Sir: While synthetic polymers can be fashioned into almost any shape, small diameter spherical beads are essentially the only form of polymers used in modern column liquid chromatography. The only significant exception may be the cartridges containing sheets of planar chromatographic separation media introduced recently by Millipore, Säulentechnik Knauer, BioRad, Cuno, and others.¹

A theoretical analysis of conditions influencing the efficiency of a column in the separation of macromolecules with molecular weight exceeding 10^5 revealed that the optimum size of porous particles in the packing medium is about $1\text{ }\mu\text{m}$.² When this size is reached, the slow diffusion of solutes within the pores does not restrict the separation quality. While even smaller sizes would theoretically be desirable, current limitations in the technology, including packing problems, column back pressure, dead volumes in detection instruments and connecting tubes, etc., make the concept of using very small beads unpractical. Current trends seem to favor particle sizes in the range $3\text{--}10\text{ }\mu\text{m}$.

In order to improve the kinetics of the separation process, perfusion chromatography, which is based on the use of packings with very large pores of up to $1\text{ }\mu\text{m}$, was developed.^{3,4} These large pores allow at least part of the mobile phase to flow through the beads, rather than around them, therefore improving the kinetics of separation in the interior of the beads by reducing the diffusional path length. It has been estimated that approximately 5% of the mobile phase flows through the porous particles in a perfusion column.³

The perfusion concept has been further improved in some ways by the development of high-performance membrane chromatography in which *all* of the mobile phase flows through the flat macroporous polymer body, which may be 2-mm thick and is held in a cartridge or cell.^{1,5} The separation proceeds by gradient elution and the method is useful in the chromatographic modes based on the on-off principle.

Hjerten has recently described a column consisting of a continuous strongly compressed plug 30-mm long and 6-mm diameter based on solvent-swollen poly(acrylic acid-co-methylenebisacrylamide). Despite the lack of a permanent pore structure, this material could be used in the separation of proteins by ion-exchange mechanism⁶ provided the flow rate was kept near 0.5 mL/min , resulting in a column back pressure of 1.4 MPa . This finding is interesting though more versatility would likely have been achieved had a permanent macroporous structure been incorporated in the polymer plug.

The main advantage of both the macroporous membrane and the compressed plug approaches is that the separation occurs as *all* the mobile phase flows through the porous structure of the separation medium. This reduces the elution pathway and facilitates diffusion in and out of small porous areas. However, the macroporous membranes have limited capacities and can only be used in a specialized form of separation. Similarly, the compressed plugs may not be suitable for use in solvents of widely different polarities as they do not possess a macroporous structure and they depend on swelling phenomena for their operation.

This report deals with the preparation of a novel continuous

bed column that incorporates both macroporosity and capacity. These rod-shaped columns, consisting of a single "molded" piece of macroporous polymer, can be used in most chromatographic modes and offer a tempting alternative to the standard columns packed with particles.

EXPERIMENTAL SECTION

Preparation of a Continuous Rod of Porous Polymer. The continuous porous polymer rod was prepared by an *in situ* polymerization within the confines of the tube of a chromatographic column $30\text{ mm} \times 8\text{-mm i.d.}$ The 40:60 vol % mixture of monomers (glycidyl methacrylate and ethylene dimethacrylate, 60:40 vol %) and porogenic solvents (cyclohexanol and dodecanol, 80:20 vol %) in which azobisisobutyronitrile (1 wt % with respect to monomers) was dissolved, was purged with nitrogen for 15 min and injected into the stainless steel column tube stoppered on one end with a steel nut plug, and the original opening was then closed with a silicon rubber septum. The polymerization was allowed to proceed for 6 h at $70\text{ }^\circ\text{C}$ within the column acting as a mold. The stopper and the septum were removed, and the excess polymer at the ends of the "molded" continuous block of porous polymer was detached; the column hardware was then assembled and connected to a HPLC pump. Several 30-mm-long columns were prepared using the same polymerization conditions. The porogenic solvents and other soluble moieties within the porous polymer block were washed out by pumping methanol at a flow rate 1 mL/min for 2 h.

Preparation of Diol-Functionalized Porous Polymer Rod. The epoxide groups of porous polymer rod were hydrolyzed by filling the column with 0.5 mol/L aqueous sulfuric acid then placing it in a water bath at $60\text{ }^\circ\text{C}$ for 3 h. The hydrolyzed column was then attached to the chromatograph and washed at a flow rate of 1 mL/min with 100 mL of water, 100 mL of 50:50 water-THF mixture, and 100 mL of THF.

Preparation of Amino-Functionalized Porous Polymer Rod. The epoxide groups of a similarly prepared porous polymer rod were aminated by injection of 2 mL of diethylamine and 3 h heating to $70\text{ }^\circ\text{C}$ to afford the corresponding polymer with 1-(*N,N*-diethylamino)-2-hydroxypropyl groups.⁷ For the chromatographic experiments, the modified column was attached again to the HPLC equipment and washed successively with 100 mL of methanol, 200 mL of 50:50 methanol-water, 200 mL of water, and 200 mL of 0.01 mol/L Tris-HCl buffer solution pH 7.6. Elemental analysis of the resulting polymer indicated that it contained 1.6 mmol of amino groups per gram. There is no difference in the nitrogen content of samples taken from the outer skin and core at the top, center, and bottom of the modified rod. As the polymer containing the (diethylamino)hydroxypropyl groups can complex metal ions,⁸ a disk cut in the rod after its removal from the column housing was stained with copper(II). Observation of the disk shows that it is homogeneously blue colored. This is confirmed by examination with a scanning electron microscope which does not show any inhomogeneity across the rod.

Chromatographic Testing of the Porous Polymer Rods. Chromatographic testing was carried out using a Nicolet LC 9560 ternary gradient liquid chromatograph provided with a Hewlett-Packard 1050 UV detector. The samples were injected through a Rheodyne valve loop injector. Following a 10-min elution period with 0.01 mol/L Tris-HCl buffer solution at pH 7.6, a 10 min linear gradient from the starting buffer to 1 mol/L NaCl in the same buffer was utilized for the chromatographic

separations. The elution profile reflects the gradient used as a change in base line.

RESULTS AND DISCUSSION

The lack of development of continuous bed chromatographic media based on porous polymer rods can be attributed in part to the lack of appropriate technology in the preparation of such materials, and to the fear that extremely high back pressures would be encountered in practical applications. This assumption was based on extrapolation of data obtained from experience with smaller and smaller particulate packings. Early work by Hjerten⁶ with compressed plugs of a solvent-swollen hydrophilic polymer has already shown that acceptable back pressures can be achieved at a moderate flow rate. However, this observation made for a swollen material cannot be assumed to hold for a macroporous structure which would normally be expected to be even more suitable for chromatographic applications. The advantages inherent to macroporosity derive from the coexistence of globules and void spaces or pores within the macroporous structure.⁹ The globules have a compact core consisting of highly cross-linked material surrounded by a layer of less cross-linked polymer chains. The cores confer rigidity to the material, while the surrounding chains may swell when they are modified or placed in an appropriate solvent. As a result of this local swelling the voids between globules are filled to different degrees depending on the exact conditions. Overall, the swelling has essentially no effect on the actual size of the separation medium but it results in a decrease in pore size.

The pores of a macroporous polymer are interconnected, and therefore the entire structure is permeable to solutes as well as eluting solvents. In addition, control over pore size and pore size distribution, based on the selection of porogenic agents, their content in the polymerization mixture, as well as on the concentration of the cross-linking agent in the monomer mixture, is available for fine tuning of the separation medium.¹⁰

The approach we use to prepare porous polymer rods is advantageous as both chemical reactivity and macrostructure are built into the material in one simple operation. In addition as the porous polymer rods are prepared in situ within the column tube, by a process somewhat akin to molding which affords a final product having the desired geometry and requiring no tedious packing operation. This is a significant advantage as the efficiency of packed bead columns is known to be affected by packing conditions, including the skills of the operator, as well as numerous other variables.¹¹ Due to their high degree of cross-linking, the macroporous poly(glycidyl methacrylate-co-ethylene dimethacrylate) rods we prepare are essentially incompressible hard materials that fully occupy the tube space. Their inner macroporous structure is readily controlled by adjustments to the composition of the polymerization mixture.¹⁰ Since the back pressure may be expected to be inversely related to pore size, we have chosen, for the first illustration of this novel approach, a composition of the polymerization mixture which provides a final material with rather large pores and a specific surface area of ca. 10 m²/g.

The permeability of the porous polymer rod is confirmed in chromatographic measurements with the hydrolyzed diol-functionalized column in THF. The retention time for both benzene and polystyrene (MW 2.9×10^6) at a flow rate of 2 mL/min are very similar, 0.63 and 0.60 min, respectively, and no exclusion effects are seen. The resulting chromatographic peaks are quite narrow. These findings suggest that the rods prepared under our experimental conditions contain almost no micropores.

The back pressure vs flow rate dependency was of prime interest. Figure 1 shows that the relationship is almost linear

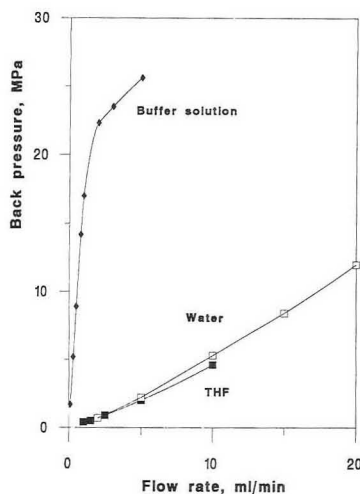


Figure 1. Effect of flow rate on back pressure in the diol (THF and water) and aminofunctionalized (buffer solution) porous polymer rod column. Conditions: column 30 mm \times 8-mm i.d. Mobile phase: water, THF, and 0.01 mol/L Tris-HCl buffer pH 7.6.

for flow rates up to 20 mL/min and proves the absence of compression of the rod. The back pressure in the hydrolyzed column is somewhat higher for water than is the case for THF due to effect of solvent viscosity. The switch from water to THF and back neither changes the structure of the rod nor causes any mechanical damage. Repeated permeability measurements in both water and THF provided identical results. These correlate to chromatographic results achieved with beads of similar composition packed in a column.¹²

For the amine-modified columns, used with the buffer solution as mobile phase, the curve is steeper but linear up to almost 2 mL/min. The higher slope of the back pressure vs flow rate for this ion-exchange column illustrates the effect of swelling. The rod is located in the tube and cannot increase its diameter; therefore, swelling results in a decrease in the overall permeability of the medium. Surprisingly, at higher flow rates the column does not plug as is observed for classical columns packed with polymer beads,¹³ but the slope of the back pressure vs flow rate curve decreases dramatically.

For the diol column, the retention volume of benzene in THF does not depend on the flow rate and is 1.26 mL on average. The volume of the empty column is 2.51 mL and the extra column volumes for connections and tubings amount to 0.11 mL. From these data, the porosity of the rod is calculated to be approximately 50%, a value which is in good agreement with that expected from the amount of porogens used. This porosity suggests that, on average, only half of the cross section of the continuous chromatographic rod is filled with the solid polymer globules. The other half constitutes the free pores through which the mobile phase can flow.

Although the calculation is not relevant to ion-exchange chromatography but to size exclusion chromatography which is our future target, a rough estimate of the plate number for the 30-mm-long continuous rod column, using the sharp benzene peak in THF at a flow rate 1 mL/min, is 3500 plates which corresponds to 117 000 plates/m or a HETP of about 9 μ m. This value compares very favorably to any bead-packed polymer column currently available.

A few model separations of protein mixtures using typical ion-exchange chromatography techniques illustrate the good separation properties of the amino functionalized porous rod

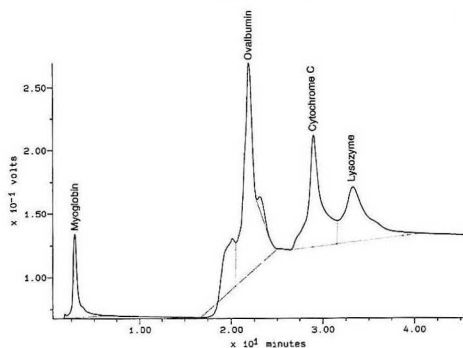


Figure 2. Ion-exchange chromatograph of model protein mixture in the porous polymer rod column. Conditions: column 30 mm X 8-mm i.d., poly(glycidyl methacrylate-co-ethylene dimethacrylate) modified with (diethylamino)hydroxypropyl groups. Mobile phase: 10 min 0.01 mol/L Tris-HCl buffer solution at pH 7.6, followed by 10 min gradient of the same buffer from 0 to 1 mol/L NaCl, flow rate 0.5 mL/min, UV detector 218 nm, injection 2 μ L of a solution containing total 16 mg/mL proteins.

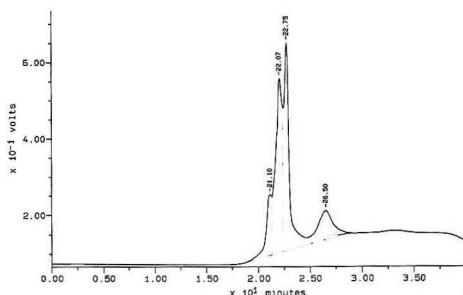


Figure 3. Ion-exchange chromatograph of egg white protein in the porous polymer rod column. Conditions: injection 0.1 μ L of a solution containing 16 mg/mL egg white; other conditions see Figure 2.

polymer columns (Figures 2-4). The myoglobin, use as a nonretained compound, elutes with the starting buffer prior to the start of the gradient. Its retention volume is 1.43 mL, in good agreement with the retention volume of benzene in the hydrolyzed diol column. Preliminary measurements of albumin recovery obtained by a comparison of the weight of injected protein and the amount determined by measurements of the UV absorption in the recovered solution shows better than 95% recovery in all cases. This value did not change in subsequent measurements.

In addition to the considerable advantages resulting from their in situ preparation within the confines of a chromatographic column, the polymerized porous polymer rod columns benefit from increased reproducibility as confirmed in parallel studies with different columns prepared under identical conditions. The chromatograms acquired on columns prepared from the same mixture are all equivalent. As the chromatographic properties of the rod column did not change over a period of 5 weeks of daily use, durability of the column can be assumed to be sufficient.

In contrast to bead materials which often require considerable size classification before use, the rod approach affords no wastes. Almost any monomer can be used, including those that are water soluble and would therefore not be useful in

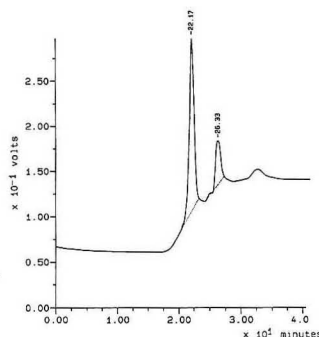


Figure 4. Ion-exchange chromatograph of chicken egg albumin in the porous polymer rod column. Conditions: injection 2 μ L of a solution containing 8 mg/mL ovalbumin; other conditions see Figure 2.

suspension polymerizations using water as the continuous phase. The copolymerization approach allows access to a variety of primary functionalities without additional chemical modification steps.

While this report is only preliminary, it demonstrates the viability of polymerized porous rod separation media. We are currently refining the preparation methods, studying structure-chromatographic properties relationships, and working on continuous columns for other chromatographic modes and prepared from different comonomers.

ACKNOWLEDGMENT

Financial support of this work through unrestricted gifts from IBM Corporation (Materials and Processing Sciences Program) is gratefully acknowledged. In addition, thanks are due to the Cornell Materials Science Center supported by the National Science Foundation (DMR-8818558) for the use of its polymer characterization facility.

REFERENCES

- (1) Tennikova, T. B.; Bleha, M.; Svec, F.; Almazova, T. B.; Belenkii, B. G. *J. Chromatogr.* **1991**, *555*, 97.
- (2) Snyder, L. R.; Stadalius, M. A. *High Performance Liquid Chromatography: Advances and Perspectives*; Academic Press: New York, 1986; Vol. 4, p 294.
- (3) Afeyan, N. B.; Gordon, N.; Maszaroff, I.; Varady, I.; Fulton, S. P.; Yang, Y.; Regnier, F. E. *J. Chromatogr.* **1990**, *519*, 1.
- (4) Afeyan, N. B.; Fulton, S. P.; Regnier, F. E. *J. Chromatogr.* **1991**, *544*, 267.
- (5) Tennikova, T. B.; Belenkii, B. G.; Svec, F. *J. Liquid Chromatogr.* **1991**, *14*, 63.
- (6) Hjerten, S.; Liao, J.-L.; Zhang, R. *J. Chromatogr.* **1989**, *473*, 273.
- (7) Svec, F.; Hrudkova, H.; Horak, D.; Kalal, J. *Angew. Makromol. Chem.* **1977**, *63*, 23.
- (8) Kalalova, E.; Radova, Z.; Svec, F.; Kalal, J. *Eur. Polym. J.* **1977**, *63*, 23.
- (9) Pelzbauer, Z.; Lukas, J.; Svec, F.; Kalal, J. *J. Chromatogr.* **1979**, *171*, 101.
- (10) Tennikova, T. B.; Horak, D.; Svec, F.; Tennikov, M. B.; Kever, E. E.; Belenkii, B. G.; *J. Chromatogr.* **1989**, *475*, 187.
- (11) Snyder, L. R.; Kirkland J. J. *Introduction to Modern Liquid Chromatography*, 2nd ed.; J. Wiley: New York, 1979; p 202.
- (12) Tennikova, T. B.; Horak, D.; Svec, F.; Kolar, J.; Coupek, J.; Trushin, S. A.; Maltsev, V. G.; Belenkii, B. G. *J. Chromatogr.* **1988**, *435*, 357.
- (13) Lloyd, L. L. *J. Chromatogr.* **1991**, *544*, 201.

Frantisek Svec
Jean M. J. Fréchet*

Department of Chemistry
Baker Laboratory
Cornell University
Ithaca, New York 14853-1301

RECEIVED for review November 5, 1991. Accepted January 9, 1992.

Mass Spectrometric Identification of Methylphosphonic Acid: The Hydrolysis Product of Isopropyl Methylphosphonofluoridate and Pinacolyl Methylphosphonofluoridate

Sir: For verification purposes, detection and identification of degradation products of nerve agents such as isopropyl methylphosphonofluoridate (sarin), pinacolyl methylphosphonofluoridate (soman), etc. are important, as the agent itself may be present at below the detection limit some time after their alleged use in war depending upon the prevailing weather conditions. To this end several efforts have been made by various groups of workers. The nerve agents (sarin, soman, and VX) are hydrolyzed ultimately to methylphosphonic acid (MPA),¹ as per Scheme I for sarin and soman.

Methylphosphonic acid being polar and nonvolatile, efforts had been made to analyze it by high-performance liquid chromatography (HPLC) or by gas chromatography (GC) and gas chromatography-mass spectrometry (GC-MS) after derivatization.¹⁻³ Derivatization has been carried out by various means such as methylation with diazomethane,^{4,5} formation of trimethylsilyl ethers or *tert*-butyldimethylsilyl ethers,^{6,7} methylation with trimethylphenylammonium hydroxide, or benzylation with 1-benzyl-3-(4-chlorophenyl)triazene.⁸ However, the derivatization process has some inherent limitations because of lengthy, cumbersome procedures and in some cases poor yields, instability of derivatizing reagents, or their sensitivity to moisture. All these limitations make the identification of methylphosphonic acid difficult even under ideal conditions.

We report here direct identification of the hydrolysis products of sarin and soman. The fragmentation patterns of sarin and soman lead to a peak at m/z 99^{9,10} whereas MPA and other intermediates like isopropyl methylphosphonate (IMPA) and 1,2,2-trimethylpropyl methylphosphonate (TMPA), if present, give a peak at m/z 97 in aqueous solution. Identifying the m/z 97 peak by direct inlet electron impact/chemical ionization (EI/CI) and fast atom bombardment (FAB) mass spectrometry using graphite fluoride as adsorbent can lead to definite confirmation for the possible presence of nerve agents in the sample since the use of graphite fluoride as an adsorbent for concentrating solute from large volumes of air and water has been shown to have promise in environmental monitoring.¹¹

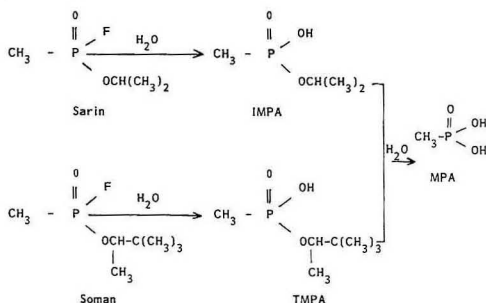
Mass spectral analysis was carried out using JEOL JMS DX-300 mass spectrometer coupled with a JMA-2000 data analysis system. The direct inlet probe temperature in EI/CI was regulated from 25 to 250 °C with a heating rate of 64 °C/min. The chamber temperature was maintained at 80 °C. EI mass spectra were recorded at 70 eV. In CI mode, isobutane (Matheson purity) was used as reagent gas. Argon (Matheson purity) was used as the bombarding atom in FAB mode.

Sarin, soman, IMPA, and MPA were synthesized in our laboratory, and the identity and the purity (>95%) were checked by analytical methods like GC (IMPA and MPA upon derivatization with diazomethane while sarin and soman directly), GC-MS (sarin and soman), and IR and ¹H and ³¹P NMR spectrometry (all compounds).

Adequate safety measures were observed during the synthesis of sarin and soman. Synthesis and solution preparation were carried out in a fume cupboard wearing protective clothing, gloves, and a face mask. No special safety measure was adopted for handling other compounds.

Graphite fluoride (C₂F)_n was obtained from Central Glass Co. Ltd., Tokyo, Japan. It is a dark gray powder which has

Scheme I



a specific surface area of 90 m²/g (determined by a Quantasorb Jr. BET surface area analyzer) and an average particle size of 12 μm. It is thermally stable up to 400 °C and is insoluble in all solvents.

The hydrolysis of sarin and soman was done using tap water, and MPA in this hydrolyzed mixture was easily detected after 4 weeks (MPA was present up to 12 weeks beyond which we did not analyze the mixture) whereas the parent compounds could not be detected after 2 weeks when analyzed by direct sampling with EI and CI mass spectrometry. MPA was further diluted with water (10 μg in 100 mL), which was less than the detection limit of the mass spectrometer (approx 1 ng in EI/CI), and adsorbed onto graphite fluoride adsorbent. A 1-μg amount of the adsorbent was then sampled on the FAB probe tip by making a paste with 1 μL of glycerol, and mass spectra were recorded.

The EI and CI mass spectra of the hydrolysis product of sarin and soman gave the protonated molecular ion peak at m/z 97. This molecular ion peak was confirmed by high-resolution/accurate mass measurement and the molecular formula was obtained as (CH₅O₃P).

In contrast to the peak at m/z 97 for MPA in aqueous solution (the peak at m/z 96 is negligible under these conditions), neat MPA gives a major peak at m/z 96 and a very minor peak at m/z 97.

The molecular ion peak and major fragments at m/z 81 (H₂PO₃), 79 (PO₃), and 47 (PO) were further confirmed by recording EI/CI mass spectra of synthesized MPA. The FAB mass spectrum of an aqueous solution of MPA also gives a major peak at m/z 97 and a similar fragmentation pattern.

The results from the above experiments show that this direct method of detection and identification of breakdown products of nerve agents by mass spectral techniques can be very useful when such toxicants have to be verified in below nanogram levels.

ACKNOWLEDGMENT

We are grateful to P. K. Ramachandran of DRDE Gwalior for encouragement and fruitful suggestions.

Registry No. MPA, 993-13-5; sarin, 107-44-8; soman, 96-64-0.

REFERENCES

- (1) Tornes, J. A.; Johnsen, B. A. *J. Chromatogr.* **1989**, *467*, 129-138.
- (2) Bossle, P. C.; Reutter, D. J.; Sarver, E. W. *J. Chromatogr.* **1987**, *407*, 399-404.
- (3) Bossle, P. C.; Martin, J. I.; Sarver, E. W.; Sommer, H. Z. *J. Chromatogr.* **1983**, *267*, 209-212.
- (4) Verweij, A.; Degenhardt, C. E. A. M.; Boter, H. L. *Chemosphere* **1979**, *3*, 115.
- (5) Verweij, A.; Boter, H. L.; Degenhardt, C. E. A. M. *Science* **1979**, *204*, 616.
- (6) Harvey, D. J.; Horning, M. G. *J. Chromatogr.* **1973**, *79*, 65.
- (7) Purdon, J. G.; Pagotto, J. G.; Miller, R. K. Report DREO-936; Defence Research Establishment: Ottawa, 1985.
- (8) Andersson, G.; Fredriksson, S. A.; Lindberg, G.; Olofsson, B. FOA 4 Report; Forsvarets Forskningsanstalt Huvudavdelning 4, S901 82 Umea, Sweden.
- (9) Tripathi, D. N.; Kaushik, M. P.; Bhattacharya, A. J. *Can. Soc. For. Sci.* **1987**, *20* (4), 151-153.
- (10) Report on identification of potential organophosphorus warfare agents; Ministry for Foreign Affairs of Finland: Helsinki, 1979 [ISBN 951-46-4063(2)].
- (11) Yao, C. C. D.; Zlatkis, A. *Chromatographia* **1987**, *23* (5), 370-72.

Durgesh N. Tripathi*

Karuna S. Pandey

Arabinda Bhattacharya

Ramamoorthy Vaidyanathaswamy

Analytical Services Wing
Defence Research & Development Establishment
Tansen Road
Gwalior-474 002 (MP), India

RECEIVED for review August 23, 1991. Accepted January 6, 1992.

TECHNICAL NOTES

Recovery of Submilligram Quantities of Carbon Dioxide from Gas Streams by Molecular Sieve for Subsequent Determination of Isotopic (^{13}C and ^{14}C) Natural Abundances

James E. Bauer*

Department of Oceanography, Florida State University, Tallahassee, Florida 32306

Peter M. Williams

Scripps Institution of Oceanography, Marine Research Division, University of California, San Diego, La Jolla, California 92093-0218

Ellen R. M. Druffel

Woods Hole Oceanographic Institution, Department of Chemistry, Woods Hole, Massachusetts 02543

INTRODUCTION

Quantitative recovery and isotopic analysis of CO_2 generated from organic and inorganic carbon is important for a variety of natural sample types. For example, the two most commonly used techniques for the oxidation of organic carbon to CO_2 are the sealed-tube method¹ and various modifications of the flow-through combustion method.² While both methods ultimately depend upon the presence of O_2 for the oxidation process, the sealed-tube method has been the method of choice for the subsequent recovery and isotopic analysis of CO_2 . This is due to the relative ease with which CO_2 (sublimation point = -78.5°C at 760 mmHg pressure) can be cryogenically removed from an otherwise noncondensable, static (i.e., non-flowing) gas mixture under vacuum. This concept has been improved upon through the use of variable-temperature cryogenic traps (VTTs)^{3,4} which allow gas components having different melting points to be sequentially frozen out and distilled off for collection of essentially pure product. In contrast, CO_2 contained in carrier gas streams is generally difficult to collect at atmospheric pressure following organic carbon combustion since this usually entails using O_2 as both the oxidant and the carrier gas. Cryogenic collection of CO_2 at liquid nitrogen temperature (bp -195.8°C) from an O_2 stream results in the condensation of liquid O_2 (bp -183.0°C), a potentially hazardous situation, and possibly in incomplete CO_2 recovery. Pumping the liquified O_2 away under vacuum, or trapping the CO_2 from the O_2 stream at temperatures below

the boiling point of O_2 using VTTs, can also result in incomplete recovery and isotopic fractionation of CO_2 . In fact, even when N_2 is used as the carrier gas at atmospheric pressure and liquid nitrogen temperature, intermittent condensation of the N_2 stream may occur,⁵ though this is much less severe than for O_2 . Finally, systems which are designed to collect CO_2 from gas streams (especially O_2) cryogenically or using partial vacuums can attain considerable complexity.

A method is therefore needed which allows CO_2 to be quantitatively recovered from O_2 and N_2 gas streams at atmospheric pressure. For isotope studies, a further requirement is that no fractionation of the carbon isotopes in the CO_2 occurs. This led us to develop a simple, convenient method which is based on the highly selective absorptive properties of aluminosilicate molecular sieves for different gases. While molecular sieves have been employed to a limited extent in some commercial organic carbon analyzers, in some cases for $\delta^{13}\text{C}$ determinations (e.g., see ref 6), a thorough assessment of the analytical capabilities of sieves has, to our knowledge, not been made. The method presented here has a low associated blank ($<0.02\ \mu\text{mol}$ of C), is robust over a wide range of O_2 and N_2 carrier gas flows (at least $100\text{--}2000\ \text{cm}^3\text{min}^{-1}$) and quantities of CO_2 (at least $0.3\text{--}50\ \mu\text{mol}$ of C), and is nonfractionating with respect to carbon isotopic (^{13}C and ^{14}C) natural abundances. Molecular sieves should have a variety of applications for CO_2 quantification and isotopic analysis.

EXPERIMENTAL SECTION

The specific molecular sieve used in these studies was a synthetic sodium aluminosilicate zeolite having the molecular formula

* Corresponding author.

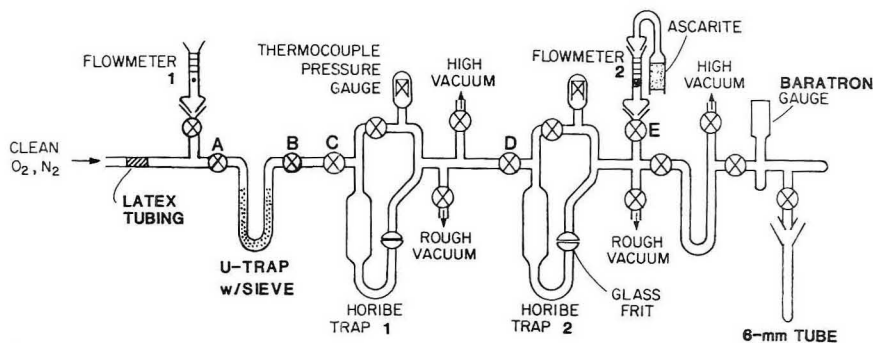


Figure 1. Schematic drawing of the gas flow/vacuum line system used in the present study for evaluation of Type 13X molecular sieve. The flow of gases in the system is from left to right.

$\text{Na}_2\text{OAl}_2\text{O}_3\text{SiO}_2$ (Type 13X, $1/16$ -in. pellets, Linde Division, Union Carbide Corporation, Danbury, CT). The sieve aperture is 10 Å in diameter, while the molecular diameters of CO_2 , O_2 , and N_2 are 3.34, 2.98, and 3.15 Å, respectively. The number of molecules of a specific compound which are retained in the sieve cavities via the sieve apertures is strongly dependent on both the molecular diameter and the temperature of the sieve.⁷ Molecular sieves are selective for specific gas molecules not only on the basis of pore size but also on the basis of molecular polarity and boiling point. In the case of Type 13X, the Na^+ -containing sieve is strongly polar, resulting in a preferential retention of CO_2 over other, less polar gases (e.g., O_2 and N_2). It is likewise imperative that molecules which could potentially displace CO_2 (e.g., H_2O) be prevented from entering the sieve. Type 13X is commonly used in industrial applications for the removal of CO_2 gas and H_2O vapor from hydrocarbon gas mixtures.

To evaluate the molecular sieve for quantitative collection and release of CO_2 , as well as the isotopic fidelity of the trapped and released CO_2 , a sieve trap was interfaced to a gas flow/vacuum extraction line. The components of the system in which Type 13X was used are shown in Figure 1. The quartz U-tube (dimensions: height, 150 mm; i.d., 9 mm; o.d., 12 mm) contains approximately 12 g of sieve which is immobilized by plugging the tube with prebaked quartz wool. The U-tube has sealing o-ring stopcocks at each end which allow it to be removed from the main line as needed without exposing the sieve to air. The sieve should be exposed to air for a minimum of time when transferring it to the U-tube in order that absorption and adsorption of atmospheric gases and contaminants are minimized. Water vapor is the most deleterious of these components, and it may reduce the efficiency of the sieve if exposure is chronic (G. Rand, personal communication). When the unit is attached to other instrumentation a trap of magnesium perchlorate upstream from the sieve trap has been found to be adequate for eliminating the H_2O before it reaches the molecular sieve. Care should also be taken to keep the sieve free of organic contaminants during handling because of the potential for their slow oxidation at elevated temperatures (see below).

When a new batch of sieve is used it should be conditioned for at least 24 h by opening the U-tube to full vacuum (10^{-6} atm) while heating at 550°C with a heating jacket (Glas-Col, Terre Haute, IN). This temperature is well below that which purportedly causes degradation of the zeolite ($\sim 700^\circ\text{C}$; G. Rand, personal communication), but it is high enough to eliminate absorbed CO_2 and H_2O from the sieve and to volatilize and combust any initially adsorbed organic contaminants. In operation, the sieve is allowed to equilibrate at room temperature (22 – 25°C) before CO_2 collection. At least temperatures, O_2 and N_2 molecules pass freely through the sieve apertures and occupy very little of the sieve's total available cavity space.⁷ Since the sieve will normally be at full vacuum following the analysis of a prior sample, it is then brought to atmospheric pressure by closing the system to vacuum and then introducing ultra-high-purity O_2 or N_2 ($400\text{ cm}^3\cdot\text{min}^{-1}$) into the U-tube by slowly opening the upstream stopcock A. The gas is then allowed to flow through the remainder of the system

and to vent by opening stopcocks B–E. At this point, if the sieve is to be used for collecting CO_2 from a remote instrument, it may be isolated by closing stopcocks A and B, and flowmeter 1 and the U-tube are removed as a unit from the flow/vacuum line. For purposes of this study, however, it was maintained intact on the flow/vacuum line.

The recovery of CO_2 from O_2 and N_2 streams was evaluated as follows. The carrier gas was adjusted to the desired flow rate with the molecular sieve trap maintained at room temperature. A quantity of pure CO_2 of known isotopic composition was injected through heavy-walled latex rubber tubing using a precision microliter syringe (Micrometrics, Shorewood, IL). The total time for all injections was 2.0 min. A period of 5 min was allowed to elapse after injection, and flow was then stopped by closing stopcocks A and E. The entire system was then brought to full vacuum. Horibe trap 1 was immersed in a bath consisting of dry ice in 2-propanol (-78.5°C) to serve as a water trap. Horibe trap 2 was immersed in liquid nitrogen to serve as the CO_2 trap. The Horibe traps were employed here because their design, with increased dead volume for greater residence time and glass frits for increased surface area, allow for quantitative collection of CO_2 even under full dynamic vacuum.⁸ The stopcocks to vacuum were then closed so that the system was under static vacuum. Preliminary tests of the retention efficiency of the sieve demonstrated that no CO_2 leaked past the U-tube following injection and none desorbed from the sieve while at room temperature under full dynamic vacuum for at least 1 h. The heating jacket was then placed around the U-tube, and the CO_2 was transferred to Horibe trap 2. Following transfer, Horibe trap 2 was evacuated again, and its contents were cryogenically transferred to the measured volume under static vacuum. The volume of gas was measured using a Baratron absolute pressure transducer (MKS Instruments, Andover, MA) which had previously been calibrated with known CO_2 gas standards.

For $\delta^{13}\text{C}$ determinations the above procedure was followed, and CO_2 standard gas samples were cryogenically collected in 6-mm glass tubing which was flame-sealed. The $\delta^{13}\text{C}$ of the samples was measured with a Nuclide 6-60RMS mass spectrometer. For $\Delta^{14}\text{C}$ determinations, oceanic humic matter of known $\Delta^{14}\text{C}$ was dissolved in ultra-high-purity artificial seawater and combusted to CO_2 using a high-temperature total organic carbon analyzer. The unit was interfaced to the sieve U-tube which trapped the CO_2 from the O_2 gas stream. The CO_2 was purified and collected as above for subsequent $\Delta^{14}\text{C}$ analysis by tandem accelerator mass spectrometry.

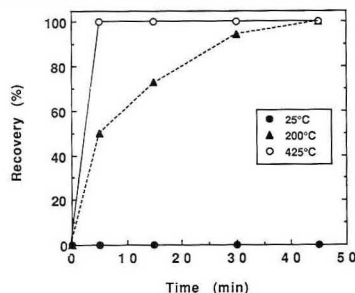
RESULTS AND DISCUSSION

A wide range of carrier gas flow rates and quantities of CO_2 was used to assess the conditions under which Type 13X sieve could be used. In addition, various operating parameters (desorption temperature, desorption time) were also evaluated in order to develop an optimized protocol for routine use of the sieve. Initial tests using O_2 and N_2 as carrier gases revealed that recoveries of CO_2 were identical using these two gases.

Table I. Recoveries (%) of Standard Amounts of CO₂ from O₂ Stream at Different Flow Rates Using Type 13X Molecular Sieve^a

O ₂ flow rate (cm ³ ·min ⁻¹)	recovery (%)
150	100.0
3-h O ₂ flow, then CO ₂ injection	100.0
CO ₂ injection, then 3-h O ₂ flow	100.0
420	100.7
1000	99.3
2000	100.0

^a CO₂ (250 μL) was injected over a 2-min interval. Standard deviation of replicate trials was ±1.0%.

**Figure 2.** Recovery of standard CO₂ gas from sieve trap as a function of time while held at room temperature (25 °C) and during heating at 200 and 425 °C. The CO₂ (250 μL) was added by 2.0-min injection to O₂ stream flowing at 150 cm³·min⁻¹. Standard deviation of replicate runs was ±1%.

Subsequently, O₂ was used as the carrier gas for further experimental evaluation both because it is normally used for flow-through organic carbon combustion and because it is more problematic in cryogenic applications. The system blank using Type 13X was insignificant (always <0.02 μmol of C), and hence sample values required no correction.

The CO₂ was trapped with 100% efficiency by Type 13X molecular sieve for quantities of CO₂ ranging over 2 orders of magnitude (0.3–50 μmol, $r^2 = 1.000$, $n = 12$). The trapping efficiency of CO₂ gas was independent of the flow rate of O₂ through the sieve and was also 100% in all cases (Table I). This demonstrates the extremely high affinity of Type 13X for CO₂ since the residence time of gas in the U-tube was less than 1 s at the greatest flow rate used here (2000 cm³·min⁻¹). The equivalent range of CO₂ concentrations over all tests was 2–130 μmol per liter of carrier gas. The sieve retained 100% of the CO₂ (10 μmol) even when followed by prolonged periods (3 h) of continuous O₂ flow (Table I). The CO₂ was also retained with 100% efficiency when it was introduced to the sieve after the sieve was subjected to prolonged periods of continuous O₂ flow (Table I). Therefore, applications which require extended periods of time to collect adequate amounts of CO₂ for a given analysis are assured of quantitative recoveries.

The time dependence of CO₂ release from Type 13X sieve under vacuum was evaluated at three temperatures (Figure 2). At room temperature (25 °C), prolonged (1 h) application of full vacuum to the sieve trap resulted in no loss of absorbed CO₂. At 200 °C, 100% release took up to 45 min. However, at 425 °C, complete release was achieved within 5 min of heating. For most applications, rapid release is preferable in order to avoid potential isotopic fractionations resulting from the kinetic effects of slow release. We routinely heat the sieve rapidly to 425 °C by maintaining the heating jacket at this temperature, even when it is not around the U-tube. Although the sieve can be heated to ~700 °C, its structure may begin

Table II. Isotopic Signatures of Injected CO₂ Standard Gas (δ¹³C) and of CO₂ Derived from High-Temperature Flow-Through Combustion of Oceanic Humic Substances (Δ¹⁴C)^a

CO ₂ derivation	δ ¹³ C (‰)	Δ ¹⁴ C (‰)
standard gas injection		
known	-35.9 ± 0.2	—
sieve	-35.8 ± 0.1	—
oceanic humics combustion		
humic no. 161		
known	—	-387 ± 26
sieve	—	-374 ± 21
humic no. 151		
known	—	-495 ± 30
sieve	—	-509 ± 29

^a The CO₂ was collected on Type 13X molecular sieve and subsequently purified for isotopic analysis (see text for details). Oxygen carrier gas flow rate was 150 cm³·min⁻¹.

to break down at such elevated temperatures, resulting in a loss of trapping efficiency (G. Rand, personal communication). The lowest blanks are attained when the sieve is kept at 425 °C, especially when it is not being used for extended periods of time.

The stable isotope ratio of CO₂ trapped and released by the sieve was identical to that of the stock CO₂ (Table II). Triplicate injections of 10 μmol of CO₂ at an O₂ flow rate of 150 cm³·min⁻¹ yielded δ¹³C = -35.8 ± 0.1‰ while the known value of stock CO₂ was δ¹³C = -35.9 ± 0.2‰ indicating that fractionation of CO₂ upon passage through the sieve did not occur. Although stable isotope ratios were measured for 10-μmol samples of CO₂ only, accurate ratios are expected for lesser and greater quantities of CO₂ and at different flow rates since recoveries were 100% in all cases. However, for very small or very large amounts of CO₂ the accuracy of isotopic values should be checked against similarly sized known gas standards which have been processed through the sieve trap. When the sieve was interfaced to a high-temperature organic carbon analyzer with O₂ as the carrier gas, the Δ¹⁴C signatures of the CO₂ (8–10 μmol) derived from combustion of oceanic humic substances were indistinguishable from the known signatures determined by sealed-tube combustion (Table II). Thus, both δ¹³C and Δ¹⁴C may be accurately determined by collection of CO₂ from the gas stream using the sieve trap. It should also be noted that for these short-term collections the associated blank was insignificant.

The simplicity of the trap and the range of conditions over which Type 13X molecular sieve can be used provide several advantages over systems which use cryogenic collection of CO₂. The sieve can be used at atmospheric pressure and at the room temperature of most laboratories to collect CO₂ from either O₂ or N₂ (and possibly other gases) carrier gas streams. The upper limits examined in this study were 2000 cm³·min⁻¹ flow rate and 50 μmol of CO₂. These ranges may well be greater in the system used here but in any case could be expanded by using collection tubes which hold a greater volume and mass of sieve or by using multiple traps arrayed in series. Under very rigorous flow conditions or extremes in amounts of CO₂ collected, retention efficiencies, as well as stable isotope ratios, should be checked periodically to ensure that the capacity of the sieve is not exceeded. We have used a single batch of Type 13X in a U-type continuously for over 12 months with no signs of performance deterioration, resulting in significant savings in both cost and maintenance over cryogenic collection systems.

ACKNOWLEDGMENT

We thank D. Des Marais for comments on the manuscript, A. Witter for help in preliminary tests, D. Des Marais and A.

Tharpe for $\delta^{13}\text{C}$ measurements, and the Center for Accelerator Mass Spectrometry of Lawrence Livermore National Laboratory for $\Delta^{14}\text{C}$ analyses. This work was supported by NSF grant nos. OCE87-16590, OCE88-40531, and OCE91-01540.

REFERENCES

- (1) Buchanan, D. L.; Corcoran, B. J. *Anal. Chem.* **1959**, *31*, 1635.
- (2) Van Hall, C. E.; Saffran, J.; Stenger, V. A. *Anal. Chem.* **1963**, *35*, 315.
- (3) Stump, R. K.; Frazer, J. W. Lawrence Livermore National Laboratory, Report UCRL-50318, 1967.
- (4) Des Marais, D. J. *Anal. Chem.* **1978**, *50*, 1405.

- (5) Bauer, J. E.; Haddad, R. E.; Des Marais, D. J. *Mar. Chem.* **1991**, *33*, 335.
- (6) Wedeking, K. W.; Hayes, J. M.; Matzigeit, U. In *Earth's Earliest Biosphere*; Schopf, J. W., Ed.; Princeton Univ. Press: Princeton, 1983; p 428.
- (7) Breck, D. W. *Zeolite Molecular Sieves: Structure, Chemistry and Use*; John Wiley & Sons: New York, 1974.
- (8) Horibe, Y.; Shigehara, K.; Takakuwa, Y. *J. Geophys. Res.* **1973**, *78*, 2625.

RECEIVED for review August 13, 1991. Revised manuscript received December 23, 1991. Accepted January 6, 1992.

Inverse Sampling Valve Interface for On-Line Process Monitoring with a Mass Spectrometer

Jennifer S. Brodbelt*

Department of Chemistry and Biochemistry, University of Texas at Austin, Austin, Texas 78712-1167

Reid S. Willis and A. Kasem Chowdhury

Dow U.S.A., P.O. Box 1398, Pittsburg, California 94565

INTRODUCTION

Advances in analytical instrumentation have led to new designs and application of on-line, real-time process monitoring,¹⁻⁶ including methods which rely on chromatographic² or spectroscopic analysis.⁶⁻⁸ With the advent of less costly, compact, and less complex mass spectrometers,⁹ increasing efforts have been directed at developing on-line mass spectrometric techniques,¹⁰⁻¹⁹ because they offer both qualitative and quantitative information about the chemical process with high sensitivity.

Mass spectrometry is particularly suitable for sampling gaseous streams. Many applications of on-line gas chromatography-mass spectrometry interfaces¹⁰ have been reported. Additionally, direct gas sampling may be achieved by use of a pulsed electromagnetic valve connected to a mass spectrometer.^{11,12} The use of a pulsed valve with a Fourier transform ion cyclotron resonance mass spectrometer¹¹ or a quadrupole ion trap mass spectrometer¹² has proven effective for intermittent introduction of volatile components. More recently, several examples of mass spectrometric liquid sampling have been demonstrated. Most rely on atmospheric pressure ionization (API) sources¹³ or membrane separators¹⁴⁻¹⁹ to accommodate the potentially high gas load when a liquid is sampled into a vacuum. Unfortunately, API sources are mechanically complex and involve additional stages of differential pumping. Although the membrane-based devices are versatile and less complex, they exhibit long or variable response times due to slow diffusion of the analyte through the membrane.

In some cases, a more direct liquid-sampling system is preferred to a membrane interface, especially if quantitative sample transfer or faster response times are needed. Microliter quantities of liquid solutions can be introduced into a mass spectrometer via a conventional direct insertion probe,²⁰ but this technique involves use of a vacuum interlock and is not suitable for on-line continuous-monitoring applications. In this report, we demonstrate for the first time direct on-line monitoring of gas or liquid samples by using an inverse sampling valve coupled to a mass spectrometer.

Standard versus Inverse Liquid-Sampling Valves. *Standard Liquid Sampling.* Liquid-sampling valves such as those made by ABB²¹ or MAT²² operate on the principle of metering microliter quantities of a liquid into a carrier gas

stream and then vaporizing the liquid rapidly and completely into a gas chromatograph (GC). To our knowledge, these liquid-sampling valves have never been used to transfer samples directly to mass spectrometers. Figure 1 is a cross-sectional view of a portion of a MAT valve attached to a gas chromatograph. Liquid sample from the process stream is directed to the valve through port 1. The sample fills the grooved slot, 2, of the piston, 3, and is transferred to the heated vaporization zone, 4, upon actuation of the piston. The seals, 5, ensure that only sample in the slot ($\sim 1 \mu\text{L}$) is transferred. Hot carrier gas, 6, flashes the sample and directs it into the GC column, 7.

Inverse Sampling. Inverse sampling²³ is a recent modification of the liquid-sampling valve, wherein the heated vaporization section is removed and the remainder of the valve is welded to the vessel holding the material to be transferred. For our purposes, this vessel is a short welded section of 2-in. pipe, which serves as the sample chamber. The valve is further modified to expose one of its seals into the sample chamber. The liquid-transfer section of the standard valve becomes an evacuation chamber or vaporization section in the modified valve. Finally, the mode of operation is opposite to the standard liquid sample; i.e., the inject position becomes the load position and vice versa. The sampling piston captures sample from the chamber or process stream into its $1/4\text{-}\mu\text{L}$ groove while in the extended (load) position and transfers it in the retracted (inject) position. Transference takes place by evacuation of the sample-filled groove into the analytical instrument, with or without a supplementary carrier gas stream. When the sample is a liquid, the "vaporization zone" must be heated and a carrier gas is recommended. These added steps are unnecessary for gas samples.

The advantage of inverse sampling is that the valve can be attached directly to the process, obviating the need for divert streams or pumps. This sampler can be used for transference of any vaporizable substance and is particularly useful for molten streams which are ordinarily difficult to sample.

EXPERIMENTAL SECTION

Two spectrometers were used, a Finnigan quadrupole ion trap mass spectrometer (ITMS)²⁴ located at the University of Texas for gas sampling and a Finnigan 4600 quadrupole mass spectrometer located at Dow U.S.A. for liquid sampling. Pentachloropyridine (PCP) was obtained from Dow Chemical. All other

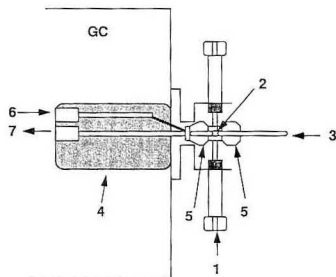
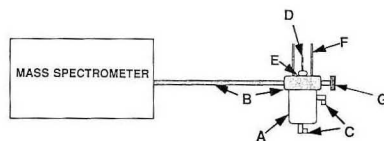


Figure 1. Cross-sectional view of MAT valve.



- A. Sampling valve body
- B. Evacuated vaporization zone
- C. Air actuation ports
- D. Piston
- E. Rulon or ceramic seal
- F. Sample chamber
- G. Plug

Figure 2. Setup for inverse sampling mass spectrometry of gas and volatile liquid samples. For molten or involatile samples, the plug is replaced by a 100 μ m i.d. fused-silica capillary which is connected to a helium cylinder.

substances were obtained from Aldrich Chemical and used without further purification.

Gas Sampling. The inverse sampling valve/mass spectrometer setup for gas sampling is illustrated in Figure 2. In this setup, one end of the vaporization section was plugged and the other connected to the mass spectrometer with $1/8$ -in. stainless steel tubing. The sampling piston was actuated into and retracted from the sample chamber by using a flow of pressurized air. In the retracted position, the sample groove is exposed directly to the vacuum chamber. In the extended position, the piston passes through a Rulon J seal and extends into the sampling chamber. Gaseous samples were introduced into the sample chamber by various means: air was injected from the atmosphere, Freon-12 (dichlorodifluoromethane) was sprayed into the air-filled chamber, and benzene was swabbed around the sampling piston. Samples were then introduced into the mass spectrometer when the piston retracted into the evacuated zone. The pressure of the ion trap mass spectrometer rose from nominally 2.0×10^{-6} to $(2.5\text{--}3.5) \times 10^{-6}$ Torr upon vaporization of the sample. The samples were electron-ionized, and the trap was operated in the mass-selective instability mode. A buffer gas pressure of 1 mTorr was used.

Liquid Sampling. For transfer of liquid or molten samples, the valve was further modified. The plug was replaced with a 5-ft. length of 100 μ m i.d. fused silica, and the end was attached to a 12 psi helium line. The $1/8$ -in. tubing was replaced with $1/16$ -in. tubing in order to minimize peak broadening. The $1/16$ -in. tubing is more flow-restrictive and permits less sample diffusion within the transfer tubing. The vaporization section was heated to 270 $^{\circ}$ C to minimize sample dispersion. A 1-g amount of pentachloropyridine (mp 125 $^{\circ}$ C, bp 250 $^{\circ}$ C) was placed in the sample chamber. Upon sample injection, the pressure of the quadrupole mass spectrometer rose from 1.0×10^{-6} to 2.3×10^{-6} Torr. The mass spectrometer was operated in the electron ionization mode.

RESULTS AND DISCUSSION

Figure 3 shows spectra from a $1/4$ - μ L injection of air and then air contaminated with Freon-12, acquired with the valve

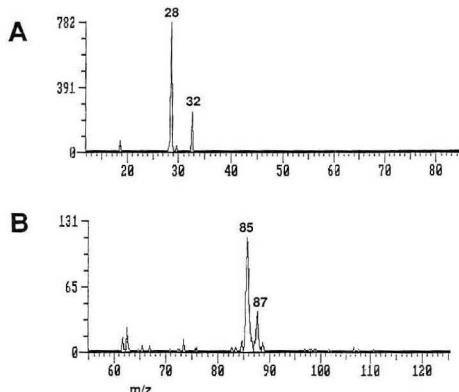


Figure 3. Mass spectra obtained with a quadrupole ion trap from sampling (A) atmosphere and (B) Freon in atmosphere.

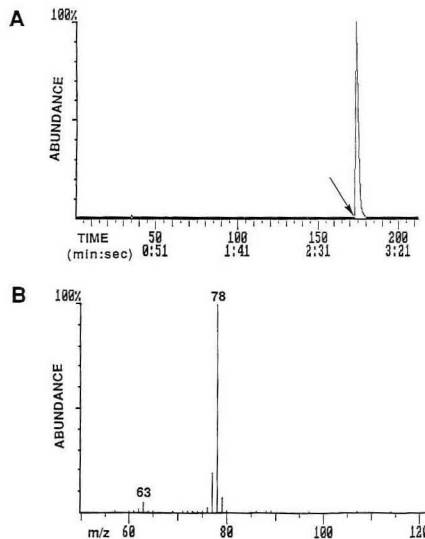


Figure 4. (A) Time vs ion intensity profile for sampling benzene with a quadrupole ion trap mass spectrometer (arrow indicates injection point). (B) Mass spectrum obtained with a quadrupole ion trap from sampling benzene.

connected to the ion trap mass spectrometer. For these samples, the base pressure of the vacuum chamber reached nominally 4.0×10^{-6} Torr, and the spectral quality remained excellent.

The valve was then used to sample benzene into the spectrometer. Shown in Figure 4A is the time versus ion intensity profile and in Figure 4B is the mass spectrum of a benzene/air mixture. The response is rapid (<100 ms) because the sample is pulled directly into the vacuum chamber without passing through a separation device or conductance limit. The peak width is 5–15 s depending on the concentration of the organic analyte in the air. Sample-to-sample reproducibility is high (relative standard deviation of 2–4%), and there is no apparent tailing or sample carryover.

The valve was then connected to the Finnigan 4600 quadrupole mass spectrometer for direct liquid sampling as de-

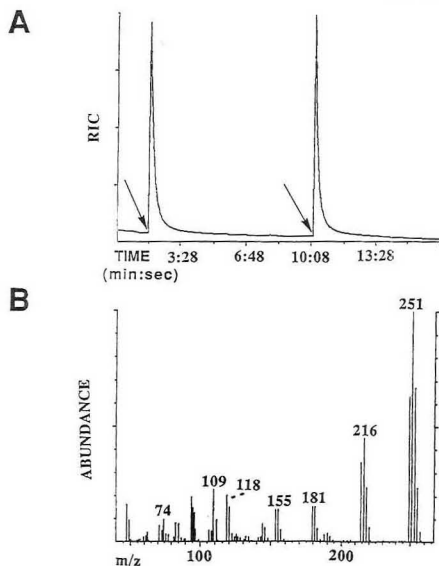


Figure 5. (A) Time vs ion intensity profile of duplicate injections of PCP in a quadrupole mass spectrometer (arrows indicate injection points). (B) Mass spectrum of PCP.

scribed in the Experimental Section. Pentachloropyridine passes rapidly through the interface and demonstrates little tailing, as seen in Figure 5A. Duplicate injections show reproducible profiles. The acquired mass spectrum, shown in Figure 5B, matches the known spectrum of PCP.

CONCLUSIONS

The simplicity of this novel sampling interface and adaptability to on-line monitoring make it an attractive alternative to membrane devices for industrial process analysis. Moreover, the mechanics of the valve make it suitable for operation in a fully automated system, and this type of interface essentially eliminates the need for sample preconditioning or dilution. Finally, an inverse valve offers several advantages over pulsed electromagnetic valves for gas sampling. First, the inverse sampling valve described in this report does not require a stable or defined back-pressure (of the process stream being monitored), as is typically necessary for

operation of a pulsed valve. Additionally, the inverse sampling valve is more rugged and is easier to clean than a pulsed valve.

ACKNOWLEDGMENT

We thank David Simeroth of Dow U.S.A., Texas Division, for developing and implementing the inverse sampling valve. This research would not have been possible without his pioneering work. J.B. acknowledges the support of the Welch Foundation (Grant F-1155) and the donors of the Petroleum Research Fund, administered by the American Chemical Society.

Registry No. Benzene, 71-43-2; pentachloropyridine, 2176-62-7.

REFERENCES

- (1) Huskins, D. J. *General Handbook of On-Line Process Analyzers*; Ellis Horwood Ltd.: Chichester, 1981.
- (2) Pitt, M. J.; Preece, P. E., Eds. *Instrumentation and Automation in Process Control*; Ellis Horwood: New York, 1990.
- (3) Mix, P. E. *Design and Application of Process Analyzer Systems*; John Wiley: New York, 1984.
- (4) Krajca, J. M., Ed. *Water Sampling*; Ellis Horwood Ltd.: Chichester, U.K., 1989.
- (5) Callis, J. B.; Illman, L.; Kowalski, B. R. *Anal. Chem.* **1987**, *59*, 624A.
- (6) Melcher, R. G.; Peters, L.; Emmel, H. W. *Topics Curr. Chem.* **1986**, *134*, 59.
- (7) Eckstein, R. J.; Owens, G. D.; Bain, M. A.; Hudson, D. A. *Anal. Chem.* **1986**, *58*, 2318.
- (8) Seitz, W. R. *Anal. Chem.* **1984**, *56*, 16A.
- (9) Stafford, G. C.; Kelley, P. E.; Bradford, D. C. *Am. Lab.* **1983**, June, 51.
- (10) McClennen, W. H.; Arnold, N. S.; Sheya, S. A. N.; Lighty, J. S.; Meuzelaar, H. L. C. *Proceedings of the 38th ASMS Conference on Mass Spectrometry and Allied Topics*, Tucson, AZ, 1990; p 611.
- (11) Carlin, T. J.; Freiser, B. S. *Anal. Chem.* **1983**, *55*, 574.
- (12) Emary, W. B.; Kaiser, R. E.; Kentamaa, H. I.; Cooks, R. G. *J. Am. Soc. Mass Spectrom.* **1990**, *1*, 308.
- (13) Kenny, D. V.; Slivon, L. E. *Proceedings of the 38th ASMS Conference on Mass Spectrometry and Allied Topics*, Tucson, AZ 1990; p 679.
- (14) Slivon, L. E.; Bayer, M. R.; Ho, J. S.; Budde, W. L. *Anal. Chem.* **1991**, *63*, 1335.
- (15) Eustache, H.; Histi, G. *J. Membr. Sci.* **1981**, *8*, 105.
- (16) Brodbelt, J. S.; Cooks, R. G.; Tou, J. C.; Kallos, G.; Dryzga, M. D. *Anal. Chem.* **1987**, *59*, 454.
- (17) Brodbelt, J. S.; Cooks, R. G. *Anal. Chem.* **1985**, *57*, 1153.
- (18) Sturara, A.; Doretti, L.; Parvoli, G.; Cecchinato, F.; Frison, G.; Traldi, P. *Biomed. Environ. Mass Spectrom.* **1989**, *18*, 707.
- (19) LaPack, M. A.; Tou, J. C.; Enke, C. G. *Anal. Chem.* **1991**, *63*, 1631.
- (20) Dougherty, R. C.; de Kanel, J. *Anal. Chem.* **1984**, *56*, 2979.
- (21) ABB Process Analytics, Inc., Model No. 3526749, 843 Jefferson St., P.O. Box 831, Lewisburg, WV 24901.
- (22) Mess and Apparatechnik, Model No. 101 290, Rudolf Friedrich, Am Wiesrain 20, D-8000 München 45, West Germany, Telex 5213426.
- (23) Dow Chemical Co. Patent application number 631533. David Simeroth of Dow U.S.A., in Freeport, TX, successfully applied inverse sampling to gas chromatography.
- (24) Louis, J. N.; Cooks, R. G.; Syka, J. E.; Kelley, P. E.; Stafford, G. C.; Todd, J. F. *J. Anal. Chem.* **1987**, *59*, 1677.

RECEIVED for review October 31, 1991. Accepted January 6, 1992.

Extraction Technique for the Determination of Oxygen-18 in Water Using Prevacuated Glass Vials

Richard A. Socki*

Lockheed ESC, C-23, 2400 NASA Road, Houston, Texas 77058

Haraldur R. Karlsson

Texas Tech University, Department of Geoscience, Box 41053, Lubbock, Texas 79409

Everett K. Gibson, Jr.

NASA-Johnson Space Center, SN-2, Houston, Texas 77058

INTRODUCTION

The need for a rapid, inexpensive technique for routine $^{18}\text{O}/^{16}\text{O}$ extraction from water has arisen recently through applications in the medical sciences¹ and in hydrology. The traditional experimental technique for determining the oxygen

*To whom all correspondence should be addressed.

isotope composition of water, the $\text{CO}_2\text{-H}_2\text{O}$ equilibration method,² is tedious, time consuming, and involves the use of custom-made glass apparatus. Furthermore, because of potential memory effects from one sample to the next, the glassware needs to be thoroughly cleaned between runs. A few attempts have been made to improve upon the method.^{3,4} Attempts to analyze water directly in the source of the mass

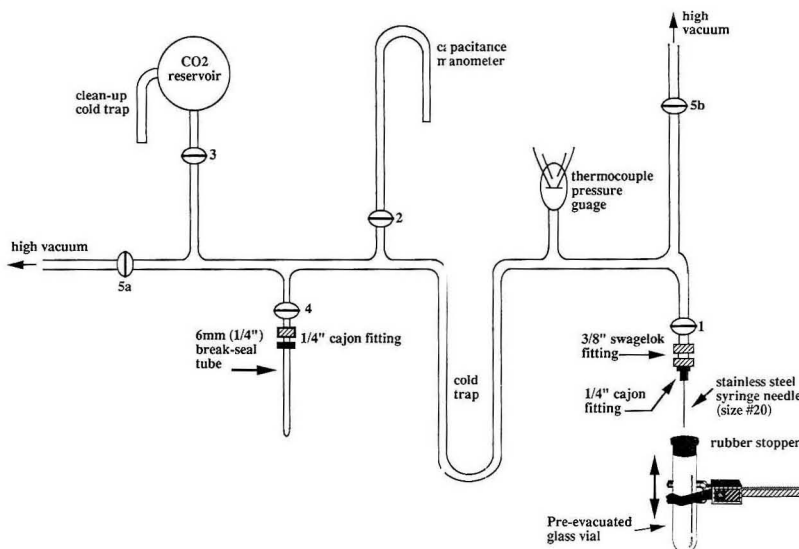


Figure 1. Diagram of the extraction line showing the position of the preevacuated vial.

spectrometer^{5,6} produced large memory effects and questionable results. Commercially available apparatus for automated extraction of $^{18}\text{O}/^{16}\text{O}$ from water is generally prohibitively expensive and often is designed to interface only with the manufacturer's own mass spectrometer. The method described in this paper utilizes inexpensive, off-the-shelf, preevacuated, glass vials. Preevacuated vials have been used by others for the isotopic analysis of breath CO_2 and are well tested.⁷ The vials can be purchased in bulk from scientific apparatus suppliers at a relatively low cost. These are coupled with a simplified extraction line consisting of a stainless steel syringe needle and a glass cold trap. Vials are filled with CO_2 and H_2O and shaken in a constant-temperature water bath for at least 90 min. Since the vials are discarded after use, no cleaning is necessary, essentially eliminating any memory effect. Reproducibility is generally better than $\pm 0.05\%$. The only reagents required are gaseous CO_2 for equilibration, a dry ice/alcohol mixture for trapping water, and liquid nitrogen for transferring the CO_2 .

EXPERIMENTAL SECTION

Experimental Details. A diagram of the preparation line is shown in Figure 1. A preevacuated vial is placed in the sample holder clamp, as shown in Figure 1. Care should be taken when choosing commercially available vacuum vials since some have rubber stoppers lubricated with silicone gel. The silicone gel lubricant has been known to produce an array of volatile components which may interfere with the isotopic analysis.⁸ We use Venject brand, 7-cm³ vials with a nonsilicone coating, available from Terumo Medical Supply, Elkton, MD 21921. The holder is a small-size steel glassware clamp with the plastic sleeves on the jaws removed. This provides a "snug" fit and prevents the vial from moving sideways while freely allowing upward movement. Vial and holder are positioned directly beneath the syringe needle on the extraction line with the vial resting on a lab jack. The jack is raised far enough so the syringe needle is embedded into the top of the vial's rubber stopper. The needle is evacuated through valve 1. The vial is then raised further so the needle punctures the rubber stopper. After pumping for a few seconds, the valves to the vacuum (valves 5a,b) are closed and 150 μmol of CO_2 is expanded into the vial by opening the CO_2 reservoir (valve 3) and opening valve 2 (manometer). The CO_2 pressure inside the vial is about 0.52 atm. Valve 1 is then closed, and the

vial is removed from the syringe needle. Off-line the vial is injected with 1.4–1.5 cm³ of water via a 5-cm³ glass syringe. Care should be taken when filling the vials with water to ensure that not too much air is let in. Since the pressure in the vial is lower than atmospheric pressure, the water sample from the glass syringe will be drawn directly into the vial.

The rubber stopper on top of the vial is designed to have 1 atm of pressure "pushing" it in. Care must be taken, however, not to force the lip on the rubber stopper from side to side, as this would result in a leak across the stopper seal. Samples should not be stored in the CO_2 -charged vials for more than a few weeks due to the probability of leaks occurring.

Once filled, the CO_2 - H_2O vessels are placed in a $25 \pm 0.1^\circ\text{C}$ constant-temperature bath. The containers are clamped sideways in a wrist action shaker and completely immersed in the bath water. Complete immersion of the vials is necessary if ambient laboratory air temperatures are significantly less than 25°C . Cool air temperatures will cause the water in the vial to condense at the portion sticking above the level of the water bath. We use a relatively low-cost oscillating motion shaker turned on its side to produce a wrist-action movement. Stroke amplitude can be adjusted on the shaker to produce the desired degree of agitation of water in the vial. Sufficient agitation breaks the surface of the water sample and facilitates quick isotopic equilibration.

After equilibration is complete, the vials are placed back in the holder on the line and the syringe needle is again pumped out as described in the filling procedure. However, this time the bottom of the vial is immersed in a dewar of liquid nitrogen. Since some of the water tends to "stick" to the bottom of the rubber stopper, the top of the vial is lightly heated with a flameless heat gun to condense all of the water to the bottom of the vial. The noncondensibles are then pumped out by raising the tube so the needle punctures the stopper. Any water vapor caught inside the syringe needle will immediately freeze and may later block the flow of CO_2 . To eliminate blockage, the syringe needle is also lightly heated with the heat gun. After sufficient pumping, valve 5 is closed and the liquid nitrogen dewar is replaced with a dry ice/alcohol dewar to keep the water frozen at the bottom of the vial. Released CO_2 is then frozen into the cold trap with liquid nitrogen, dried again by exchanging the liquid nitrogen dewar with one containing dry ice/alcohol, and transferred to a 6-mm Pyrex break-seal tube (valve 4) where it can be stored for analysis later.

Analytical Details. All CO_2 in this study was analyzed for oxygen and carbon isotopes on a triple-collecting Finnigan MAT 251 stable-isotope mass spectrometer at NASA-JSC. All oxygen

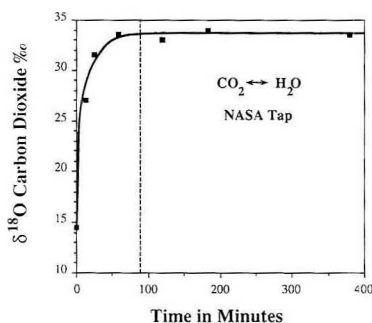


Figure 2. Variation with time of the $\delta^{18}\text{O}$ composition of CO_2 equilibrated with our laboratory working standard (NASA tap water). Oxygen isotope exchange equilibration is complete in about 1.5 h (broken line).

Table I. $\delta^{18}\text{O}$ Results for Three International Water Standards and Three Laboratory Standards

sample name	no. of preparations	std dev 1σ , ‰	meas ^a $\delta^{18}\text{O}$ SMOW, ‰	normalized ^b $\delta^{18}\text{O}$ SMOW, ‰
International Standards				
V-SMOW	5	± 0.05	+0.04	0.00
GISP	6	± 0.02	-24.85	-24.83
SLAP	5	± 0.03	-55.59	-55.50
Laboratory Standards				
GOMS	24	± 0.05	+0.36	
NASA tap	33	± 0.02	-6.63	
ADAM	20	± 0.05	-41.34	

^aThese data were calculated using the $\text{CO}_2\text{-H}_2\text{O}$ fractionation factor of 1.04120 recommended by Friedman and O'Neil (1977).¹⁰

^bThese data were normalized to $\Delta(\text{V-SMOW} - \text{SLAP}) = -55.50\%$.

isotopic ratio results are reported relative to SMOW.⁹

RESULTS AND DISCUSSION

Equilibration Time. Figure 2 is a plot of $\delta^{18}\text{O}$ of our laboratory working standard water (NASA tap) versus time and indicates the time needed to reach isotopic equilibrium between CO_2 and H_2O . Seven vials were filled with 1.5 cm³ of NASA tap and 150 μmol of CO_2 . These were shaken in a 25 °C water bath for up to 380 min. The $\delta^{18}\text{O}$ value at time = 0 is the initial oxygen isotope composition of the injected CO_2 . With increasing time, the $\delta^{18}\text{O}$ composition of the CO_2 approaches an equilibrium value with that of the water in the vial. Data indicate that equilibration is completed in at least 90 min if the vials are placed sideways and shaken. The process of shaking the vials sideways breaks the surface of the

water sample and facilitates more rapid oxygen isotope exchange.

Accuracy and Precision. Data for the oxygen isotope composition of six different water standards using the technique described in this paper are reported in Table I. Our three laboratory standards consist of an isotopically light water (ADAM, acronym for average depleted Antarctic meltwater) prepared by filtering a block of Antarctic ice, a water of intermediate isotopic composition (NASA tap, distilled Houston tap water), and a water relatively enriched in $\delta^{18}\text{O}$ (GOMS, acronym for Gulf of Mexico sea water, distilled sea water taken from the south shore of Galveston Island, TX). International standards provided by the IAEA, Vienna, that were analyzed include V-SMOW, SLAP, and GISP.

On the basis of the number of analyses, reproducibility of all six standards using our technique is generally better than $\pm 0.05\%$ at the 1 σ level of confidence. Furthermore, the oxygen isotope composition of the international standards V-SMOW, SLAP, and GISP are well within the mean of reported values.¹¹

CONCLUSIONS

The method described in this paper satisfies the need for a rapid and inexpensive $^{18}\text{O}/^{16}\text{O}$ water extraction technique. Since the preevacuated vials are discarded after use, the potential for memory effects during extraction is eliminated. Furthermore, good sample reproducibility makes our method acceptable for routine $^{18}\text{O}/^{16}\text{O}$ water extractions.

ACKNOWLEDGMENT

We thank Dale Schoeller for drawing our attention to the use of preevacuated vials. This research was supported by the NASA Planetary Biology Program. Use of trade names and manufacturers/suppliers in this publication is for descriptive purposes only and does not constitute endorsement by Lockheed Engineering and Sciences Co. or NASA.

Registry No. ^{18}O , 14797-71-8; water, 7732-18-5.

REFERENCES

- (1) Schoeller, D. J. *Nutr.* **1988**, *118*, 1278.
- (2) Epstein, S.; Mayeda, T. *Geochim. Cosmochim. Acta* **1953**, *4*, 213.
- (3) Yoshida, N.; Mizutani, Y. *Anal. Chem.* **1986**, *58*, 1273.
- (4) Roether, W. *Int. J. Appl. Radiat. Isot.* **1970**, *21*, 379.
- (5) Majzoub, M.; Nief, G. *Adv. Mass Spectrom.* **1968**, *4*, 511.
- (6) Hagemann, R.; Lohez, P. *Adv. Mass Spectrom.* **1978**, *7A*, 504.
- (7) Schoeller, D. A.; Klein, P. D. *Biomed. Mass Spectrom.* **1978**, *5*, 29.
- (8) Ajami, A. M.; Watkins, J. B. *Clin. Chem.* **1983**, *29*, 725.
- (9) Craig, H. *Geochim. Cosmochim. Acta* **1957**, *12*, 133-149.
- (10) Friedman, I.; O'Neil, J. R. *U.S. Geol. Surv. Prof. Pap.* **1977**, No. 440-KK.
- (11) Hut, G. *Report to the Director General, Consultant's Group Meeting on Stable Isotope Reference Standards*, Vienna, Sep 16-18, 1985; IAEA: Vienna, 1987; 42 pp.

RECEIVED for review September 30, 1991. Accepted January 8, 1992.

CORRECTION

Enzymatic Flow Injection Analysis in Nonaqueous Media

Lorenzo Braco, José A. Darós, Miguel de la Guardia (*Anal. Chem.* **1992**, *64*, 129-133).

On page 129, on the first line under the Experimental Section, the word *spiralis* should be species.

AUTHOR INDEX

- Akagi, T., 737
 Archambault, J.-F., 810

 Bartsch, R. A., 815
 Bauer, J. E., 824
 Benincasa, M. A., 790
 Bhattacharya, A., 823
 Bouchonnet, S., 743
 Braco, L., 831
 Brodbelt, J. S., 827
 Buckley, W. T., 724
 Budac, J. J., 724

 Chowdhury, A. K., 827
 Cooper, L. M., 802

 Darós, J. A., 831
 de la Guardia, M., 831
 Denhez, J.-P., 743
 Dorsey, J. G., 785
 Druffel, E. R. M., 824

 Fréchet, J. M. J., 820
 Fuchigami, T., 711
 Fujii, T., 775

 Gibson, E. K., Jr., 829
 Giddings, J. C., 790
 Godfrey, D. V., 724
 Griffiths, P. R., 705

 Hankins, M. G., 815

 Hasenoehrl, E. J., 705
 Hayashita, T., 815
 Higashijima, T., 711
 Hogan, J. D., 763
 Hoppiliard, Y., 743

 Imasaka, T., 711
 Ishibashi, N., 711

 Kaneta, T., 798
 Karlsson, H. R., 829
 Kim, J. S., 815
 Knobeloch, J. M., 815
 Koenig, K. M., 724
 Kooser, R. G., 785

 Lamb, E., 785
 Lang, J. C., 715
 Laude, D. A., Jr., 763
 Lee, J. C., 815
 Lee, J. H., 815
 Lépine, L., 810
 Li, L., 769
 Liu, H., 802
 Loscalzo, J., 779
 Lunte, C. E., 806

 Masuda, A., 737
 Mauriac, C., 743
 Missel, P. J., 715

 Pandey, K. S., 823

 Perkins, J. H., 705
 Pinkston, J. D., 802
 Preston, L. M., 754

 Raynie, D. E., 802
 Russell, D. H., 754

 Schechter, I., 729
 Scott, D. O., 806
 Shabani, M. B., 737
 Socki, R. A., 829
 Stamlar, J. S., 779
 Stevens, L. E., 715
 Strobel, F. H., 754
 Svec, F., 820

 Taga, M., 798
 Tanaka, S., 798
 Telting-Diaz, M., 806
 Tripathi, D. N., 823

 Vaidyanathaswamy, R., 823

 Wang, A. P. L., 769
 Washburn, K. S., 754
 Wehmeyer, K. R., 802
 Williams, P. M., 824
 Willis, R. S., 827
 Wright, P. B., 785

 Yoshida, H., 798

JOURNAL OF CHEMICAL & ENGINEERING DATA



Get A World Of Precise, Accurate Data In This International, Quarterly Journal

Multidisciplinary in nature and international in scope, the *Journal of Chemical and Engineering Data (JCED)* features contributions by distinguished physicists, chemists, chemical engineers, mechanical engineers, biological scientists, and applied mathematicians from the world over. Their expert reports represent numerical data bases for private technical information systems, particularly in industry, that will broaden your scientific horizons and improve the quality of your work.

This unique journal offers you precise, accurate data on physical, thermodynamic, and transport

properties of well-defined materials. It also keeps you informed about the latest international standards on symbols, terminology, and units of measurement for reporting data properly.

You'll find numerical property data measurements on:

- pure substances of defined purity
- well-defined gaseous, liquid, and solid mixtures
- semi-empirical and theoretical correlations useful in interpolating, extrapolating, and predicting properties of scientific and technological importance

- new substances — the physical and spectral properties of inorganic, organic, and biochemical substances and other complex substances prepared by established synthetic procedures that may have major scientific and technological applications

Editor

Kenneth N. Marsh
Texas A&M University

Associate Editors

Henry V. Kehiaian
University of Paris VII-CNRS, France
Randolph C. Wilhoit
Texas A&M University

1992 SUBSCRIPTION INFORMATION

Volume 37
4 Issues Per Year
ISSN 0021-9568



		U.S.	Canada and Mexico	Europe*	All Other Countries*
ACS Members	1 year	\$ 33	\$ 38	\$ 42	\$ 45
	2 years	\$ 59	\$ 69	\$ 77	\$ 83
Nonmembers	1 year	\$289	\$294	\$298	\$301
Supplementary Material on Microfiche		\$ 12	\$ 16	\$ 16	\$ 16

*Air service included.

Member subscription rates are for personal use only.
For nonmember rates in Japan, contact Maruzen Co., Ltd.

Journal subscriptions start January 1992 and are based on a calendar year.

Foreign payment must be made in U.S. currency, by international money order, UNESCO coupons, or U.S. bank draft, or order through your subscription agency.

Address your orders to:

American Chemical Society
Department L0011
Columbus, OH 43268-0011

Toll free: (800) 333-9511

Outside U.S.: (614) 447-3776

Telex: 440159 ACSP UI or
892582 ACSPUBS

Fax: (614) 447-3671

This publication is available on microfilm,
microfiche, and electronically through Chemical
Journals Online on STN International.

*Add Speed and
Precision to Your
Macrosample
Carbon, Hydrogen
and Nitrogen
Analyses with
the LECO®
CHN-1000*

The LECO® CHN-1000 is designed to provide rapid analysis results for non-homogeneous materials such as coal, coke, oil, rubber, and a wide variety of other organic materials.

The 200 milligram nominal sample size allows a more representative sample to be used, providing precise results within minutes.

LECO®'s icon-driven, touch-screen software is interfaced with a powerful 386 computer base for ultimate ease of operation.

Optional automatic sample loading carousels can be incorporated to allow unattended operation for extended time periods. The 35 sample carousels can be stacked allowing larger runs to be performed.

For more information, call or write today!

CIRCLE 80 ON READER SERVICE CARD



LECO® Corporation 3000 Lakeview Avenue
St. Joseph, MI 49085-2396 U.S.A.
Phone: (616) 983-5531 Facsimile: (616) 983-3850